Synthesis, Characterization and Spectroscopic Studies of Transition Metal Complexes with Chalcogen (O, S, Se and Te) Bridged Non–innocent Ligands

A Dissertation Presented in Partial Fulfillment of the Requirement for the Degree
of
Doctor of Philosophy
at
IIT Guwahati

by

Manas Kumar Mondal

Roll No. 126122004

Department of Chemistry
Indian Institute of Technology Guwahati
Guwahati–781039, Assam
India

December 2016

To my parents

"Chemistry is necessarily an experimental science: its conclusions are drawn from data, and its principles supported by evidence from facts."

Michael Faraday

भारतीय प्रौद्योगिकी संस्थान गुवाहाटी
Indian Institute of Technology Guwahati

Indian Institute of Technology Guwahati
Department of Chemistry

DECLARATION

I do hereby declare that the research work embodied in this thesis entitled "***Synthesis, Characterization and Spectroscopic Studies of Transition Metal Complexes with Chalcogen (O, S, Se and Te) Bridged Non–innocent Ligands***" has been carried out by me under the supervision of **Dr. Chandan Mukherjee**, Department of Chemistry, Indian Institute of Technology Guwahati, Assam–781039, India. The research works have been carried out in the period of August 2012 to November 2016.

In keeping with the general practice of reporting scientific observations, due acknowledgements have been made wherever the work described is based on the findings of other investigators.

IIT Guwahati
December, 2016

Manas Kumar Mondal
Roll No. 126122004

Dr. Chandan Mukherjee
Associate Professor
Department of Chemistry
Indian Institute of Technology Guwahati
Guwahati, 781039, Assam, India

Phone no. +91–361–258–2327(O)
Fax no. +91–361–258–2349
Email: cmukherjee@iitg.ernet.in

CERTIFICATE

This is to certify that the research work presented in this thesis entitled "***Synthesis, Characterization and Spectroscopic Studies of Transition Metal Complexes with Chalcogen (O, S, Se and Te) Bridged Non–innocent Ligands***" is an authentic record of the results obtained from the research work carried out by **Mr. Manas Kumar Mondal** (**Roll No. 126122004**) under my supervision in Department of Chemistry, Indian Institute of technology Guwahati, India. This work is original and has not been submitted elsewhere for a degree or award.

Place: IIT Guwahati
Date: 02/12/2016

Dr. Chandan Mukherjee
(Thesis Supervisor)

Acknowledgements

I would like to admit that the submission of the thesis would not be possible without the help of some well–wisher to me who extended their immense support, encouragement, and help during my research period. I would like to express my heartfelt thanks to all of them.

- *First of all, I express my deep sense of gratitude and appreciation to my supervisor* ***Dr. Chandan Mukherjee*** *who introduced me to the field of coordination chemistry of redox active non–innocent ligands. His constant guidance, professional inspiration and scientific knowledge discussions always acted as catalyst during my research work.*
- *I am highly obliged to* ***Prof. Gopal Das*** *(IIT Guwahati),* ***Prof. V. Manivannan*** *(IIT Guwahati) and* ***Dr. A. S. Achalkumar*** *(IIT Guwahati) for their valuable time to share my research knowledge.*
- *I am highly indebted to Department of Chemistry (IIT Guwahati), Department of Chemical Engineering (IIT Guwahati) and Central Instrumental Facility (IIT Guwahati) for the instrumental help during my research work.*
- *I am highly gratified to "****Indian Institute of Technology Guwahati****" for the doctoral fellowship.*
- *I am highly grateful to* ***Prof. Thorsten Glaser*** *(Universität Bielefeld) and* ***Dr. Archana Tiwari*** *(Sikkim University) for the measurement of SQUID.*
- *Thanks to* ***Dr. Biswajit Ganguly*** *(CSIR–Central Salt & Marine Chemical Research Institute) for TDDFT calculation.*
- *I obliged to* ***Prof. Tapan K. Paine*** *(IACS Kolkata) for the elemental analysis of my samples.*
- *Thanks to* ***Dr. Babulal Das****,* ***Mr. Imdadul Islam****,* ***Mr. Harsaraj Biswanath****, and* ***Mr. Kh. Kesho Singh*** *for their support at instrumental laboratory during the research work.*
- *I express my heartfelt thanks to my lab mates and some of my friends (****Dr. Samir Ghorai****,* ***Mr. Hemanta Deka, Mr. Prasenjit Barman****,* ***Mr. Utpal Nath****,* ***Mr. Suman Kalyan Das****,* ***Mr. Subhasish Jana****, Late* ***Ms. Richa Rakshit****,* ***Mrs. Bedika Phukan****,* ***Mr. Surajit Halder****,* ***Mr. Keshab Mondal****,* ***Mr. Ujjal Ghosh****,* ***Mr. Ganesh Chandra Paul****,* ***Ms. Mahmuda Khannam,*** *and* ***Mr. Prasenjit Sarkar****) for their well wises, heartfelt encouragement, and constant support during the research period at IIT Guwahati.*

❖ *Finally, I wish to express my heartiest gratitude to my father, mother, elder brother and younger sister for their constant inspiration, encouragement and inestimable affection towards me.*

Manas Kumar Mondal

Present Address

Room No. 008
Married Scholar Hostel
Indian Institute of Technology Guwahati
Guwahati–781039, Assam, India
Phone: +91 361 2583307

Permanent Address

Vill+Post: Mayurhat
P.S.: Hanskhali
Nadia–741502
West Bengal, India
Mobile: +91 8133917545

Email: manas.mondal@iitg.ernet.in
manasmondal17@gmail.com

Thesis Title:

"Synthesis, Characterization and Spectroscopic Studies of Transition Metal Complexes with Chalcogen (O, S, Se and Te) Bridged Non–innocent Ligands"

Date of Submission of Thesis:

02–12–2016

Education:

2014–till date	Senior Research Fellow at 'Department of Chemistry, IITG)
2012–2014	Junior Research Fellow at 'Department of Chemistry, IITG)
2012	**Master of Science** (in Chemistry) Indian Institute of Technology Guwahati Assam, India
2009	**Bachelor of Science** (Chemistry Hons.) Dinabandhu Andrews Collage, University of Calcutta West Bengal, India

Honors/Awards:

1. Qualified '**JAM 2010**' examination.

2. Qualified '**GATE–2011**' examination.

3. Qualified CSIR–UGC combined test for "National Eligibility Test for Lectureship (NET) and Junior Research Fellowship (JRF)–2012 (June)" under '**Lectureship'** scheme in Chemical Science.

4. Qualified CSIR–UGC combined test for "National Eligibility Test for Lectureship (NET) and Junior Research Fellowship (JRF)–2013 (December)" under '**UGC'** scheme in Chemical Science.

List of Conferences/Symposiums

1. "ChemConvene 2015" Department of Chemistry, Indian Institute of Technology Guwahati.

2. "18th CRSI National Symposium in Chemistry" 2016, Institute of Nano Science and Technology and Punjab University.

Published Papers:

(1) "Unprecedented Iminobenzosemiquinone and Iminobenzoquinone Coordinated Mononuclear Cu(II) Complex Formation under Air", **Manas Kumar Mondal**, Abul Kalam Biswas, Bishwajit Ganguly,* and Chandan Mukherjee*, ***Dalton Trans.***, 2015, **44**, 9375-9381. (Full Paper)

(2) "An Unprecedented One-Step Synthesis of Octahedral Cu(II)–Bis(iminoquinone) Complexes and their Reactivity with $NaBH_4$", **Manas Kumar Mondal**, and Chandan Mukherjee*, ***Dalton Trans.***, 2016, **45**, 13532. (Full Paper)

(3) "A Solid–State Valence Tautomeric Octahedral $\{Co^{II}[(BQ–N–Cat)]_2\}^0$ Complex Formation *via* Ligand-Centered Phenolic C–O Bond breaking and Co–O Bond making", **Manas Kumar Mondal**, Archana Tiwari and Chandan Mukherjee*. ***Chem. Commun.***, 2016, **52**, 11995. (Communication)

Doctoral Committee:

Prof. Gopal Das (Chairman)

Prof. V. Manivannan (member)

Dr. A. S. Achalkumar (member)

Dr. Chandan Mukherjee (supervisor)

Abstract

भारतीय प्रौद्योगिकी संस्थान गुवाहाटी
Indian Institute of Technology Guwahati

Chapter I

General Introduction and Motivation

Involvement of π–radical species mainly, tyrosyl radical in several metalloenzymes *e.g.* Galactose Oxidase, Catechol Oxidase, Photosystem I and Photosystem II, Cu–assisted organic cofactor formation in Amine Oxidases, Cytochrome c Oxidase, Cytochrome P450, Ribonucleotide Reductase have motivated chemists to develop bio-mimetic enzyme models using redox active non–innocent ligands. *o*–Aminophenol is a better choice of non–innocent ligand for synthesizing the mimicking model of metalloenzyme/s.

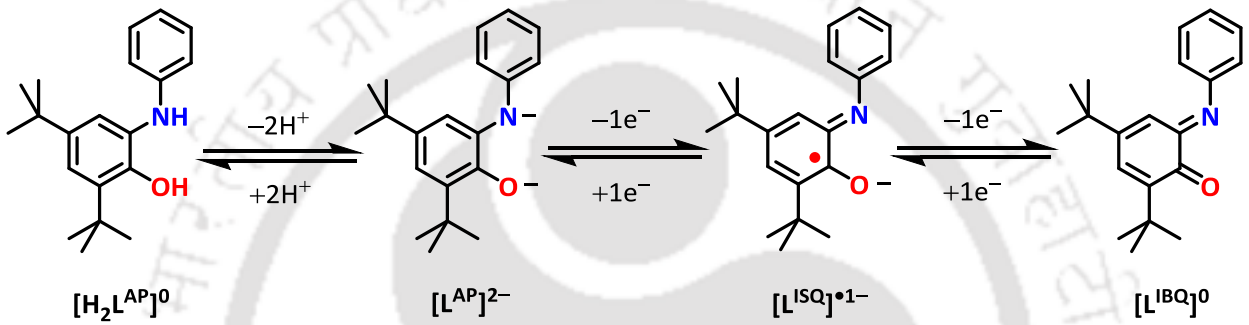

Scheme 1: *Various possible oxidation states of an o–aminophenol ligand (**H_2L^{AP}**).*

Apart from the utilization, structural and electronic importance as a mimicking model, metal complexes derived from such kind of non–innocent ligands are very much effective for catalytic C–C cross coupling reaction, $–CF_3$ group transferring agent, C–O/N/S bond activation, valence tautomeric species formation etc. Noteworthy, the redox reversibility of non–innocent ligand fragment enables it to behave as a reversible electron reservoir. Thus, the non–innocent ligands and their corresponding metal complexes show great potential to explode in the field of chemical, electronics and energy storage systems.

Chapter II

Synthesis and Characterization of Chalcogen–Bridged Non–Innocent Ligands and the Corresponding Cu(II) Complexes

A non–innocent ligand backbone consisted of two orthogonally placed aminophenol units was designed and synthesized by placing a common chalcogen (O, S, Se and Te) bridge between two $\mathbf{H_2L^{AP}}$ [N(2–hydroxy–3,5–di–*tert*–butyl phenyl) aniline] ligand units. The bridging atom

was attached at the *ortho*–position of the aniline ring and thus, a series of four potentially non–innocent ligands was developed.

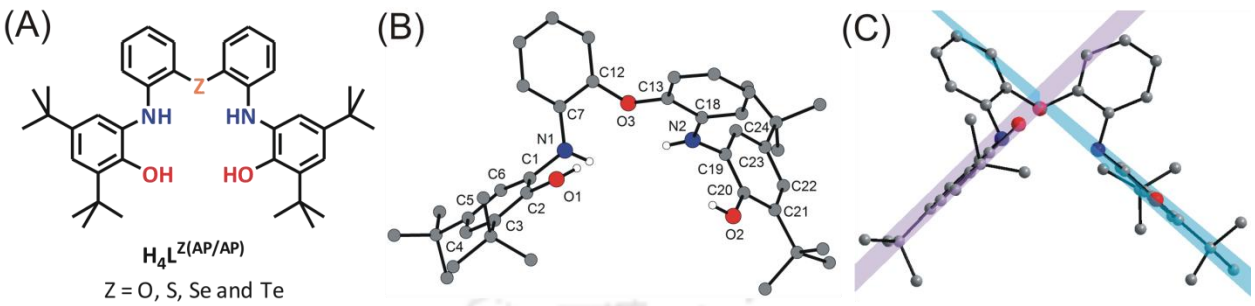

Figure 1: *(A) Schematic presentation of chalcogen bridged ligand* $\boldsymbol{H_4L^{Z(AP/AP)}}$*, where Z = O, S, Se and Te; (B) Crystal structure of ligand* $\boldsymbol{H_4L^{O(AP/AP)}}$*; (C) Perpendicular orientation of two aminophenol moieties in ligand* $\boldsymbol{H_4L^{O(AP/AP)}}$*.*

The presence of two orthogonally oriented aminophenol units within a single molecule of $\mathbf{H_4L^{Z(AP/AP)}}$ make the model attractive for the tuning of the electronic structure of corresponding Cu complexes by placing two radical units to the orthogonal position to each other.

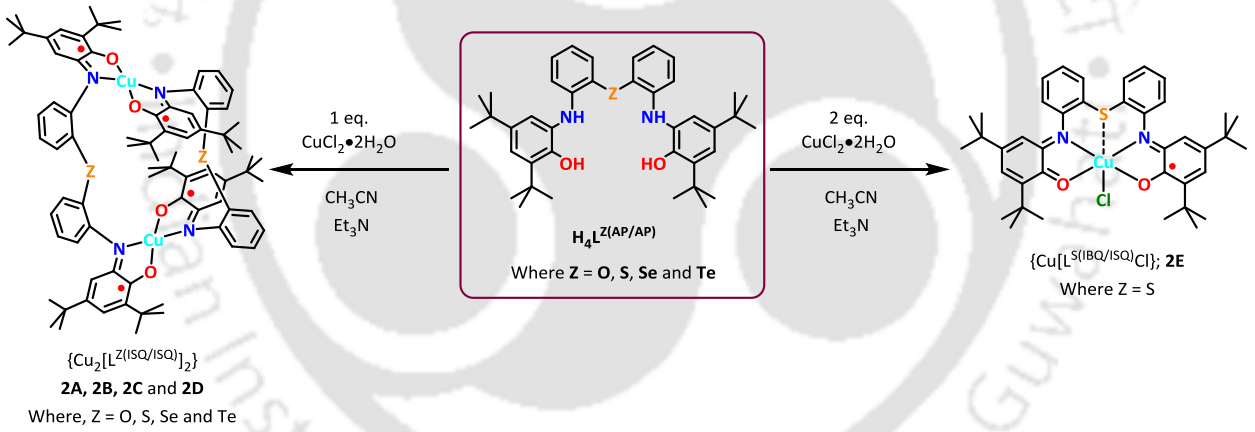

Scheme 2: *Schematic presentation of complexeation of chalcogen bridge ligand* $\boldsymbol{H_4L^{Z(AP/AP)}}$ *with* $CuCl_2•2H_2O$*.*

The equimolar reaction between ligand $\mathbf{H_4L^{Z(AP/AP)}}$ with $CuCl_2•2H_2O$ in the presence of Et_3N provided tetraradical–containing dinuclear Cu(II) complex, where each of the two Cu(II)–ions were situated at the center of a square planar environment made up by two iminosemiquinone $[(ISQ)^{\bullet 1-}]$ units (Scheme 2; $\mathbf{\{Cu_2[L^{Z(ISQ/ISQ)}]_2\}}$). By changing the metal ion concentration, an octahedral mononuclear Cu(II) complex (**2E**) was developed from ligand $\mathbf{H_4L^{S(AP/AP)}}$. In the novel complex (**2E**), one of the two coordinated amidophenolate units was present in its two electron oxidized iminoquinone $\{[IBQ]^0\}$ form and other was in its one–electron oxidized iminosemiquinone $\{[ISQ]^{\bullet 1-}\}$ form. The formation of complex **2E** was

proceeded through the initial generation of tetraradical–containing dinuclear Cu(II) complex (**2B**), which underwent oxidation by $CuCl_2$•$2H_2O$ and Et_3N as well as air.

Chapter III

Synthesis and Characterization of Co Complexes from Chalcogen Bridged Non–Innocent Ligands

The orthogonally placed two aminophenol units within a single molecule is an authentic demand for non–innocent ligand assisted C–C cross–coupling, valence tautomeric complex formation and C–O/S/Se bond activation. On this perspective issues, ligand $\mathbf{H_4L^{Z(AP/AP)}}$ become a novel model to synthesize corresponding Co complexes.

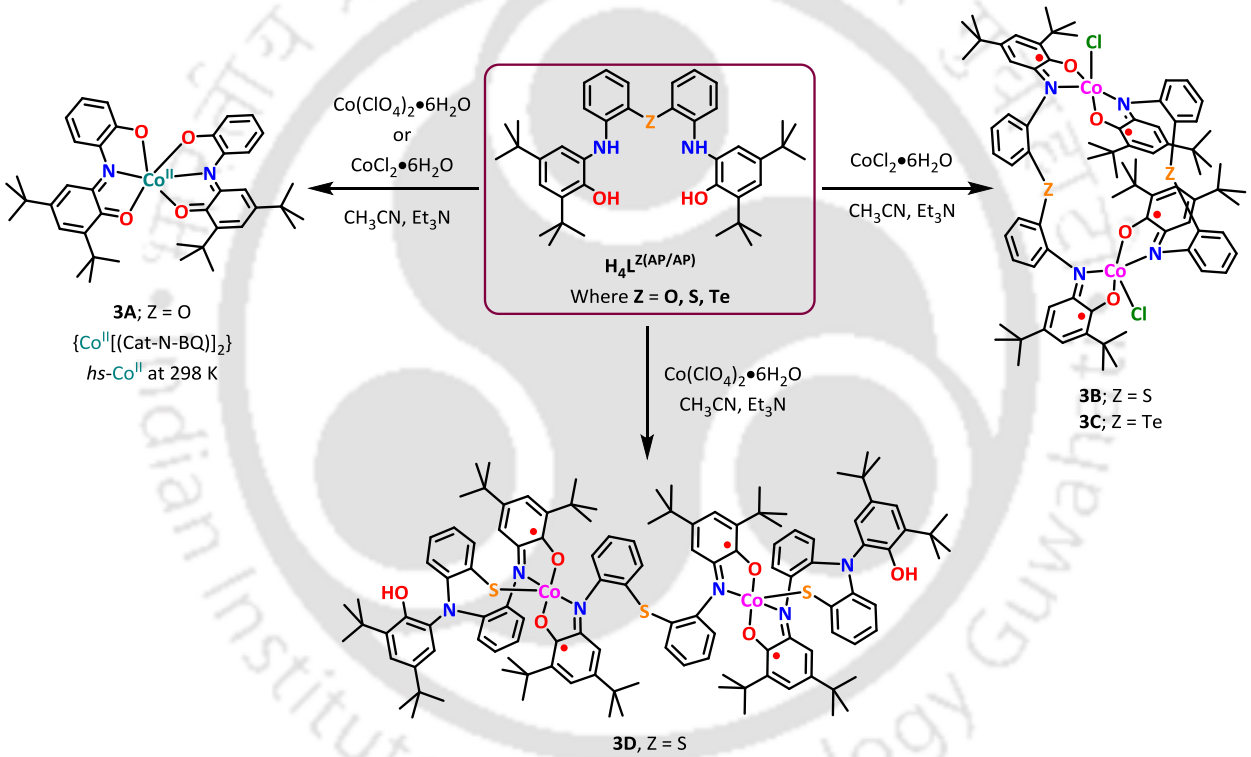

Scheme 3: *Chalcogen bridge ligand* $\boldsymbol{H_4L^{Z(AP/AP)}}$ *(Z = O, S, and Te) and its reactivity toward Co–salts.*

The O−bridge ligand $\mathbf{H_4L^{O(AP/AP)}}$ provided a mononuclear octahedral cobalt complex **3A** by two set of successive homolytic C_{aryl}–O_{bridge} bond breaking and homolytic Co–O_{bridge} bond making. Complex **3A** has shown solvent and solid phase thermal tautomeric conversion, where the solid phase tautomeric conversion depended upon the availability of the lattice solvent molecules within the crystalline matrix. The S and Te bridge ligand provided tetraradical–containing dinuclear Co(III) complexes (**3B** and **3C**) on treatment with $CoCl_2$•$6H_2O$. On changing the counter anion, *i.e.*, the lack of chloride ion, caused an activation of C–S bond and provided complex **3D** from ligand $\mathbf{H_4L^{S(AP/AP)}}$.

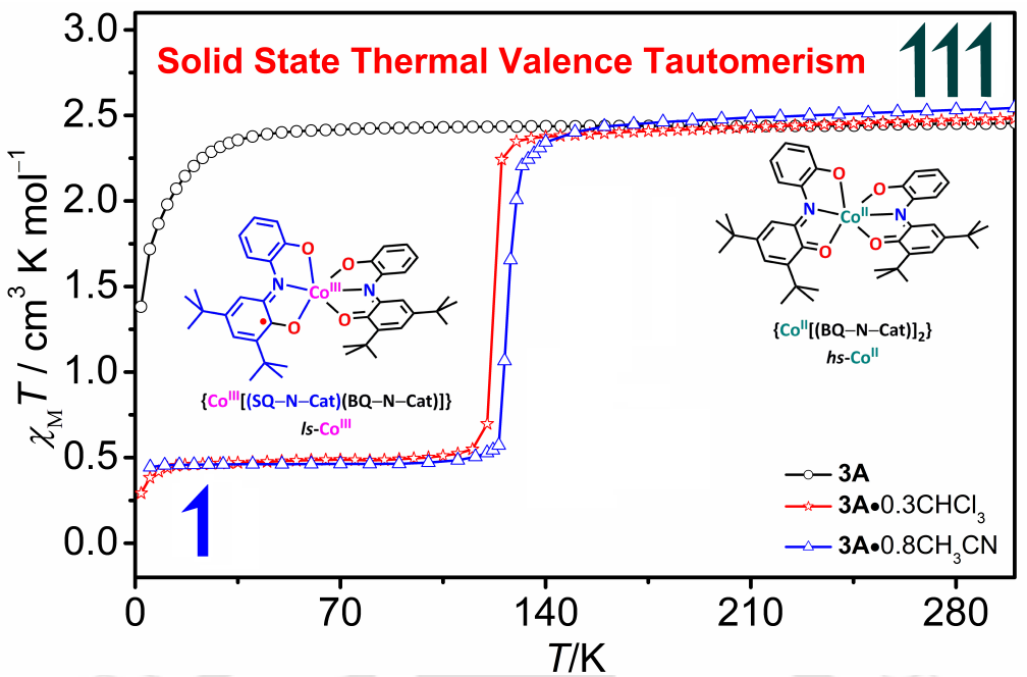

Figure 2: *$\chi_M T$ vs. T plots of complex **3A** (in solid state) crystalized from different solvent systems.*

Chapter IV

Synthesis and Characterization of a Distal–NO_2 group Appended Aminophenol–Based Ligand and its Corresponding First–Row Transition Metal Complexes

A distal –NO_2 group–appended aminophenol–based ligand $\mathbf{H_2L^{AP(o\text{–}NO_2\text{–}OPh)}}$ was designed and synthesized to generate iminosemiquinone [$(ISQ)^{\bullet 1-}$] and/ iminoquinone [$(IBQ)^0$]–coordinated metal complexes. The electron withdrawing –NO_2 group was appended within the ligand backbone for: (I) tuning the electronic structure of corresponding metal complex, (II) attach the organic fragment to some solid support and (III) for further modification of the ligand skeleton.

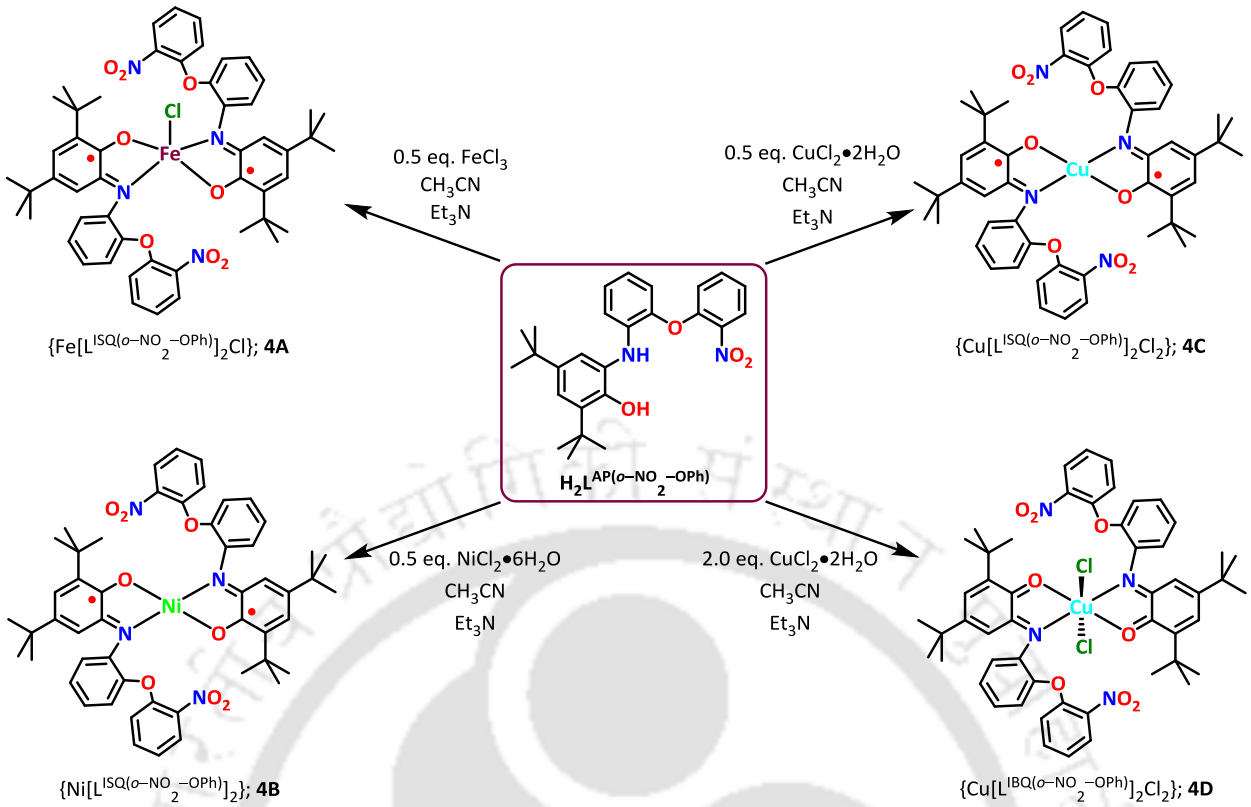

Scheme 4: *Ligand* $\boldsymbol{H_2L^{AP(o–NO_2–OPh)}}$ *and the corresponding Fe, Ni and Cu complexes.*

The ligand $\mathbf{H_2L^{AP(o–NO_2–OPh)}}$ behaved as a non–innocent bidentate one and generated bis(iminosemiquinone)M (M = Fe, Ni and Cu) complexes on reacting with the corresponding metal–chloride salt. In complex **4A**, the unpaired spins of *hs*–Fe(III)–center and coordinated radical anions underwent antiferromagnetic coupling and resulted an S_t = 3/2 spin state as the ground state.

The non–innocent ligand fragment can also able to exist as its zero oxidation state (iminoquinone), which was rarely abundant. An efficient one–step method for the generation of Cu(II)–bis(iminoquinone) complex using amidophenolate based non–innocent ligands with 2 equivalents of $CuCl_2•2H_2O$ in the presence of Et_3N and air has been established. The electrophilicity of the iminoquinone complex has been utilized to generate H_2 gas from a source hydride ion ($NaBH_4$) in anhydrous acetonitrile.

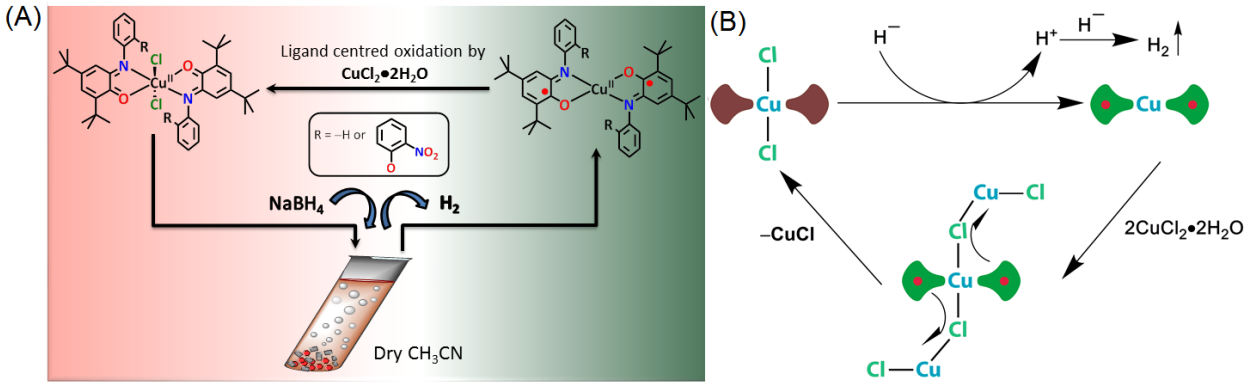

Figure 3: *Cu(II)–bis(iminoquinone) assisted H_2 production from $NaBH_4$ and the regeneration of quinone complex.*

Chapter V

A Hemilabile –NH_2 Group Appended Aminophenol–Based Bidentate Non–Innocent Ligand: Synthesis, Characterization and Corresponding Radical–Containing Transition Metal Complexes

The extent of structural distortion due to secondary coordination left the resultant unpaired spin to the ligand site in Cu(II)–bis(iminosemiquinone) complexes. A hemilabile –NH_2 group appended aminophenol based ligand $\mathbf{H_2L^{AP(o\text{–}NH_2\text{–}OPh)}}$ was designed and synthesized to generate corresponding Co, Ni and Cu complexes.

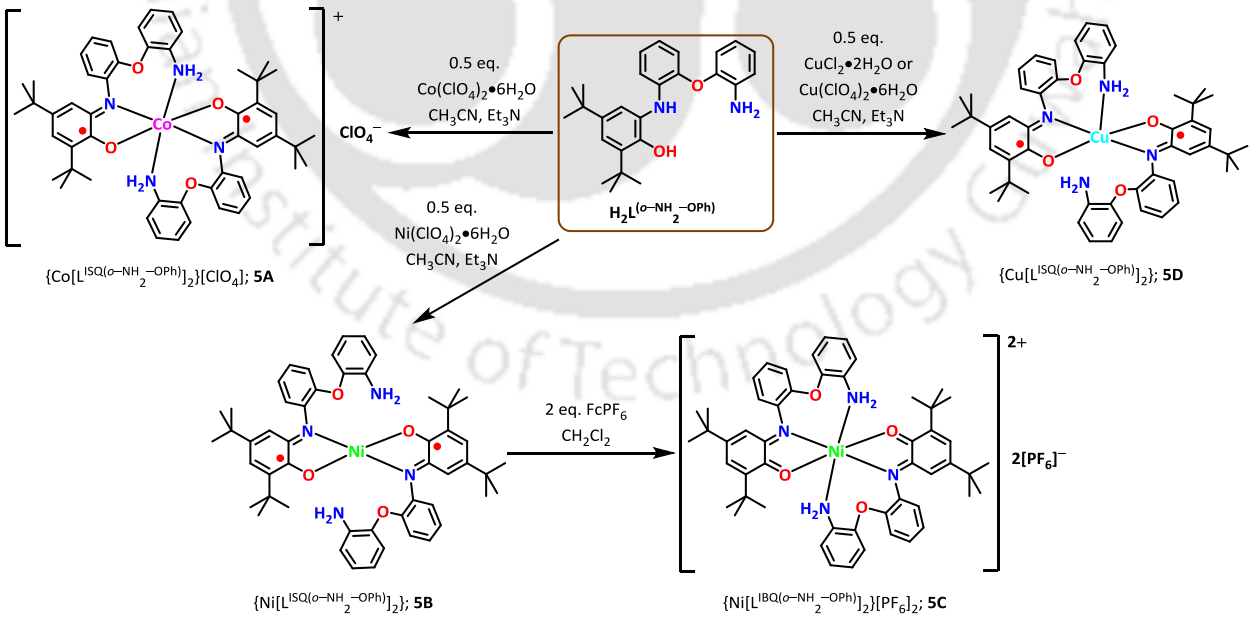

Scheme 5: *Ligand $\boldsymbol{H_2L^{AP(o\text{–}NH_2\text{–}OPh)}}$ and the corresponding Co, Ni and Cu complexes.*

The ligand provided bis(iminosemiquinone)–coordinated metal (Co, Ni and Cu) complexes. The diradical–containing Ni complex **5B** underwent ligand centered oxidations on

treatment with 2 eq. ferrocenium hexafluorophosphate ($FcPF_6$). The oxidation led an elongation of Ni–L bond lengths (along amidophenolate sites), which facilitated the axial approach of aryl amines toward the metal ion (**5C**). In complex **5D**, an aryl–NH_2 coordination through axial direction caused 16.1(1)° dihedral angle in between the two ligating iminosemiquinone radical anion [$(ISQ)^{\bullet 1-}$] planes. Simulation to the experimental variable tempetature magnetic susceptibility data revelaed that the square pyramidal complex (**5D**) having two energitically close (1/2, 1) and (1/2, 0) spin states (Figure 4B).

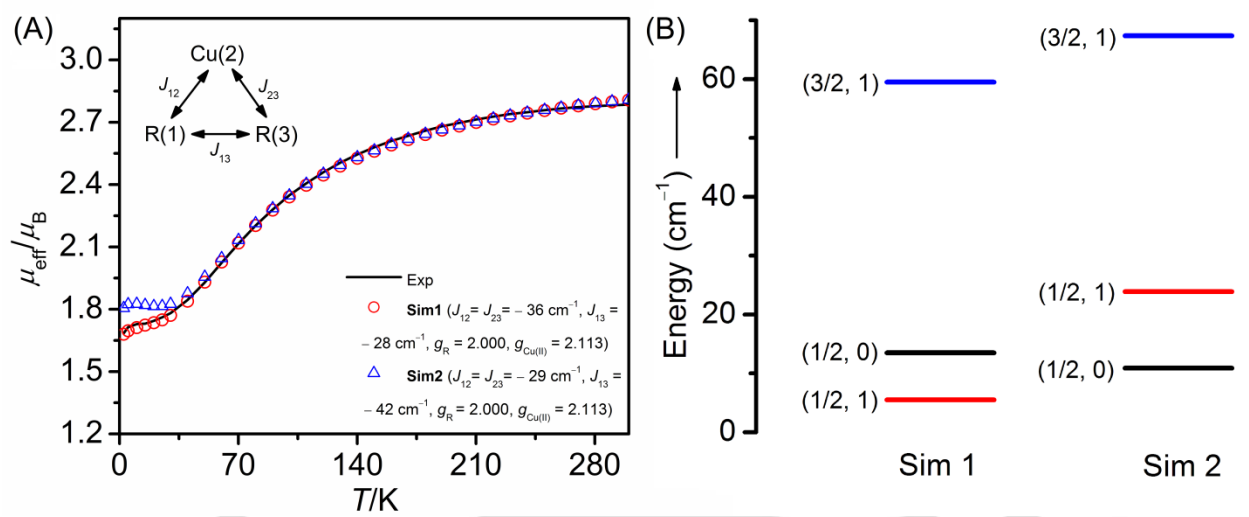

Figure 4: *(A) Experimental and simulated μ_{eff} vs. T plot for complex **5D**; (B) Calculated energy level based on resultant simulated values.*

CONTENTS

Chapter IV

Synthesis and Characterization of a Distal–NO_2 group Appended Aminophenol–Based Ligand and its Corresponding First–Row Transition Metal Complexes

Chapter V

A Hemilabile –NH_2 Group Appended Aminophenol–Based Bidentate Non–Innocent Ligand: Synthesis and Characterization of its Corresponding Radical–Containing Transition Metal Complexes

Chapter VI

Equipment and Experimental Section

Appendices

ABBREVIATIONS

Technical terms:

av. : average
B : magnetic field
LMCT : ligand–to–metal charge transfer
MLCT : metal–to–ligand charge transfer
LLCT : ligand–to–ligand charge transfer
IET : intramolecular electron transfer
SET : single electron transfer
D : zero–field splitting
deg. : degree (°)
e^-: electron
E : total energy
Exp : experimental
Sim : simulated
H : Hamiltonian
J : coupling constant (cm^{-1}) /or Hz
hs : high spin
ls : low spin
I : nuclear spin
HOMO : highest occupied molecular orbital
LUMO : lowest unoccupied molecular orbital
m/z : mass per charge
RT : room temperature (30 ℃)
S : electron spin
s : singlet
d : doublet
t : triplet
q : quartet

Units:

Å : angstrom (10^{-10} m)
cm : centimetre
emu : electromagnetic unit
G : gauss
h : hour
K : Kelvin
M : molar
m / min. : minute
mm : millimeter
nm : nanometer (10^{-9} m)
s : second
T : tesla
μ_B : bohr magnetron
B : magnetic field
° : degree

Symbols:

λ : wavelength (nm)
ε : extinction coefficient ($M^{-1}cm^{-1}$)
μ_{eff} : magnetic moment (μ_B)
δ : Isomer shift
× : multiplication

Solvents and reagents:

TBAP : tetrabutylammonium perchlorate
Cat : catechol
SQ : semiquinone
ISQ : iminosemiquinone
IBQ : iminoquinone
CH_2Cl_2 : dichloromethane
$CHCl_3$: chloroform
Et_2O : diethylether
Et_3N : triethylamine
EtOAc : ethylacetate
$Et_4N^+Cl^-$: tetraethylammonium chloride
EtOH : ethanol
KBr : potassium bromide
MeOH : methanol

THF : tetrahydrofuran

CH_3CN : acetonitrile

Techniques:

EA : elemental analysis
EI : electron ionisation
EPR : electron paramagnetic resonance
NMR : nuclear magnetic resonance
SQUID : superconducting quantum interface device

ESI : electrospray ionisation
IR : infrared
MS: mass spectrometry
UV–vis/NIR : ultraviolet–visible/near infrared

Latin expressions:

ca. : around
et al. : and co−workers
e.g. : for example
i.e. : namely

tert : tertiary
vs. : versus, against
via : through
vide infra : see below

Chapter I

General Introduction, Motivation, and Objectives

1.1: General Introduction, Motivation and Objectives

In bioinorganic chemistry, the role of metal ions and the interaction of metal ion(s) with the surrounding organic ligands in various biological processes are studied. Metal ion–containing enzymes are known as metalloenzymes. It has been found that in most of the metalloenzymes the active site, where the enzymatic reactivity occurs, are the metal centers. Widespread occurrence and involvement of amino acid radicals, mainly tyrosine radical, in metalloenzymatic catalysis, for example; Galactose Oxidase,[1] Catechol Oxidase,[2] Photosystem I and Photosystem II,[3] Cu–assisted organic cofactor formation in Amine Oxidases,[4] Cytochrome c Oxidase,[5] Cytochrome P450,[6] Ribonucleotide Reductase,[7] etc, have motivated chemists and biologists to the synthesis of radical–containing transition metal complexes.

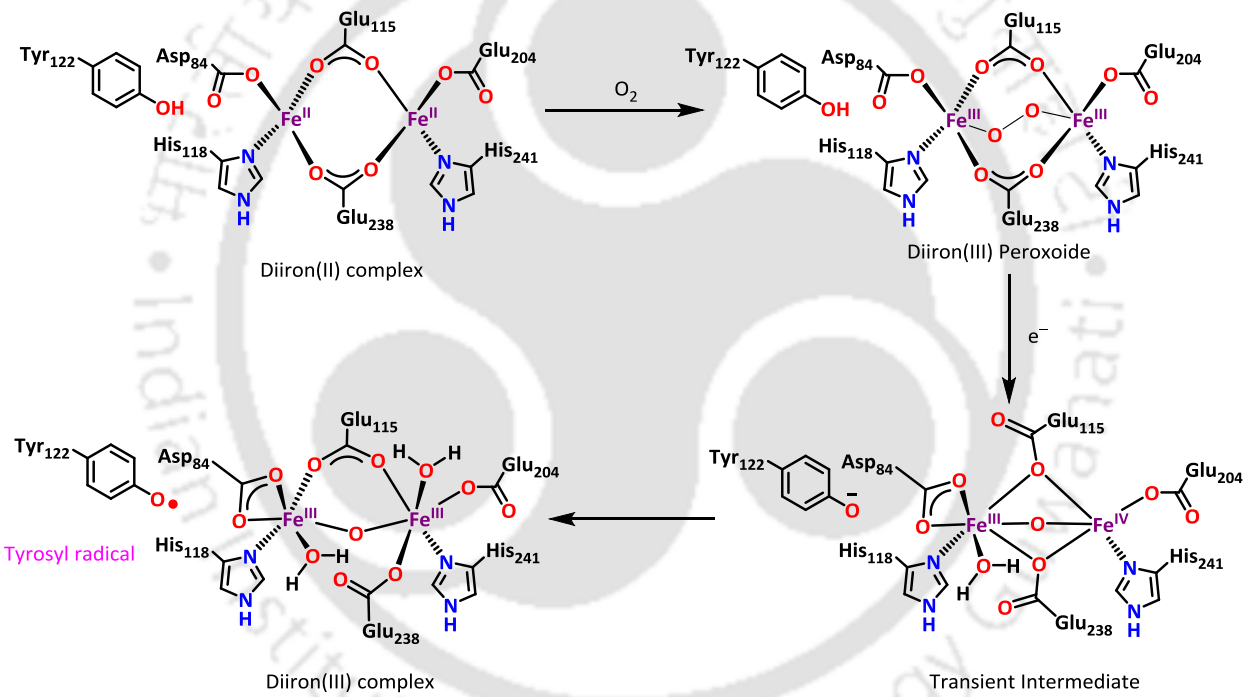

Scheme 1.1: *Generation of tyrosyl radical in ribonucleotide reductase.*[7g]

In 1972, A. Ehrenberg and P. Reichard have shown the existence of tyrosyl radical in R2 subunit of ribonucleotide reductase, a non–heme metalloprotein.[7a] The enzyme catalyze the conversion of a ribonucleosides to deoxyribonucleosides in all organism and thus, it serves in the essential step of DNA replication and repair. The redox states of both the metal ions as well as the tyrosyl radical cooperatively play the crucial role during the conversion.

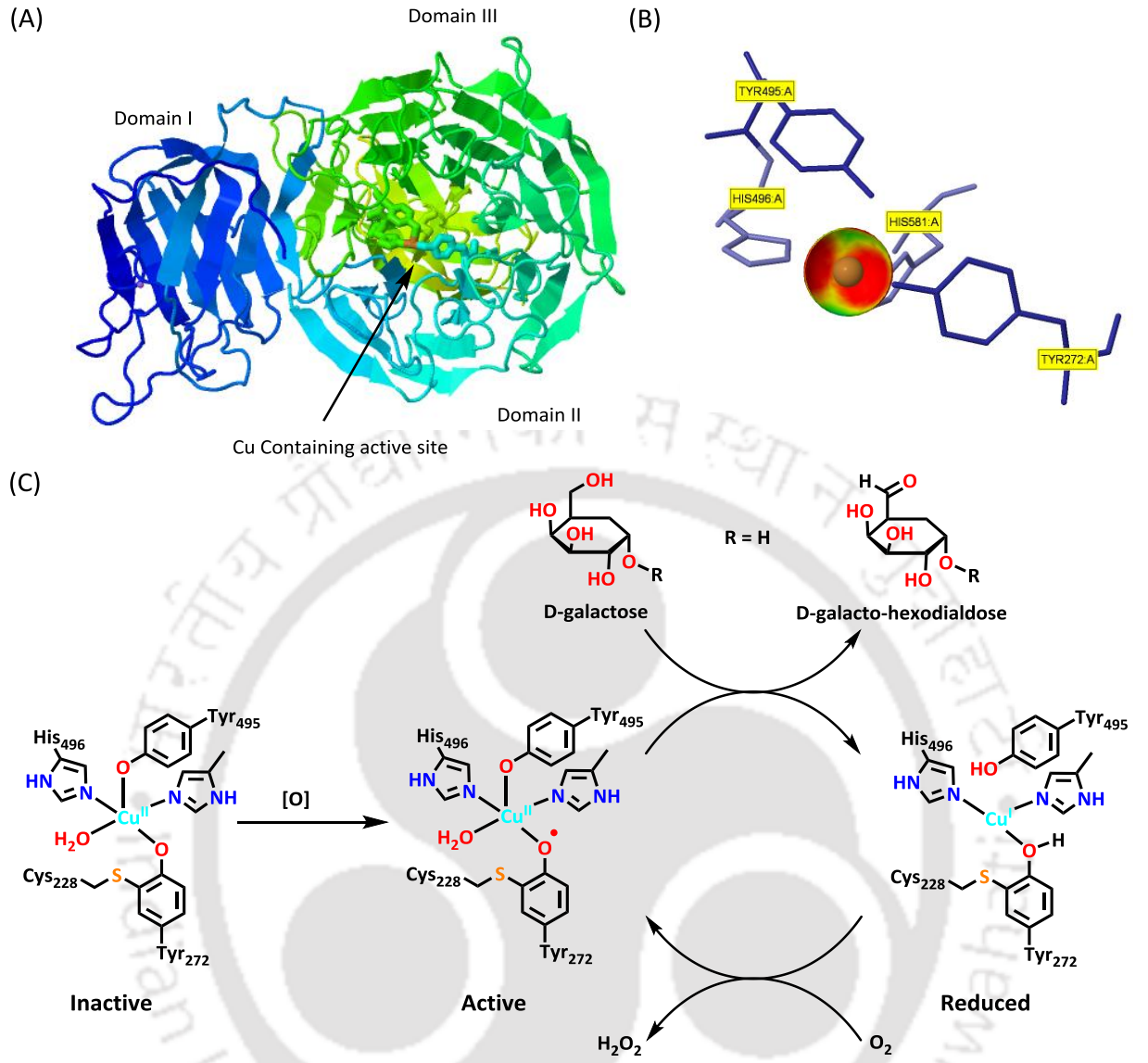

Scheme 1.2: *(A) Structural representation of Galactose Oxidase*[1a] *with specification of domains and Cu containing active site; (B) Cu pocket interaction in the active site and (C) Reaction profile of the active site during the catalytic oxidation of D–galactose.*

Galactose Oxidase (GO) is a fungal mononuclear Cu–containing polypeptide chain consisting of 639 amino acids with a molecular weight 68 kDa.[1] The enzyme has three domains and the Cu–containing active site is located at domain II. In the active site, Cu(II)–ion is firmly coordinated with two histidines (His496, His581), two tyrosines (Tyr272, Tyr495) and a solvent (H_2O) molecule. Tyr272 has a thioether coordination with Cys228 and during the catalytic oxidation of D–galactose to corresponding aldehyde, it acts as a cofactor.[1] During the catalytic oxidation process, both of the Cu(II)–ion and tyrosyl radical motif accept one–electron each. To note, the structural simplicity and catalytic efficiency inspired chemists to synthesize the mimicking model of Galactose Oxidase.

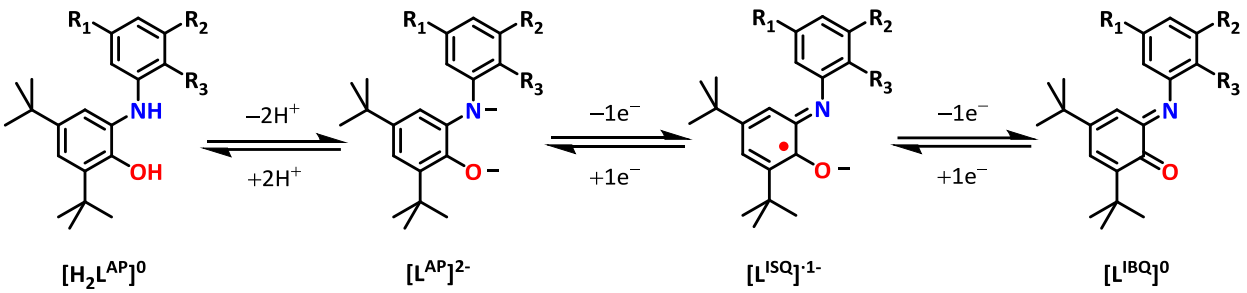

Where R_1, R_2, R_3 = H; R_1, R_2= H and R_3 = OMe, SMe, SePh; R_1, R_2= ^{t}Bu and R_3 = OH; R_1= Cl, R_2= H and R_3 = OH

Scheme 1.3: *Probable oxidation states of substituted* $\boldsymbol{H_2L^{AP}}$.

The aminophenol based non–innocent ligand $\mathbf{H_2L^{AP}}$ [N(2–hydroxy–3,5–di–*tert*–butyl phenyl) aniline] is a basic constituent of several radical–containing transition metal complexes.[8a] Several substituted ligands and their corresponded metal complexes are developed. Depending upon the reacting metal salt and the reaction condition, the metal coordinated amidophenolate moieties in the complex can be existed in its 2– and/or 1– and/or 0 oxidation states (Scheme 1.3).[8] It is reported that such kind of non–innocent ligands provide radical–containing transition metal (Mn, Fe, Co, Ni, Pd, V, Cr, Cu, etc) complexes under air.[8,9,10] Thus obtained metal complexes have got a considerable attention due to its versatile applications (*e.g.* mimic enzymatic reaction,[8c–d,10] catalytic C–C coupling reaction,[8d–e] –CF_3 group transferring agent,[8f] C–N bond formation reaction[8g] etc).

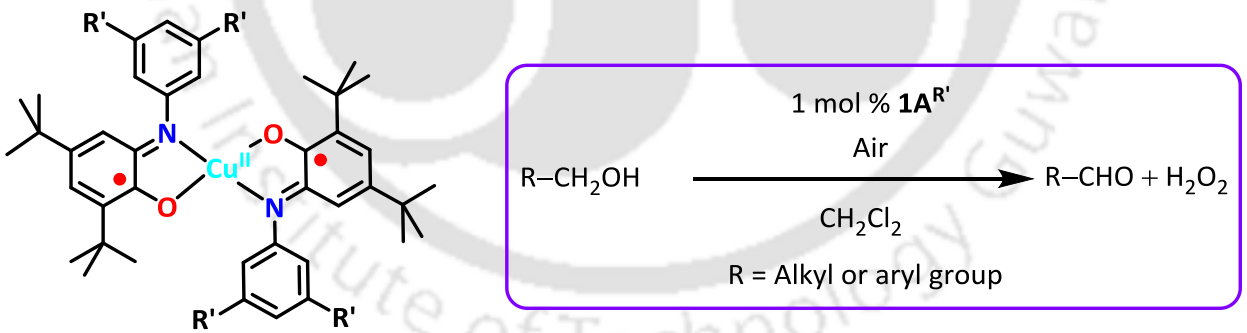

$\mathbf{1A^{R'}}$;Where R' = –CF_3, –Cl, –OCH_3, –^{t}Bu, –H

Scheme 1.4: *Mimicking model of Galactose Oxidase derived from aminophenol based ligand.*[8c]

A series of Cu–containing diradical Cu(II)–bis(iminosemiquinone) complex derived from substituted $\mathbf{H_2L^{AP}}$ ligands are effective for catalytic alcohol oxidation *i.e.* mimic the function of Galactose Oxidase (Scheme 1.4).[11] The oxidation procedure is facilitated by redox activity of the non–innocent ligand fragment, whereas *α*–H abstraction is the rate determining step. The

catalytic activity of Cu(II)–bis(iminosemiquinone) complex is invigorated by the electron withdrawing substituents at aniline ring of the ligand fragment *i.e.* by complex $\mathbf{1A^{CF_3}}$.[11]

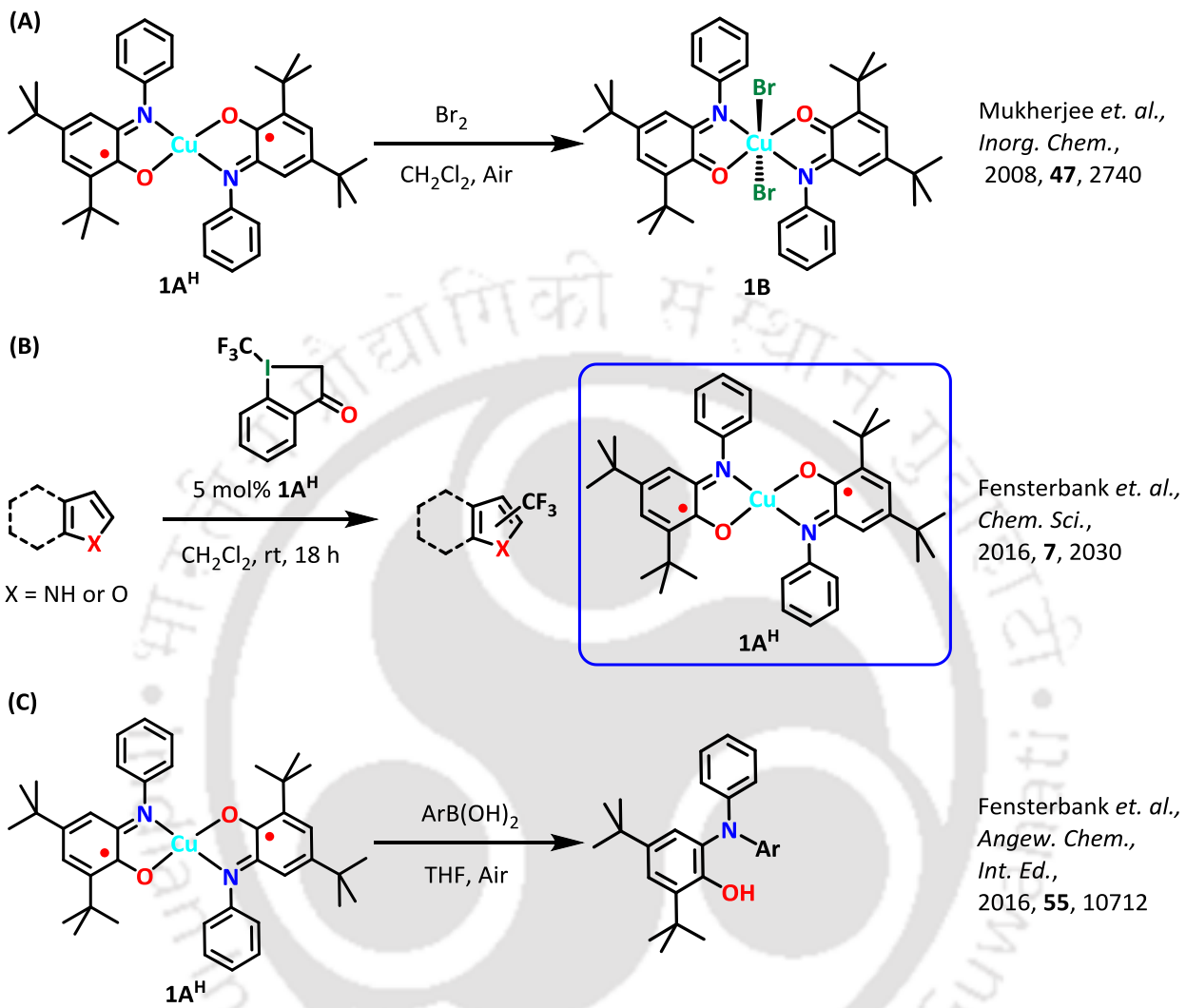

Scheme 1.5: *Utilizations of Cu(II)–bis(iminosemiquinone) complex; (A) generation of Cu(II)–bis(iminoquinone) complex,(B) –CF_3 group transfer reaction and (C) C–N bond forming reaction.*

The ligand centered oxidation of Cu(II)–bis(iminosemiquinone) complex [$\mathbf{1A^H}$] by using molecular bromine provides an octahedral Cu(II)–complex [**1B**] (Scheme 1.5A) where each of the coordinated ligands are in fully oxidized iminoquinone form and the charge of the metal ion are compensated by two axially coordinated bromide ions.[8c] Recently, Fensterbank *et. al.* reported the generation of $CF_3^{\bullet}$ radical from a source CF_3^{+} by utilising the Cu(II)–bis(iminosemiquinone) complex [$\mathbf{1A^H}$].[8f] One–electron reduction of CF_3^{+}–ion is assisted by the ligand centered single electron transfer (SET) of complex $\mathbf{1A^H}$. Thus obtained $CF_3^{\bullet}$ radical can be utilized in trifluoromethylation of heteroaromatics (Scheme 5.B), trifluoromethylation of silyl enol ethers and hydrotrifluoromethylation of alkynes.[8f] Another application of Cu(II)–

bis(iminosemiquinone) complex (**1A^{H}**) has been recently reported by Fensterbank *et. al.* where C–N bond forming reaction occurs under air (Scheme 1.5C).[8g]

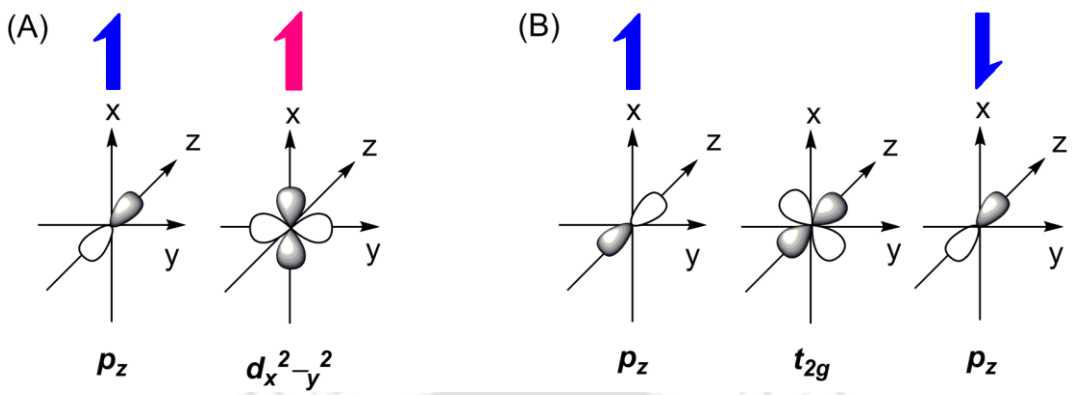

Scheme 1.6: *Spin interaction in (A) between two orthogonal metal and radical spin orbitals and (B) Cu(II) mediated antiferromagnetic coupling between two radical spins of the square planar Cu(II)–bis(iminosemiquinone) complex.*

In addition to understanding the catalytic reactivity of the radical–containing metal complexes, details study of metal ion(s)–radical(s) interactions have got considerable attention. In this context, the study of the origin of paramagnetic nature of three spins–containing four–coordinate diradical Cu(II)–bis(iminosemiquinone) complexes have achieved special interest. In the complexes, an electronic spin frustrating situation is developed by the antiferromagnetic interaction between two amongst the three spins. In the square planar coordination sphere, spin containing ligand and metal orbitals are orthogonally orientated. According to Goodenough–Kanamori rule,[13] such orientation facilitates ferromagnetic coupling between the radical center and metal center spins (Scheme 1.6A). At this situation, two radical spins undergo antiferromagnetic coupling through metal centered t_{2g} orbital and resulting Cu(II)–site doublet ground state (Scheme 1.6B).

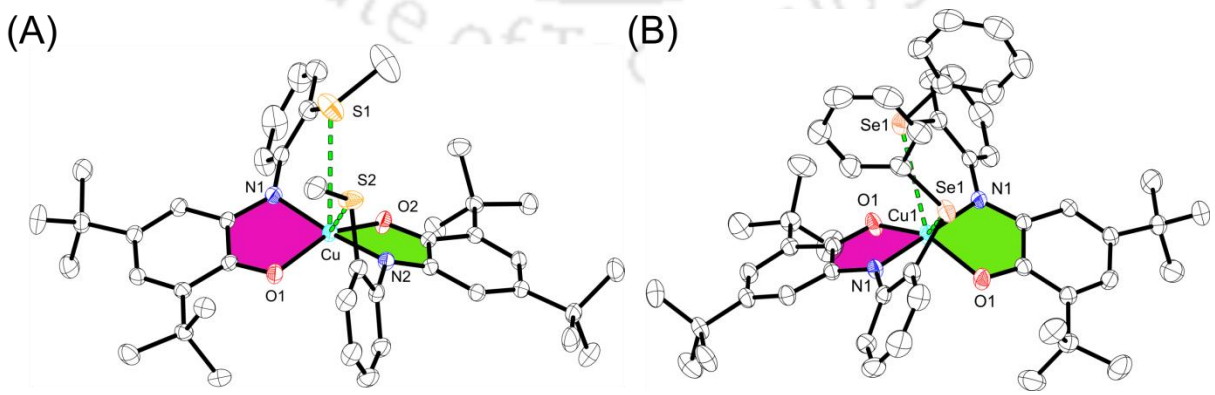

Figure 1: *(A) Complex **1C**, {Cu[L$^{ISQ(S–Me)}$]$_2$} and (B) complex **1D**, {Cu[L$^{ISQ(Se–Ph)}$]$_2$} represented with the secondary coordination (green dashed line), which caused the distortion in the ligating plane by 32.2 and 36.6 °, respectively.*[13]

Secondary coordination from soft coordinating site to the metal–center at Cu(II)–bis(iminosemiquinone) complexes caused an alteration of ground state electronic configuration. In 2005, Kaim *et al.* reported a soft coordination caused a bent angle 32.2° between two ligating iminosemiquinone units.[13*a*] Another example with axial secondary interaction was reported by Mukherjee *et al.* where Cu(II)–coordinated two iminosemiquinone units having a twist angle equal to 36.6°.[13*b*] The axial secondary interaction led to a distortion around the metal ion and thus, the spin containing ligand (p_z) and Cu(II) orbital ($d_{x^2-y^2}$) became non–orthogonal. This situation predominantly facilitated the metal–radical antiferromagnetic interaction over radical–radical interaction and the resultant unpaired electron located on the ligand site.

It has been realized that the introduction of soft hemilabile entities (–SMe, –SePh) at the close proximity to the metal ion (Cu^{II}) provide ligand site doublet ground state.[13] The twist and/or bent angle between two ligating iminosemiquinone [$(ISQ)^{\bullet 1-}$] radical units facilitate higher extent of antiferromagnetic coupling between ligand and metal site spins compared to two radical spins and resulting unpaired electron is located on ligand site. Those reported observations interpret the electronic structure of such kind of complexes and leave an implication regarding tuning parameter of radical–containing metal complexes. Thus, a detail study and finding of actual fact, *i.e*. twist angle *vs*. bent angle seeks special attention and development of new non–innocent ligands. Thus, ligands $\mathbf{H_4L^{Z(AP/AP)}}$ [where Z = O, S, Se and Te] and $\mathbf{H_2L^{AP(}}$*o*$\mathbf{–NH_2–OPh)}$ (*vide infra*) [Scheme 1.10] are synthesized and the corresponding Cu(II)–complexes have been studied for the understanding of metal–radical interactions. In case of ligand $\mathbf{H_2L^{AP(}}$*o*$\mathbf{–NH_2–OPh)}$, it was expected that the $–NH_2$ group will coordinate to the Cu(II)–center and will lift the Cu(II) ion above the basal plane and generate distortion around the metal center. Thus, the distortion effect in coupling–fashion can be further studied.

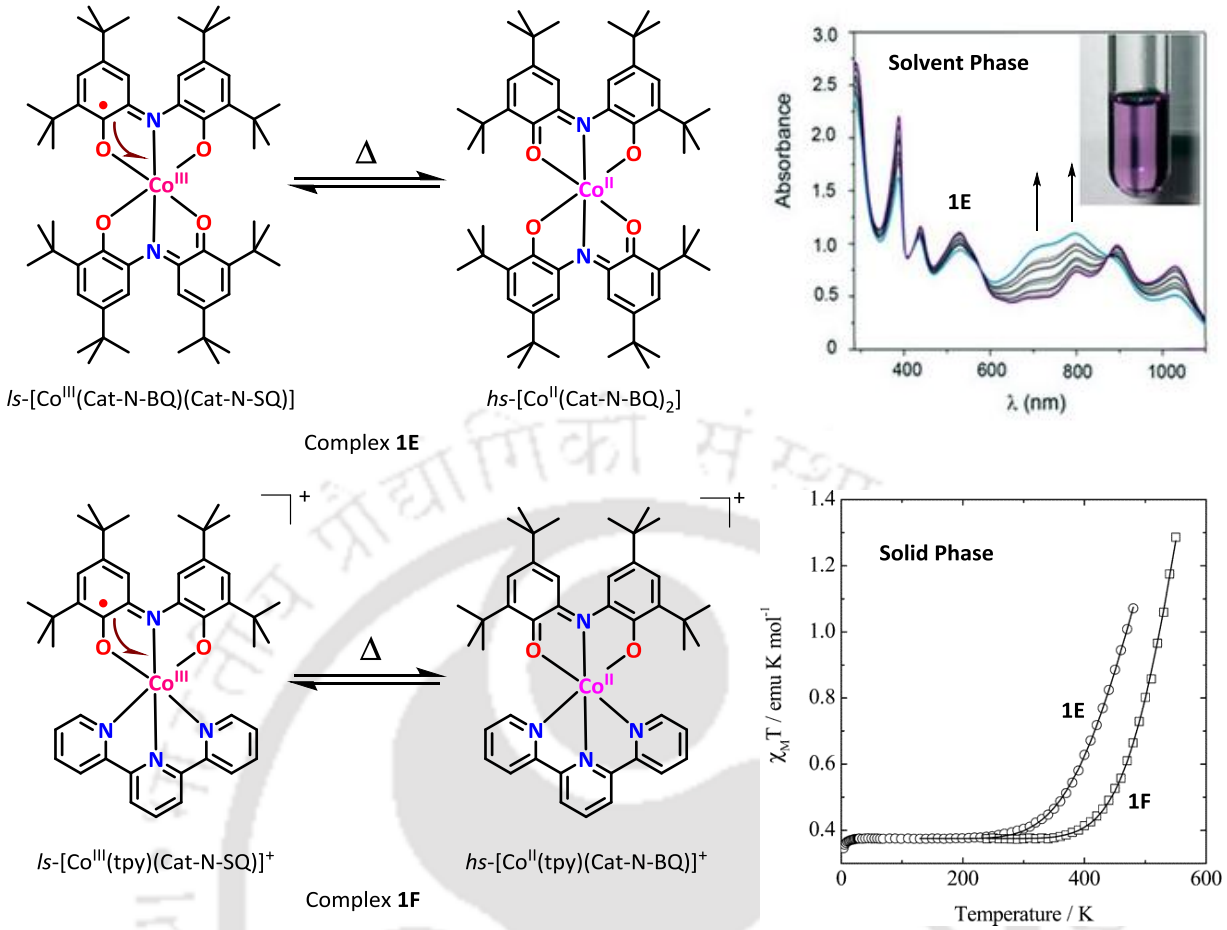

Scheme 1.7: *Thermal tautomeric conversion of complex **1E** and **1F**; solvent and solid phase valence tautomerism.*[14b,c]

The cobalt complexes derived from amidophenolate based non–innocent ligands have versatile utility in homogeneous catalysis,[8e] molecular level switching material,[14] magnetic materials[14] etc. The flexibility in several redox states of the amidophenolate moieties facilitated the activity of those Co–complexes. The ligand fragment can be used as electron reservoir and the intramolecular electron transfer from the ligand site to the Co ion or *vice versa* leads to a valence tautomeric conversion (Scheme 1.7).[14] Such kind of valence tautomerism is driven by several external stimuli, like temperature, pressure, electric field and light. So those complexes can be utilized as molecular based switches.

The thermal driven intramolecular electron transfer (IET) leads to the transformation of the complex **1E** from its *ls*–Co(III) form to *hs*–Co(II) form in solution.[14b,c] The temperature dependent electronic absorption spectra as well as solution phase magnetic moment measurement employing Evan's method were supportive for such kind of tautomeric conversion. The absorption spectra supports the increment of *hs*–Co(II) concentration with increase in temperature (Scheme 1.7). The complex **1F** is another similar kind of six–coordinate Co–

complex. It is reported both the complexes show valence tautomeric conversion in solid phase (Scheme 1.7).[14c] Thus, the non–innocent ligand coordinated paramagnetic Co–complexes are very much effective for the generation and development of electronic devices.

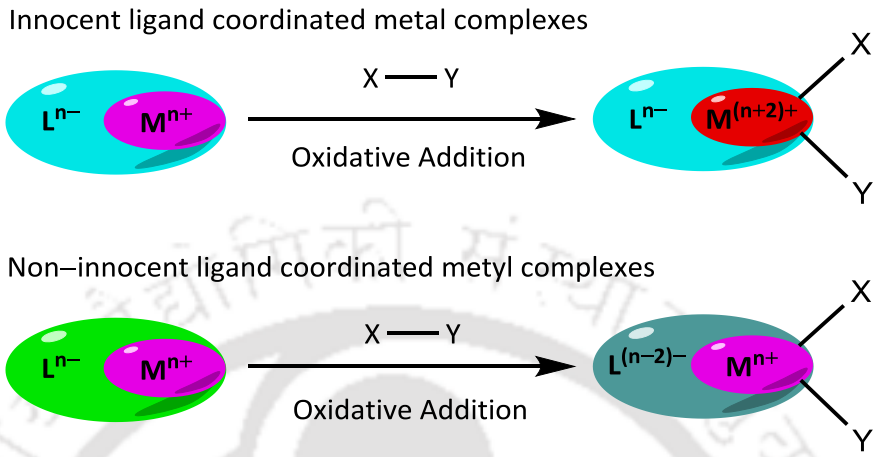

Scheme 1.8: *Schematic presentation of oxidative addition to innocent and non–innocent ligand coordinated metal complexes.*

Group 10 metal (mainly, Ni and Pd) are widely used for C–C cross coupling reaction as their easily feasible redox couple (M^{2+}/M) facilitates the preliminary oxidative addition. The required transfer of two electrons during the oxidative addition comes from the metal ion. However, for metal like cobalt is less conspicuous choice for such kind of reaction. The coordination of non–innocent ligand fragment with Co–ion could capable the molecular entity to participate in cross coupling reaction. The metal ion and the redox active ligand fragments are corporately interacted with the substrate during the catalytic C–C coupling reaction.

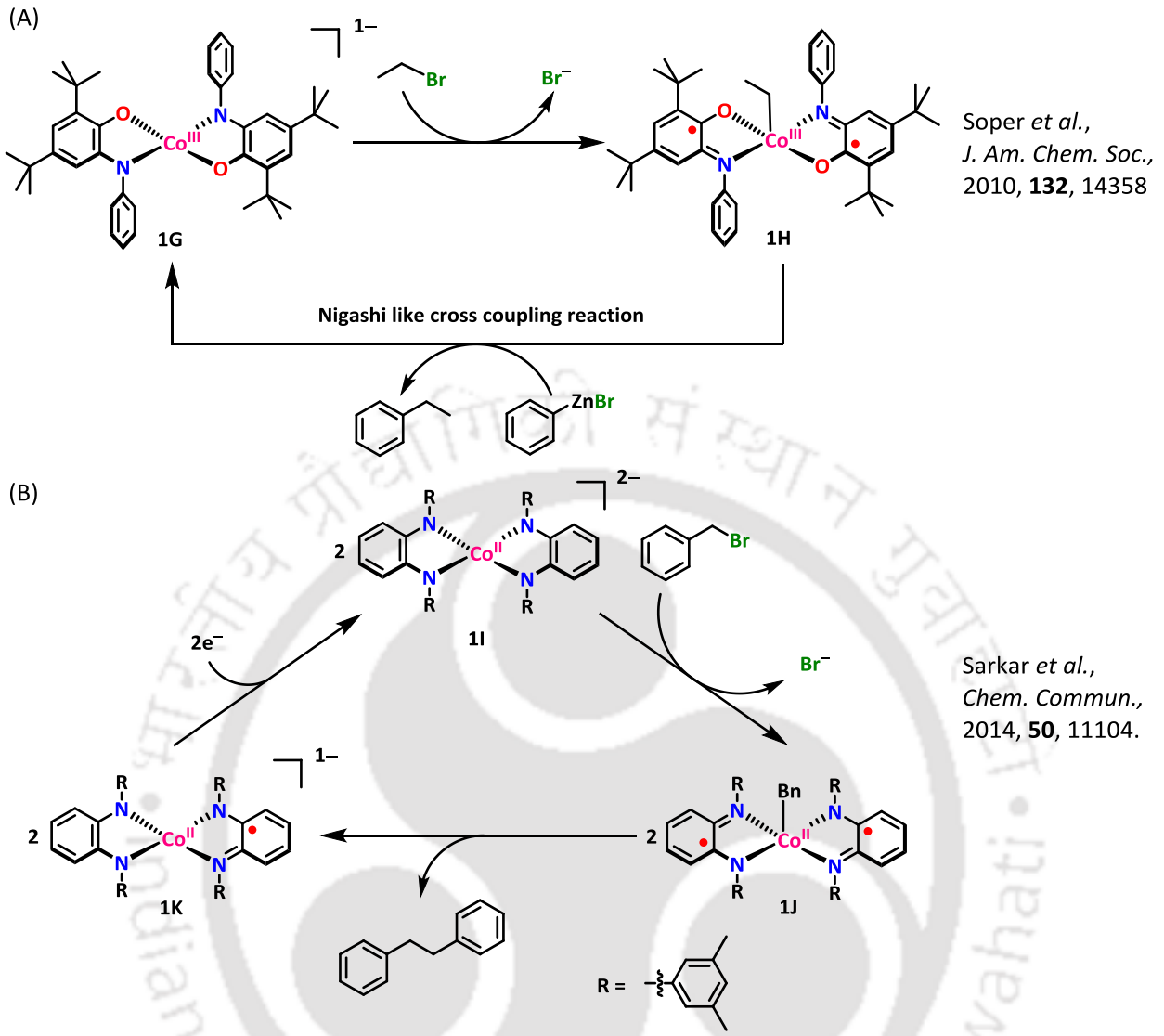

Scheme 1.9: *Utilization of Co complexes derived from non–innocent ligands.*

In 2010, Soper *et al.* reported a square planar Co(III)–bis(amidopenolate) complex [**1G**], which behaves as a nucleophile during the reaction with alkyl halide and provides a square pyramidal Co(III)–bis(iminosemiquinone) complex [**1H**] (Scheme 1.9A), where alkyl fragment is coordinated at the apex position.[8e] The coordinated non–innocent moieties provide two electrons during the oxidative addition and thus, each of the amidophenolate [$(AP)^{2-}$] unit transformed to its one–electron oxidized iminosemiquinone [$(ISQ)^{\bullet 1-}$] form. Upon treatment of the complex with organozine halide *e.g.* PhZnBr, a C–C couple product appeared and the regeneration of complex Co(III)–bis(amidopenolate) is happened. However, the rate of transformation of the C–C coupled product is quite low (10–15%).

The four–coordinate Co(II) complex [**1I**] reported by Sarkar *et al.* is capable for electrocatlytic C−C cross coupling reaction (Scheme 1.9B).[15] The ligand assisted oxidative addition of benzyl bromide to the metal ion provide a diradical–containing square pyramidal complex [**1J]**, where $-CH_2Ph$ (Bn) is axially coordinated to the metal ion. The formation of C−C coupled dibenzyl product results the complex [**1K]**, which upon one–electron reduction regenerates the active catalyst [**1I]**.

In both of the cases, the percentage of yield and the turnover number for the C–C coupling reaction are low and demand further improvement. This might be due to the lack of suitable *cis*– accommodation for the preliminary oxidative addition of the alkyl halide to the metal ion (Scheme 1.8).

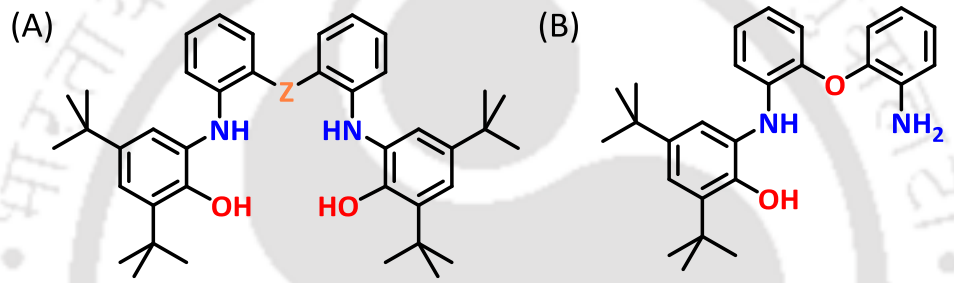

Scheme 1.10: *Schematic presentation of (A) ligand* $\boldsymbol{H_4L^{Z(AP/AP)}}$*, where Z = O, S, Se and Te and (B) ligand* $\boldsymbol{H_2L^{AP(o–NH_2–OPh)}}$.

Based on the above stated facts, non–innocent ligands that are consisted of two orthogonally situated aminophenol moieties within a single molecule can be designed and investigated. To serve the purpose two $\mathbf{H_2L^{AP}}$ [N(2–hydroxy–3,5–di–*tert*–butyl phenyl) aniline] molecules have been connected through a common chalcogen atom at the *ortho*–position to the aniline fragments (Scheme 1.10A). Thus, a series of four ligands has been developed $\mathbf{H_4L^{Z(AP/AP)}}$ [where Z = O, S, Se and Te].

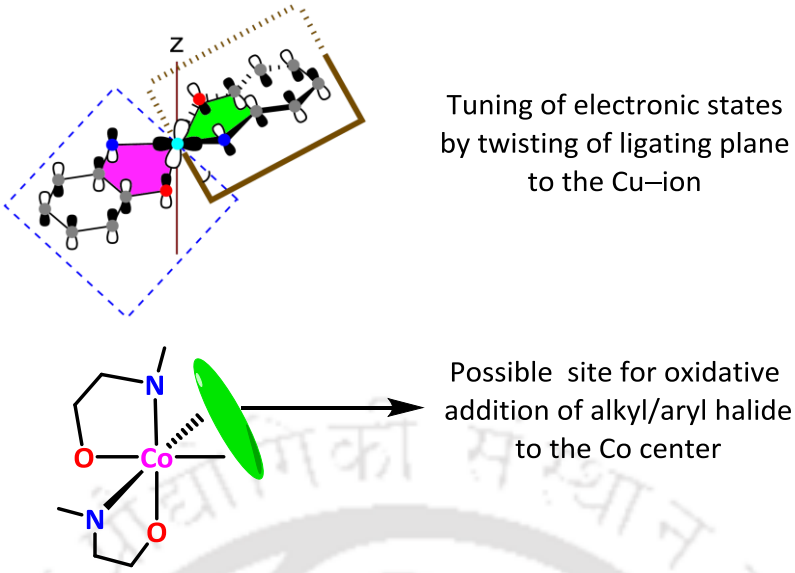

Scheme 1.11: *Probable benefits on the metalation of chalcogen bridged ligand* $\boldsymbol{H_4L^{Z(AP/AP)}}$ *by Cu– and Co–ion.*

The presence of chalcogen linkage makes two equal halves within the tetradentate ligand and the ligand has a set of two nearly orthogonal aminophenol groups. Thus, the developed ligand would be the better model for: (I) the tuning of the electronic structure of the Cu complexes by placing two radical units at an orthogonal position to each other, and (II) the generation of Co–complexes with suitable *cis*– accommodation sites for the substrate.

The significant importance of quinone moiety is observed in Cu–containing enzyme primary Amine Oxidase, which catalyzes the oxidative deamination of primary amine to corresponding aldehyde with concomitant formation of one equivalent of H_2O_2 and one equivalent of NH_3.[16]

$$RCH_2NH_2 + H_2O + O_2 \longrightarrow RCHO + NH_3 + H_2O_2$$

The active site of E. Coli Amine Oxidase (Scheme 1.12) is comprised of three histidine coordinated Cu(II)–ion and an organic cofactor TPQ (topaquinone).[14] The non–involvement of Cu(II)–ion during the oxidative half reaction is well established and during the oxidation of primary amine, the quinone moiety is getting reduced to aminophenol. The Asp383 unit behaves as a base during the oxidation cycle. Cu(II)–ion participates in the aerial oxidation of aminophenol moiety to its active TPQ form.

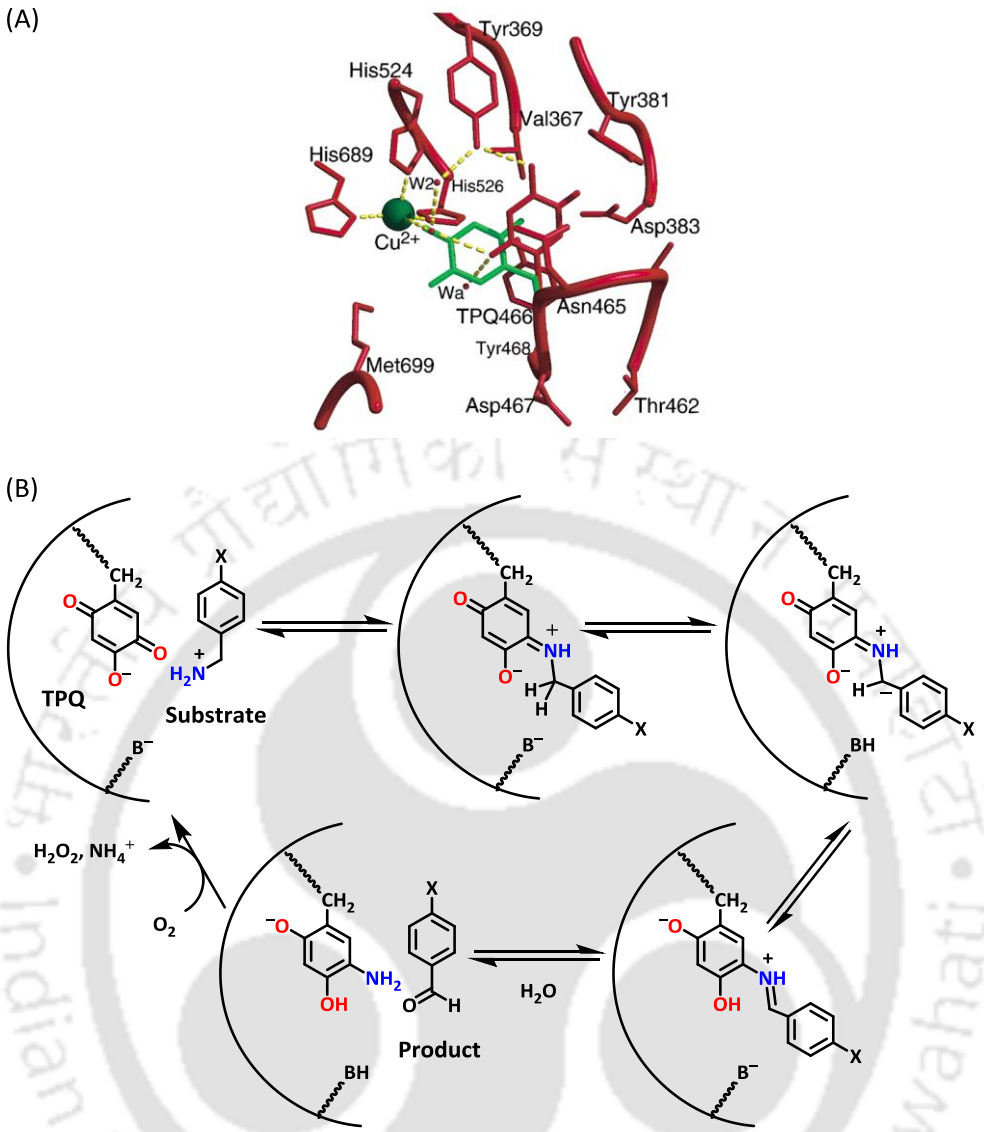

Scheme 1.12: *(A) Active site of E. coli Amine Oxidase*[16]*; (B) The mechanistic pathway of Cu–containing E. coli Amine Oxidase.*[16]

The amidophenolate based non–innocent ligand can also exist in its two–electron oxidized iminoquinone form in metal complexes. In 2008, Chaudhuri *et al.* reported ligand–assisted oxidative addition of bromine to the Cu–ion in Cu(II)–bis(iminosemiquinone) complex (**1B**) where Cu–ion retains its 2+ oxidation state and the iminosemiquinone radical anions undergoes one–electron oxidation each (Scheme 1.5A).[8c] Thus developed octahedral Cu(II)–bis(iminoquinone) complex is effective for the oxidation of triethylamine to acetaldehyde and diethylamine in dichloromethane under air. X–band EPR spectra of the reaction mixture indicated the existence of ligand centered radical, which is suggestive of reduction of coordinated–ligand by triethylamine.[8c]

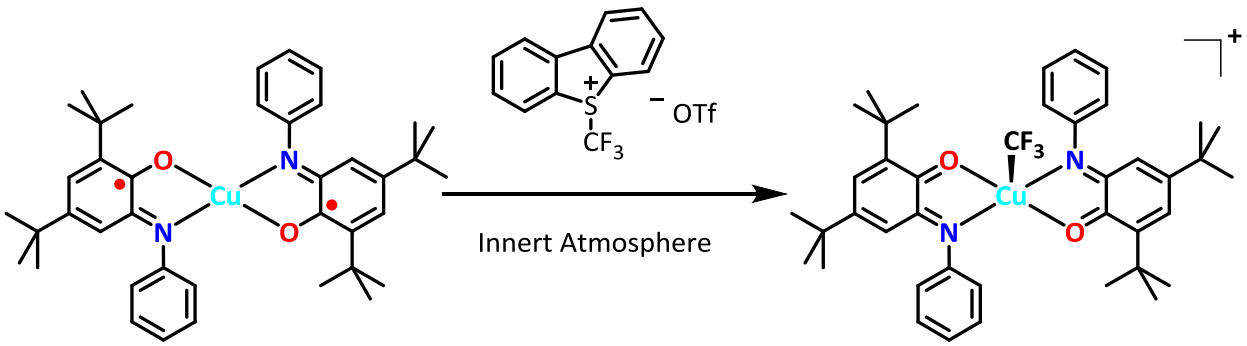

Scheme 1.13: *Ligand assisted oxidative addition of CF_3^+ to Cu–center in Cu(II)−bis(iminosemiquinone) complex.*[17]

In 2014, Fensterbank *et al.* reported another synthetic strategy of the generation of Cu(II)–bis(iminoquinone) complex by using Umemoto reagent (Scheme 1.13).[17] Oxidative addition of electrophilic CF_3^+ group to the Cu–ion is assisted by ligand centered oxidation, where the oxidation state of metal ion remains as 2+ in the resultant square pyramidal complex. Recently, the complex has been utilized in $–CF_3$ group transferring reaction and C–N bond formation reaction.

The reported synthetic strategies are not friendly as the used reagents are highly toxic in nature and commercially expensive. Hence, the development of a new strategy for the one–step synthesis of Cu(II)–bis(iminosemiquinone) complex seeks interest. In order to investigate in the regards, a new ligand $\mathbf{H_2L^{AP(o–NO_2–OPh)}}$ that contains a redox active aminophenol unit, an ethereal linked *o*–nitrobenzene moiety (Scheme 1.14) has been employed. Generally, this kind of aminophenol–based ligands provided radical–containing metal complexes under air. The presence of $–NO_2$ substituent may affect on the electronic and redox states of the resultant metal complexes and can promote oxidation of the complex at lower potential. Thus, employing only mild oxidants, the two–electron oxidation of the formed Cu(II) complex can be done. Furthermore, the $–NO_2$ group can be utilized: (I) as the anchor to attach the ligand fragment to a solid support like electrode[18] for exploring better homogeneous catalytic or electrocatalytic properties**,** and (II) for the further modification of ligand skeleton or generation of new ligand.

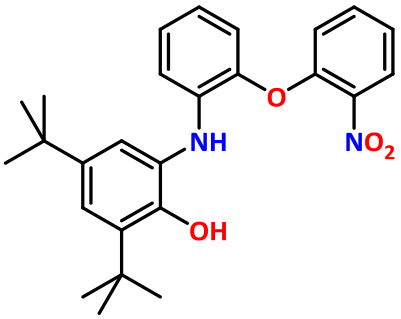

Scheme 1.14: *Schematic presentation of ligand* $H_2L^{AP(o-NO_2-OPh)}$.

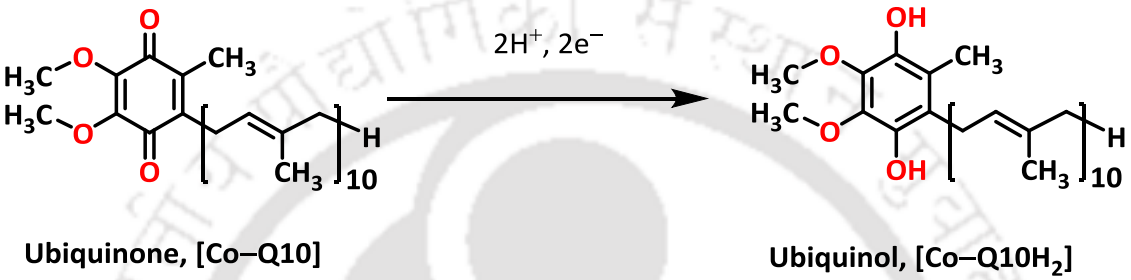

Scheme 1.15: *Coenzyme ubiquinone and its electrophilic behavior.*

In addition, the iminoquinone–coordinated Cu(II)–complexes can be utilized as electrophiles like ubiquinone coenzyme,[19] which acts as two–electron transporter at respiratory chain in living cell and generates protons (Scheme 1.15). Thus, the electrophilic behavior of the metal–coordinated iminoquinone species, generated from ligand $\mathbf{H_2L^{AP(o-NO_2-OPh)}}$, can be utilized as hydrogen generator from a hydride source like $NaBH_4$ (Scheme 1.16). In the reaction, Cu(II)–bis(iminoquinone) complex will be reduced to Cu(II)–bis(iminosemiquinone) species and thus generated proton will couple with another hydride anion to produce hydrogen gas (Scheme 1.16). Reaction under moisture free condition will refrain the production of $NaBO_2$.

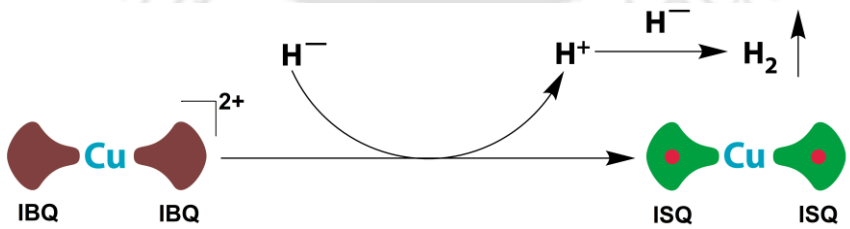

Scheme 1.16: *Schematic presentation of Cu(II)–bis(iminoquinone) assisted hydrogen production from a hydride source ($NaBH_4$).*

References

1. (*a*) N. Ito, S. E. V. Phillips, C. Stevens, Z. B. Ogel, M. J. McPherson, J. N. Keen, K. D. S. Yadav and P. F. Knowles, *Nature*, 1991, **350**, 87; (*b*) Y. Wang, J. L. DuBois, B. Hedman, K. O. Hodgson and T. D. P. Stack, *Science*, 1998, **279**, 537; (*c*) M. M. Whittaker and J. W. Whittaker, *J. Biol. Chem.*, 1990, **265**, 9610; (*d*) F. Himo, L. A. Friksson, F. Maseras and P. E. M. Siegbahn, *J. Am. Chem. Soc.*, 2000, **122**, 8031; (*e*) L. Que, Jr. and W. B. Tolman, *Nature*, 2008, **455**, 333 (*f*) J. W. Whittaker, *Chem. Rev.*, 2003, **103**, 2347.

2. (*a*) E. I. Solomon, U. M. Sundaram and T. E. Machonkin, *Chem. Rev.*, 1996, **96**, 2563; (*b*) E. I. Solomon, M. J. Baldwin and M. D. Lowery, *Chem. Rev.*, 1992, **92**, 521; (*c*) I. A. Koval, P. Gamez, C. Belle, K. Selmeczib and J. Reedijk, *Chem. Soc. Rev.*, 2006, **35**, 814; (*d*) P. E. M. Siegbahn, *J. Biol. Inorg. Chem.*, 2004, **9**, 577.

3. (*a*) J. Stubbe and W. A. van der Donk, *Chem. Rev*., 1998, **98**, 705; (*b*) B. A. Barry and G. T. Babcock, *Proc. Natl. Acad. Sci. USA*, 1987, **84**, 7099.

4. (*a*) S. M. Janes, D. Mu, D. Wemmer, A. J. Smith, S. Kaur, D. Maltby, A. L. Burlingame and J. P. Klinman, *Science*, 1990, **248**, 981; (*b*) D. M. Dooley, M. A. McGuirl, D. E. Brown, P. N. Turowski, W. S. McIntire and P. F. Knowles, *Nature*, 1991, **349**, 262; (*c*) J. P. Klinman, *J. Biol. Chem.*, 1996, **271**, 27189.

5. M. T. T. Wong–Riley, H. L. Liang, J. T. Eells, B. Chance, M. M. Henry, E. Buchmann, M. Kane and H. T. Whelan, *J. Biol. Chem.*, 2005, **280**, 4761.

6. (*a*) F. Peter Guengerich, *Chem. Res. Toxicol.*, 2008, **21**, 70; (*b*) J. T. Groves, *PNAS*, 2003, **100**, 3569; (*c*) H. Isobe, K. Yamaguchi, M. Okumura and J. Shimada, *J. Phys. Chem. B*, 2012, **116**, 4713.

7. (*a*) A. Gräslund and A. Ehrenberg, *Appl. Magn. Reson.*, 2007, **31**, 447; (*b*) M. A. S. Perez, P. A. Fernandes and M. J. Ramos, *J. Chem. Theory Comput.*, 2010, **6**, 2770; (*c*) T. P. Dang, A. J. Sobczak, A. M. Mebel, C. Chatgilialoglu and S. F. Wnuk, *Tetrahedron*, 2012, **68**, 5655; (*d*) E. C. Minnihan, D. G. Nocera and J. Stubbe, *Acc. Chem. Res.*, 2013, **46**, 2524; (*e*) J. Stubbe, D. G. Nocera, C. S. Yee and M. C. Y. Chang, *Chem. Rev.*, 2003, **103**, 2167; (*f*) A. Ehrenberg and P. Reichard, *J. Biol. Chem.*, 1972, **247**, 3485; (*g*) J. Stubbe and P. Riggs–Gelasco, *Trends Biochem.*

Sci., 1998, **23**, 438; (*h*) M. D. Sintchak, G. Arjara, B. A. Kellogg, J. Stubbe and C. L. Drennan, *Nat. Struct. Biol.*, 2002, **9**, 293.

8. (*a*) P. Chaudhuri, C. N. Verani, E. Bill, E. Bothe, T. Weyhermüller and K. Wieghardt, *J. Am. Chem. Soc.*, 2001, **123**, 2213; (*b*) M. K. Mondal, A. K. Biswas, B. Ganguly and C. Mukherjee, *Dalton Trans.*, 2015, **44**, 9375; (*c*) C. Mukherjee, U. Pieper, E. Bothe, V. Bachler, E. Bill, T. Weyhermüller and P. Chaudhuri, *Inorg. Chem.*, 2008, **47**, 2740; (*d*) S. Mukherjee, T. Weyhermüller, E. Bothe, K. Wieghardt and P. Chaudhuri, *Dalton Trans.*, 2004, 3842 ; (*e*) A. L. Smith, K. I. Hardcastle and J. D. Soper, *J. Am. Chem. Soc.*, 2010, **132**, 14358; (*f*) J. Jacquet, S. Blanchard, E. Derat, M. Murr and L. Fensterbank, *Chem. Sci.*, 2016, **7**, 2030; (*g*) J. Jacquet, P. Chaumont, G. Gontard, M. Orio, H. Vezin, S. Blanchard, M. Murr, and L. Fensterbank, *Angew. Chem., Int. Ed.*, 2016, **55**, 10712.

9. (*a*) H. Chun, T. Weyhermüller, E. Bill and K. Wieghardt, *Angew. Chem., Int. Ed.*, 2001, **40**, 2489; (*b*) H. Chun, C. N. Verani, P. Chaudhuri, E. Bothe, E. Bill, T. Weyhermüller and K. Wieghardt, *Inorg. Chem.*, 2001, **40**, 4157.

10. C. Mukherjee, T. Weyhermüller, E. Bothe and P. Chaudhuri, *C.R. Chim.*, 2007, **10**, 313.

11. C. Mukherjee, U. Pieper, E. Bothe, V. Bachler, E. Bill, T. Weyhermüller and P. Chaudhuri, *Inorg. Chem.*, 2008, **47**, 8943.

12. (*a*) J. B. Goodenough, *Scholarpedia*, 2008, **3,** 7382; (*b*) J. B. Goodenough, *J. Phys. Chem. Solids*, 1958, **6**, 287; (*c*) J. Kanamori, *J. Phys. Chem. Solids*, 1959, **10**, 87.

13. (*a*) S. Ye, B. Sarkar, F. Lissner, T. Schleid, J. van Slageren, J. Fiedler and W. Kaim, *Angew. Chem., Int. Ed.*, 2005, **44**, 2103; (*b*) R. Rakshit, S. Ghorai, S. Biswas and C. Mukherjee, *Inorg. Chem.*, 2014, **53**, 3333.

14. (*a*) S. K. Larsen and C. G. Pierpont, *J. Am. Chem. SOC.*, 1988, **110**, 1827; (*b*) F. Novio, E. Evangelio, N. Vazquez–Mera, P. Gonzalez–Monje, E. Bellido, S. Mendes, N. Kehagias and D. Ruiz–Molina, *Sci. Rep.*, 2013, **3**, 1708; (*c*) O. Cador, F. Chabre, A. Dei, C. Sangregorio, J. V. Slageren and M. G. F. Vaz, *Inorg. Chem.*, 2003, **42**, 6432.

15. M. van der Meer, Y. Rechkemmer, I. Peremykin, S. Hohloch, J. van Slageren and B. Sarkar, *Chem. Commun.*, 2014, **50**, 11104.

16. (*a*) M. R. Parsons, M. A. Convery, C. M. Wilmot, K. D. S. Yadav, V. Blakeley, A. S. Corner, S. E. V. Phillips, M. J. McPherson and P. F. Knowles, *Structure*, 1995, **3**, 1191; (*b*) J. M. Murray, C. G. Saysell, C. M. Wilmot, W. S. Tambyrajah, J. Jaeger, P. F. Knowles, S. E. V. Phillips and M. J. McPherson, *Biochemistry*, 1999, **38**, 8217.

17. J. Jacquet, E. Salanouve, M. Orio, H. Vezin, S. Blanchard, E. Derat, M. Desage–El Murr and L. Fensterbank, *Chem. Commun.*, 2014, **50**, 10394.

18. (*a*) L. Zhang and J. M. Cole, *ACS Appl. Mater. Interfaces*, 2015, **7**, 3427; (*b*) L. A. Zotti, T. Kirchner, J. Cuevas, F. Pauly, T. Huhn, E. Scheer and A. Erbe, *Small*, 2010, **6**, 1529.

19. (*a*) R. Dhingra and L. A. Kirshenbaum, *Cell Death Dis.*, 2015, **6**, e1956; (*b*) G. Cecchini, *Annu. Rev. Biochem.*, 2003, **72**, 77; (*c*) E. Tomitsuka1, H. Hirawake1, Y. Goto, M. Taniwaki, S. Harada and K. Kita, *J. Biochem.*, 2003, **134**, 191.

Chapter II

*Synthesis and Characterization of Chalcogen–Bridged Non–Innocent Ligands and the Corresponding Cu(II) Complexes**

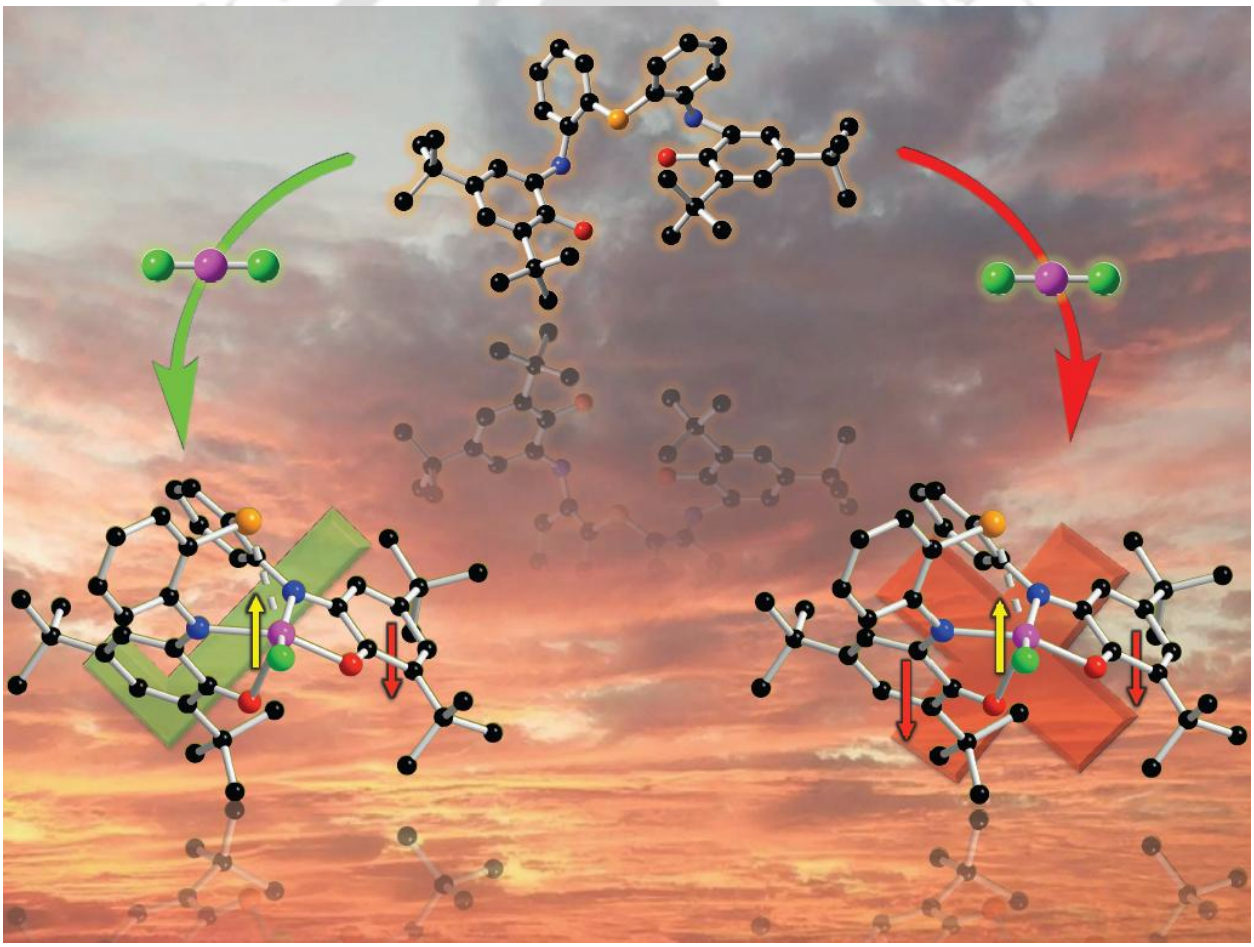

* Some results have been reported in *Dalton Trans.*, 2015, **44**, 9375.

2.1: Introduction

Galactose Oxidase (GO) is a fungal copper–containing mononuclear metalloenzyme that catalyses aerial oxidation of primary alcohols to the corresponding aldehydes with a concomitant reduction of oxygen to hydrogen peroxide.[1] The active site of GO is composed of a Cu(II) ion that is surrounded by two histidine imidazole units and two tyrosinate units (Protein Data Bank identity 1GOG).[1b–e] In the catalytically active form, Cu(II) ion ($3d^9$) is coordinated to the Tyr272 radical in a distorted square pyramidal geometry. Both the paramagnetic centers participate in the catalysis and undergo one–electron reduction each and, consequently, the substrate primary alcohol is oxidized to an aldehyde.

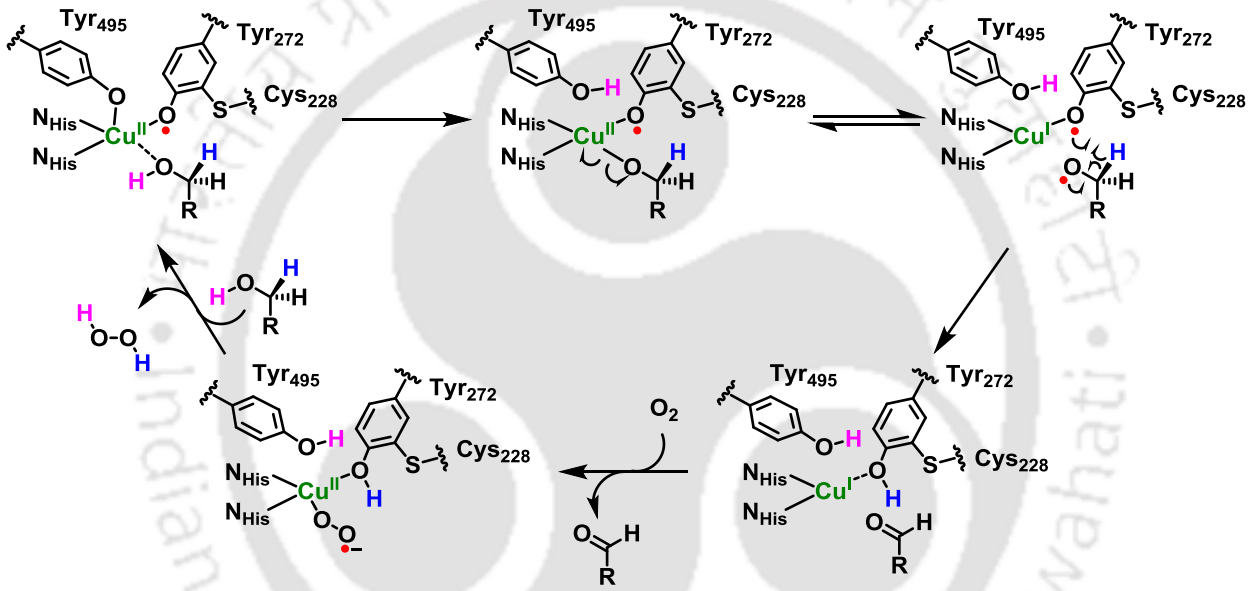

Scheme 2.1: *The catalytic cycle of Galactose Oxidase (GO).*

The high catalytic efficiency and the structural simplicity motivated chemists to synthesize functional and/or structural models of GO; (i) to have efficient enzyme–like alcohol–oxidation catalysts, and (ii) to gain insight into the electronic structure. Several GOase inspired catalytic systems are well established and they efficiently oxidize primary alcohols to corresponding aldehydes.[2] In this regard, a number of non–innocent ligands, which are defined as the organic moieties capable of changing their oxidation state upon coordination to metal ions, and their corresponding diradical–containing square planar or distorted square planar Cu(II) complexes have been synthesized and studied by X–ray crystallography and various other spectroscopic techniques, *e.g.* NMR, EPR, UV–Vis/NIR, etc.[3a] In those reported complexes, the non–innocent ligand moiety aminophenol undergoes one–electron oxidation on metalation with copper ion and diradical–containing Cu(II) complexes are formed.[3]

A non–innocent ligand 2–anilino–4,6–di–*tert*–butylphenol {$\mathbf{H_2L^{AP}}$; Scheme 2.2} reacts with copper ion under air and provides a diradical–containing square planar $[\mathbf{Cu(L^{ISQ})_2}]^0$ complex where $[L^{ISQ}]^{\bullet 1-}$ represents monoanionic iminosemiquinone ligand (Scheme 2.2).[3a]

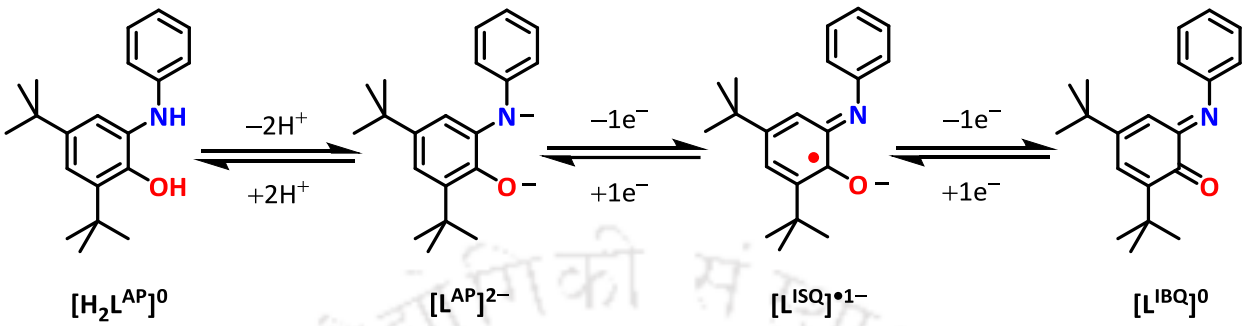

Scheme 2.2: *Several oxidation states of 2–Anilino–4,6–di–tert–butylphenol* ($\boldsymbol{H_2L^{AP}}$).[3a]

The square planar complex; $\mathbf{[Cu(L^{ISQ})_2]^0}$ hold three unpaired electrons and their coupling fashion make the complex paramagnetic in nature. Experimental data reveals the existence of strong antiferromagnetic coupling between two radicals *i.e.* radical–radical antiferromagnetic coupling predominates over radical–copper coupling and the resultant unpaired electron resides on Cu(II)–ions.

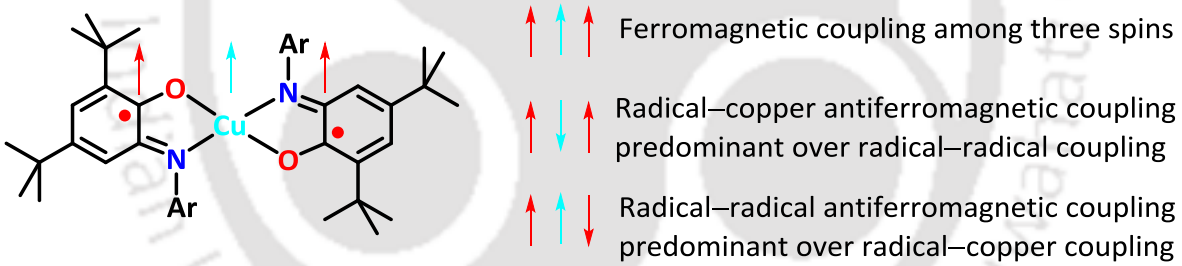

Scheme 2.3: *The square planar complex;* $\boldsymbol{[Cu\{L^{(ISQ)}\}^2]^0}$ *and its probable coupling fashions.*

A series of substituted 2–anilino–4,6–di–*tert*–butylphenol and their corresponding Cu(II)–diradical complexes have been reported.[3] In those complexes, the effective antiferromagnetic radical–radical interaction dominate over Cu(II)–radical interaction and results S_t = 1/2 as the ground state attributable to an almost "isolated" copper(II) spin character.[3a–d]

By introducing a soft coordinating entity (*e.g.* –SMe, –SePh) at the *ortho*– position of the aniline phenyl ring, the structure of the metal complex can be deviated from its regular geometry. The resulted paramagnetic complex has a different coupling pattern among its unpaired electrons *i.e.* resultant unpaired electron is on ligand–centered.[3e,f]

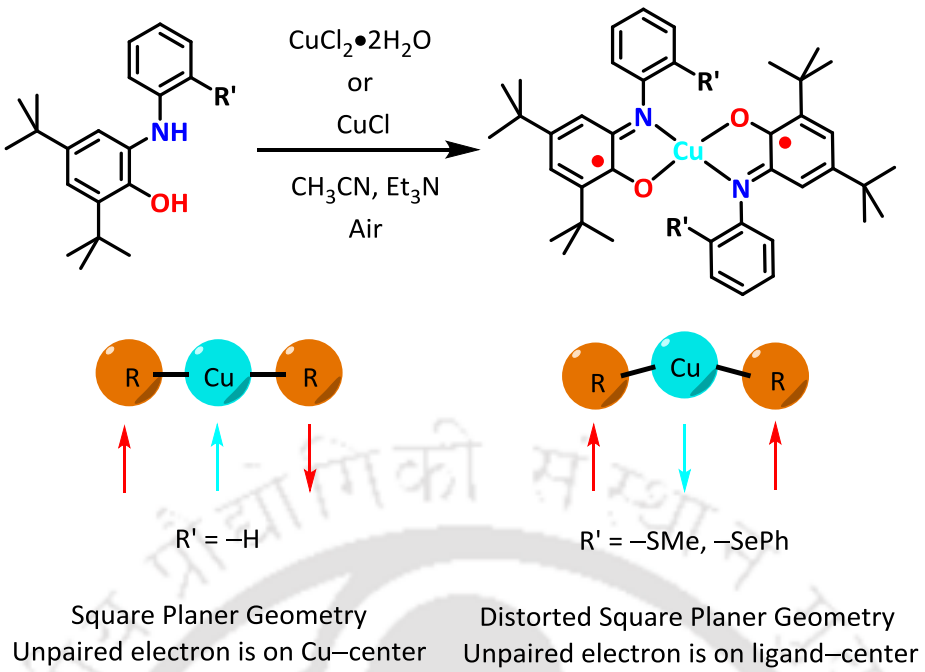

Figure 2.1: *Reported Cu(II)–bis(iminosemiquinone) complexes and their coupling fashion.*[3]

The coupling fashion among the radicals and Cu(II) center depends upon the structure and the secondary interaction present in the complex.[3] In the square planar complex **[Cu(L^{ISQ})$_2$]^0**, the orthogonality between the radical–centered magnetic orbital (p_z) and Cu(II) centered magnetic orbital ($d_{x^2-y^2}$) reinforces the antiferromagnetic coupling between two radical moieties through Cu(II) centered t_{2g} orbital. The structural deviation due to secondary coordination(s) break the orthogonality between the radical centered and Cu(II) centered magnetic orbitals and hence, Cu(II)–radical antiferromagnetic coupling predominates over radical–radical antiferromagnetic coupling.

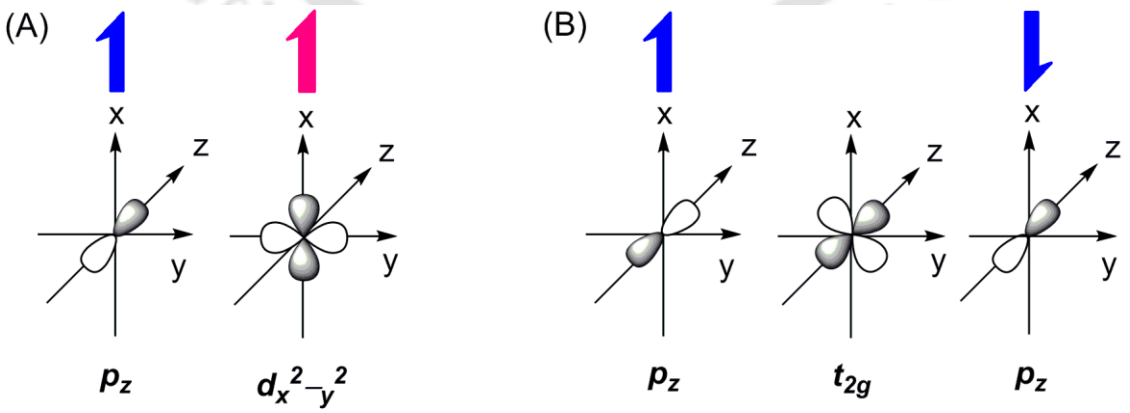

Figure 2.2: *(A) Orthogonality between radical centered magnetic orbital (p_z) and Cu(II) centered magnetic orbital ($d_{x^2-y^2}$) in square planar* ***[Cu(L^{ISQ})$_2$]^0*** *complex; (B) Radical–radical antiferromagnetic coupling through Cu(II) centered t_{2g} orbital.*

In this regards, a ligand backbone–containing two orthogonally placed aminophenol units was planned to synthesize. Hence, $\mathbf{H_4L^{Z(AP/AP)}}$ was synthesized by placing a chalcogen (O, or S, or Se, or Te) bridge between two $\mathbf{H_2L^{AP}}$ ligand units. The bridging atom was attached at the *ortho*– position of the aniline ring. Thus, obtained ligand $\mathbf{H_4L^{Z(AP/AP)}}$ having two ligating aminophenol units at nearly orthogonal to each other. In this chapter, the synthesis and characterization of chalcogen bridged ligands [$\mathbf{H_4L^{Z(AP/AP)}}$] and their corresponding copper complexes are reported.

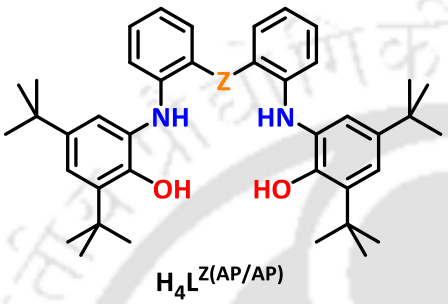

$\mathbf{H_4L^{Z(AP/AP)}}$

Where Z =O, S, Se or Te

When
Z = O, $\mathbf{H_4L^{O(AP/AP)}}$
Z = S, $\mathbf{H_4L^{S(AP/AP)}}$
Z = Se, $\mathbf{H_4L^{Se(AP/AP)}}$
Z = Te, $\mathbf{H_4L^{Te(AP/AP)}}$

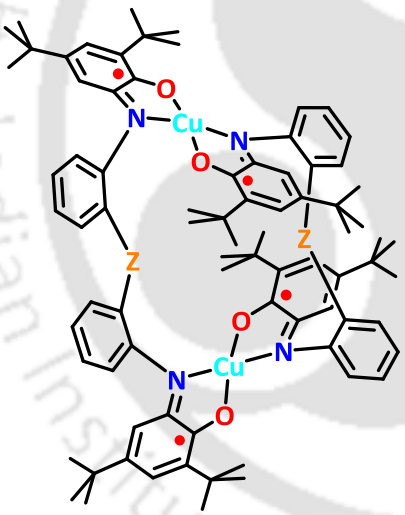

$\{Cu_2[L^{Z(ISQ/ISQ)}]_2\}$

Where Z =O, S, Se or Te

When
Z = O, $\{Cu_2[L^{O(ISQ/ISQ)}]_2\}$; **2A**
Z = S, $\{Cu_2[L^{S(ISQ/ISQ)}]_2\}$; **2B**
Z = Se, $\{Cu_2[L^{Se(ISQ/ISQ)}]_2\}$; **2C**
Z = Te, $\{Cu_2[L^{Te(ISQ/ISQ)}]_2\}$; **2D**

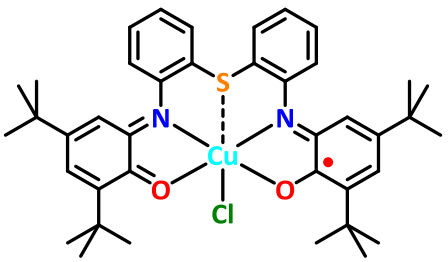

$\{Cu[L^{S(IBQ/ISQ)}]Cl\}$; **2E**

Here,
Bridging atom = S
$\{Cu[L^{S(IBQ/ISQ)}]Cl\}$; **2E**

Scheme 2.4: *Different chalcogen–bridge ligands and their corresponding Cu complexes.*

2.2: *Synthesis and Characterizations of Chalcogen Bridged Non–innocent Ligand $H_4L^{Z(AP/AP)}$, where Z = O, S, Se and Te*

The chalcogen bridged ligands, $\mathbf{H_4L^{Z(AP/AP)}}$ (Z = O, S, Se, Te) were synthesized by following a common synthetic route (Scheme 2.5). A reaction between 2:1 3,5–di–*tert*–butylcatechol and bis(*o*–aminophenyl)Z in hexane provided ligand $\mathbf{H_4L^{Z(AP/AP)}}$ in good yield.[4] Small amount of Et_3N was used as the initiator.

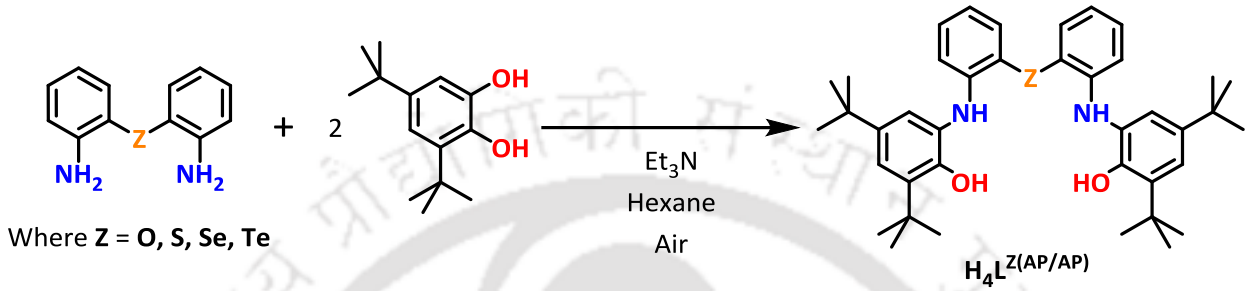

Scheme 2.5: *General synthetic route to the formation of ligand* $\boldsymbol{H_4L^{Z(AP/AP)}}$*, where* ***Z = O, S, Se*** *and* ***Te*** .

The formation aminophenol containing ligand from catechol is going through benzoquinone and iminobenzoquinone intermediates and the mechanism is well established[5] and shown in Scheme 2.6.

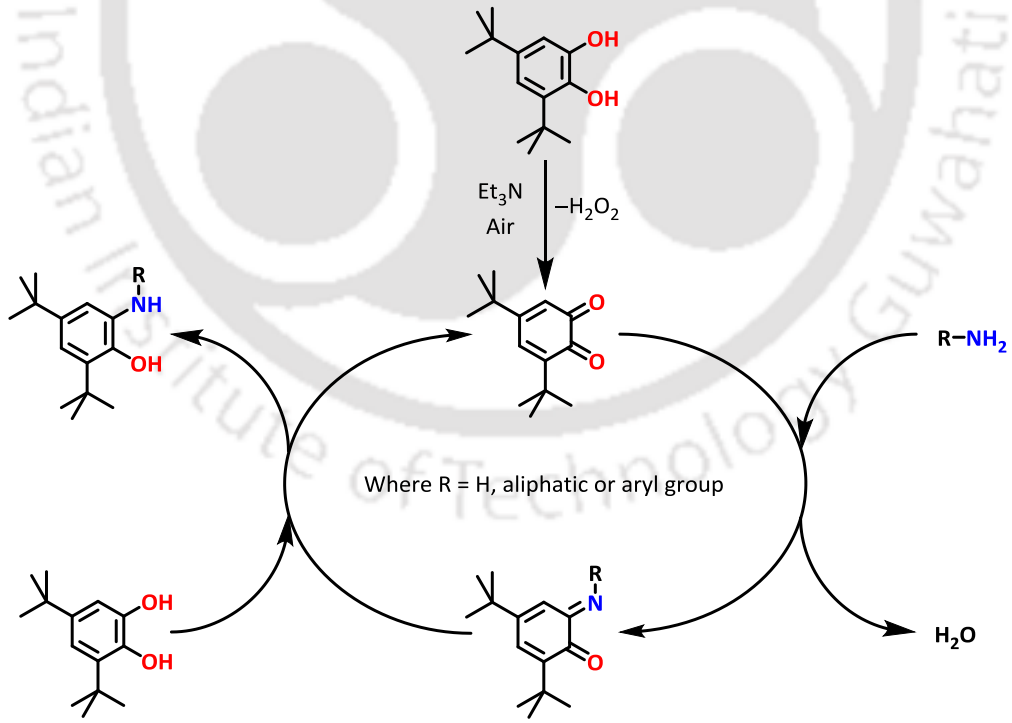

Scheme 2.6: *Plausible mechanism of the formation of aminophenol containing ligand from 3,5–di–tert–butylcatechol.*[5]

All the ligands were characterized by FTIR spectroscopy, NMR spectroscopy and mass spectrometry techniques.

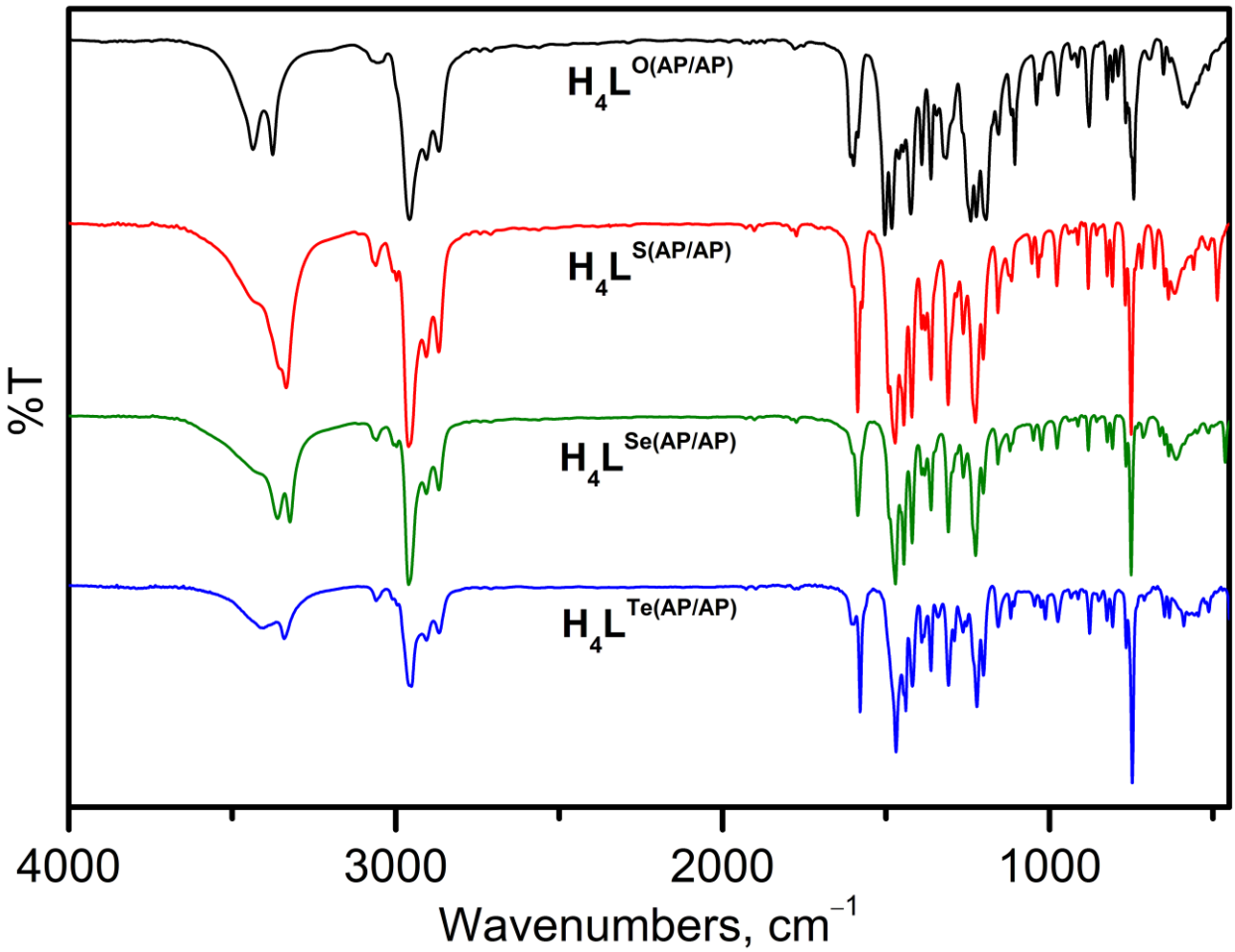

Figure 2.3: *IR spectra of ligand* $H_4L^{Z(AP/AP)}$*, where Z = O, S, Se and Te.*

In IR spectra of $H_4L^{Z(AP/AP)}$, existence of aminophenol moieties were confirmed by the presence of sharp bands at the region 3450−3320 cm^{-1} and those bands corresponded to ν(O−H) and ν(N−H) stretches.[6a,b] A weak band for the stretching of aryl C−H was appeared at 3060 cm^{-1}.[6a] The asymmetric, overtone and symmetric ν(C–H) stretching vibration bands, corresponded to the *tert*−butyl groups, appeared at the region 2960−2860 cm^{-1}.[6a,c,d] In addition to this, the bands corresponded to ν(C–H) bending vibrations of methyl groups were appeared at ~ 1480 cm^{-1} and ~ 1364 cm^{-1}.[6a] The infrared stretching bands at ~1587, 1504 and 1483 cm^{-1} ascribed as ν(C=C) stretches of the aromatic rings.[6a] Two bands at around 1310 and 1225 cm^{-1} appeared due to aminophenol ν(C–N) and ν(C–O) stretches, respectively.[6a] Compound $H_4L^{O(AP/AP)}$ has shown two distinct bands at 1241 and 1194 cm^{-1} and those bands corresponded to the asymmetric and symmetric stretching of aryl ethereal ν(C–O) stretching vibrations.[6e]

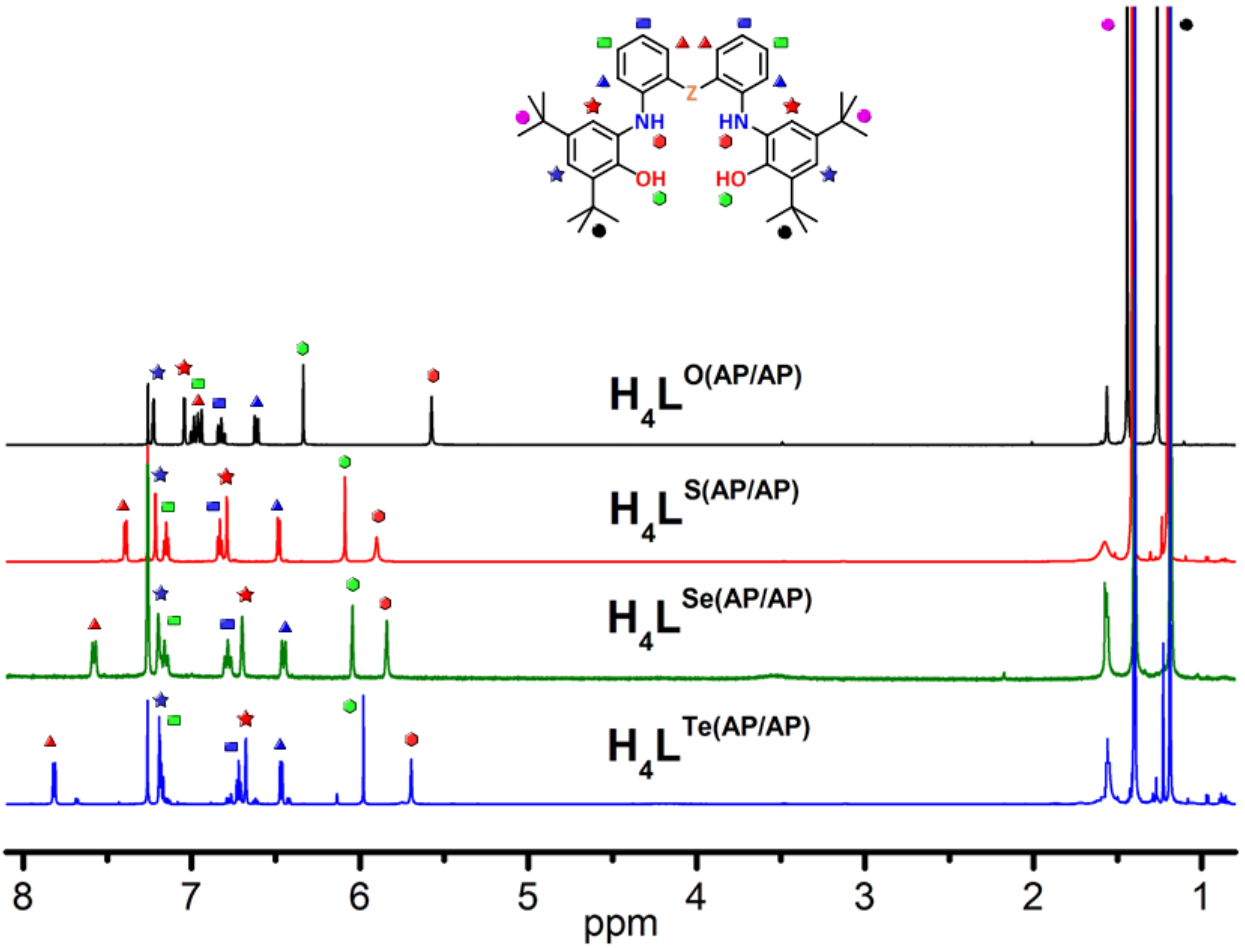

Figure 2.4: *^{1}H NMR spectra of ligand* $\boldsymbol{H_4L^{Z(AP/AP)}}$*, where Z = O, S, Se and Te.*

^{1}H NMR spectra of all four ligands were measured in $CDCl_3$ at 298 K. The existence of a chalcogen bridge produced two equal halves within the ligand molecule. The resonance signals for all the six type of aryl protons appeared at the range 7.85−6.40 ppm. Two distinct singlet peaks in the range 6.35−5.55 ppm were attributed for –OH and –NH protons, respectively. All the aliphatic protons from two types of *tert*–butyl group appeared in the range 1.45−1.18 ppm. A peak around ~1.56 ppm was due H_2O in the solvent or sample.^{13}C NMR and details of the carbons peaks annotations of each of the ligands are shown in 'Equipment and Experimental Section'.

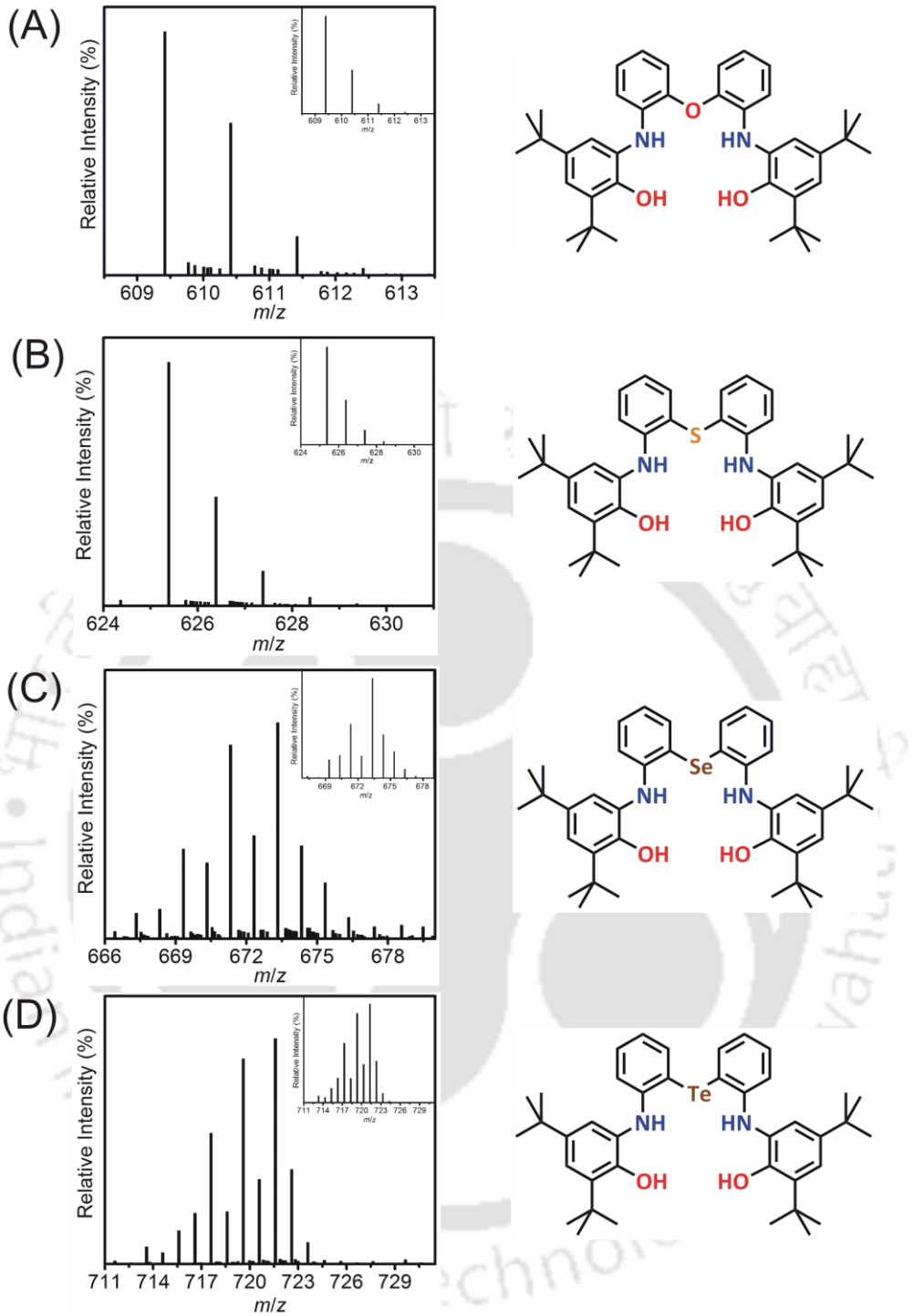

Figure 2.5: *ESI–mass spectra of [A] ligand* $\boldsymbol{H_4L^{O(AP/AP)}}$*, [B] ligand* $\boldsymbol{H_4L^{S(AP/AP)}}$*, [C] ligand* $\boldsymbol{H_4L^{Se(AP/AP)}}$*, and [D] ligand* $\boldsymbol{H_4L^{Te(AP/AP)}}$*; experimental and simulated isotope distribution pattern (inset).*

Electrospray ionization mass spectra (ESI–MS) of $\mathbf{H_4L^{O(AP/AP)}}$ and $\mathbf{H_4L^{S(AP/AP)}}$ were measured in CH_3CN (HPLC grade) solution in positive mode. 100% molecular ion peak corresponded to $[L+H]^+$ (L = molecular mass of the ligand) was appeared at *m/z* = 609.41 for $\mathbf{H_4L^{O(AP/AP)}}$; 625.38 for $\mathbf{H_4L^{S(AP/AP)}}$. ESI–MS spectra of ligand $\mathbf{H_4L^{Se(AP/AP)}}$ and $\mathbf{H_4L^{Te(AP/AP)}}$ were measured in CH_3CN (HPLC grade) solution in negative mode. Molecular ion peak

corresponded to $[L-H]^-$ was appeared at *m/z* = 671.62 (100 %) for $\mathbf{H_4L^{Se(AP/AP)}}$; 721.59 (25 %) for $\mathbf{H_4L^{Te(AP/AP)}}$. Isotope distribution pattern of the observed mass peaks confirmed the composition as $[C_{40}H_{52}N_2O_3+H]^+$ for $\mathbf{H_4L^{O(AP/AP)}}$; $[C_{40}H_{52}N_2O_2S+H]^+$ for $\mathbf{H_4L^{S(AP/AP)}}$; $[C_{40}H_{52}N_2O_2Se-H]^-$ for $\mathbf{H_4L^{Se(AP/AP)}}$; and $[C_{40}H_{52}N_2O_2Te-H]^-$ for $\mathbf{H_4L^{Te(AP/AP)}}$, respectively.

Ligand $\mathbf{H_4L^{O(AP/AP)}}$ was characterized by X–ray diffraction analysis. Suitable crystal was obtained from a dichloromethane:methanol (3:1) solvent mixture. Crystal structure of the ligand implied composition as well as the envisaged perpendicular orientation of two aminophenol moieties in the ligand molecule (Fig. 2.6).

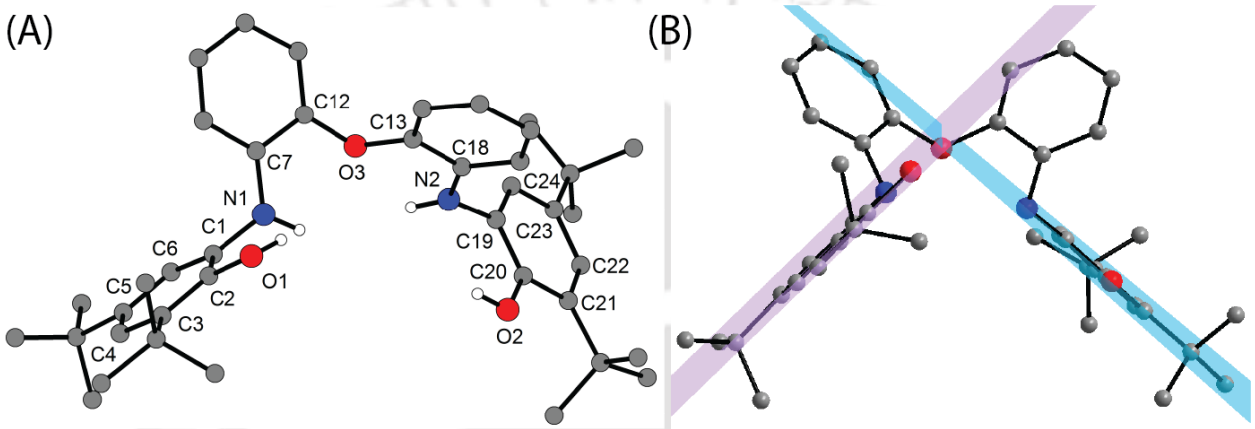

Figure 2.6: *(A) Ball and Stick presentation of ligand* $\boldsymbol{H_4L^{O(AP/AP)}}$*; (B) Perpendicular orientation of two aminophenol moieties in the ligand molecule.*

The crystal structure of $\mathbf{H_4L^{O(AP/AP)}}$ has been measured at 293(2) K by single crystal X–ray crystallography. The ligand was crystallized in the triclinic space group '*P–1*'. In the ligand two $\mathbf{H_2L^{AP}}$ units were connected through an ether linkage at the *–ortho* position of two aniline moieties. All aryl C–C bond lengths were found in the range of 1.357–1.408(7) Å, which suggested the benzonoid type of all the aryl rings. The O3–C12 = 1.393(7) and O3–C13 = 1.404(8) Å bond lengths were resembles with several reported aryl ether compound.[7] The ethereal angle (∠C12–O3–C13) was found as 120.3(5)°. Such linkage provided nearly perpendicular (84.4°) orientation between two aminophenol units [C1–to–C6 and C19–to–C24 rings] (Fig. 2.6B). The structure provided a brief idea on similar type of other chalcogen bridged ligands.

Table 2.1: *Selected bond distances (Å) and angels (°) for complex* $\boldsymbol{H_4L^{O(AP/AP)}}$ *.*

C1–C2	1.382(7)	C17–C18	1.368(8)
C2–C3	1.384(7)	C18–C13	1.408(8)

C3–C4	1.395(7)	C19–C20	1.374(8)
C4–C5	1.408(7)	C20–C21	1.412(7)
C5–C6	1.390(7)	C21–C22	1.388(7)
C6–C1	1.385(7)	C22–C23	1.372(7)
C7–C8	1.380(7)	C23–C24	1.388(7)
C8–C9	1.378(8)	C24–C19	1.394(7)
C9–C10	1.342(9)	N1–C1	1.447(6)
C10–C11	1.357(10)	N1–C7	1.394(7)
C11–C12	1.387(9)	N2–C18	1.394(7)
C7–C12	1.379(7)	N2–C19	1.435(6)
C13–C14	1.366(8)	O1–C2	1.393(7)
C14–C15	1.364(10)	O2–C20	1.369(6)
C15–C16	1.396(10)	O3–C12	1.393(7)
C16–C17	1.393(8)	O3–C13	1.404(8)
C12–O3–C13	120.3(5)	C18–N2–C19	121.9(5)
C7–N1–C1	121.6(4)		

Incorporation of two non−innocent aminophenol units within a single molecular entity make the ligand potentially non−innocent in character and its possible various oxidation states are shown in Scheme 2.7.

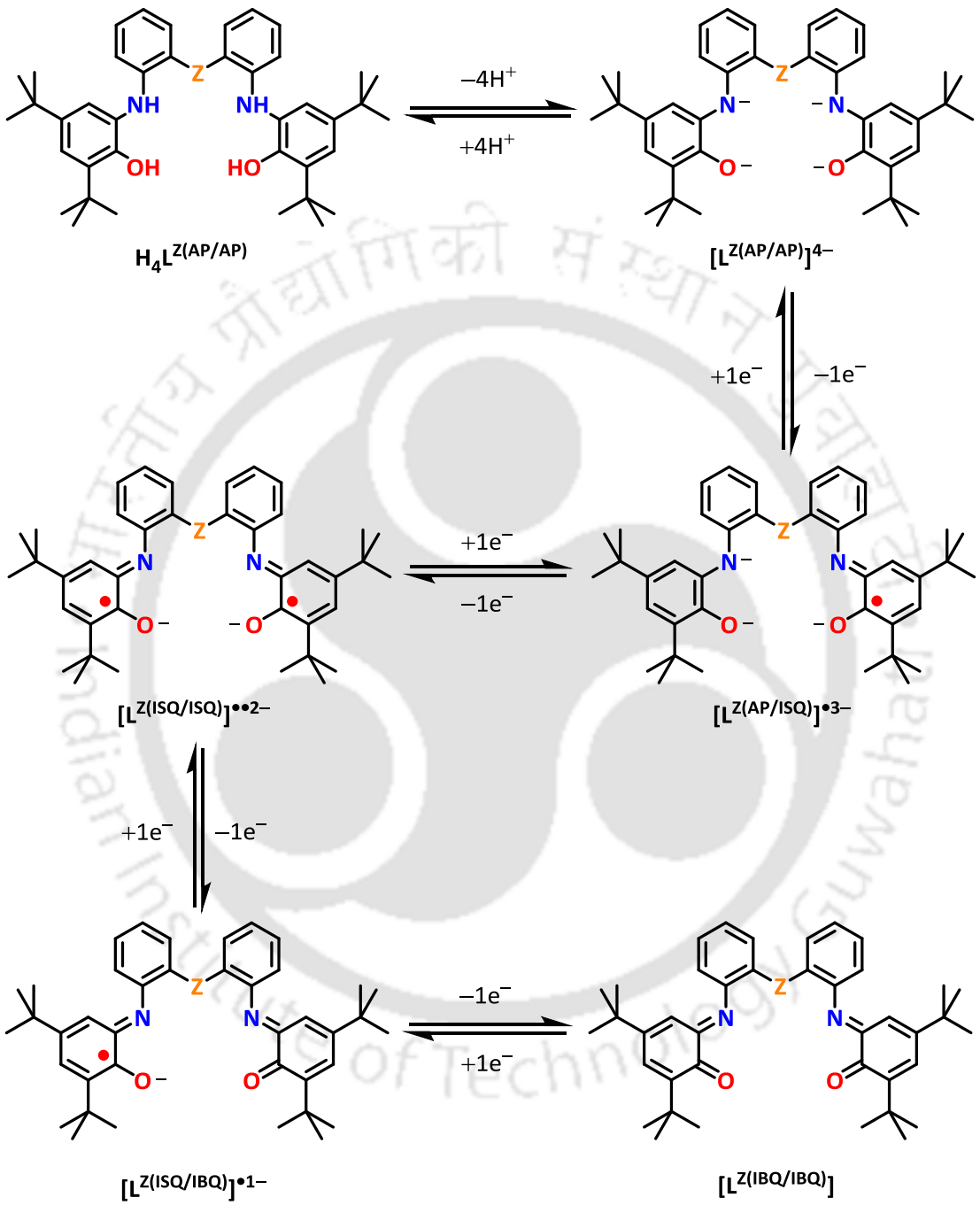

Scheme 2.7: *Different oxidation states of* $H_4L^{Z(AP/AP)}$ *ligands, where Z = O, S, Se and Te.*

2.3: Synthesis and Characterizations of Cu(II) Complexes by Equimolar Reaction between $CuCl_2•2H_2O$ and $H_4L^{Z(AP/AP)}$

An equimolar reaction between ligand $\mathbf{H_4L^{O(AP/AP)}}$ and $CuCl_2•2H_2O$ in CH_3CN in the presence of Et_3N produced green color complex (**2A**) in good yield. The other three analogous green color complexes **2B**, **2C** and **2D** were also synthesized by employing $\mathbf{H_4L^{Z(AP/AP)}}$ (Z = S, Se and Te) ligands, respectively, under the same reaction conditions.

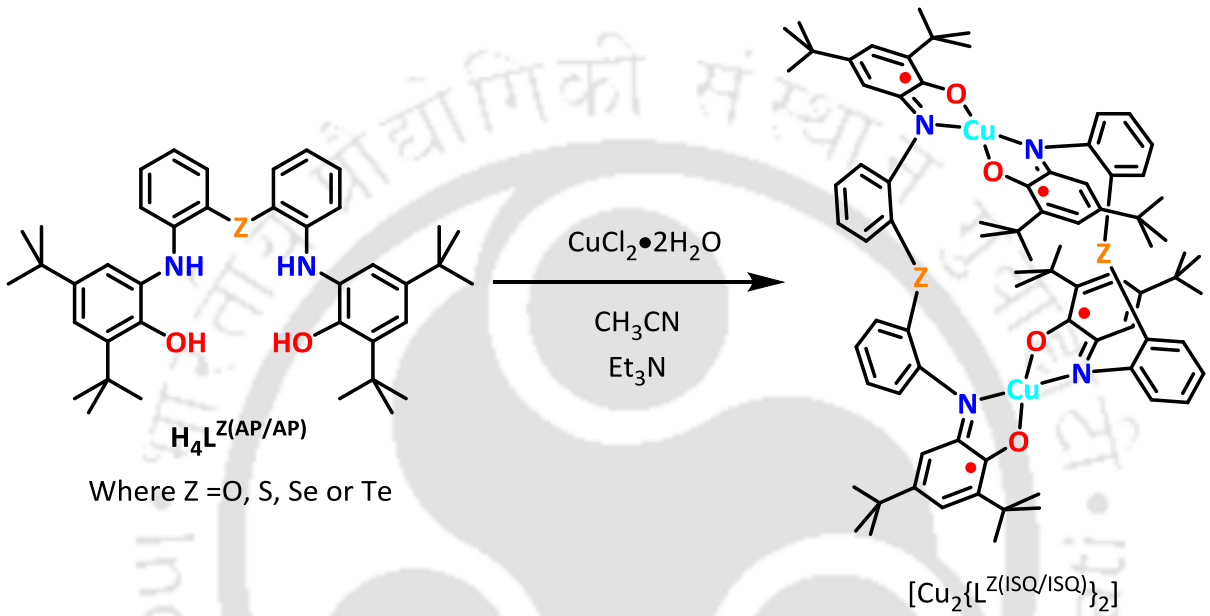

Scheme 2.8: *General synthetic route of complex **2A**, **2B**, **2C** and **2D**.*

X−ray diffraction analysis revealed that complex **2C** was dinuclear in nature and each of the two Cu(II)−ions was situated at the center of a square planar environment made up by two iminosemiquinone [$(ISQ)^{\bullet 1-}$] units (*vide infra*). Isolation of suitable single crystals for X−ray diffraction analysis of other three analogues (**2B**, **2C** and **2D**) was unsuccessful. However, several spectroscopic studies (*vide infra*) emphasized that all four complexes have same type of bonding mode and might have similar type of structure *i.e.* dinuclear tetraradical–containing Cu(II) structure as found for **2C**.

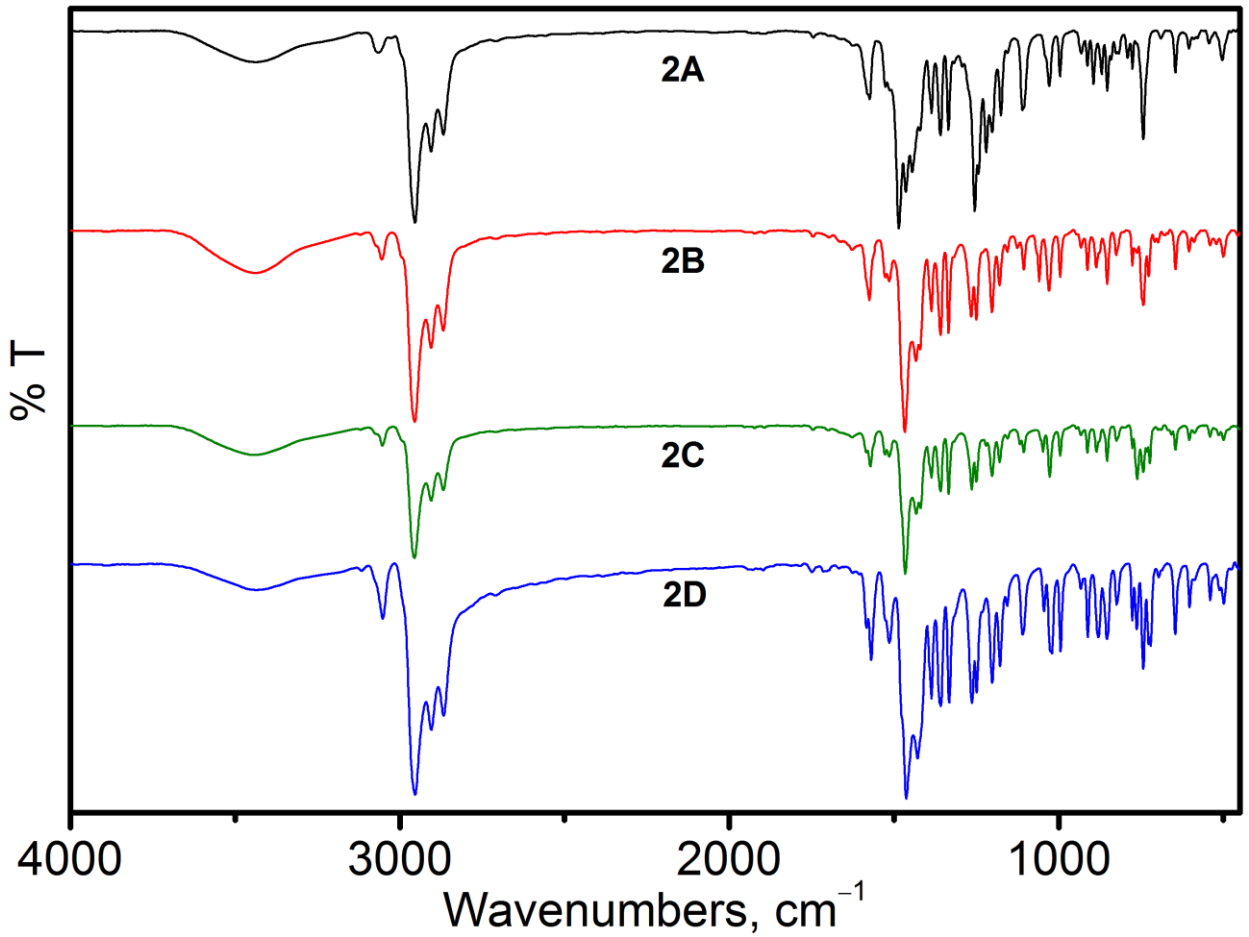

Figure 2.7: *IR spectra of **2A**, **2B**, **2C** and **2D**.*

Coordination of copper ion with N–H and O–H deprotonated aminophenol unit, *i.e.*, amidophenolate, was indicated by the absence of sharp peaks at the range 3100–3600 cm^{-1} in infrared spectra (Fig. 2.7). A weak band corresponding to aryl ν(C−H) stretching observed at around 3055 cm^{-1}.[6a] The existences of three sharp bands at around 2905, 2868 and 2905 cm^{-1} were due to asymmetric, overtone and symmetric stretching of ν(C−H).[6a,c,d] Those bands implied the coordination of the copper ion with *tert*–butyl group containing ligand backbone. Two peaks at around 1572 cm^{-1} and 1470 cm^{-1} were due to ν(C⋯N) and ν(C⋯O) stretching, respectively.[8] Those bands implied that the existence of aminophenolate moieties as its one–electron oxidized iminosemiquinone [(ISQ)$^{\bullet 1-}$] form.

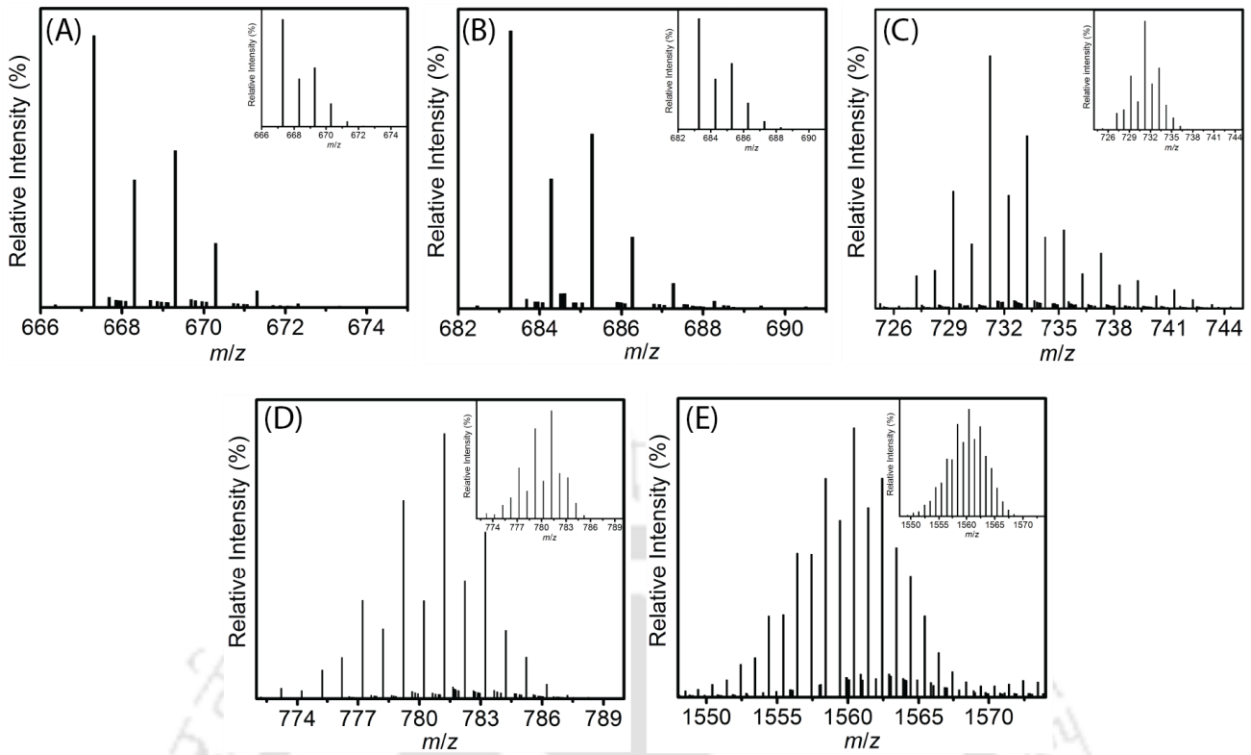

Figure 2.8: *ESI–mass spectra of [A] for complex **2A**, [B] for complex **2B**, [C] for complex **2C** (30%), [D] for complex **2D** and **[E]** for complex **2D** (5 %); experimental and simulated isotope distribution pattern (inset).*

Electrospray ionization mass spectrometry (ESI–MS) measurement of the complexes in CH_3CN provided a 100% molecular ion peaks at *m*/*z* = 667.30 [**2A**]; 683.28 [**2B]**; 781.22 [**2D**] and a 30% peak at *m*/*z* = 731.23 [**2C**]. Parenthesis indicated the complexes. Experimental and simulated isotope distribution pattern supported the composition as $[C_{40}H_{48}N_2O_2ZCu]^+$ and the composition were corresponded to half fragmented part of the dinuclear complex. Only for the case of **2D**, a peak corresponding to the dinuclear copper complex was found at *m*/*z* = 1560.43 but the relative intensity was only 5%. Isotope distribution pattern of the observed mass peak at *m*/*z* = 1560.43 confirmed the composition of **2D** as $[C_{80}H_{96}N_4O_4Te_2Cu_2]^+$.

An aerial reaction of $\mathbf{H_4L^{Se(AP/AP)}}$ with $CuCl_2{\bullet}2H_2O$ (1:1) in CH_3CN in presence of Et_3N produced an X−band EPR inactive green solid (**2C**). Recrystallization of the solid from a $CHCl_3/CH_3CN$ (3:1) solvent mixture provide a crystalline compound suitable for single−crystal X−ray diffraction study. ORTEP presentation of the molecular structure of complex **2C** is depicted in Fig. 2.9.

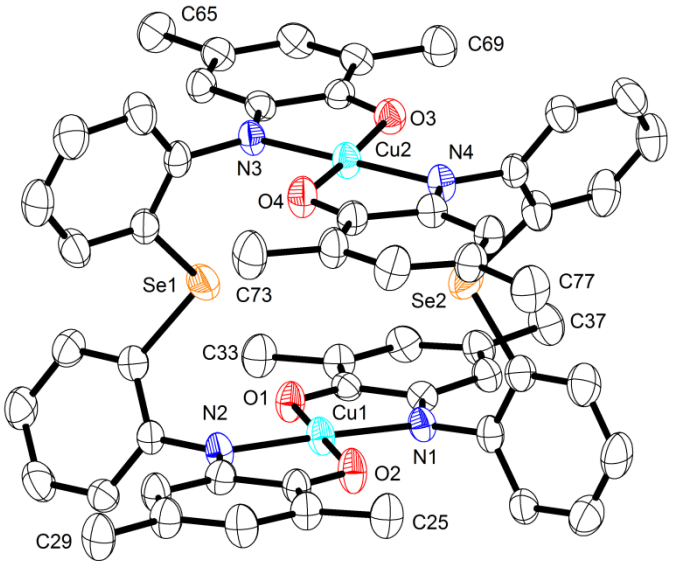

Figure 2.9: *ORTEP representation of complex **2C**; thermal ellipsoids were drawn at 40 % probability level; H atoms, solvent molecule and methyl groups attached to C25, C29, C33, C37, C65, C69, C73 and C77 were omitted for clarity.*

The crystal structure of **2C** has been measured at 293(2) K by single crystal X–ray diffraction technique. The complex was crystallized in the triclinic space group *'P–1'*. The neutral complex was consisted of two similar tetra–coordinated Cu geometry, where each Cu atom was coordinated to two amidophenolate units that belonged to two different ligand molecules. Due to such type of binding, each Cu–ion was situated at center of square planar binding core. The bond length between the metal ions and ligating atoms were found as Cu1–O1 = 1.917(4), Cu1–O2 = 1.907(4), Cu2–O3 = 1.930(4), Cu2–O4 = 1.915(4), Cu1–N1 = 1.936(4), Cu1–N2 = 1.939(4), Cu2–N3 = 1.925(4) and Cu2–N4 = 1.934(4) Å. Those values suggested the +II oxidation state of each of the coordinated metal ion in the complex **2C**.[2b,3,9] Each ligand–backbone was composed of four C_6 rings and among them, two C_6 rings (*i.e.* aminophenolate units) contained two *tert*–butyl groups. Quinoid–type distortion *i.e.* short–long–short C–C bonds followed by three successive long C–C bond distances were observed in the *tert*–butyl groups containing C_6 rings. All the C–N and C–O bonds attached to the *tert*–butyl groups–containing C_6 rings have bond distances 1.334±0.003 Å and 1.293±0.002 Å, respectively. This implied partial double bond character of those bonds.[2b,3,9] Quinoid–distortion of those C_6 rings and the partial double bond character of attached C–N and C–O bonds emphasized that all the four amidophenolate units existed in their one electron oxidized iminosemiquinone ($ISQ^{\bullet 1-}$) form in the complex. All the four other C_6 rings having C–C bond distances in the range 1.388±0.019 Å, which were indicative of phenyl form of the rings. Those four C_6 rings and the two bridging Se

atoms were involved as two bridging units between two square planar Cu(II) units. Thus the dinuclear Cu(II) complex (**2C**) achieved a double decker type of structure.

Table 2.2: *Selected bond distances (Å) and angels (°) for complex* ***2C.***

Cu1–O2	1.907(4)	C1–C2	1.453(7)
Cu1–O1	1.917(4)	C2–C3	1.419(7)
Cu1–N1	1.936(4)	C4–C3	1.366(8)
Cu1–N2	1.939(4)	C4–C5	1.421(8)
Cu2–O4	1.915(4)	C6 C5	1.365(8)
Cu2–N3	1.925(4)	C6–C1	1.417(7)
Cu2–O3	1.930(4)	C13–C14	1.426(8)
Cu2–N4	1.934(4)	C14–C15	1.362(8)
Se1–C48	1.920(6)	C16–C15	1.422(8)
Se1–C24	1.920(6)	C17–C16	1.367(8)
Se2–C12	1.917(6)	C18–C17	1.423(7)
Se2–C60	1.923(6)	C18–C13	1.447(7)
O2–C18	1.292(6)	C42–C41	1.418(7)
O1–C2	1.295(6)	C42–C43	1.355(8)
O3–C46	1.295(6)	C44–C43	1.424(8)
O4–C58	1.293(6)	C44–C45	1.372(8)
N1–C1	1.333(6)	C46–C45	1.429(8)
N1–C7	1.422(6)	C41–C46	1.459(7)
N2–C13	1.337(7)	C53–C54	1.411(8)
N2–C19	1.417(6)	C54–C55	1.369(8)
N3–C41	1.331(7)	C55 C56	1.420(8)
N3–C47	1.436(7)	C56–C57	1.370(8)
N4–C53	1.331(7)	C58–C57	1.425(8)
N4–C59	1.423(7)	C53–C58	1.451(8)
O2–Cu1–O1	179.1 (2)	O4–Cu2–O3	176.1(2)
O2–Cu1–N1	95. 8(2)	N3–Cu2–O3	83.3(2)
O1–Cu1–N1	83.5(2)	O4–Cu2–N4	83.6(2)
O2–Cu1–N2	83.7(2)	N3–Cu2–N4	179.5(2)
O1–Cu1–N2	97.0 (2)	O3–Cu2–N4	97.2(2)
N1–Cu1–N2	178.0(2)	C48–Se1–C24	100.0(2)
O4–Cu2–N3	95.9(2)	C12–Se2–C60	100.2(3)

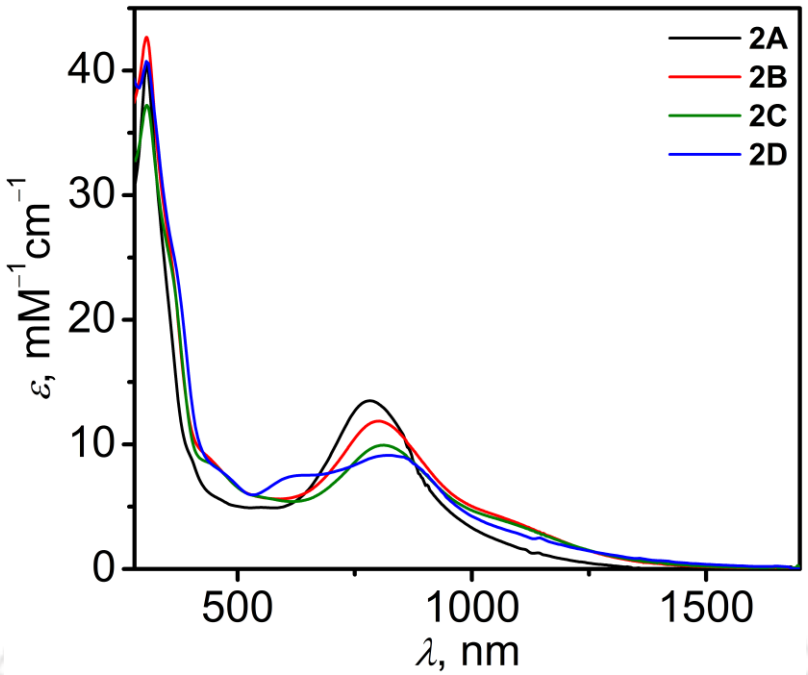

Figure 2.10: *UV−Vis/NIR spectra of complex **2A**, **2B**, **2C** and **2D**.*

Electronic absorption spectra of **2A**, **2B**, **2C** and **2D** were measured in dichloromethane at room temperature and all of them have shown almost similar type of spectrum feature (Fig. 2.10). The absorption bands at around λ_{max} = 450 nm corresponded to metal–to–ligand charge transfer. A very intense (ε > 5350 $M^{-1}cm^{-1}$) absorption maximum was observed at a range 780−830 nm for each of the complexes. The band was due to spin– and dipole– allowed ligand–to–ligand charge transfer.[3a,e,9b] The broad band above 1000 nm were due to intraligand (IL) charge transfer. [3a,e,9b] Thus the electronic absorption spectra suggested the existence of Cu(II)–bis(iminosemiquinone) moiety in the molecule.

Table 2.3: *UV–Vis/NIR data of complex **2A, 2B, 2C** and **2D**.*

Complex	λ, nm (ε, $M^{-1}cm^{-1}$)
2A	1072^{br} (2100), 784 (13500), 403^{sh} (8400)
2B	1080^{br} (3950), 802 (11850), 450^{sh} (8500)
2C	1074^{br} (3800), 811 (9950), 452^{sh} (8250)
2D	1070^{br} (3200), 825 (9100), 620 (7500), 460^{sh} (8000)

Superscript ‘sh’ and ‘br’ stands for shoulder and broad band respectively.

2.4: Synthesis and Characterizations of an Unprecedented Cu(II) Complex Obtained from Ligand $H_4L^{S(AP/AP)}$

An 1:2 reaction between ligand $\mathbf{H_4L^{S(AP/AP)}}$ and $CuCl_2{\bullet}2H_2O$ in CH_3CN in presence of Et_3N provided an distorted octahedral Cu(II) complex **2E** in 52% of yield under air (Scheme 2.9).

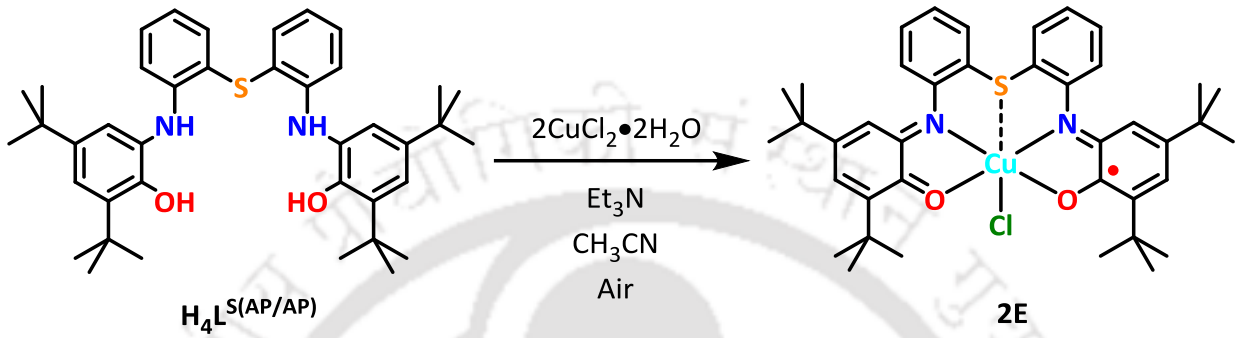

Scheme 2.9: *Synthetic route of complex **2E**.*

Generally, non–innocent ligand moiety aminophenolate undergo coordination with metal centre as its one–electron oxidised iminosemiquinone $[ISQ]^{\bullet 1-}$ form. [2b,3,9] However, the single crystal X–ray diffraction analysis confirmed that in the complex, one of the two 2–anilido–4,6–di–*tert*–butylphenol arms was present in its one–electron oxidized iminosemiquinone$[ISQ]^{\bullet 1-}$ form, while, the other was in its two electron oxidized iminoquinone $[IBQ]^0$ form. This type of coordination was not observed at normal condition. The monoradical–containing Cu(II) complex was diamagnetic in nature owing to a strong antiferromagnetic coupling between the single electron containing $d_{x^2-y^2}$ magnetic orbital of Cu(II)–ion and the radical–centered unpaired electron. Formation of complex **2E** proceeded through the initial generation of an air stable green solid (**2B**). The several spectroscopic techniques revealed the similarity of complex **2B** with dinuclear copper complex **2C** (discussed at section 2.2).

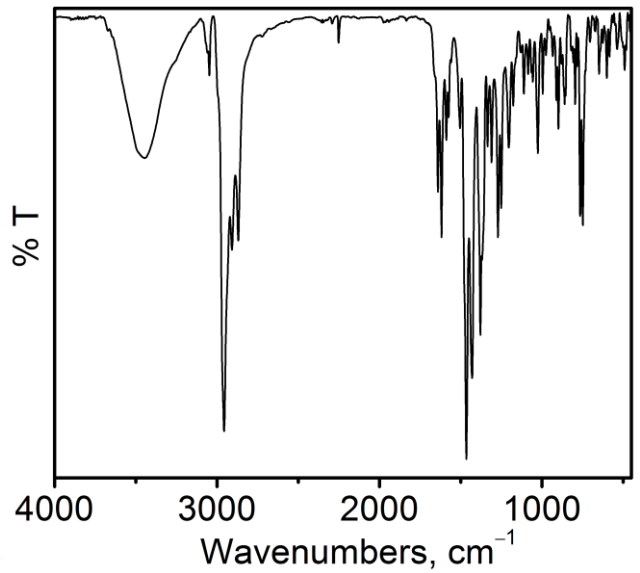

Figure 2.11: *IR spectrum of* ***2E*****.**

Infrared (IR) spectroscopic analysis indicated that Cu(II) was coordinated with the deprotonated aminophenol units and this type of coordination was confirmed by the disappearance of ν(O–H), ν(N–H) stretching bands at 3434, 3358 and 3335 cm^{-1}. The presence of bands at 2956, 2908 and 2869 cm^{-1} further emphasized the metal coordination with the *tert*–butyl group–containing ligand backbone.[6a,c,d] The presence of free acetonitrile molecule in crystal–void space was confirmed by a weak band at 2242 cm^{-1}. The coordination of Cu(II) center with a iminoquinone $[IBQ]^0$ moiety was confirmed by presence of ν(C=O), ν(C=N) stretching bands at 1640 and 1618 cm^{-1}, respectively.[10a] In addition with this, the existence of iminosemiquinone $[ISQ]^{\bullet 1-}$ unit was further revealed by the presence of peaks at around 1589 cm^{-1} and 1465 cm^{-1}. The peaks were due to ν(C⋯N) and ν(C⋯O) stretching unis, respectively.[8] Thus, infrared spectroscopic analysis revealed the presence of metal coordinated iminoquinone $[IBQ]^0$ and iminosemiquinone $[ISQ]^{\bullet 1-}$ moieties within the molecule.

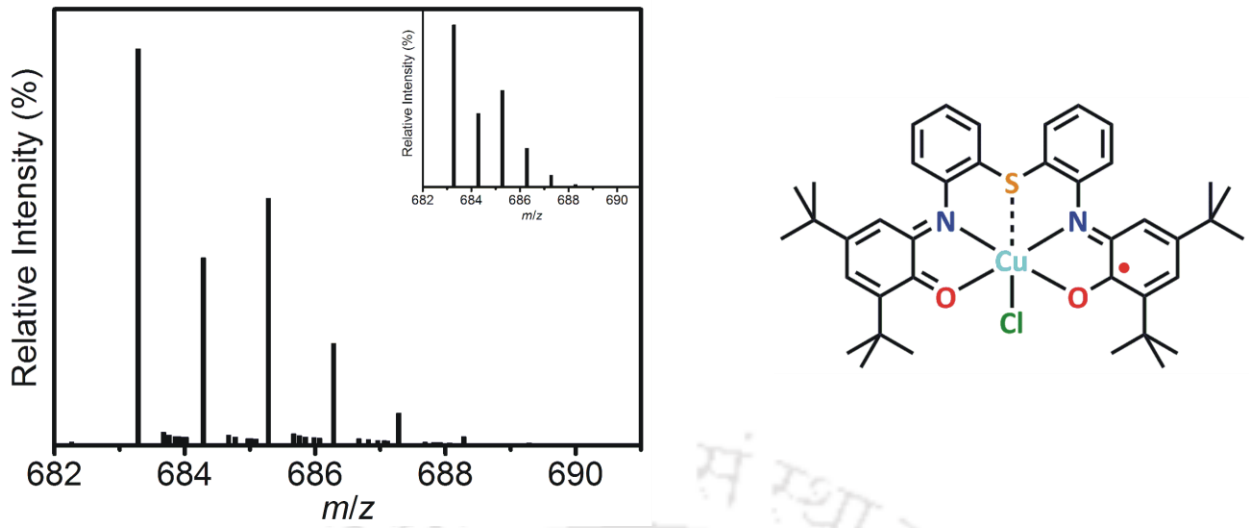

Figure 2.12: *ESI–mass spectrum of **2E** in +ve mode; experimental and simulated isotope distribution pattern (inset).*

Electrospray ionization mass spectrum (ESI–MS) of complex **2E** in CH_3CN (Fig. 2.12) provided a 100% molecular ion peak at *m/z* = 683.28 in positive mode. Experimental and simulated isotope distribution pattern confirmed the molecular ion peak as $[M–Cl]^+$ with the composition $[C_{40}H_{48}CuN_2O_2S]^+$.

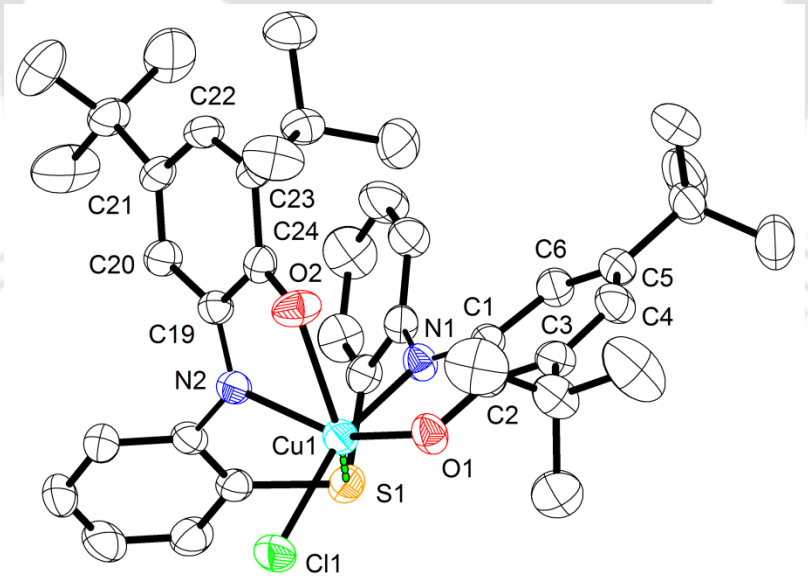

Figure 2.13: *ORTEP representation of **2E;** thermal ellipsoids were drawn at 50 % probability level. H atoms and solvent molecule were omitted for clarity.*

Crystal suitable for X–ray crystallographic analysis was obtained by slow evaporation of solution of **2E** from a 5:2 CH_2Cl_2/CH_3CN solvent mixture and crystal structure was measured at 296(2) K. The complex crystallized in the monoclinic space group '$P2_1/n$'. The ORTEP presentation of the molecular structure of complex **2E** is depicted in Fig. 2.13.

In the neutral complex, the central Cu1 atom was six–coordinate with a highly distorted octahedral geometry. The ligand backbone was composed of mainly four C_6 rings. Among them, two C_6 rings each contained two *tert*–butyl groups, while the other two did not. Interestingly, alternating short–long–short C–C bond distances followed by three long bond distances were observed in the *tert*–butyl group–containing two C_6 rings. This type of distortion is known as quinoid–type distortion and has previously been observed for one–electron as well as two–electron oxidized phenyl ring systems.[2*b*,3,10,11] All the C–C bond distances of the other two C_6 rings were almost the same and were within the 1.39 ± 0.01 Å range as expected for fully reduced phenyl rings. The C1–N1 = 1.354(3) and C2–O1 = 1.284(4) Å bond distances were in between of their characteristic single bond and double bond values and indicated a partial double bond character for both the bonds.[3] These partial double bond characterizing C–N and C–O bonds along with the quinoid–type distortion emphasized an one–electron oxidized iminosemiquinone $[ISQ]^{\bullet 1-}$ form for the C6 ring composed of C1–to–C6 atoms.[3] The C19–N2 = 1.303(4) and C24–O2 = 1.229(3) Å bond distances were in accord with their characteristic double bond values, and hence, the quinoid–type distortion acquiring C6 ring, which is constituted by C19–to–C24 atoms, along with C19–N2 and C24–O2 represented its two electron oxidized iminoquinone $[IBQ^0]$ form.[10] Note that the angle between the iminosemiquinone C6 (C1–to–C6) plane and the iminoquinone C6 (C19–to–C24) plane was ∼58°.

Two different oxidation states of the *tert*–butyl group containing two C_6 rings were further reflected by Cu–N and Cu–O bond distances. The Cu1–N1 = 1.973(3) and Cu1–O1 = 1.967(2) Å bond distances were expectably found to be much shorter compared to Cu1–N2 = 2.108(2) and Cu1–O2 = 2.418(2) Å bond distances, and were in accord with the previously reported Cu(II)–O_{ISQ} and Cu(II)–N_{ISQ} bonds [O_{ISQ} and N_{ISQ} represent the O atom and the N atom of an iminosemiquinone moiety attached to the Cu(II) atom], and Cu(II)–O_{IBQ} and Cu(II)–N_{IBQ} bonds [O_{IBQ} and N_{IBQ} represent the O atom and the N atom of an iminoquinone moiety attached to the central Cu(II) atom], respectively.[2*b*,3,10,11] Hence, from the X–ray crystallographic analysis it was evident that the two non–innocent 2–anilido–4,6–di–*tert*–butylphenolate moieties, which were bridged by the S1 atom with a bridging angle of ∼100°, were present in complex **2E** in two different oxidation states. The overall formal charge of the ligand in the complex was –I and the neutrality of the complex was maintained by the coordination of a mononegative chloride ion [Cu(II)–Cl1 = 2.219(1)].

Table 2.4: *Selected bond distances (Å) and angels (°) for complex* ***2E*****.**

Cu1–O1	1.967(2)	C1–C6	1.415(4)
Cu1–N1	1.973(3)	C1–C2	1.443(4)
Cu1–N2	2.108(2)	C2–C3	1.440(4)
Cu1–Cl1	2.219(1)	C3–C4	1.364(5)
Cu1–O2	2.418(2)	C5–C4	1.426(5)
S1–C13	1.774(3)	C6–C5	1.358(4)
S1–C12	1.776(3)	C19–C20	1.435(4)
O1–C2	1.284(4)	C19–C24	1.515(4)
O2–C24	1.229(3)	C21–C20	1.336(4)
N1–C1	1.354(3)	C21–C22	1.470(4)
N1–C7	1.405(4)	C23–C22	1.344(4)
N2–C19	1.303(4)	C23–C24	1.470(4)
N2–C18	1.432(4)		
O1–Cu1–N1	82.1(1)	C13–S1–C12	99.8(1)
O1–Cu1–N2	153.6(1)	C2–O1–Cu1	113.2(2)
N1–Cu1–N2	93.6(1)	C1–N1–C7	123.6(3)
O1–Cu1–Cl1	98.2(1)	C1–N1–Cu1	112.6(2)
N1–Cu1–Cl1	160.4(1)	C7–N1–Cu1	122.8(2)
N2–Cu1–Cl1	94.4(1)	C24–O2–Cu1	107.6(2)
O1–Cu1–O2	82.2(1)	C19–N2–C18	120.4(2)
N1–Cu1–O2	84.9(1)	C19–N2–Cu1	118.8(2)
N2–Cu1–O2	71.4(1)	C18–N2–Cu1	120.3(2)
Cl1–Cu1–O2	114.6(1)		

The electronic absorption spectrum was recorded in dichloromethane solution (Fig. 2.14) and the electronic transition along with the extension coefficient has been summarized in Table 2.5.

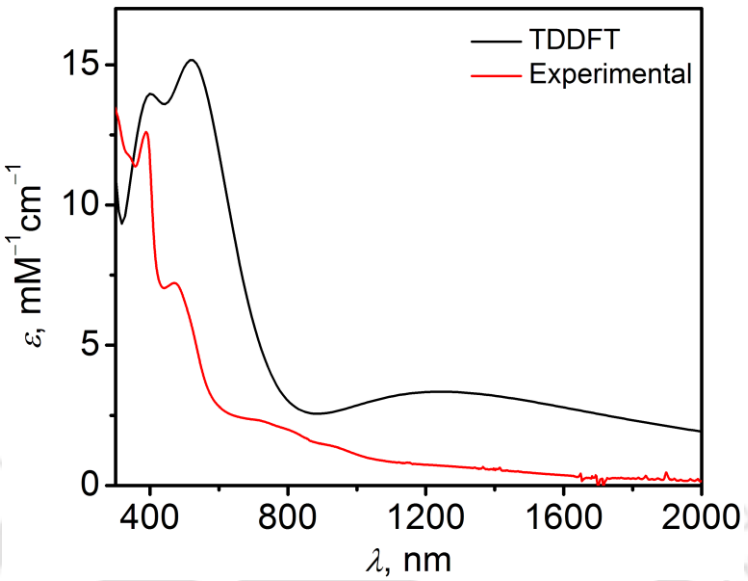

Figure 2.14: *Experimental UV–Vis/NIR spectrum of **2E** (red line) in CH_2Cl_2; theoretically (TDDFT) obtained spectrum (black line).*

Time dependent density functional theory (TDDFT) calculations have been performed in the dichloromethane solvent (ε = 8.93) with the optimized geometry (Fig. 2.15) using 50 singlet states at the B3LYP/6−31G(d,p) level of theory in order to rationalize the experimentally observed UV−Vis/NIR absorption bands (Fig. 2.14) of **2E**. The bond length parameter of the optimized geometry is summarized in 'Appendices' section. The selection of CH_2Cl_2 for TDDFT calculations was due to the record of experimental absorption spectra in the medium.

Table 2.5: *UV–Vis/NIR data of complex **2E**.*

Complex	λ, nm (ε, $M^{-1}cm^{-1}$)
2E	1180^{br}(800), 940^{sh}(1400), 800^{sh}(2000), 720^{sh}(2300), 475(7250), 385 (12550)

Superscript 'sh' and 'br' stands for shoulder and broad band, respectively.

The absorption wavelength at 381 nm (experimental absorption = 386 nm) corresponded to the intraligand charge transfer.[12a,b] The experimental absorption band at 475 nm was because of ligand–to–metal charge transfer (LMCT) as obtained with TDDFT calculations at 490 nm. The frontier molecular orbitals responsible for the electronic transition at λ = 490 nm were HOMO–4 to LUMO+1 (Fig. 2.15). The absorption band at 941 nm was due to metal–to–ligand charge transfer, and the frontier molecular orbitals showed the electronic transition from HOMO−1 to LUMO+1 (Fig. 2.15) for the band. The TDDFT results also showed an absorption

band at 1172 nm. The frontier molecular orbital analysis suggested that the band appeared due to an intramolecular ligand–to–ligand charge transfer process where a transition occurs from the HOMO of one *tert*–butyl group–containing phenyl ring A to the other *tert*–butyl group–containing phenyl ring B (LUMO+1) (Fig. 2.15).

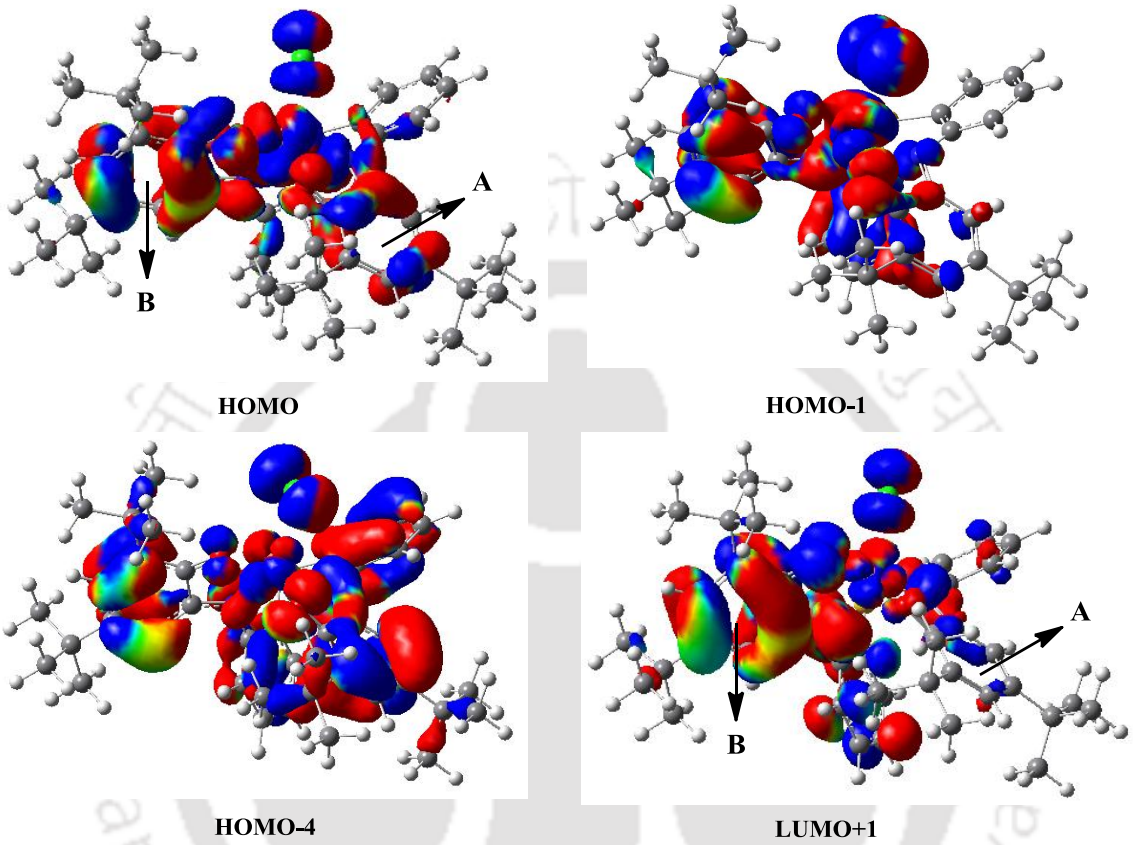

Figure 2.15: *B3LYP/6–31G (d,p) calculated frontier molecular orbitals for a complex in dichloromethane (white = H, gray = C, blue = N, red = O, lime = Cl, and coral = Cu).*

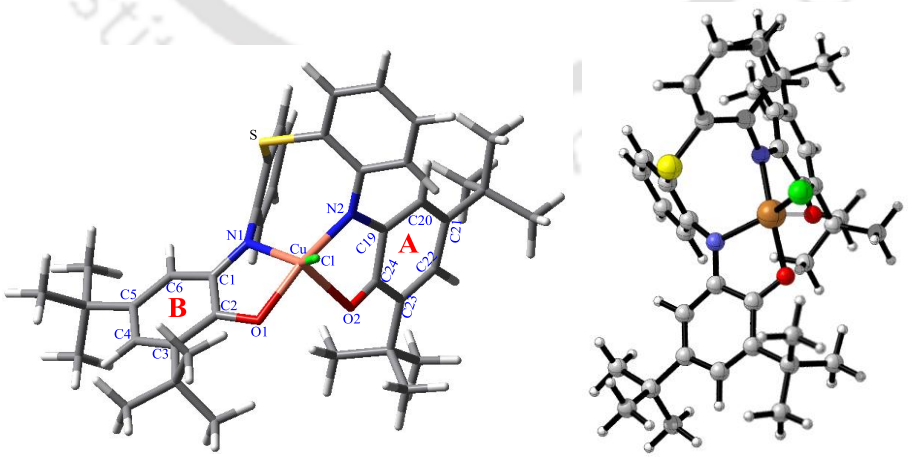

Figure 2.16: *The optimized geometry of complex **2E** at the B3LYP/6–31G (d, p) level of theory (white = hydrogen, gray = carbon, blue = nitrogen, red = oxygen, lime = chlorine and coral = copper).*

Complex **2E** acquired two paramagnetic centers; (i) a Cu(II) center ($3d^9$, $S_{Cu(II)} = 1/2$) and (ii) a radical ($S_R = 1/2$). Depending on their coupling fashions, $S_t = 1$ or $S_t = 0$ ground states would be formed. Magnetic susceptibility measurement of the complex in solid state has been measured at 1T and resulted μ_{eff} *vs.* T plot is represented on Fig. 2.17.

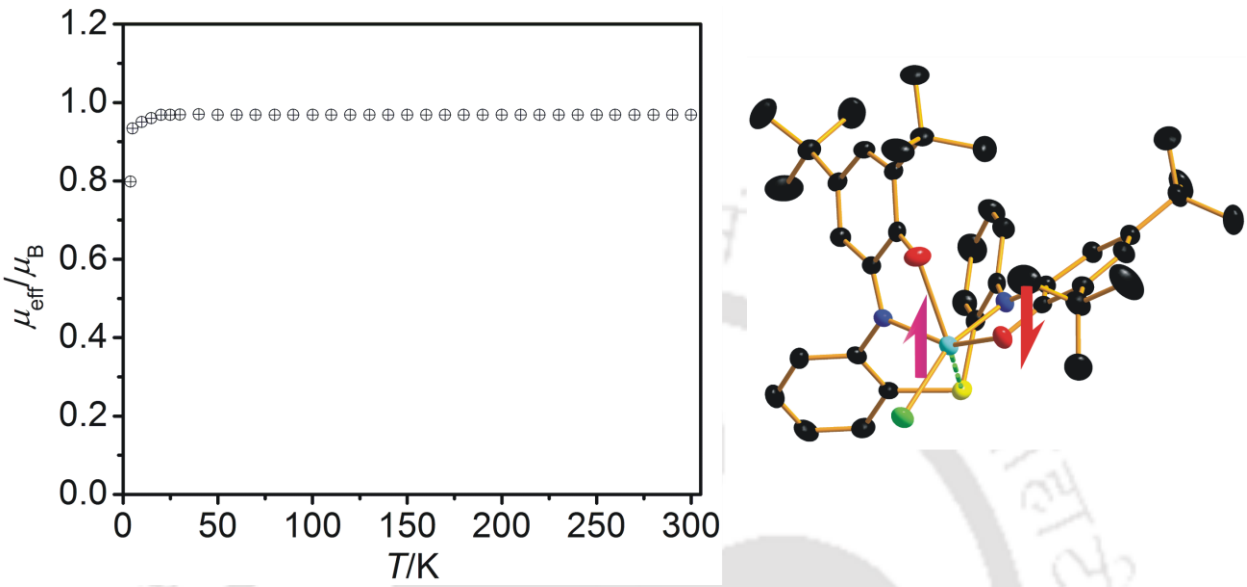

Figure 2.17: *The μ_{eff} vs. T plot of complex **2E** and corresponding coupling patterns among the spins.*

Variable–temperature (2–300 K) magnetic susceptibility measurements showed a constant effective magnetic moment value ($\mu_{eff} = 0.96\ \mu_B$) in the temperature range (Fig. 2.17). This lower value was the indication of existences of antiferromagnetic coupling between the two paramagnetic centers. Thus, the magnetic susceptibility measurement of the mononuclear Cu(II) complex **2E** suggest the diamagnetic nature of the complex.

The electrochemical behavior of complex **2E** was studied by cyclic voltammetry. Cyclic voltammograms (CVs) have been recorded in CH_2Cl_2 solutions containing 0.10 M $[(^nBu)_4N]ClO_4$ as a supporting electrolyte at a glassy carbon working electrode, a platinum wire counter electrode and an $Ag/AgNO_3$ reference electrode. Ferrocenium hexafluorophosphate ($FcPF_6$) was used as an internal standard and all the potentials have been referenced *vs.* Fc^+/Fc couple.

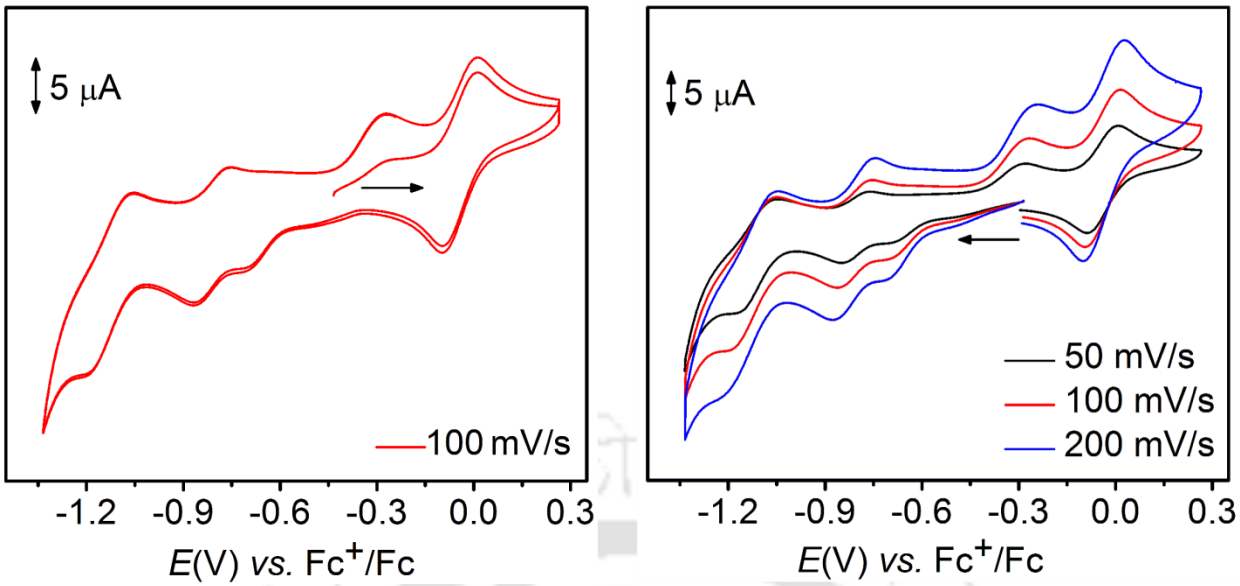

Figure 2.18: *Cyclic voltammograms of complex **2E** measured in a CH_2Cl_2 solution. Left: two consecutive cycles. Right: rate dependence.*

Complex **2E** was composed of one fully oxidized iminoquinone, one one–electron oxidized iminosemiquinone, and one chloride unit. The complex underwent a one–electron oxidation at +0.02 V (Fig. 2.18) and, consequently, the formation of a fully oxidized Cu(II)–diquinone species took place. This species underwent four successive one–electron reductions at −0.10, −0.27, −0.88, and −1.21 V, respectively (Fig. 2.18), and presumably generated a Cu(II)–diamidophenolate species.[3] While the first two oxidation potentials of the reduced species were separated by 0.15 V and 0.13 V than those of the corresponding reduction potentials, the third oxidation potential had a 0.44 V separation than that of the corresponding reduction potential. This could be due to structural changes, *i.e.* loss of chloride ions followed by reduction or vice versa.

2.5: Probable Pathways of Formation of 2E from ligand $H_4L^{S(AP/AP)}$

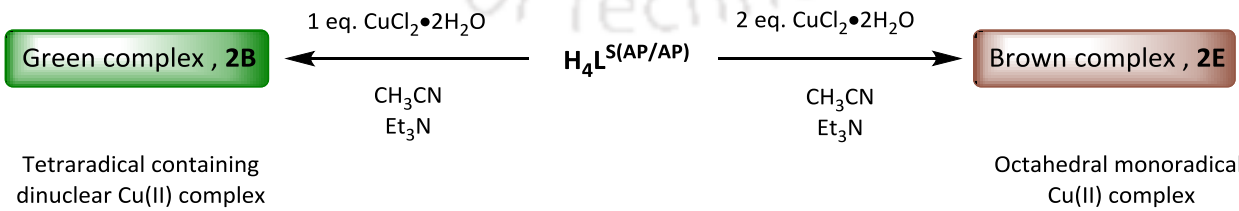

Scheme 2.10: *Reactivity of ligand $H_4L^{S(AP/AP)}$ with $CuCl_2•2H_2O$ in CH_3CN in presence of Et_3N.*

The formation of complex **2E** required two equivalents of $CuCl_2•2H_2O$ compared to one equivalent of ligand $\mathbf{H_4L^{S(AP/AP)}}$ and the formation of **2E** was preceded through the initial

generation of green complex (**2B**), which was X–band EPR silent. Structural determination of the complex has not been possible due to solubility problems and the unsatisfactory single crystal quality. However, a very close resemblance of the UV–Vis/NIR spectrum of the green solid (**2B**) to that of the X–band EPR inactive dinuclear tetraradical–containing Cu(II) complex (**2C**) formed with the analogous $\mathbf{H_4L}^{\mathbf{Se(AP/AP)}}$ ligand ($L^{Se(ISQ/ISQ)}$: Cu = 2 : 2; each ligand is coordinated to both Cu(II) centers) supported indirectly the dinuclear nature of the green solid.

The aerial oxidation of complex **2B** (Fig. 2.19A) was recorded by UV–Vis/NIR spectroscopic technique. In a reaction set up, O_2 gas was continuously purge through the CH_2Cl_2 solution of complex **2B**. The band at λ_{max} = 800 nm that corresponded to ligand–to–ligand charge transfer[3a,e,8b] diminished with time and a new band appeared at λ_{max} = 475 nm. The band at λ_{max} = 475 nm was assigned to π–π^* transition of the iminoquinone moiety. The spectra found after full oxidation was quite resemble with the complex **2E**. Thus, the dinuclear complex **2B** underwent ligand–centered oxidation and mononuclear complex **2E** has been formed in dichloromethane solution.

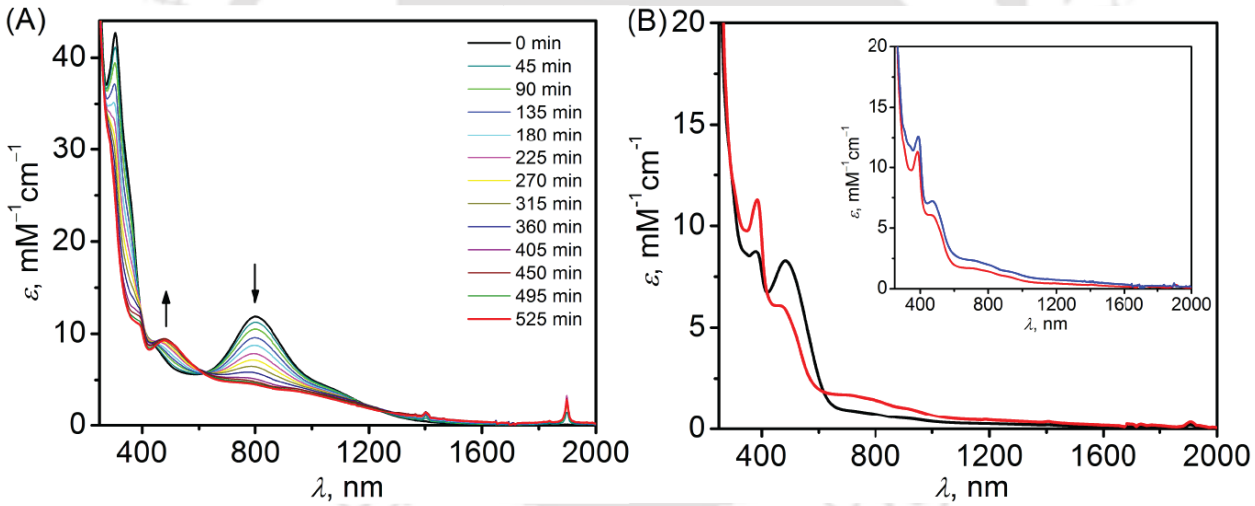

Figure 2.19: *[A] Time dependent UV–Vis/NIR change of complex **2B** in air. [B] UV–Vis/NIR spectra of; Black: Complex **2B** + 2 equivalents $CuCl_2$•$2H_2O$ in CH_3CN; Red: formed red solution + 10 μL Et_3N. Inset: Red: formed red solution + 10 μL Et_3N, blue: complex **2E** in CH_2Cl_2.*

It has been mention earlier that the formation of complex **2E** required two equivalents of $CuCl_2$•$2H_2O$ compared to one equivalent of the $\mathbf{H_4L}^{\mathbf{S(AP/AP)}}$ ligand. In order to understand the role of excess $CuCl_2$•$2H_2O$ in complex **2E** formation, 0.50 equivalent of **2B** was added in a CH_3CN solution of $CuCl_2$•$2H_2O$. The colour of the solution instantaneously became dark–red and the green solid disappeared (Fig. 2.19B, black line). The UV–Vis/NIR spectrum of the dark–red solution showed the formation of a strong band at 480 nm (ε = 8400 $M^{-1}cm^{-1}$) and indicated

the generation of a diquinone species. In fact, the spectrum corroborated the previously reported Cu(II)–diquinone species.[10] Upon addition of 10 μL of Et_3N to the red solution, the colour of the solution changed immediately to brown (Fig. 2.19B, red line) and a precipitation started slowly. The UV–Vis/NIR spectrum of the solution implied the formation of complex **2E** by a one–electron reduction of the initially formed Cu(II)–diquinone species (Fig. 2.19B, inset). Hence, it can be argued that the concentration of $CuCl_2•2H_2O$ along with Et_3N played a vital role in the formation of complex **2E** from the green compound.

Furthermore, to understand the mechanism of formation of complex **2E**, CuCl was used in place of excess amount $CuCl_2•2H_2O$. However, Cu(I) salt was unable to produce the product as well as the Cu(II)–diquinone intermediate. Therefore, it could be assumed that the reaction has followed the inner sphere mechanism.

The oxidation of intermediate **2B** led to the formation of complex **2E**. The electrochemical behaviour of **2B** was also supportive for the feasible oxidation process, which was triggered by air and $CuCl_2•2H_2O$. Cyclic voltamograms **2B** was measured in dichloromethane and depicted in Fig. 2.20. Ferrocenium hexafluorophosphate ($FcPF_6$) was used as an internal standard and all the potentials have been referenced *vs.* Fc^+/Fc couple.

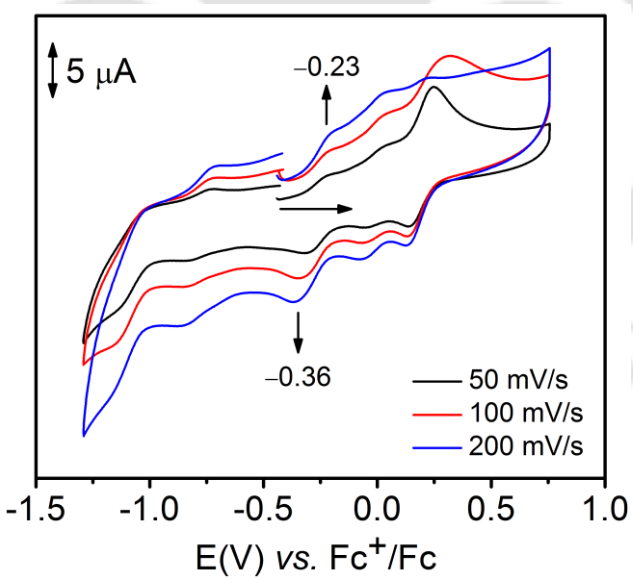

Figure 2.20: *Cyclic voltammograms of the green compound (**2B**) in CH_2Cl_2 using glassy carbon working electrode and Pt as counter electrode.*

In complex **2B**, each of the Cu(II)–ion was coordinated with two iminosemiquinone moieties. The resulted cyclic voltammograms (CV) of **2B** was not resembled with any mononuclear diradical–containing Cu(II)–bis(iminosemiquinone) form.[3a] This probably due to

existence of **2B** as the dinuclear tetraradical–containing Cu(II) complex like **2C**. All the redox waves were not well discernable but the first oxidation potential of **2B** was found quite low (–0.23 V). Thus, the oxidation of the green compound (**2B**) proceeded by the $CuCl_2 \bullet 2H_2O$ and Et_3N duo as well as air and the process was possibly favored because of low oxidation potentials of the initially formed compound.

The schematic path of the formation of complex **2E** from ligand $\mathbf{H_4L^{S(AP/AP)}}$ has been shown in Scheme 2.11.

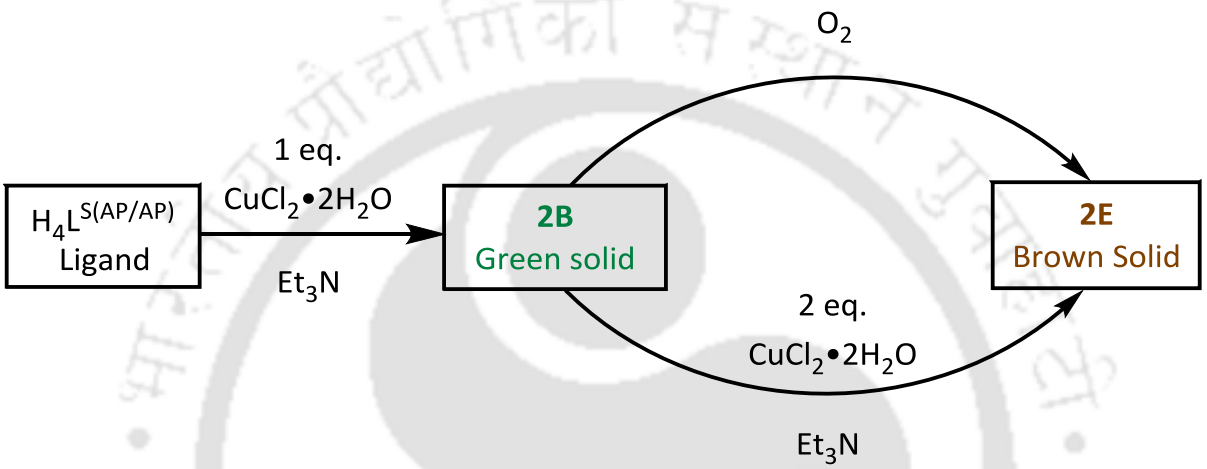

Scheme 2.11: *Proposed pathway for the generation of complex **2E**.*

2.6: Conclusions

- Orthogonality between two coordinable bidentate $\mathbf{H_2L^{AP}}$ units is achieved by placing a chalcogen (O, or S, or Se, or Te) atom as a bridge between the *ortho* positions of the aniline rings.
- Equimolar reaction between ligand $\mathbf{H_4L^{Z(AP/AP)}}$ (Where Z = O, S, Se and Te) with $CuCl_2{\bullet}2H_2O$ in CH_3CN in the presence of Et_3N provides tetraradical–containing dinuclear Cu(II) complex where each of the Cu(II)−ion is situated at the center of a square planar core, constituted by two iminosemiquinone $[(ISQ)^{\bullet 1-}]$ units.
- Ligand $\mathbf{H_4L^{S(AP/AP)}}$ provides a mononuclear pseudo octahedral Cu(II) complex (**2E**) by reacting with two equivalent $CuCl_2{\bullet}2H_2O$ in CH_3CN in presence of Et_3N at air.
- In complex **2E**, one of the two coordinated amidophenolate units is present in its two electron oxidized iminoquinone $\{[IBQ]^0\}$ form and other is in its one–electron oxidized iminosemiquinone $\{[ISQ]^{\bullet 1-}\}$ form.
- The formation of complex **2E** is proceeded through the initial generation of tetraredical–containing dinuclear Cu(II) complex (**2B**), which underwent oxidation by $CuCl_2{\bullet}2H_2O$ and Et_3N as well as air. The oxidation process is favored because of low oxidation potential of complex **2B**.

References

1. (*a*) J. Stubbe and W. A. van der Donk, *Chem. Rev.*, 1998, **98**, 705; (*b*) R. H. Holm, P. Kennepohl and E. I. Solomon, *Chem. Rev.*, 1996, **96**, 2239; (*c*) J. W. Whittaker, *Chem. Rev.*, 2003, **103**, 2347; (*d*) F. Himo, L. A. Eriksson, F. Maseras, and Per E. M. Siegbahn, *J. Am. Chem. Soc.*, 2000, **122**, 8031; (*e*) N. Ito, S. E. V. Phillips, C. Stevens, Z. B. Ogel, M. J. Mcpherson, J. N. Keen, K. D. S. Yadav and P. F. Knowles, *Nature*, 1991, **350**, 87; (*f*) N. Ito, S. E. V. Phillips, K. D. S. Yadav and P. F. Knowles, *J. Mol. Biol.*, 1994, **238**, 794; (*g*) R. Banerjee, *Chem. Rev.*, 2003, **103**, 2081; (*h*) L. Que Jr. and W. B. Tolman, *Nature*, 2008, **455**, 333; (*i*) D. L. Yin, S. Urresti, M. Lafond, E. M. Johnston, F. Derikvand, L. Ciano, J. Berrin, B. Henrissat, P. H. Walton, G. J. Davies and H. Brumer, *Nat. Commun.*,2015, 6:10197 doi: 10.1038.

2. (*a*) E. Zueva, P. H. Walton and J. E. McGrady, *Dalton Trans.*, 2006, 159; (*b*) C. Mukherjee, U. Pieper, E. Bothe, V. Bachler, E. Bill, T. Weyhermüller and P. Chaudhuri, *Inorg. Chem.*, 2008, **47**, 8943; (*c*) J–L. Pierre, *Chem. Soc. Rev.*, 2000, **29**, 251; (*d*) K. Asami, A. Takashina, M. Kobayashi, S. Iwatsuki, T. Yajima, A. Kochem, M. Gastel, F. Tani, T. Kohzuma, F. Thomas and Y. Shimazaki, *Dalton Trans.*, 2014, **43** 2283; (*e*) P. Mondal, S. P. Parua, P. Pattanayak, U. Das, and S. Chattopadhyay, *J. Chem. Sci.*, 2016, **128**, 803.

3. (*a*) P. Chaudhuri, C. N. Verani, E. Bill, E. Bothe, T. Weyhermüller and K. Wieghardt, *J. Am. Chem. Soc.*, 2001, **123**, 2213; (*b*) P. Chaudhuri and K. Wieghardt, *Prog. Inorg. Chem.*, 2001, **50**, 151; (*c*) P. Chaudhuri, K. Wieghardt, T. Weyhermüller, T. K. Paine, S. Mukherjee and C. Mukherjee, *Biol. Chem.*, 2005, **386**, 1023; (*d*) C. Mukherjee *et al.*, unpublished results; (*e*) Ye, B. Sarkar, F. Lissner, T. Schleid, J. van Slageren, J. Fiedler and W. Kaim, *Angew. Chem., Int. Ed.*, 2005, **44**, 2103; (*f*). R. Rakshit, S. Ghorai, S. Biswas and C. Mukherjee, *Inorg. Chem.*, 2014, **53**, 3333.

4. R. Metzinger, S. Demeshko and C. Limberg, *Chem. Eur. J.*, 2014, **20**, 4721.

5. (*a*) E. J. Corei and K. Achiwa, *J. Am. Chem. Soc.***,** 1969, **91**, 1429; (*b*) A. Y. Girgis, A. L. Balch, *Inorg. Chem.*, 1975, **14**, 2724.

6. (*a*) G. R. Pandhare, V. M. Shinde and Y. H. Deshpande, *Rasayan J. Chem.*, 2008, **1**, 337; (*b*) J. Coates, *Interpretation of Infrared Spectra: A Practical Approach*, John Wiley & Sons Ltd, Chichester, 2000; (*c*) D. L. Pavia, G. M. Lampman, G. S. Kriz and J. R. Vyvyan, *Introduction to Spectroscopy*, 4th edition, 31; (*d*) P. K. Kipkemboi, P. C. Kiprono and J. J. Sanga, *Bull. Chem.*

Soc. Ethiop., 2003, **17**, 211; (*e*) S. Sahoo, C. K. Chakraborti, P. K. Behera, S. C. Mishra, *Int. J. Drug Dev. & Res.*, 2011, **3**, 261.

7. (*a*) A. R. Choudhury, K. Islam, M. T. Kirchner, G. Mehta and T. N. Guru Row, *J. Am. Chem. Soc.*, 2004, **126**, 12274; (*b*) A. Lennartson, A. Hedström and M. Håkansson, *Chirality*, 2015, **27**, 425.

8. (*a*) G. Hastings and V. Sivakumar, *Biochemistry*, 2001, **40**, 3681; (*b*) J. Breton, J. Burie, C. Berthomieu, G. Berger and E. Nabedryk, *Biochemistry*, 1994, **33**, 4953; (*c*) H. Suzuki, M. A. Nagasaka, M. Sugiura and T. Noguchi, *Biochemistry*, 2005, **44**, 11323;

9. (*a*) F. Thomas, *Eur. J. Inorg. Chem.*, 2007, 2379; (*b*) C. Mukherjee, T. Weyhermüller, E. Bothe and P. Chaudhuri, *Inorg. Chem.*, 2008, **47**, 11620; (*c*) S. Ghorai and C. Mukherjee, *Chem. Asian J.*, 2014, **9**, 3518; (*d*) C. Mukherjee, T. Weyhermüller, E. Bothe, E. Rentschler and P. Chaudhuri, *Inorg. Chem.*, 2007, **46**, 9895; (*e*) A. I. Poddel'sky, V. K. Cherkasov and G. A. Abakumov, *Coord. Chem. Rev.*, 2009, **253**, 291; (*f*) S. Ghorai, A. Sarmah, R. K. Roy, A. Tiwari and C. Mukherjee, *Inorg. Chem.*, 2016, **55**, 1370; (*g*) A. Paretzki, R. Hübner, S. Ye, M. Bubrin, S. Kämper and W. Kaim, *J. Mater. Chem. C*, 2015, **3**, 4801; (*h*) D. L. J. Broere, R. Plessius and J. I. van der Vlugt, *Chem. Soc. Rev.*, 2015, **44**, 6886.

10. C. Mukherjee, U. Pieper, E. Bothe, V. Bachler, E. Bill, T. Weyhermüller and P. Chaudhuri, *Inorg. Chem.*, 2008, **47**, 2740.

11. (*a*) G. A. Abakumov, V. K. Cherkasov, V. I. Nevodchikov, V. A. Kuropatov, G. T. Yee and C. G. Pierpont, *Inorg. Chem.*, 2001, **40**, 2434; (*b*) K. J. Blackmore, J. W. Ziller and A. F. Heyduk, *Inorg. Chem.*, 2005, **44**, 5559; (*c*) C. Mukherjee, T. Weyhermüller, K. Wieghardt and P. Chaudhuri, *Dalton Trans.*, 2006, **18**, 2169; (*d*) S. Ghorai and C. Mukherjee, *Dalton Trans.*, 2014, **43**, 394.

12. (*a*) W. Li, F. Yang and Z. Wang, *Int. J. Quantum Chem.*, 2011, **111**, 2099; (*b*) S. Torres, G. Ferraudi, M. J. Aguirrea, M. Isaacsc, B. Matsuhiro, N. P. Chandĭa and L. Mendoza, *Helv. Chim. Acta*, 2011, **94**, 293.

Chapter III

*Synthesis and Characterization of Co Complexes from Chalcogen Bridged Non–Innocent Ligands**

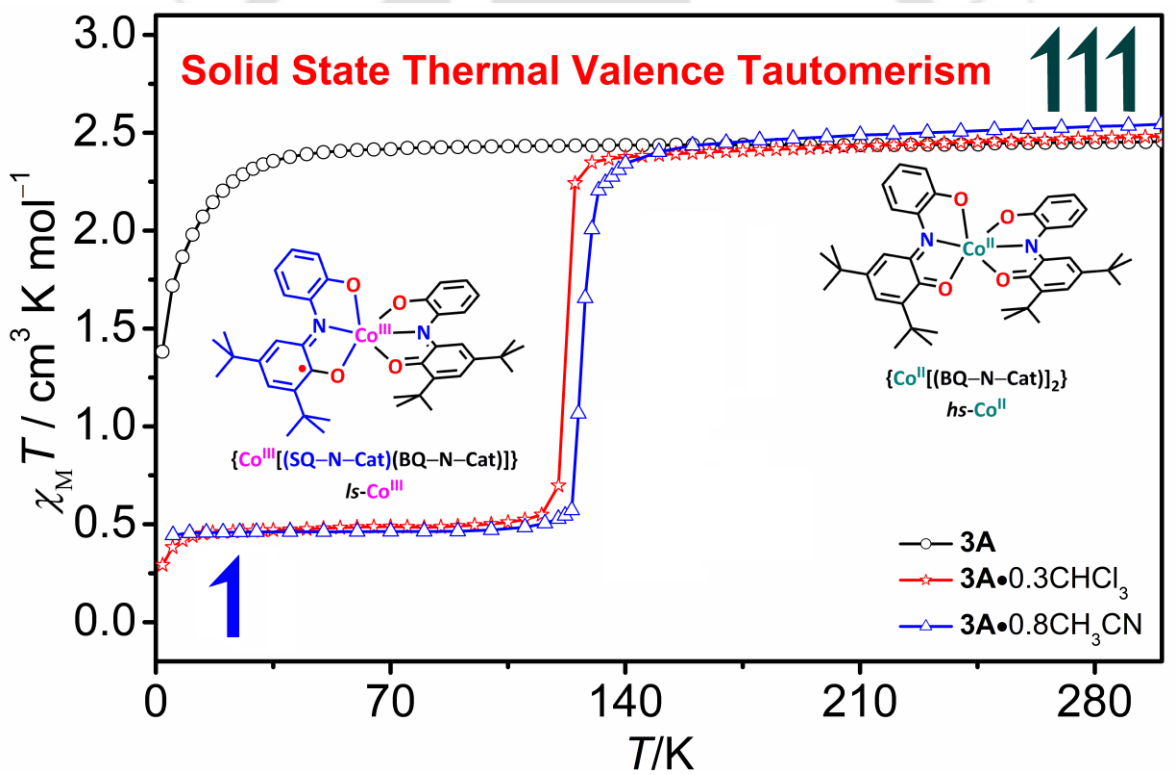

* Some results have been reported in *Chem. Commun.*, 2016, **52**, 11995.

3.1: Introduction

The reactivity of the metal complexes derived from traditional redox–inactive or innocent ligands depends upon the suitable vacant sites and the flexible oxidation states of the metal ion, while, the ligand oxidation state remains unaffected. However, the metallation of redox–active or non–innocent ligands[1] provide corresponding metal complexes, where the change in oxidation state of both metal and coordinated non–innocent ligands are feasible for oxidative addition reactions.[1,2] A schematic representation of oxidative addition to both innocent and non–innocent ligands–coordinated metal complexes[2a,3] are shown in Scheme 3.1. In the complexes, non–innocent ligands: (I) act as electron reservoir, (II) modify the Lewis acidity of the central metal ion, (III) generate ligand–centered radical moiety and (IV) participate in single–electron transfer to metal or substrate.[2a]

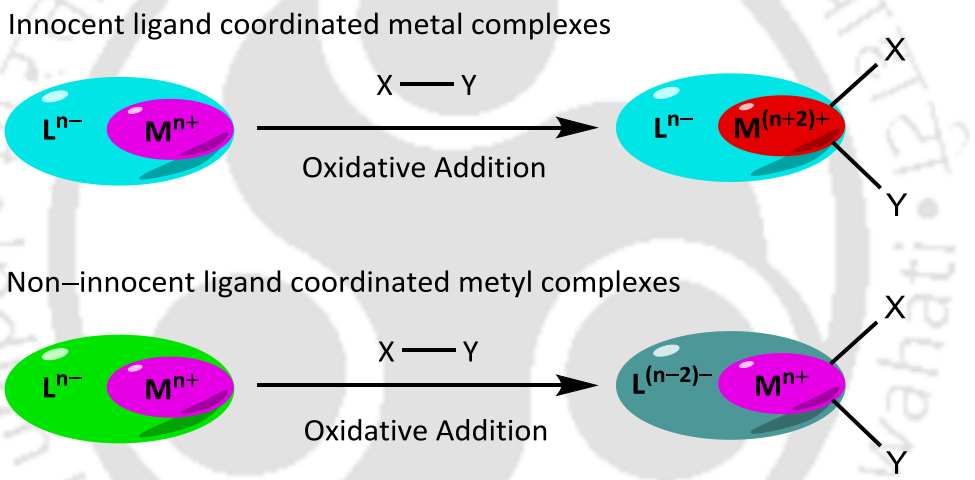

Scheme 3.1: *Schematic presentation of oxidative addition to innocent and non–innocent ligand coordinated metal complexes.*

Noteworthy, the non–innocent ligands coordinated Co–complexes have achieved great importance in the field of biomimetic catalysis, C–H bond activation, C–C cross coupling, C–N bond activation, bistable as well as valence tautometic complex formation, etc.[4–6] Soper *et al.* have reported that the electrophilic and nucleophilic behaviors of square planar Co(III) complexes depend on the redox state of the coordinated redox–active ligands (Scheme 3.2).[5a] Redox–active ligand–coordinated cobalt complexes have recently been reported as catalysts for C–C coupling reactions.[5a,c]

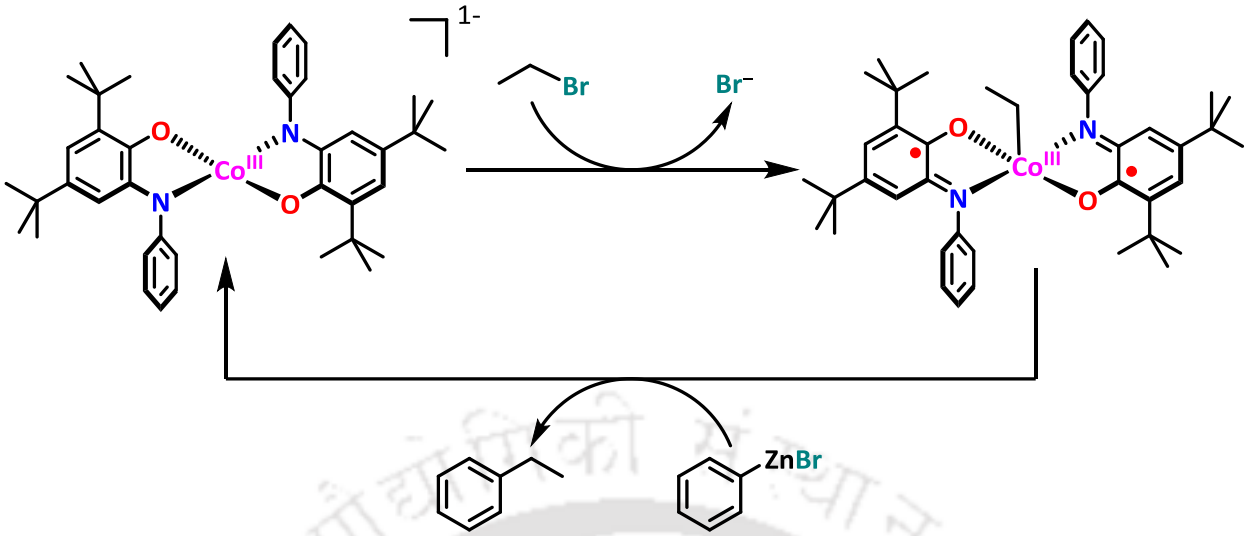

Scheme 3.2: *Schematic presentation of Negishi–like C–C cross–coupling reaction reported by Soper et al.*[5a]

Apart from the catalytic reactivity, valence tautomerization between Co(III)–semiquinone to Co(II)–quinone electronic isomers are under progressive investigation for the demand of logic gates, bistable and spin–switch materials developments.[6] Thus, the study of cobalt complexes that are coordinated to redox–active ligands has drawn special attention.

2–Anilino–4,6–di–*tert*–butylphenol ($\mathbf{H_2L^{AP}}$) is an established bidentate non–innocent ligand.[7] The square planar Co(III) complex that formed by the coordination of two equivalents of $[\mathbf{L^{AP}}]^{2-}$ ligand, $[\mathbf{Co^{III}([L^{AP}]^{2-})_2}]^-$, is known to behave as a strong nucleophile and undergoes $2e^-$ oxidative addition with alkyl halides. In this process, each $[L^{AP}]^{2-}$ ligand undergoes one–electron oxidation and consequently, alkyl–coordinated square pyramidal complexes having general formula of $[\mathbf{Co^{III}E([L^{ISQ}]^{\bullet 1-})_2}]$ (where E = CH_2Cl, alkyl) form. To initiate an oxidative C–C cross coupling reaction *via* the oxidative addition of both alkyl and halide units to the metal center in a Co complex requires *cis*– orientated accommodation site for alkyl halide (Scheme 3.3). Therefore, *cis*– orientation is necessary between the two coordinated non–innocent ligands to create such a vacant site for the accommodation of alkyl halide. In square planar $[\mathbf{Co^{III}([L^{AP}]^{2-})_2}]^-$ complex, the two coordinating–ligands orient in *trans*– fashion. Thus, oxidative addition of both alkyl and halide units was not possible in the system.

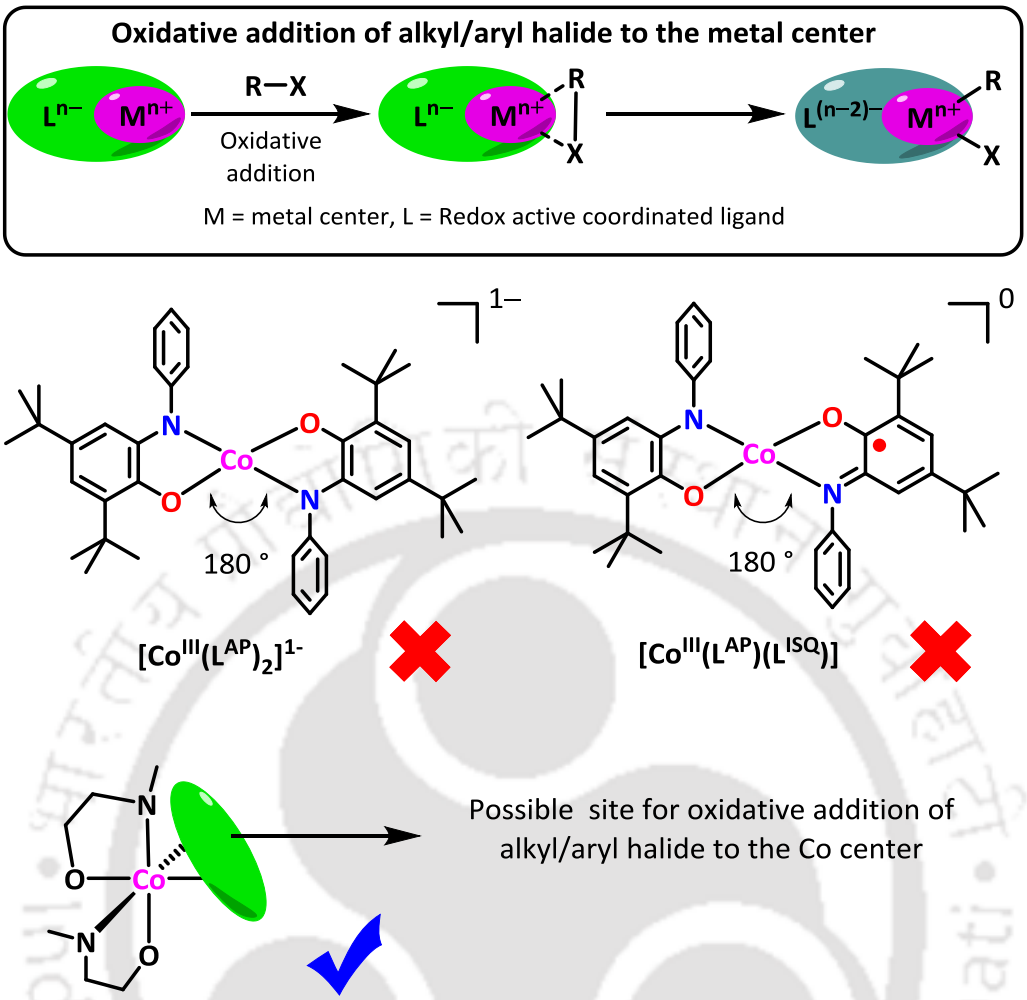

Scheme 3.3: *Required orientation of coordinated redox active ligand in oxidative addition of alkyl/aryl halide to the metal center.*

As a foremost step to impose non–coplanar arrangement between two radical–generation units, two $\mathbf{H_2L^{AP}}$ ligands were combined by a bridging chalcogen atom that connects two ligands *via* the *–ortho* carbon atom of the two aniline moieties. Thus formed new ligand will be designated here as $\mathbf{H_4L^{Z(AP/AP)}}$. Hence, coplanar and *trans*–alignment of the radical–generating 3,5–di–*tert*–butyl amidophenolate units could be restricted and the required vacant site for *cis*–coordination might be availed.

In this chapter, the synthesis and characterization of Co–complexes from chalcogen bridge ligands; $\mathbf{H_4L^{Z(AP/AP)}}$ where Z = O, S and Te have been reported. To note, the synthesis and characterization of ligands have already been discussed in chapter II.

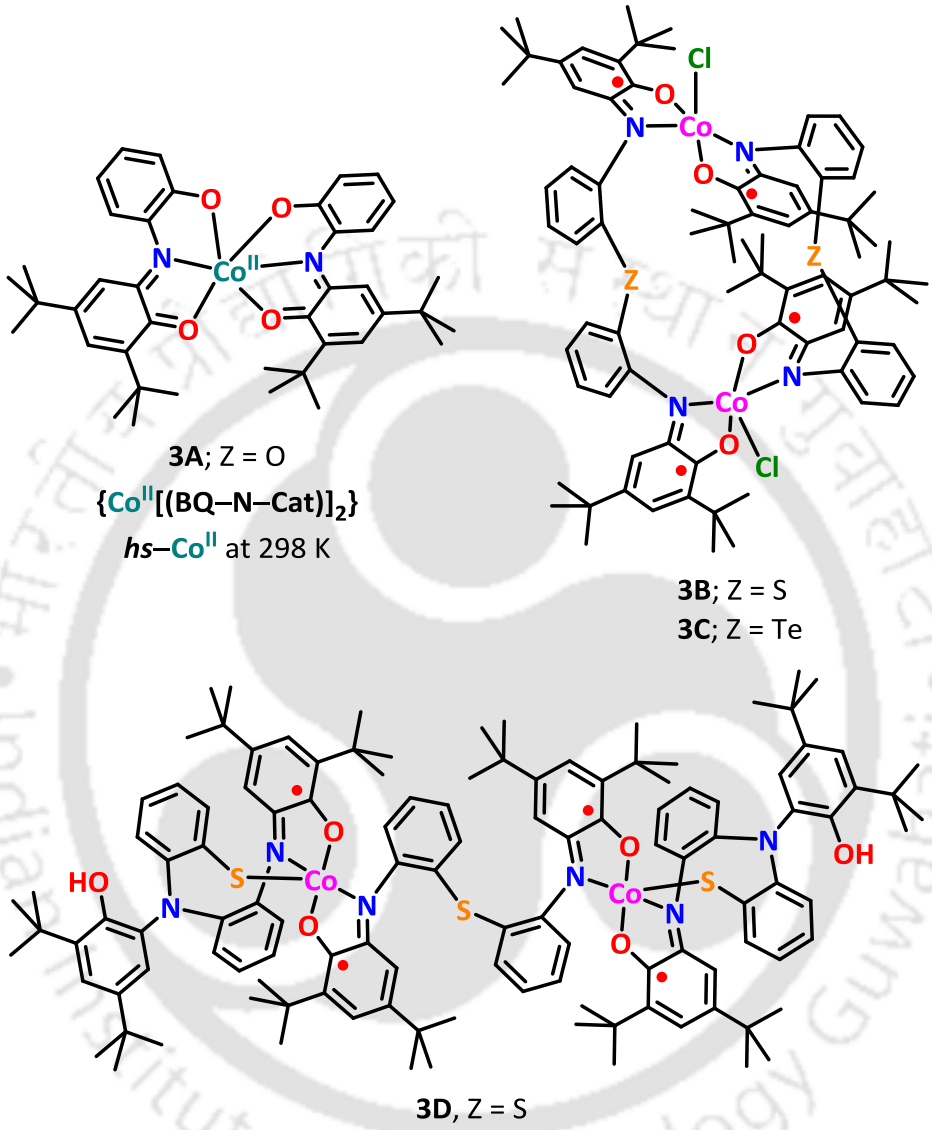

Scheme 3.4: *Several complexes derived from ligand* $\boldsymbol{H_4L^{Z(AP/AP)}}$ *where Z = O, S and Te.*

3.2: Synthesis and Characterizations of Cobalt Complex (3A) from Ligand $H_4L^{O(AP/AP)}$

An equimolar reaction between ligand $\mathbf{H_4L^{O(AP/AP)}}$ and $Co(ClO_4)_2 \bullet 6H_2O$ or $CoCl_2 \bullet 6H_2O$ in CH_3CN in the presence of Et_3N under air provided a blue–green solid **3A** (Scheme 3.5). The formation of complex **3A** proceeded through an initial generation of a brown–black intermediate (**A**, *vide infra*).

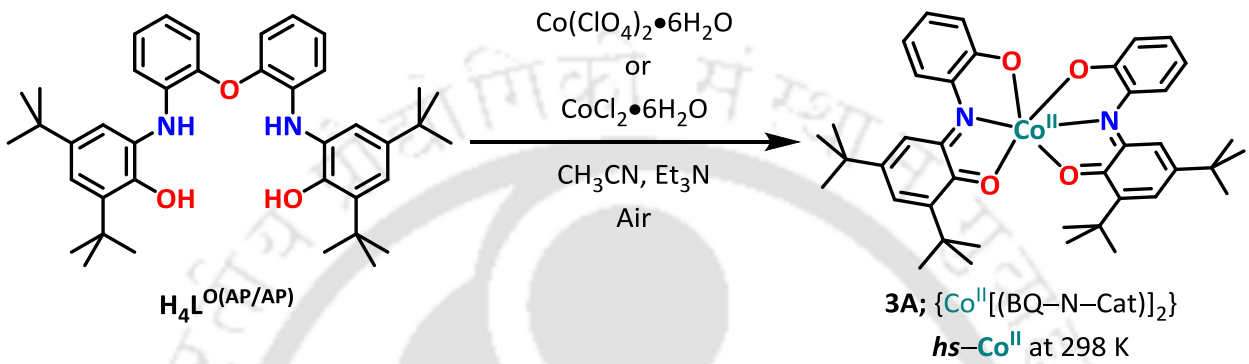

Scheme 3.5: *Synthetic route of complex* ***3A*** *from ligand* $\boldsymbol{H_4L^{O(AP/AP)}}$.

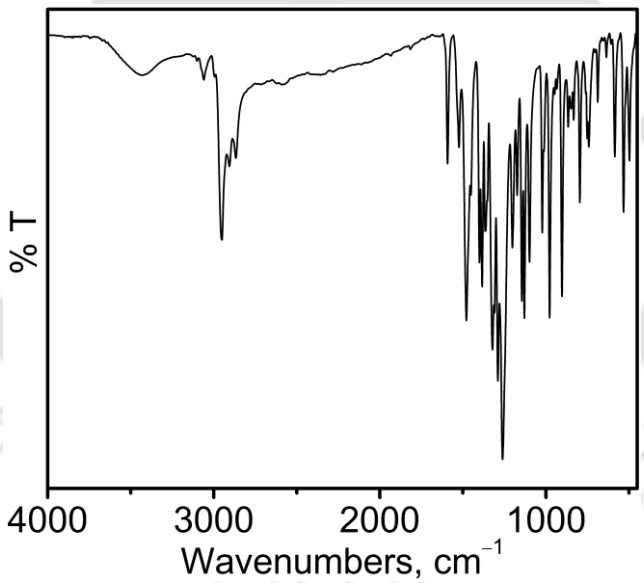

Figure 3.1: *IR spectrum of complex* ***3A***.

The infrared spectrum of complex **3A** (Fig. 3.1) was recorded on KBr pallet at 300 K. The metal coordination with the deprotonated amidophenolate units was confirmed by the disappearance of the ν(O–H) and ν(N–H) stretching bands.[8a–b] A weak band corresponding to $\nu(C_{Ar}–H)$ [Ar stands for aromatic] stretch was observed at 3060 cm^{-1}. Three bands at 2951, 2906 and 2867 cm^{-1} were attributed for asymmetric, overtone and symmetric bands of $\nu(C_{Al}–H)$ [Al stands for aliphatic] stretches of *tert*–butyl groups, respectively.[8c,d] In addition to this, the $\nu(C_{Al}–$

H) bending vibration of methyl groups appeared at 1479 and 1367 cm^{-1}. The strong bands in the region of 1322–1221 cm^{-1} were attributed to ν(C–N) and ν(C–O) stretches.[9a]

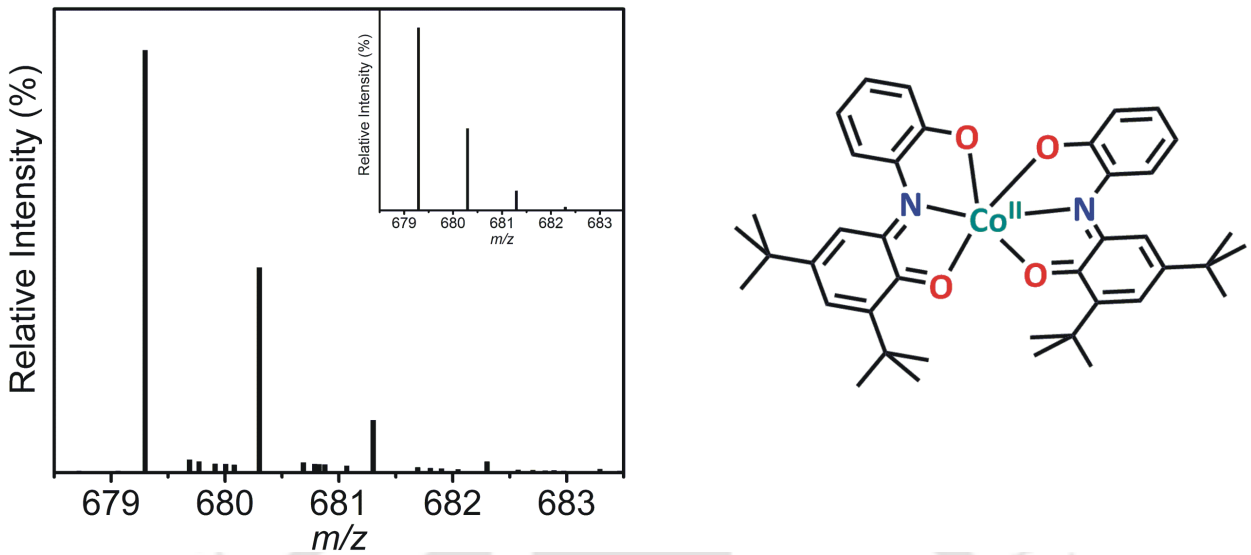

Figure 3.2: *ESI–mass spectrum (+ve mode) of complex **3A** with experimental and simulated (inset) isotope distribution pattern.*

Electrospray ionization mass spectrum (ESI–MS) of a solution of complex **3A** in CH_3CN provided a 100% molecular ion peaks at *m/z* = 679.31 ($[M]^+$; M = molecular mass) in the positive mode. Experimental and simulated isotope distribution pattern confirmed the composition as $C_{40}H_{48}N_2O_4Co$.

The green complex (complex **3A**) upon crystallization from toluene appeared as rectangular shaped crystal. X–ray diffraction measurement of the crystal was recorded at 100 K. However, due to poor crystallinity, the obtained data quality was not worthy enough for accurate determination of the oxidation states of the metal and the ligand centers. The ball and stick diagram of the molecular structure of complex **3A** is shown in Fig. 3.3.

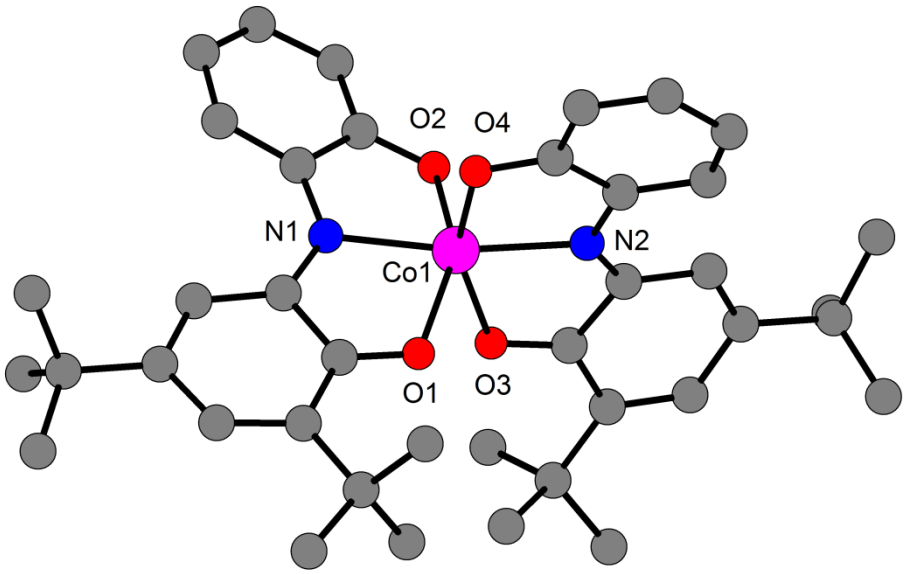

Figure 3.3: *Ball and stick presentation of complex **3A** (crystalized from toluene), H–atoms were omitted for clarity.*

The crystallographic analysis revealed that the complex was neutral, mononuclear–octahedral (*mer*) and the coordinated ligand backbone was different from that of the initially employed ligand [$\mathbf{H_4L^{O(AP/AP)}}$]. The measurement pointed out the formation of new tridentate ligand form $\mathbf{H_4L^{O(AP/AP)}}$ *via* ligand–centered phenolic C–O bond cleavage during the complexation reaction. In the complex, the Co center was coordinated with two similar kind of *O,N,O*–coordinated type ligand. But the data quality of the crystal was not good enough to determine the exact oxidation state of the ligand fragment and the metal ion.

Two more crystallization methods have been applied from two different solvents system. Structural determinations of thus obtained crystals were measured by X–ray diffraction study at 295 K. The incorporation of $CHCl_3$ and CH_3CN as lattice solvents with complex **3A** was observed when the complex was crystalized from chloroform/acetonitrile (3:1) and diethyl ether/acetonitrile (2:1) solvent mixture, respectively. However, there was no lattice solvent when complex was crystalized from toluene (Fig. 3.4). The information regarding the presence of H–bonding and/or short interactions within the complex is presented in Fig 3.4. X–ray diffraction analysis was not worthy enough for determining the oxidation states of metal and ligand centers. The selective bond lengths are shown in Table 3.1 and the crystalline parameters with the quality–limitations are summarized at Table 3.2.

The crystalline packing of complex **3A** (crystalized from different solvent system) is shown in Fig. 3.4.

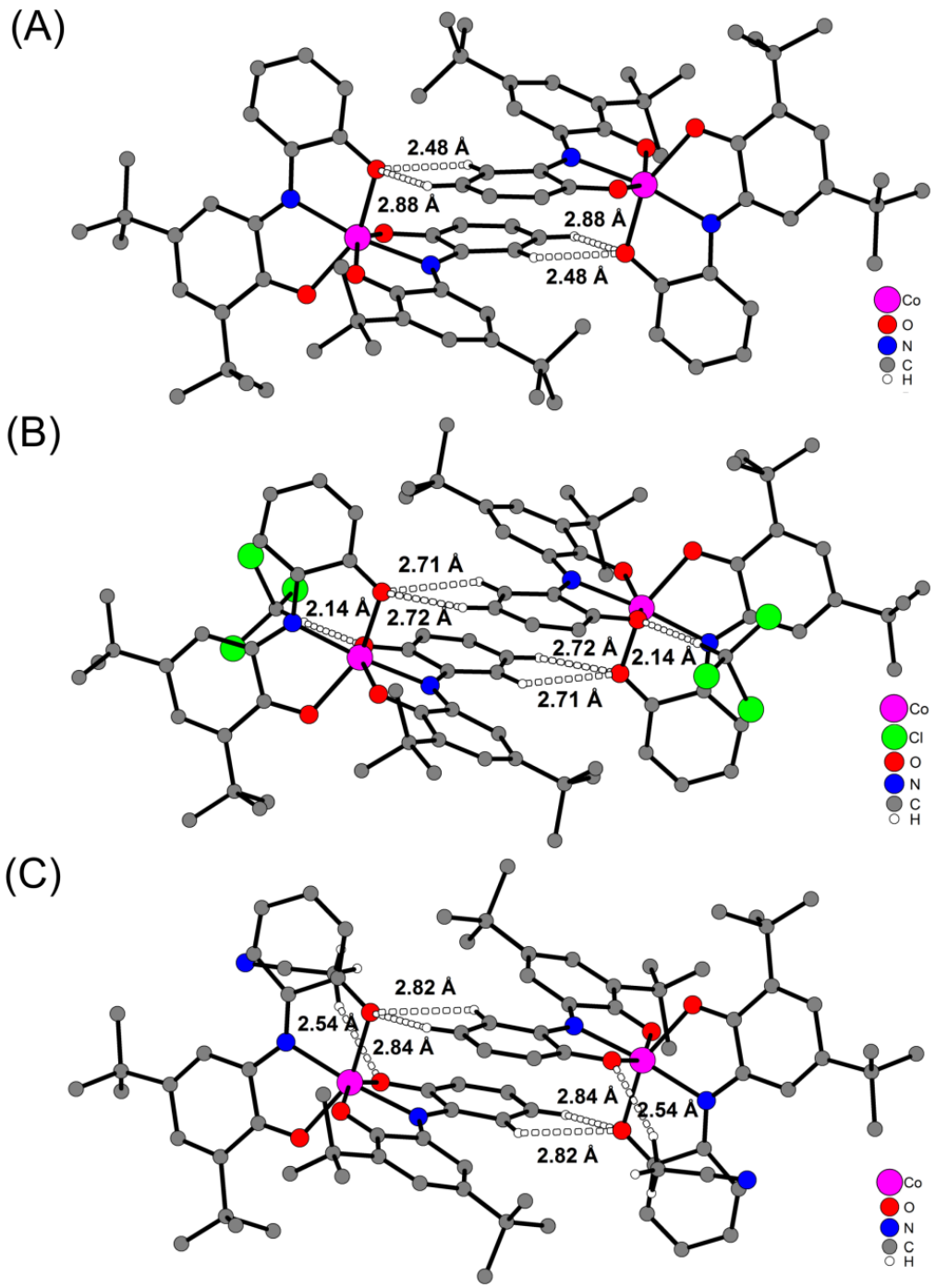

Figure 3.4: *H bond between two adjacent molecules (A) complex **3A**; (B) complex **3A**•1$CHCl_3$, and (C) complex **3A**•1CH_3CN. H atoms (except involved in H–bonding and attached with solvent molecule) in the metal complex were omitted for clarity.*

It has been found that complex **3A** crystalized from toluene have stronger intermolecular interaction (H–bonding) in the crystal packing compare to the crystals found from other solvent

systems (Fig. 3.4). On the other hand, incorporation of lattice solvent and the existence of solvent–solute interaction/H–bonding in the crystal packing have been observed for crystals found from other solvent systems.

Table 3.1: *Selected bond distances (Å) for the Co complexes.*

Bond Type	**3A**•1$CHCl_3$ (293 K)	**3A** (100 K)	**3A**•1CH_3CN (293 K)
Co1–O1	2.113(10)	2.103(5)	2.113(6)
Co1–O2	2.027(12)	2.049(5)	2.049(7)
Co1–O3	2.089(9)	2.107(5)	2.056(9)
Co1–O4	2.017(10)	2.032(6)	2.063(9)
Co1–N1	2.082(11)	2.062(6)	2.082(6)
Co1–N2	2.083(10)	2.064(6)	2.085(7)
O1–C2	1.266(16)	1.267(8)	1.255(10)
O2–C12	1.292(16)	1.299(8)	1.301(10)
O3–C14	1.271(15)	1.257(8)	1.270(10)
O4–C24	1.234(16)	1.295(9)	1.293(11)
N1–C1	1.287(16)	1.348(9)	1.314(10)
N1–C7	1.391(17)	1.345(9)	1.362(11)
N2–C13	1.355(15)	1.317(9)	1.335(12)
N2–C19	1.393(16)	1.377(9)	1.324(13)

Table 3.2: *Crystallographic data and its quality–limitations (in red and yellow–highlights) for the complexes.*

	3A•1$CHCl_3$	**3A**	**3A**•1CH_3CN
CCDC No.	1511019	1511021	1511022
Empirical formula	$C_{41}H_{49}CoN_2O_4Cl_3$	$C_{40}H_{48}CoN_2O_4$	$C_{42}H_{51}CoN_3O_4$
Formula weight	799.10	679.73	720.79
Unit cell dimensions	a = 11.6599(17) Å	a = 10.741(2) Å	a = 11.9760(11) Å
	b = 13.780(3) Å	b = 13.763(3) Å	b = 13.4487(11) Å
	c = 14.5966(9) Å	c = 14.309(3) Å	c = 14.6400(7) Å
	α = 78.503(10)°	α = 64.820(5)°	α = 67.872(6)°
	β = 88.721(8)°	β = 86.451(5)°	β = 88.335(6)°
	γ = 81.580(14)°	γ = 72.227(6)°	γ = 65.421(9)°
Volume, V (Å^3)	2273.4(5)	1817.2(6)	1963.4(3)
Z	2	2	2
Temperature, *T(K)*	293(2)	100(2)	293(2)
θ range for data collection	2.95° to 25.00°	1.58° to 18.81°	3.02° to 25.00°
Completeness to θ	99.4% (θ = 25.00°)	97.6% (θ = 18.81°)	95.6% (θ = 25.00°)
Goodness–of–fit on F^2	0.929	1.036	1.172
R(int)	0.1846	0.0689	0.1275
R(sigma)	0.2595	0.0950	0.1469
Final *R* indices [$I > 2\sigma(I)$]	*R1* = 0.1794, *wR2* = 0.3740	*R1* = 0.0566, *wR2* = 0.1267	*R1* = 0.1193, *wR2* = 0.2998
R indices (all data)	*R1* = 0.2901, *wR2* = 0.4418	*R1* = 0.0986, *wR2* = 0.1506	*R1* = 0.2027, *wR2* = 0.4067

The presence of lattice solvent in the crystal packing was also confirmed by elemental analysis (Table 3.3). Depending on the presence of lattice solvent in the crystal–packing, the complex crystalized from toluene, chloroform/acetonitrile (3:1) and diethyl ether/acetonitrile (3:1) were abbreviated now onwards as **3A**, **3A**•0.3 $CHCl_3$ and **3A**•0.8 CH_3CN, respectively.

Table 3.3: *Elemental data of Co complexes crystalized from different solvent system.*

Crystalizing system	% C		%H		%N		Composition/ Abbreviation
	Exp	Calcd	Exp	Calcd	Exp	Calcd	
Toluene	70.03	70.68	6.99	7.12	4.23	4.12	$C_{40}H_{48}N_2O_4Co$/ **3A**
Chloroform: Acetonitrile (3:1)	67.64	67.68	6.80	7.00	3.91	4.01	$C_{40}H_{48}N_2O_4Co$•0.3$CHCl_3$/ **3A**•0.3 $CHCl_3$
Diethyl ether: Acetonitrile (2:1)	70.12	71.21	7.13	7.00	5.50	5.52	$C_{40}H_{48}N_2O_4Co$•0.8CH_3CN/ **3A**•0.8 CH_3CN

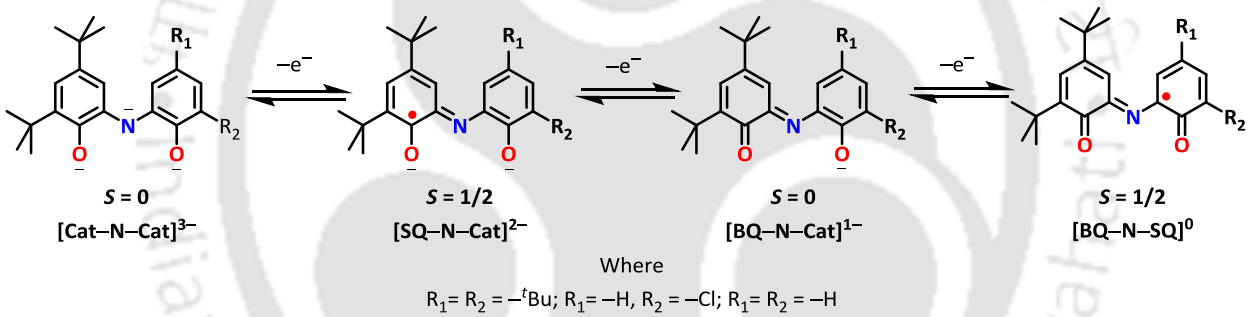

Scheme 3.6: *Probable several oxidation states of coordinated O,N,O– type ligand.*

Crystal structure and elemental studies supported the coordination of O,N,O type tridentate ligand to the metal ion. Two analogous tridentate ligands were already available in the literature[10] and the probable oxidation states of the tridentate moieties are shown in Scheme 3.6. Therefore, the composition of the neutral complex **3A** can be either (a) a Co(II) ($S_{Co(II)}$ = 3/2, high–spin) ion with two coordinated diamagnetic $(BQ–N–Cat)^{1–}$ ligands, *i.e.*, $\{Co^{II}[(BQ–N–Cat)]_2\}^0$ or (b) a Co(III) ($S_{Co(III)}$ = 0, low–spin) ion with coordinated paramagnetic $(SQ–N– Cat)^{2–}$ [S_L = 1/2] and $(BQ–N– Cat)^{1–}$ ($S_{L'}$ = 0) ligands, *i.e.*, $\{Co^{III}[(SQ–N–Cat)(BQ–N–Cat)]\}^0$ (Scheme 3.7). The assumption is well supported by some previously reported literature[10] and the charge neutrality of the complex. Due to having low potential gap between chromophore $[SQ–N–Cat]^{2–}$ and $[BQ–N–Cat]^{1–}$, those two forms were inter–convertible by single IET (intermolecular electron transfer). The IET may be caused by several external stimuli (like thermal, light and

pressure). Several reports are also suggestive for the existence of thermal tautomeric conversion between the assumed two conformations.[6,10]

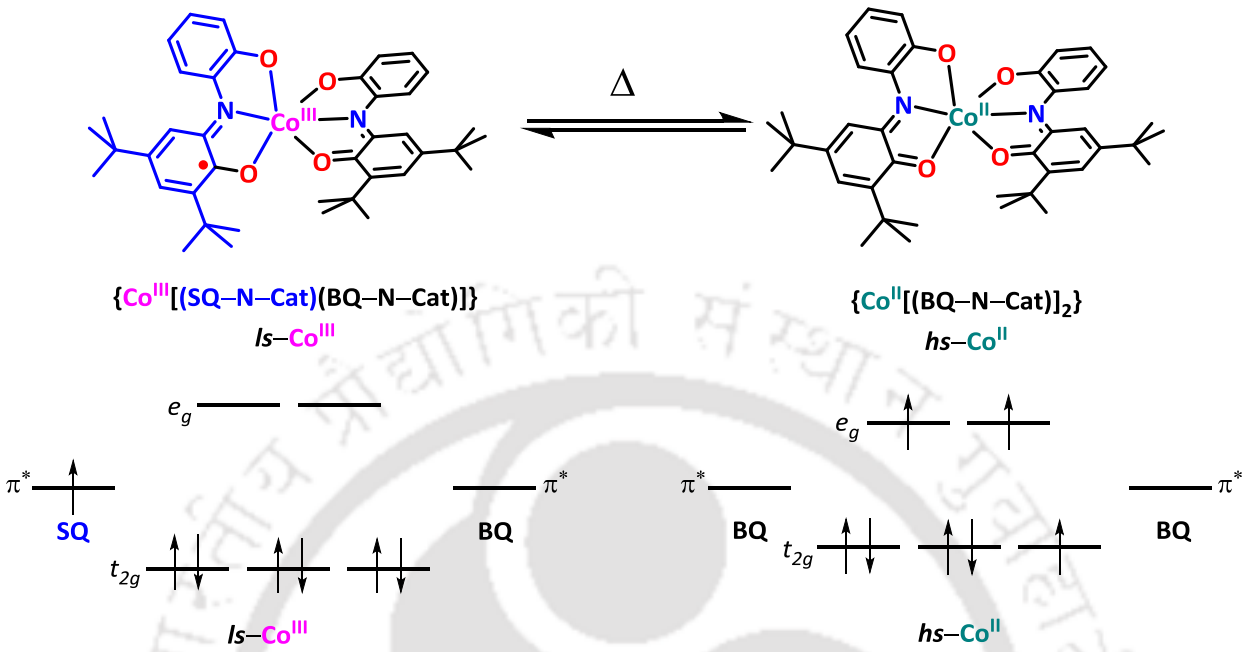

Scheme 3.7: *Thermal valence tautomeric conversion between two isomers*.

3.3: Solvent and Solid Phase Valence Tautomism of Complex 3A

It was previously reported that some analogous complexes of **3A** shown thermal tautomeric conversion in solution phase.[10] Thus, the Co complex **3A** derived from ligand [$\mathbf{H_4L^{O(AP/AP)}}$] might exist either as {*ls*–Co^{III}[(SQ–N–Cat)(BQ–N–Cat)]}^{0} or as {*hs*–Co^{II}[(BQ–N–Cat)]$_2$}^{0}and the tautomeric conversion would dependent upon the temperature (Scheme 3.7).

Temperature dependent electronic absorption spectra of complex **3A**•0.3$CHCl_3$ was recorded in toluene in the temperature range from 20 to 70 K. The spectra are depicted on Fig. 3.5.

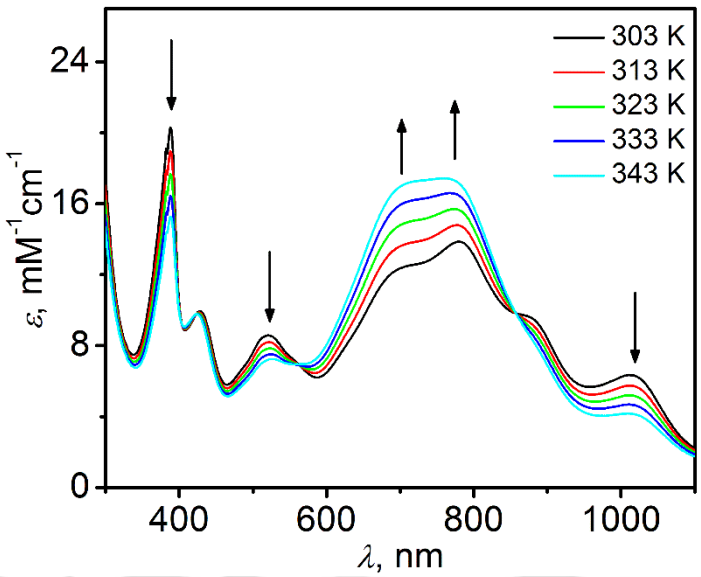

Figure 3.5: *Temperature dependent electronic absorption spectra of complex* ***3A****•0.3CHCl*$_3$ *in toluene over a temperature range 303–343 K.*

Variable temperature absorption spectrum of complex **3A**•0.3CHCl$_3$[12] in toluene emphasized the existence of equilibrium involving two chromophores as indicated by the presence of two isosbestic points at 856 and 560 nm. The bands at 779 and 697 nm were due to chromophore [BQ–N–Cat]$^{1-}$.[11*a–c*] Thus, the increase in absorption of the bands with temperature implied the thermal driven VT conversion toward {*hs*–Co^{II}(BQ–N–Cat)$_2$} at high temperature. The depletion of bands at 505, 433, 387 nm that corresponded to metal coordinated chromophore [SQ–N–Cat]$^{2-}$ indicated the decrease in concentration of the unit with increase in temperature of the solution.[11*d*] Thus, the thermal electronic spectrum complex **3A** was evidenced for thermal valence tautomerism conversion in solution phase.

The solvent phase thermal tautomeric conversion was also supported by X–band EPR measurement. The measurement on **3A**•0.3CHCl$_3$[12] was performed at 77 K in a CH_2Cl_2/toluene solvent mixture (Fig. 3.6A). A ligand–centered S = 1/2 signal with a reasonable ^{59}Co (I = 7/2) super–hyperfine interaction was established by the simulation of the experimental spectrum. The parameters obtained by the simulation were g_1 = 2.007, g_2 = 2.007, and g_3 = 1.998; g_{iso} = 2.004; ^{59}Co(A_1, A_2, A_3) = (7, 7, 27)×10^{-4} cm^{-1}. Interestingly, it was observed that the signal vanished at 295 K. The temperature–dependent signal also held true for solid–state X–band EPR measurements of the complex (Fig. 3.6B). The intensity of the signal decreases drastically at 295 K. In fact, the nature of the observed EPR signal was different than that of ligand–centered S = 1/2 and indeed, very weak in intensity, *i.e.*, almost X–band EPR silent. Therefore, it can be argued that in solution as well as in the solid state the complex underwent valence

tautomerization; at low temperature (77 K) the complex existed as {*ls*–Co^{III}[(SQ–N–Cat)(BQ–N–Cat)]}^{0}, while at 295 K it existed as {*hs*–Co^{II}[(BQ–N–Cat)]$_2$}^{0}. Vanishing of the X–band EPR signal at 295 K was due to zero field splitting (>0.3 cm^{-1}) that resulted upon high spin–orbit coupling at Co(II). Herein, it is noteworthy that valence tautomerization between octahedral {*ls*–Co^{III}[(SQ–N–Cat)(BQ–N–Cat)]}^{0} and {*hs*–Co^{II}[(BQ–N–Cat)]$_2$}^{0} is well known in solution; however, the phenomenon is absent in the solid state within the 2–295 K temperature range.[9, 11*a,c*] It should be noted that complex **3A**•0.8CH_3CN also provided similar kind of X–band EPR signals at solid state (Fig. 3.6C) while complex **3A** (crystalized from toluene) was X–band EPR silent at both 77 K and 295 K. The X–band EPR silence feature of complex **3A** (crystalized from toluene) was suggestive for its existence as {*hs*–Co^{II}[(BQ–N–Cat)]$_2$}^{0} at the mentioned temperate range.

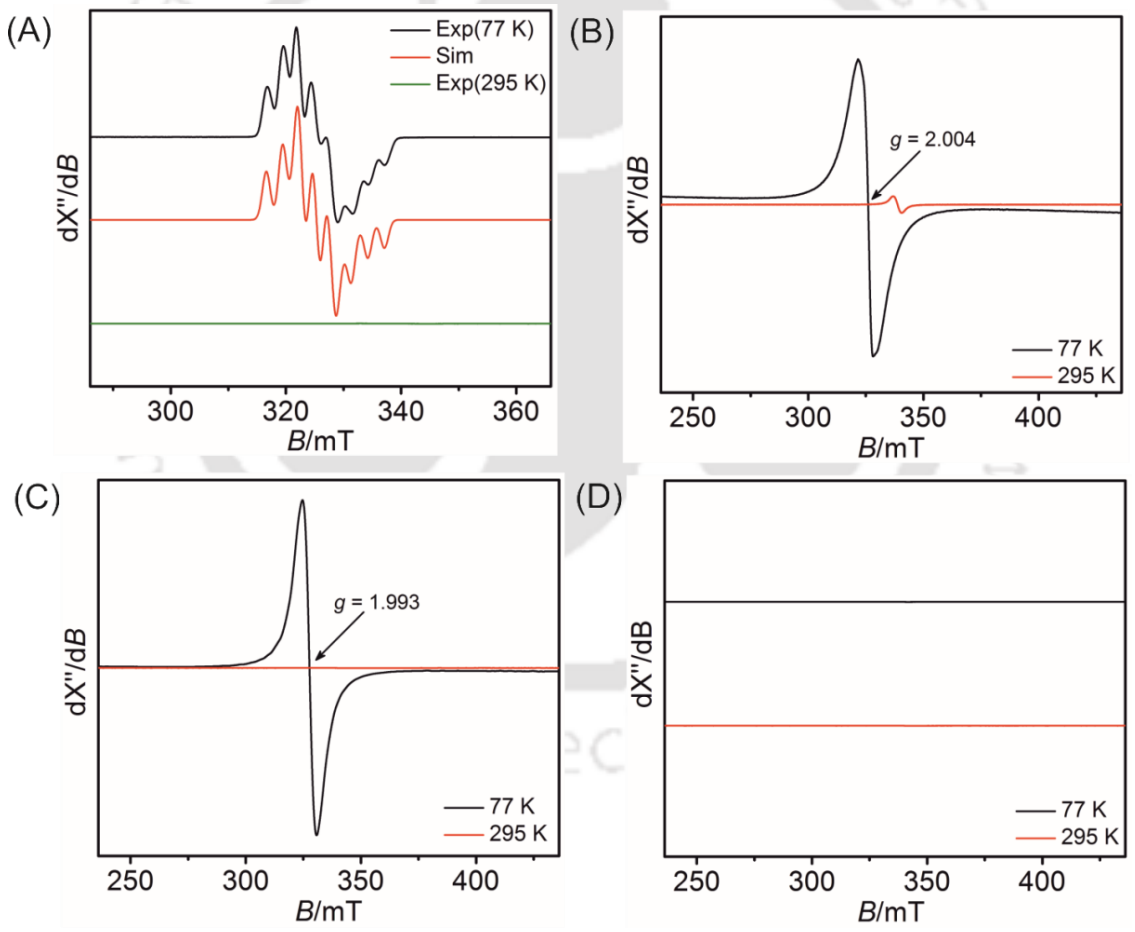

Figure 3.6: *X–band EPR spectra measured at 77 and 295 K; (A) complex **3A**•0.3$CHCl_3$ in a CH_2Cl_2/toluene (2:1) solvent mixture; microwave frequency (GHz): 9.444; modulation frequency (kHz): 100; amplitude = 1.0; (B) complex **3A**•0.3$CHCl_3$ in the solid state; microwave frequency (GHz): 9.142; modulation frequency (kHz): 100; amplitude (G) = 0.3; (C) complex **3A**•0.8CH_3CN in solid state; microwave frequency (GHz): 9.138; modulation frequency (kHz): 100; amplitude (G) = 1.0; and (D) complex **3A** in solid state; X–band microwave frequency (GHz): 9.143; modulation frequency (kHz): 100; amplitude (G) = 1.0.*

Inspired by X–band EPR results, variable–temperature magnetic susceptibility measurement was carried out on a solid sample of complex **3A**•0.3$CHCl_3$[12] at 1 T external magnetic field to reinforce the solid–state valence tautomeric nature of the complex. The $\chi_M T$ *vs.* *T* plot is depicted in Fig. 3.7. At 10 K, $\chi_M T$ = 0.44 emu K mol^{-1} was observed. This value was closely commensurate with the system having one–unpaired electron (an *S* = 1/2 spin). The value remained almost unchanged up to 118 K. Interestingly, in the 118 to 125 K temperature range a sharp transition in the magnetic moment to $\chi_M T$ = 2.34 emu K mol^{-1} was observed. The magnetic moment attained at 125 K remained almost constant up to 300 K. This feature supported a valence tautomeric phenomenon in the system, where low–spin diamagnetic Co(III) was reduced to high spin Co(II) by the ligand–centric SQ unit that then transformed to its one–electron oxidized BQ form (Scheme 3.7). Therefore, it can be argued that till 118 K the complex was existing in the $\{ls\text{–}Co^{III}[(SQ\text{–}N\text{–}Cat)(\ BQ\text{–}N\text{–}Cat)]\}^0$ form, while above 125 K the complex continued to exist in the $\{hs\text{–}Co^{II}[(BQ\text{–}N\text{–}Cat)]_2\}^0$ form.

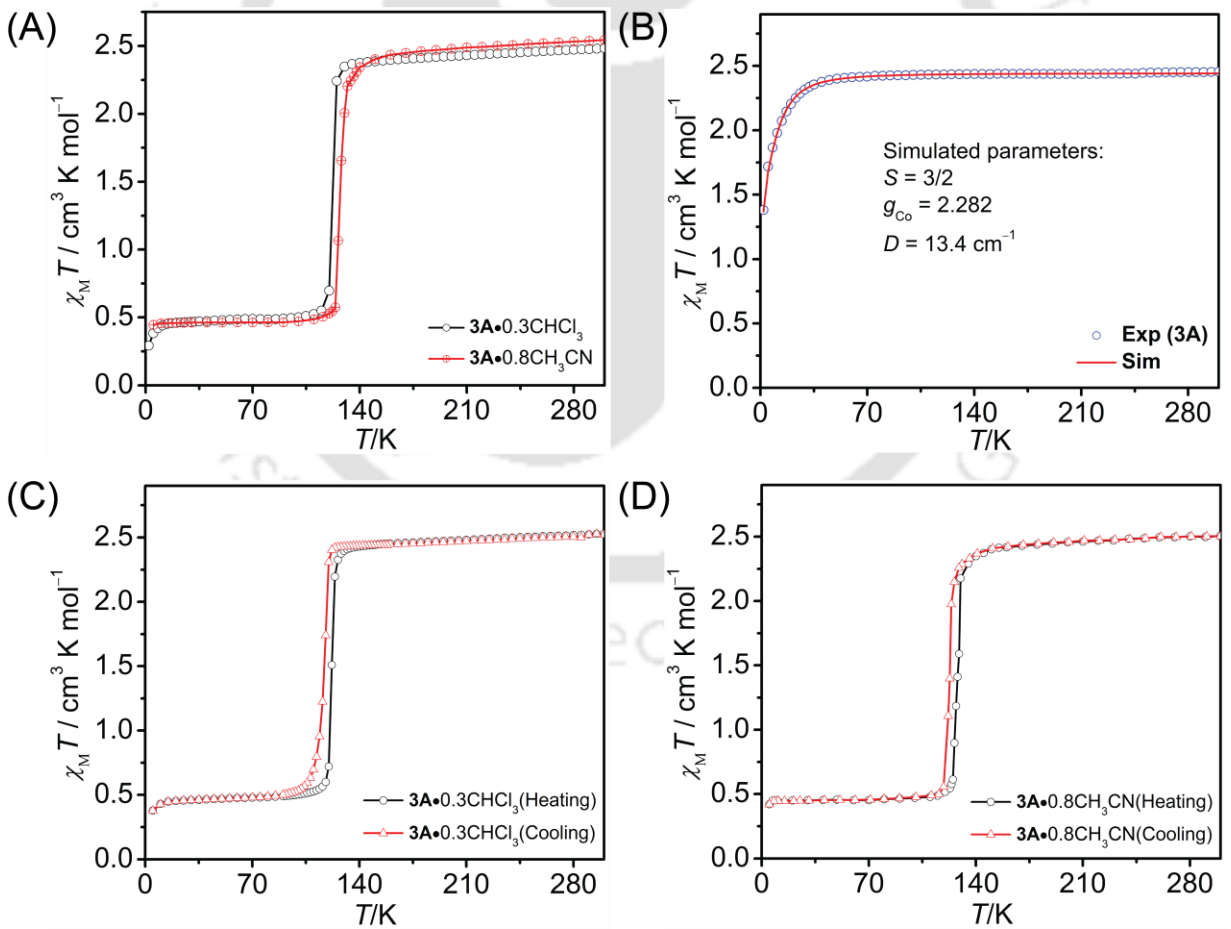

Figure 3.7: *$\chi_M T$ vs. T plots: (A) **3A**•0.3$CHCl_3$ and **3A**•0.8CH_3CN, (B) **3A**, (C) hysteresis measurement of **3A**•0.3$CHCl_3$ and (D) hysteresis measurement of **3A**•0.8$CHCl_3$.*

The thermodynamic parameters corresponding to the tautomeric conversion was calculated based on the following relation[6e,11c]:

$$\chi_M T = \chi_M T_{SQ} + \gamma_{hs\text{-}Co(II)}(\chi_M T_{hs\text{-}Co(II)} - \chi_M T_{SQ}) \qquad \text{Eq. 3.1}$$

$$\text{With } \gamma_{hs\text{-}Co(II)} = \frac{1}{\exp\left(\frac{\Delta H}{RT} - \frac{\Delta S}{R}\right)+1}$$

Where $\chi_M T$ is the product of magnetic susceptibility with corresponding temperature; $\chi_M T_{SQ}$ and $\chi_M T_{hs\text{-}Co(II)}$ stand for $\chi_M T$ values of isolated {*ls*–Co^{III}[(SQ–N–Cat)(BQ–N–Cat)]}^{0} and {*hs*–Co^{II}[(BQ–N–Cat)]$_2$}^{0} conformers, respectively; $\gamma_{hs\text{-}Co(II)}$ is the mole faction of {*hs*–Co^{II}[(BQ–N–Cat)]$_2$}^{0} conformer; ΔH and ΔS are respectively the change of enthalpy and entropy associated with tautomeric conversion.

Based on eq. 3.1, the critical temperature (T_c), which is defined as the temperature at which the free energy difference (ΔG) between the two inter–convertible species is nil, was 122 K for complex **3A**•0.3$CHCl_3$. Such type of solid–state tautomeric conversion was also observed for crystalline **3A**•0.8 CH_3CN (red line, Fig. 3.7A). However, T_c of **3A**•0.8 CH_3CN was slightly higher (5.4 K) compared to that of **3A**•0.3$CHCl_3$. The calculated thermodynamic parameters were found as ΔH = 101 kJ mol^{-1} and ΔS = 825 J K^{-1} mol^{-1} for complex 3A•0.3$CHCl_3$; ΔH = 79 kJ mol^{-1} and ΔS = 618 J K–1 mol^{-1} for complex **3A**•0.8 CH_3CN. However, the calculated values were abruptly high and thus, those values have no physical meaning.

Unlike solvated crystals **3A**•0.3$CHCl_3$ and **3A**•0.8 CH_3CN, in the case of complex **3A**, the $\chi_M T$ = 2.46 emu K mol^{-1} value remained almost constant in the temperature range 50–300 K. Upon further lowering the temperature, the $\chi_M T$ value decreased and reached 1.71 emu K mol^{-1} at 5 K. Herein, the decrease in the $\chi_M T$ value was due to zero–field splitting (D = 13.4 cm^{-1}, Fig. 3.7B) that arose because of strong spin–orbit coupling at the Co(II) center. Thus, it was apparently evident that in the absence of lattice solvent, the complex remained in the {*hs*–Co^{II}[(BQ–N–Cat)]$_2$}^{0} form and no valence tautomerization took place.

Thus, the magnetic susceptibility measurement of all the three samples (**3A**, **3A**•0.3$CHCl_3$ and **3A**•0.8 CH_3CN) rationalized the requirement of lattice solvent with in the crystalline packing.

The tautomeric conversion from *ls*–Co^{III} to *hs*–Co^{II} species proceeded through intermolecular electron transfer (IET) from electron rich ligand site to the metal center. Herein,

ligand fragment $[(SQ–N–Cat)^{2–}]$ promoted one–electron to the coordinated Co(III)–ion during the tautomeric conversion and thus $\{ls–Co^{III}[(SQ–N–Cat)(BQ–N–Cat)]\}^{0}$ transformed to $\{hs–\{Co^{II}[(BQ–N–Cat)]_2\}^{0}$. The intermolecular electron transfer is associated with the change in metal–ligand bond length and molecular volume (Scheme 3.8).

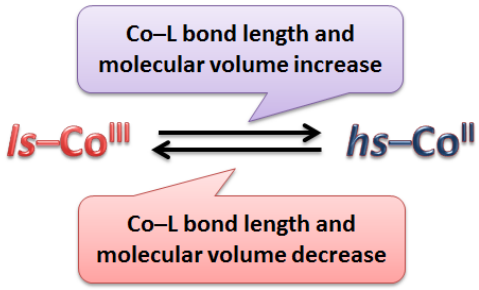

Scheme 3.8: *Schematic presentation of molecular change during tautomeric conversion.*

The single–crystal volume of **3A** increased with the incorporation of lattice solvent (Table 3.2) Therefore, it was evident that the presence of lattice solvent molecules within the crystal lattice promoted flexibility or softness[3a,n] in the systems (Fig. 3.9 and 3.12) and favored the required structural changes during the valence tautomeric transition. Crystal–structure packing analyses revealed that in complex **3A** two adjacent molecules were firmly held by strong intermolecular H–bonds, while, in complex **3A**•1$CHCl_3$ and complex **3A**•1CH_3CN the intermolecular H–bonds were weak in nature (Fig. 3.4). The strong H–bonds, which can be considered as a stabilizing factor, presumably prevented complex **3A** from undergoing any required structural change for valence tautomerization. The abrupt transition within a very small (7 K) temperature range (Fig. 3.7) for **3A**•1$CHCl_3$ and **3A**•1CH_3CN reinforced a strong cooperative effect[3a,n] that was propagated through the lattice solvent network (Fig. 3.9 and 3.10).

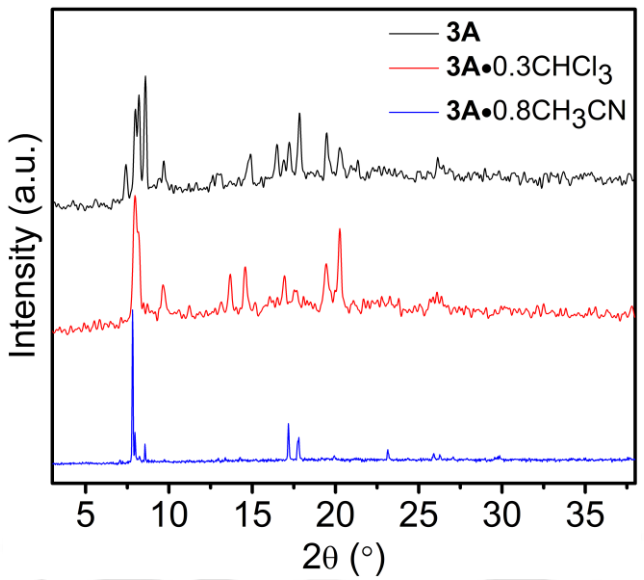

Figure 3.8: *X–ray powder diffractograms of crystalline samples*[12] *of the Co complexes.*

Although, the crystallographic phases and the nature of the lattice solvent molecule were different for the different complexes (Fig. 3.8), no consequence on the nature of transition, transition temperature, and hysteresis effect (Fig. 3.7C and 3.7D) was discerned. These experimental facts reinforced that no correlative inference can be formulated amongst T_c, solvent nature and crystallographic phases.

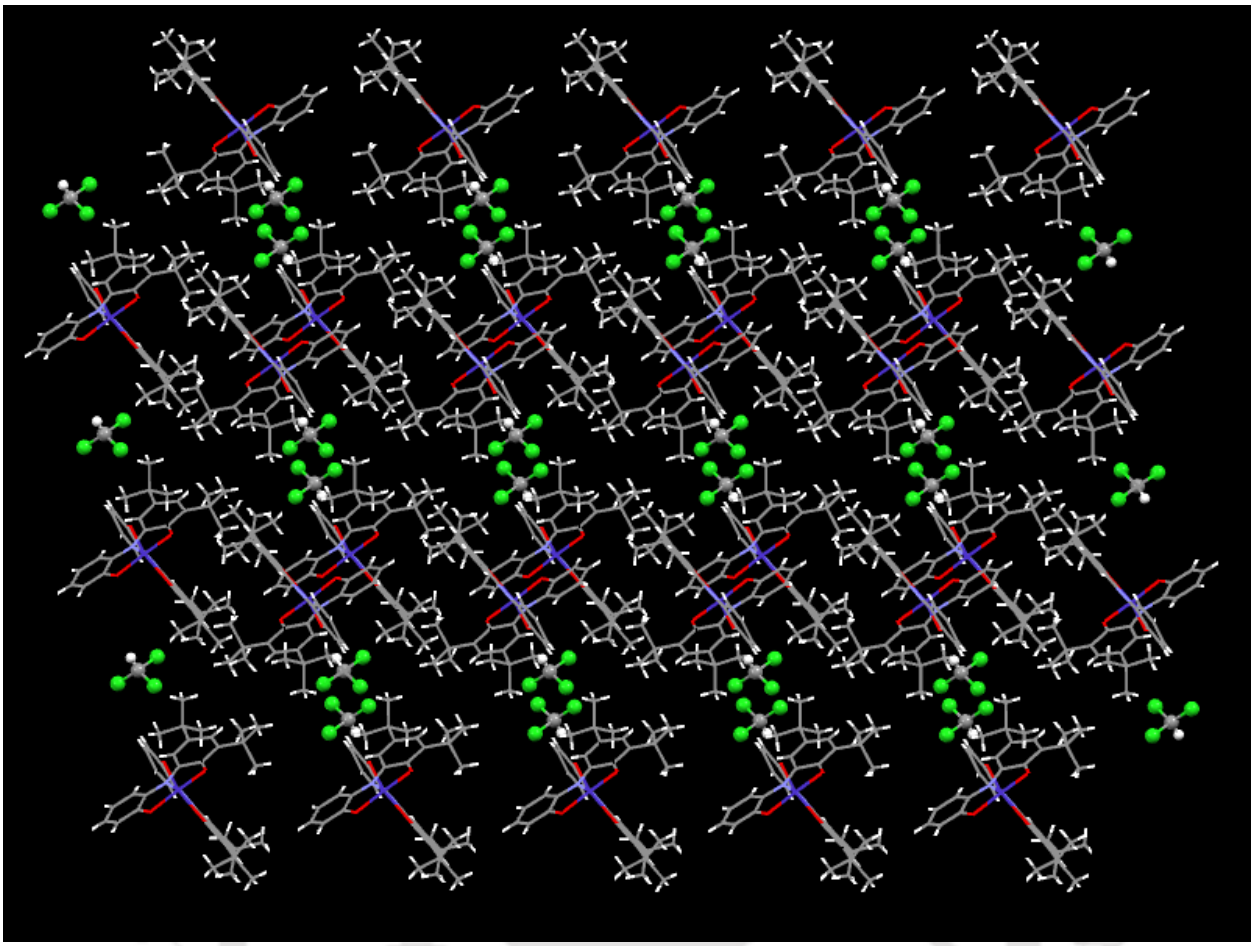

Figure 3.9: *Crystal packing diagram of complex* ***3A•****1*$CHCl_3$ *along c–axis. The elements C, Co, Cl, H, O and N are represented as gray, blue, green, white, red and violet color, respectively.*

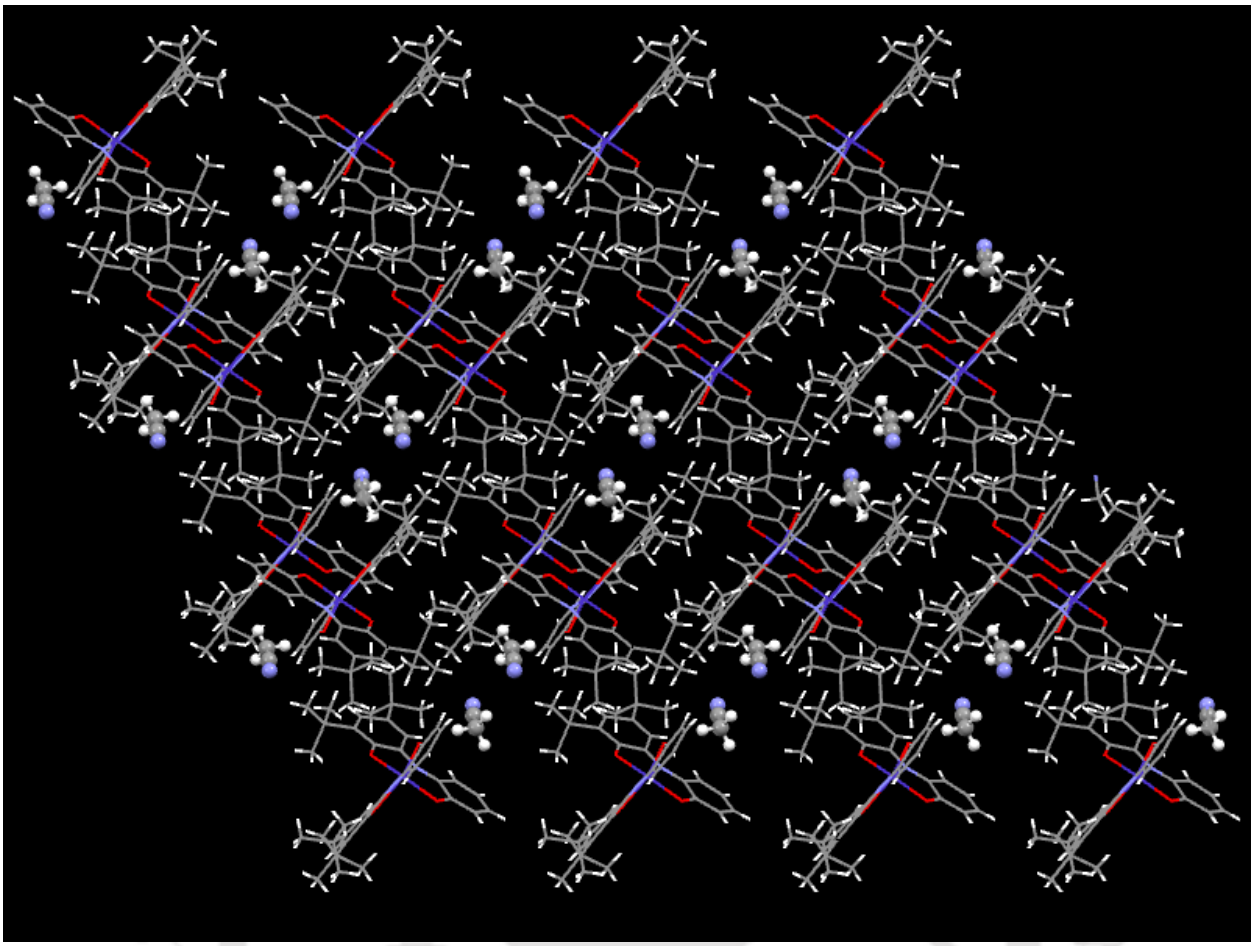

Figure 3.10: *Crystal packing diagram of complex* ***3A*****•***1CH$_3$CN along c–axis. The elements C, Co, H, O and N are represented as gray, blue, white, red and violet color, respectively.*

3.4: Probable Pathway of Generation of Complex 3A from Ligand $H_4L^{O(AP/AP)}$

It was previously mentioned that the coordinated ligand backbone in complex **3A** was different from the initially employed ligand, $\mathbf{H_4L^{O(AP/AP)}}$ (Section 3.2). During the reaction, the initially generated brown crude (**A**) was isolated and characterized by several spectroscopic/spectrometric techniques (Fig. 3.11). Structural characterization of the intermediate **A** was not possible as it readily underwent formation of complex **3A** during crystallization. The presence of ν(O–H) = 3368 and ν(N–H) = 3224 cm^{-1} bands in the infrared spectrum of intermediate **A** conjectured the existence of free aminophenol unit within the complex. ESI–MS(+) analysis of the intermediate in CH_3CN showed a 100% molecular ion peak at *m*/*z* = 1269.69, which corresponded to 2:1 ligand:Co complex having one free aminophenol unit. Experimental and simulated isotope distribution pattern confirmed the composition as $[C_{80}H_{98}N_4O_6Co]^+$. The solid phase X–band EPR spectrum of intermediate **A** (Fig. 3.11D) was

supportive for the existence ligand centered single unpaired electron (S_t = 1/2). The charge neutrality and the mentioned spectroscopic evidences revealed that the intermediate was composed by an octahedral Co(III)–ion coordinated with three iminsemiquinone [$(ISQ)^{\bullet 1-}$] moieties comes from two ligand molecules (Fig. 3.11A).

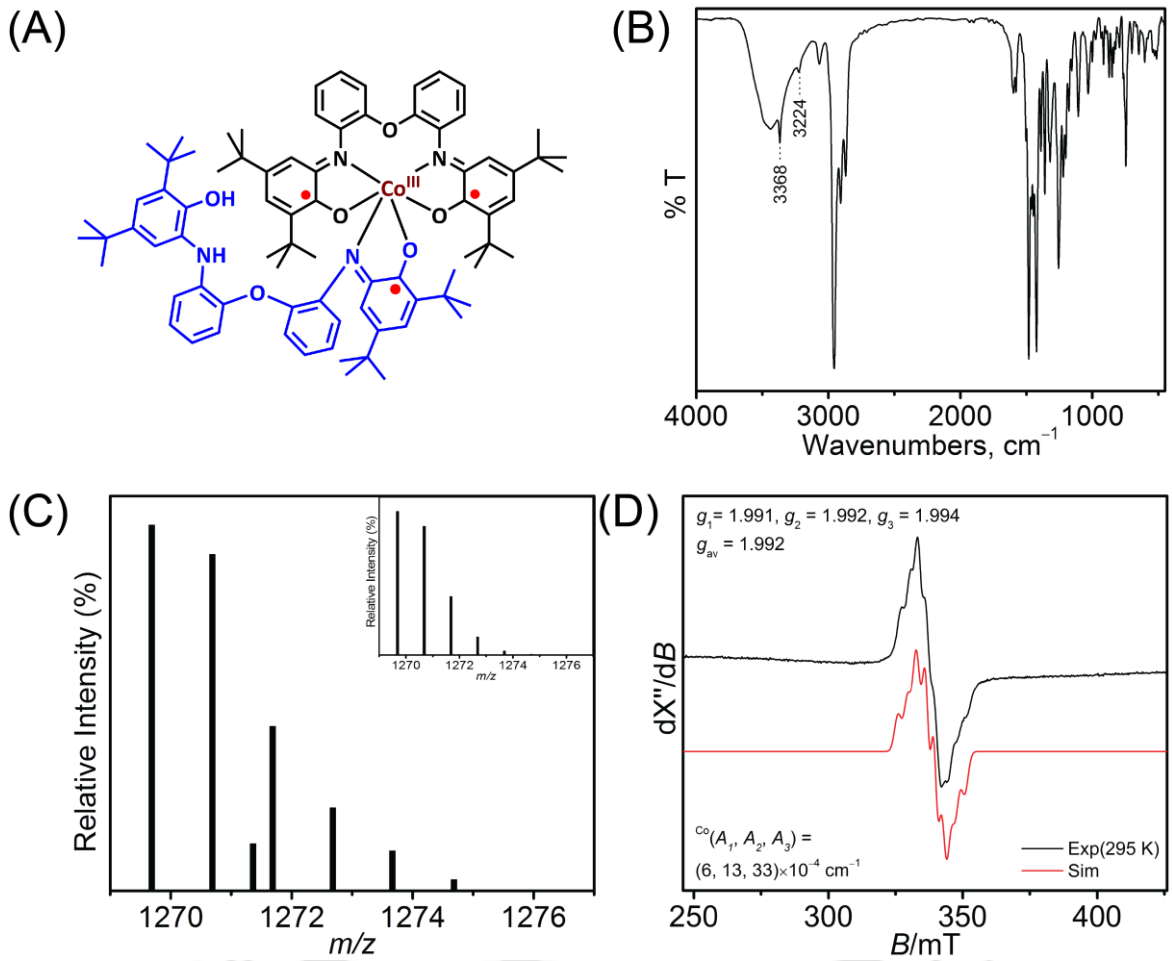

Figure 3.11: *Intermediate **A** and its characterizations.*

In addition to characterization of the isolated brown–intermediate, mass spectrometry analysis (Fig. 3.12) of the reaction solution was carried out further in order to better understanding of the reaction path.

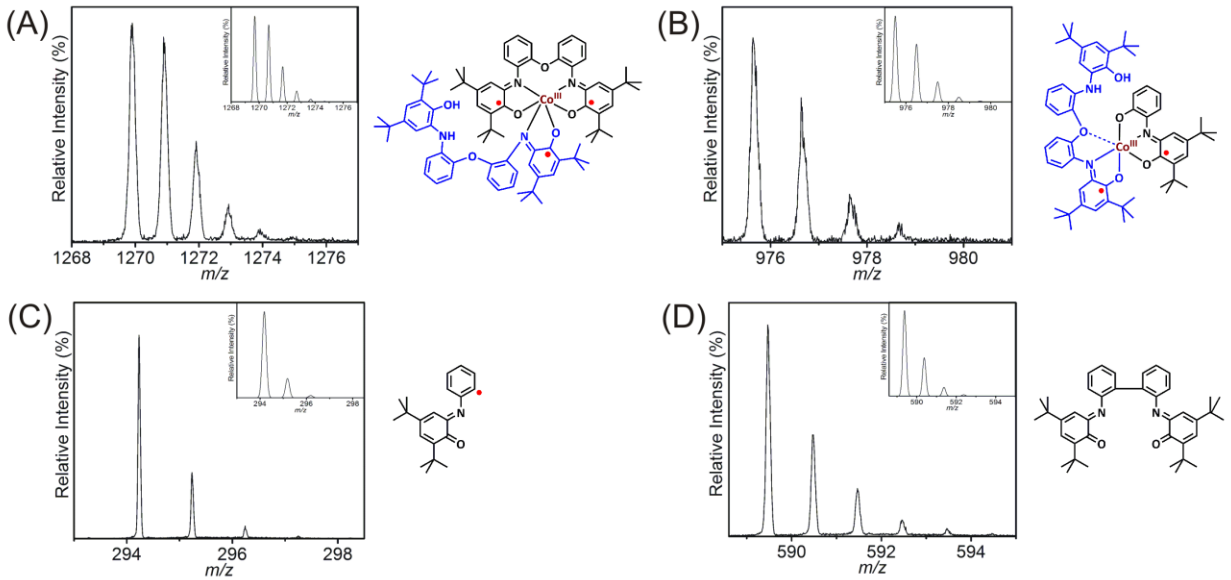

Figure 3.12: *ESI–mass spectrum (+ve mode) of the reaction mixture with experimental and simulated (inset) isotope distribution patterns.*

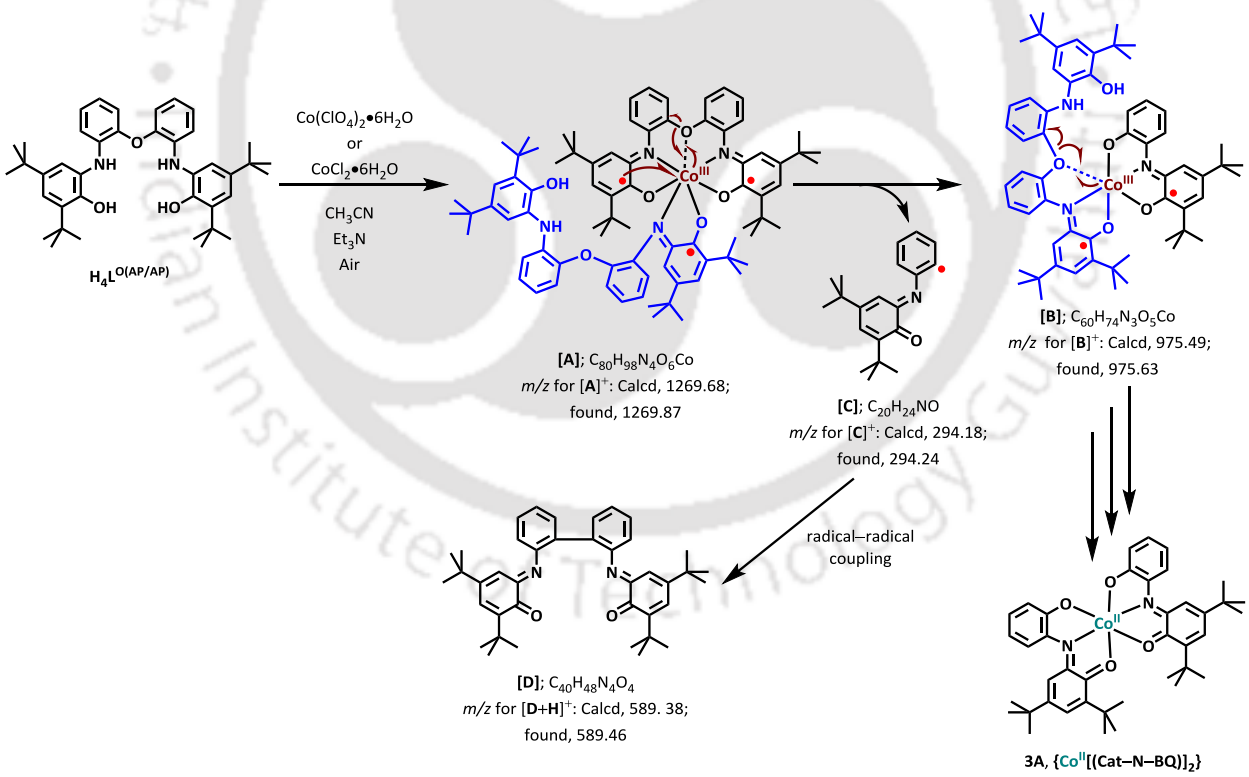

Scheme 3.9: *Proposed mechanism of the formation of complex **3A** from* $H_4L^{O(AP/AP)}$.

In mass spectrum of the reaction mixture, a peak at *m*/*z* = 1269.87 was attributed the generation of intermediate **A**. The existence of species **B** (*m*/*z* = 975.63) and **C** (*m*/*z* = 294.24) in the reaction mixture implied the C_{aryl}–O_{bridge} activation and thereafter homolytic C_{aryl}–O_{bridge} bond breaking and homolytic Co–O_{bridge} bond formation. Those homolytic bond breaking and formation inside the intermediates (**A** and **B**) proceeded through simultaneous oxidation of iminosemiquinone [$(ISQ)^{\bullet 1-}$] to the corresponding iminoquinone [$(IBQ)^{0}$] in the progress of complex **3A** formation. The mechanistic proposal has been shown in scheme 3.9.

3.5: Synthesis and Characterization of Co Complexes from S (3B), Te (3C) Bridged Ligands by Using $CoCl_2$•$6H_2O$ as the Metal ion Source

Ligands having same structural motif, however, with different bridging atom (S and Te) produced X–band EPR inactive binuclear complexes on reacting with equimolar amount of $CoCl_2$•$2H_2O$ in CH_3CN at presence of Et_3N (Scheme 3.10). Those complexes are designated as **3B** and **3C**, respectively. Similar analogue from Se bridged ligand was not able to produce in good yield.

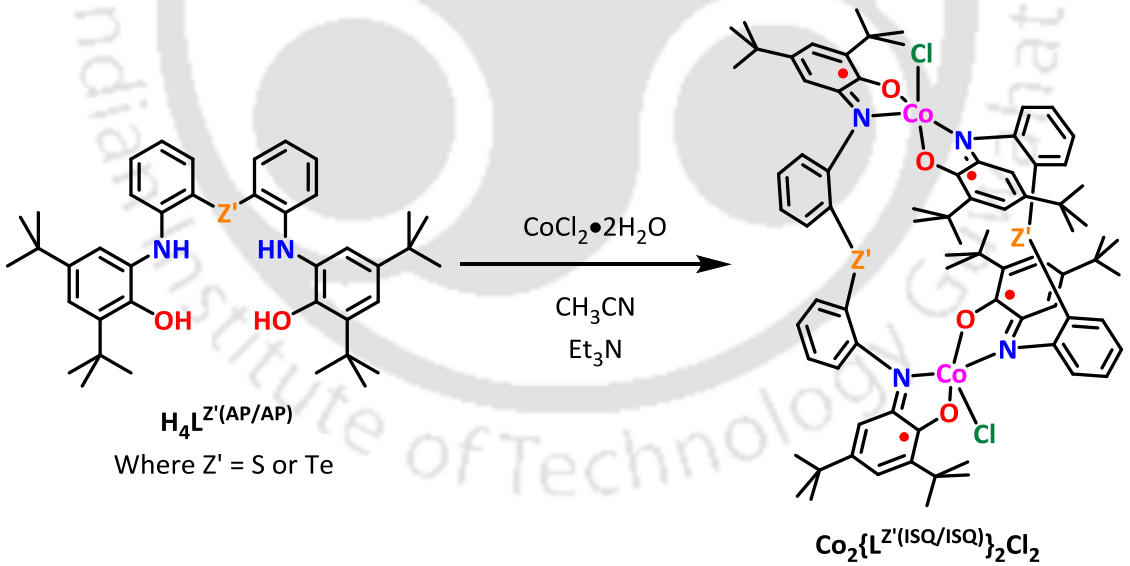

Scheme 3.10: *General synthetic route for formation of* ***$Co_2\{L^{Z'(ISQ/ISQ)}\}_2Cl_2$****; where Z′ = S or Te.*

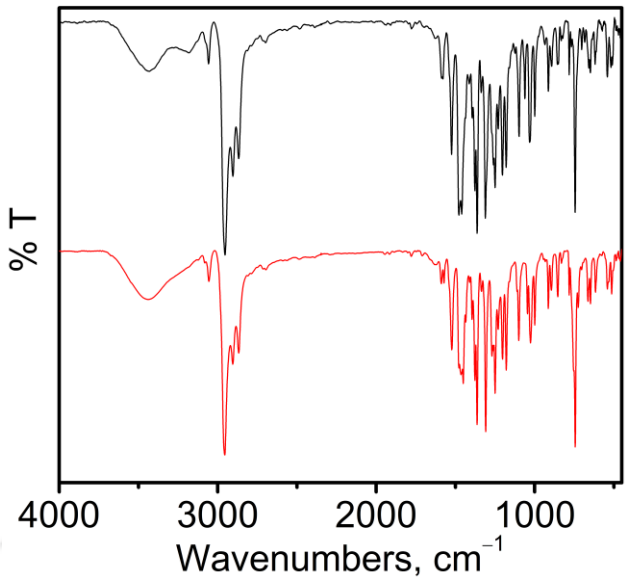

Figure 3.13: *FTIR spectrum of complex **3B** (black line) and complex **3C** (red line).*

Complex **3B** and **3C** have shown similar type of infrared spectrums (Fig. 3.13). The absence of sharp peaks at the region 3200–3500 cm^{-1} indicates the metal coordination with the deprotonated –OH and –NH groups. A band around 3056 cm^{-1} was observed due to ν(C_{ph}–H) stretching frequencies. The bands at 3179 cm^{-1} (**3B**) was attributed as ν(C_{ph}–H) stretching frequencies.[13*a*] Three distinct bands at the range 2960–2865 cm^{-1} ascribed for asymmetric, overtone and symmetric type of ν(C–H) stretches for *tert*–butyl group. A set of band at around 1587 and 1363 cm^{-1} was corresponded to ν(C⋯N) and ν(C⋯O) stretches of the iminosemiquinone anion ($ISQ^{\bullet 1-}$).[13*b–d*]

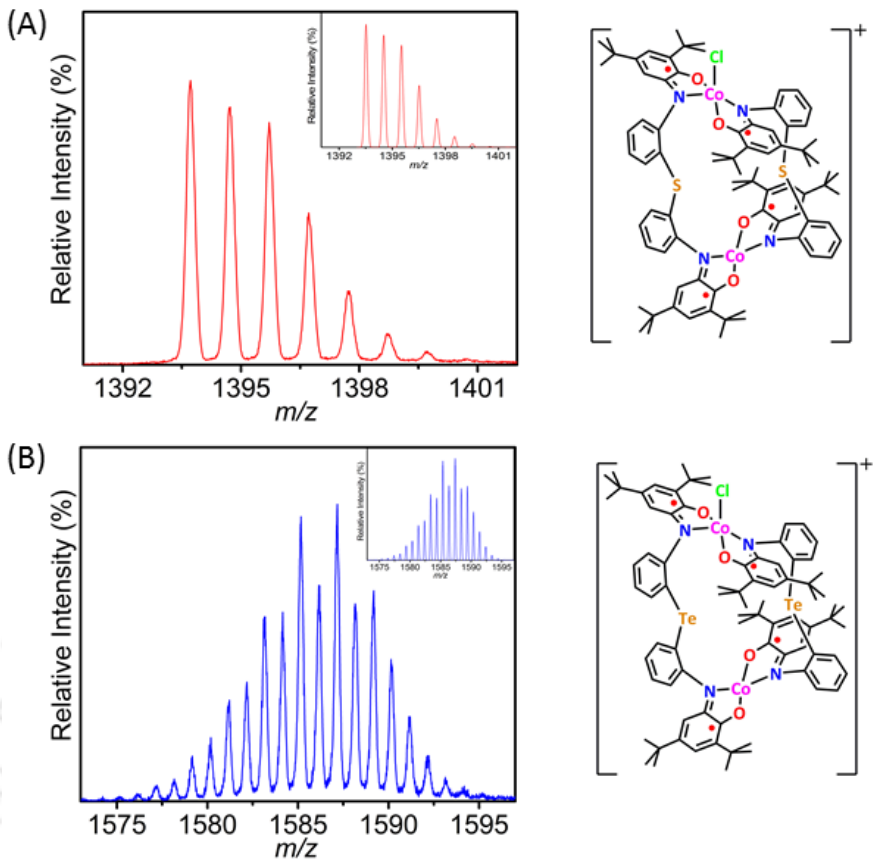

Figure 3.14: *ESI–mass spectrum of [A] complex **3B** and [B]complex **3C** in +ve mode corresponded to $[M–Cl]^+$ molecular ion peak; experimental and calculated isotope distribution pattern (inset).*

Electrospray ionization (+ve) mass spectrum in acetonitrile for the complex **3B** and **3C** have been shown in Fig. 3.14. For complex **3B**, a 100% molecular ion peak at *m/z* 1393.72 corresponded to $[M–Cl]^+$. Calculated isotope distribution pattern endorsed the composition as $[C_{80}H_{96}Co_2N_4O_4S_2Cl]^+$. Complex **3C** also shown similar kind of mass peaks at *m/z* 1587.16 but the relative intensity was only 5%. Isotope distribution pattern confirmed the composition as $[C_{80}H_{96}Co_2N_4O_4Te_2Cl]^+$.

The ORTEP representation of molecular structures of complex **3B** and **3C** are shown in Fig. 3.15. Single crystal X–ray diffraction analyses are suggestive for structural similarity and binuclear nature of the species.

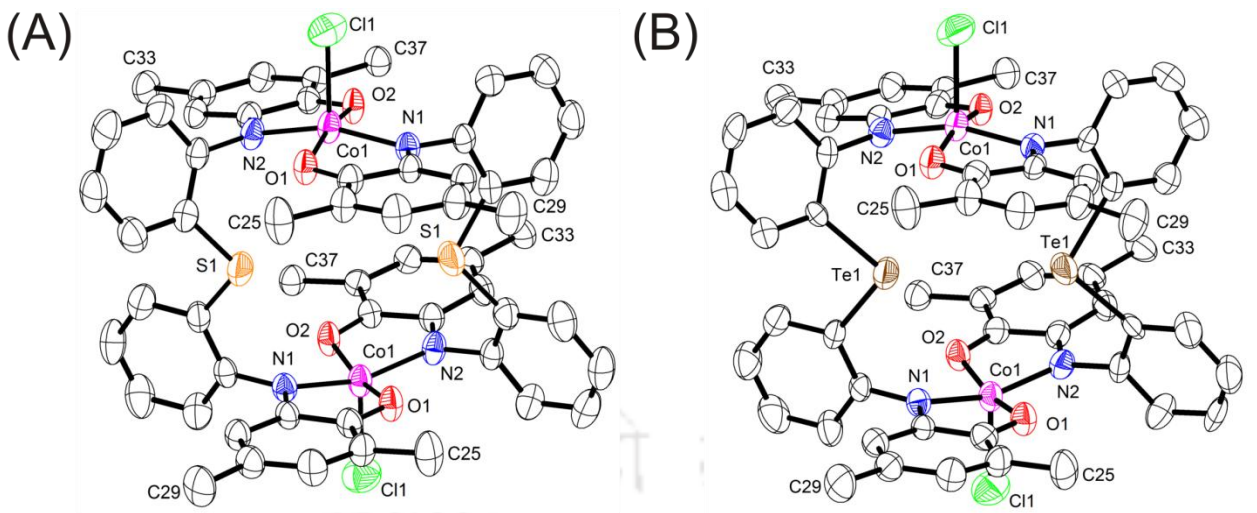

Figure 3.15: *ORTEP representation of (A) complex **3B** and (B) complex **3C**; thermal ellipsoids were drawn at 40 % probability level; H atom, solvent molecule and methyl groups attached with C25, C29, C33 and C37 were omitted for clarity.*

The crystal structure of **3B** was measured at 293(2) K by single crystal X–ray diffraction technique. The complex was crystallized in the orthorhombic crystal system having space group *'Pbcn'*. The neutral complex consisted of two Co(III)–ion coordinated with two ligand molecules. Selected bond distances and bond angles are presented in Table 3.5.

The double–decker type of structure was composed by two oppositely orientated square pyramidal Co(III)–diradical units. In each of the square pyramidal unit (τ ~ 0.1),[14] the Co–ion was coordinated with two amidophenolate moieties at the basal plane and the apex position was occupied by chloride ion. Due to the axial coordination, Co(III)–ions pulled by 0.273 Å from the basal plane composed by O1, N1, O2 and N2 atoms. The dihedral angle between two planes passing through two pentagonal chelate rings (plane1 containing Co1, N1, C1, C2, O1 atoms and plane2 Co1, N2, C19, C24, O2 atoms) was 16.97°. The average bond distance of Co–O and Co–N were 1.868 and 1.848 Å, respectively, while, the bond distance of Co1–Cl1 was found as ~2.250 Å. Those values suggested +III oxidation state and low spin state of the Co ions.[15*a–c*] In each of the coordinating amidophenolate unit, the bond distances of C–O and C–N bonds were in the range of 1.356±0.007 Å and 1.290±0.002 Å, respectively. Those values implied the partial double bond character of those C–O and C–N bonds.[15*d,e*] In addition to this, quinoid–type distortion *i.e.* short–long–short C–C bond followed by three successive long C–C bond was observed in the *tert*–butyl groups containing amidophenolate type C_6 rings. These structural features were suggestive for the existence of aminophenolate unit to its one–electron oxidized π–

radical anion *i.e.* $ISQ^{\bullet 1-}$ form. All the C–C bond distances for all others C_6 rings were found in the range of 1.363 ± 0.020 Å, as expected for normal aromatic phenyl rings.

Complex **2C** (Fig. 3.15B) also have shown similar structure like **3B**. The Co1–Co1* bond length was found as 6.035(1) [**3B**] and 6.544(1) [**3C**] Å. The distance between two bridging atoms was found as 4.598(1) [S1–S1*] and 3.979(1) [Te1–Te1*] for complex **3B** and **3C**, respectively.

Table 3.4: *Selected Bond Distances (Å) and Angles (deg) for Complexes **3B** and **3C**.*

	Complex 3B	**Complex 3C**
Co1–N1	1.855(3)	1.853(5)
Co1–N2	1.842(4)	1.851(5)
Co1–O1	1.867(3)	1.873(4)
Co1–O2	1.870(3)	1.861(4)
Co1–Cl1	2.250(2)	2.241(2)
O1–C2	1.292(5)	1.300(7)
O2–C24	1.288(5)	1.286(7)
N1–C1	1.349(5)	1.332(7)
N1–C7	1.426(5)	1.439(7)
N2–C18	1.420(5)	1.433(7)
N2–C19	1.362(5)	1.336(7)
Z1–C12	1.771(5)	2.122(7)
Z1–C13	1.764(5)	2.105(6)
C1–C2	1.433(6)	1.434(8)
C2–C3	1.441(6)	1.423(8)
C3–C4	1.355(6)	1.362(9)
C4– C5	1.414(7)	1.443(9)
C5–C6	1.384(6)	1.362(9)
C1–C6	1.415(6)	1.422(8)
C7–C8	1.370(6)	1.370(9)
C8–C9	1.403(7)	1.377(10)
C9– C10	1.361(8)	1.352(10)
C10–C11	1.368(7)	1.367(9)
C11–C12	1.399(6)	1.415(8)
C7–C12	1.379(6)	1.350(8)
C13–C14	1.402(7)	1.383(9)
C14–C15	1.379(8)	1.392(10)
C15– C16	1.366(8)	1.354(10)
C16–C17	1.395(7)	1.380(9)
C17–C18	1.371(6)	1.392(9)
C18–C13	1.376(7)	1.389(9)
C19–C20	1.420(6)	1.427(8)
C20–C21	1.389(6)	1.355(9)
C21–C22	1.426(6)	1.421(8)

C22–C23	1.367(6)	1.374(8)
C23– C24	1.445(6)	1.439(8)
C19–C24	1.428(6)	1.445(8)
N2–Co1–N1	160.18(17)	160.0(2)
N2–Co1–O1	93.12(15)	93.4(2)
N1–Co1–O1	83.65(14)	83.7(2)
N2–Co1–O2	84.01(14)	83.6(2)
N1–Co1–O2	94.39(14)	94.3(2)
O1–Co1–O2	165.95(15)	165.6(2)
N2–Co1–Cl1	102.03(13)	101.9(2)
N1–Co1–Cl1	97.77(12)	98.1(2)
O1–Co1–Cl1	97.54(12)	97.69(17)
O2–Co1–Cl1	96.51(11)	96.8(2)
C13–Z1–C12	104.9(2)	98.7(2)
C1–N1–C7	118.5(3)	119.3(5)
C1–N1–Co1	113.7(3)	114.1(4)
C7–N1–Co1	127.5(3)	126.4(4)
C19–N2–C18	118.7(4)	117.8(5)
C19–N2–Co1	114.4(3)	115.0(4)
C18–N2–Co1	126.9(3)	127.2(4)
C2–O1–Co1	114.2(3)	113.9(4)
C24–O2–Co1	114.0(3)	114.6(4)

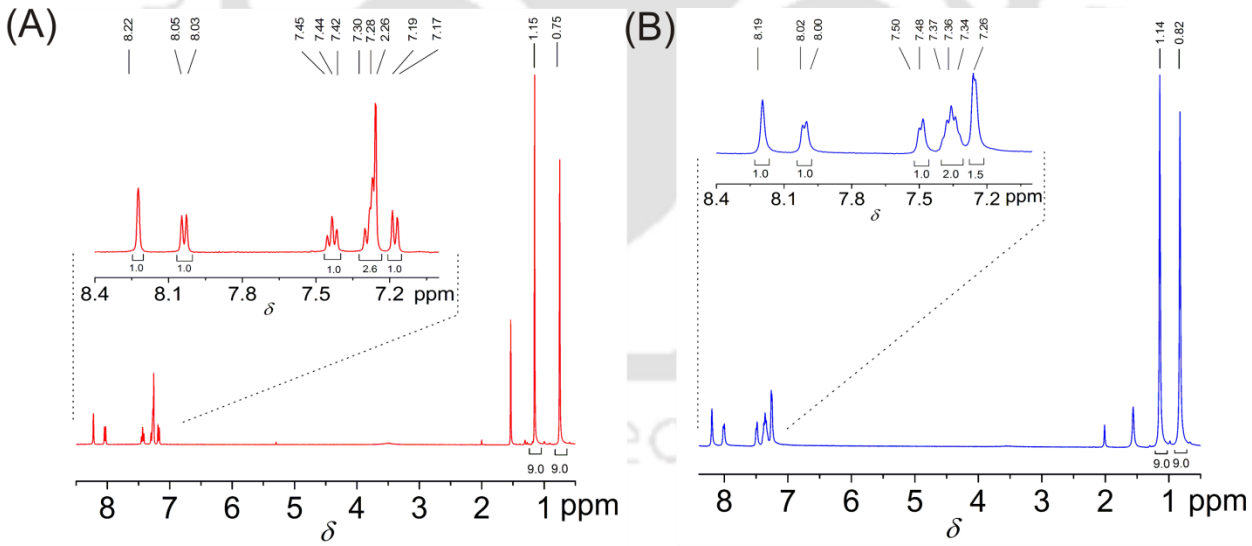

Figure 3.16: *[1]HNMR spectrum of [A]complex **3B** and [B] complex **3C** in CD_3Cl.*

In the complex, each of the square pyramidal moiety experienced an antiferromagnetic coupling between two Co(III)–coordinating π–radicals [$ISQ^{\bullet 1-}$] and thus, the entire molecule was diamagnetic. This argument was also supported by ^{1}H NMR ($CDCl_3$, 399.85 MHz) analysis at 298 K. In the spectrum, no major negative shift for the protons associated within the complex was observed.. ^{1}H NMR measurement of complex **3B** provided the signals at δ 8.22 (s, 4H), 8.04

(d, *J* = 7.6 Hz, 4H), 7.45–7.41 (m, 4H), 7.30–7.26 (m, 8H), 7.18 (d, *J* = 7.6 Hz, 4H), 1.15 (s, 36H), 0.75 (s, 36H) ppm (Fig. 3.16). Complex **3C** also provided the ^{1}H NMR signals at δ 8.19 (s, 4H), 8.01 (d, *J* = 6.0 Hz, 4H), 7.49 (d, *J* = 7.2 Hz, 4H), 7.37–7.34 (m, 8 H), 7.26 (s, 4H), 1.14 (s, 36H), 0.82 (s, 36H) ppm with no peak at high field.

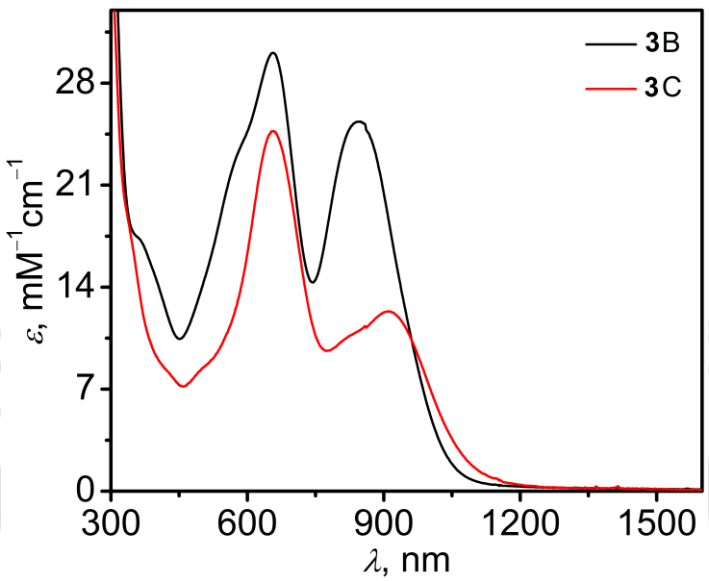

Figure 3.17: *UV–Vis/NIR spectrums of complex **3B** (black line) and complex **3C** (red line) in dichloromethane at 298 K.*

The electronic absorption spectra of complex **3B** and complex **3C** were measured in dichloromethane at room temperature and shown in Fig 3.19. The band positions along with the extinction coefficient values were summarized in Table 3.5. The absorption bands at 656 (**3B**), 909 (**3C**) and 657 (**3C**) nm were assigned as ligand–to–metal charge transfer (LMCT).[15a,b] The absorption maxima at 843 (**3B**) and 834 (**3C**) nm (parenthesis indicates the complex) corresponded to ligand–to–ligand charge transfer.[15c,d]

Table 3.5: *Electronic absorption data for complex **3B** and **3C**.*

Complex	λ_{max}, nm (ε, M^{-1} cm^{-1})
3B	842(25300), 655(30100), 573^{sh}(22700), 365(17200).
3C	909(12350), 834^{sh}(10800), 657(24700), 498^{sh}(8300).

*superscript 'sh' stands for shoulder band.

3.6: Synthesis and Characterization of Co Complex (3D) from S Bridged Ligand by Using $Co(ClO_4)_2•6H_2O$ as the Metal Source

The dinuclear Co complex (**3B**) formation proceeded by the metalation with $CoCl_2•2H_2O$. The square pyramidal coordination sphere around each of Co(III)–ion was same and the axial coordination was occupied by a chloride ion comes from the metal salt. A normal curiosity was developed regarding the effect of counter anion on similar kind of reaction. Herein, the complexation of ligand $H_2L^{S(AP/AP)}$ with $Co(ClO_4)_2•6H_2O$ provided complex **3D**. The lack of axial chloride ion led C_{Ar}–S activation and provided a 3L(ligand):2M(Co^{III}) complex, **3D**.

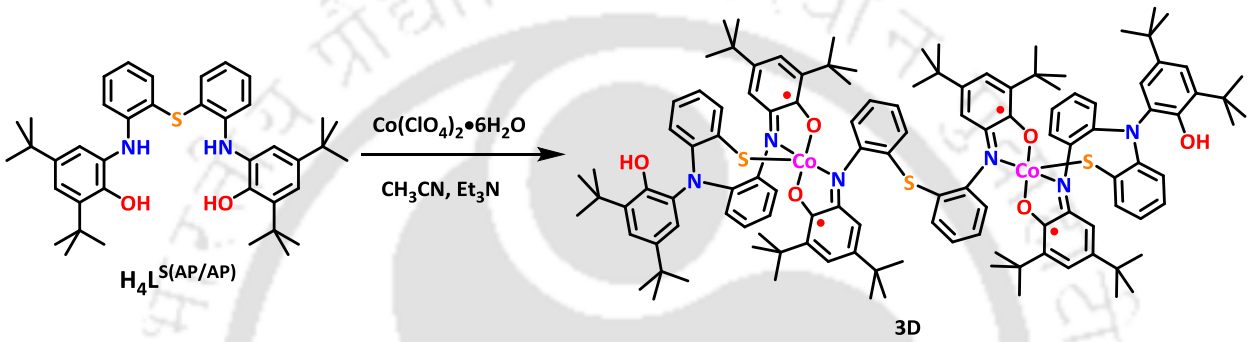

Scheme 3.11: *Synthetic route of complex **3D** from $H_2L^{S(AP/AP)}$.*

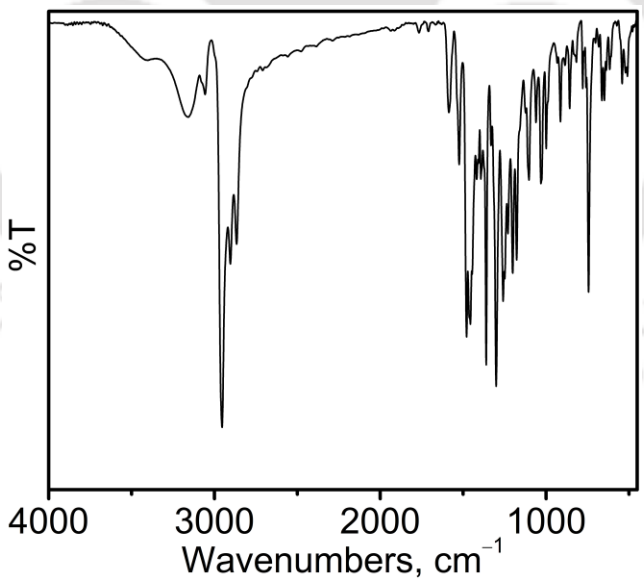

Figure 3.18: *FTIR spectrum of complex **3D**.*

FTIR spectrum of the complex is suggestive for the metal coordination along with the charge of coordinating amidophenolate moieties. In the spectrum, three bands at the range 2960–2865 cm^{-1} ascribed for asymmetric, overtone and symmetric type of ν(C–H) stretches for *tert*–butyl group.[8c–e] Those bands implied the metal coordination with the *tert*–butyl group

containing ligand fragment. Two bands at 1587 and 1363 cm^{-1} were corresponded to ν(C⋯N) and ν(C⋯O) stretches of the metal coordinated iminosemiquinone anion ($ISQ^{\bullet 1-}$) moieties.[13b–d]

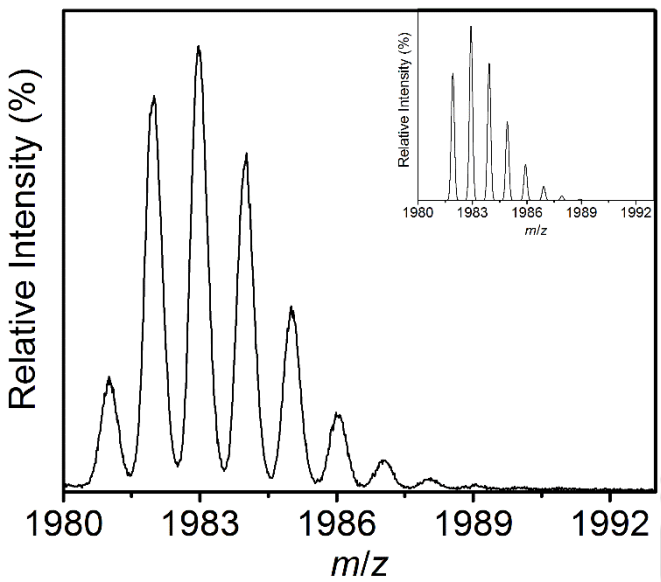

Figure 3.19: *ESI–mass spectrum of complex **3D** in +ve mode corresponded to $[M+H]^+$ molecular ion peak; experimental and calculated isotope distribution pattern (inset).*

Electrospray ionization mass spectrum (ESI–MS) of a solution of complex **3D** in CH_3CN provided a 100% molecular ion peaks at *m/z* = 1982.98 at positive mode. The observed peak corresponded to the $[M+H]^+$ ion and the isotope distribution pattern confirmed the composition as $[C_{120}H_{147}Co_2N_6O_6S_3]^+$.

The complex was crystalized from a diethyl ether:acetonitrile (3:1) solvent mixture and the resultant crystal was measured by single crystal X–ray diffractometer at 293(2) K. The molecular structure of complex **3D** is shown in Fig. 3.20. The selective bond length and angle parameters are given in Table 3.6.

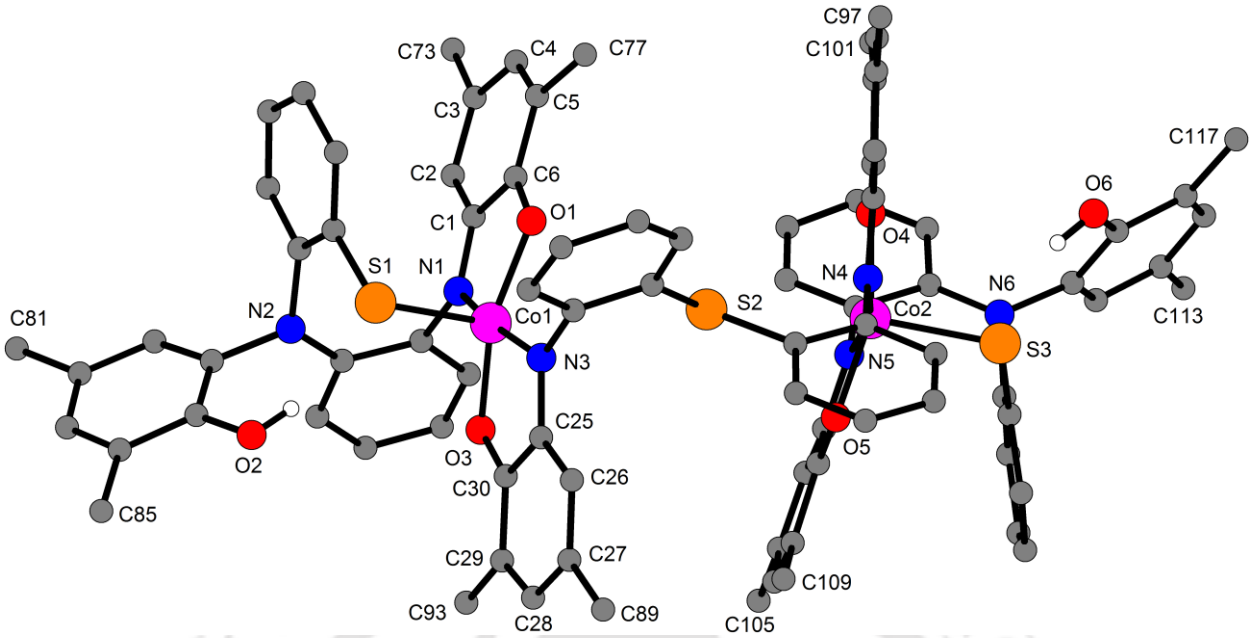

Figure 3.20: *Ball and stick presentation of complex **3D**; H–atoms (except attached with O2 and O6), methyl groups (attached with C73, C77, C81, C85, C89, C93, C97, C101, C105, C109, C113 and C117) were omitted for clarity.*

The complex was crystalized in the triclinic '*P*–1' space group. The neutral molecule consisted of two Co(III)–ions and three ligand molecules. The square pyramidal coordination sphere around each of the metal ion was same. Each of the Co–ion was coordinated with two amidophenolate units (from two different ligand molecules) at basal plane and the axial site was occupied by an aryl sulfide fragment. The average bond length of Co–N, Co–O and Co–S bonds were found as 1.865, 1.850 and 2.255 Å, respectively. The metal coordinated amidophenolate unit having C–N and C–O bond distances equal to 1.352±0.015 and 1.298±0.008 Å, respectively. Those values implied the partial double bond character of those C–O and C–N bonds.[15d,e] In addition to this, quinoid–distortion *i.e.* short–long–short C–C bond followed by three successive long C–C bond was observed in those metal coordinated amidophenolate C_6 rings. Thus, the structural feature was suggestive for the existence of those aminophenolate units to its one–electron oxidized π–radical anion *i.e.* $ISQ^{\bullet 1-}$ form. The terminal ligand provided the axial coordination through S–atom (Co–S = 2.255 Å). The axial S–coordination led a rearrangement within the terminal ligand moiety, which involved C_{Ar}–S bond cleavage and C_{Ar}–N bond formation. Thus, the terminal ligand contained a non–coordinated phenolic –OH group. However, in case of the connecting ligand between two square pyramidal Co(III) entities, the S–bridge didn't involve any coordination or interaction with the metal ion.

Table 3.6: *Selected Bond Distances (Å) and Angles (deg) for Complex **3D** (As the metal surrounding for each of the metal ion is nearly same, only Co1 coordination sphere is mentioned)*

Co1–N1	1.851(6)	C5–C6	1.439(10)
Co1–N3	1.840(6)	C1–C6	1.454(11)
Co1–O1	1.873(5)	C25–C26	1.399(10)
Co1–O3	1.866(4)	C26–C27	1.361(9)
Co1–S1	2.252(2)	C28–C27	1.431(10)
O1–C6	1.293(9)	C29–C28	1.352(10)
N3–C25	1.367(9)	C30–C29	1.438(9)
N1–C1	1.334(8)	C30–C25	1.439(10)
O3–C30	1.306(8)	S1–C18	1.744(9)
C1–C2	1.392(11)	S2–C36	1.766(8)
C3–C2	1.387(11)	S2–C37	1.777(8)
C4–C3	1.417(11)	S3–C66	1.737(10)
C5–C4	1.363(11)		
N1–Co1–N3	168.9(3)	O1–Co1–S1	98.7 (2)
N1–Co1–O3	94.4(2)	N3–Co1–S1	94.1(2)
N1–Co1–O1	84.0(2)	O3–Co1–S1	99.3(2)
O1–Co1–O3	162.0(2)	C36–S2–C37	100.9(4)
O1–Co1–N3	94.3(2)	C18–S1–Co1	101.4(3)
N3–Co1–O3	83.8(2)	C66–S3–Co2	100.8(4)
N1–Co1–S1	97.1(2)		

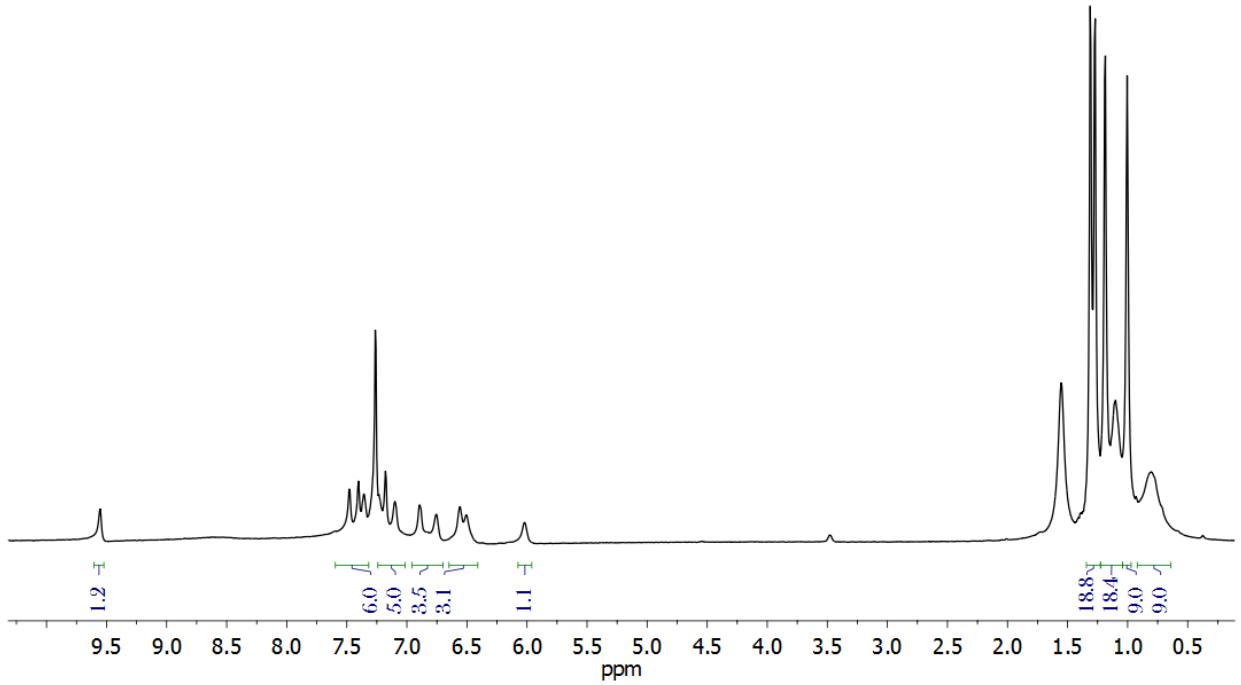

Figure 3.21: *^{1}H NMR spectrum of complex **3D** in CD_3Cl.*

The presence of strong antiferromagnetic coupling between Co(III) coordinated two π–radicals at the basal plane provided S_t = 0 in each of the square pyramidal moiety. Thus the overall compound was magnetically diamagnetic. This argument was also supported by ^{1}H NMR ($CDCl_3$, 399.85 MHz) analysis. No negative shift for the protons associated within the complex was observed in ^{1}H NMR measurement. ^{1}H NMR measurement of complex **3D** provided the signals at δ 9.55 (s, 2H), 7.48−7.36 (m, 12H), 7.23–7.10 (m, 10 H), 6.89–6.36 (m, 6H), 6.56−6.51 (m, 6H), 6.02 (s, 2H), 1.31−0.80 (s, 108H) ppm (Fig. 3.21).

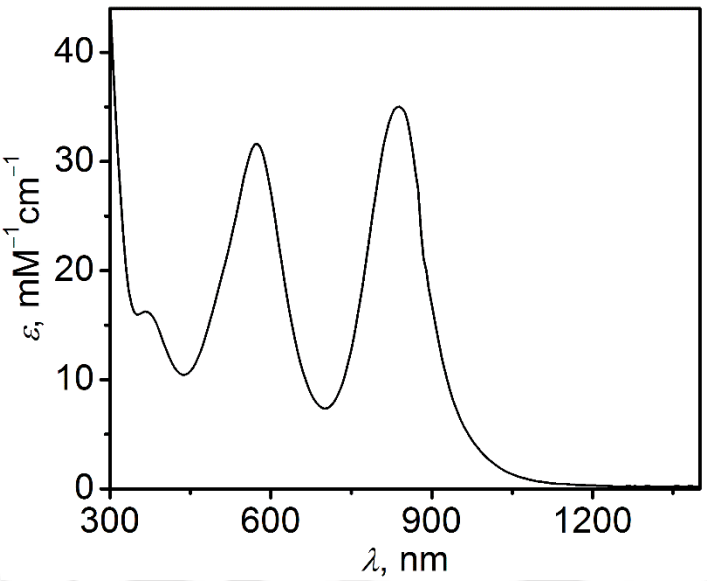

Figure 3.22: *UV–Vis/NIR spectrums of complex **3D** in dichloromethane at 298 K.*

The electronic absorption spectrum of complex **3D** was measured in dichloromethane at room temperature and shown in Fig 3.24. The band positions along with the extinction coefficient values were summarized in Table 3.7. The intense absorption band at 843 nm was corresponded to ligand–to–ligand charge transfer which was resemble with Co(III)–bis(iminosemiquinone) species.[15] Another absorption band at 575 nm was assigned as ligand–to–metal charge transfer (LMCT).[15a,b]

Table 3.7: *Electronic absorption data of **3D**.*

Complex	**λ_{max}, nm (ε, M^{-1} cm^{-1})**
3D	840(35000), 575(31500), 365(16200)

3.7: Conclusions

- The O−bridge ligand $\mathbf{H_4L^{O(AP/AP)}}$ provides a mononuclear octahedral cobalt complex **3A** through an initial generation of intermediate **A** upon reacting with $CoCl_2•6H_2O$ or $Co(ClO_4)_2•6H_2O$.
- The formation of complex **3A** from intermediate **A** proceeds by two set of successive homolytic $C_{aryl}–O_{bridge}$ bond breaking and homolytic $Co–O_{bridge}$ bond formation.
- Crystalline complex **3A** shows solution as well as solid phase thermal valence tautomerism where the solid phase tautomeric conversion depends upon the availability of the lattice solvent within the crystalline matrix.
- Similar type of ligand with different bridging atom (S and Te) provided double–decker type tetraradical–containing binuclear Co^{III} complex during the reaction with $CoCl_2•6H_2O$. The resultant complex **3B** and **3C** are diamagnetic in nature.
- The S−bridged ligand $\mathbf{H_4L^{S(AP/AP)}}$ provides an tetraradical–containing binuclear Co^{III} complex **3D** upon reacting with $Co(ClO_4)_2•6H_2O$ in CH_3CN. In the complex, the axial S coordination to the metal ion is caused by $C_{Ar}–S$ bond cleavage and $C_{Ar}–N$ bond formation in the terminal ligand fragments.
- The bridging Ar−Z (Z = O, S, and Te) bond distance is found to determine the nuclearity of the generated Co complexes.

References

1. (*a*) W. Kaim and B. Schwederski, *Coord. Chem. Rev.*, 2010, **254**, 1580; (*b*) W. Kaim, *Coord. Chem. Rev.*, 1987, **76**, 187; (*c*) P. J. Chirik and K.Wieghardt, *Science*, 2010, **327**, 794; (*d*) P. J. Chirik, *Inorg. Chem.*, 2011, **50**, 9737.

2. (*a*) D. L. J. Broere, R. Plessius and J. I. van der Vlugt, *Chem. Soc. Rev.*, 2015, **44**, 6886; (*b*) F. Dénès, M. Pichowicz, G. Povie and P. Renaud, *Chem. Rev.*, 2014, **114**, 2587.

3. (*a*) M. Findlater, W. H. Bernskoetter, and M. Brookhart, *J. Am. Chem. Soc.*, 2010, **132**, 4534; (*b*) C. C. C. J. Seechurn, M. O. Kitching, T. J. Colacot and V. Snieckus, *Angew. Chem., Int. Ed.*, 2012, **51**, 5062.

4. (*a*) A. L. Smith, L. A. Clapp, K. I. Hardcastle and J. D. Soper, *Polyhedron*, 2010, **29**, 164. (*b*) S. Ghorai and C. Mukherjee, *Chem. Commun.*, 2012, **48**, 10180; (*c*) S. H. A. M. Leenders, R. Gramage–Doria, B. de Bruin and J. N. H. Reek, *Chem. Soc. Rev.*, 2015, **44**, 433; (*e*) S. Ghorai and C. Mukherjee, *Dalton Trans.*, 2014, **43**, 394; (*f*) V. Lyaskovskyy and B. de Bruin, *ACS Catal.*, 2012, **2**, 270; (*g*) S. Ghorai, C. Mukherjee, *Chem. Asian J.*, 2014, 3518; (*h*) S. Ghorai, C. Mukherjee, *RSC Advances*, 2014**, 4**, 24698.

5. (*a*) A. L. Smith, K. I. Hardcastle and J. D. Soper, *J. Am. Chem. Soc.*, 2010, **132**, 14358; (*b*) A. R. Corcos, O. Villanueva, R. C. Walroth, S. K. Sharma, J. Bacsa, K. M. Lancaster, C. E. MacBeth and J. F. Berry, *J. Am. Chem. Soc.*, 2016, **138**, 1796; (*c*) M. van der Meer, Y. Rechkemmer, I. Peremykin, S. Hohloch, J. van Slageren and B. Sarkar, *Chem. Commun.*, 2014, **50**, 11104.

6. (*a*) E. Evangelio, C. Rodriguez–Blanco, Y. Coppel, D. N. Hendrickson, J. P. Sutter, J. Campo and D. Ruiz–Molina, *Solid State Sci.*, 2009, **11**, 793; (*b*) H. Spiering, T. Kohlhaas, H. Romstedt, A. Hauser, C. Bruns–Yilmaz, J. Kusz and P. Gütlich, *Coord. Chem. Rev.*, 1991, **111**, 275; (*c*) P. Gütlich, A. B. Gaspar and Y. Garcia, *Beilstein J. Org. Chem.*, 2013, **9**, 342; (*d*) N. Azzaroli, A. Lapini, M. D. Donato, A. Dei, and R. Righini, *J. Phys. Chem. B.*, 2013, **117**, 15492; (*e*) D. M. Adams and D. N. Hendrickson, *J. Am. Chem. Soc.*, 1996, **118**, 11515; (*f*) F. Novio, E. Evangelio, N. Vazquez–Mera, P. González– Monje, E. Bellido, S. Mendes, N. Kehagias and D. Ruiz–Molina, *Sci. Rep.*, 2013, **3**, 1708.

7. P. Chaudhuri, C. N. Verani, E. Bill, E. Bothe, T. Weyhermüller and K. Wieghardt, *J. Am. Chem. Soc.*, 2001, **123**, 2213.

8. (*a*) J. Coates, *Interpretation of Infrared Spectra: A Practical Approach*, John Wiley & Sons Ltd, Chichester, 2000; (*b*) G. R. Pandhare, V.M. Shinde and Y. H. Deshpande, *Rasayan J. Chem.*, 2008, **1**, 337; (*c*) P. K. Kipkemboi, P. C. Kiprono and J. J. Sanga, *Bull. Chem. Soc. Ethiop.*, 2003, **17**, 211; (*d*) D. L. Pavia, G. M. Lampman, G. S. Kriz and J. R. Vyvyan, *Introduction to Spectroscopy*, 4th edition, 31.

9. S. K. Larsen and C. G. Pierpont, *J. Am. Chem. Soc.*, 1988, **110**, 1827.

10. (a) C. L. Simpson, S. R. Boone and C. G. Pierpont, *Inorg. Chem.*, 1989, **28**, 4379; (b) A. Sasmal, E. Garribba, C. J. Gómez–García, C. Desplanches and S. Mitra, *Dalton Trans.*, 2014, **43**, 15958.

11. (*a*) O. Cador, F. Chabre, A. Dei, C. Sangregorio, J. V. Slageren, and M. G. F. Vaz, *Inorg. Chem.*, 2003, **42**, 6432; (*b*) A. Y. Girgis and A. L. Balch, *Inorg. Chem.*, 1975, **14**, 2724; (*c*) A. Caneschi, A. Cornia, and A. Dei, *Inorg. Chem.*, 1998, **37,** 3419; (*d*) S. Bruni, A. Caneschi, F. Cariati, C. Delfs, A. Dei, and D. Gatteschi, *J. Am. Chem. Soc.* 1994, **116**, 1388.

12. As obtained by microanalysis (C, H, N values).

13. (*a*) S. Senthil, S. Arulmozhi, and J. Madhavan, *Der Pharma Chemica*, 2013, **5,** 228; (*b*) A. V. Piskunov, A. V. Lado, G. A. Abakumov, V. K. Cherkasov, O. V. Kuznetsova, G. K. Fukin, and E. V. Baranov, *Russ. Chem. Bull., Int. Ed.*, 2007, **56**, 97; (*c*) C. W. Lange and C. G. Pierpont, *Inorg. Chim. Acta*, 1997, **263**, 219 ; (*d*) G. A. Abakumov, V. K. Cherkasov, M. P. Bubnov,a L. G. Abakumova, V. N. Ikorskii, G. V. Romanenko and A. I. Poddel´sky, *Russ. Chem. Bull., Int. Ed.*, 2006, **55**, 44.

14. A. W. Addison, N. T. Rao, J. Reedijk, J. van Rijn, G. C. Verschoor, *J. Chem. Soc. Dalton Trans.*, 1984. 1349.

15. (*a*) E. Bill, E. Bothe, P. Chaudhuri, K. Chlopek, D. Herebian, S. Kokatam, K. Ray, T. Weyhermüller, F. Neese and K. Wieghardt, *Chem. Eur. J.*, 2005, **11**, 204; (*b*) A. I. Poddel'sky, V. K. Cherkasov, G. K. Fukin, M. P. Bubnov, L. G. Abakumova and G. A. Abakumov, *Inorg. Chim. Acta.*, 2004, **357**, 3632; (*c*) C. N. Verani, S. Gallert, E. Bill, T. Weyhermüller, K. Wieghardt and P. Chaudhuri, *Chem. Commun.*, 1999, 1747; (*d*) M. M. Khusniyarov, K. Harms, O. Burghaus, J. Sundermeyer, B. Sarkar, W. Kaim, J. van Slageren, C. Duboc and J. Fiedler, *Dalton Trans.*, 2008, 1355; (*e*) S. Kokatam, T. Weyhermüller, E. Bothe, P. Chaudhuri and K. Wieghardt, *Inorg. Chem.*, 2005, **44**, 3709.

Chapter IV

*Synthesis and Characterization of a Distal–NO_2 group Appended Aminophenol–Based Ligand and its Corresponding First–Row Transition Metal Complexes**

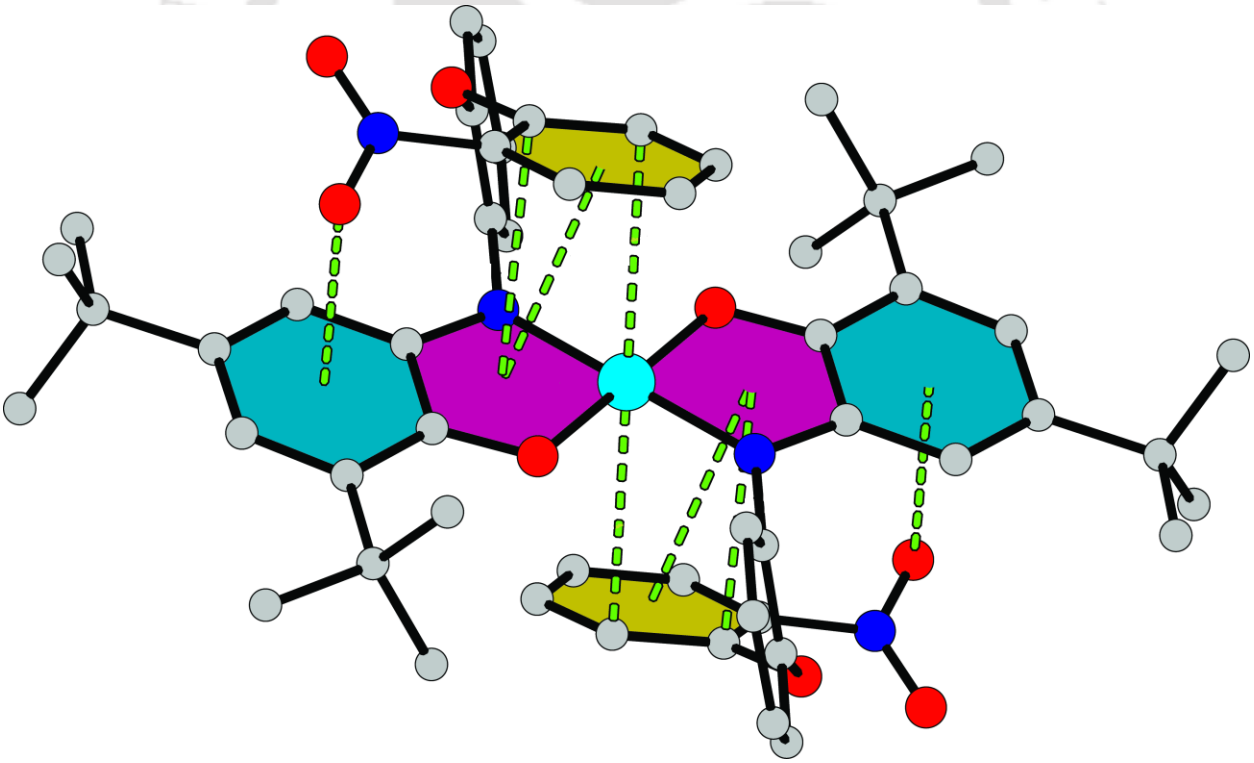

* Some results have been reported in *Dalton Trans.*, 2016, **45**, 13532.

4.1: Introduction

Organic quinone derivatives have vast importance in several biological, medicinal, laboratorial and industrial perspectives.[1] Co–enzyme ubiquinone (Q–10) is an essential compound for the life and health of every living cell.[2] In structural sense, it is actually a *para* quinone derivatives associated with a long isoperonoid tail, which help to diffuse the enzyme in the hydrophobic phase of the inner mitochondrial membrane. The non–innocent attitude of the quinone moiety makes the enzyme a suitable two–electron transporter at respiratory electron transfer chain.

In the respiratory complex II (Succinate dehydrogenase), the catalytic succinate to fumarate oxidation at inner mitochondrial matrix proceeded by means of reduction of Q–10 to ubiquinol.[2] The oxidation–reduction reaction is a part of membrane associated electron transport in citric acid cycle. The procedure is essential for the transfer of proton across the membrane, which promotes the synthesis of ATP (adenosine triphosphate).

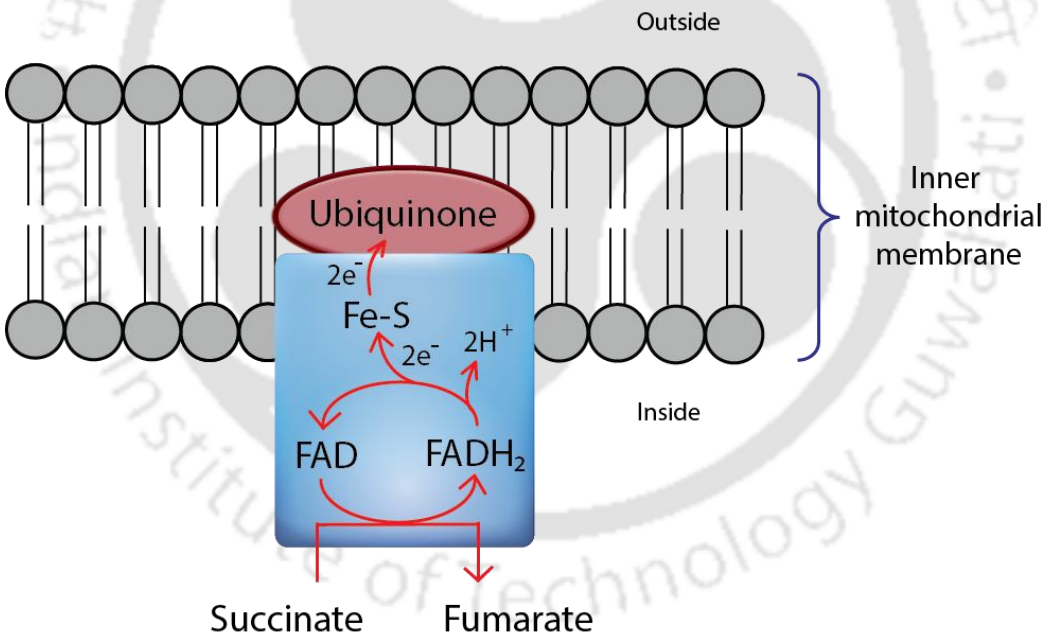

Scheme 4.1: *Schematic representation of Succinate Dehydrogenase.*

During the succinate oxidation, FAD (flavin adenine dinucleotide) undergoes the formation of $FADH_2$ (flavin adenine dinucleotide dihydride) (Scheme 4.2). The electron transfer from $FADH_2$ to an ubiquinone proceeded through three Fe–S cluster and resulted an ubiquinol as the reduced product (Scheme 4.2).[2c]

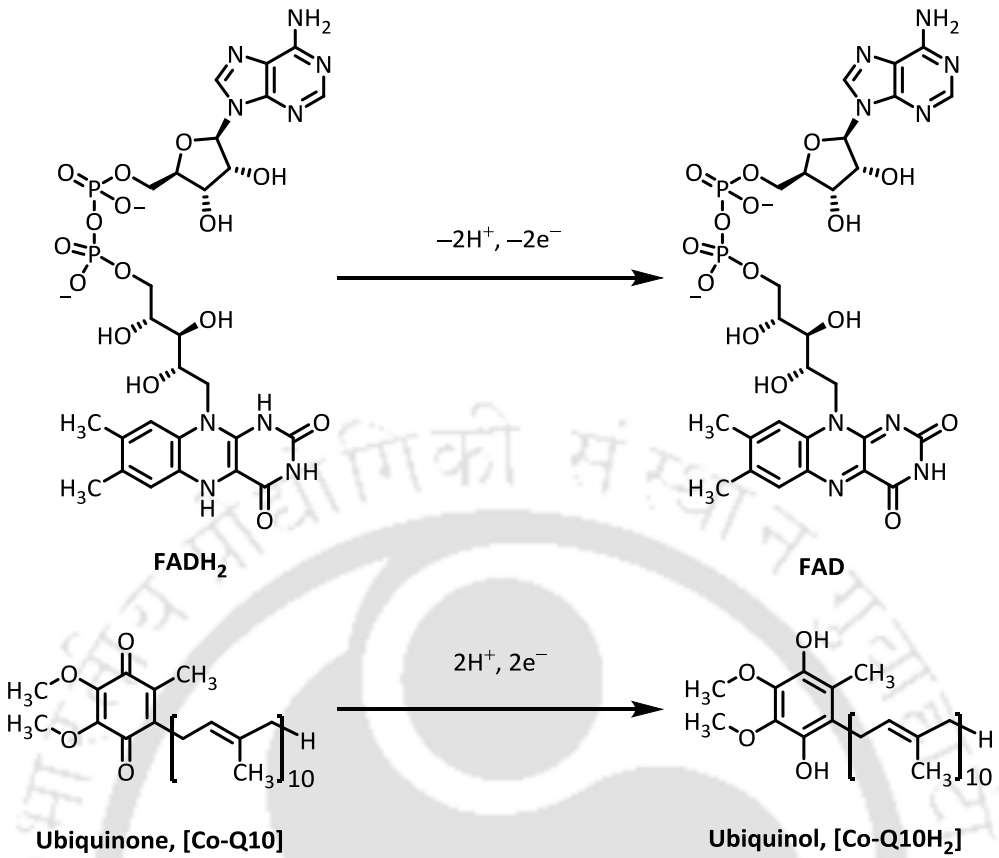

Scheme 4.2: *Two major redox reactions in complex II of respiratory chain.*

The reactivity of quinone species in biological field are raised due to the electron affinity of quinone moiety and all the redox states are reversibly feasible under mild condition. However, utilisation of organic quinone derivatives in laboratory and industrial perspective is quite unfavourable due to the synthetic and stability issue of its several redox states. Introduction of metal coordination with quinone derivatives solve of the problem and resultant metal–quinone complexes have got a considerable attention due to the several utilities, such as; valence tautomeric (VT) complexes,[3a,b] magnetic switch materials,[3c,d] $–CF_3$ group transferring agent,[3e,f] C–N bond formation agent[3g] etc.

Ligand $\mathbf{H_2L^{AP}}$ is an amidophenolate based non–innocent ligand and its coordination with transition metal provided several radical–containing transition metal complexes.[4a] Several substituted ligands and their corresponded metal complexes have got a considerable attention due to their versatile utilities such as mimic enzymatic reaction, $–CF_3$ group transferring agent, C–N bond formation reaction etc.[4a–e] In those metal complexes, the non–innocent amidophenolate units are in their 2– or 1– oxidation states. Amidophenolate may also be existed as zero oxidation state,[3e,f] which is quite uncommon for most of the first–row based transition metal complexes. At

zero oxidation state *i.e.* in the form of iminobenzoquinone [$(IBQ)^0$], the ligand moiety act as an electron acceptor like several organic quinone derivatives.[1]

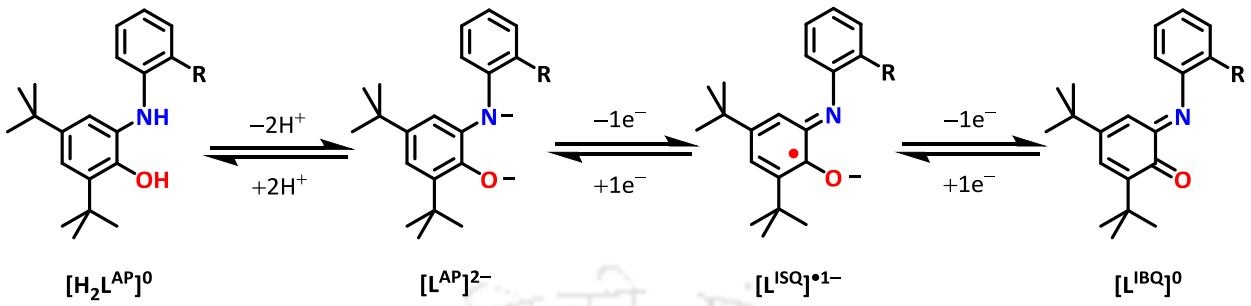

Scheme 4.3: *Probable oxidation states of* H_2L^{AP}.[4a]

Several Cu–quinone species were previously reported and their involvement in various biological phenomena,[5] C–N bond formation[3g] and $–CF_3$ group transferring agent[3e–g] have motivated chemist to the synthesis of Cu–quinone complexes. Amidophenolate based non–innocent ligands have been employed in this preoperative issue. These ligands in the presence of Cu–salt, air and base, provide Cu(II)–radical complexes, which upon further oxidation using external oxidants (*e.g.* molecular bromine,[4d] Umemoto reagent[3e]) can be converted into the corresponding Cu(II)–quinone species.

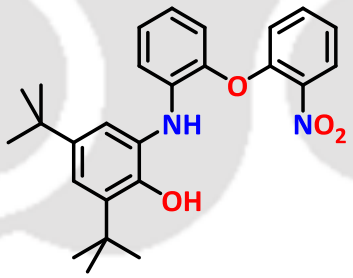

Scheme 4.4: *Schematic representation of ligand* $H_2L^{AP(o–NO_2–OPh)}$.

In this chapter, an amidophenolate based ligand $\mathbf{H_2L^{AP(o–NO_2–OPh)}}$ has been reported. The ligand was designed by replacing an *ortho*– hydrogen atom from the aniline moiety of ligand $\mathbf{H_2L^{AP}}$ with *o*–nitrophenolate unit. The introduction of nitro group in the structural skeleton is employed due to probable attachment of the organic ligand unit to solid support *e.g.* solid electrode for future perspective (electrocatalysis). Furthermore, the understanding of the effect of polar $–NO_2$ group to the geometry and thereafter to the electronic state of the corresponding radical–containing complexes is intended.

In this chapter the single step synthesis of Cu(II)–bis(iminoquinone) complexes and their utilization as hydrogen gas evaluator from $NaBH_4$ under inert gas atmosphere has also been focused. Furthermore, the synthesis and characterization of M–bis(iminosemiquinone) (M = Fe, Ni and Cu) complexes have been discussed.

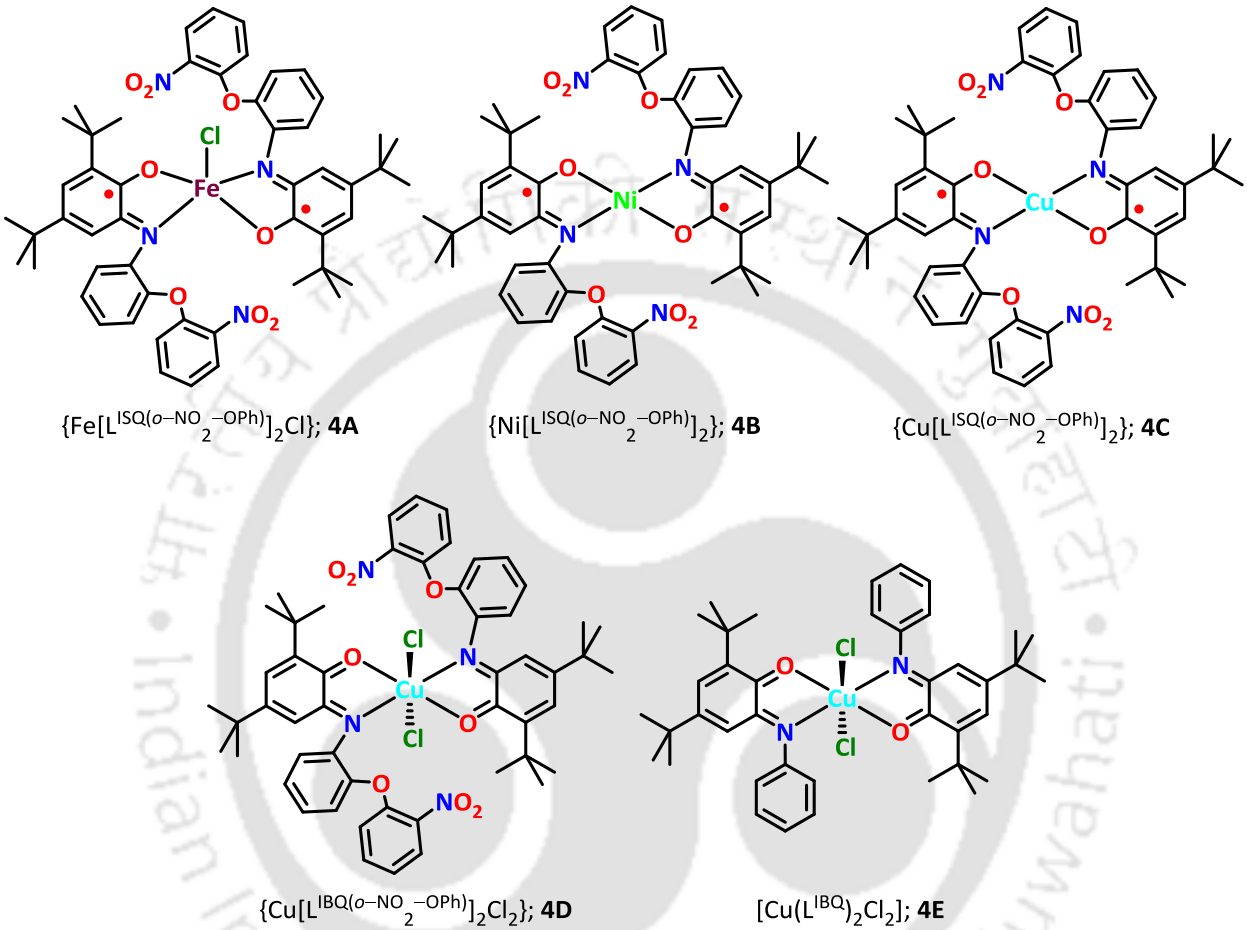

Scheme 4.5: *Several complexes derived from ligand* $H_2L^{AP(o\text{–}NO_2\text{–}OPh)}$.

4.2: Synthesis and Characterization of Ligand $H_2L^{AP(o–NO_2–OPh)}$

An equimolar reaction between 3,5–di–*tert*–butylcatechol with 2–(2–nitrophenoxy)aniline in hexane provided ligand $\mathbf{H_2L^{AP(o–NO_2–OPh)}}$ as a light yellow powder (Scheme 4.6). In the reaction catalytic amount of Et_3N was used as 3,5–di–*tert*–butyl benzoquinone initiator.

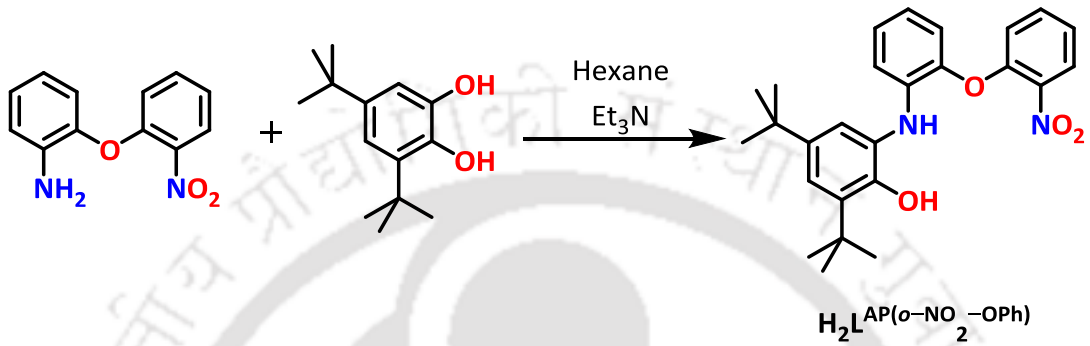

Scheme 4.6: *Synthetic route of ligand* $H_2L^{AP(o–NO_2–OPh)}$.

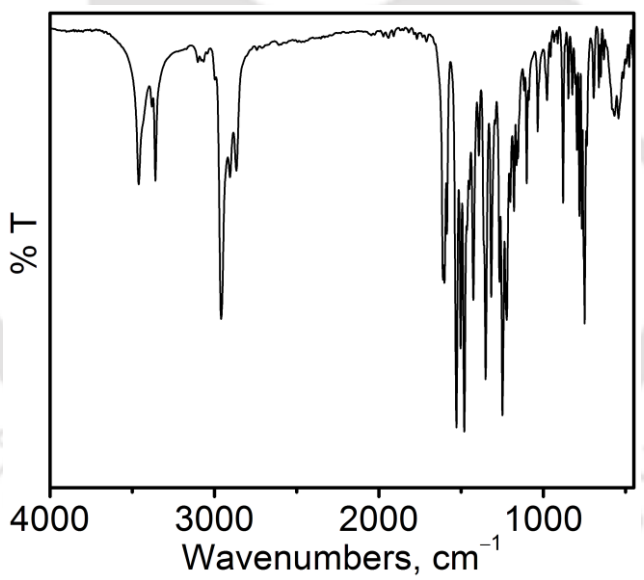

Figure 4.1: *FTIR spectrum of* $H_2L^{AP(o–NO_2–OPh)}$.

In the infrared spectrum of ligand $\mathbf{H_2L^{AP(o–NO_2–OPh)}}$ (Fig. 4.1), two sharp bands at 3460 and 3359 cm^{-1} corresponded to ν(O–H) and ν(N–H) stretching, respectively.[6a,b] The asymmetric, overtone and symmetric bands of ν(C–H) stretches for the *tert*–butyl groups appeared at 2960, 2905 and 2866 cm^{-1}, respectively.[6c,d] The bending ν(C–H) stretches for *tert*–butyl groups appeared at 1480 and 1364 cm^{-1}. The presence of nitro group in the ligand backbone was confirmed by the existence of two sharp bands at 1528 and 1351 cm^{-1}, which

appeared due to respective asymmetric and symmetric ν(N–O) stretching of –NO_2 group.[6e] A strong and sharp band at 1248 cm^{-1} was attributed as ν(C–O) stretching of –NO_2–substituted phenol linkage.[6f] The phenolic ν(C–O) and the ν(C–N) stretching bands appeared at 1316 and 1223 cm^{-1}, respectively, for the *tert*–butyl groups–containing 2–aminophenol unit.[6b]

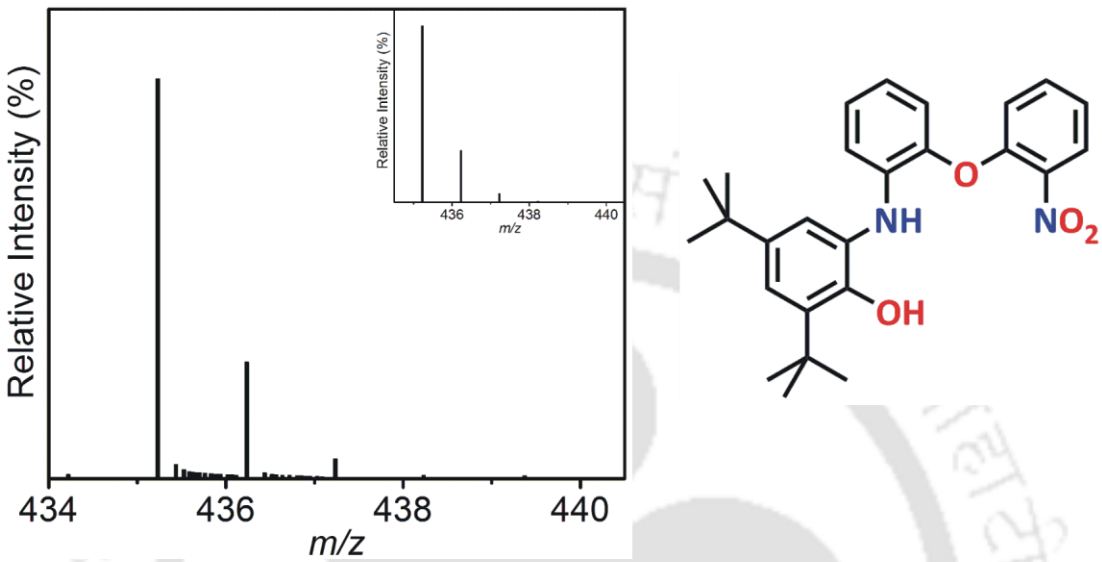

Figure 4.2: *ESI–mass spectrum (+ve mode) of ligand* $\boldsymbol{H_2L^{AP(o\text{–}NO_2\text{–}OPh)}}$ *with experimental and simulated (inset) isotope distribution pattern.*

Electrospray ionization mass spectrum (ESI–MS) of a solution containing ligand $\mathbf{H_2L^{AP(o\text{–}NO_2\text{–}OPh)}}$ in CH_3CN provided a 100% molecular ion peak at *m*/*z* = 435.23 (Fig 4.2). Simulated isotope distribution pattern (inset) confirmed the composition as $[C_{26}H_{30}N_2O_4+H]^+$.

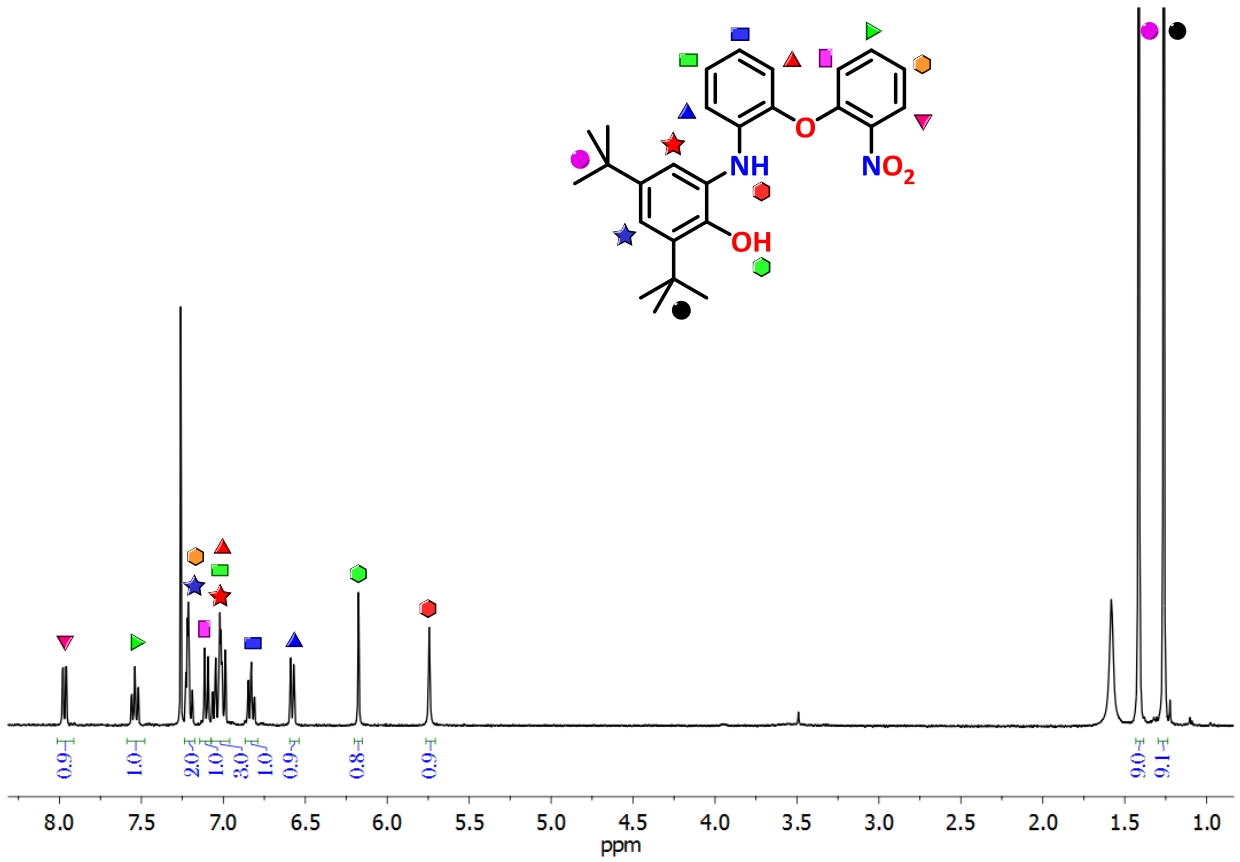

Figure 4.3: *^{1}H NMR spectrum of* $\boldsymbol{H_2L^{AP(o-NO_2-OPh)}}$ *in* $CDCl_3$.

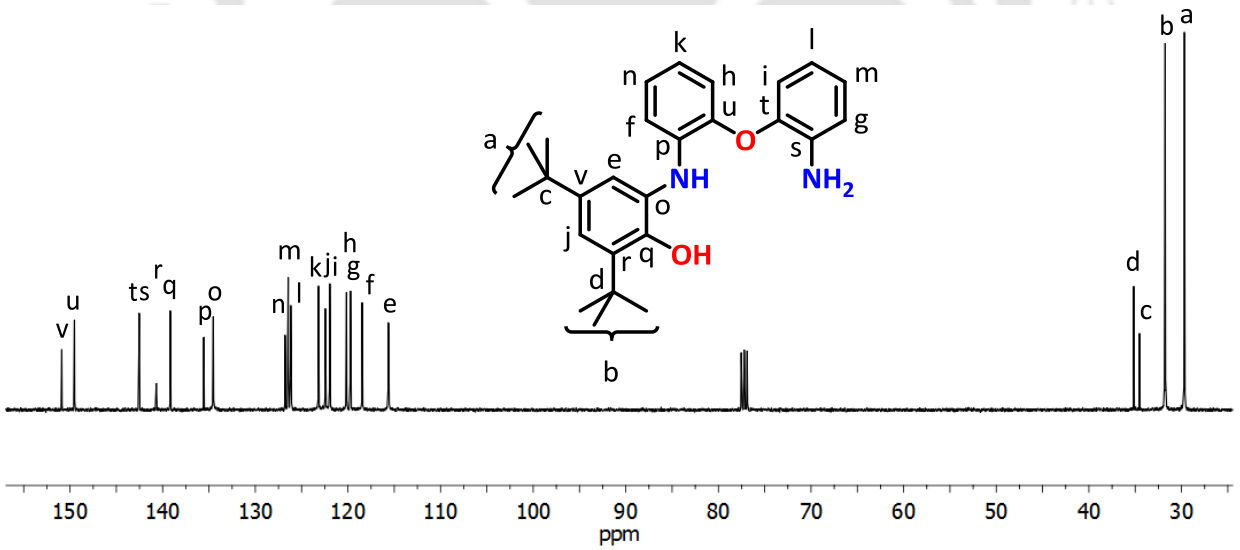

Figure 4.4: *^{13}C NMR spectrum of* $\boldsymbol{H_2L^{AP(o-NO_2-OPh)}}$ *in* $CDCl_3$.

^{1}H NMR spectrum of $\mathbf{H_2L^{AP(o-NO_2-OPh)}}$ was recorded in $CDCl_3$ at 399.853 MHz (Fig. 4.3). Resonance signals at 1.26 and 1.42 ppm appeared as singlet and each peak corresponded to the nine hydrogen atom attached to *tert*–butyl groups. Two singlet peaks at 5.74 and 6.18 ppm

were corresponded to N–H and O–H protons, respectively. Apart from this, signals for 10 aromatic protons appeared in the range 6.5–8.0 ppm. Resonance signal at 1.60 and 7.26 ppm were corresponded to the water and $CHCl_3$ molecule from the solvent and or the sample.

The ^{13}C NMR spectrum of ligand $\mathbf{H_2L^{AP(o–NO_2–OPh)}}$ was recorded in $CDCl_3$ at 150.151 MHz (Fig. 4.4). The resonance signal for four aliphatic type of carbon appeared at a region of 29–to–36 ppm and all the aryl carbon appeared at a region of 115–to–152 ppm. Three peaks near about 77.2 ppm corresponded to the solvent molecule.

The aminophenol based ligand $\mathbf{H_2L^{AP(o–NO_2–OPh)}}$ is potentially redox active in character and its probable oxidation states are shown in Scheme 4.7.

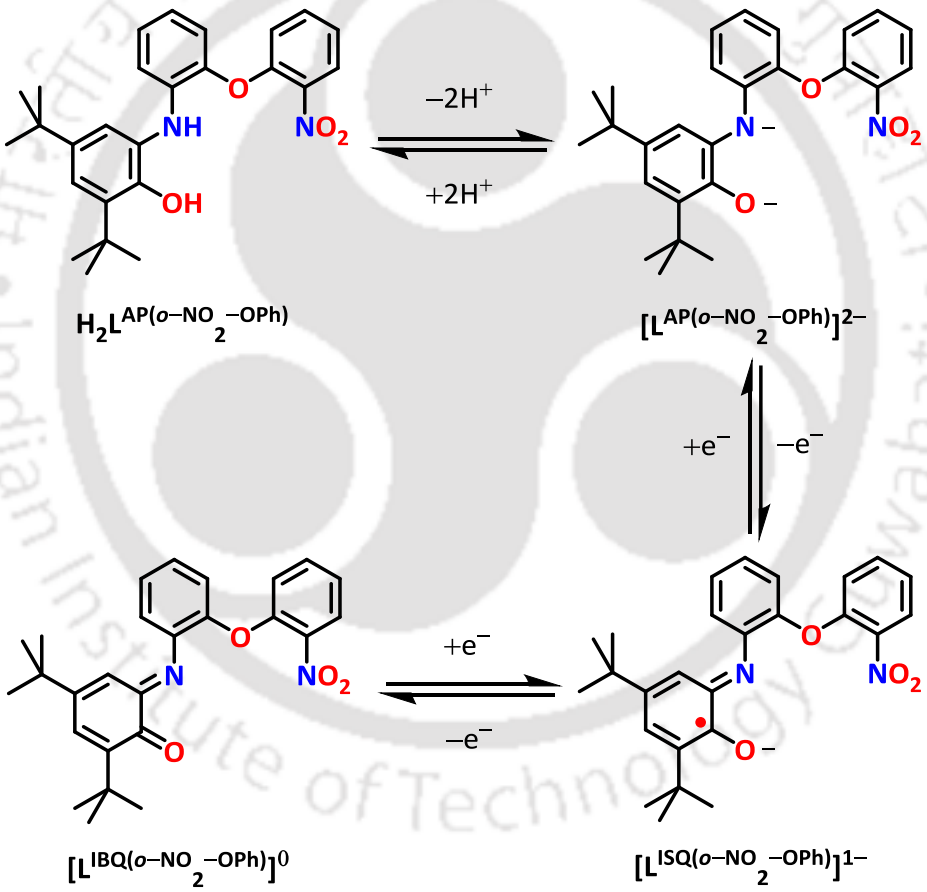

Scheme 4.7: *Possible oxidation states of* $\boldsymbol{H_2L^{AP(o–NO_2–OPh)}}$.

4.3: Synthesis and Characterization of a Square Pyramidal Fe(III) Complex from Ligand $H_2L^{AP(o–NO_2–OPh)}$

Ligand $\mathbf{H_2L^{AP(o–NO_2–OPh)}}$ upon reacting with 0.5 equivalent amount of anhydrous $FeCl_3$ in CH_3CN in presence of Et_3N under aerial atmosphere provided a square pyramidal diradical–containing mononuclear iron complex (**4A**) in 52% yield (Scheme 4.8).

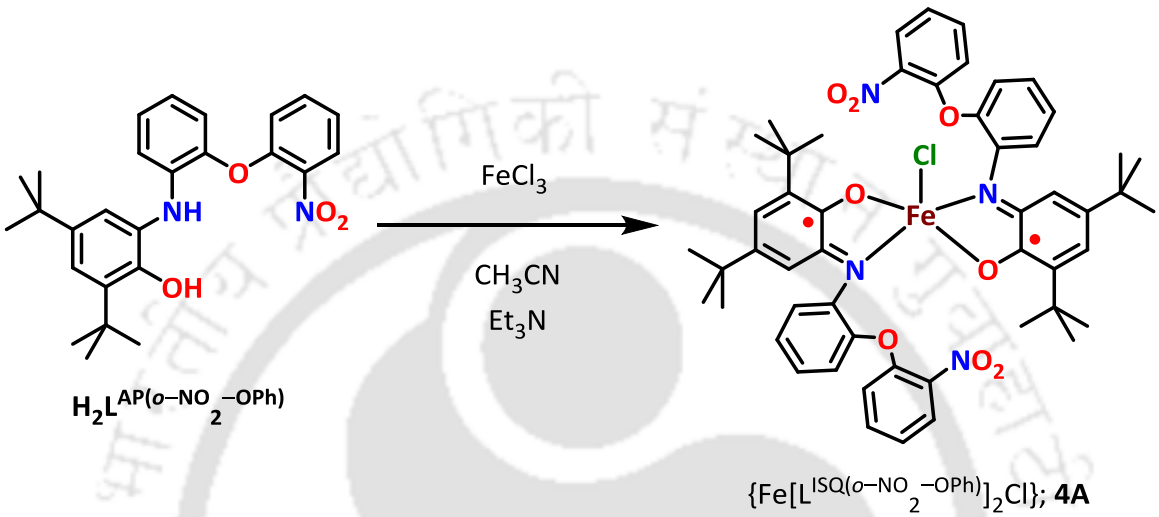

Scheme 4.8: *Synthetic route of complex **4A** from ligand $\boldsymbol{H_2L^{AP(o–NO_2–OPh)}}$.*

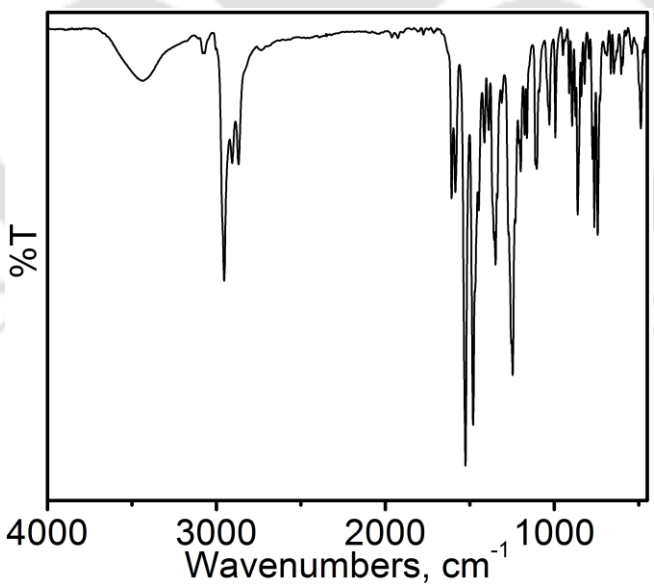

Figure 4.5: *FTIR spectrum of complex **4A**.*

The disappearance of infrared bands at a region of 3100–3500 cm^{-1} was suggestive for the metal coordination with the N–H and O–H deprotonated aminophenol units of ligand $\mathbf{H_2L^{AP(o–NO_2–OPh)}}$ (Fig 4.5). Stretching frequency corresponding to the *tert*–butyl groups, $–NO_2$

group and ethereal linkage did not alter significantly after the complex formation. Two bands at 1585 cm^{-1} and 1480 cm^{-1} were due to ν(C=N) and ν(C⋯O) stretching, respectively.[7a,b] Those bands implied that the aminophenol existed as its one–electron oxidized iminobenzosemiquinone [$(ISQ)^{\bullet 1-}$] form.

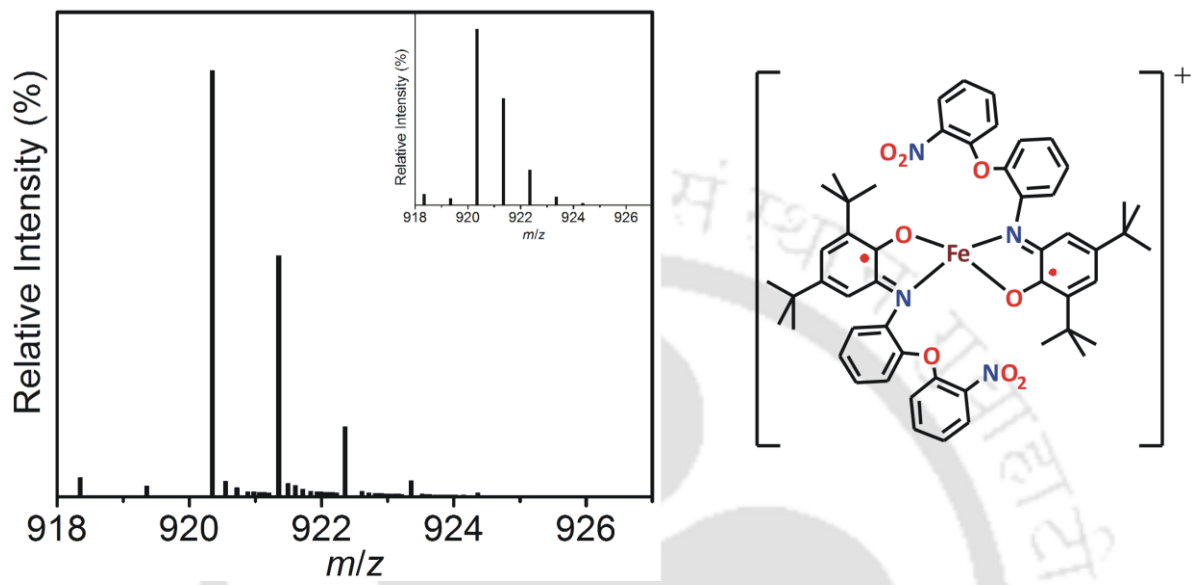

Figure 4.6: *ESI–mass spectrum (+ve mode) of complex* ***4A*** *with experimental and simulated (inset) isotope distribution pattern.*

Electrospray ionization mass spectrum (ESI–MS) of a solution of complex **4A** in CH_3CN provided a 100% molecular ion peak at *m*/*z* = 920.35 in positive mode, which was corresponded to $[M–Cl]^+$. Isotope distribution pattern of the experimental and simulated spectrum revealed $[C_{52}H_{56}FeN_4O_8]^+$ composition for the molecular ion peak.

The block–shaped crystal of complex **4A** was obtained by slow evaporation of a dichloromethane:acetonitrile (2:1) solution. The molecular structure was determined by single crystal X–ray diffraction analysis at 296(2) K. The complex was crystallized in the monoclinic space group '$P2_1/c$'. ORTEP diagram of the molecular structure of the complex is shown in Fig. 4.7 and selected bond distances and bond angles were given in Table 4.1.

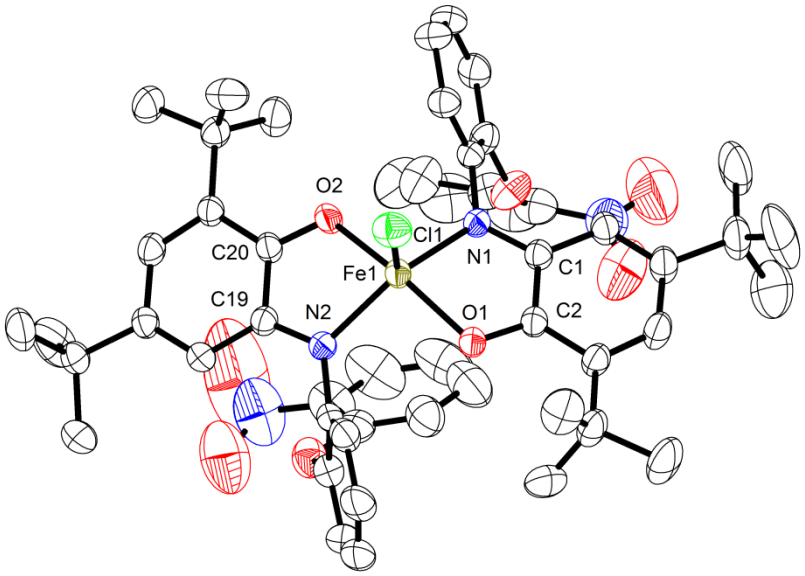

Figure 4.7: *ORTEP presentation of complex **4A**; thermal ellipsoids were drawn at 40% probability level. H–atoms were omitted for clarity.*

In the five–coordinate neutral complex, two N–H and O–H deprotonated aminophenol units that formed basal N2O2 plane coordinated the central Fe atom. Coordination of apical chloride ion lifted the iron atom by 0.534(1) Å from the basal plane constituted by the N2O2 donor set. This type of coordination promoted the system in distorted square pyramidal geometry with τ_5 = 0.22.[8] The bond distances of Fe1–Cl1, Fe1–N1, Fe1–N2, Fe1–O1 and Fe1–O2 were found as 2.237(1), 2.023(2), 2.034(2), 1.958(2) and 1.950(2) Å, respectively. Those values were comparable with the high–spin complex $[Fe^{III}(L^{ISQ})_2Cl]$, reported by H. Chun *et. al.*[9a] The bond distances of N1–C1, O1–C2, N2–C19 and O2–C20 were found as 1.337(3), 1.293(3), 1.343(3) and 1.292(3) Å, respectively. These values implied the partial double bond nature of those bonds. Additionally, quinoid–distortion in the amidophenolate rings (C1–to–C6, C19–to–C24) was also observed. This clearly indicated that each of the deprotonated ligand was in its one–electron oxidized iminosemiquinone $[(L^{ISQ(o\text{–}NO_2\text{–}OPh)}]^{\bullet 1-}$ form.[9a–d] The axial chloride coordination balanced the charged of the neutral complex. To note, the other C_6 rings were in fully reduced phenyl form (C–C = 1.36–1.40 Å).

Table 4.1: *Selected bond distances (Å) and angles (°) for complex **4A**.*

Fe1–O1	1.958(2)	C3–C4	1.368(4)
Fe1–O2	1.950(2)	C4–C5	1.435(5)
Fe1–N1	2.023(2)	C5–C6	1.355(4)
Fe1–N2	2.034(2)	C6–C1	1.421(4)
Fe1–Cl1	2.237(1)	C19–C20	1.448(4)

O1–C2	1.293(3)	C20–C21	1.427(4)
N1–C1	1.337(3)	C21–C22	1.369(4)
O2–C20	1.292(3)	C22–C23	1.437(4)
N2–C19	1.343(3)	C23–C24	1.363(4)
C1–C2	1.455(4)	C24–C19	1.418(4)
C2–C3	1.422(4)		
O2–Fe–O1	155.4 (1)	N1–Fe1–N2	142.4 (1)
O2–Fe1–N1	91.8 (1)	O2–Fe1–Cl1	102.6 (1)
O1–Fe1–N1	79.4(1)	O1–Fe1–Cl1	101.9 (1)
O2–Fe1–N2	79.0 (1)	N1–Fe1–Cl1	106.4 (1)
O1–Fe1–N2	94.0(1)	N2–Fe1–Cl1	111.1(1)

The electronic absorption spectrum of complex **4A** was recorded in CH_2Cl_2 at room temperature and depicted in Fig. 4.8. The electronic absorption bands along with corresponding coefficient value were summarized in Table 4.2

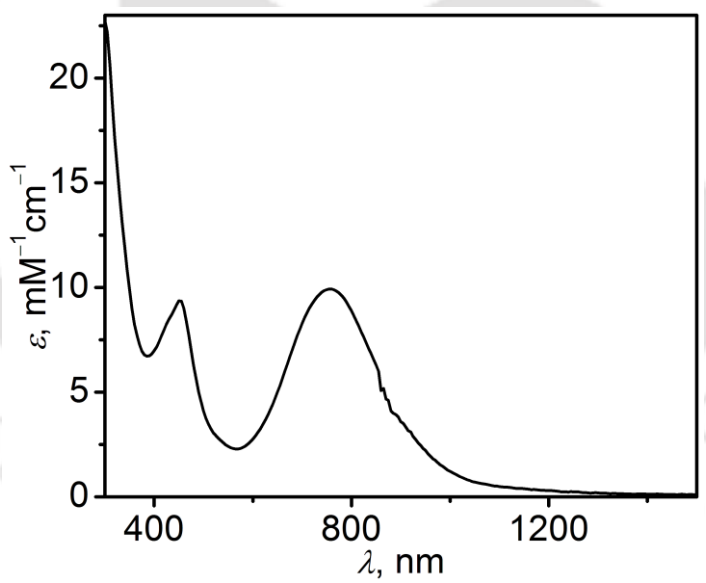

Figure 4.8: *UV–Vis/NIR spectra of complex **4A** in 300–1500 nm range.*

The observed broad band at 1097 nm corresponded to charge transfer transition. The strong characteristic intraligand charge transfer band appeared at 755 nm and the band reinforced the existence of iron coordinated iminosemiquinone moieties in the complex.[9d,10] A band near 450 nm was attributed as semiquinonate based ligand–to–metal charge transfer (LMCT).[9b,10]

Table 4.2: *Electronic absorption data of complex **4A**.*

Complex	λ_{max}, nm (ε, M^{-1} cm^{-1})
4A	1040^{br}(750), 755 (9900), 450 (9350)

* The superscript 'br' stands for broad band.

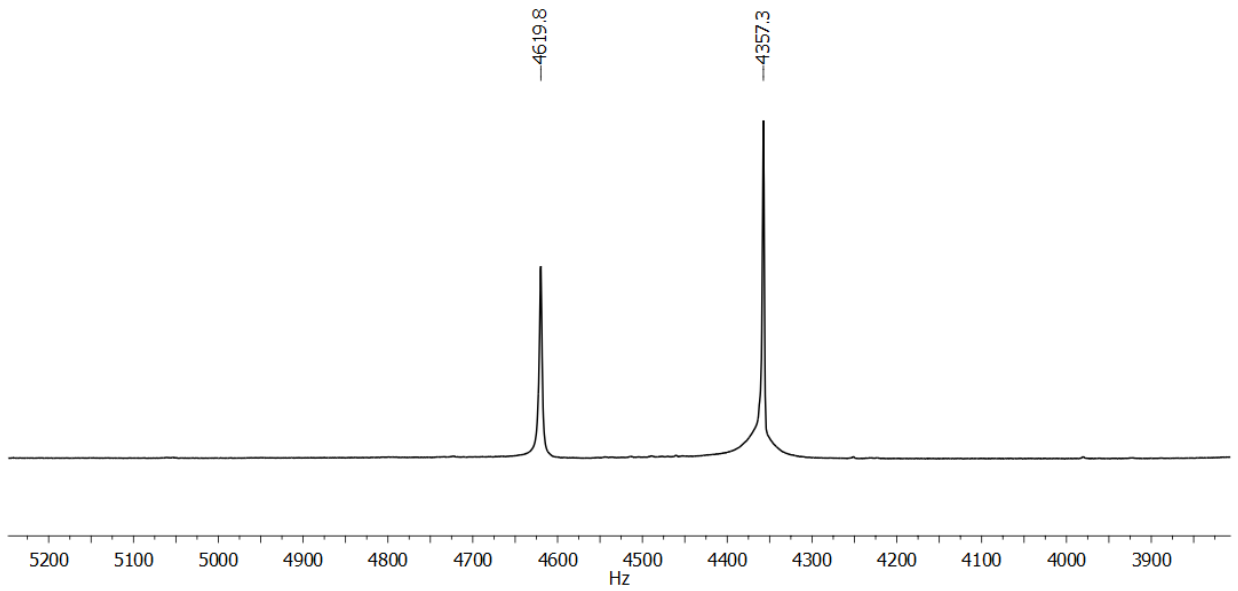

Figure 4.9: *Evans method ^{1}H NMR spectrum[11] of complex **4A** in CDCl3 at 600 MHz. μ_{eff} = 3.91μ_B at 298 K.*

Evans method ^{1}H NMR measurement[11] of complex **4A** in $CDCl_3$ has been recorded at 600 MHz. For the measurement, complex **4A** was taken in $CDCl_3$ at a concentration of 0.017 g/mL. The positive shift (paramagnetic) in resonance signal (δ_v) of the used solvent was found by 262.5 Hz (Fig. 4.9) at 298 K. Thus, from the resultant data, the effective magnetic moment μ_{eff} of complex **4A** was found as 3.91 μ_B, which was corresponding to three unpaired electrons within a single molecule.

Structural parameter as obtained from the X–ray diffraction study suggested that the maximum available unpaired electrons within the molecule would be seven (five unpaired electrons on Fe(III) and two radical–based unpaired electrons). If ferromagnetic coupling among the spins prevails, then magnetic moment corresponds to seven unpaired electrons would result. However, Evens method ^{1}H NMR measurement directly suggested the existence of three unpaired electrons within a molecule. Therefore, an antiferromagnetic coupling between the metal centered unpaired electrons and radical–based unpaired electrons has been realized in the complex.

Furthermore, for better understanding of the spin coupling within the molecule, X–band EPR study has been done in CH_2Cl_2/toluene solvent mixture at 77 K and the resultant spectrum is presented on Fig. 4.10.

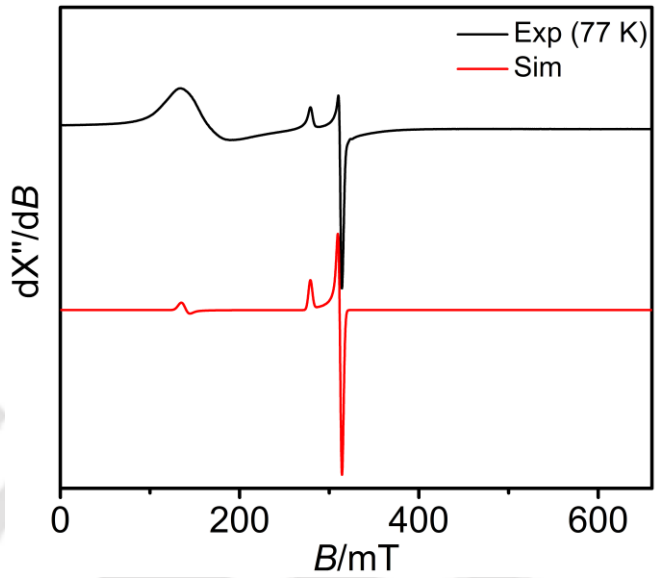

Figure 4.10: *X–band EPR spectrum of complex* ***4A****. X–band microwave frequency (GHz): 9.138; modulation frequency (kHz): 100; microwave power (mW): 0.995; amplitude (G): 1.0.*

In complex **4A**, the Fe(III)–ion as well as each of the coordinated iminosemiquinone [$(ISQ)^{\bullet 1-}$] units possessed paramagnetic spin/s. Experimentally obtained X–band EPR spectra was a signature of Fe(III)–centered unpaired electrons. The experimental data corresponded to an S_t = 3/2 spin state as the ground state, which was simulated by using the following parameters: g_1 = 2.085; g_2 = 4.750; g_3 = 2.340; g_{iso} = 2.994; $^{57}Fe(A_1, A_2, A_3) = (1, 31, 1) \times 10^{-4}$ cm^{-1}. Thus, the simulated data reinforced the existence of unpaired spins on Fe(III)–ion.

4.4: Synthesis and Characterization of a Square Planar Ni(II) Complex from Ligand $H_2L^{AP(o–NO_2–OPh)}$

Ligand $\mathbf{H_2L^{AP(o–NO_2–OPh)}}$ upon reacting with 0.5 equivalent amount of $NiCl_2 \bullet 6H_2O$ in CH_3CN in the presence of Et_3N under aerial atmosphere provided a square planar diradical–containing mononuclear Ni(II) complex (**4B**) in 18% yield (Scheme 4.9). Although, the reaction was carried out under refluxing condition, 56% ligand was isolated as unreacted.

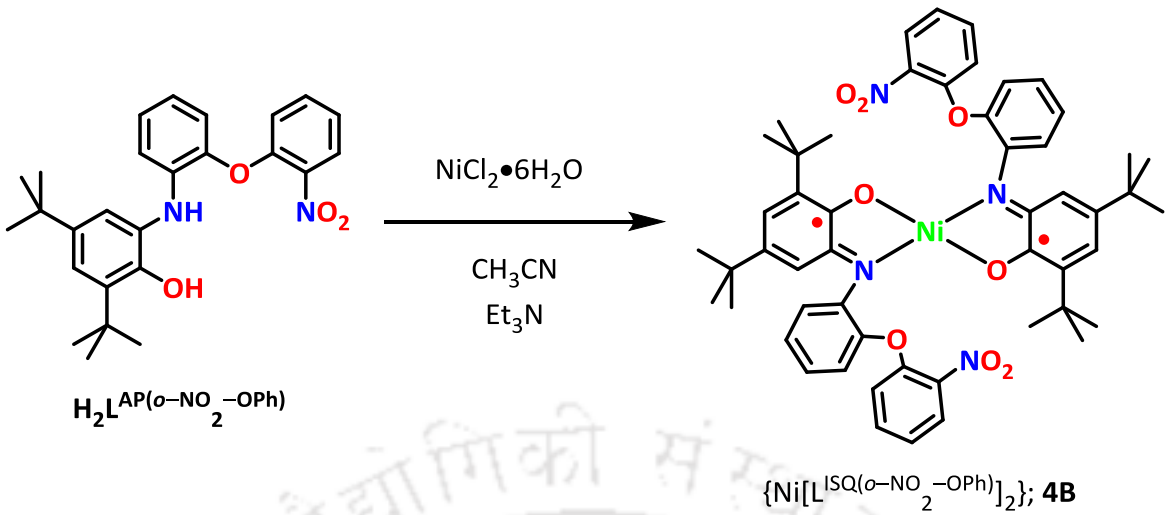

Scheme 4.9: *Synthetic route of complex **4B** from ligand* $H_2L^{AP(o-NO_2-OPh)}$.

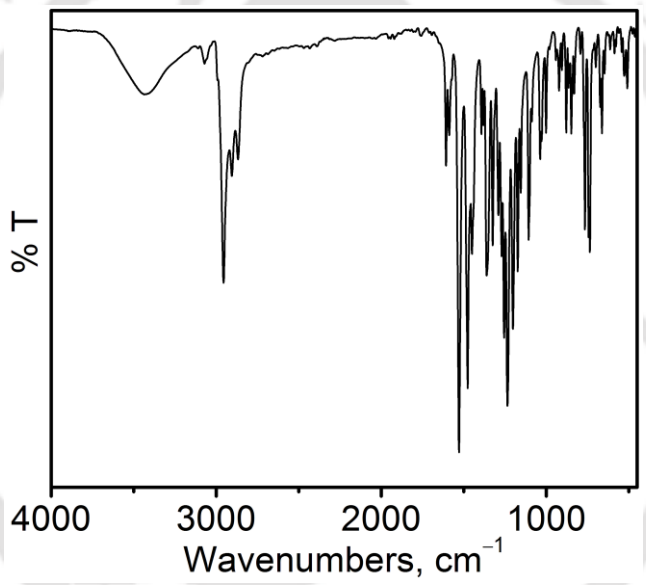

Figure 4.11: *FTIR spectrum of complex **4B**.*

Infrared spectrum of complex **4B** has been shown in Fig. 4.11. Ni–ion coordination with deprotonated aminophenol moiety was confirmed by the disappearance of characteristic sharp bands at 3460 and 3359 cm^{-1}. Characteristic bands for *tart*–butyl groups appeared at 2955, 2905 and 2868 cm^{-1}.[6c,d] The bands at 1588 and 1440 cm^{-1} attributed to ν(C=N) and ν(C⋯O) stretching respectively.[7] The existence of strong bands at 1529 and 1361 cm^{-1} were due to asymmetric and symmetric ν(N⋯O) stretches for the $–NO_2$ group.[6e]

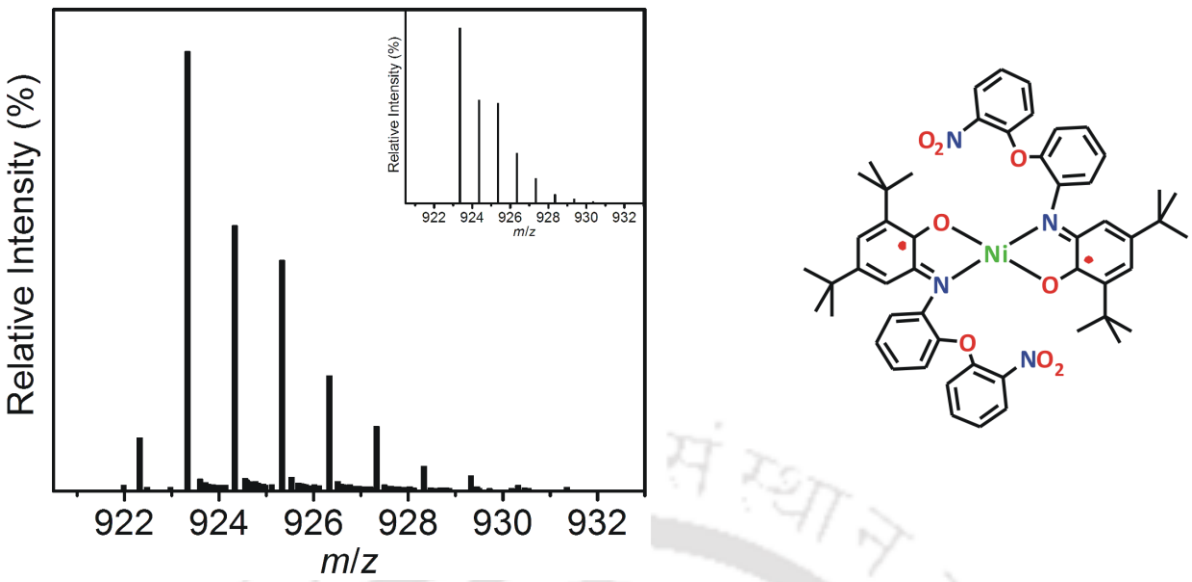

Figure 4.12: *ESI–mass spectrum (+ve mode) of complex **4B** with experimental and simulated (inset) isotope distribution pattern.*

Electrospray ionization mass spectrum (ESI–MS) of a solution of complex **4B** in CHN provided a 100% molecular ion peak at *m*/*z* = 923.35 at positive mode. The peak corresponded to $[M+H]^+$, M = stands for complex **4B**. Simulated isotope distribution pattern revealed the composition of the peak as $[C_{52}H_{56}NiN_4O_8+H]^+$.

Crystals suitable for single crystal X–ray diffraction analysis were obtained by slow evaporation of a CH_2Cl_2/CH_3CN (6:1) solvent mixture. The complex crystalized in the monoclinic space group '*C*2/*c*'. ORTEP diagram of the molecular structure of the complex has been portrayed in Fig. 4.13 and selected bond distances and bond angles are given in Table 4.3.

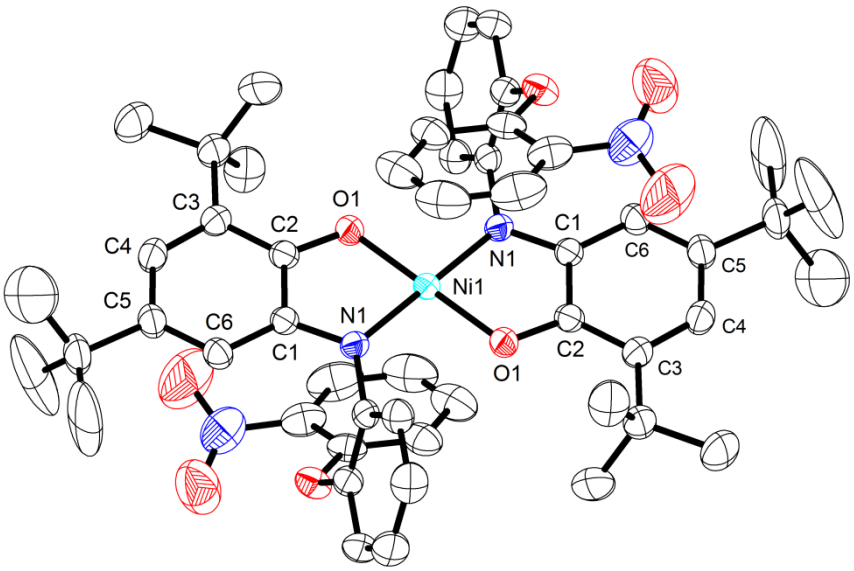

Figure 4.13: *ORTEP presentation of complex **4B**; thermal ellipsoids were drawn at 40% probability level. H–atoms were omitted for clarity.*

In the neutral complex, the central Ni–ion was four–coordinate, where two deprotonated aminophenol moieties from two individual ligands occupied the coordination sites. The complex acquired an inversion center located on Ni1 atom and coordination of two amidophenolate moieties to Ni1 was *trans*– in fashion. The coordination environment of Ni1 was square planar in nature (τ_4 = 0.0)[12]. The Ni1–N1 = 1.840(2) Å and Ni1–O1 = 1.839(2) Å bond distances corresponded to +II oxidation state of the central Ni–ion.[4a] The bond length of C1–N1 and C2–O1 were found as 1.358(4) and 1.313(4) Å, respectively. This indicated that the bonds are in their partial double bond nature.[4a,] The partial double bond character of C1–N1, C2–O1 bonds and observed quinoid distortion (short–long–short C–C bond followed by three successive long C–C bonds) of the *tert*–butyl groups–containing C_6 ring (C1–to–C6) suggested the existence of the amidophenolate unit as its one–electron oxidized iminosemiquinone [$(ISQ)^{\bullet 1-}$] form. The C–C bond length for all others C_6 rings were found in the range of 1.380±0.014 Å, which implied their phenyl form. Noteworthy, the ethereal oxygen did not take part any coordination/interaction in the crystal.

Effect of –NO_2 group on the structure of complex 4B:

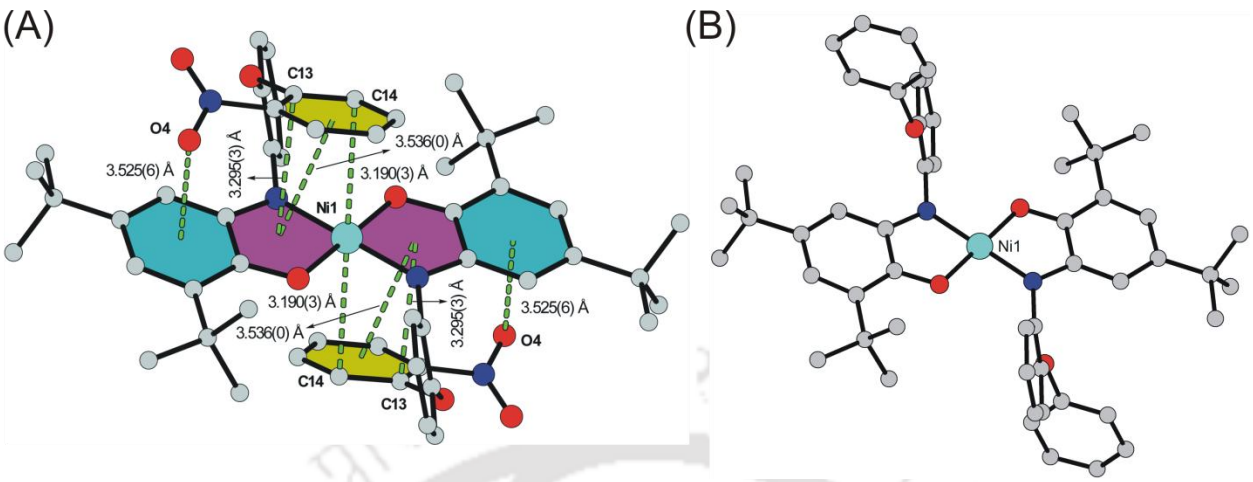

Figure 4.14: *(A) Short interaction in complex **4B**; (B) Ni(II)–bis(iminosemiquinone) complex synthesized from ligand* $H_2L^{AP(OPh)}$.[13]

A similar ligand analogue (without NO_2 group) and corresponding Ni(II)–bis(iminosemiquinone) complex were reported by C. Mukherjee *et. al*.[13] It was observed that there were no short intramolecular interactions in the complex (Fig. 4.14B). In ligand $\mathbf{H_2L^{AP(o\text{–}NO_2\text{–}OPh)}}$, the presence of –$NO_2$ group at *ortho* to the ethereal linkage facilitated several short intramolecular interactions in complex **4B** (Fig. 4.14A). Due to the presence of a short interaction [3.190(3) Å] between Ni1 and a distal carbon atom (C14), complex **4B** could be even described as an axially elongated octahedral.

Table 4.3: *Selected bond distances (Å) and angles (°) for complex **4B**.*

Ni1–O1	1.839(2)	C2–C3	1.419(4)
Ni1–N1	1.840(2)	C3–C4	1.376(5)
N1–C1	1.358(4)	C4–C5	1.423(5)
O1–C1	1.313(4)	C5–C6	1.367(4)
C1–C2	1.419(4)	C6–C1	1.409(4)
O1–Ni1–O1*	180.0(1)	O1–Ni1–N1*	94.5(1)
N1–Ni1–N1*	180.0(0)	Ni1–N1–C1	113. 7(2)
O1–Ni1–N1	85.5(1)	Ni1–O1–C2	113. 7(2)

The asterisk (*) symbol stands for symmetry operation, inversion center.

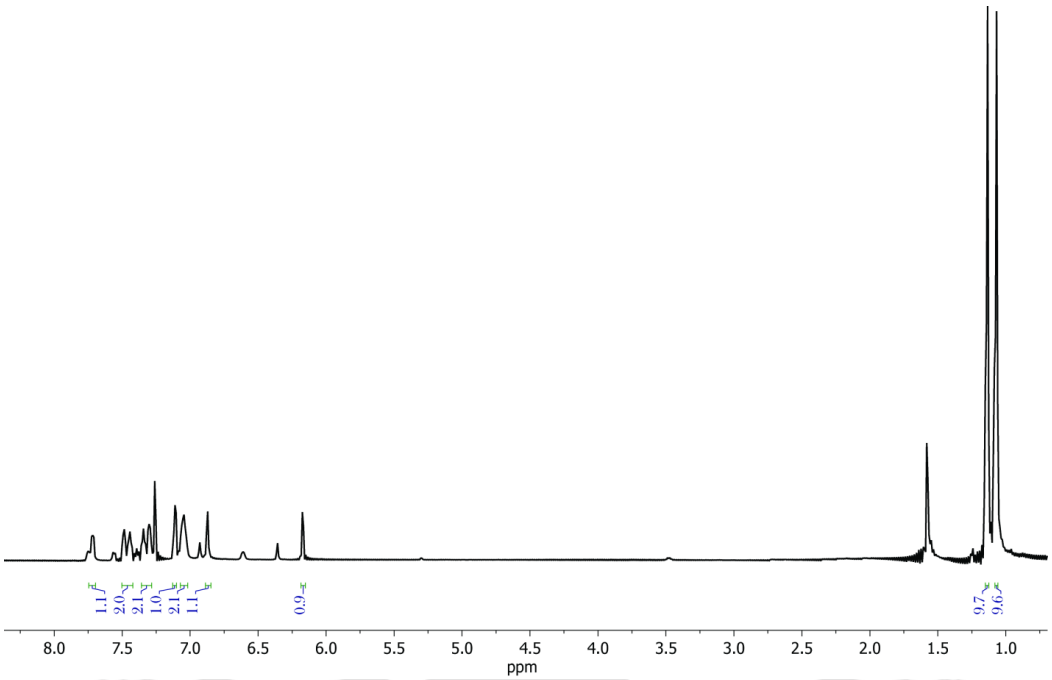

Figure 4.15: *^{1}H NMR of complex **4B**.*

In the complex, presence of strong antiferromagnetic coupling between two coordinated π–radical resulted S_t = 0 ground state. Thus obtained diamagnetism was confirmed by ^{1}H NMR (Fig. 4.15). The resonance signal for the *tert*–butyl groups were appeared at 1.07 and 1.13 ppm, whereas the resonance signals for the aryl protons were appeared at a range of 6.17–7.72 ppm.

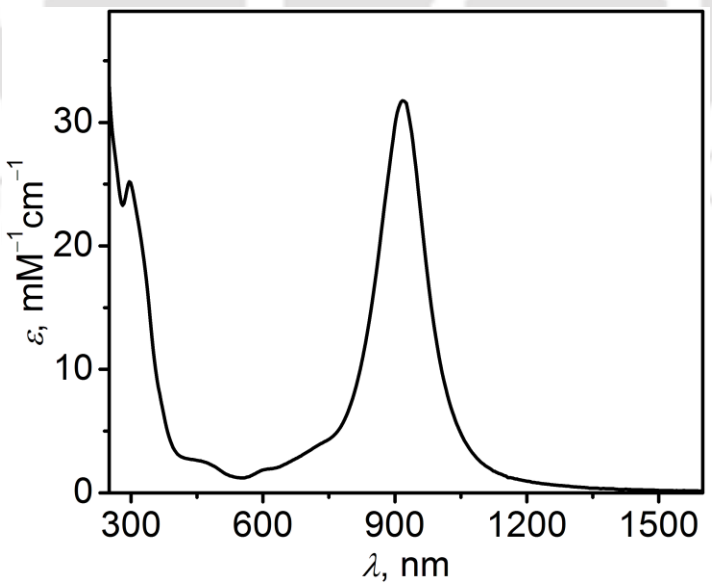

Figure 4.16: *UV–Vis/NIR spectra of complex **4B** in 300–1700 nm range.*

The electronic absorption spectrum of complex **4B** was recorded in CH_2Cl_2 at room temperature and shown in Fig. 4.16. The electronic absorption bands along with corresponding

coefficient value are summarized in Table 4.4. The observed sharp band at λ_{max} = 917 nm corresponded to ligand–to–ligand charge transfer (LLCT) in nature.[4a,14a,b] The band is the characteristic for Ni(II)–bis(iminosemiquinone) complex. Some charge transfer bands were observed at 728, 605 and 461 nm.

Table 4.4: *Electronic absorption data of complex **4B**.*

Complex	λ_{max}, nm (ε, M^{-1} cm^{-1})
4B	917(31750), 728^{sh}(3900), 605^{sh}(1900), 461^{sh}(2550), 296(25200)

* The superscript 'sh' stands for shoulder band.

4.5: Synthesis and Characterization of a Square Planar Cu(II) Complex from Ligand $H_2L^{AP(o–NO_2–OPh)}$

Ligand $\mathbf{H_2L^{AP(o–NO_2–OPh)}}$ upon reacting with 0.5 equivalent amount of $CuCl_2$•$2H_2O$ in CH_3CN in the presence of Et_3N under aerial atmosphere in 2 hours provided the square planar diradical–containing mononuclear complex **4C** in 68% yield (Scheme 4.10).

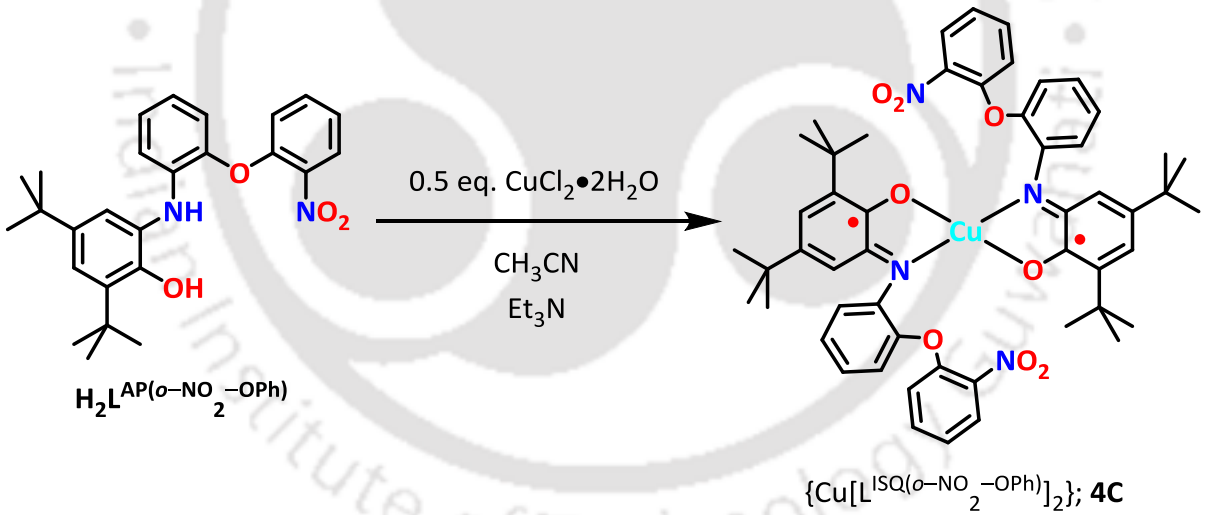

Scheme 4.10: *Synthetic route of complex **4C** from ligand $H_2L^{AP(o–NO_2–OPh)}$.*

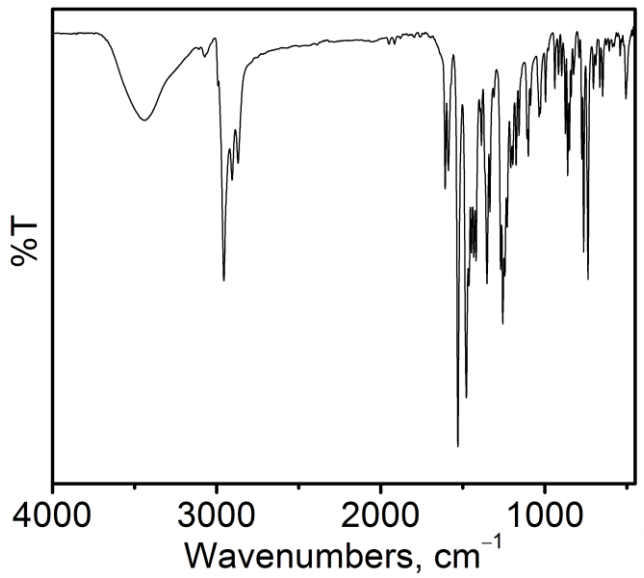

Figure 4.17: *FTIR spectrum of complex **4C**.*

The infrared spectrum of complex **4C** (Fig. 4.17) endorsed the basic coordination of the ligand with the metal ion. The disappearance of bands at 3460 [ν(N–H)] and 3359 cm^{-1} [ν(O–H)] clarified the copper coordination with the N–H and O–H deprotonated aminophenol. The asymmetric, overtone and symmetric ν(C–H) bands appeared at 2956, 2870 and 2906 cm^{-1}, respectively. Those bands corresponded to the *tert*–butyl group of the ligand backbone.[6c,d] The bands at 1588 and 1448 cm^{-1} were ascribed as ν(C⋯N) and ν(C⋯O) stretching, respectively.[7,15] Those bands implied the iminosemiquinone [(ISQ)$^{\bullet 1-}$] coordination with the Cu–ion. The band positions for the nitro groups and the ethereal linkage have not been altered during the complexation.

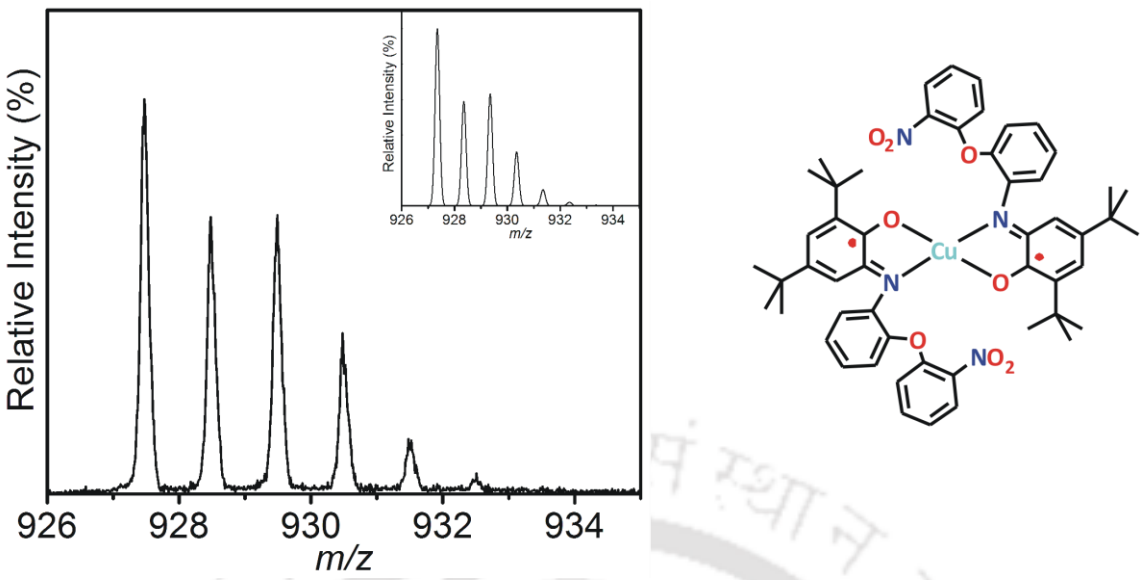

Figure 4.18: *ESI–mass spectrum (+ve mode) of complex **4C** with experimental and simulated (inset) isotope distribution pattern.*

Electrospray ionization mass spectrum (ESI–MS) of a solution of complex **4C** in CH_3CN provided a 100% molecular ion peak at *m*/*z* = 927.47 in positive mode. The observed mass corresponded to $[M]^+$. Isotope distribution pattern of the experiment and simulation data suggested the composition as $[C_{52}H_{56}CuN_4O_8]^+$ for the molecular ion peak.

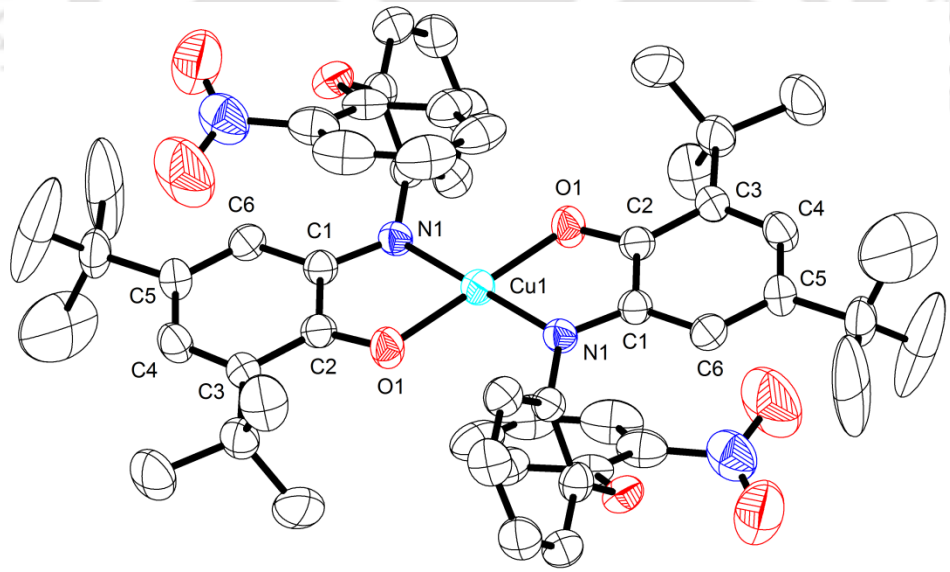

Figure 4.19: *ORTEP presentation of complex **4C**; thermal ellipsoids were drawn at 40% probability level. H–atoms were omitted for clarity.*

The X– ray diffraction analysis of green crystalline solid obtained from a CH_2Cl_2/CH_3CN (6:1) solvent mixture was carried out at 293 K. The complex crystalized in the monoclinic space group

'*C*2/*c*'. ORTEP diagram of the molecular structure of the complex has been portrayed in Fig. 4.19 and selected bond distances and bond angles were given in Table 4.7.

The crystal structure of complex **4C** was almost similar to complex **4B**. The complex was neutral in charge and the central Cu atom was four–coordinated with two NO donor sets from two individual ligands. Thus obtained complex molecule acquired an inversion center at Cu1 atom. Hence, the nature of the both coordinated–ligands was same. The geometry around the Cu atom was square planar as evident by (τ_4) = 0.00[16] value. The Cu1–O1 = 1.929(3) Å and Cu1–N1 = 1.934(3) Å bond distances suggested +II oxidation state of the Cu atom.[4a,9d,17] The C–C bond distances of the *tert*–butyl groups–containing C_6 rings were different than those of the other C_6 rings. The C–C bonds of the without *tert*–butyl groups–containing C_6 rings were ranging in between 1.362–1.399 Å and indicated phenyl form of the C_6 rings. Contrarily, three alternating short–long–short C–C bonds [C3–C4 = 1.371(5), C4–C5 = 1.430(6), C5–C6 = 1.361(5) Å] followed by other three long C–C bonds [C1–C6 = 1.416(5), C1–C2 = 1.454(5), C2–C3 = 1.431(5) Å] were present in the *tert*–butyl groups–containing C_6 rings. This type of distortion is known as *quinoid–distortion* and implied the non–aromatic character of the C_6 rings, *i.e.*, oxidation of phenyl rings. The C1–N1 = 1.340(4) and C2–O1 = 1.301(4) Å bonds were ranging in between of single bond (C–N = 1.45, C–O = 1.36 Å) and double bond (C=N = 1.30, C=O = 1.22 Å) values, which implied an one–electron oxidized iminosemiquinone form {[$L^{ISQ(o\text{–}NO_2\text{–}OPh)}$]$^{\bullet 1-}$} of the coordinating ligands. In short, the neutral mononuclear complex was a Cu(II)–bis(iminosemiquinone). [4a,9d,17]

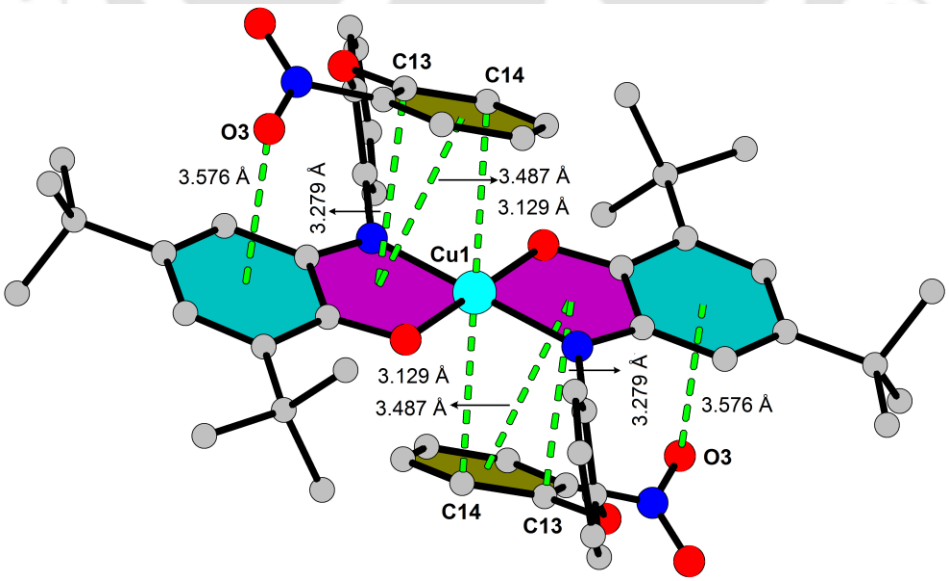

Figure 4.20: *Representation of short intamolecular interaction in complex **4C**.*

In complex **4C**, two distal C atoms (C14) from two different phenyl rings (Fig. 4.20) occupied the axial positions. The complex also possessed several short intermolecular interactions like complex **4B**. The Cu(II)–C^{Ph} (C^{Ph} stands for C14 atoms belonging to phenyl rings) units were having a distance of 4.13 Å. Therefore, the short interaction caused a pseudo octahedral surrounding around the metal ion.[18]

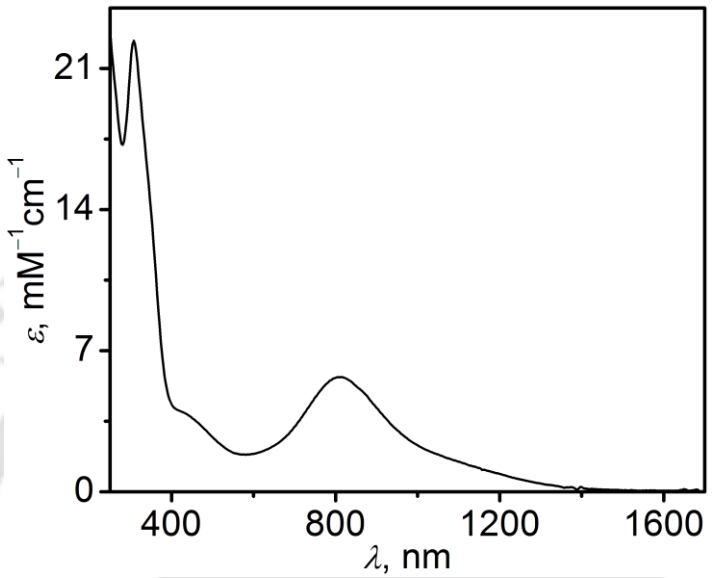

Figure 4.21: *UV–Vis/NIR spectra of complex **4C** in 300–1700 nm range.*

The electronic absorption (UV–Vis/NIR) spectra of complex **4C** were recorded in dichloromethane at room temperature (25 °C). The spectra are shown in Fig. 4.21. The absorption band position along with the extinction coefficient values are summarized in Table 4.5.

In case of complex **4C**, an intense band corresponding to spin– and dipole– allowed ligand–to–ligand charge transfer appeared at 812 nm (ε = 5700 $M^{-1}cm^{-1}$). This band is typical of four coordinate Cu(II)–bis(iminosemiquinone) complexes.[4a,9d,14e] The bands at 1049 nm (ε = 2400 $M^{-1}cm^{-1}$) was due to intraligand (IL) charge transfer[17e] whereas another band at 431 nm (ε = 3900 $M^{-1}cm^{-1}$) was attributed as metal–to–ligand charge transfer (MLCT). Thus, the electronic absorption feature of complex **4C** further supported its Cu(II)–bis(iminosemiquinone) form.

Table 4.5: *Electronic absorption data of complex **4C**.*

Complex	λ_{max}, nm (ε, M^{-1} cm^{-1})
4C	1049^{br}(1850), 812 (5700), 431^{sh}(3900), 308 (22400)

***** The superscript 'br' and 'sh' stands for broad and solder band respectively.

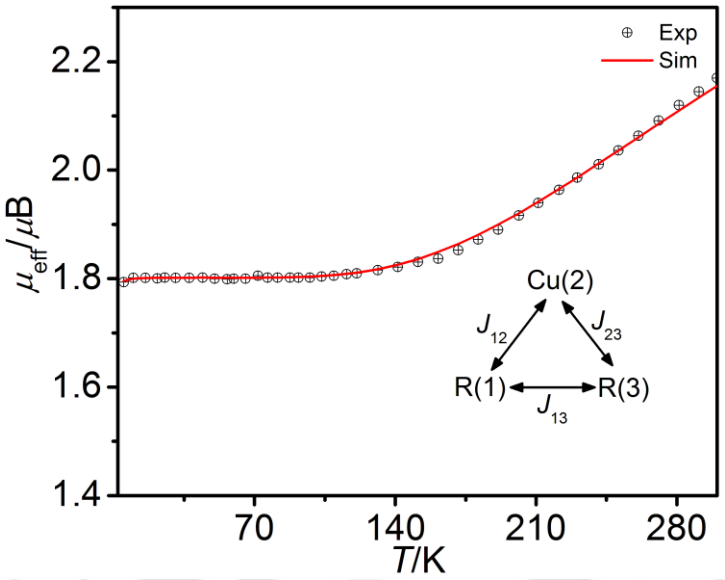

Figure 4.22: *μ_{eff} vs. T plot for complex **4C** at B = 1.0 T.*

The temperature dependent magnetic susceptibility analysis of complex **4C** was recorded at an external field 1 T on solid sample and resulting μ_{eff} *vs.* T plot has been presented in Fig. 4.22. The effective magnetic moment value remained constant at 1.80 μ_B over a temperature range 2 to 140 K. Above the temperature, the value increased gradually and reached μ_{eff} = 2.17 μ_B at 300 K. The μ_{eff} = 1.80 μ_B at 5 K indicated that complex **4C** had an S_t = 1/2 ground state with g > 2.00 (μ_{eff} = 1.73 μ_B; g = 2.00) and the increase of magnetic moment with temperature emphasized the presence of multi−paramagnetic centers in the molecule and the existences of antiferromagnetic coupling among the spins.

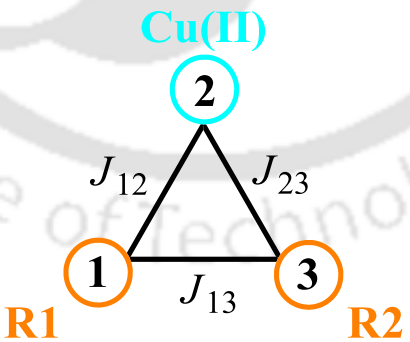

Structurally complex **4C** have possessed one spin at Cu(II) ($S_{Cu(II)}$ = 1/2) and two spins at coordinated iminosemiquinone [$(ISQ)^{\bullet 1-}$] (S_{R1} = S_{R2} = 1/2). The interactions among three spins will provided three electron spin states (S_t, S*) = (3/2, 1), (1/2, 1) and (1/2, 0) symbolically represented as (↑↑↑), (↑↓↑) and (↑↑↓), respectively, where S_t = S_{Cu} + S_{rad1} + S_{rad2} and S* = S_{rad1} + S_{rad2}. The experimental result was simulated by using the parameters: S_{Cu} = 1/2, S_R = 1/2, $g_{Cu(II)}$

= 2.08, g_R = 2.00, J_{12} = J_{23} = –10.0 cm^{-1}, J_{13} = −270.0 cm^{-1} where J_{12} or J_{23} stand for coupling between a radical and adjacent Cu(II) ion and J_{13} stands for radical–radical coupling. For such a system, the energy of coupled spin states were given by *E* (3/2, 1) = [(–7J_{12}–8J_{13})/8], E (1/2, 1) = [(5J_{12}–8J_{13})/8] and E (1/2, 0) = –3J_{12}/8.[19] Thus, the energy of the ground state was found as 3.75 cm^{-1}, which corresponded to a single unpaired electron with (1/2, 0) spin state *i.e.* radical–radical antiferromagnetic coupling predominant over radical–copper antiferromagnetic coupling and resultant unpaired electron resided on Cu(II)–ion.

To consolidate the Cu–center location of the unpaired electron, EPR measurement was done. The solubility of crystalline complex **4C** was very low in most of the organic solvent *e.g.* CH_2Cl_2, $CHCl_3$, MeOH, EtOH, CH_3CN, $PhCH_3$ and therefore, X–band EPR analysis of complex **4C** was recorded in solid state at 77 K.

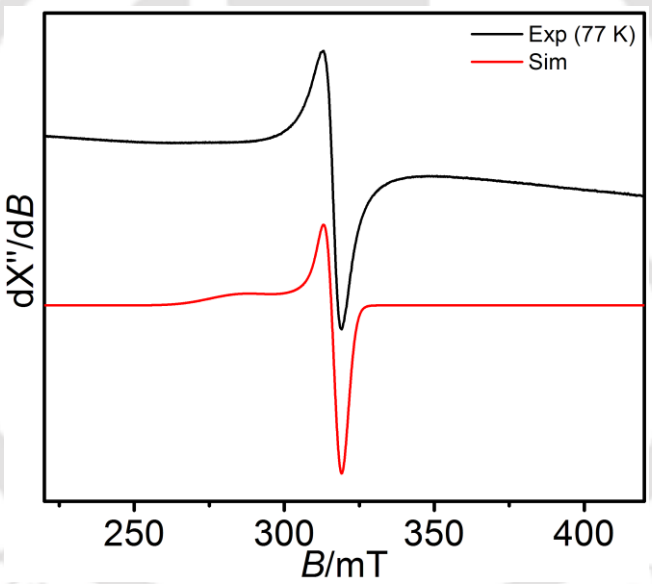

Figure 4.23: *X–band EPR spectrum of complex* ***4C****. X–band microwave frequency (GHz): 9.145; modulation frequency (kHz): 100; microwave power (mW): 0.998; amplitude (G): 1.0.*

The broad and unresolved nature of the spectrum was due to solid state measurement. Nevertheless, the experimentally obtained axial spectrum was well simulated using the following parameters: g_1 = g_2 = 2.065; g_3 = 2.230; g_{iso} = 2.120; $^{63/65}$Cu (A_1, A_2, A_3) = (0, 0, 133)×10^{-4} cm^{-1}. The g_{iso} > 2.00 and g_3 > g_1 = g_2 > 2.00 values indicated the existence of the unpaired–electron on 3d_x^2–$_y^2$ orbital of Cu(II) center. The observed *g*–parameters (g_1 = g_2 < g_3) implied axial elongation of around Cu(II) center, which also supported by short intramolecular interactions (Fig. 4.20) as described earlier.

Cyclic voltammograms of complex **4C** was measured in CH_2Cl_2 solution containing 0.10 M[(^{n}Bu)$_4$N]ClO_4 as the supporting electrolyte at a glassy carbon working electrode and Ag/AgCl reference electrode. Ferrocenium hexafluorophosphate was used as an internal standard and all the potentials have been referenced versus Fc^+/Fc couple. The cyclic voltammograms of complex **4C** was shown in Fig. 4.24 and the corresponding redox potentials were summarized in Table 4.6.

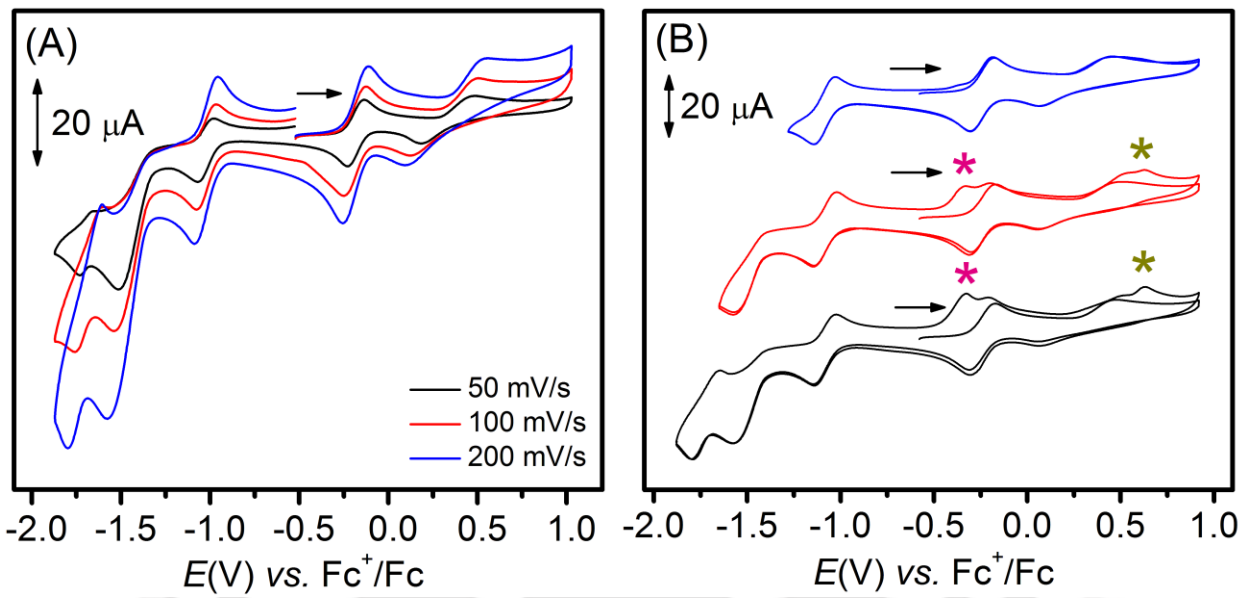

Figure 4.24: *Cyclic voltammograms of (A) complex **4C** measured in dichloromethane; (B) complex **4C** at three different potentials range and two consecutive cycles.*

The complex **4C** underwent two successive ligand–centered oxidations at −0.129 and 0.492 V and a fully oxidized Cu(II)–bis(iminoquinone) species was developed.[4a,17c,f,g] Thus obtained Cu(II)–bis(iminoquinone) species underwent five successive reductions at 0.119, −0.253, −1.074, −1.538 and −1.765 V during the cathodic scan. Two coordinated– iminoquinone moieties can accept a maximum of four electrons. Thus, the fifth reduction process corresponded to the reduction of Cu(II) to Cu(I). Therefore, it was apparent that a Cu(I)–bis(amidophenolate) species was formed after five successive reductions. During the oxidation of Cu(I)–bis(amidophenolate) species, two additional oxidation waves appeared at −0.285 and 0.669 V as observed by two successive cyclic voltammograms measurement (Fig. 4.24B). The reduction potential beyond −1.288 V was responsible for the appearance of those two additional oxidation waves (Fig. 4.24B). Thus the irreversible reduction wave at −1.538 V was attributed to the process of the $[Cu^{II}\{L^{AP(o\text{–}NO_2\text{–}OPh)}\}\{L^{ISQ(o\text{–}NO_2\text{–}OPh)}\}]^-$/$[Cu^{I}\{L^{AP(o\text{–}NO_2\text{–}OPh)}\}\{L^{ISQ(o\text{–}NO_2\text{–}OPh)}\}]^{2-}$ couple (Schemes 4.11). Hence, the reduction at −1.685 V was due to the Cu(I)–coordinated

ligand–centered reduction of iminosemiquinone species to the corresponding amidophenolate species.

Table 4.6: *Summary of redox potential in volts vs. Ferrocenium/Ferrocene (Fc^+/Fc).*

Complex	E_{Ox} (V) *vs.* Fc^+/Fc	E_{Red} (V) *vs.* Fc^+/Fc	ΔE (V) *vs.* Fc^+/Fc	$E_{1/2}$ (V) *vs.* Fc^+/Fc
	–1.605	–1.765	0.160	–1.685
		–1.538		
4C	–0.964	–1.074	0.110	–1.019
	–0.129	–0.253	0.124	–0.191
	0.492	0.119	0.373	0.306

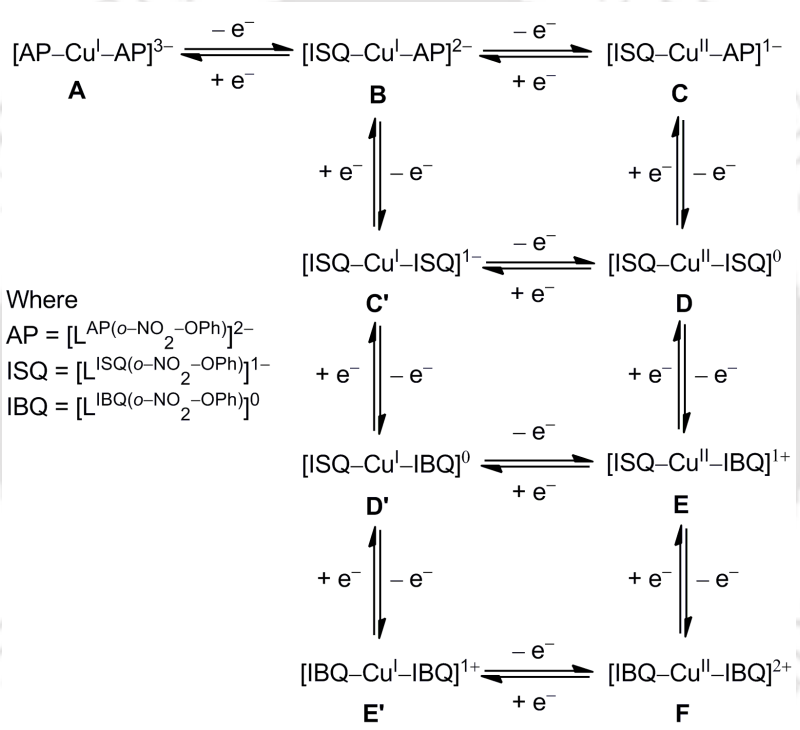

Scheme 4.11: *Redox path of complex **4C** during electrochemical analysis by cyclic voltammograms.*

4.6: One Step Synthesis of Octahedral Cu(II)–Bis(iminoquinone) Complexes

Instead of using 0.5 eq. $CuCl_2•2H_2O$, ligand $\mathbf{H_2L^{AP(o–NO_2–OPh)}}$ upon reacting with 2.0 equivalent amount of $CuCl_2•2H_2O$ in CH_3CN in the presence of Et_3N under aerial atmosphere in 2 hours provided an octahedral mononuclear Cu(II)–bis(iminoquinone) [**4D**] in 39% yield. It was a single step Cu(II)–bis(iminoquinone) synthesis, where each of coordinated amidophenolate units were in fully oxidised iminoquinone [$(IBQ)^0$] form. Inspired by the method, another common non–innocent ligand $\mathbf{H_2L^{AP}}$ has been introduced for crosschecking the one step Cu(II)–bis(iminoquinone) synthesis and it also provided diquinone–coordinated Cu(II) complex [**4E**•CH_2Cl_2**]** in 65% yield. The formation of Cu(II)–bis(iminoquinone) was proceeded with the generation of CuCl salt.

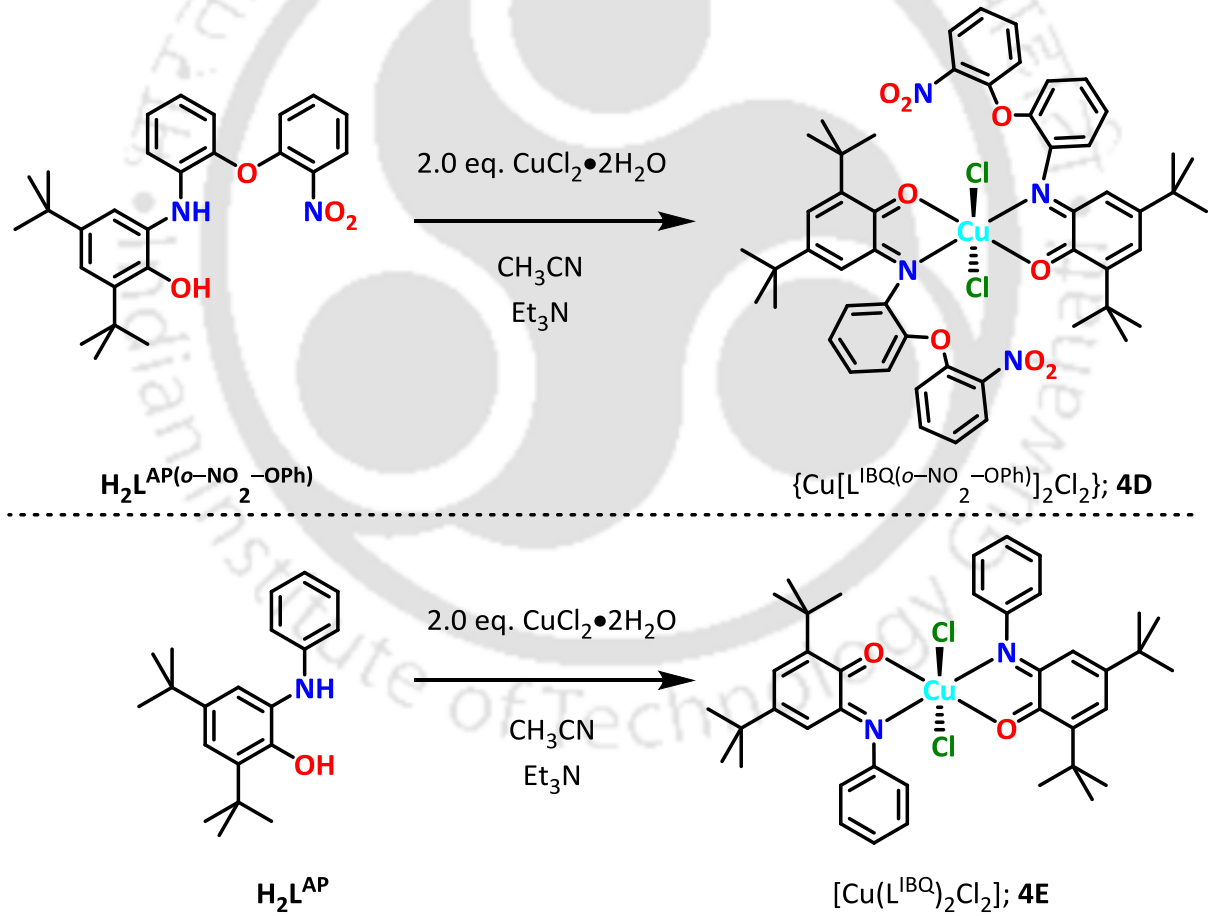

Scheme 4.12: *One step synthesis of Cu(II)–bis(iminoquinone) complexes **4D** and **4E**.*

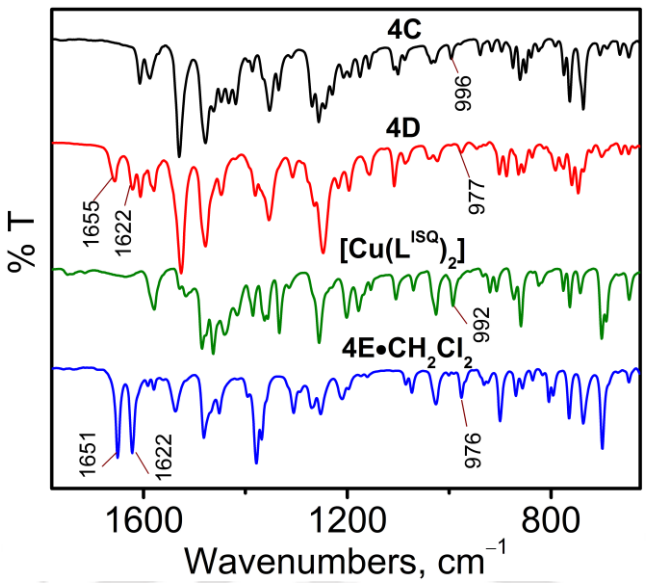

Figure 4.25: *FTIR spectra of complex **4D** and **4E**•CH_2Cl_2 along with corresponded Cu(II)–bis(iminosemiquinone) complex **4C** and **[Cu(L^{ISQ})$_2$]**[4a], respectively.*

The oxidation state of the non–innocent amidophenolate moieties [$(AP)^{2-}$] were confirmed by FTIR spectroscopy. IR spectra (1680–625 cm^{-1}) of complex **4D** and **4E**•CH_2Cl_2 along with the corresponded Cu(II)–bis(iminosemiquinone) complex **4C** and **[Cu(L^{ISQ})$_2$]**[4a] have been shown in Fig 4.26. IR absorption bands for ν(C=O) stretching was appeared at 1655[**4D**], 1651[**4E**•CH_2Cl_2] cm^{-1} whereas ν(C=N) stretching band appeared at 1622 cm^{-1} [**4D**, **4E**•CH_2Cl_2]. Parenthesis indicated the complexes. The ν(C=O) and ν(C=N) stretching modes revealed the existence of iminoquinone [$(IBQ)^0$] in the metal coordinated ligand moiety.[4d,20] A weak band at 996 [**4C**], 992 [**Cu(L^{ISQ})$_2$]** cm^{-1} corresponded to ν[(Cu–O(ISQ)] stretch shifted to 975[**4D**], 976 [**4E**•CH_2Cl_2**]** cm^{-1}, which would attributed as ν[(Cu–O(IBQ)] stretch.[4d]

The Cu(II)–bis(iminoquinone) complex was crystalized from 2:1 CH_2Cl_2/hexane solvent mixture. Single crystal X–ray diffraction measurements for complex **4D** and complex **4E**•CH_2Cl_2 were measured at 296(2) K. ORTEP drawings of the molecular structures of the complexes are shown in Fig. 4.26. Selected bond distances and bond angles were given in Table 4.7. Complex **4D** and complex **4E**•CH_2Cl_2 crystallized in the monoclinic space group '*C*2/*c*' and '$P2_1/c$', respectively.

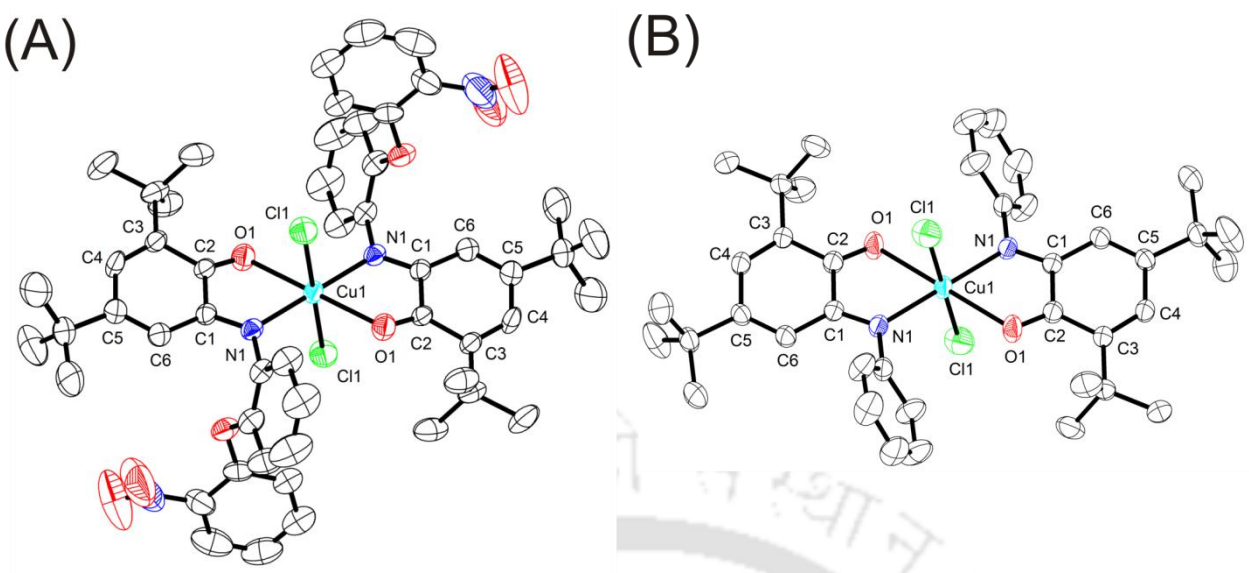

Figure 4.26: *ORTEP presentation of (A) complex **4D** and (B) **4E**•CH_2Cl_2; thermal ellipsoids were drawn at 50% probability level. H–atoms (for both of the complex) and solvent molecule (for complex **4E**•CH_2Cl_2) were omitted for clarity.*

Both the complexes were neutral and the central Cu atom was six–coordinate. Coordinated Cl, N, and O atoms were attached to the central Cu atom in *trans*– fashion. The Cu1–N1 = 2.025(4)[**4D**], 2.020(3)[**4E**•CH_2Cl_2]; Cu1–O1 = 2.344(3)[**4D**], 2.414(2)[**4E**•CH_2Cl_2]; Cu1–Cl1 = 2.273(1)[**4D**], 2.294(1)[**4E**•CH_2Cl_2] (parenthesis indicates the complex) bond distances indicated a distorted octahedral geometry around the Cu centre.[4d] While, Cu1–N1 bond distances were close to the bond distances found in complex **4C**, Cu1–O1 bonds were significantly long compared to those found in complex **4C**. This further implied that the oxidation state of the coordinated ligands in complex **4D** as well as in complex **4E**•CH_2Cl_2 was different than that in complex **4C**, *i.e.*, the ligands were not in their one–electron oxidized iminosemiquinone forms. Indeed, double bond characterizing C1–N1 = 1.298(5)[**4D**], 1.286(4)[**4E**•CH_2Cl_2] and C2–O1 = 1.215(5)[**4D**], 1.215(4)[**4E**•CH_2Cl_2] Å bond distances along with *quinoid–distortion* of the *tert*–butyl groups–containing phenyl rings (Table 4.7) confirmed two–electron oxidized iminoquinone {[$L^{IBQ(o-NO_2-OPh)}$]^0, [**4D**]; (L^{IBQ}), [**4E**•CH_2Cl_2]} form of the coordinated ligands.[4d,20] Thus, both complex **4D** and complex **4E**•CH_2Cl_2 were comprised of two chloride ions, two iminoquinone ligands and a Cu(II) ion.

Table 4.7: *Selected bond distances (Å) and bond angles (°) for the complexes.*

	4C	**4D**	**4E**•CH_2Cl_2
Cu1–O1	1.929(3)	2.344(3)	2.414(2)
Cu1–N1	1.934(3)	2.025(4)	2.020(3)
Cu1–Cl1		2.273(1)	2.294(1)
O1–C2	1.301(4)	1.215(5)	1.215(4)
O2–C12	1.399(4)	1.386(6)	
O2–C13	1.372(4)	1.379(6)	
N1–C1	1.340(4)	1.298(5)	1.286(4)
N1–C7	1.422(4)	1.426(6)	1.432(4)
N2–O3	1.197(5)	1.234(8)	
N2–O4	1.186(5)	1.181(8)	
N2–C18	1.487(6)	1.444(9)	
C1–C2	1.454(5)	1.525(6)	1.522(4)
C2–C3	1.431(5)	1.471(6)	1.469(5)
C4–C3	1.371(5)	1.343(7)	1.342(4)
C4–C5	1.430(6)	1.464(7)	1.463(4)
C5–C6	1.361(5)	1.332(7)	1.341(5)
C1–C6	1.416(5)	1.436(6)	1.441(4)
O1–Cu1–O1*	180.0(2)	180.0(1)	180.0(1)
O1–Cu1–N1	83.4(1)	74.5(1)	73.5(1)
O1–Cu1–N1*	96.6(1)	105.5(1)	106.5(1)
N1–Cu1–Cl1		89.9(1)	88.2(1)
N1–Cu1–Cl1*		90.1 (1)	91.8(1)
Cl1–Cu1–Cl1*		180.0(1)	180.0(1)
Cl1–Cu1–O1*		92.13(9)	91.8(1)
Cl1–Cu1–O1		87.87(9)	88.2(1)
N1–Cu1–N1*	180.0(1)	180.0(1)	180.0(1)
C2–O1–Cu1	113.1(2)	108.7(3)	108.8(2)
C13–O2–C12	117.7(3)	118.0(4)	
C1–N1–C7	120.7(3)	122.7(4)	120.3(3)
C1–N1–Cu1	113.3(2)	120.4(3)	121.7(2)
C7–N1–Cu1	125.2(2)	116.9(3)	117.8(2)
O3–N2–C18	116.1(5)	117.4(8)	
O4–N2–C18	119.4(5)	119.9(8)	
O4–N2–O3	124.6(6)	122.6(8)	

The asterisk (*) symbol stands for symmetry operation, inversion center.

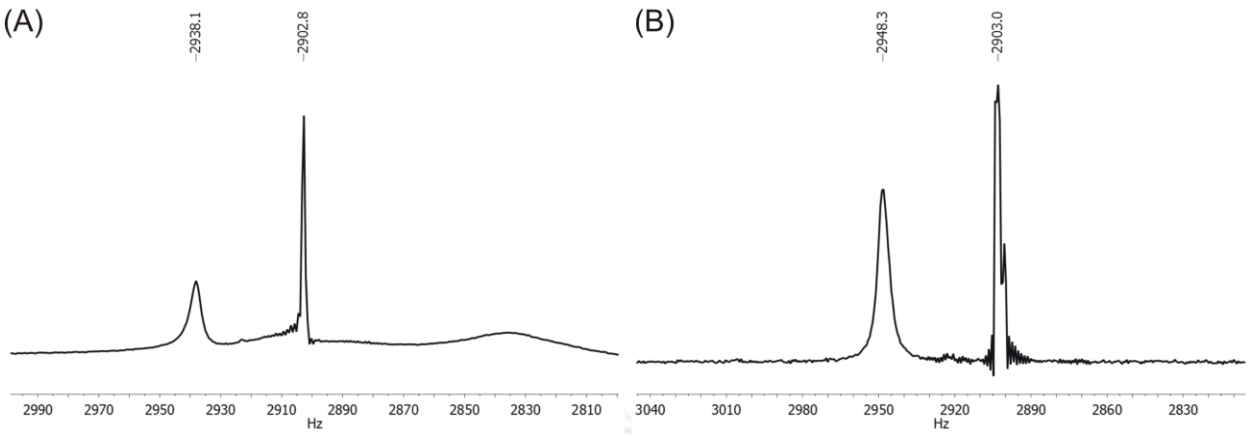

Figure 4.27: *Evans method ^{1}H NMR spectrum[11] of (A) complex **4D** in $CDCl_3$ at 400 MHz (μ_{eff} = 2.05 μ_B at 298 K); (B) complex **4E**•CH_2Cl_2 in $CDCl_3$ at 400 MHz (μ_{eff} = 1.95 μ_B at 298 K).*

In case of both complex **4D** and **4E**•CH_2Cl_2, the geometrical details pointed on the Cu(II)–coordination with two iminoquinone [$(IBQ)^0$] units in an octahedral coordination sphere. Such coordination comprised single spin on the metal ion in both of the complex. Evans method ^{1}H NMR measurement[11] of complex **4D** and **4E**•CH_2Cl_2 were performed in $CDCl_3$ at 400 MHz. In the analysis, concentration of complex **4D** and **4E**•CH_2Cl_2 were taken by 0.017 and 0.020 g/mL, respectively. The positive shift (paramagnetic) in resonance signal (δ_v) of the used solvent was found by 35.3 (**4D**) and 45.3 Hz (**4E**•CH_2Cl_2) (Fig. 4.27) at 298 K. Thus, from the resultant data, the effective magnetic moment μ_{eff} of complex **4D** and **4E**•CH_2Cl_2 were found as 2.05 and 1.95 μ_B, respectively. The resultant magnetic moments (>1.73 μ_B) were suggestive for metal centered single unpaired electron for both of the complexes.

To consolidate the Cu–center location of the unpaired electron, EPR measurement for each of the Cu(II)–bis(iminoquinone) complex was done. X–band EPR spectrum of complex **4D** and **4E**•CH_2Cl_2 were recorded in a 2:1 CH_2Cl_2/toluene solvent mixture at 77 K. Experimental and simulated spectra were shown in Figure 4.28.

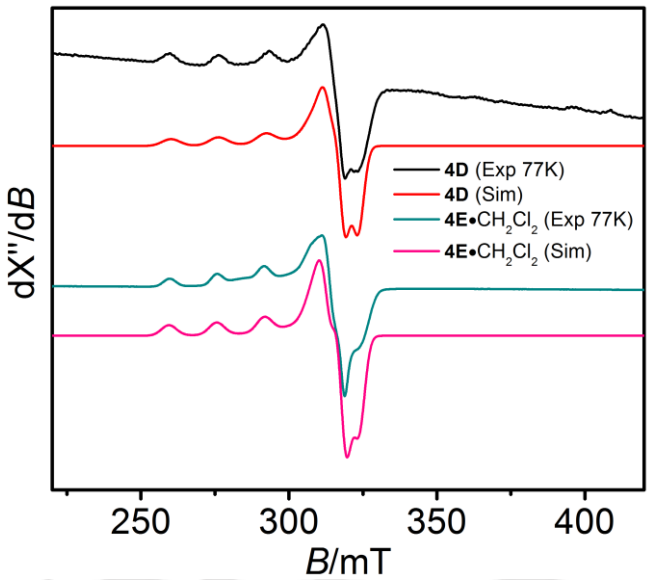

Figure 4.28: *X–band EPR spectrum of the complexes measured at 77 K. Conditions: X–band microwave frequency (GHz): 9.143 [**4D**], 9.142 [**4E**•CH_2Cl_2]; modulation frequency (kHz): 100 [**4D**, **4E**•CH_2Cl_2]; microwave power (mW): 0.995 [**4D**, **4E**•CH_2Cl_2]; amplitude (G): 3.0 [**4D**], 1.0 [**4E**•CH_2Cl_2].*

In both complex**es**, Cu(II) ion was the only paramagnetic centre as the coordinated non–innocent ligand moieties were in fully oxidised state. Experimentally obtained EPR spectra were also signature of Cu(II)–centered unpaired–electron. The spectra were simulated using the following parameters: g_1 = 2.058[**4D**], 2.057[**4E**•CH_2Cl_2]; g_2 = 2.080[**4D**], 2.085[**4E**•CH_2Cl_2]; g_3 = 2.300[**4D**], 2.303[**4E**•CH_2Cl_2]; g_{iso} = 2.146[**4D**], 2.148[**4E**•CH_2Cl_2]; $^{63/65}$Cu(A_1, A_2, A_3) = (0, 0, 160) × 10^{-4} cm^{-1}[**4D**], (3, 3, 162) × 10^{-4} cm^{-1}[**4E**•CH_2Cl_2]. The simulated–data reinforced the location of unpaired–electron on Cu(II) centre (g_{iso} > 2.00) and the EPR signals were appeared for axial Cu(II) systems with slight rhombic distortions. The $g_3 > g_1, g_2$, and $A_3 >> A_1$, A_2 further indicated the presence of unpaired electron on $d_x^2–_y^2$ orbital of the Cu(II) ion.[18c,d]

The electronic absorption spectra of Cu(II)–bis(iminoquinone) complexes (**4D** and **4E**•CH_2Cl_2) were recorded in dichloromethane solution at room temperature and the spectra were shown in Fig. 4.29. The λ_{max} and corresponding absorption coefficient value were summarised in Table 4.8.

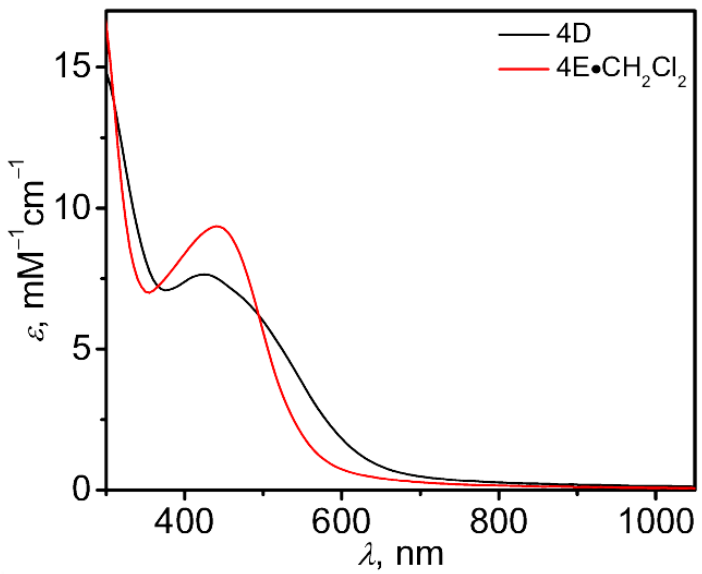

Figure 4.29: *UV–Vis/NIR spectra of complex* ***4D*** *and* ***4E****•CH_2Cl_2 in 300–1050 nm range.*

A broad band near 650 nm with low extension coefficient was observed for both of the complexes. The band was corresponded to the Cu^{II} [$3d^9$]–centered *d–d* electronic transition. The bands at 425 (**4D**) and 440(**4E**•CH_2Cl_2) were due to benzoquinone based charge transfer (π–π* transition).[4a,d]

Table 4.8: *The summary of electronic absorption spectra of* ***4D*** *and* ***4E****•CH_2Cl_2.*

Complex	λ_{max}, nm (ε, M^{-1} cm^{-1})
4D	650^{br}(850), 485^{sh}(6500), 425(7650), 305(14350)
4E•CH_2Cl_2	650^{br}(400), 440 (9350), 295 (17200)

* The superscript 'br' and 'sh' stands for broad and solder band respectively.

4.7: Proposed Pathway of the Formation of Cu(II)–bis(iminoquinone) Complexes

In order to understand the pathway, solvent effect and salt effect were investigated in a sequential manner. It was found that Cu(II)–bis(iminoquinone) complex (**4D**) formation also proceeded in EtOH with 46% yield. Hence, it can be argued that the Cu(II)–bis(iminoquinone) complex formation–reaction was indifferent to the nature of the used solvent, *i.e.* the reaction was not a solvent driven–process.

Cu(II) salt (2 eq.) with different counter anion (like Br^- , AcO^- or ClO_4^-) were unable to produce Cu(II)–bis(iminoquinone) species under similar reaction condition as described in Scheme 4.12. Those reactions leaded ligand $\mathbf{H_2L^{AP(o\text{–}NO_2\text{–}OPh)}}$ or $\mathbf{H_2L^{AP}}$ to their one electron oxidized state and resulted corresponding diradical Cu(II)–bis(iminosemiquinone) species as green solid. This indicated that the Cu(II)–bis(iminoquinone) complex formation depended on the nature of the employed salt *i.e*. $CuCl_2•2H_2O$. The anion, associated to the Cu(II) ion, was then postulated to participate in the electron transfer,[21] *i.e*. in the oxidation of iminosemiquinone to iminoquinone.

The formation of Cu(II)–bis(iminoquinone) complexes (**4D** and **4E**•CH_2Cl_2) were proceeded through the initial generation of corresponding diradical Cu(II)–bis(iminosemiquinone) species. The ligand centre radical anions were oxidised by the excess $CuCl_2•2H_2O$ in the reaction medium and a white Cu(I) salt was appeared with the desired product. The white solid was insoluble in most of the organic solvents like CH_3CN, CH_2Cl_2, $CHCl_3$ and it was turned to greenish with time under air. The colourless isolated solid was X–band EPR silent, while the light green solid showed a Cu(II)–centered EPR spectrum (Fig. 4.31). This implied that the initially isolated solid was CuCl, which under an aerial atmosphere changed to its Cu(II) form. Hence, it was evident that during the reaction Cu(II) was reduced to Cu(I). The electron–transfer was possibly an inner sphere process,[21] where at the initial stage two chloride ions from two individual $CuCl_2$ molecules formed two bridges with the central Cu(II) atom of a diradical–containing Cu(II) complex in *trans*– fashion (Scheme 4.13). After that, an electron was transferred to each bound $CuCl_2$ unit from the two iminosemiquinone moieties through the Cu(II) centre and produced the octahedral *trans*–dichloride–bound mononuclear Cu(II)–bis(iminoquinone) complexes along with CuCl. The mechanistic proposal is depicted in Scheme 4.13.

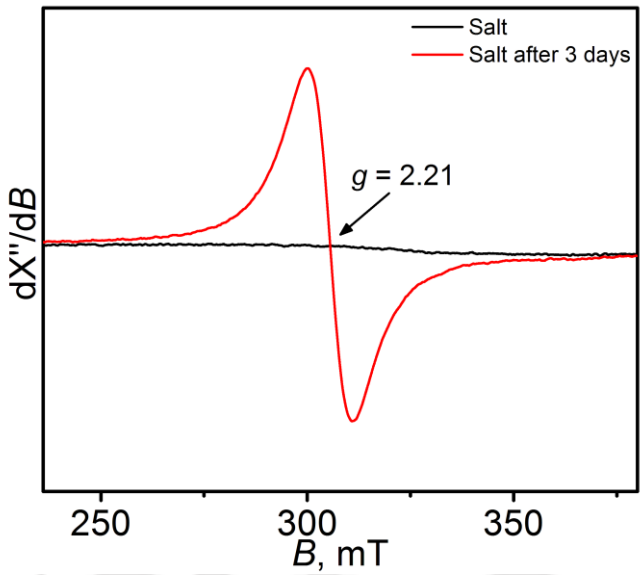

Figure 4.30: *Experimental X–band EPR spectra for the salt found during the synthesis of complex **4D** at room temperature; X–band microwave frequency (GHz): 9.450, modulation frequency (kHz): 100, microwave power (mW): 0.998, amplitude: 100.0.*

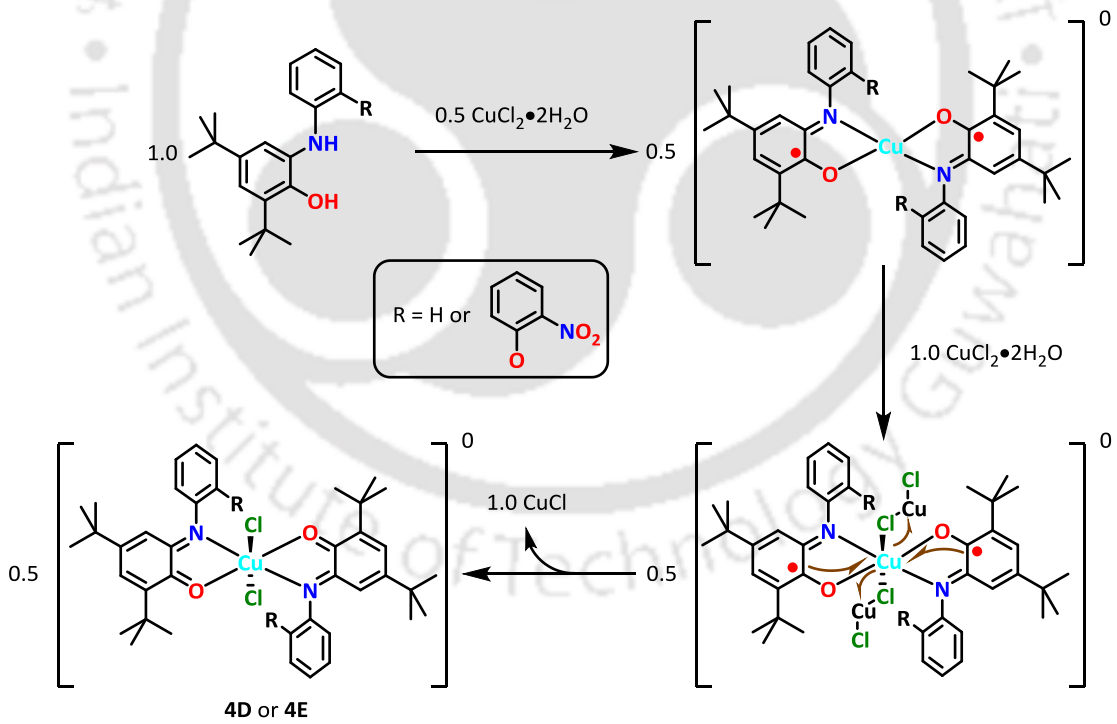

Scheme 4.13: *Proposed mechanism for the formation of octahedral Cu(II)–bis(iminoquinone) species.*

4.8: Generation of Hydrogen from $NaBH_4$ in Anhydrous Acetonitrile

Iminoquinone moiety can accept two–electrons, hence, Cu(II)–bis(iminoquinone) complexes can be used as electrons–acceptor or as multi–electron oxidising agents. Therefore, the complexes can be examined as catalysts or promoters for the generation of H_2 gas from BH_4^- species. Thus, such catalytic property was preliminarily investigated employing the Cu(II)–bis(iminoquinone) complex **4E**•CH_2Cl_2. In dry CH_3CN, 1:5 complex **4E**•CH_2Cl_2 and $NaBH_4$ were added. Instantaneously, H_2 gas started forming and was coming out from the reaction medium in bubbler form (Fig. 4.31A). The gas was characterized by gas chromatography (GC) technique (Fig. 4.31B).

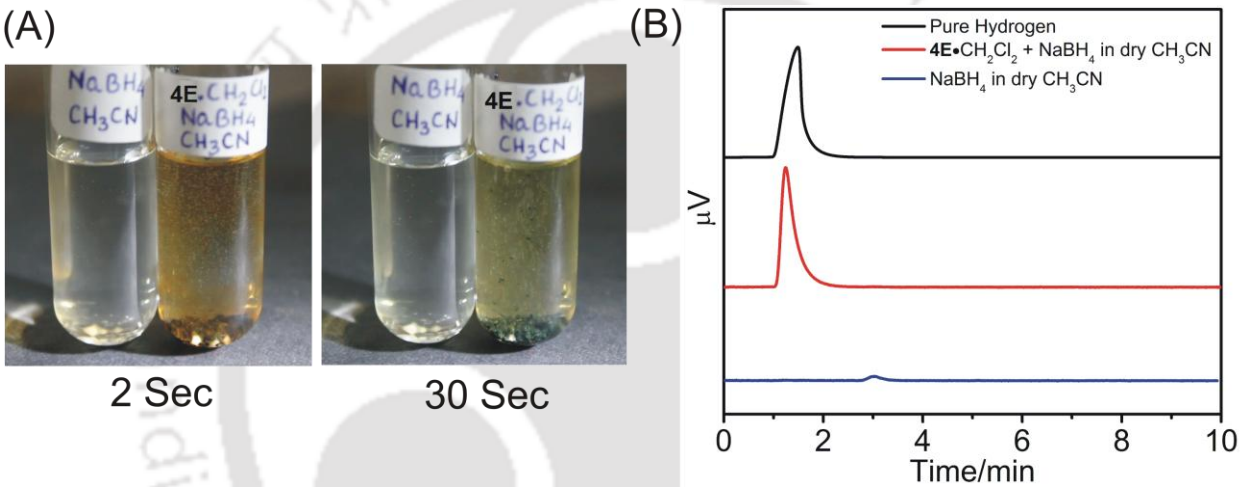

Figure 4.31: *(A) Complex **4E**•CH_2Cl_2 assisted formation of H_2 gas from $NaBH_4$ in dry CH_3CN; (B) Gas chromatographic (GC) analysis of the evolved gas.*

To note, under the same reaction condition almost no H_2 gas was formed in the absence of the complex. In due course the brown Cu(II)–bis(iminoquinone) complex **4E**•CH_2Cl_2 transformed to a green precipitate, which was characterized by mass, IR and UV–Vis/NIR spectroscopic techniques as the corresponding Cu(II)–bis(iminosemiquinone) species $[Cu(L^{ISQ})_2]$[4a] (Scheme 4.14A). To note, the isolated yield of the crystalline Cu(II)–bis(iminosemiquinone) species after the reaction was 78% and can be converted to complex **4E**•CH_2Cl_2 again by using 3.0 equivalents of $CuCl_2$•$2H_2O$ in CH_3CN (Scheme 4.14A). Complex **4D** was also shown such type of hydrogen evolution capability from $NaBH_4$ in dry acetonitrile and transformed to corresponding Cu(II)–bis(iminosemiquinone) species (**4C**).

In the reaction mixture, probably hydride ion transformed to proton during the interaction with Cu(II)–bis(iminoquinone) species and the generated proton transformed to

hydrogen in presence of excess hydride ion (Scheme 4.14B). Thus, the function of two–electron transporter ubiquinone coenzyme has been mimicked by Cu(II) coordinated iminoquinone entity.

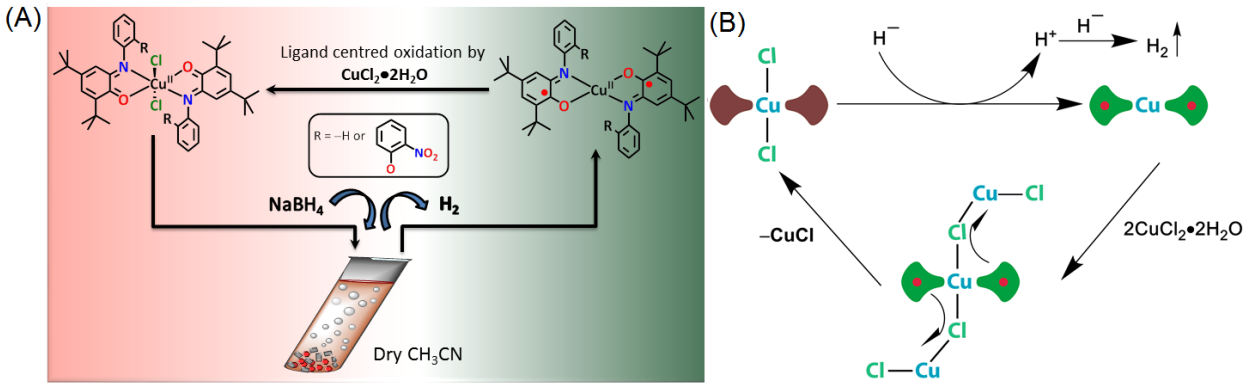

Scheme 4.14: *Schematic representation (A) and proposed pathway (B) of complex Cu(II)–bis(iminoquinone) assisted evolution of H_2 gas with generation of diradical containing Cu(II)–bis(iminosemiquinone) species and regeneration of Cu(II)–bis(iminoquinone) by using $CuCl_2•2H_2O$.*

4.9: Conclusion

- Ligand $\mathbf{H_2L^{AP(o-NO_2-OPh)}}$ results a square pyramidal iron(III)–bis(iminosemiquinato)chloride complex (**4A**) on reacting with anhydrous $FeCl_3$ in presence of Et_3N under air. In the complex, both radicals are antiferromagnetically coupled with the high–spin Fe(III) center.
- Reaction of 0.5 equivalent Ni or Cu salt with the ligand results the corresponding diradical–containing square planar Ni(II) or Cu(II) complex.
- An efficient method for the generation of Cu(II)–bis(iminoquinone) complex using amidophenolate based non–innocent ligand and 2 equivalents of $CuCl_2 \bullet 2H_2O$ in the presence of Et_3N and air has been established in one step.
- The generation of Cu(II)–bis(iminoquinone) complex is proceeded through initial generation of diradical–containing Cu(II) complex, which on reacting with excess $CuCl_2 \bullet 2H_2O$ results the final complex.
- $CuCl_2 \bullet 2H_2O$ acts as an oxidant and the oxidation of iminosemiquinone[$(ISQ)^{\bullet 1-}$] moieties was proceeded through inner sphere mechanism. This results Cu(I)Cl as the reduced–product.
- The electrophilic behaviour of Cu(II)–bis(iminoquinone) species helps to produce hydrogen gas from $NaBH_4$ in the anhydrous acetonitrile medium.

References

1. (*a*) K. Overvad, B. Diamant, L. Holm, G. Hølmer, S. A. Mortensen and S. Stender, *Eur. J. Clin. Nutr.*, 1999, **53**, 764; (*b*) F. L. Crane, *J. Am. Coll. Nutr.*, 2001, **20**, 591; (*c*) A. Varela–López, P. Bullón, F. Giampieri and J. L. Quiles, *Antioxidants.*, 2015, **4**, 447; (*d*) R. Rucker, W. Chowanadisai and M. Nakano, *Altern. Med. Rev.*, 2009, **14**, 268; (*e*) M. Miroshnikov, K. P. Divya, G. Babu, A. Meiyazhagan, L. M. R. Arava, P. M. Ajayan and G. John, *J. Mater. Chem. A*, 2016, **4**, 12370; (*f*) S. S. Stahl and A. E. Wendlandt, *Angew. Chem., Int. Ed.*, 2015, **54**, 14638; (*g*) B. Yang, L. Hoober–Burkhardt, S. Krishnamoorthy, A. Murali, G. K. S. Prakash and S. R. Narayanan, *J. Electrochem. Soc.*, 2016, **163**, A1442.

2. (*a*) R Dhingra and L. A. Kirshenbaum, *Cell Death Dis.*, 2015, **6**, e1956; (*b*) G. Cecchini, *Annu. Rev. Biochem.*, 2003, **72**, 77; (*c*) E. Tomitsuka1, H. Hirawake1, Yu–ichi Goto, M. Taniwaki, S. Harada and K. Kita, *J. Biochem.*, 2003, **134**, 191.

3. (*a*) F. Novio, E. Evangelio, N. Vazquez–Mera, P. Gonzalez–Monje, E. Bellido, S. Mendes, N. Kehagias and D. Ruiz–Molina, *Sci. Rep.*, 2013, **3**, 1708; (*b*) O. Cador, F. Chabre, A. Dei, C. Sangregorio, J. V. Slageren and M. G. F. Vaz, *Inorg. Chem.*, 2003, **42**, 6432; (*c*) B. Gui, X. Meng, Y. Chen, J. Tian, G. Liu, C. Shen, M. Zeller, D. Yuan and C. Wang, *Chem. Mater.*, 2015, **27**, 6426; (*d*) P. Yan, M. W. Holman, P. Robustelli, A. Chowdhury, F. I. Ishak, and D. M. Adams, *J. Phys. Chem. B*, 2005, **109**, 130; (*e*) J. Jacquet, E. Salanouve, M. Orio, H. Vezin, S. Blanchard, E. Derat, M. Desage–El Murr and L. Fensterbank, *Chem. Commun.*, 2014, **50**, 10394; (*f*) J. Jacquet, S. Blanchard, E. Derat, M. Desage–El Murr and L. Fensterbank, *Chem. Sci.*, 2016, **7**, 2030; (*g*) J. Jacquet, P. Chaumont, G. Gontard, M. Orio, H. Vezin, S. Blanchard, M. Desage–El Murr, and L. Fensterbank, *Angew. Chem., Int. Ed.*, 2016, **55**, 10712.

4. (*a*) P. Chaudhuri, C. N. Verani, E. Bill, E. Bothe, T. Weyhermüller and K. Wieghardt, *J. Am. Chem. Soc.*, 2001, **123**, 2213; (*b*) A. L. Smith, L. A. Clapp, K. I. Hardcastle and J. D. Soper, *Polyhedron*, 2010, **29**, 164; (*c*) A. L. Smith, K. I. Hardcastle and J. D. Soper, *J. Am. Chem. Soc.*, 2010, **132**, 14358; (*d*) C. Mukherjee, T. Weyhermüller, E. Bothe and P. Chaudhuri, Inorg. Chem., 2008, **47**, 2740; (*e*) S. Mukherjee, T. Weyhermüller, E. Bothe, K. Wieghardt and P. Chaudhuri, *Dalton Trans.*, 2004, 3842.

5. (*a*) Y. Izumi, H. Sawada, N. Sakka, N. Yamamoto, T. Kume, H. Katsuki, S. Shimohama and A. Akaike, *J. Neurosci. Res.*, 2005, **79**, 849; (*b*) G. F. Z. da Silva and L.–J. Ming, *Angew. Chem., Int. Ed.*, 2007, **46**, 3337; (*c*) R. Liu, B. Goodell, J. Jellison and A. Amirbahman, *Environ. Sci.*

Technol., 2005, **39**, 175; (*d*) T. Klabunde, C. Eicken, J. C. Sacchettini and B. Krebs, *Nat. Struct. Biol.*, 1998, **5**, 1084; (*e*) E. I. Solomon, U. M. Sundaram and T. E. Machonkin, *Chem. Rev.*, 1996, **96**, 2563; (*f*) H. Decker, T. Schweikardt and F. Tuczek, *Angew. Chem., Int. Ed.*, 2006, **45**, 4546; (*g*) C. M. Wilmot, *Biochem. Soc. Trans.*, 2003, **31**, 493.

6. (*a*) G. R. Pandhare, V. M. Shinde and Y. H. Deshpande, *Rasayan J. Chem.*, 2008, 1, 337; (*b*) J. Coates, *Interpretation of Infrared Spectra: A Practical Approach*, John Wiley & Sons Ltd, Chichester, 2000; (*c*) D. L. Pavia, G. M. Lampman, G. S. Kriz and J. R. Vyvyan, *Introduction to Spectroscopy*, 4th edition, 31; (*d*) P. K. Kipkemboi, P. C. Kiprono and J. J. Sanga, *Bull. Chem. Soc. Ethiop.*, 2003, **17**, 211; (*e*) C. W. M. Yuen, S. K. A. Ku, P. S. R. Choi, C. W. Kan and S. Y. Tsang, *RJTA.*, 2005, **9**, 26; (*f*) S. Sahoo, C. K. Chakraborti, P. K. Behera and S. C. Mishra, *Int. J. Drug Dev. & Res.*, 2011, **3**, 261.

7. (*a*) G. Hastings and V. Sivakumar, *Biochemistry*, 2001, **40**, 3681; (*b*) J. Breton, J. Burie, C. Berthomieu, G. Berger and E. Nabedryk, *Biochemistry*, 1994, **33**, 4953.

8. A. W. Addison, N. T. Rao, J. Reedijk, J. van Rijn, G. C. Verschoor, *J. Chem. Soc. Dalton Trans.*, 1984, 1349.

9. (*a*) H. Chun, T. Weyhermüller, E. Bill and K. Wieghardt, *Angew. Chem., Int. Ed.*, 2001, **40**, 2489; (*b*) J. L. Wong, R. F. Higgins, I. Bhowmick, D. Xi Cao, G. Szigethy, J. W. Ziller, M. P. Shores and A. F. Heyduk, *Chem. Sci.*, 2016, 7, 1594; (*c*) H. Chun, C. N. Verani, P. Chaudhuri, E. Bothe, E. Bill, T. Weyhermüller and K. Wieghardt, *Inorg. Chem.*, 2001, **40**, 4157; (*d*) C. Mukherjee, T. Weyhermüller, E. Bothe and P. Chaudhuri, *Inorg. Chem.*, 2008, **47**, 11620.

10. E. Evangelio, M.–L. Bonnet, M. Cabanas, M. Nakano, J.–P. Sutter, A. Dei, V. Robert and D. Ruiz–Molina, *Chem. Eur. J.*, 2010, **16**, 6666.

11. (*a*) D. F. Evans, *J. Chem. Soc.*, 1959, 2003; (*b*) D. F. Evans, G. V. Fazakerley and R. F. Phillips, *J. Chem. Soc. A*, 1971, 1931; (*c*) C. Piguet, *J. Chem. Educ.*, 1997, **74**, 815.

12. A. Okuniewski, D. Rosiak, J. Chojnacki and B. Becker, *Polyhedron*, 2015, **90**, 47.

13. C. Mukherjee *et al.*, unpublished results.

14 (*a*) K. Ray, T. Weyhermüller, F. Neese and K. Wieghardt, *Inorg. Chem.*, 2005, **44**, 5345; (*b*) A. Mukherjee and R. N. Mukherjee, *Indian J. Chem.*, 2011, **504**, 484.

15. H. Suzuki, M.A. Nagasaka, M. Sugiura and T. Noguchi, *Biochemistry*, 2005, **44**, 11323.

16. L. Yang, D. R. Powella and R. P. Houser, *Dalton Trans.*, 2007, 955.

17. (*a*) F. Thomas, *Eur. J. Inorg. Chem.*, 2007, 2379; (*b*) P. Chaudhuri and K. Wieghardt, *Prog. Inorg. Chem.*, 2002, **50**, 151; (*c*) R. Rakshit, S. Ghorai, S. Biswas and C. Mukherjee, *Inorg. Chem.*, 2014, **53**, 3333; (*d*) P. Chaudhuri, K. Wieghardt, T. Weyhermüller, T. K. Paine, S. Mukherjee and C. Mukherjee, *Biol. Chem.*, 2005, **386**, 1023; (*e*) S. Ye, B. Sarkar, F. Lissner, T. Schleid, J. van Slageren, J. Fiedler and W. Kaim, *Angew. Chem., Int. Ed.*, 2005, **44**, 2103; (*f*) S. Ghorai and C. Mukherjee, *Chem. Asian J.*, 2014, **9**, 3518; (*g*) C. Mukherjee, U. Pieper, E. Bothe, V. Bachler, E. Bill, T. Weyhermüller and P. Chaudhuri, *Inorg. Chem.*, 2008, **47**, 8943; (*h*) C. Mukherjee, T. Weyhermüller, E. Bothe, E. Rentschler and P. Chaudhuri, *Inorg. Chem.*, 2007, **46**, 9895; (*i*) A. I. Poddel'sky, V. K. Cherkasov and G. A. Abakumov, *Coord. Chem. Rev.*, 2009, **253**, 291; (*j*) S. Ghorai, A. Sarmah, R. K. Roy, A. Tiwari and C. Mukherjee, *Inorg. Chem.*, 2016, **55**, 1370; (*k*) A. Paretzki, R. Hübner, S. Ye, M. Bubrin, S. Kämper and W. Kaim, *J. Mater. Chem. C*, 2015, **3**, 4801; (*l*) D. L. J. Broere, R. Plessius and J. I. van der Vlugt, *Chem. Soc. Rev.*, 2015, **44**, 6886.

18. (*a*) I. M. Procter, B. J. Hathaway and P. J. Nichollos, *J. Chem. Soc. A*, 1968, 1678; (*b*) R. S. Drago, *Physical Methods in Chemistry*, Philadelphia, 1977; (*c*) B. J. Hathaway and D. E. Billing, *Coord. Chem. Rev.*, 1970, **5**, 1; (*d*) E. Garribba and G. Micera, *J. Chem. Educ.*, 2006, **83**, 1229; (*e*) R. Rakshit and C. Mukherjee, *Eur. J. Inorg. Chem.*, 2016, 2731.

19. O. Kahn, *Molecular Magnetism*, Wiley–VCH, New York, 1993.

20. M. K. Mondal, A. K. Biswas, B. Ganguly and C. Mukherjee, *Dalton Trans.*, 2015, **44**, 9375.

21. H. –C. Chang, F. –C. Lo, W. –C. Liu, T. –H. Lin, W. –F. Liaw, T. –S. Kuo and W. –Z. Lee, *Inorg. Chem.*, 2015, **54**, 5527.

Chapter V

A Hemilabile –NH_2 Group Appended Aminophenol–Based Bidentate Non–Innocent Ligand: Synthesis and Characterization of its Corresponding Radical–Containing Transition Metal Complexes

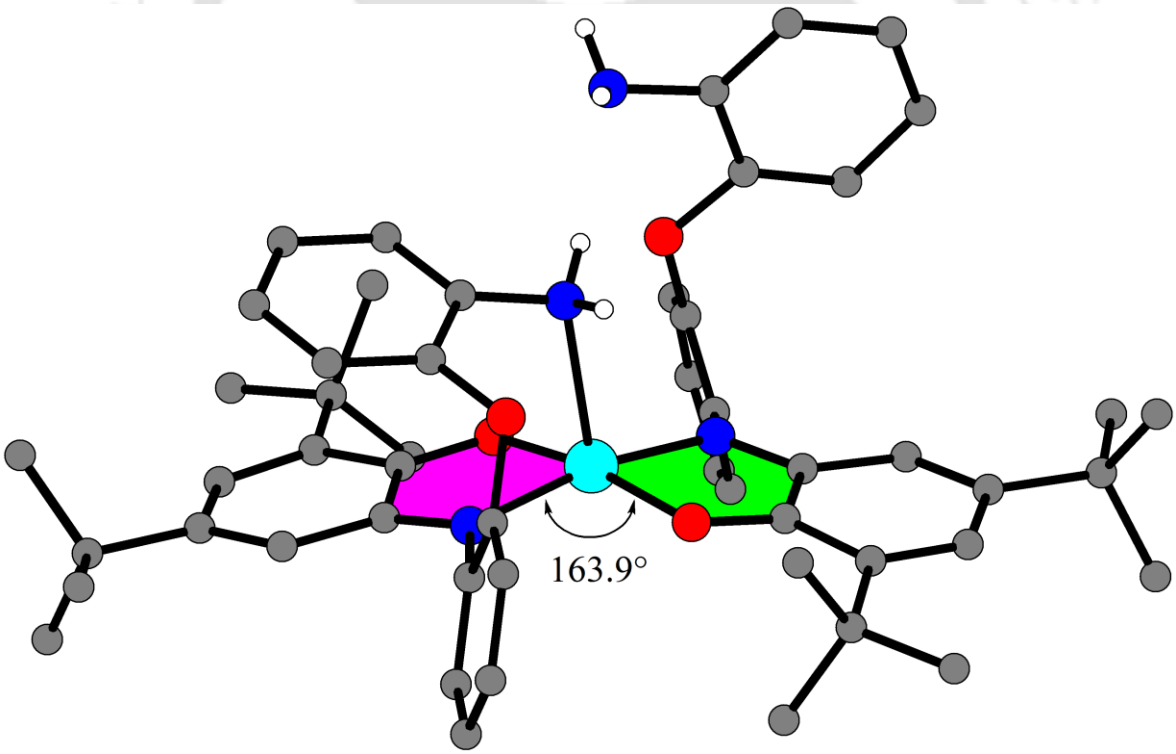

5.1: Introduction

Because of structural simplicity and possible biomimetic applications, synthesis and characterization of functional and structural model–complexes of Type–I and Type–II mononuclear Cu–based proteins (*e.g.*, plastocyanin,[1] galactose oxidase,[2] amine oxidase[3] etc) have attain special attention

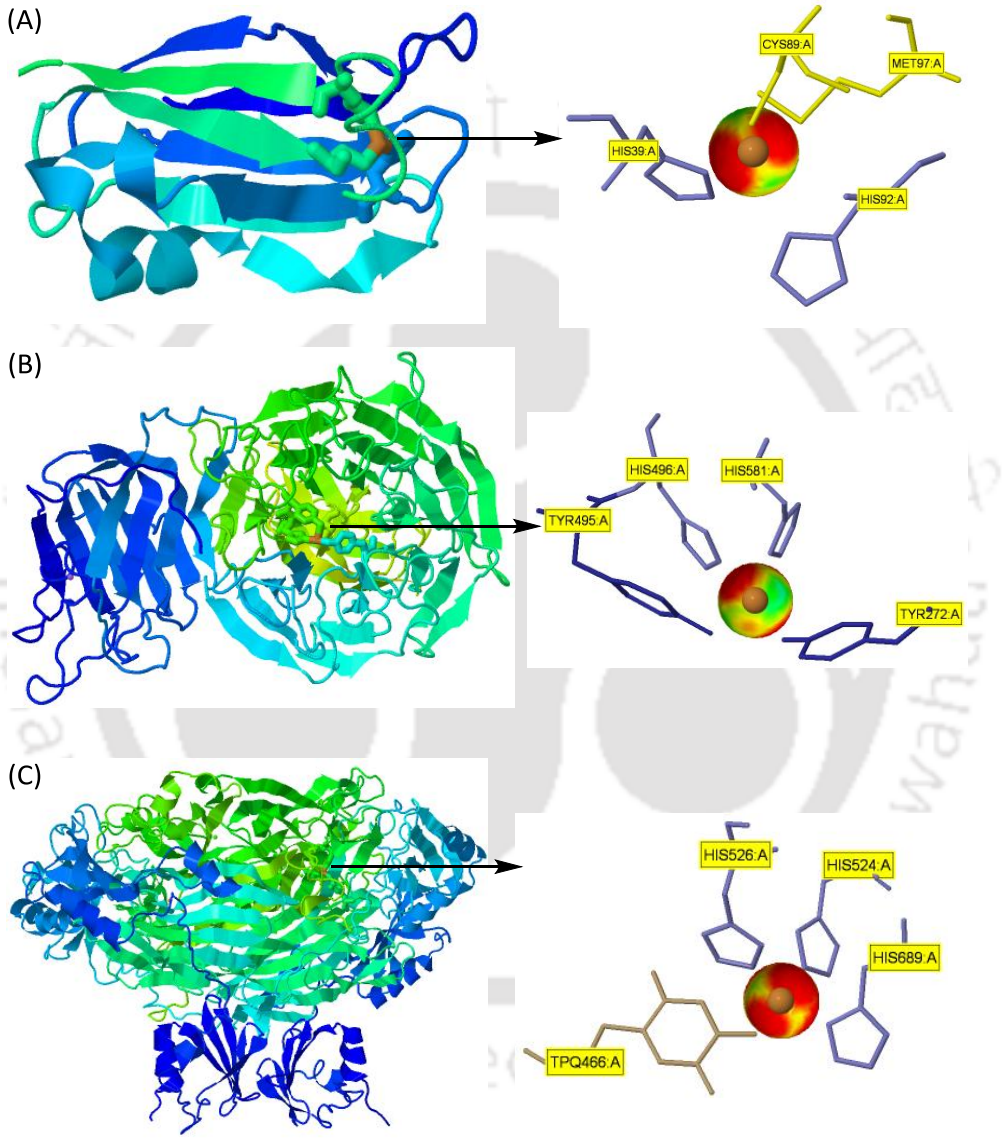

Figure 5.1: *Cu–containing mononuclear enzymes and their active site Cu–pocket interaction: (A) Plastocyanin (3BQV);[1a] (B) Galactose Oxidase (1GOG)[2a] and (c) Amine Oxidase (1OAC)[3a].*

In this context, to mimic the function of Galactose Oxidase (GO), a few four–coordinate Cu^{II}–diradical complexes are synthesized employing 2–aminophenol derivative–based ligands.[4] In the presence of base, air and Cu–salt, the aminophenol unit undergoes one–electron oxidation and results the expected Cu^{II}–diradical complex. Coordination of two radical units with a Cu(II)–

ion in a four–coordinate complex results a spin–frustrating situation in the molecule. The spin–coupling mechanism in such type of four–coordinate square planer complexes ([Cu(L^{ISQ})$_2$]) has been previously formulated by Chaudhuri *et al*.[4a]

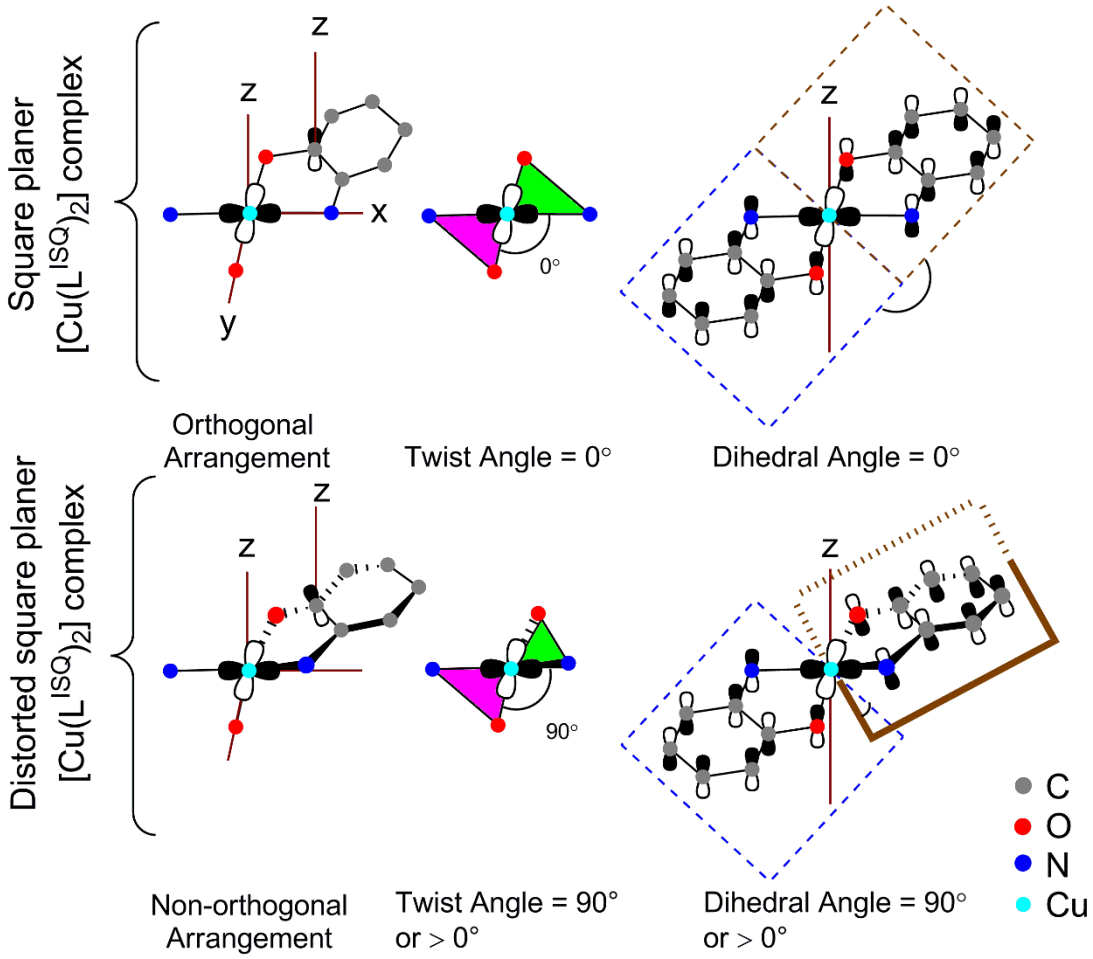

Figure 5.2: *Orthogonal and non–orthogonal arrangement between Cu(II)–centered $d_{x^2-y^2}$ and ligand centered p_z orbitals (left side); Twist angle between the biting plane (middle) and the dihedral angle between two iminosemiquinone moieties through common Cu(II) center.*

In the square planner Cu(II)–diradical complexes, single electron–containing metal orbital ($d_{x^2-y^2}$) and ligand centered (p_z) orbital are orthogonal to each other. This orthogonal relation promotes a ferromagnetic coupling between the Cu(II) center and the coordinated radical centers. However, a strong antiferromagnetic coupling between the two radical centers propagates *via* the Cu(II)–centered filled t_{2g} set of orbitals. A higher antiferromagnetic coupling compared to the ferromagnetic coupling leads to (↑↑↓) as the ground state electronic configuration, where the single electron resides on the metal center.

However, in some cases, axial secondary coordination leads to an alteration in coupling fashion and provides (↑↓↑) as the ground state electronic configuration, *i.e.* ligand–centered unpaired electron. The structural distortion generates non–orthogonally between metal centered magnetic orbital ($d_{x^2-y^2}$) and ligand centered (p_z) orbitals, which predominantly facilitate the metal–radical antiferromagnetic interaction over the radical–radical interaction. In this note, the question arises regarding the limiting deviation that would shift predominance of antiferromagnetic coupling to the Cu(II)–radical unit from the radical–radical unit. It has been found that an axial soft coordination caused a major distortion in the basal plane as reported by Kaim *et al*[4c] and Mukherjee *et al*. [4d]

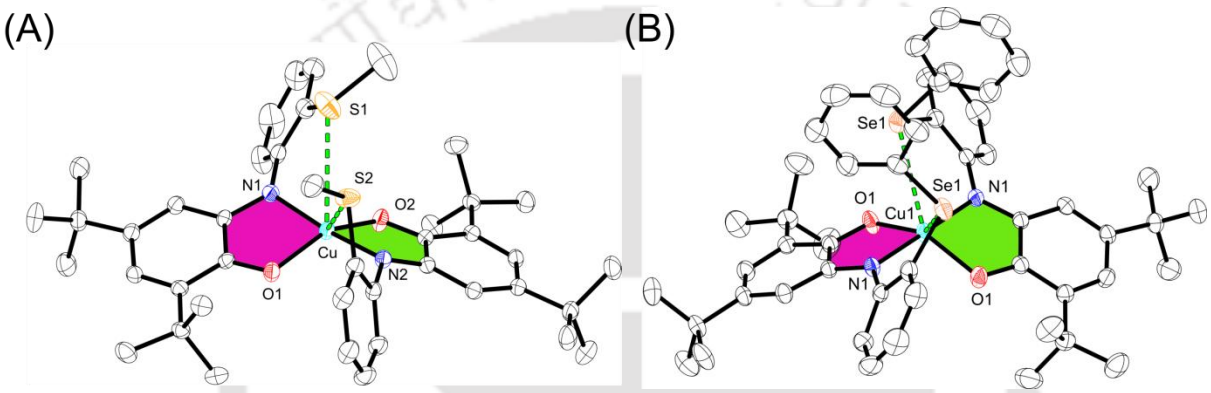

Figure 5.3: *(A) Complex {Cu[$L^{ISQ(S-Me)}$]$_2$} and (B) complex {Cu[$L^{ISQ(Se-Ph)}$]$_2$} represented with the secondary coordination (green dashed line) which caused the distortion in the ligating plane by 32.2 and 36.6 °, respectively.*[4c,d]

Thus, the extent of structural distortions as well as the secondary coordination get a considerable attention in determining the coupling fashion between the Cu(II) and a radical center.[2c,d] Herein, we have introduced harder entity (–NH_2) in the ligand backbone to find out the effect of interaction in the electronic behavior of corresponding Cu–complex. In this perspective, ligand $\mathbf{H_2L^{AP(o-NH_2-OPh)}}$ has designed by introducing an *o*–amidophenolate moiety at an *ortho*– position of the anilino unit of ligand H_2L^{AP}.

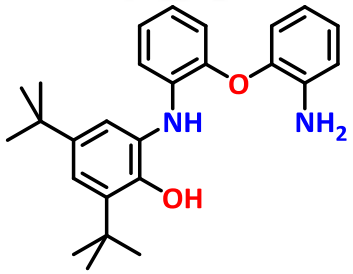

Scheme 5.1: *Schematic representation of ligand* $\boldsymbol{H_2L^{AP(o-NH_2-OPh)}}$.

In this chapter, the synthesis and characterization of ligand $\mathbf{H_2L^{AP(o\text{–}NH_2\text{–}OPh)}}$ and corresponding metal complexes (Co, Ni and Cu) have been reported.

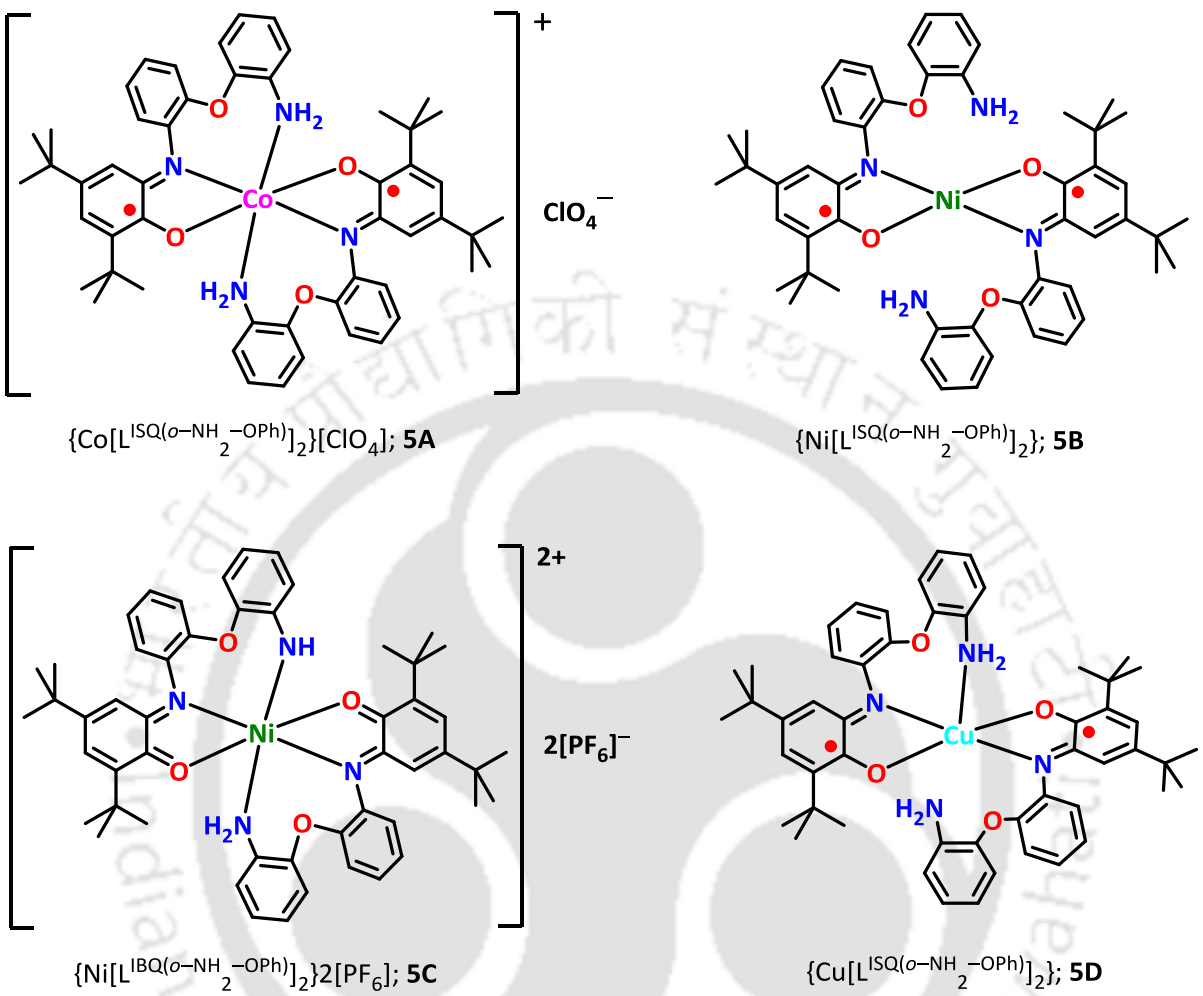

{Co[$L^{ISQ(o\text{–}NH_2\text{–}OPh)}$]$_2$}[$ClO_4$]; **5A**

{Ni[$L^{ISQ(o\text{–}NH_2\text{–}OPh)}$]$_2$}; **5B**

{Ni[$L^{IBQ(o\text{–}NH_2\text{–}OPh)}$]$_2$}2[$PF_6$]; **5C**

{Cu[$L^{ISQ(o\text{–}NH_2\text{–}OPh)}$]$_2$}; **5D**

Scheme 5.2: *Several Complexes derived from ligand* $\boldsymbol{H_2L^{AP(o\text{–}NH_2\text{–}OPh)}}$.

5.2: Synthesis of Ligand $H_2L^{AP(o–NH_2–OPh)}$

Ligand $\mathbf{H_2L^{AP(o–NH_2–OPh)}}$ was synthesized from $\mathbf{H_2L^{AP(o–NO_2–OPh)}}$ by reduction of $–NO_2$ group using ammonium formate in presence of Pd–C (10 %) in CH_3OH (Scheme 5.3). The reaction was preceded with the formation of 84 % corresponding amine under N_2 atmosphere.

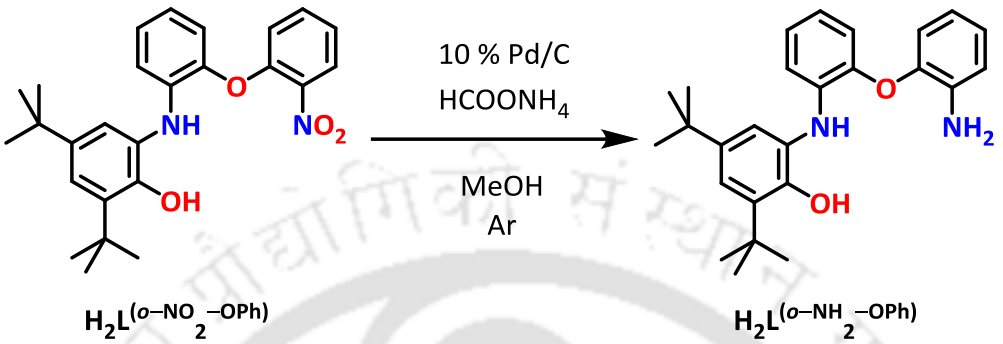

Scheme 5.3: *Synthetic route of ligand* $H_2L^{AP(o–NO_2–OPh)}$.

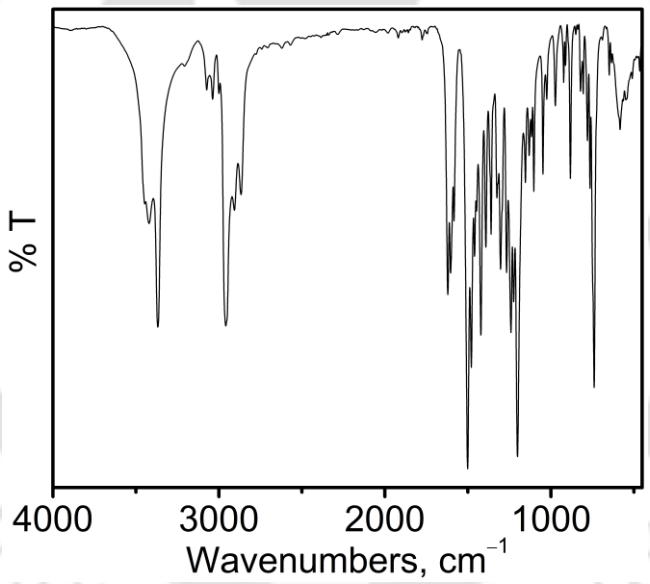

Figure 5.4: *FTIR spectrum of* $H_2L^{AP(o–NH_2–OPh)}$.

Infrared spectrum of $\mathbf{H_2L^{AP(o–NH_2–OPh)}}$ provided sharp bands at 3448, 3421 and 3367 cm^{-1}. Those bands were due to ν(O–H) and ν(N–H) stretching.[5a–b] Weak band at 3039 and 3073 cm^{-1} corresponded to $\nu(C_{Ar}–H)$ stretching for the aryls rings. The presence of *tert*–butyl substitution to the aryl rings was confirmed by three sharp bands at 2959, 2905 and 2865 cm^{-1}.[5d–e] Those bands corresponded to asymmetric, overtone and symmetric ν(C–H) stretches, respectively. The incorporation of $–NH_2$ group in the ligand backbone was further revealed by the presence of a sharp band at 1621 cm^{-1} that corresponded to ν(N–H) bending mode. The phenolic ν(C–O) and

the ν(C–N) stretching appeared at 1303 and 1224 cm^{-1}, respectively.[5a] A strong and sharp band at 1201 cm^{-1} was attributed to ν(C–O) stretching of ether linkage.[5e]

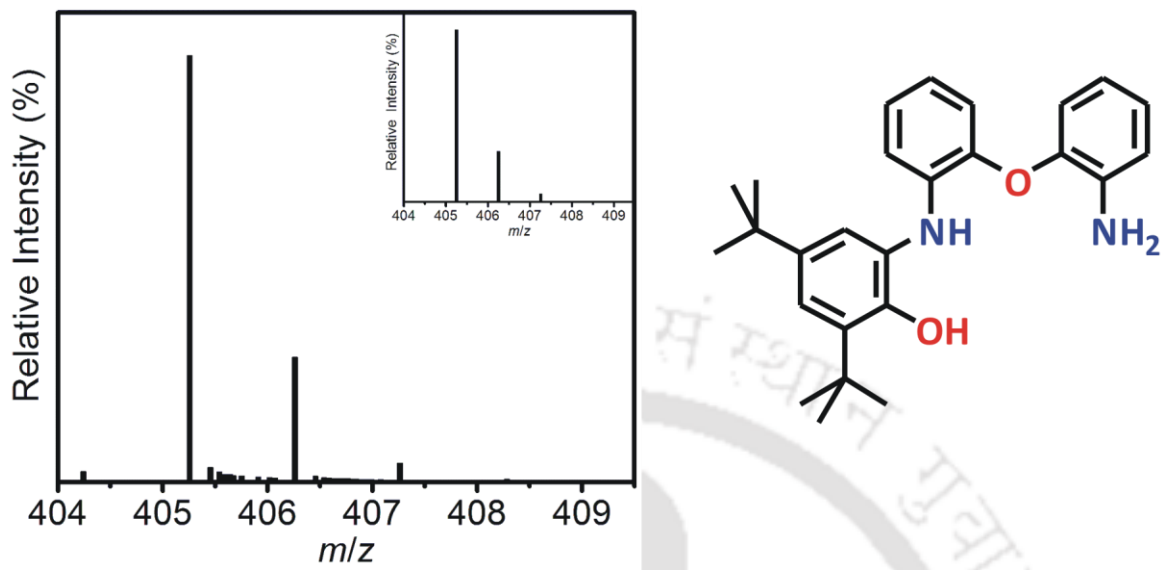

Figure 5.5: *ESI–mass spectrum (+ve mode) of ligand* $\boldsymbol{H_2L^{AP(o\text{–}NH_2\text{–}OPh)}}$ *with experimental and simulated (inset) isotope distribution pattern.*

Electrospray ionization mass spectrum (ESI–MS) of a CH_3CN solution of ligand $\mathbf{H_2L^{AP(o\text{–}NH_2\text{–}OPh)}}$ provided a 100% molecular ion peak at *m*/*z* = 405.26. Simulated isotope distribution pattern (inset) confirmed the composition as $[C_{26}H_{32}N_2O_2+H]^+$ for the observed mass peaks.

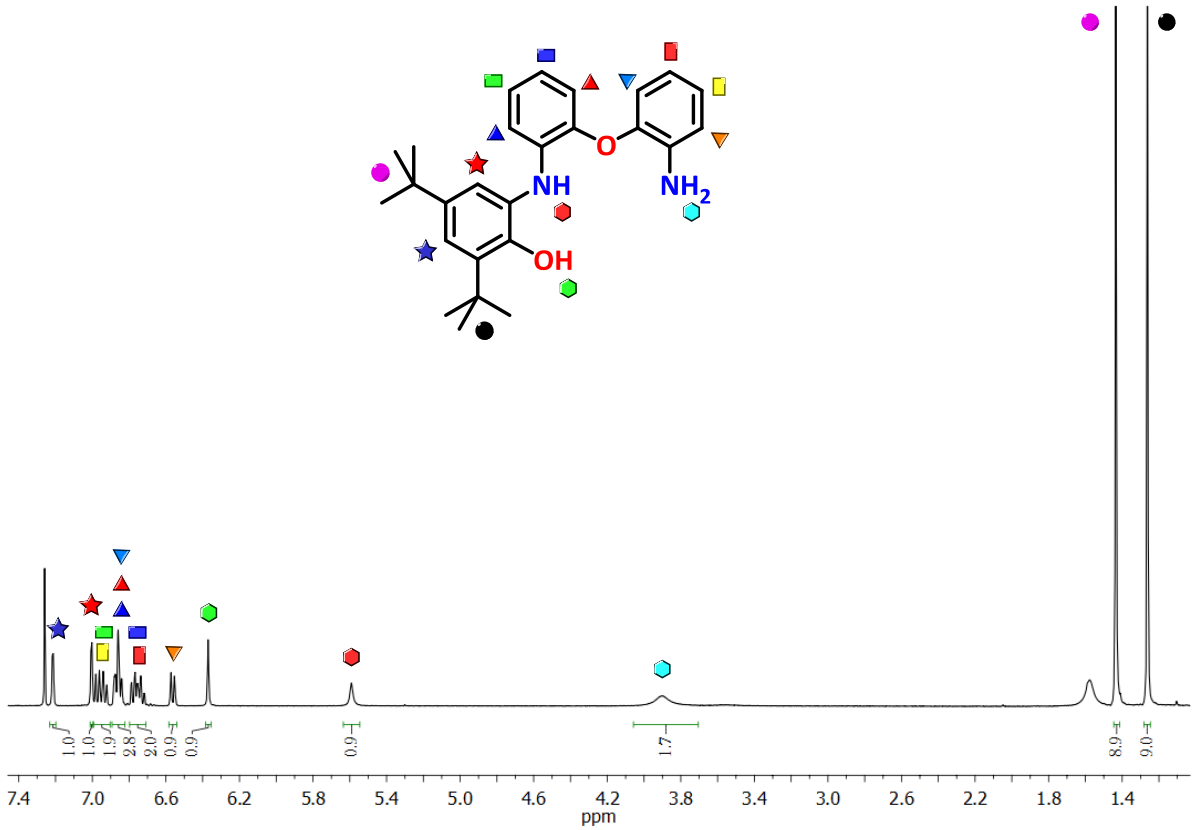

Figure 5.6: *^{1}H NMR spectrum of $H_2L^{AP(o–NH_2–OPh)}$ in $CDCl_3$.*

^{1}H NMR spectrum of $\mathbf{H_2L^{AP(o–NH_2–OPh)}}$ was recorded in $CDCl_3$ at 399.853 MHz. Resonance signals at 1.26 and 1.44 ppm were appeared as singlet and corresponded to the hydrogen atoms attached to the *tert*–butyl groups. Presence of a broad resonance signal at 3.90 ppm revealed the incorporation of primary aryl amine in the ligand skeleton. Two singlet peaks at 5.59 and 6.37 ppm were corresponded to NH and OH protons, respectively. Apart from those signals, signals for 10 aromatic protons were appeared in the 6.5–7.3 ppm range.

^{13}C NMR spectrum of $\mathbf{H_2L^{AP(o–NH_2–OPh)}}$ was recorded in $CDCl_3$ at 150.913 MHz. Four resonance signals at a region of 29.8–35.2 ppm were corresponded to two different types of *tert*–butyl substituents in the ligand back bone. Characteristic eighteen aryl peaks for 18 aryl carbon centers were appeared in the 115–150 ppm region.

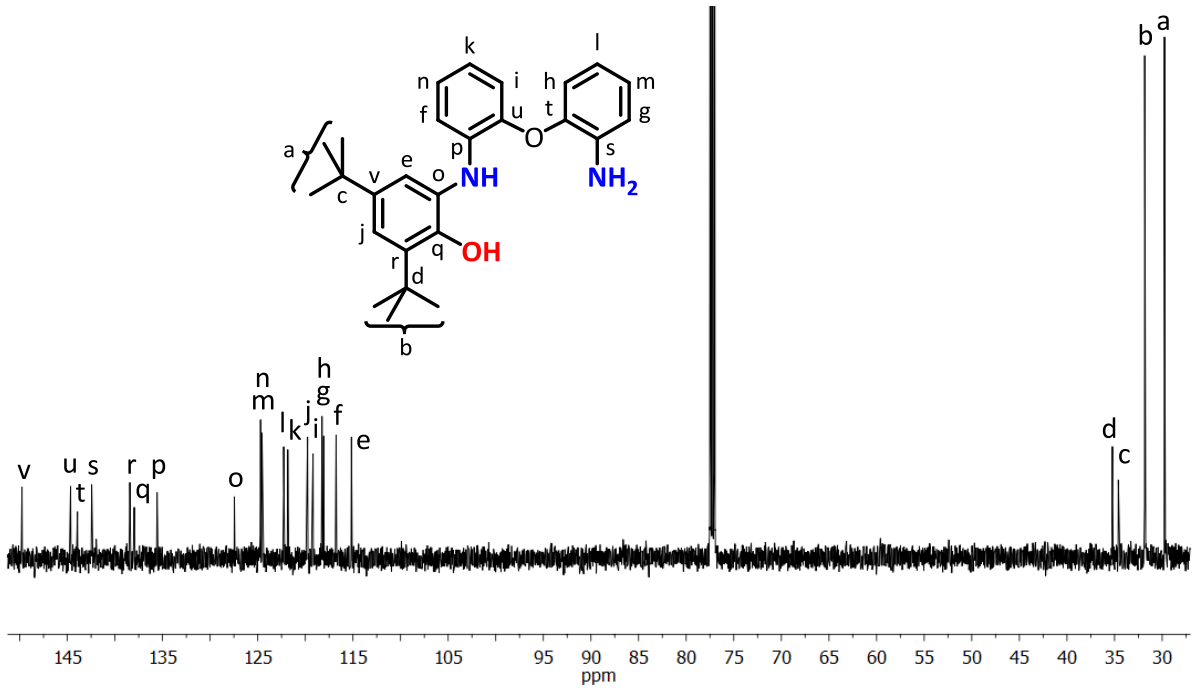

Figure 5.7: *^{13}C NMR spectrum of $H_2L^{AP(o–NH_2–OPh)}$ in $CDCl_3$*

The ligand $H_2L^{AP(o–NH_2–OPh)}$ contains a 2–aminophenol unit, which may exist in several oxidation states in its corresponding metal complexes as shown in Scheme 5.4.

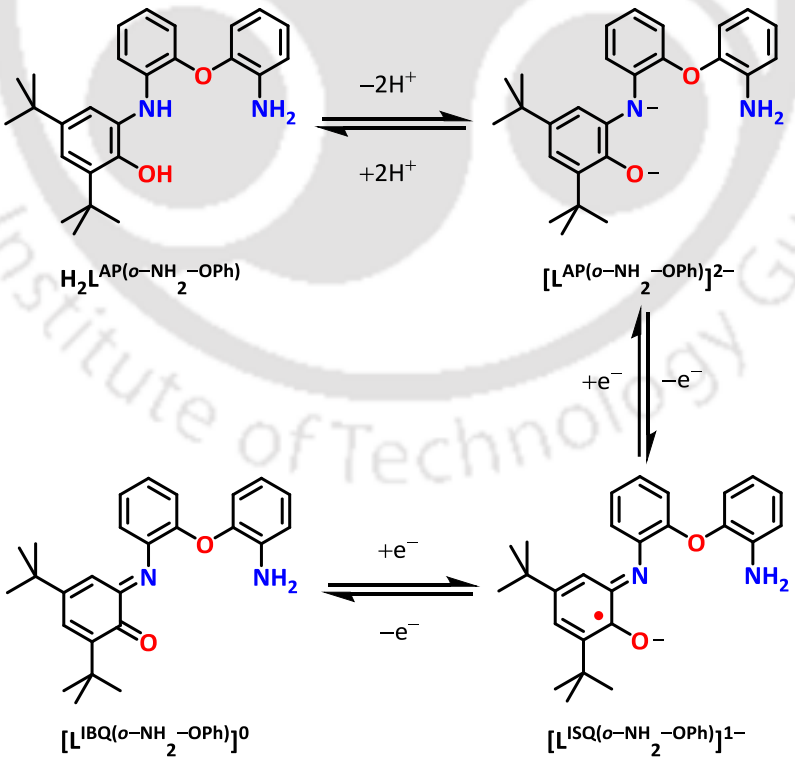

Scheme 5.4: *Different probable oxidation states of the $H_2L^{AP(o–NH_2–OPh)}$.*

5.3: Formation of Octahedral Co(III) Complex from Ligand $H_2L^{AP(o–NH_2–OPh)}$

The ligand $\mathbf{H_2L^{AP(o–NH_2–OPh)}}$ reacted with half equivalent of $Co(ClO_4)_2•6H_2O$ in CH_3CN in presence of Et_3N and provided a diamagnetic green solid (**5A**). The green solid was crystalized from an acetonitrile solution by slow evaporation technique.

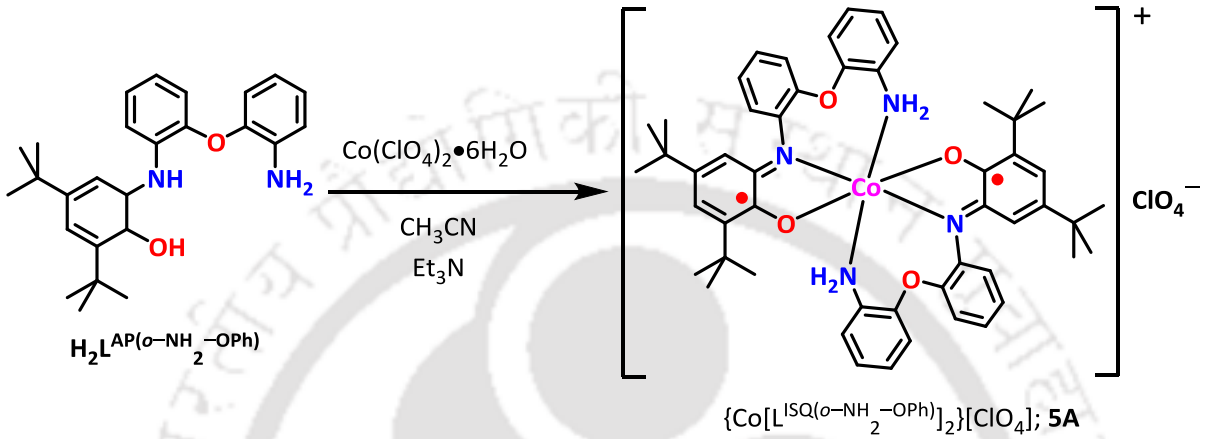

Scheme 5.5: *Synthetic route of complex* ***5A*** *from ligand* $\boldsymbol{H_2L^{AP(o–NH_2–OPh)}}$.

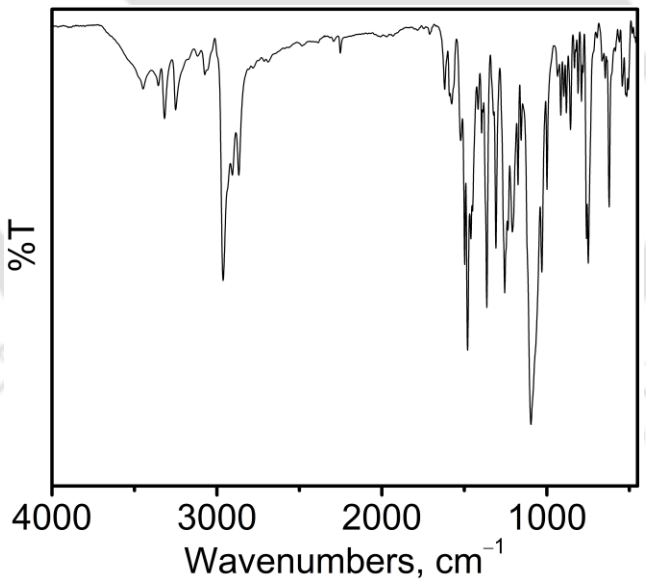

Figure 5.8: *FTIR spectrum of complex* ***5A****.*

In the FTIR spectrum of complex **5A**, the sharp bands at the region 3450–3250 cm^{-1} were appeared due to asymmetric and symmetric ν(N–H) stretches of amine group.[5a,b] Another band at 1619 cm^{-1} corresponded to ν(N–H) bending vibration confirmed the existence of aryl amine in the complex.[5a,b] Two sharp bands at 1577 and 1363 cm^{-1} corresponded to ν(C=N) and ν(C⋯O) stretches, respectively.[6a] Those bands indirectly implied the iminosemiquinone,

[$(ISQ)^{\bullet 1-}$] coordination to the metal ion. The incorporation of perchlorate ion as the counter anion was evident by the presence of strong band at 1095 cm^{-1} and 622 cm^{-1}.[6b]

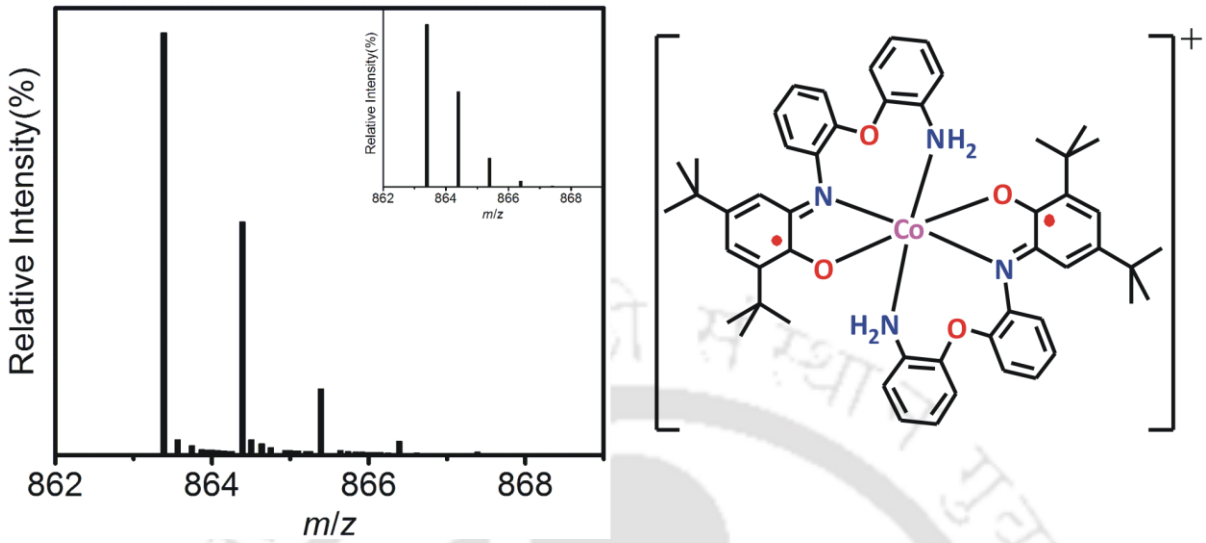

Figure 5.9: *ESI–mass spectrum of complex **5A**; experimental and simulated isotope distribution pattern (inset).*

Electrospray ionization mass spectrum (ESI–MS) of a solution containing complex **5A** in CH_3CN provided a 100% molecular ion peak at *m*/*z* = 863.38. Simulated isotope distribution pattern ascribed the molecular ion peak as $[M–ClO_4]^+$ ion with the composition of $[C_{26}H_{30}N_2O_2Co]^+$.

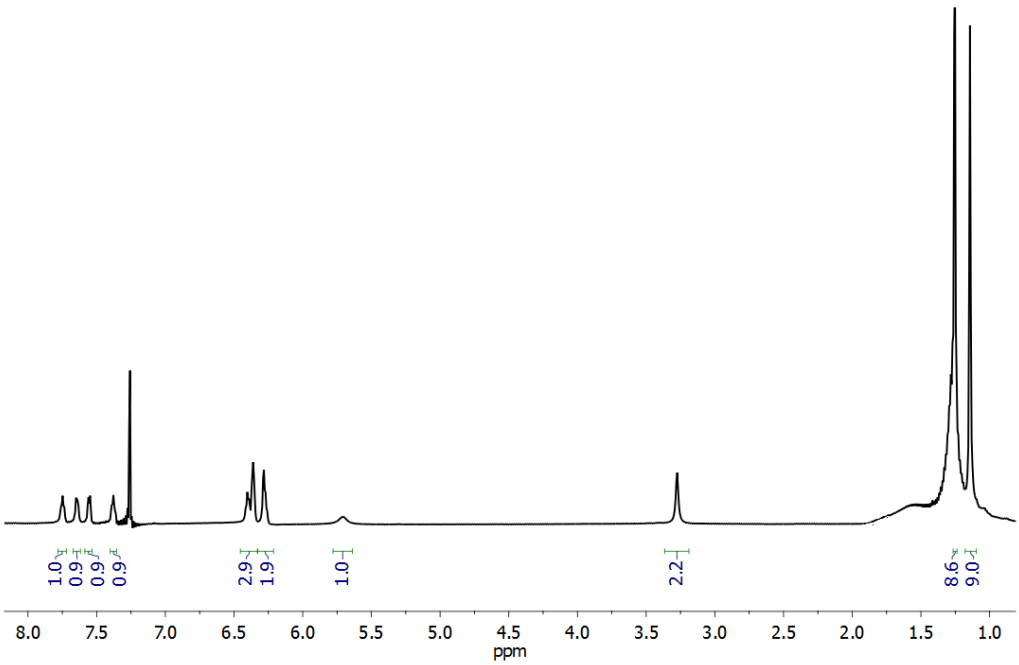

Figure 5.10: *^1H NMR spectrum of complex **5A** in $CDCl_3$.*

The ^{1}H NMR spectrum of the complex was recorded in $CDCl_3$ at 400 MHz (Fig. 5.10) and the observed proton NMR signals confirmed the diamagnetic nature of complex **5A.** The resonance signal for the *tert*–butyl groups were appeared at 1.14 (18H) and 1.25 (18H) ppm and the metal coordinated free amine signal at 3.27 (4H) ppm. The resonance signal for all the ring attached protons were observed at the region of 5.71–7.75 (20H) ppm.

Suitable crystals for X–ray diffraction studies were obtained by slow evaporation of a concentrated CH_3CN solution of complex **5A**. Single crystal X–ray diffraction analysis at 293(2) K provided the molecular structure of complex **5A**. The ORTEP presentation of the complex has been shown in Fig.5.11.

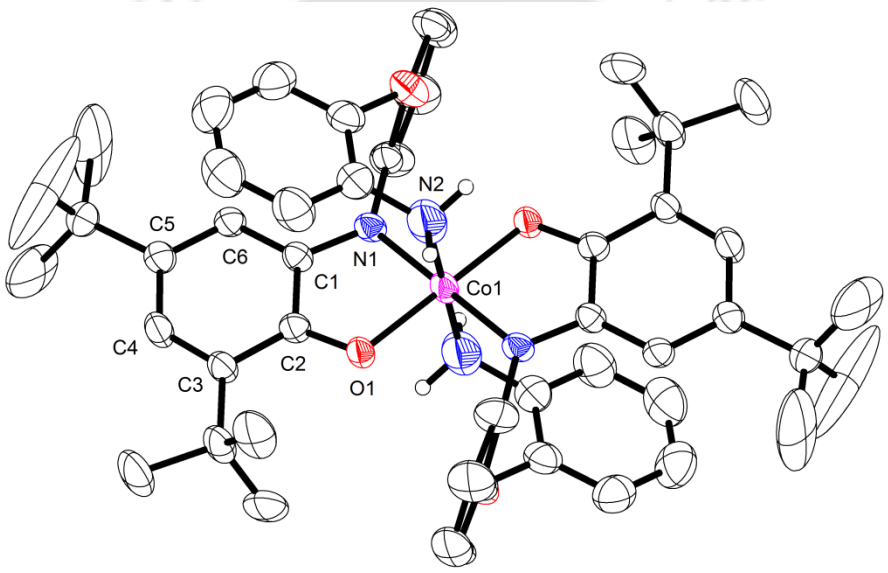

Figure 5.11: *ORTEP presentation of complex* ***5A****; thermal ellipsoids were drawn at 40% probability level. Counter anion* $(ClO_4)^-$ *and H–atoms (except attached with primary amine) were omitted for clarity.*

The complex crystallized in the monoclinic space group '*C2/c'*. In the complex, the ligand coordinated unit was monopositive in nature. The counter anion was a perchlorate unit. In the monopositive unit, the basal plane was constituted by two NO donor sets that belonged to two different amidophenolate ligand moieties. The coordination pattern of the ligand was *–trans* in nature. The Co1–O1, Co1–N1 and Co1–N2 bands have the bond distances of 1.873(3), 1.873(4) and 2.203(7) Å, respectively. The bond lengths toward the amidophenolate ligating site suggested +III oxidation state of the metal center.[7] The observed bond distances for N1–C1 and O1–C2 bonds were 1.357(6) and 1.306(5) Å respectively, indicated the partial double bond character of those bonds. In addition, three alternating short–long–short C–C bonds [C3–C4 = 1.365(7), C4–C5 = 1.433(7) and C5–C6 = 1.378(7) Å] followed by other three long C–C bonds

[C6–C1 = 1.411(6), C1–C2 = 1.431(6) and C2–C3 = 1.435(6) Å]} were observed for the *tert*–butyl containing C_6 rings.[7a–d,8] Thus, the non–aromaticity of those C_6 ring and partial double bond character of attached N1–C1 and O1–C2 bonds indicated the existences of amodiphenolate moieties in its one–electron oxidized iminosemiquinone [$(ISQ)^{\bullet 1-}$] form (Scheme 5.4).

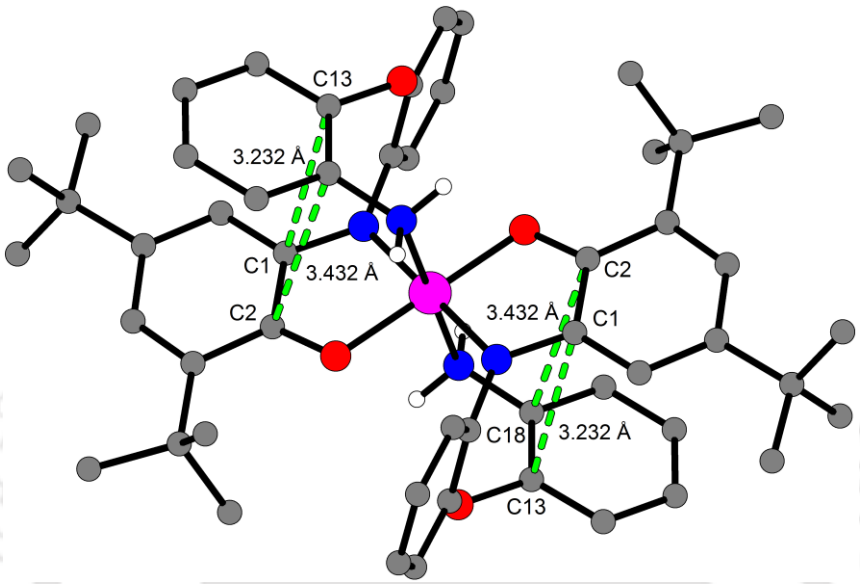

Figure 5.12: *Representation of short intamolecular interaction in complex* ***5A****.*

The neutral aryl amine group attached with atom C18 provided an axial coordination [Co1–N2 = 2.203(7) Å] to the metal center and caused an octahedral surrounding around the metal ion. The axial coordination of the aryl amine was facilitated by some short intramolecular interaction (Fig. 5.12). This axial amine coordination prevented the closer approach of the ethereal oxygen to the metal center as observed in cobalt complexation with ligand $\mathbf{H_2L^{O(AP/AP)}}$ (Chapter II).[9]

Table 5.1: *Selected bond distances (Å) and angels (°) for complex* ***5A.***

Co1–N1	1.873(4)	C18–N2	1.429(8)
Co1–O1	1.873(3)	C1–C2	1.431(6)
Co1–N2	2.203(7)	C2–C3	1.435(6)
O1–C2	1.306(5)	C3–C4	1.365(7)
N1–C1	1.357(6)	C4–C5	1.433(7)
N1–C7	1.426(6)	C5–C6	1.378(7)
O2–C12	1.383(7)	C6–C1	1.411(6)
O2–C13	1.384(7)		
N1–Co1–N1*	180.0(3)	N2–Co1–O1	88.0(2)
N1–Co1–O1	95.7(1)	N2–Co1–O1*	92.0(2)
N1–Co1–O1*	84.3 (1)	C2–O1–Co1	113.7(3)

O1–Co1–O1*	180.0 (0)	C12–O2–C13	117.5(4)
N2–Co1–N2*	180.0(0)	C1–N1–C7	121.9(4)
N2–Co1–N1	88.6(2)	C1–N1–Co1	113.9(3)
N2–Co1–N1*	91.4(2)	C7–N1–Co1	124.1(3)

The asterisk (*) symbol stands for symmetry operation, inversion center.

The electronic absorption spectrum of complex **5A** was recorded in CH_2Cl_2 at ambient temperature and shown in Fig. 5.13. The band positions along with the extension coefficient are given in Table 5.2.

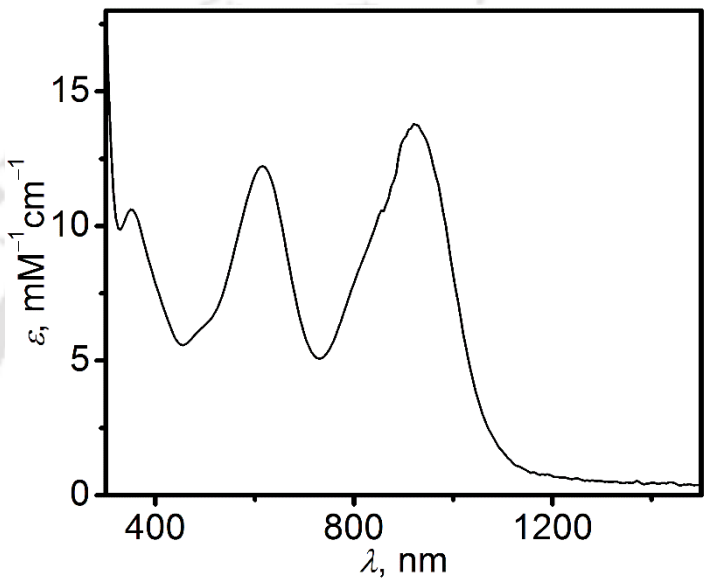

Figure 5.13: *UV–Vis/NIR spectrum of complex* ***5A*** *in* CH_2Cl_2 *at 300–1500 nm range.*

The octahedral cobalt complex **5A** provided strong bands at 924 and 614 nm. Those bands corresponding to ligand–to–metal charge transfer (LMCT).[7b,d] A shoulder band at 824 nm was due to ligand–to–ligand charge transfer.[7a,10]

Table 5.2: *Electronic absorption data of Complex* ***5A***.

Complex	λ_{max} (ε, $M^{-1}cm^{-1}$)
5A	924 (14400), 824^{sh} (9150), 614 (12750), 352 (11350)

*superscript 'sh' stands for shoulder band.

5.4: Synthesis and Characterization of Ni(II)–bis(iminosemiquinone) Complex from Ligand $H_2L^{AP(o–NH_2–OPh)}$

A reaction between 2:1 ligand $\mathbf{H_2L^{AP(o–NH_2–OPh)}}$ and $Ni(ClO_4)_2•6H_2O$ in CH_3CN in the presence of Et_3N produced a diamagnetic green solid (**5B**). The green solid was recrystallized from a dichloromethane:acetonitrile (3:1) solvent mixture.

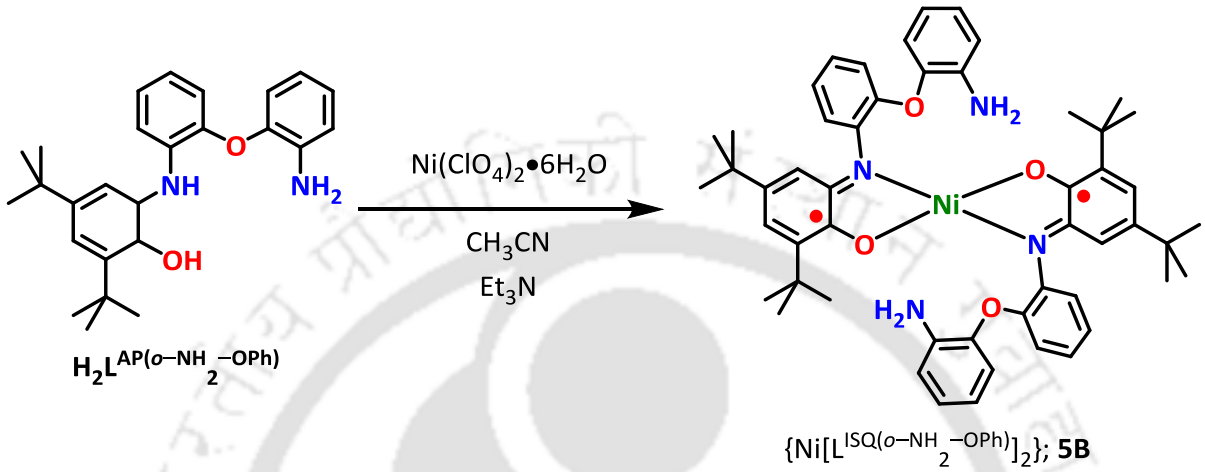

$H_2L^{AP(o–NH_2–OPh)}$

$\{Ni[L^{ISQ(o–NH_2–OPh)}]_2\}$; **5B**

Scheme 5.6: *Synthetic route of complex **5B** from ligand $H_2L^{AP(o–NH2–OPh)}$.*

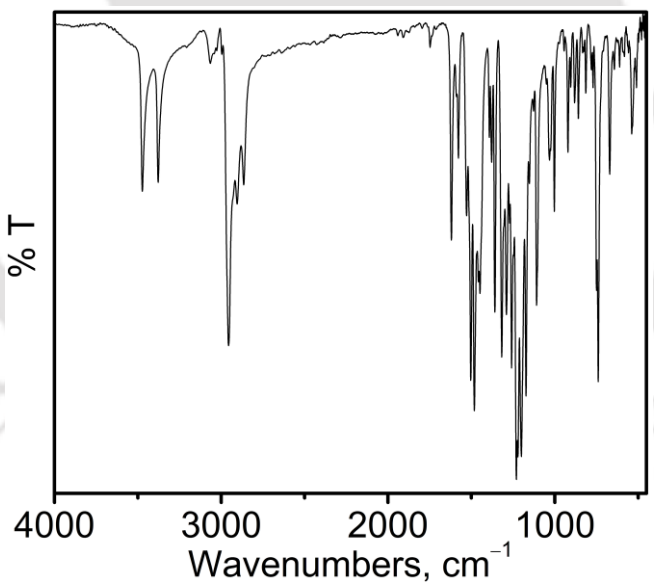

Figure 5.14: *FTIR spectrum of complex **5B**.*

In FTIR spectrum of complex **5B**, strong bands at 3473 and 3378 cm^{-1} corresponded to asymmetric and symmetric ν(N–H) stretches, respectively.[11a] This related to the presence of non–coordinated primary amine in the ligand backbone. The fact was also supported by ν(N–H) bending vibration at 1620 cm^{-1}.[11a] The bands at 1578 and 1447 cm^{-1} were attributed for ν(C=N) and ν(C⋯O) stretches, respectively.[11b–c] It revealed the existence of metal coordinated

iminosemiquinone [(ISQ)$^{\bullet 1-}$] moieties in the complex. The characteristic asymmetric ethereal stretching band was appeared at 1248 cm^{-1}.[11d–e]

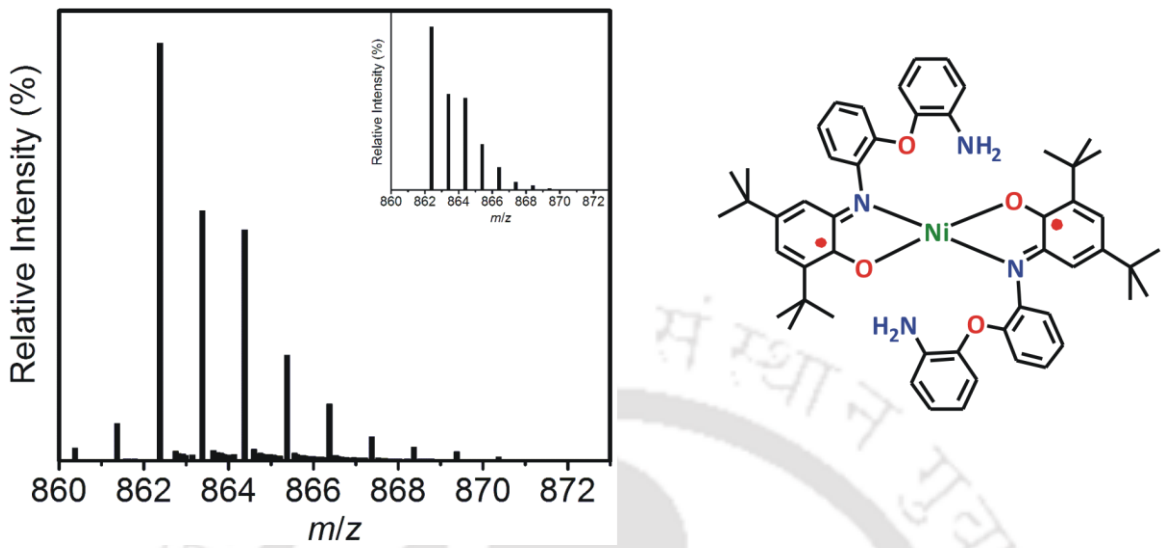

Figure 5.15: *ESI–mass spectrum (+ve) of complex **5B**; experimental and simulated isotope distribution pattern (inset).*

Electrospray ionization mass spectrum (ESI–MS) of a solution containing complex **5B** in CH_3CN provided a 100% molecular ion peak at *m*/*z* = 862.38. Simulated isotope distribution pattern (inset) identified the 100% molecular ion peak as $[M]^+$ with the composition of $[C_{52}H_{60}N_4O_4Ni]^+$.

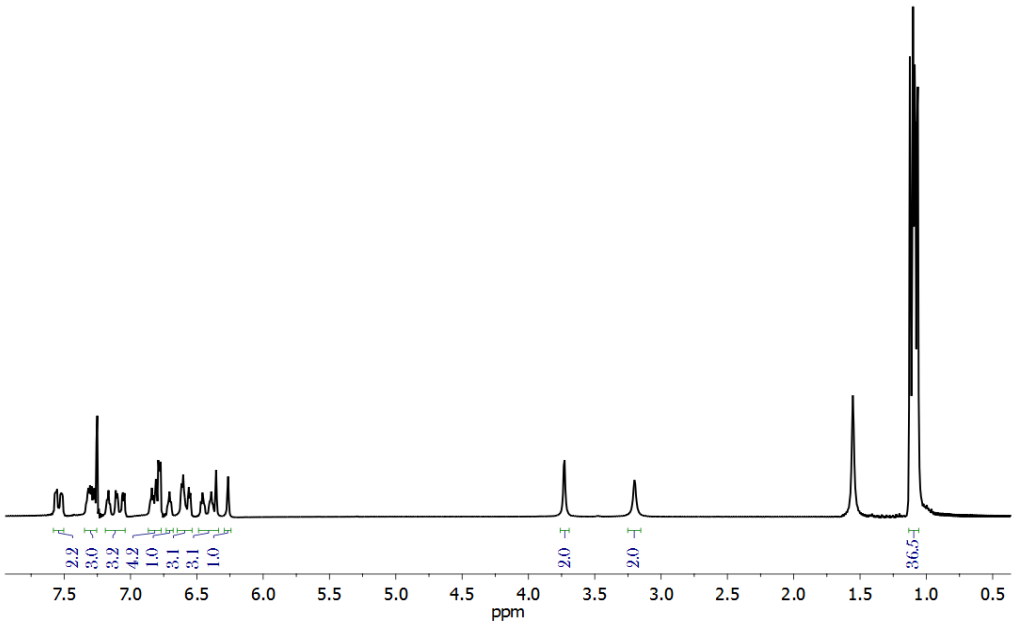

Figure 5.16: *^{1}H NMR spectrum of complex **5B**.*

The diamagnetic nature of complex **5B** was confirmed by ^{1}H NMR spectrum that recorded in $CDCl_3$ at 400 MHz. The resonance signals for *tert*–butyl groups were appeared at δ = 1.07–1.12 (36H) ppm and the signals for free amines were appeared at 3.20 (2H) and 3.73 (2H) ppm. All of the aromatic protons showed resonance signals in the range of 6.26–7.56 (20H) ppm.

Complex **5B** was crystalized from a dichloromethane:acetonitrile (3:1) solvent mixture and the crystal structure of complex **5B** has been determined by single crystal X–ray diffractometer analysis at 293 K. The ORTEP presentation of the complex is shown in Fig. 5.17. Selected bond distances and angles are given in Table 5.3.

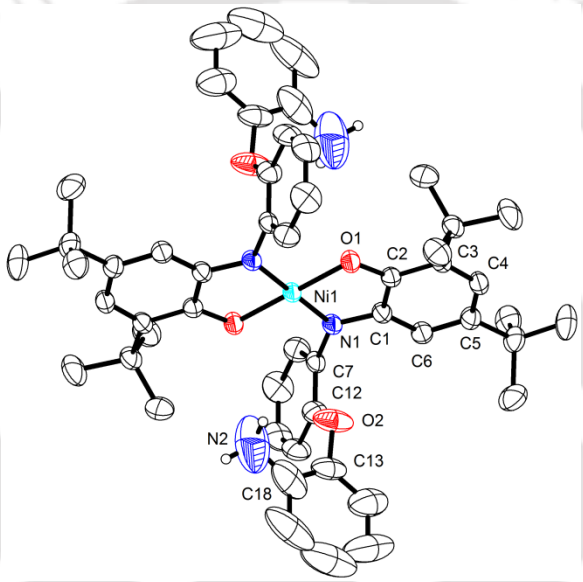

Figure 5.17: *ORTEP presentation of complex **5B**; thermal ellipsoids were drawn at 50% probability level. H–atoms (except attached with N2 atom) were omitted for clarity.*

Complex **5B** crystallized in the triclinic space group '*P–1*'. X–ray diffraction analysis revealed that the coordinated two amidophenolate units belonged to two different ligand units and coordinated to the metal ion in *trans*– fashion. Noteworthy, the ethereal oxygen and the primary amine in the ligand backbone have not participated in coordination. The tetra–coordination to the metal ion created a square planer surrounding with τ_4[13] value equal to 0.0. The Ni1–N1 = 1.829(2) and Ni1–O1 = 1.843(2) Å bond distances resembled closely to the previously reported Ni complexes where the central Ni was present in +II oxidation state.[4a,7c,12] The bond distances for C1–N1 = 1.355(3) and C2–O1 = 1.313(3) Å were in between their single bond and double bond values *i.e.* the bonds were partially double bond in nature.[4a,7c,8,12] Along with this, *tert*–butyl group containing C_6 rings exhibited a quinoid type of distortion (short–long–

short C–C bonds followed by three successive long C–C bond distances). The above structural feature revealed the existence of the *tert*–butyl group containing amidophenolate rings in its one–electron oxidized iminosemiquinone([ISQ]$^{\bullet 1-}$) form. The primary amines as well as the ethereal oxygen atoms were not involved in any coordination with the metal ion and any short type of intramolecular interaction. Thus, complex **5B** has been well described as square planner Ni(II)–bis(iminosemiquinone) complex.

Table 5.3: *Selected bond distances (Å) and angels (°) for complex **5B.***

Ni1–N1	1.829(2)	C18–N2	1.356(7)
Ni1–O1	1.843(2)	C1–C2	1.430(4)
O1–C2	1.313(3)	C2–C3	1.420(4)
N1–C1	1.355(3)	C4–C3	1.383(4)
N1–C7	1.422(3)	C5–C4	1.423(4)
O2–C12	1.381(4)	C6–C1	1.404(4)
O2–C13	1.387(4)		
N1–Ni1–N1*	180.0(1)	C12–O2–C13	118.9(2)
N1–Ni1–O1	85.69(8)	C1–N1–C7	120.9(2)
N1–Ni1–O1*	94.31(8)	C1–N1–Ni1	113.8 (2)
O1–Ni1–O1*	180.0(1)	C7–N1–Ni1	124.9 (2)
C2–O1–Ni1	113.2 (2)		

The asterisk (*) symbol stands for symmetry operation, inversion center.

The redox behavior of the Ni(II)–bis(iminosemiquinone) complex (**5B)** was measured in CH_2Cl_2 solution containing 0.10 M $[(^nBu)_4N]ClO_4$ as the supporting electrolyte at a glassy carbon working electrode and Ag/AgCl reference electrode. Ferrocenium hexafluorophosphate ($FcPF_6$) was used as an internal standard and all the potentials have been referenced *vs.* Fc^+/Fc couple. The cyclic voltammograms of complex **5B** is depicted in Fig. 5.18 and all of the redox potentials are summarized in Table 5.4.

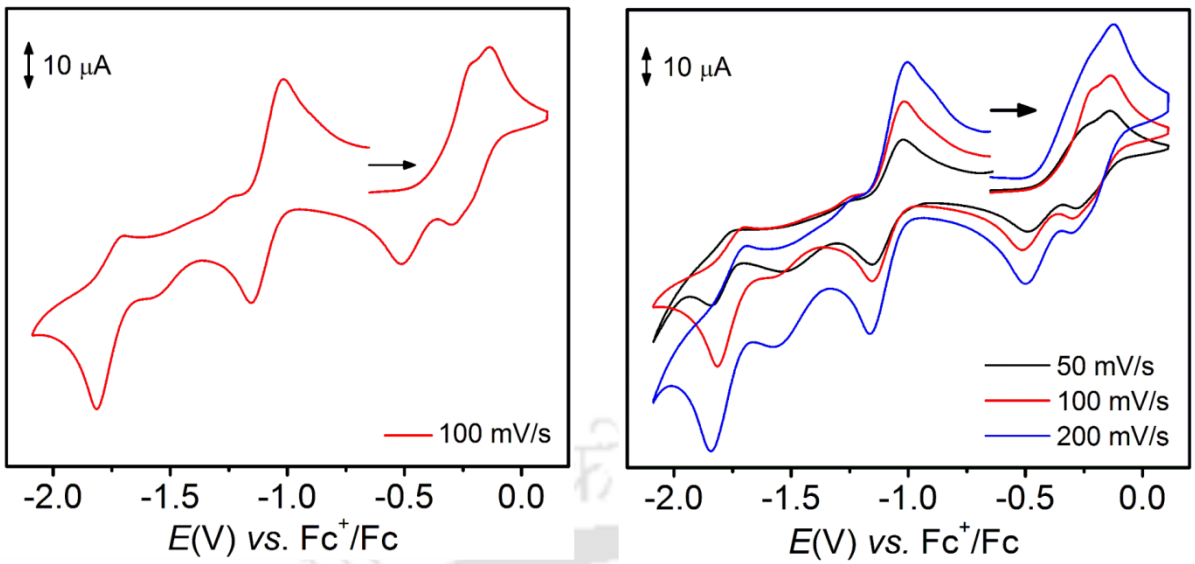

Figure 5.18: *Cyclic voltammograms of complex **4B** measured in dichloromethane; (A) single cycle at 100 mV/s scan rate and (B) rate dependence.*

During the anodic scan from –0.65 V, two successive oxidation at –0.215 and –0.135 V led the complex **5B** to its fully oxidized Ni(II)–bis(iminoquinone) form (at 100 mV/s scan rate).[4a] The energy difference (ΔE) between first two oxidation potentials depended upon the scan rate. This might be due to the involvement of metal ion on the development of Ni(II)–bis(iminoquinone) species during those two oxidation processes.[4a] Those oxidation potential values (–0.365 and –0.217 V) were very negative compare to Fc^+/Fc couple. Hence, an additional attempt regarding the oxidation of complex **5B** by ferrocenium hexafluorophosphate has been taken to find out the intermediate or Ni(II)–bis(iminoquinone) complex (*vide infra*). Thus developed oxidized species underwent four successive reduction and generated Ni(II)–bis(amidophenolate) species. The observed reduction potential at –1.086 and –1.755 V were due to the ligand–centered reduction as reported previously.[4a]

Table 5.4: *Summary of Redox Potentials of Complexes **5B** in Volts vs. Ferrocenium/Ferrocene (Fc^+/Fc).*

Complex	$E_{1/2}$(ox1)	$E_{1/2}$(ox2)	$E_{1/2}$(red1)	$E_{1/2}$(red2)
5B	–0.365	–0.217	–1.086	–1.755

* All of the potentials were calculated at 100 mV/s scan rate.

5.5: *Oxidation of Complex 5B by Ferrocenium Hexafluorophosphate ($FcPF_6$); Synthesis and Characterization of Ni(II)–bis(iminoquinone) Complex*

The first two oxidation potentials of complex **5B** have been found as negative *vs.* Fc^+/Fc redox couple. Thus, there would be a possibility of generation of one– as well as two–electron oxidized Ni–complex from **5B** by treatment with one and two equivalents of $FcPF_6$ ['Fc' refer ferrocenium ion], respectively. However, experimentally, one–electron oxidized species could not be isolated as it readily underwent disproportionation reaction during the reaction. Two electron oxidized Ni(II)–bis(iminoquinone) complex **5C** was obtained during the treatment of **5B** with two equivalent of $FcPF_6$ in dichloromethane under air.

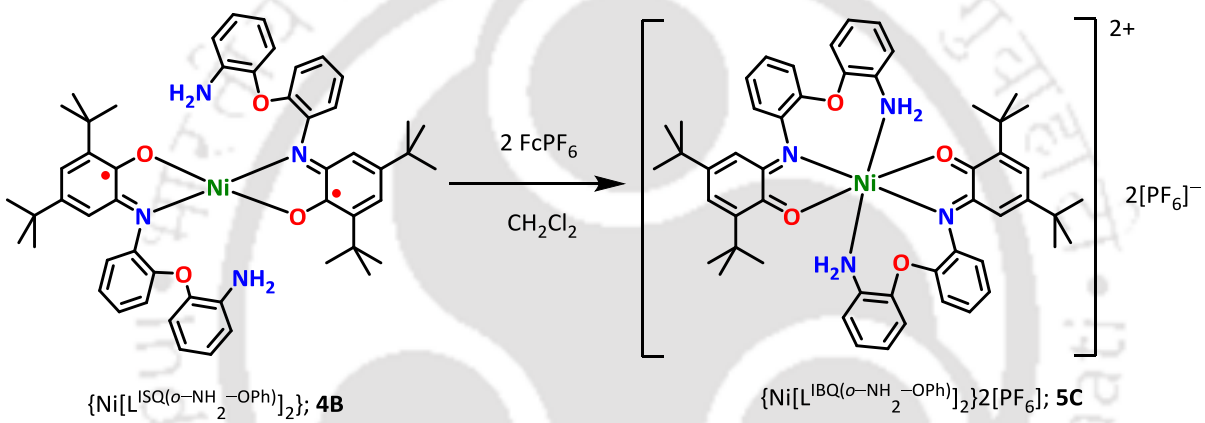

Scheme 5.7: *Synthetic route of complex 5C from 5B.*

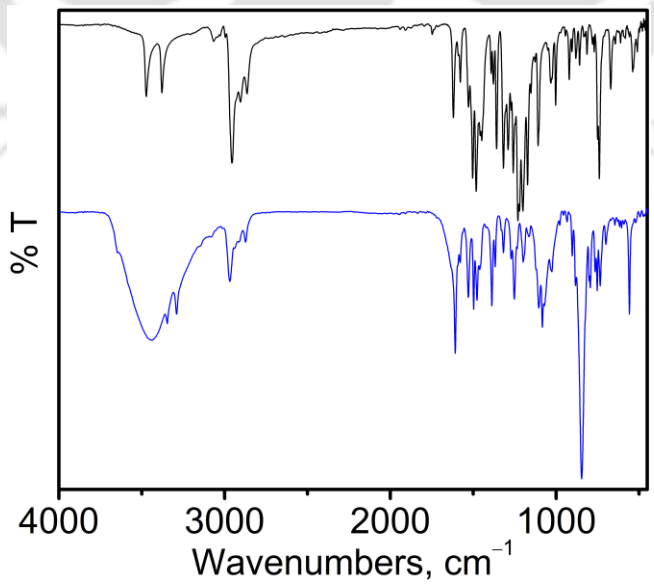

Figure 5.19: *FTIR spectrum of complex **5B** (black line) and **5C** (blue line).*

In the recorded FTIR spectrum of complex **5C** (Fig.4.19, blue line), the observed asymmetric and symmetric ν(N–H) stretches were appeared at 3346 and 3290 cm^{-1}, respectively.[14a] Along with this, a sharp band corresponded to ν(N–H) bending vibration was appeared at 1609 cm^{-1}. Those stretching and bending vibrations were appeared quite lower in values compare to iminosemiquinone coordinated Ni(II) complex (**5B**). This might be due to the involvement of aryl amine group with the metal center. Asymmetric ethereal stretching band was appeared at 1253 cm^{-1}. The presence of a strong and sharp band at 845 cm^{-1} corresponded to the presence of counter anion $[PF_6]^-$ in the complex.[6b,14b]

Complex **5C** was crystalized from a dichloromethane:hexane (3:1) solvent mixture. The molecular structure of the complex was obtained by single crystal X–ray diffraction analysis at 293(2) K. ORTEP view of the molecular structure is shown in Fig. 5.20 and selected bond distances (Å) and angles (°) are summarized in Table 5.5.

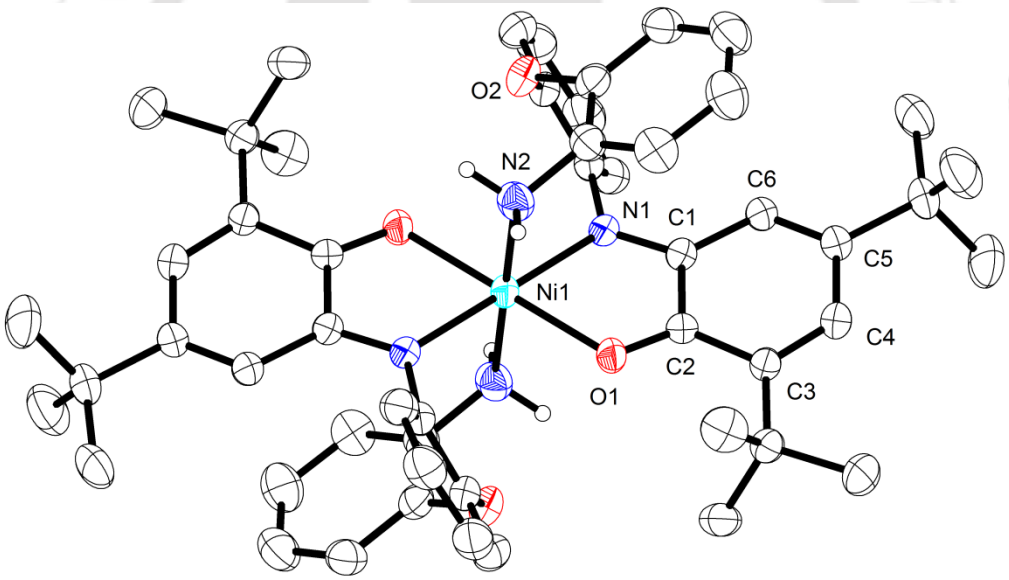

Figure 5.20: *ORTEP presentation of complex **5C**; thermal ellipsoids were drawn at 40% probability level. Lattice solvent, counter anion and H–atoms (except attached with N2 atom) were omitted for clarity.*

Complex **5C** crystalized in the triclinic space group '*P*–1'. The octahedral coordination sphere around the central Ni(II)–ion was composed of two ligand molecules. In the complex Ni1–N1 = 2.069(3) and Ni1–O1 = 2.057(3) Å bonds were significantly long compare to the corresponding iminosemiquinone complex **5B** [Ni1–N1 = 1.829(2) and Ni1–O1 = 1.843(2) Å]. The elongation of the bonds indicated the lower formal charge of the coordinating ligand units. In the complex, the aryl amine provided apex coordination [Ni1–N2 = 2.160(4) Å] to the metal center and resulted the octahedral coordination sphere.

The double bond characterizing N1–C1 = 1.292(5) and O1–C2 = 1.243(5) Å bonds along with the quinoid–distortion of the *tert*–butyl group–containing C_6 ring revealed the existence of amidophenolate moieties in its two–electron oxidized iminobenzoquinone [$(IBQ)^0$] form (Scheme 5.4).[12a,14b] Thus, the obtained iminobenzoquinone have shown weak coordination (long interatomic distances) to the metal ion, which allowed the aryl amine to coordinate to the metal ion. The axial coordination of the aryl amine to the metal ion was also facilitated by short intramolecular interaction (Fig. 5.21). The dipositive charge of the coordination sphere was neutralized by the presence of two PF_6^- anions within the crystalline lattice. Thus, the oxidation of **5B** by ferrocenium hexafluorophosphate ($FcPF_6$) led to a bis(iminobenzoquinone) coordinated octahedral Ni(II) complex.

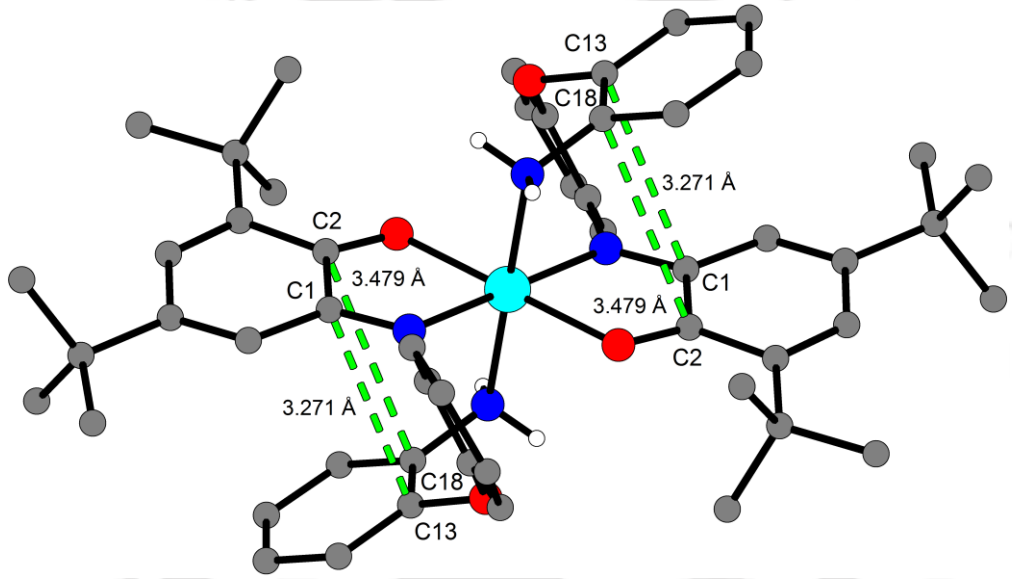

Figure 5.21: *Representation of short intamolecular interaction in complex **5C**.*

Table 5.5: *Selected bond distances (Å) and angels (°) for complex **5C**.*

Ni1–N1	2.069(3)	C18–N2	1.440(5)
Ni1–O1	2.057(3)	C1–C2	1.513(6)
Ni1–N2	2.160(4)	C2–C3	1.466(5)
O1–C2	1.243(5)	C3–C4	1.350(6)
N1–C1	1.292(5)	C4–C5	1.470(6)
N1–C7	1.429(5)	C5–C6	1.345(6)
O2–C12	1.395(5)	C6–C1	1.435(5)
O2–C13	1.403(5)		
N1–Ni1–N1*	180.0(0)	N2–Ni1–O1	88.8(1)
N1– Ni1–O1	101.7(1)	N2–Ni1–O1*	91.2(1)
N1– Ni 1–O1*	78.3(1)	C2–O1–Ni1	115.0(3)
O1– Ni1–O1*	180.0(0)	C12–O2–C13	115.2(3)

N2–Ni1–N2*	180.0(0)	C1–N1–C7	122.0(3)
N2–Ni1–N1	91.2(1)	C1–N1–Ni1	115.4(3)
N2–Ni1–N1*	88.8(1)	C7–N1–Ni1	122.5(2)

The asterisk (*) symbol stands for symmetry operation, inversion center.

The electronic absorption spectrum of complex **5B** and **5C** were recorded in CH_2Cl_2 (Fig. 5.22) and the absorption maxima with the extension coefficient are summarized in Table 5.6.

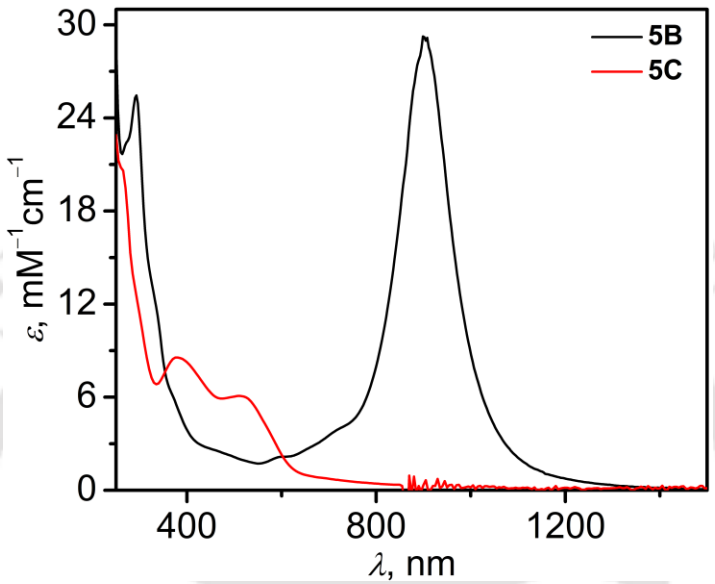

Figure 5.22: *UV–Vis/NIR spectrum of complex **5B** (black line) and **5C** (red line) in CH_2Cl_2 at 250–1500 nm range.*

In the recorded UV–Vis/NIR spectrum, the characteristic strong band for complex **5B** was appeared at 908 nm. The band was assigned as spin and dipole allowed ligand–to–ligand charge transfer.[4a] The absences of corresponding band for complex **5C** reconfirmed the generation of ligand–centered oxidized species by ferrocenium hexafluorophosphate ($FcPF_6$). The observed bands at 515 and 382 nm were due to iminobenzoquinoe based π–π* charge transfers.[14b]

Table 5.6: *Electronic absorption data for complex **5B** and **5C**.*

Complex	λ_{max} (ε, $M^{-1}cm^{-1}$)
5B	908 (29150), 728^{sh}(4050), 593^{sh}(2150), 293(25450)
5C	700^{br}(800), 515 (6150), 382 (8650), 264(20500)

* Superscript sh and br stand for shoulder and broad bands, respectively.

5.6: Synthesis and Characterization of Square Pyramidal Cu(II)–bis(iminosemiquinone) Complex from Ligand $H_2L^{AP(o–NH_2–OPh)}$

A 2:1 aerial reaction between the ligand $\mathbf{H_2L^{AP(o–NH2–OPh)}}$ and $CuCl_2•2H_2O$ or $Cu(ClO_4)_2•6H_2O$ in CH_3CN in presence of Et_3N provided a square pyramidal Cu(II)–bis(iminosemiquinone) complex (**5D**) as green solid (Scheme 5.8).

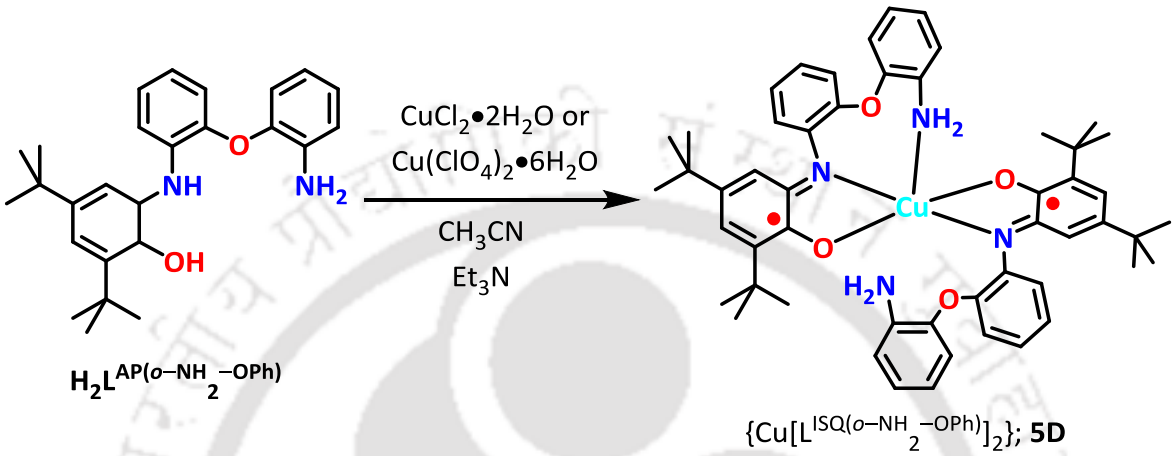

Scheme 5.8: *Synthetic route of complex **5D** from ligand $H_2L^{AP(o–NH_2–OPh)}$.*

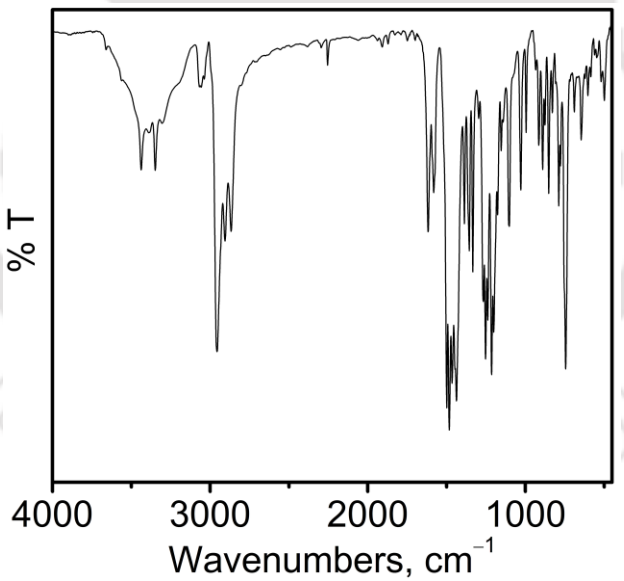

Figure 5.23: *FTIR spectrum of complex **5D**.*

In FTIR spectrum of the complex, four stretching bands corresponded to asymmetric and symmetric ν(N–H) stretches were appeared in the resign of 3440–3305 cm^{-1}.[5a,14a] The metal coordination with the ligand backbone was confirmed by the presence of sharp bands at 2956, 2905 and 2867 cm^{-1}. Those bands were characteristic for the presence of *tert*–butyl groups at the ligand backbone. A sharp and strong band at 1617 cm^{-1} corresponded to ν(N–H) bending

vibration indicated the existence of primary amine within the molecule. Existence of two bands at 1581 and 1483 cm^{-1} exposed the presence of metal coordinated amidophenolate moiety in its one–electron oxidized iminosemiquinone [$(ISQ)^{\bullet 1-}$] form. A weak band at 2255 cm^{-1} corresponded to the ν(C≡N) has been appeared due to presence of acetonitrile in the crystal lattice. The strong and sharp bands at 1252 and 1214 cm^{-1} were corresponded to ν(C–O) stretches of the aryl ethereal linkage that was present in the ligand skeleton.[5e]

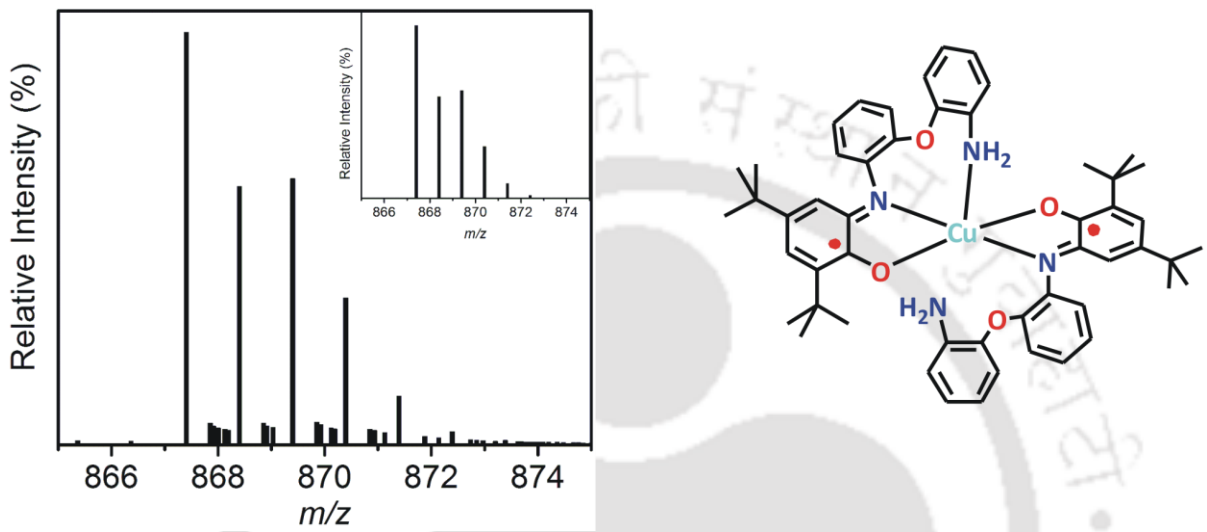

Figure 5.24: *ESI–mass spectrum (+ve) of complex **5D**; experimental and simulated isotope distribution pattern (inset).*

Electrospray ionization mass spectrum (ESI–MS) of a CH_3CN solution of complex **5D** provided a 100% molecular ion peak at *m*/*z* = 867.40. Simulated isotope distribution pattern (inset) confirmed that the molecular ion peak corresponded to $[M]^+$ with the composition of $[C_{52}H_{60}CuN_4O_4]^+$.

Single crystal suitable for X–ray diffraction analysis was obtained by recrystallizing complex **5D** from a CH_2Cl_2/CH_3CN (5:2) solvent mixture and the X−ray diffraction measurement was performed at 293(2) K. The ORTEP presentation of the molecular structure of complex **5D** is shown in Fig. 5.25 and the selected bond distances (Å) and angles (°) are summarized in Table 5.7.

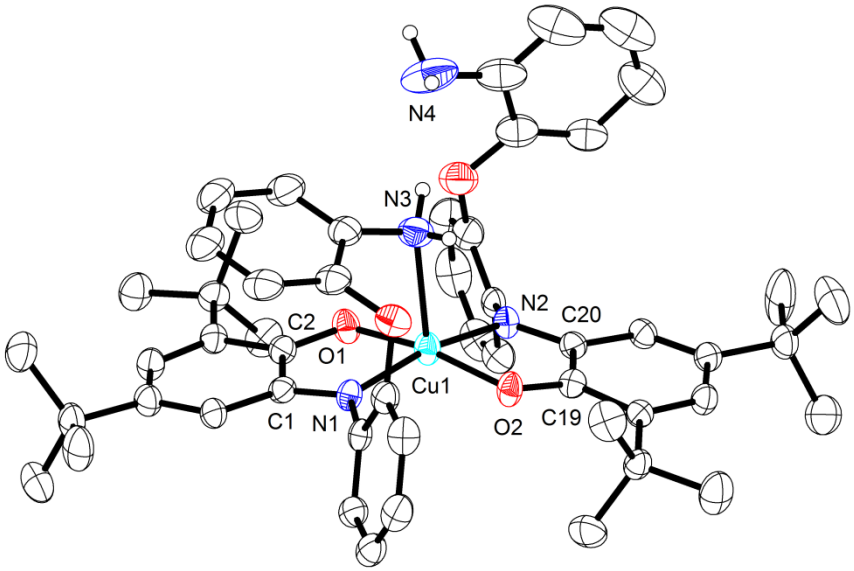

Figure 5.25: *ORTEP presentation of complex **5D**; thermal ellipsoids were drawn at 40% probability level. Solvent molecule and H–atoms (except attached with primary amine) were omitted for clarity.*

The complex was crystallized in the triclinic space group '*P–1*'. In the neutral complex, Cu center was five–coordinate with τ_5[13a] value of 0.02. The basal plane was constituted by two NO donor sets of two amidophenolate units that belonged to two different ligand entities. The central Cu atom was coordinated to both NO donor sets. The apical position was occupied by amine group–belonging N3 atom [Cu1–N3 = 2.485(7) Å]. The central Cu atom was situated 0.197(1) Å above the basal plane. The Cu1–L(N/O) [Cu1–N1 = 1.966(3), Cu1–N2 = 1.972(3), Cu1–O1 = 1.922(3) and Cu1–O2 = 1.945(3)] bond distances (along basal plane) were commensurate with the previously reported Cu(II)–N and Cu(II)–O bond distances of similar systems.[4,15] The bond distances of N1–C1, O1–C2, N2–C20 and O2–C19 were found as 1.334(5), 1.299(5), 1.334(5) and 1.285(5) Å, respectively. Those values were in between of their single bond and double bond characterizing values. Along with this, *tert*–butyl group containing C_6 rings exhibited a quinoid–distortion (short–long–short C–C bonds followed by three successive long C–C bonds). The above structural feature revealed the existence of the *tert*–butyl group containing amidophenolate rings in its one–electron oxidized iminosemiquinone ($[ISQ]^{\bullet 1-}$) form (Scheme 5.4). The other C_6 rings (except attached with *tert*–butyl groups) have C–C bond distance within the range of 1.38±0.02 Å as prospective for fully reduced phenyl rings. Thus obtained pentacoordinated Cu(II)–bis(iminosemiquinone) complex having an axial hard ($–NH_2$) coordination to the metal center and it caused an dihedral angle in between two ligating O1–Cu1–N1 and O2–Cu1–N2 planes by 16.1(1)°.

Table 5.7: *Selected Bond Distances (Å) and Angles (°) for Complex **5D**.*

Cu1–O1	1.922(3)	N3–C18	1.413(6)
Cu1–O2	1.945(3)	N4–C36	1.408(9)
Cu1–N1	1.966(3)	C1–C2	1.458(6)
Cu1–N2	1.972(3)	C2–C3	1.433(6)
Cu1–N3	2.485(7)	C4–C3	1.367(6)
O1–C2	1.299(5)	C4–C5	1.422(6)
O2–C19	1.285(5)	C6–C5	1.360(6)
O3–C13	1.382(6)	C1–C6	1.419(5)
O3–C12	1.386(5)	C19–C20	1.457(6)
O4–C30	1.384(6)	C20–C21	1.430(5)
O4–C31	1.378(7)	C21–C22	1.362(6)
N1–C1	1.334(5)	C22–C23	1.433(6)
N1–C7	1.417(5)	C23–C24	1.377(5)
N2–C20	1.334(5)	C24–C19	1.428(6)
N2–C25	1.424(5)		
O1–Cu1–O2	169.1(1)	C13–O3–C12	116.8(4)
O1–Cu1–N1	83.5(1)	C31–O4–C30	117.7(4)
O2–Cu1–N1	95.3(1)	C1–N1–C7	121.4(3)
O1–Cu1–N2	95.7(1)	C1–N1–Cu1	112.3(3)
O2–Cu1–N2	83.1(1)	C7–N1–Cu1	126.2(3)
N1–Cu1–N2	167.8(1)	C20–N2–C25	121.1(3)
N1–Cu1–N2	167.8(1)	C20–N2–Cu1	112.2(3)
C2–O1–Cu1	113.3(3)	C25–N2–Cu1	124.3(3)
C19–O2–Cu1	112.9(2)		

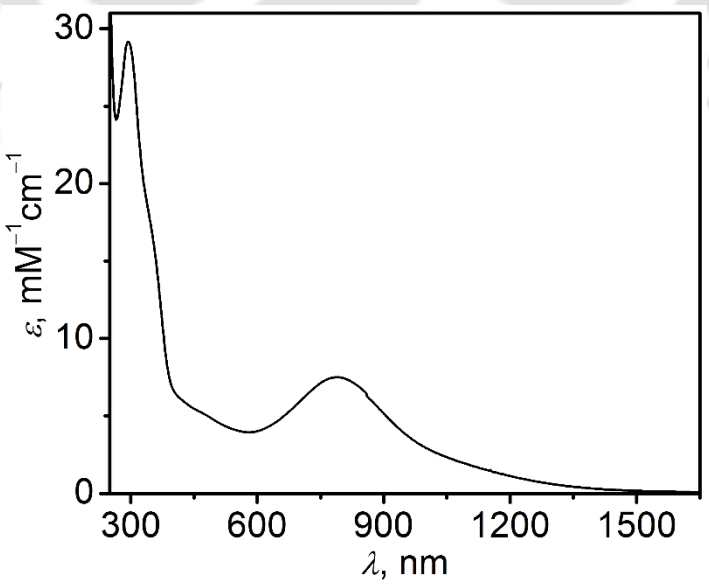

Figure 5.26: *UV–Vis/NIR spectrum of complex **5D** in CH_2Cl_2 at 250–1650 nm range.*

The electronic absorption spectrum of the complex **5D** was recorded in dichloromethane at room temperature (Fig. 5.26) and the absorption maxima with the extension coefficient were summarized in Table 5.8.

The absorption band at 790 nm (ε = 7500 $M^{-1}cm^{-1}$) was the characteristic of Cu–iminobenzosemiquinato species.[4a] The band was attributed as spin– and dipole–allowed ligand–to–ligand charge transfer. The bands at 1050 nm (ε = 2350 $M^{-1}cm^{-1}$) and 457 nm (ε = 5350 $M^{-1}cm^{-1}$) were corresponding to intraligand charge transfer (ILCT) and metal–to–ligand charge transfer, respectively.[4c]

Table 5.8: *Electronic absorption data of complex **5D**.*

Complex	λ_{max} (ε, $M^{-1}cm^{-1}$)
5D	1050^{br}(2350), 790 (7500), 457(5350), 359^{sh}(15150), 293 (29150)

* Superscript sh and br stand for shoulder and broad bands, respectively.

The redox behavior of the square pyramidal Cu(II)–bis(iminosemiquinone) complex (**5D)** was measured in CH_2Cl_2 solution containing 0.10 M $[(^nBu)_4N]ClO_4$ as the supporting electrolyte at a glassy carbon working electrode and Ag/AgCl reference electrode. Ferrocenium hexafluorophosphate ($FcPF_6$) was used as an internal standard and all the potentials have been referenced *vs.* Fc^+/Fc couple. The cyclic voltammograms of complex **5D** is depicted in Fig. 5.27 and all of the redox potentials are summarized in Table 5.9.

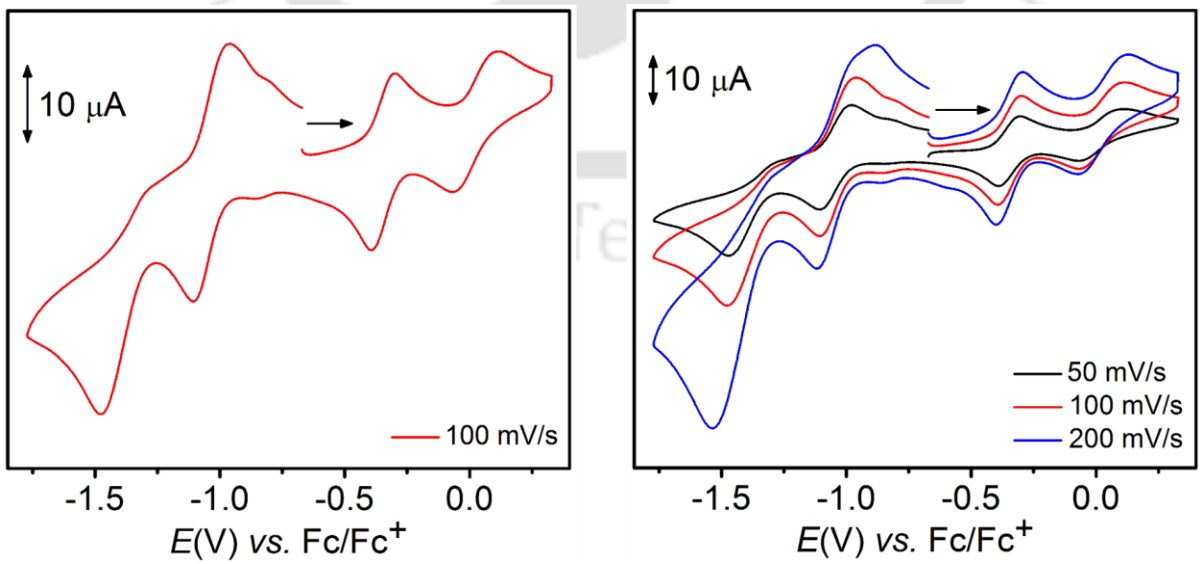

Figure 5.27: *Cyclic voltammograms of complex **5D** measured in dichloromethane; (A) single cycle at 100 mV/s scan rate and (B) rate dependence.*

During the anodic scan, two successive oxidation at –0.346 and 0.021 V led the neutral complex (**5D)** to its fully oxidized Cu(II)–diquinone form (Scheme 5.9). Interestingly, the second oxidation potential (0.021 V *vs.* Fc^{+}/Fc) was nearly 0.30 V lower compare to several square planer diradical Cu(II) complex (Table 5.10). This might be due to higher electron density and or lack of electronic conjugation of the corresponding redox center. Complex **5D** underwent four successive one–electron reductions and resulted Cu(II)–diamidophenolate species. The two redox process at –1.036 and –1.381 V were resembled with several Cu(II)–diradical species and corresponded to Cu(II)–bound ligand centered reductions.[4*a-c*, 8*f*]

Table 5.9: *Summary of Redox Potentials of Complexes **5D** in Volts vs. Fc^{+}/Fc redox couple.*

Complex	$E_{1/2}$(ox1)	$E_{1/2}$(ox2)	$E_{1/2}$(red1)	$E_{1/2}$(red2)
5D	–0.346	0.021	–1.036	–1.381

Table 5.10: *Comparison of second oxidation potential of several Cu(II)–bis(iminosemiquinone) complexes.*

Complex	$E_{1/2}$(ox2)	Reference
$[Cu(L^{ISQ})_2]$	0.370	4*a*
$[Cu\{L^{ISQ(R)}\}_2]$, R represent the substitution/s at aniline ring	>0.320	4*b*
$[Cu\{L^{ISQ(SMe)}\}_2]$	0.37	4*c*
$[Cu(L^{ISQ/ISQ})]$	0.347	8*f*
5D	0.021	This work

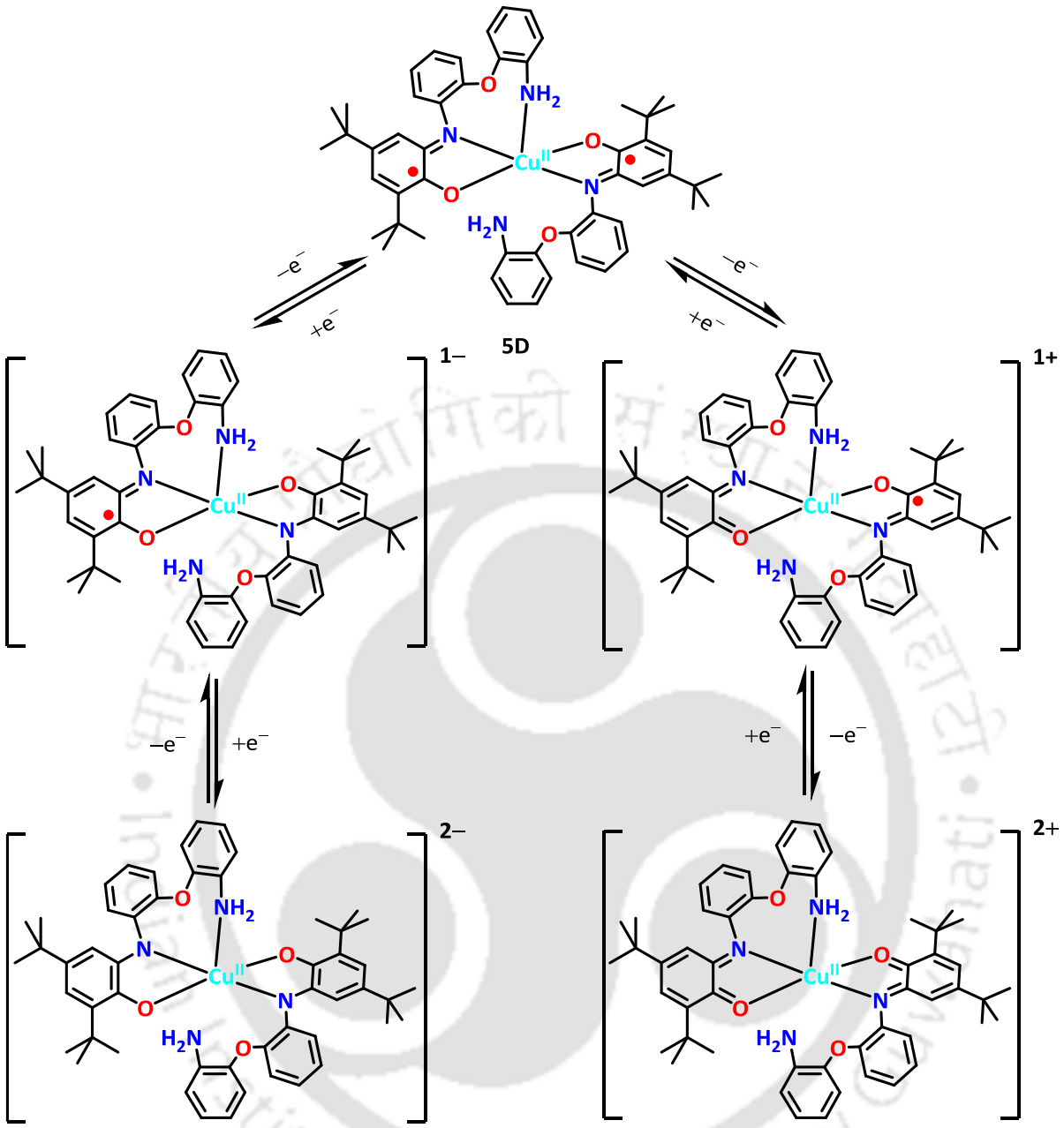

Scheme 5.9: *Different possible redox states of complex* ***5D***.

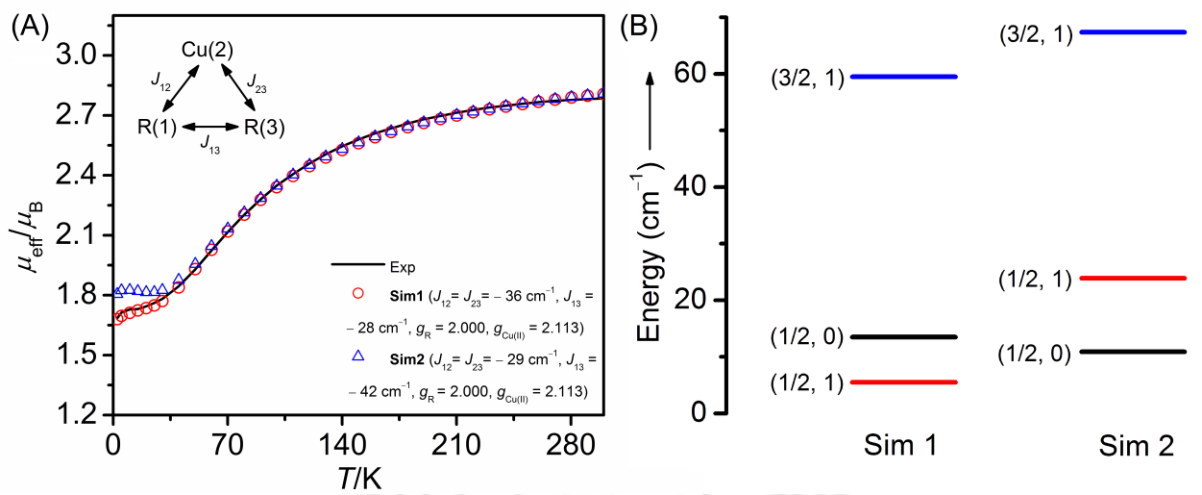

Figure 5.28: *(A) Experimental and simulated μ_{eff} vs. T plot for complex **5D**; (B) Calculated energy level based on resultant simulated values.*

The magnetic susceptibility data for complex **5D** (Fig. 5.28A) was collected on solid sample in the temperature range 2–300 K in an applied magnetic field of 1.0 T. Experimental data revealed the existence of single unpaired electron at the ground state as the value of μ_{eff} was found 1.71 μ_B. The initial magnetic moment value increased gradually from 15 K and reached to a maximum of 2.78 μ_B at 300 K. This magnetic behavior was characteristic of antiferromagnetic coupling between the spins and the nature of the curve indicated the presence of multi–paramagnetic centers. The complex has three S = 1/2 spins with one spin at Cu(II) ($S_{Cu(II)}$ = 1/2) and two spins at two ligand–based radicals (S_{R1} = S_{R2} = 1/2). The interactions amongst the spins will provide electron spin states (S_t, S*) = (3/2, 1), (1/2, 1) and (1/2, 0). It can be symbolically represented as (↑↑↑), (↑↓↑), and (↑↑↓), respectively, where, S_t = S_{Cu} + S_{rad1} + S_{rad2} and S* = S_{rad1} + S_{rad2}.[16a] A very good agreement with the experimental data has been obtained by simulation[16b] (Sim1) using the following parameters: J_{12} = J_{13} = −36 cm^{-1}; J_{23} = −28 cm^{-1}; $g_{Cu(II)}$ = 2.113 and g_R = 2.000 (Sim1, Fig. 5.28). This simulation (Sim1) suggested state (1/2, 1) as the ground state. Another simulation (Sim2) with the following parameters: J_{12} = J_{13} = −29 cm^{-1}; J_{23} = −42 cm^{-1}; $g_{Cu(II)}$ = 2.113 and g_R = 2.000 provided (1/2, 0) spin state as the ground state. The close value of exchange interaction for complex **5D** revealed the existence of close location between (1/2, 1) and (1/2, 0) spin states. However, Sim2 was not fully resembled with the experimental data at the temperature range 2–40 K. The μ_{eff} = 1.73 μ_B at 10 K indicated the ground state to be S_t = 1/2, hence, to find out the exact location of the unpaired electron EPR analysis was performed at 77 K.

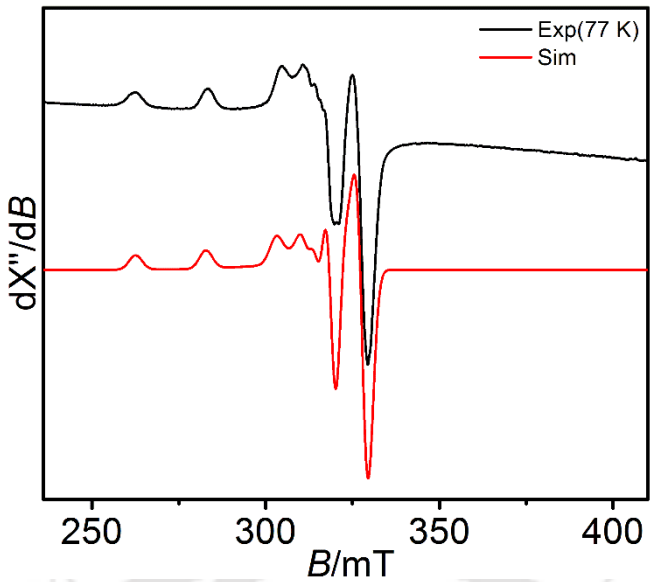

Figure 5.29: *Experimental (Exp) X–band EPR spectrum of complex **5D** presented with the simulation (Sim). X–band microwave frequency (GHz): 9.143; microwave power (mW):0.995; modulation frequency (KHz): 100; amplitude (G) = 2.5.*

The square pyramidal diradical Cu(II) complex **5D** contains three paramagnetic centers in its molecular skeleton. EPR measurement of the complex has been measured in a 10:1 mixture of CH_2Cl_2 and toluene at 77 K. The EPR data was simulated by using W95EPR program[17] and the simulation was done by using the following parameters; g_1 = 2.050; g_2 = 2.060, g_3 = 2.230; g_{av} = 2.113; $^{Cu}(A_1, A_2, A_3) = (20, 30, 197) \times 10^{-4}$ cm^{-1}, $^{N}(A_1, A_2, A_3) = (3, 6, 0) \times 10^{-4}$ cm^{-1}. Those values clearly consolidated that the radical–radical antiferromagnetic interaction predominant over metal–radical interaction and S_t = 1/2 as the ground state attributable as Cu(II)–centred spin character. However, it was not well agreed with more perfectly matched simulation data (Sim1, Fig. 5.28) of SQUID measurement. It might be due to lower energy difference between E(1/2, 0) and E(1/2, 1) spin states. Thus at 77 K, the resultant spin exhibited on $(d_{x^2-y^2})^1$ magnetic orbital of Cu(II)–ion.

5.7: Conclusion

- The ligand $\mathbf{H_2L^{AP(o–NH_2–OPh)}}$ behaves as a tridentate coordination entity during the complexation with $Co(ClO_4)_2 \cdot 6H_2O$ and provide an octahedral Co(III)–bis(iminosemiquinone) complex (**5A**). The involvements of aryl amine through axial direction prevent the closer approach of ethereal oxygen toward the metal center.
- In diradical square planer NI(II)–bis(iminosemiquinone) complex (**5B**), the aryl amines are not involved any coordination with the metal ion.
- On treatment with 2 eq. ferrocenium hexafluorophosphate ($FcPF_6$), complex **5B** provide an octahedral Ni(II)–bis(iminobenzoquinone) complex (**5C**). The elongation of Ni1–O1 and Ni1–N1 bond lengths allows the aryl amine for axial approach toward the metal ion.
- Ligand $\mathbf{H_2L^{AP(o–NH_2–OPh)}}$ provide a square pyramidal Cu(II)–bis(iminosemiquinone) complex **5D** where an aryl–NH_2 coordination through axial direction caused a dihedral angle in between two ligating O1–Cu1–N1 and O2–Cu1–N2 planes by 16.1(1)°.
- The magnetic susceptibility data with computer simulation for complex **5D** revealed the existence of closely located (1/2, 1) and (1/2, 0) spin states.

References

1. (*a*) R. Fromme, Y. S. Bukhman–deRuyter, H. Mi, P. Fromme, RCSB PDB, *DOI: 10.2210/pdb3bqv/pdb*; (*b*) E. I. Solomon, R. K. Szilagyi, S. D. George and L. Basumallick, *Chem. Rev.*, 2004, **104**, 419.

2. (*a*) N. Ito, S. E. V. Phillips, C. Stevens, Z. B. Ogel, M. J. McPherson, J. N. Keen, K. D. S. Yadav and P. F. Knowles, *Nature*, 1991, **350**, 87; (*b*) Y. Wang, J. L. DuBois, B. Hedman, K. O. Hodgson and T. D. P. Stack, *Science*, 1998, **279**, 537; (*c*) M. M. Whittaker and J. W. Whittaker, *J. Biol. Chem.*, 1990, **265**, 9610; (*d*) F. Himo, L. A. Friksson, F. Maseras and P. E. M. Siegbahn, *J. Am. Chem. Soc.*, 2000, **122**, 8031; (e) L. Que, Jr. and W. B. Tolman, *Nature*, 2008, **455**, 333 (*d*) J. W. Whittaker, *Chem. Rev.*, 2003, **103**, 2347.

3. (*a*) M. R. Parsons, M. A. Convery, C. M. Wilmot, K. D. Yadav, V. Blakeley, A. S. Corner, S. E. Phillips, M. J. McPherson, P. F. Knowles, *Structure*, 1995, **3**, 1171; (*b*) S. M. Janes, D. Mu, D. Wemmer, A. J. Smith, S. Kaur, D. Maltby, A. L. Burlingame and J. P. Klinman, *Science*, 1990, **248**, 981; (*c*) D. M. Dooley, M. A. McGuirl, D. E. Brown, P. N. Turowski, W. S. McIntire and P. F. Knowles, *Nature*, 1991, **349**, 262; (*d*) J. P. Klinman, *J. Biol. Chem.*, 1996, **271**, 27189.

4**.** (*a*) P. Chaudhuri, C. N. Verani, E. Bill, E. Bothe, T. Weyhermüller and K. Wieghardt, *J. Am. Chem. Soc.*, 2001, **123**, 2213; (*b*) C. Mukherjee, U. Pieper, E. Bothe, V. Bachler, E. Bill, T. Weyhermüller and P. Chaudhuri, *Inorg. Chem.*, 2008, **47**, 8943; (*c*) S. Ye, B. Sarkar, F. Lissner, T. Schleid, J. van Slageren, J. Fiedler and W. Kaim, *Angew. Chem., Int. Ed.* 2005, **44**, 2103; (*d*) R. Rakshit, S. Ghorai, S. Biswas and C. Mukherjee, *Inorg. Chem.*, 2014, **53**, 3333.

5. (*a*) J. Coates, *Interpretation of Infrared Spectra: A Practical Approach*, John Wiley & Sons Ltd, Chichester, 2000; (*b*) G. R. Pandhare, V.M. Shinde and Y. H. Deshpande, *Rasayan J. Chem.*, 2008, **1**, 337; (*c*) P. K. Kipkemboi, P. C. Kiprono and J. J. Sanga, *Bull. Chem. Soc. Ethiop.*, 2003, **17**, 211; (*d*) D. L. Pavia, G. M. Lampman, G. S. Kriz and J. R. Vyvyan, *Introduction to Spectroscopy*, 4th edition, 31; (*e*) S. Sahoo, C. K. Chakraborti, P. K. Behera, S.C. Mishra, *Int. J. Drug Dev. & Res.*, 2011, **3**, 261.

6. (*a*) A. V. Piskunov, A. V. Lado, G. A. Abakumov, V. K. Cherkasov, O. V. Kuznetsova, G. K. Fukin and E. V. Baranov, *Russ. Chem. Bull., Int. Ed.*, 2007, **56**, 97; (*b*) F. A. Miller

and C. H. Wilkins, *Anal. Chem.*, 1952, **24**, 1253.

7. (*a*) C. N. Verani, S. Gallert, E. Bill, T. Weyhermüller, K. Wieghardt and P. Chaudhuri, Chem. Commun., 1999, 1747; (*b*) E. Bill, E. Bothe, P. Chaudhuri, K. Chlopek, D. Herebian, S. Kokatam, K. Ray, T. Weyhermüller, F. Neese and K. Wieghardt, *Chem. Eur. J.*, 2005, **11**, 204; (*c*) A. L. Smith, K. I. Hardcastle and J. D. Soper, *J. Am. Chem. Soc.*, 2010, **132**, 14358; (*d*) A. I. Poddel'sky, V. K. Cherkasov, G. K. Fukin, M. P. Bubnov, L. G. Abakumova and G. A. Abakumov, *Inor. Chim. Acta.*, 2004, **357**, 3632 ; (*e*) R. K. Sherwood, C. L. Kent, B. O. Patrickb and W. S. McNeil, *Chem. Commun.*, 2010, **46**, 2456.

8. (*a*) D. L. J. Broere, B. de Bruin, J. N. H. Reek, M. Lutz, S. Dechert and J. I. van der Vlugt, *J. Am. Chem. Soc.*, 2014, **136**, 11574; (*b*) C. Mukherjee, T. Weyhermüller, K. Wieghardt and P. Chaudhuri, *Dalton Trans.*, 2006, 2169; (*c*) M. E. Cass, Greene, D. L. Greene, R. M. Buchanan and C. G. Pierpont, *J. Am. Chem. Soc.*, 1983, **105**, 2680; (*d*) S. N. Brown, *Inorg. Chem.*, 2012, **51**, 1251; (*e*) H. Chun, P. Chaudhuri, T. Weyhermüller and K. Wieghardt, *Inorg. Chem.*, 2002, **41**, 790; (*f*) C. Mukherjee. T. Weyhermüller, E. Bother and P. Chaudhuri, *Inorg. Chem.*, 2008, **47**, 11620.

9. M. K. Mondal, A. Tiwari and C. Mukherjee, *Chem. Cummun.*, 2016, **52**, 11995.

10. (*a*) M. M. Khusniyarov, K. Harms, O. Burghaus, J. Sundermeyer, B. Sarkar, W. Kaim, J. van Slageren, C. Duboc and J. Fiedler, *Dalton Trans.*, 2008, 1355.

11. (*a*) A. A. El–Hendawy, *J. Anal. Appl. Pyrolysis*, 2006, **75**, 159; (b) G. Hastings and V. Sivakumar, *Biochemistry*, 2001, **40**, 3681; (c) J. Breton, J. Burie, C. Berthomieu, G. Berger and E. Nabedryk, *Biochemistry*, 1994, **33**, 4953; (d) Y.–N. Kwon and J.O. Leckie, *J. Membr. Sci.*, 2006, **282**, 456; (e) L. H. Briggs and L. D. Colebrook, *Anal. Chem.*, 1957, **29**, 904.

12. (*a*) C. Mukherjee, T. Weyhermüller, E. Bothe and P. Chaudhuri, Inorg. Chem., 2008, **47**, 2740; (*b*) S. Mukherjee, T. Weyhermüller, E. Bothe, K. Wieghardt and P. Chaudhuri, *Dalton Trans.*, 2004, 3842.

13. (*a*) A. Addison, T. Rao, J. Reedijk, J. van Rijn and G. Verschoor, *J. Chem. Soc., Dalton Trans.*, 1984, 1349; (*b*) L. Yang, D. R. Powell and R. P. Houser, Dalton Trans., 2007, 955.

14. (*a*) R. Sikari, S. Sinha, U. Jash, S. Das, P. Brandão, B. de Bruin and N. D. Paul, *Inorg. Chem.*, 2016, **55**, 6114; (*b*) A. Ali, D. Dhar, S. K. Barman, F. Lloret and R. Mukherjee, *Inorg. Chem.*, 2016, **55**, 5759.

15. (*a*) F. Thomas, *Eur. J. Inorg. Chem.*, 2007, 2379; (*b*) S. Ghorai and C. Mukherjee, *Chem. Asian J.*, 2014, **9**, 3518; (*c*) C. Mukherjee, T. Weyhermüller, E. Bothe, E. Rentschler and P. Chaudhuri, *Inorg. Chem.*, 2007, **46**, 9895; (*d*) A. I. Poddel'sky, V. K. Cherkasov and G. A. Abakumov, *Coord. Chem. Rev.*, 2009, **253**, 291; (*e*) S. Ghorai, A. Sarmah, R. K. Roy, A. Tiwari and C. Mukherjee, *Inorg. Chem.*, 2016, **55**, 1370; (*f*) A. Paretzki, R. Hübner, S. Ye, M. Bubrin, S. Kämper and W. Kaim, *J. Mater. Chem. C*, 2015, **3**, 4801; (*g*) D. L. J. Broere, R. Plessius and J. I. van der Vlugt, *Chem. Soc. Rev.*, 2015, **44**, 6886.

16. (*a*) O. Kahn, *Molecular Magnetism*, VCH Publishers, Inc, New York, 1993; (*b*) E. Bill, JulX version 1.4.1, Magnetic susceptibility simulation software, Max–Planck Institute, Germany.

17. W95EPR program was developed by Frank Neese (MPI for Bioinorganic Chemistry, Mülheim, and University of Bonn).

Thesis Perspectives

1. Complexation of ligand $\mathbf{H_4L^{Z(AP/AP)}}$ (Z = O and S) with $Co(ClO_4)_2 \cdot 6H_2O$ has been found to activate and cleave C–O and C–S bonds. This phenomena open up the possibility to employ the amidophenolate coordinated Co complexes in activation of C–O/N/S/Se bonds in various organic compounds. In addition, the following ligands ($\mathbf{H_4L^{SS(AP/AP)}}$ and $\mathbf{H_4L^{SS(AP/NH_2)}}$) can be synthesized to understand the hemolytic bond cleavage *in situ*.

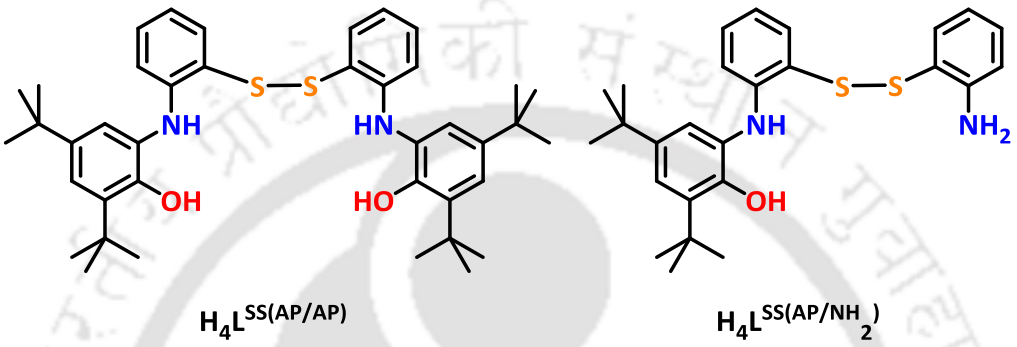

$\mathbf{H_4L^{SS(AP/AP)}}$ $\mathbf{H_4L^{SS(AP/NH_2)}}$

Scheme: Proposed ligand $\mathbf{H_4L^{SS(AP/AP)}}$ and $\mathbf{H_4L^{SS(AP/NH_2)}}$.

2. Redox reversibility of non–innocent amidophenolate based ligand in the corresponding Co complexes enables those molecular entities to show external stimuli driven valence tautomerism. Such type of complexes can be employed to design molecular level switch, molecular based electro–magnetic device etc. Furthermore, it has been observed that the valence tautomerism is driven by the cooperative effect of the crystal solvent molecules. Thus, synthesis of non-innocent ligands by incorporating of various groups, which are having solvent like units, in the ligand backbone could be perform in the near future for the synthesis of the corresponding valence tautomeric complexes.

3. The salt $CuCl_2 \cdot 2H_2O$ has acted as an oxidant and potentially oxidized the Cu–coordinated non-innocent ligand center and resulted Cu–quinone species. The electrophilicity of such Cu–quinone species can be exploited (I) to design energy serving molecular systems and (II) laboratory based electrophiles.

4. The nitro group at ligands $\mathbf{H_2L^{AP(o\text{–}NO_2\text{–}OPh)}}$ can be utilized to attach the organic moieties to a solid support like electrode and/or nanoparticle to furnish new solid supported non–innocent ligand. Thus, the ligand will be very much effective for the generation of solid-supported heterogeneous catalyst and electron reservoir.

भारतीय प्रौद्योगिकी संस्थान गुवाहाटी
Indian Institute of Technology Guwahati

Chapter VI

Equipment and Experimental Section

6.1: Methods and Equipments

All the analyses were performed at 'Instrumental Lab, Department of Chemistry' and 'Central Instrumental Facility' IITG, unless otherwise mentioned.

Chemicals and Solvents

All the chemicals and solvents were obtained from commercial sources and were used as supplied, unless noted otherwise. DMSO and DMF were dried before use.

Infrared Spectroscopy

Solid state FTIR spectra were recorded (4000–400 cm^{-1}) on 'Perkin Elmer Instrument' at room temperature. The pallet has been made by grinding the sample with IR grade KBr powder.

NMR Spectroscopy

^{1}H, ^{13}C NMR spectra were recorded on 'Varian Mercury plus 400 MHz' and on 'Bruker Ascend^{Tm} 600 MHz' nuclear magnetic resonance (NMR) spectrometer at 298 K. Chemical shifts, δ (in ppm), are reported relative to TMS [δ (^{1}H) 0.0 ppm, δ (^{13}C) 0.0 ppm] which was used as the inner reference. Otherwise, the solvents ($CHCl_3$) residual proton resonance and carbon resonance appeared at, δ 7.26, 77.2 ppm, respectively. The resultant spectrums were drawn by using 'MestReNova' NMR data processing software.

Mass Spectrometry

Mass spectra were recorded on QTOF–MS Spectrometer ('Waters, Model: Q–Tof Premier') or 'Agilent Accurate–Mass Q–TOF LC/MS 6520' spectrometer and peaks were given in *m*/*z* (% of basis peak). Mass spectra were taken in HPLC grade CH_3CN solvent.

Elemental analysis

The determination of the C, H, N was performed on 'FLASH EA 1112 series' CHN Analyzer at SAIF, Mumbai, on 'Perkin–Elmer 2400 series II' CHN Analyzer at IACS, Kolkata and on 'EuroEA3000' Elemental Analyzer at Guwahati Biotech Park, Guwahati.

UV–Vis/NIR Spectroscopy

The electronic absorption spectrum (UV–Vis/NIR) of the sample(s) was recorded on 'Perkin Elmer, Lamda 750, UV/Vis/NIR spectrometer' in HPLC grade CH_2Cl_2 at room temperature using cuvette of 1 cm width. Thermal electronic absorption spectrum of the complex

(**2A**) was recorded on 'Perkin Elmer, Lamda 350, UV/Vis/NIR spectrometer' in HPLC grade toluene at a range of 30–70 ° C.

Electrochemistry

Cyclic voltammetry was performed by using a 'VersaSTAT 3 Potentiostat'. A standard three electrode–cell was employed with a glass-carbon working electrode, a platinum-wire auxiliary electrode and Ag/AgCl (saturated NaCl in water) reference electrode. Measurements were made under an inert atmosphere at room temperature. The potential of the reference electrode was determined using Fc^{+}/Fc as the internal standard.

Magnetic Susceptibility Measurement by SQUID Magnetometer

Temperature dependent magnetic susceptibility of the powder sample was recorded by using 'Quantum Design SQUID Magnetometer MPMS' at 1T external magnetic field in the range of 2 to 300 K temperature range. The powdered samples were placed in oval Gelatin capsules and fixed in a plastic tube. The resulting volume magnetization from the samples had its diamagnetic contribution compensated and was recalculated as volume susceptibility. Diamagnetic contributions were estimated for each compound by using Pascal's constants. The resultant data was simulated by using 'JulX_v141' software. The program JulX is based on the "full matrix diagonalization" and is used for the calculation of static molar magnetic susceptibilities is based on the usual spin Hamiltonian approach for up to four spins with local multiplicities up to S = 5/2:

$$\hat{H} = \hat{H}_{ex} + \hat{H}_{ZFS} + \hat{H}_{Zee}$$

Where, $\hat{H}_{ex}$ = Exchange Hamiltonian

$$\hat{H}_{ex} = -2\sum_{i=1}^{ns-1}\sum_{j=i+1}^{ns} j_{ij}\hat{S}_i \bullet \hat{S}_j$$

$\hat{H}_{ZFS}$= Zero field splitting Hamiltonian

$$\hat{H}_{ZFS} = \sum_{i=1}^{ns} D_i\left[\hat{S}_{z,i} - \frac{1}{3}\hat{S}_i(\hat{S}_i + 1) + \frac{E_i}{D_i}(\hat{S}_{x,i}^2 - \hat{S}_{y,i}^2)\right]$$

$\hat{H}_{zee}$= Zeeman interaction Hamiltonian

$$\hat{H}_{zee} = \sum_{i=1}^{ns} g\beta\hat{S}_i \bullet \hat{B}$$

J_{ij} are the exchange coupling constants of spins i and j, ns is the number of spins (max. four), D_i, E/D_i and g_i are the local axial and rhombic zero field splitting parameters and g–values (isotropic average).

Magnetic Susceptibility Measurement by Evans Method

Effective magnetic moment of the paramagnetic complex was determined by Evans method ^{1}H NMR measurement at 298 K. A standard solution of paramagnetic complex in $CDCl_3$ was taken in the inner tube capacity (200 µL) and the required height of outer tube capacity was filled by pure $CDCl_3$ (~300 µL). The chemical shift of the solvent in presence of paramagnetic complex was measured by ^{1}H NMR measurement. The effective molar magnetic susceptibility was calculated based on the following equation:

$$\chi_M = \frac{\delta \times 3 \times MW}{4\pi f C} - \chi_{dia}$$

Where, χ_M = molar magnetic susceptibility (in the unit of emu mol^{-1}), MW = molecular weight of the complex, f = spectrometer frequency in Hz, C = concentration of the complex in g/mL and χ_{dia} is the diamagnetic contribution from the complex.

X–Band EPR Spectroscopy

First derivative X–Band EPR spectra of powdered or frozen solution samples were measured with a 'JEOL JES–FA200 Spectrometer'. The resulting data was simulated by using W95EPR–program written by Frank Neese (MPI for Bioinorganic Chemistry, Mülheim, and University of Bonn).

X-ray Powder Diffraction

X–ray powder diffraction analysis for phase identification of crystalline materials was done by using 'Bruker, D8–Advance' diffractometer at 298 K in 'Department of Chemical Engineering, IITG'. MoK_α was used as a source to produce X–ray with a wavelength of 0.78 Å. The interaction of the incident rays with the sample produces constructive interference, when conditions satisfy Bragg's Law ($n\lambda = 2d \sin\theta$). The data is collected at 2θ from ~1° to 50°, angles that are preset in the X–ray scan.

Single Crystal X-ray Crystallography

Suitable crystal for X–ray diffraction study was obtained from solvent evaporation or solvent diffusion method. X−ray crystallographic data were collected by using either a 'Bruker

SMART APEX−II CCD diffractometer', equipped with a fine focus 1.75 kW sealed tube Mo−K_α radiation (λ = 0.71073 Å) at 296(2) or 293(2) K, with increasing w (width of 0.3° per frame) at a scan speed of 3 s/frame or a 'Super Nova, Single source at offset, Eos diffractometer'. Structure was solved with the Superflip, structure solution program using Charge Flipping and refined by direct methods using 'SHELXS–97' and with full–matrix least squares on F2 using 'SHELXL–97', or with the Superflip structure solution program using Charge Flipping and refined with the olex2.refine refinement package using Gauss–Newton minimization. All then non−hydrogen atoms were refined anisotropically.

6.2: Experimental section

6.2.1: Synthesis of ligand $H_4L^{O(AP/AP)}$

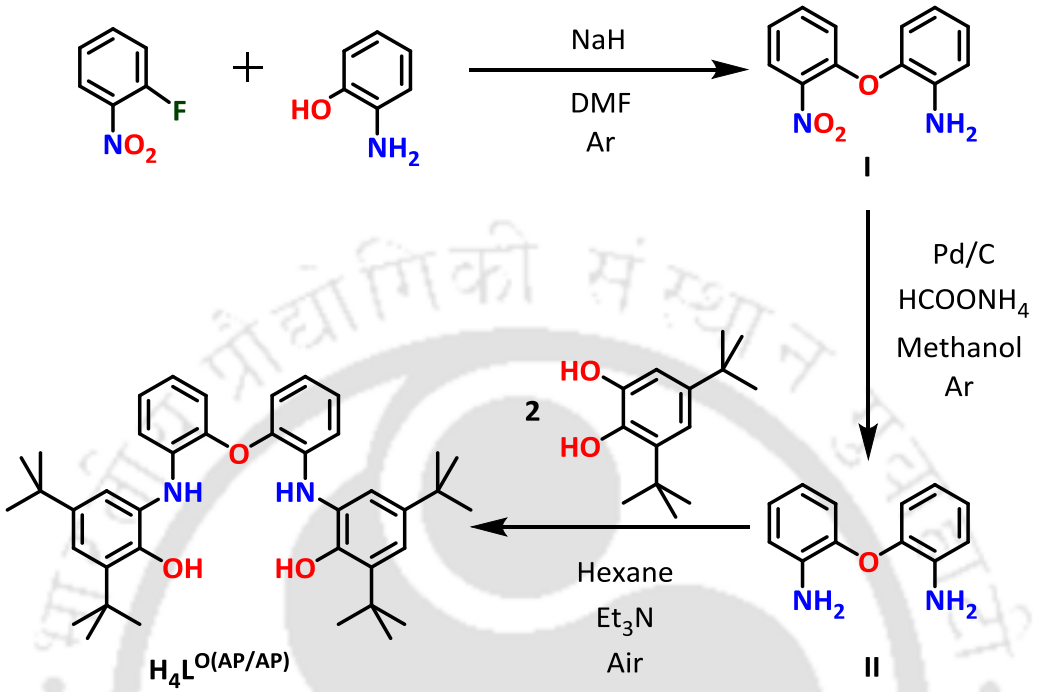

Scheme 6.1: *Synthetic route of ligand* $H_4L^{O(AP/AP)}$.

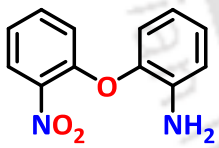

Step 1: Synthesis of 2–(2–nitrophenoxy)aniline; I. To a solution of 2–fluoronitrobenzene (0.987 g, 7 mmol) in dry DMF (4 mL), *o*–aminophenol (0.763 g, 7 mmol) and sodium hydride (0.336 g, 14 mmol) were added sequentially under Ar–atmosphere at ice cold condition. The reaction mixture was turned to reddish in due course. After 15 min, the reaction mixture was allowed to stir at room temperature for 18 h. Then it was quenched with water under ice cold condition and the product was extracted with CH_2Cl_2 (3 × 40 mL). The combined organic portion was then washed with water and brine solution and dried over anhydrous Na_2SO_4. Solvent was removed and the residue was dried under high vacuum. Thus obtained oily residue was purified by column chromatography on silica gel with an eluent consisting of hexane/ethyl acetate (9:1). 2–(2–nitrophenoxy)aniline was appeared as orange liquid.

Yield: 1.432 g, 89%.

FTIR (KBr pellet, cm^{-1}): 3462, 3384, 1624, 1605, 1586, 1525, 1500, 1352, 1307, 1270, 1238, 1186, 889, 777, 742, 665.

^{1}H NMR ($CDCl_3$, 399.853 MHz): δ 7.91 (dd, J = 8.0 Hz, J = 1.6 Hz, 1H), 7.47–7.43 (m, 1H), 7.15–7.11 (m, 1H), 7.08–7.04 (m, 1H), 6.96–6.93 (m, 2H), 6.86–6.84 (m, 1H), 6.77–6.73 (m, 1H), 3.95 (s, 2H) ppm.

ESI–MS (CH_3CN) *m/z* for $[C_{12}H_{10}N_2O_3+H]^+$: Calcd, 231.08; Found, 231.08.

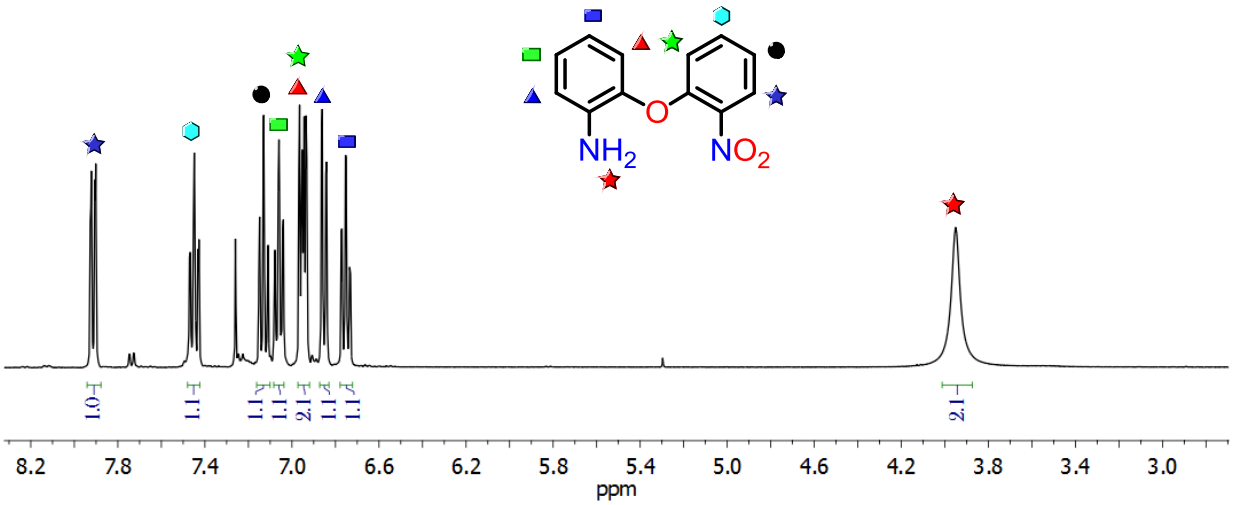

Figure 6.1: *^{1}H NMR 2–(2–nitrophenoxy)aniline;(**I**).*

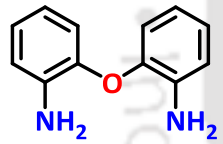

Step 2: Synthesis of bis(o–aminophenyl) ether; II. To a methanolic solution (15 mL) of 2–(2–nitrophenoxy)aniline (1.217 g, 5.29 mmol), 10% Pd in charcoal (35 mg) was added under argon atmosphere at ice cold condition. After a while (5 min), ammoniumformate (3.066 g, 48.6 mmol) was added to the reaction solution. The reaction mixture was then allowed to stir at room temperature for 4 h under argon atmosphere. It was then filtered through a pad of celite. The pad was washed with CH_2Cl_2 (50 mL). The filtrate was then extracted with CH_2Cl_2 (3×40 mL). The combined organic portion was washed with water and brine solution and dried over anhydrous Na_2SO_4. After evaporating the solvent, an off–white solid was obtained as the product.

Yield: 0.941 g, 89%.

FTIR (KBr pellet, cm^{-1}): 3469, 3426, 3379, 3348, 3200, 3061, 3034, 1615, 1580, 1499, 1454, 1303, 1263, 1199, 1185, 1156, 1137, 1033, 886, 794, 754, 678.

^{1}H NMR (399.850 MHz, $CDCl_3$): δ 6.98–6.94 (m, 2H), 6.83–6.80 (m, 2H), 6.72–6.69 (m, 2H), 3.89 (s, 4H) ppm.

^{13}C NMR (100.55 MHz, $CDCl_3$): δ 143.9, 138.0, 124.3, 118.8, 118.3, 116.4 ppm.

ESI–MS (+) for $[C_{12}H_{12}N_2O+H]^+$: Calcd, 201.10; found, 201.10.

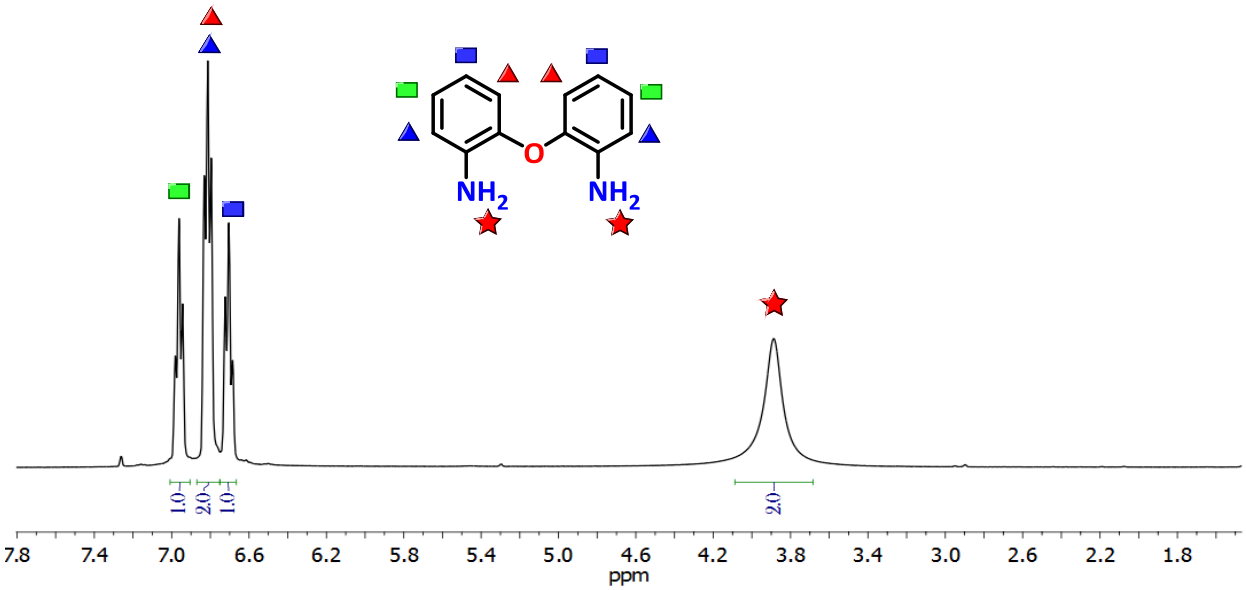

Figure 6.2: *^{1}H NMR bis(o–aminophenyl) ether; (**II**).*

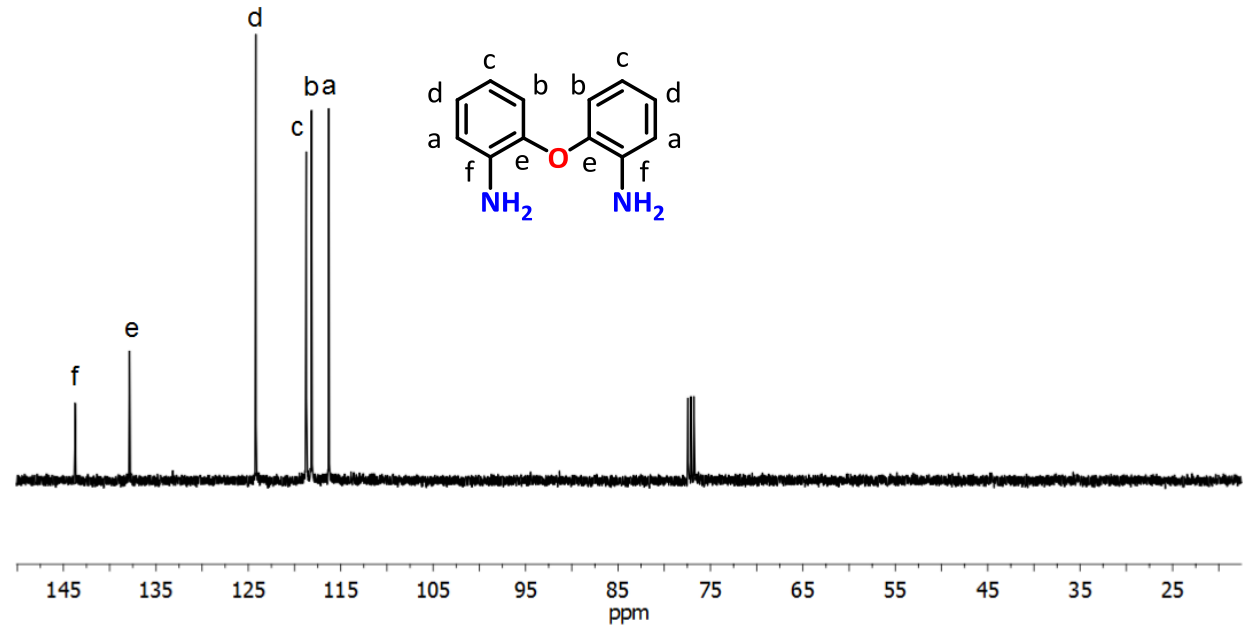

Figure 6.3: *^{13}C NMR bis(o–aminophenyl) ether; (**II**).*

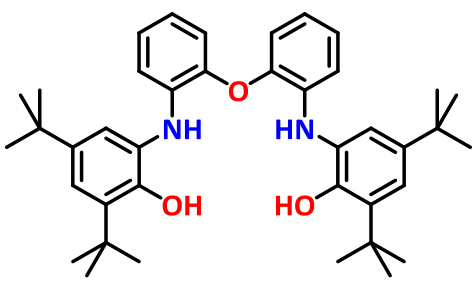

Step 3: Synthesis of ligand $H_4L^{O(AP/AP)}$. To a suspension of bis(*o*–aminophenyl) ether (0.891 g, 4.45 mmol) in hexane (15 mL), 3,5–di–*tert*–butylcatechol (1.979 g, 8.90 mmol) and Et_3N (0.05 mL) were added sequentially and the reaction mixture was refluxed for 30 min. After that the solution was stirred at room temperature (30 °C) for another 24 h. The solvent was evaporated and dried. The residue was the dissolved in hot methanol. A white precipitate was

separated out from the methanolic solution. The solid was filtered and washed with methanol (10 mL) and dried.

Yield: 1.731 g, 64 %.

FTIR (KBr pellet, cm^{-1}): 3437, 3377, 3056, 2958, 2906, 2868, 1609, 1599, 1587, 1504, 1483, 1460, 1448, 1425, 1391, 1363, 1316, 1241, 1224, 1195, 1156, 1117, 1106, 1040, 975, 879, 824, 767, 742, 579.

^{1}H NMR (399.893 MHz, $CDCl_3$): δ 7.23 (d, J = 2.0 Hz, 2H), 7.04 (d, J = 2.0 Hz, 2H), 7.00–6.94 (m, 4H), 6.84–6.80 (m, 2H), 6.63–6.60 (m, 2H), 6.34 (s, 2H), 5.58 (s, 2H), 1.44 (s, 18H), 1.26 (s, 18H) ppm.

^{13}C NMR (150.93 MHz, $CDCl_3$): δ 149.7, 144.5, 142.5, 138.4, 135.7, 127.4, 124.8, 122.3, 121.7, 120.0, 117.9, 115.5, 35.2, 34.6, 31.8, 29.8 ppm.

ESI–MS (+) *m/z* for $[C_{40}H_{52}N_2O_3+H]^+$: Calcd, 609.40; found, 609.41.

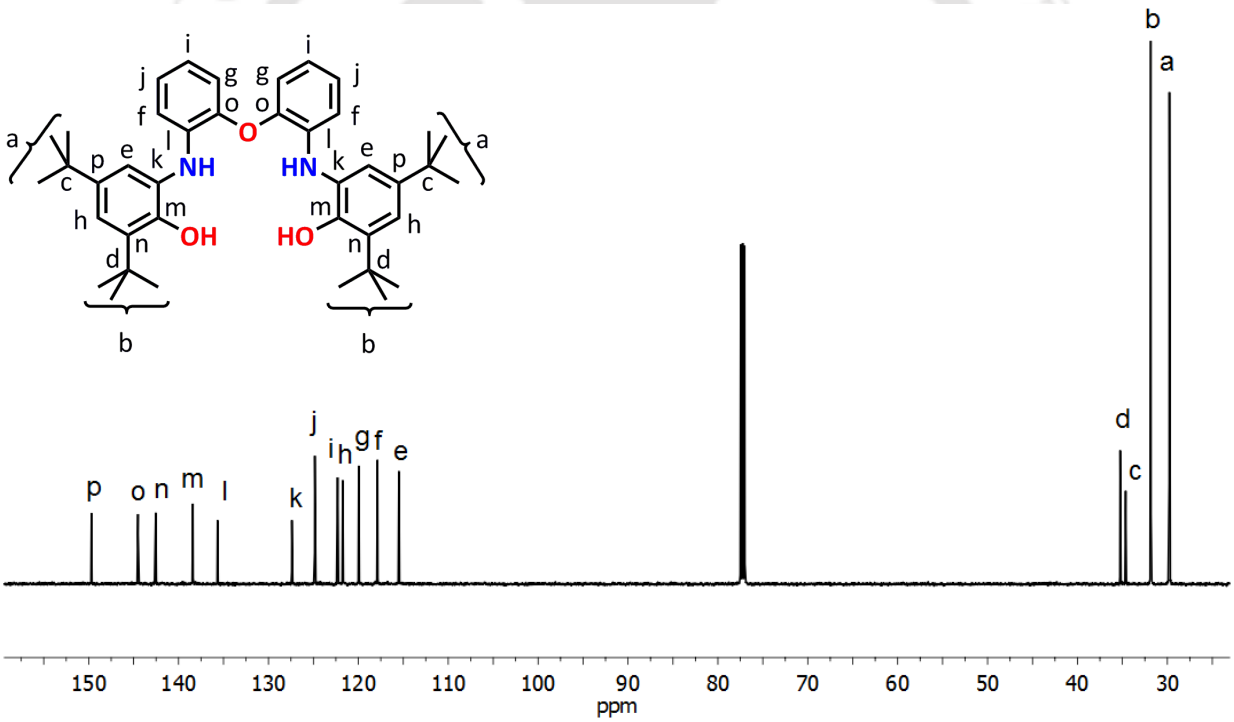

Figure 6.4: *^{13}C NMR of* $H_4L^{O(AP/AP)}$.

6.2.2: Synthesis of ligand $H_4L^{S(AP/AP)}$

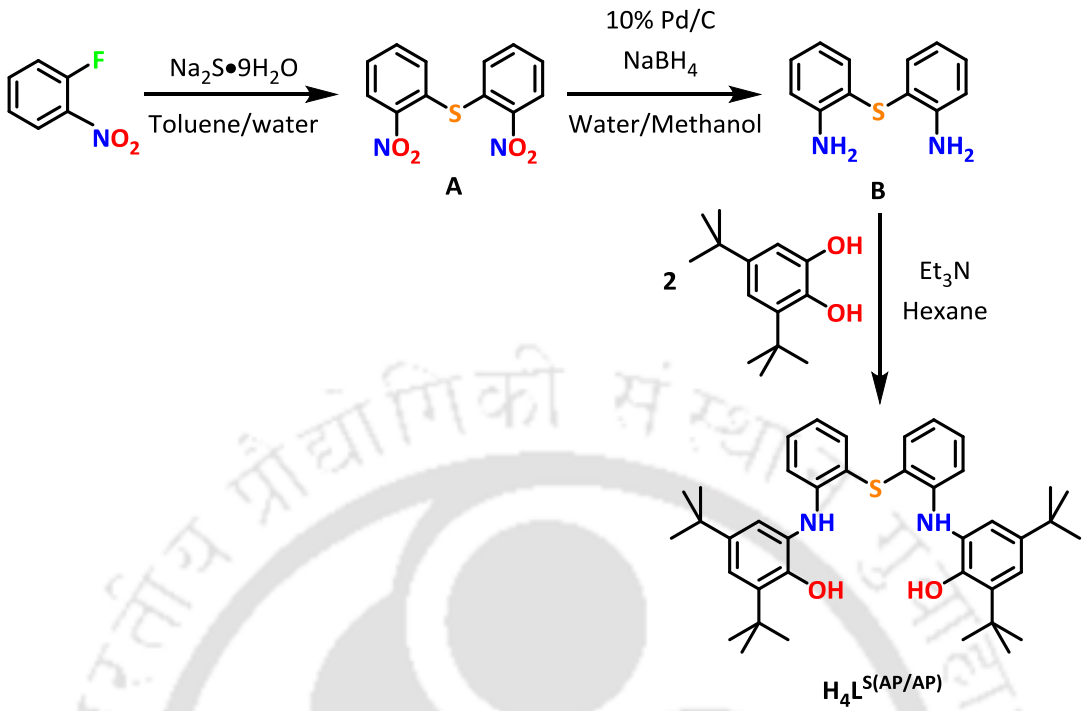

Scheme 6.2: *Synthetic route of ligand* $H_4L^{S(AP/AP)}$.

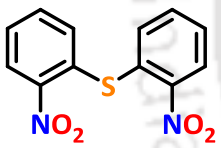

Step1: Synthesis of bis(o-nitrobenzene)sulfide; A. Bis(*o*–nitrobenzene) sulfide was synthesized by using a reported procedure (J.–Y. Liu *et al*., *J. Mol. Catal. A: Chem.*, 2006, **244**, 99). Despite using *o*–chloronitrobenzene, as reported, here we have used *o*–fluoronitrobenzene.

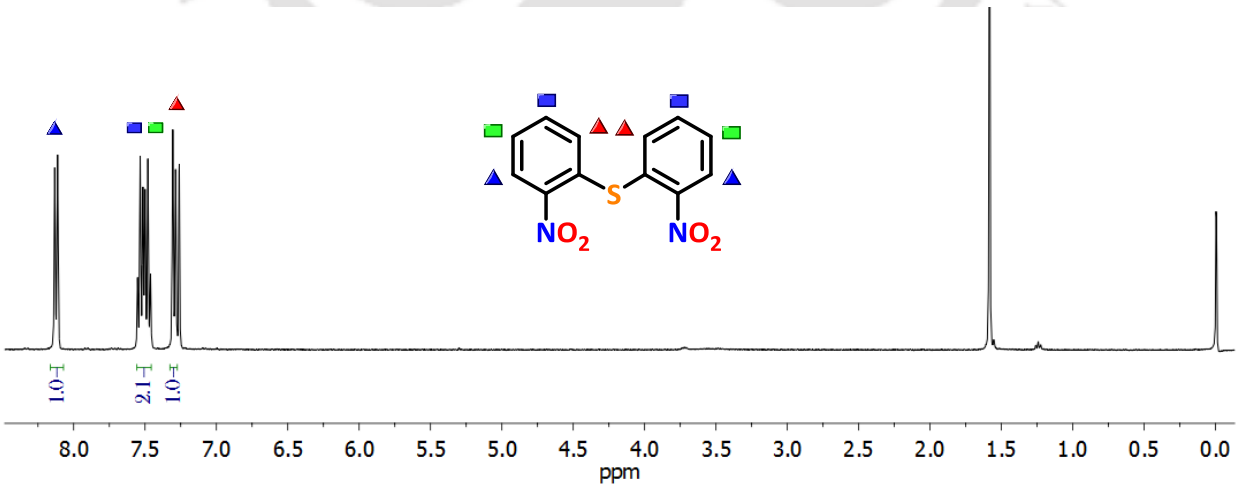

Figure 6.5: *^{1}H NMR of bis(o–nitrobenzene)sulfide;* ***(A).***

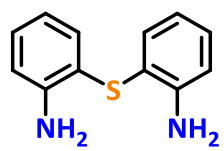

Step2: Synthesis of bis(o-aminophenyl)sulfide; B. To a suspension of finely grained bis(*o*–nitrobenzene) sulfide (0.658 g, 2.38 mmol) in a water and methanol mixture (7 : 3; 15 mL), 10% Pd–charcoal (22 mg) was added, followed by the addition of sodium borohydride (1.085 g, 28.56 mmol) under an Ar atmosphere at 0 °C. The suspension was stirred at room temperature (30 °C) for 15 minutes and then stirred at 50 °C overnight under an Ar atmosphere. The reaction mixture was then cooled to room temperature and filtered through a celite pad. The filtrate was extracted with CH_2Cl_2 (3 × 30 mL), and the combined organic layer was washed with water followed by brine and, finally, dried over anhydrous Na_2SO_4. The solvent was evaporated to afford a white solid.

Yield: 0.490 g, 95%.

FTIR (KBr pellet, cm^{-1}): 3457, 3417, 3357, 3340, 1611, 1584, 1570, 1477, 1446, 1315, 1289, 1255, 1157, 1138, 1030, 1018, 759, 754, 686, 675, 668, 540, 498, 464.

^{1}H NMR (399.85 MHz, $CDCl_3$): δ 7.21 (d, J = 7.6 Hz, 2H), 7.12–7.09 (m, 2H), 6.73–6.67 (m, 4H), 4.20 (s, 4H) ppm.

ESI–MS(CH_3CN) *m/z* for[$C_{12}H_{12}N_2S$+H]$^+$: Calcd, 217.08; found, 217.08.

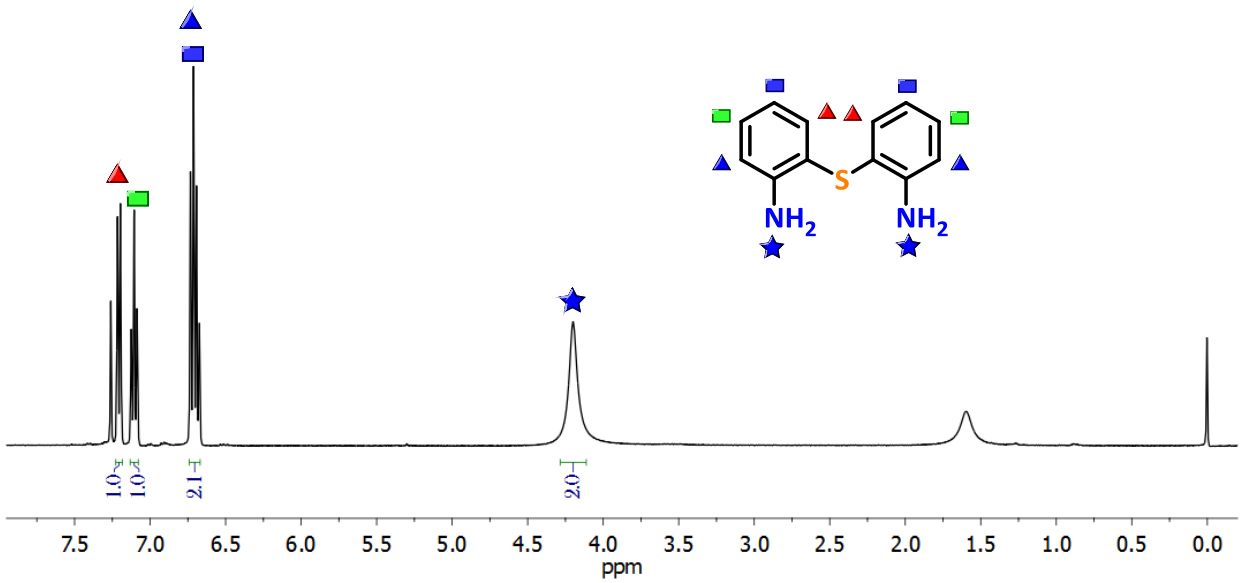

Figure 6.6: *^{1}H NMR of bis(o-aminophenyl)sulfide; (**B**).*

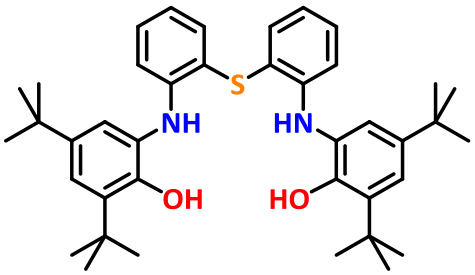

Step3: Synthesis of ligand $H_4L^{S(AP/AP)}$. To a suspension of bis(*o*–aminophenyl) sulfide (0.489 g, 2.26 mmol) in hexane (20 mL), 3,5–di–*tert*–butylcatechol (1.005 g, 4.52 mmol) was added, followed by the addition of Et_3N (0.05 mL). The reaction mixture was then refluxed for 30 minutes and then stirred at room temperature (30 °C) for 5 h. A white precipitate was obtained in due course. The solid was filtered, washed with hexane (20 mL), and dried under air.

Yield: 1.010 g, 71%.

FTIR(KBr pellet, cm^{-1}): 3434, 3358, 3335, 3061, 2961, 2906, 2868, 1602, 1587, 1574, 1492, 1472, 1446, 1421, 1391, 1380, 1362, 1310, 1264, 1227, 1203, 1158, 1116, 1054, 1035, 977, 882, 824, 808, 768, 750, 718, 679, 648, 636, 617, 560, 487.

^{1}H NMR(600.17 MHz, $CDCl_3$): δ 7.40–7.38 (m, 2H), 7.21 (d, J = 2.4 Hz, 2H), 7.16–7.14 (m, 2H), 6.84–6.82 (m, 2H), 6.79 (d, J = 1.8 Hz, 2H), 6.48 (d, J = 7.8 Hz, 2H), 6.09 (s, 2H), 5.90 (s, 2H), 1.41 (s, 18H), 1.20 (s, 18H) ppm.

^{13}C NMR (100.55 MHz, $CDCl_3$): δ 149.7, 147.2, 142.6, 135.7, 133.4, 130.0, 127.1, 122.7, 122.0, 120.3, 118.5, 114.8, 35.2, 34.5, 31.8, 29.7 ppm.

ESI-MS (+) m/z for $[C_{40}H_{52}N_2O_2S + H]^+$: Calcd, 625.38; found, 625.38.

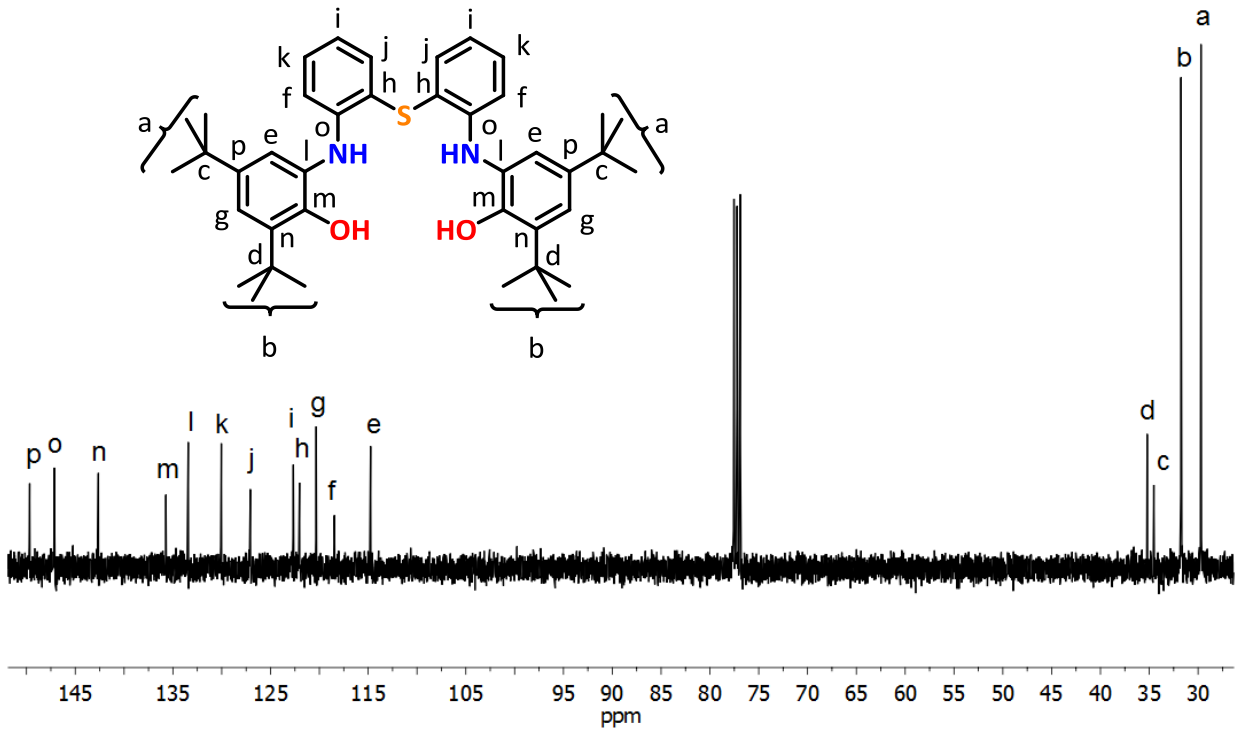

Figure 6.7: *^{13}C NMR of $H_4L^{S(AP/AP)}$.*

6.2.3: Synthesis of $H_4L^{Se(AP/AP)}$

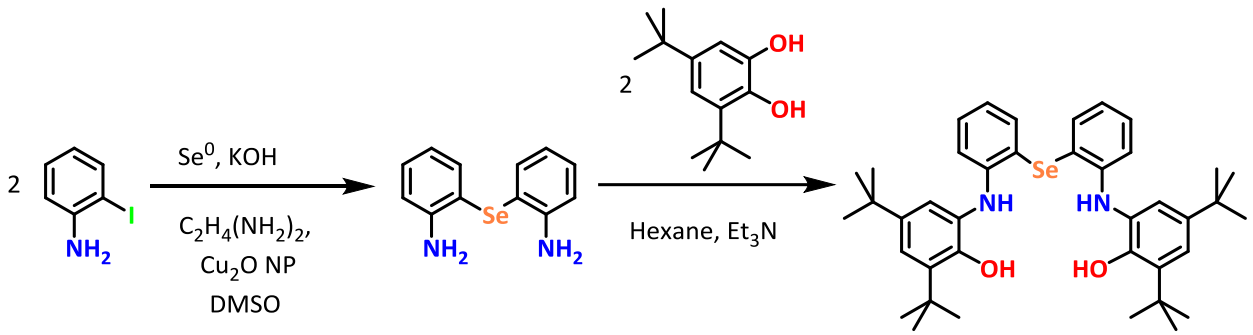

Scheme 6.3: *Synthetic route of ligand* $H_4L^{Se(AP/AP)}$.

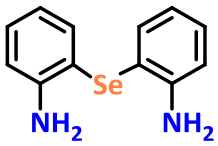

Step1: Synthesis of bis(o–aminophenyl)selenide. It was synthesized by a modified procdure.[1] A pressure tube was charged with 2–iodoaniline (0.876 g, 4.0 mmol), Se(0) (0.316 g, 4.0 mmol), Cu_2O–nano particle (0.064 g, 0.8mmol), ethylene diamine (54 μL, 0.8 mmol), KOH (0.449 g, 8.0 mmol) and DMSO (8 mL) under argon atmosphere. The reaction mixture was heated for 24 h at 120 °C. The reaction mixture was then allowed to cool and extracted with CH_2Cl_2. The organic layer was washed with brine, dried over anhydrous Na_2SO_4 and concentrated under vacuum. The residue was purified by column chromatography on silica gel with an eluent consisting of hexane and ethyl acetate (9:1) affording bis(*o*–aminophenyl)selenide.

Yield: 0.200 g, 38 %.

FTIR (KBr pellet, cm^{-1}): 3448, 3428, 3341, 3324, 3203, 3055, 3009, 2926, 2854, 1607, 1581, 1563, 1475, 1442, 1308, 1298, 1253, 1155, 1140, 1018, 754, 655, 530, 460, 434.

^{1}H NMR (399.85 MHz, $CDCl_3$): δ 7.38 (d, J = 7.6 Hz, 2H), 7.14–7.10 (m, 2H), 6.73 (d, J = 8.4 Hz, 2H), 6.67–6.64 (m, 2H), 4.18 (s, 4H) ppm.

^{13}C NMR (100.55 MHz, $CDCl_3$): δ 147.5, 135.6, 129.9, 119.4, 115.6, 114.4 ppm.

ESI–MS (+) *m/z* for $[C_{12}H_{12}N_2Se+H]^+$: Calcd, 265.03; found, 265.02.

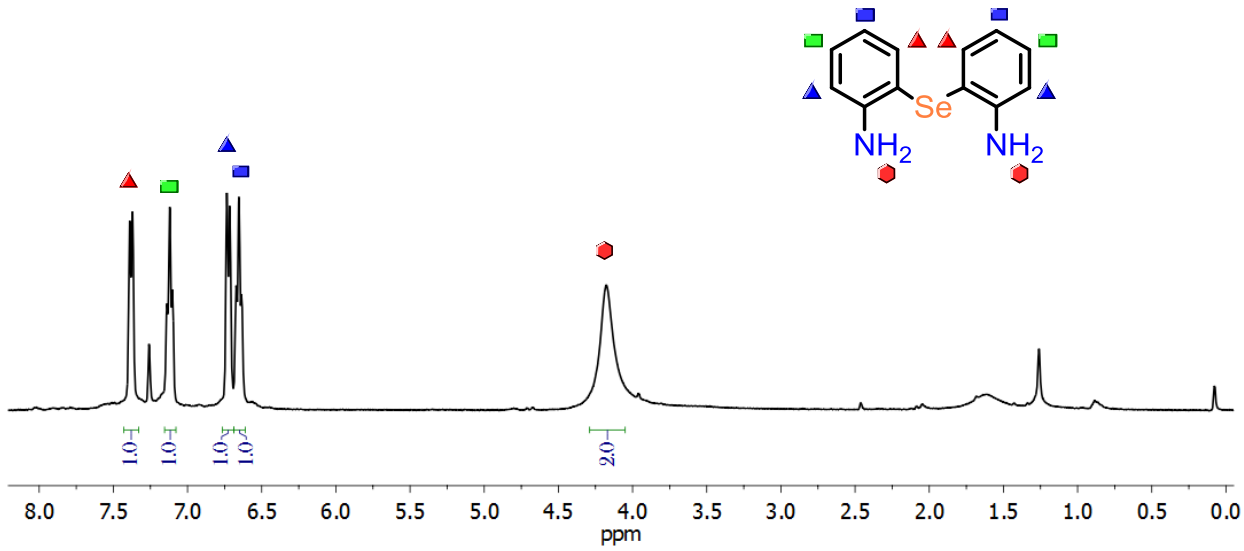

Figure 6.8: *^{1}H NMR of Bis(o–aminophenyl)selenide.*

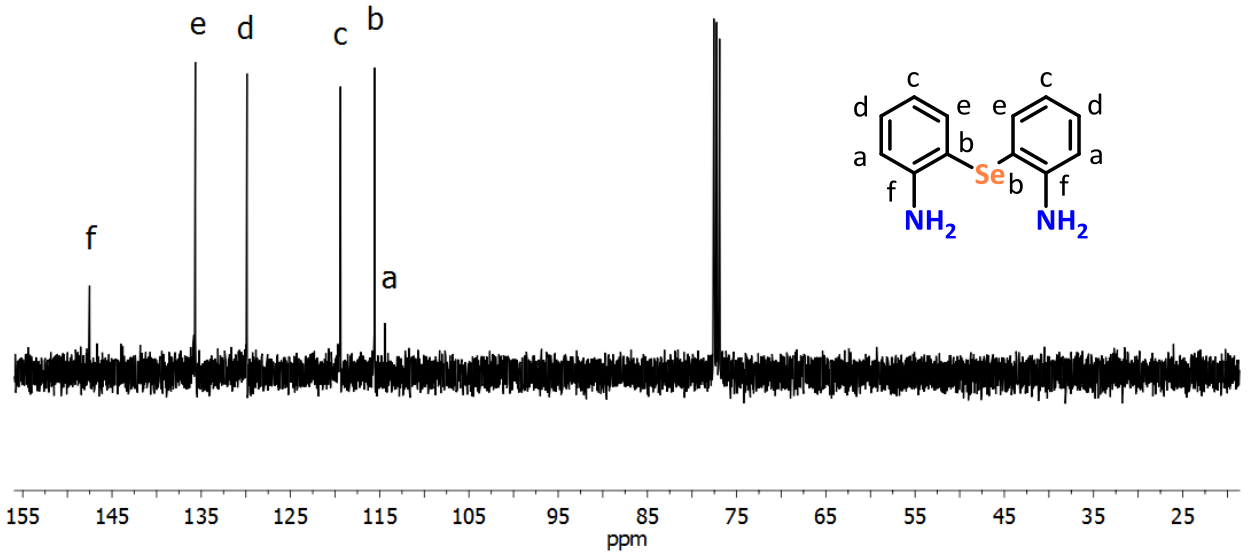

Figure 6.9: *^{13}C NMR of Bis(o–aminophenyl)selenide.*

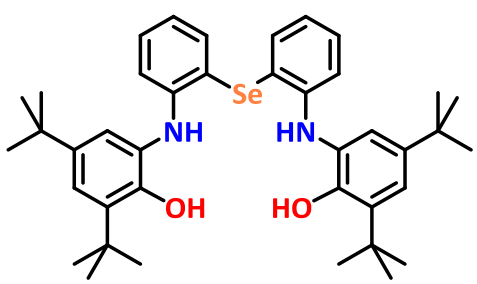

Step2: Synthesis of $H_4L^{Se(AP/AP)}$. To a mixture of bis(*o*–aminophenyl) selenide (0.380 g, 1.44 mmol) and 3,5–di–*tert*–butylcatechol (0.640 g, 2.88 mmol) in hexane (12 mL), Et_3N (0.01 mL) was added. The reaction mixture was then refluxed for 30 minutes and stirred at room temperature (30 °C) for 5 h. A white precipitate was obtained which was filtered, washed with hexane (20 mL) and dried.

Yield: 0.721 g, 75 %.

FTIR (KBr pellet, cm^{-1}): 3432, 3362, 3324, 3059, 2961, 2903, 2868, 1587, 1471, 1445, 1420, 1382, 1362, 1310, 1264, 1226, 1203, 1158, 881, 766, 750, 612, 463.

^{1}H NMR (399.853 MHz, $CDCl_3$): δ 7.58 (d, J =7.6 Hz, 2H), 7.20–7.14 (m, 4H), 6.80–6.77 (m, 2H), 6.70 (s, 2H), 6.45 (d, J =8.0 Hz, 2H), 6.04 (s, 2H), 5.84 (s, 2H), 1.40 (s, 18H), 1.18 (s, 18H), ppm.

^{13}C NMR (150.928 MHz, $CDCl_3$): δ 149.6, 147.8, 142.6, 135.7, 130.6, 127.3, 122.6, 122.0, 120.6, 115.8, 114.9, 35.2, 34.5, 31.8, 29.7 ppm.

ESI–MS (+) *m/z* for $[C_{40}H_{52}N_2O_2Se+H]^+$: Calcd, 673.33; found, 673.33.

ESI–MS (–) *m/z* for $[C_{40}H_{52}N_2O_2Se–H]^-$: Calcd, 671.32; found, 671.62.

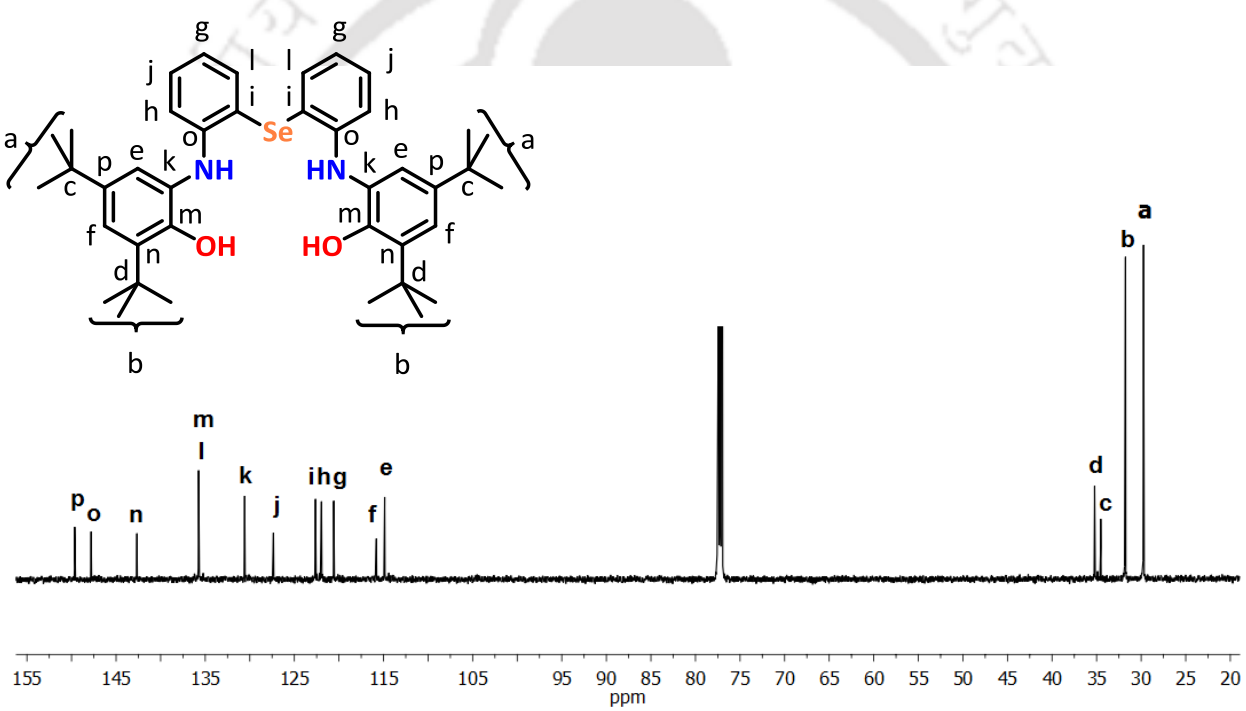

Figure 6.10: *^{13}C NMR spectrum of $H_4L^{Se(AP/AP)}$ with peak annotation.*

6.2.4: Synthesis of ligand $H_4L^{Te(AP/AP)}$

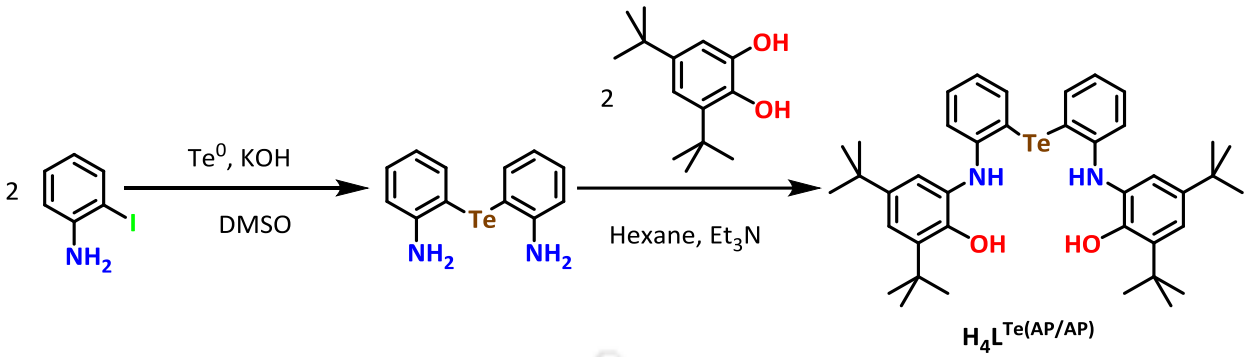

Scheme 6.4: *Synthetic route of* $H_4L^{Te(AP/AP)}$.

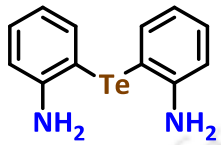

Step1: Synthesis of bis(o-aminophenyl)telluride. Dry DMSO (8 mL) was taken in a seal tube and degassed with argon. 2–iodoaniline (1.095 g, 5.0 mmol), Te^0 (0.638 g, 5.0 mmol) and KOH (0.561 g, 10.0 mmol) were taken in the tube and sealed the tube under Ar. The reaction mixture was heated in an oil bath at 110 °C and stirred at this temperature for 22 h. The mixture was allowed to cool, and treated with CH_2Cl_2 and H_2O. The extracted organic layer was washed with saturated NH_4Cl, brine solution and dried over anhydrous Na_2SO_4. On concentrating under vacuum, a brown residue was found and it was purified by column chromatography on silica gel with an eluent consisting of hexanes and ethyl acetate (9:1) to afford the bis(*o*–aminophenyl)telluride as faint brown solid.

Yield: 0.514 g, 66 %.

FTIR (KBr pellet, cm^{-1}): 3397, 3315, 3185, 3054, 1626, 1578, 1469, 1434, 1298, 1245, 1161, 1151, 1008, 854, 757, 686, 668, 642, 527, 463.

^{1}H NMR (600.174 MHz, $CDCl_3$): δ 7.66–7.64 (m, 2H), 7.16–7.13(m, 2H), 6.76–6.75(m, 2H), 6.60–6.57(m, 2H), 4.16 (s, 4H) ppm.

ESI–MS (+) *m/z* for $[C_{12}H_{12}TeN_2]^+$: Calcd, 314.00; found, 314.01.

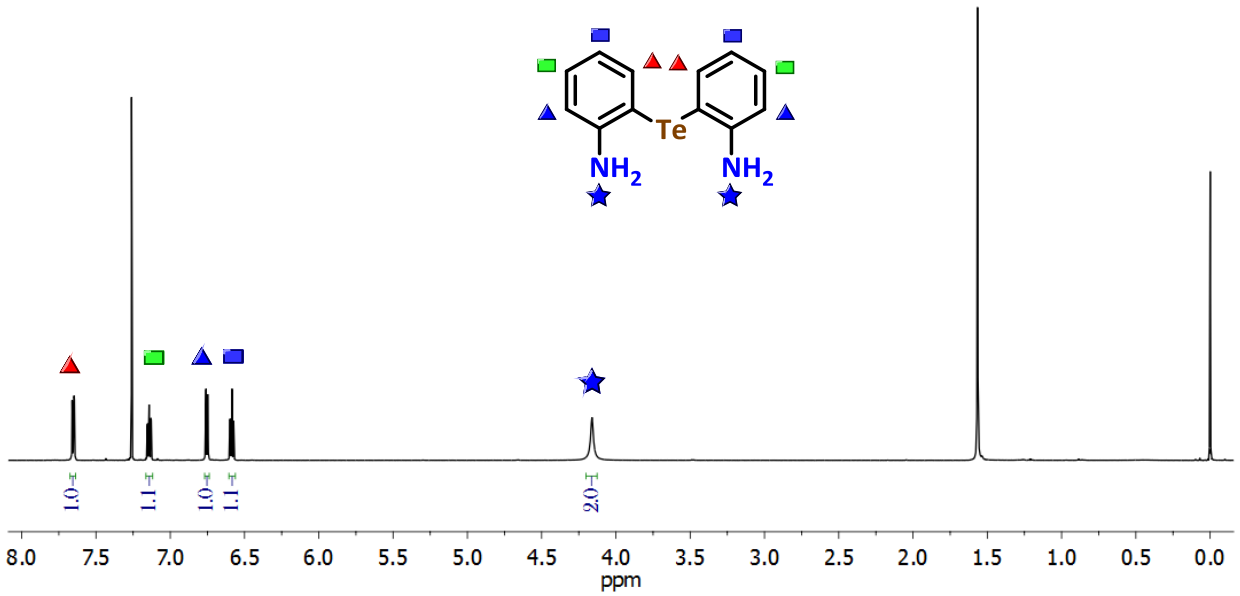

Figure 6.11: *^{1}H NMR of bis(o-aminophenyl)telluride.*

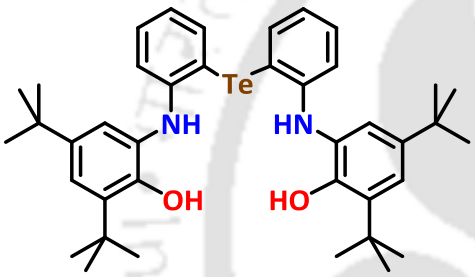

Step2: Synthesis of $H_4L^{Te(AP/AP)}$. To a suspension of bis(*o*-aminophenyl)telluride (0.312 g, 1.0mmol) in hexane (12 mL), 3,5–di–*tert*–butylcatechol (0.445 g, 1.0 mmol) was added. Et_3N (0.02 mL) was added to it and the reaction mixture was stirred for 5 h at room temperature. The resultant white product was collected through filtration and washed properly with hexane.

Yield: 0.525 g, 73 %.

FTIR (KBr pellet, cm^{-1}): 3410, 3343, 3060, 2958, 2906, 2868, 1599, 1579, 1470, 1440, 1419, 1391, 1363, 1341, 1309, 1291, 1265, 1254, 1222, 1202, 1157, 1026, 1046, 974, 877, 824, 807, 765, 747, 648, 633, 512, 449.

^{1}H NMR (600.174 MHz, $CDCl_3$): δ 7.82 (d, J = 7.2 Hz, 2H), 7.19–7.17 (m, 4H), 6.73–6.71(m, 2H), 6.68 (d, J = 2.4 Hz, 2H), 6.47 (d, J = 8.4 Hz, 2H), 5.98 (s, 2H), 5.70 (s, 2H), 1.40 (s, 18 H), 1.19 (s, 18H) ppm.

^{13}C NMR (100.54 MHz, $CDCl_3$): δ 149.6, 149.5, 142.6, 140.9, 135.7, 131.2, 127.8, 122.5, 121.8, 121.3, 114.5, 102.8, 35.2, 34.5, 31.8, 29.7 ppm.

ESI–MS (–) *m/z* for $[C_{40}H_{52}N_2O_2Te–H]^-$: Calcd, 721.2990; found, 721.5907.

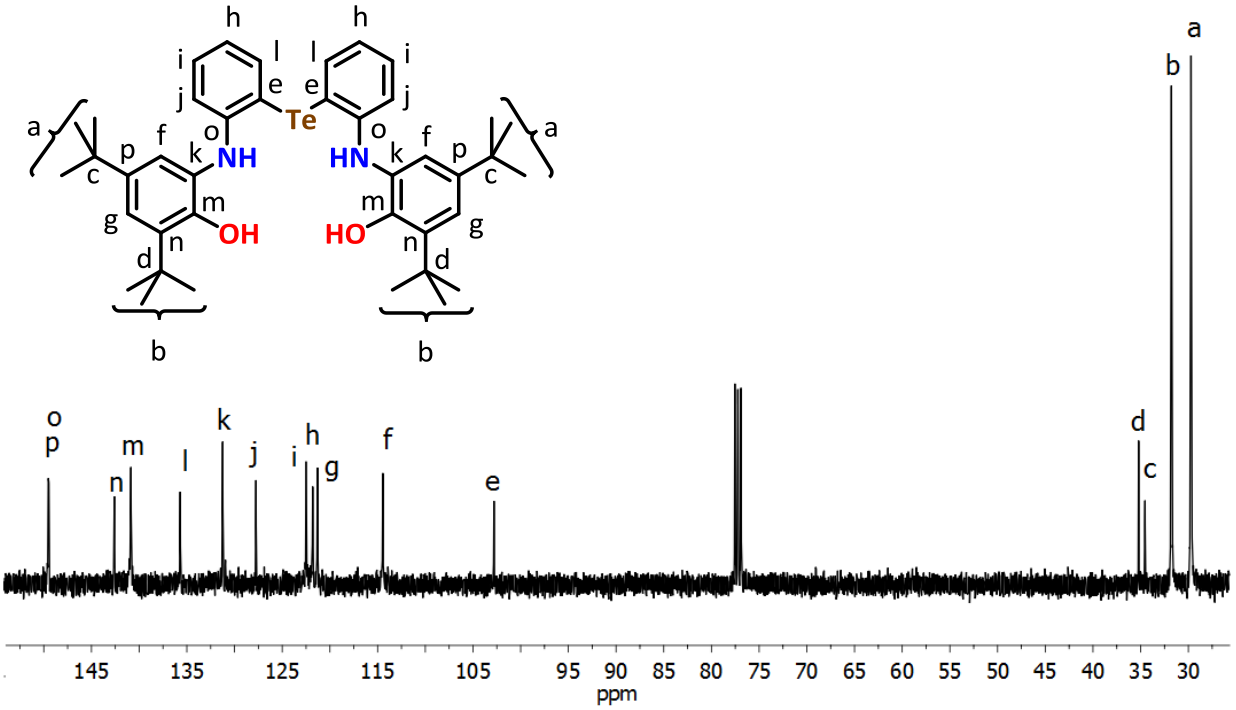

Figure 6.12: *^{13}H NMR of* $H_4L^{Te(AP/AP)}$.

6.2.5: Synthesis of ligand $H_2L^{AP(o–NO_2–OPh)}$

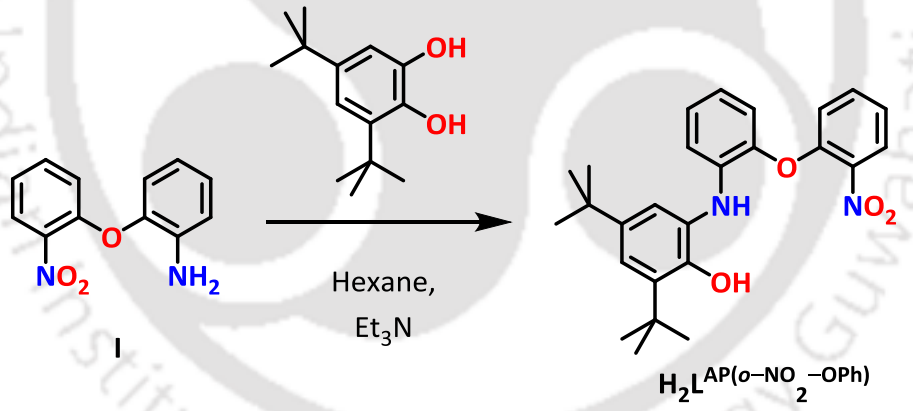

Scheme 6.5: *Synthetic route of* $H_2L^{AP(o–NO_2–OPh)}$.

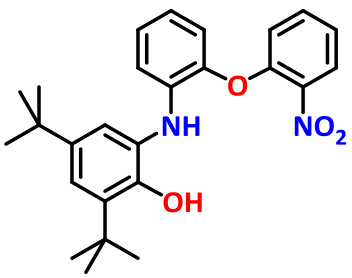

Synthesis of $H_2L^{AP(o–NO_2–OPh)}$**.** To a stirred solution of 2–(2–nitrophenoxy)aniline (2.798 g, 12.15 mmol) in hexane (20 mL), 3,5–di–*tert*–butylcatechol (2.701 g, 12.15 mmol) and Et_3N (0.02 ml) were added sequentially at room temperature (25 °C) under air. A reddish homogeneous solution was obtained on refluxing the reaction mixture for 14 h. Then it was allowed to attain room temperature and the stirring was continued for another 26 h. Pale yellow crude was obtained on evaporation of the solvent and the product was crystallized from hot methanol.

Yield: 3.87 g, 73%.

FTIR (KBr pellet, cm^{-1}): 3460, 3382, 3359, 2960, 2905, 2866, 1611, 1602, 1586, 1528, 1503, 1481, 1426, 1392, 1351, 1316, 1267, 1249, 1223, 1178, 1101, 1034, 978, 880, 796, 781, 749, 693, 568, 543.

^{1}H NMR (399.853 MHz, $CDCl_3$): δ 7.97 (dd, J = 8.4 Hz, J = 1.6 Hz, 1H), 7.57–7.51 (m, 1H), 7.23–7.19 (m, 2H), 7.10 (d, J = 8.0 Hz, 1H), 7.06–6.99 (m, 3H), 6.85–6.81 (m, 1H), 6.59–6.57 (m, 1H), 6.18 (s, 1H), 5.74 (s, 1H), 1.42 (s, 9H), 1.26 (s, 9H) ppm.

^{13}C NMR (100.542 MHz, $CDCl_3$): δ 151.0, 149.5, 142.6, 140.8, 139.2, 135.6, 134.5, 126.8, 126.5, 126.2, 123.2, 122.5, 122.0, 120.2, 119.7, 118.5, 115.7, 35.2, 34.6, 31.8, 29.7 ppm.

ESI-MS (+) m/z for $[C_{26}H_{30}N_2O_4+H]^+$: Calcd, 435.22; found, 435.23.

6.2.6: Synthesis of ligand $H_2L^{AP(o–NH_2–OPh)}$

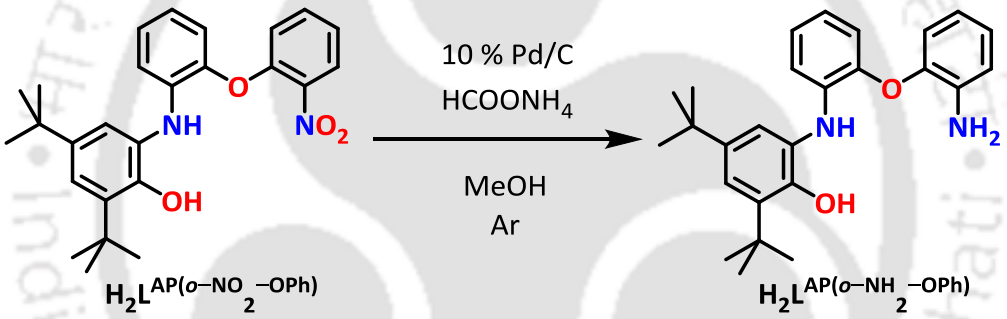

Scheme 6.6: *Synthetic route of* $H_2L^{AP(o–NH_2–OPh)}$.

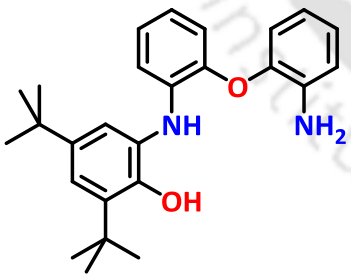

Synthesis of $H_2L^{AP(o–NH_2–OPh)}$. To a suspension of $H_2L^{AP(o–NO_2–OPh)}$ (1.847 g, 4.25 mmol) in degased methanol (30 mL), Pd/C (0.155 g) was added under Ar atmosphere at ice cold condition. After 10 minutes of stirring, ammonium formate (2.594 g, 41.15 mmol) was added to the mixture by maintaining the same condition. It was then allowed to attain room temperature and stirring was continued for 3 h 30 min. An amount of 15 mL water was added to it and the whole mixture was passed through a pad of celite. The filtrate was then extracted with CH_2Cl_2 (3×30 mL) and combined organic layer was washed with water, brine and finally dried over anhydrous Na_2SO_4. Solvent was evaporated to dryness and an off–white product was crystalized from hexane.

Yield: 1.495 g, 87 %.

FTIR (KBr pellet, cm^{-1}): 3448, 3421, 3368, 3074, 3038, 2959, 2907, 2867, 1621, 1604, 1584, 1501, 1479, 1460, 1422, 1392, 1360, 1325, 1303, 1266, 1240, 1225, 1201, 1102,1047, 883, 765, 739, 583.

^{1}H NMR (399.851 MHz, $CDCl_3$): δ 7.22 (d, J = 2.4 Hz, 1H), 7.00 (d, J = 2.4 Hz, 1H), 6.98–6.92 (m, 2H), 6.88–6.84 (m, 3H), 6.79–6.72 (m, 2H), 6.57–6.55 (m, 1H), 6.37 (s, 1H), 5.59 (s, 1H), 3.90 (s, 2H), 1.44 (s, 9H), 1.26 (s, 9H) ppm.

^{13}C NMR (150.928 MHz, $CDCl_3$): δ 149.8, 144.7, 143.9, 142.4, 138.4, 138.0, 135.6, 127.4, 124.7, 124.6, 122.3, 121.8, 119.8, 119.2, 118.2, 118.1, 116.8, 115.2, 35.2, 34.6, 31.8, 29.8 ppm.

ESI–MS (+) *m/z* for $[C_{26}H_{32}N_2O_2+H]^+$: Calcd, 405.2536 ; found, 405.2577.

6.2.7: General synthesis of complex $\{Cu_2[L^{Z(ISQ/ISQ)}]_2\}$ from ligand $H_4L^{Z(AP/AP)}$; where Z = O, S, Se and Te

To a 1:1 mixture of ligand $\mathbf{H_4L^{Z(AP/AP)}}$ (0.5 mmol) and $CuCl_2{\bullet}2H_2O$(0.086 g, 0.5 mmol)in CH_3CN (15 mL), Et_3N (0.2 mL) was added and stirred at room temperature for 5 h under air. The resultant green precipitate filtered and washed with CH_3CN.

Complex $\{Cu_2[L^{O(ISQ/ISQ)}]_2\}$; 2A.

Crude yield: 0.163 g, 49%.

FTIR (KBr pellet, cm^{-1}): 3066, 2954, 2905, 2868, 1574, 1486, 1464, 1445, 1386, 1359, 1335, 1255, 1243, 1220, 1202, 1175, 1110, 996, 894, 852, 743.

UV-Vis/NIR (CH_2Cl_2) λ_{max}, nm (ε, $M^{-1}cm^{-1}$): 1221(800), 769(5350), 545(4250), 394(7350).

ESI–MS (+) *m/z* for $[C_{40}H_{48}N_2O_3Cu]^+$: Calcd,667.31; found, 667.30.

Complex $\{Cu_2[L^{S(ISQ/ISQ)}]_2\}$; 2B.

Crude yield: 0.184 g, 54%.

FTIR (KBr pellet, cm^{-1}): 3055, 2955, 2905, 2868, 1575, 1515, 1467, 1433, 1386, 1358, 1335, 1266, 1250, 1203, 1180, 1030, 853, 743, 727, 645.

UV-Vis/NIR (CH_2Cl_2) λ_{max}, nm (ε, $M^{-1}cm^{-1}$): 1038(3850), 799(11850), 447(8650)

ESI–MS (+) *m/z* for $[C_{40}H_{48}N_2O_2SCu]^+$: Calcd, 683.28; found, 683.28.

Complex $\{Cu_2[L^{Se(ISQ/ISQ)}]_2\}$; 2C.

Yield: 0.150 g, 38%

FTIR (KBr pellet, cm^{-1}): 3053, 2956, 2905, 2868, 1585, 1571, 1528, 1515, 1466, 1432, 1419, 1386, 1334, 1263, 1250, 1202, 1179, 1027, 996, 852, 761, 743, 723.

UV-Vis/NIR (CH_2Cl_2) λ_{max}, nm (ε, $M^{-1}cm^{-1}$): 1094(3550), 810(9950), 457(8100), 363(23350).

ESI–MS (+) *m/z* for $[C_{40}H_{48}N_2O_2SeCu]^+$: Calcd, 731.23; found, 731.23.

Anal. Calcd for $C_{80}H_{96}Cu_2N_4O_4Se_2 \bullet CHCl_3$: C, 61.50; H, 6.18; N, 3.54. Found: C, 62.07; H, 6.15; N, 3.54 %.

Complex $\{Cu_2[L^{Te(ISQ/ISQ)}]_2\}$; 2D.

Crude yield: 0.165 g, 42%.

FTIR (KBr pellet, cm^{-1}): 3051, 2955, 2905, 2868, 1570, 1515, 1463, 1429, 1387, 1359, 1332, 1263, 1250, 1202, 1179, 1109, 1025, 995, 882, 853, 743, 720, 646.

UV-Vis/NIR (CH_2Cl_2) λ_{max}, nm (ε, $M^{-1}cm^{-1}$): 1079(4700), 816(10800), 622(9150), 473(9700).

ESI–MS (+) *m/z* for $[C_{40}H_{48}N_2O_2TeCu]^+$: Calcd,781.22; found, 781.22.

ESI–MS (+) *m/z* for $[C_{80}H_{96}N_4O_4Te_2Cu_2]^+$: Calcd, 1560.43; found, 1560.43.

6.2.8: Synthesis of $[CuL^{S(IBQ/ISQ)}Cl] \bullet 1CH_3CN$ (2E•1CH_3CN)

To a suspension of $H_4L^{S(AP/AP)}$ (0.287 g, 0.46 mmol) in CH_3CN (5 mL), $CuCl_2 \bullet 2H_2O$ (0.157 g, 0.92 mmol) and Et_3N (0.2 mL) were added sequentially. The resulting reaction mixture was stirred for 24 h at room temperature (30 °C) under air when the initially formed blue–green precipitate was gradually transformed to a brown solid. The thus formed brown precipitate was filtered and washed with CH_3CN (10 mL). Recrystallization of the solid from a CH_2Cl_2–CH_3CN (5 : 2) solvent mixture provided a cube-shaped crystalline solid suitable for single-crystal X-ray diffraction study. The solid was separated and washed with CH_3CN (5 mL).

Yield: 0.181 g, 52%.

FTIR (KBr pellet, cm^{-1}): 3443, 3252, 3050, 2956, 2908, 2869, 2252, 1640, 1618, 1589, 1504, 1465, 1430, 1379, 1335, 1310, 1271, 1250, 1204, 1025, 899, 765, 748.

ESI–MS (+) *m/z* for $[C_{40}H_{48}CuN_2O_2S]^+$: Calcd, 683.28; found, 683.28.

UV–Vis/NIR (CH_2Cl_2) λ_{max}, nm (ε, $M^{-1}cm^{-1}$): 1180(800), 940(1400), 800(2000), 720(2300), 475(7250), 388(12250).

Anal. Calcd for $C_{40}H_{48}ClCuN_2O_2S \bullet 1CH_3CN$: C, 66.37; H, 6.76; N, 5.53. Found: C, 66.29; H, 6.72; N, 5.39%.

6.2.9: Synthesis of $[Co^{II}(Cat\text{–}N\text{–}BQ)_2]$, 3A from Ligand $H_4L^{O(AP/AP)}$

$Co(ClO_4)_2 \bullet 6H_2O$ (0.366 g, 1.0 mmol) and Et_3N (0.4 mL) were added sequentially to a suspension of $H_4L^{O(AP/AP)}$ (0.608 g, 1.0 mmol) in CH_3CN (20 mL). A brown precipitate was observed initially within 10 min which turned black with time. After stirring for 7 h at room

temperature, the resulting precipitate was filtered and washed with acetonitrile. The solid was crystalized from a mixture of chloroform/acetonitrile (3:1) solution by slow evaporation process.

Yield: 0.204 g, 57 %; 0.161 g, 45 % (when $CoCl_2•6H_2O$ was used as the metal ion source).

FTIR (KBr pellet, cm^{-1}): 3060, 2951, 2906, 2867, 1592, 1523, 1479, 1451, 1400, 1384, 1367, 1322, 1310, 1289, 1261, 1202, 1173, 1145, 1130, 1099, 1022, 978, 903, 796, 741, 585, 532, 497.

ESI–MS (+) m/z for $[C_{40}H_{48}CoN_2O_4]^+$: Calcd, 679.29; found, 679.30.

UV–Vis/NIR (CH_2Cl_2, 300 K) λ_{max}, nm (ε, $M^{-1}cm^{-1}$): 1200(1200), 1001(6650), 762(14400), 688(13700), 511(11300), 428(14750), 387(25700).

Anal. Calcd for $C_{40}H_{48}N_2O_4Co•0.3CHCl_3$ [crystallized from chloroform/acetonitrile (3:1) solvent mixture]: C, 67.64; H, 6.80; N, 3.91.Found: C, 67.68; H, 7.00; N, 4.01.

Anal. Calcd for $C_{40}H_{48}N_2O_4Co•0.8CH_3CN$ [crystallized from a diethyl ether/acetonitrile (2:1) solvent mixture]: C, 70.12; H, 7.13; N, 5.50. Found: C, 71.71; H, 7.00; N, 5.52.

Anal. Calcd for $C_{40}H_{48}N_2O_4Co$ (crystalized from toluene): C, 70.68; H, 7.12; N, 4.12. Found: C, 70.03; H, 6.99; N, 4.23.

6.2.10: Synthesis of intermediate A from Ligand $H_4L^{O(AP/AP)}$

To a suspension of ligand $\mathbf{H_4L^{O(AP/AP)}}$ (0.304 g, 0.5 mmol) in CH_3CN (15 mL), $CoCl_2•6H_2O$ (0.118 g, 0.5 mmol) and Et_3N (0.2 mL) were added sequentially under air. The reaction mixture was allowed to stir at room temperature for 10 min. The precipitate was filtered and washed with acetonitrile. The green crude (**A**) was an intermediate and the structural determination was not possible due to the transformation of intermediate to complex **3A** in solution.

Crude yield: 0.166 g, 52%.

FTIR (KBr pellet, cm^{-1}): 3368, 324, 3068, 2956, 2906, 2869, 1598, 1582, 1482, 1448, 1424, 1390, 1360, 1319, 1255, 1220, 1176, 1106, 1031, 746.

ESI–MS (+) *m/z* for $[C_{80}H_{98}N_4O_6Co]^+$: Calcd,1269.68; found, 1269.68.

6.2.11: Synthesis of $\{Co_2[L^{S(ISQ/ISQ)}]_2Cl_2\}$,3B from Ligand $H_4L^{S(AP/AP)}$

To a suspension of $\mathbf{H_4L^{S(AP/AP)}}$ (0.188 g, 0.30 mmol) in CH_3CN (10 mL), $CoCl_2•6H_2O$ (0.072 g, 0.30 mmol) and Et_3N (0.10 mL) were added sequentially under air. The reaction mixture was refluxed for 2 h and the reaction mixture was allowed to stir at room temperature for overnight. The resulting precipitate was filtered and washed with CH_3CN. The solid was

crystalized from a mixture of dichloromethane/acetonitrile (4:1) solution by slow evaporation techniques.

Yield: 0.118 g, 53 %.

FTIR (KBr pellet, cm^{-1}): 3429, 3181, 3058, 2954, 2904, 2867, 1586, 1579, 1524, 1478, 1460, 1377, 1363, 1311, 1260, 1250, 1203, 1180, 1098, 1032, 999, 744.

^{1}H NMR (399.85 MHz, $CDCl_3$): δ 8.22 (s, 4H), 8.04 (d, J = 7.6 Hz, 4H), 7.45–7.41 (m, 4H), 7.30–7.26 (m, 8H), 7.18 (d, J = 7.6 Hz, 4H), 1.15 (s, 36H), 0.75 (s, 36H) ppm.

ESI–MS (+) *m/z* for $[C_{40}H_{48}CoN_2O_2S]^+$: Calcd, 679.2768; found, 679.3490. **ESI–MS (+) *m/z* for $[C_{80}H_{96}Co_2N_4O_4S_2Cl]^+$:** Calcd, 1393.5225; found, 1393.7194.

UV–Vis/NIR (CH_2Cl_2) λ_{max}, nm (ε, M^{-1} cm^{-1}): 842(25300), 655(30100), 573(22700), 365(17200).

Anal.Calcd for $C_{80}H_{96}N_4O_4S_2Co_2Cl_2$•0.1$CH_2Cl_2$: C, 66.85; H, 6.74; N, 3.89. Found: C, 66.83; H, 6.62; N, 4.08.

6.2.12: Synthesis of $\{Co_2[L^{Te(ISQ/ISQ)}]_2Cl_2\}$,3C from Ligand $H_4L^{Te(AP/AP)}$

To a suspension of $\mathbf{H_4L^{Te(AP/AP)}}$ (0.180 g, 0.25 mmol) in CH_3CN (10 mL), $CoCl_2$•$6H_2O$ (0.072 g, 0.30 mmol) and Et_3N (0.10 mL) were added sequentially under air. The reaction mixture was refluxed for 2 h and the reaction mixture was allowed to stir at room temperature for overnight. The resulting precipitate was filtered and washed with CH_3CN. The solid was crystalized from a mixture of dichloromethane/acetonitrile (4:1) solution by slow evaporation techniques.

Yield: 0.035 g, 14 %.

FTIR (KBr pellet, cm^{-1}): 3056, 2955, 2906, 2867, 1589, 1572, 1523, 1478, 1465, 1451, 1395, 1377, 1363, 1309, 1269, 1250, 1202, 1178, 1100, 1025, 999, 743.

^{1}H NMR (399.85 MHz, $CDCl_3$): δ 8.19 (s, 4H), 8.01 (d, J = 8.0 Hz, 4H), 7.49 (d, J = 8.0 Hz, 4H), 7.37–7.34 (m, 8H), 7.26 (s, 4H), 1.14 (s, 36H), 0.82 (s, 36H) ppm.

ESI–MS (+) *m/z* for $[C_{80}H_{96}Co_2N_4O_4Te_2Cl]^+$: Calcd, 1587.38; found, 1587.16.

UV–Vis/NIR (CH_2Cl_2) λ_{max}, nm (ε, M^{-1} cm^{-1}): 909(12350), 834(10800), 657(24700), 498(8300).

Anal. Calcd for $C_{80}H_{96}N_4O_4Te_2Co_2Cl_2$•1.8$CHCl_3$: C, 53.50; H, 5.37; N, 3.05. Found: C, 53.60; H, 5.35; N, 3.12

6.2.13: Synthesis of complex 3D from Ligand $H_4L^{S(AP/AP)}$

To a suspension of $\mathbf{H_4L^{S(AP/AP)}}$ (0.156 g, 0.25 mmol) in CH_3CN (10 mL), $Co(ClO_4)_2 \bullet 6H_2O$ (0.092 g, 0.25mmol) and Et_3N (0.15 mL) were added sequentially under air. The reaction mixture was allowed to stir at room temperature for 16 h. The resulting precipitate was filtered and washed with CH_3CN. The solid was crystalized from a mixture of diethyl ether/acetonitrile (3:1) solution by slow evaporation techniques.

Yield: 0.49 g, 30 %.

FTIR (KBr pellet, cm^{-1}): 3163, 3056, 2957, 2906, 2868, 1585, 1524, 1480, 1456, 1362, 1299, 1261, 1201, 1178, 1104, 1062, 1031, 997, 913, 856, 743.

UV-Vis/NIR (CH_2Cl_2) λ_{max}, nm (ε, M^{-1} cm^{-1}): 840(35000), 575(31500), 365(16200).

ESI–MS (+) *m/z* for $[C_{120}H_{146}Co_2N_6O_6S_3+H]^+$: Calcd, 1982.92; found, 1982.98.

6.2.14: Synthesis of $\{Fe[L^{ISQ(o\text{-}NO_2\text{-}OPh)}]_2Cl\}$, 4A

To a solution of ligand $\mathbf{H_2L^{AP(o–NO_2–OPh)}}$ (0.218 g, 0.5 mmol) in acetonitrile (5 mL), anhydrous $FeCl_3$ (0.082 g, 0.5 mmol) was added at room temperature. Addition of Et_3N (0.1 mL) to the stirred solution caused an immediate green coloration. The reaction mixture was stirred at room temperature for 3 h. During the period a green solid was precipitate out. The precipitate was filtered out and washed with acetonitrile. Suitable X–ray quality crystal was obtained from a 2:1 mixture of dichloromethane and acetonitrile.

Yield: 0.123 g, 52 %.

FTIR (KBr pellet, cm^{-1}): 3075, 2954, 2906, 2869, 1608, 1585, 1525, 1480, 1447, 1348, 1246, 1198, 1103, 994, 862, 774, 763, 483.

UV-Vis/NIR (CH_2Cl_2) λ_{max}, nm (ε, M^{-1} cm^{-1}): 1040(750), 755(9900), 450(9350).

ESI–MS (+) *m/z* for $[C_{52}H_{56}FeN_4O_8]^+$: Calcd, 920.35; found, 920.35.

6.2.15: Synthesis of $\{Ni[L^{ISQ(o\text{-}NO_2\text{-}OPh)}]_2\}$, 4B

A solution of ligand $\mathbf{H_2L^{AP(o–NO_2–OPh)}}$ (0.110 g, 0.25 mmol) with $NiCl_2 \bullet 6H_2O$ (0.060 g, 0.25mmol) and Et_3N (0.05 mL) was treated at reflux condition for 12 h in CH_3CN (12 mL). After overnight stirring at room temperature, the green precipitate was filtered and washed with CH_3CN. Crystals suitable for single crystal X–ray diffraction analysis were obtained from a $CHCl_3/CH_3CN$ (3:1) solvent mixture.

Yield: 0.20 g, 18%.

FTIR (KBr pellet, cm^{-1}): 3071, 2955, 2905, 2868, 1607, 1588, 1529, 1476, 1450, 1361, 1325, 1271, 1256, 1236, 1202, 1173, 1107, 766, 744, 736.

UV–Vis/NIR (CH_2Cl_2) λ_{max}, nm (ε, M^{-1} cm^{-1}): 917(31750), 728(3900), 605(1900), 461 (2550), 296(25200).

ESI–MS (+) *m/z* for $[C_{52}H_{56}NiN_4O_8+H]^+$: Calcd, 923.35; found, 923.35.

Anal. Calcd for $C_{52}H_{56}NiN_4O_8$: C, 67.613; H, 6.111; N, 6.065. Found: C, 66.831; H, 6.118; N, 6.156.

6.2.16: Synthesis of {Cu[$L^{ISQ(o\text{-}NO_2\text{-}OPh)}$]$_2$}, 4C

$CuCl_2$•$2H_2O$ (0.022 g, 0.125 mmol) was added to a stirred solution of ligand $H_2L^{AP(o–NO_2–OPh)}$ (0.109 g, 0.25 mmol) in CH_3CN (10 mL) at room temperature under air. To the solution Et_3N (0.05 mL) was added and the stirring was continued for 5 h. During the period, a green solid was precipitated out. The precipitate was filtered and washed with CH_3CN (10 mL). Recrystallization of the solid from a CH_2Cl_2/CH_3CN (10:1) solvent mixture provided green crystals suitable for single crystal X–ray diffraction analysis.

Yield: 0.079 g, 68%.

FTIR (KBr pellet, cm^{-1}): 3072, 2956, 2906, 2870, 1607, 1588, 1529, 1478, 1462, 1448, 1433, 1419, 1353, 1335, 1269, 1256, 1244, 1230, 1101, 861, 850, 764, 737.

ESI-MS (+) m/z for $[C_{52}H_{56}N_4O_8Cu]^+$: Calcd, 927.35; found, 927.47.

UV–Vis/NIR (CH_2Cl_2) λ_{max}, nm (ε, $M^{-1}cm^{-1}$): 1049(1850), 812(5700), 431(3900), 308(22 400).

Anal. Calcd for $C_{52}H_{56}CuN_4O_8$: C, 67.26; H, 6.08; N, 6.03. Found: C, 66.94; H, 6.10; N, 6.18.

6.2.17: Synthesis of {Cu[$L^{IBQ(o\text{-}NO_2\text{-}OPh)}$]$_2$$Cl_2$}, 4D

To a solution of ligand $H_2L^{AP(o–NO_2–OPh)}$ (0.217 g, 0.5 mmol) in CH_3CN (10 mL), $CuCl_2$•$2H_2O$ (0.171 g, 1.0 mmol) was added at room temperature under air. Addition of Et_3N (0.1 mL) to the stirred solution caused a green precipitation. It changed to brown within 30 min of stirring. The stirring was continued for further 1.5 h. To the mixture, dichloromethane (20 mL) was added and the solution was then filtered through a Whatman filter paper. Evaporation of the solvent under reduced pressure yielded a brown solid, which was washed with CH_3CN (5 mL). The residue was then dissolved in a 2:1 CH_2Cl_2/hexane solvent mixture. Slow evaporation of the solvent mixture provided suitable crystals for single crystal X-ray diffraction analysis.

Yield: 0.098 g, 39%. 0.116 g, 46% (when EtOH was used as a solvent in place of CH_3CN).

FTIR (KBr pellet, cm^{-1}): 3070, 3037, 2964, 2938, 2910, 2870, 1656, 1622, 1606, 1580, 1526, 1478, 1447, 1381, 1354, 1307, 1247, 1217, 1196, 1108, 902, 888, 864, 854, 791, 776, 759, 747, 467.

ESI-MS (+) m/z for $[C_{52}H_{56}N_4O_8Cu]^+$: Calcd, 927.35; found, 927.35.

UV–Vis/NIR (CH_2Cl_2) λ_{max}, nm (ε, $M^{-1}cm^{-1}$): 650(850), 485(6500), 425(7650), 305(14 350).

Effective magnetic moment (μ_{eff}) at 25 °C: 2.05 μ_B (Evan's method).

Anal. Calcd for $C_{52}H_{56}Cl_2CuN_4O_8 \cdot 0.33C_6H_{14}$: C, 63.15; H, 5.96; N, 5.46. Found: C, 64.01; H, 6.11; N, 5.87.

6.2.18: Synthesis of {Cu[L^{IBQ}]$_2$}, 4E

To a stirred solution of ligand $\mathbf{H_2L^{AP}}$ (0.074 g, 0.25 mmol) in CH_3CN (10 mL), $CuCl_2 \cdot 2H_2O$ (0.86 g, 0.5 mmol) and Et_3N (0.05 mL) were added at room temperature under air. A green precipitate appeared in due course. The precipitate changed to brown within 30 min and the stirring was further continued for 1.5 h. The thus formed precipitate was filtered and washed with CH_3CN (5 mL). Crystals suitable for single crystal X-ray diffraction analysis were grown by slow evaporation of a 2:1 CH_2Cl_2/hexane solvent mixture.

Yield: 0.066 g, 65%.

Alternative Procedure: To a stirred solution of ligand $\mathbf{H_2L^{AP}}$ (0.150 g, 0.5 mmol) in CH_3CN (10 mL), $CuCl_2 \cdot 2H_2O$ (0.043 g, 0.25 mmol) was added at room temperature under air. Addition of Et_3N (0.10 mL) to the solution caused a green precipitation and the stirring was continued for 1 h. The precipitate was filtered and washed with CH_3CN (10 mL). Yield: 0.124 g, 0.19 mmol, 76%. The green precipitate was taken in CH_3CN (10 mL) and $CuCl_2 \cdot 2H_2O$ (0.099 g, 0.58 mmol) was added at room temperature under air. The reaction mixture was stirred for 1.5 h. A brown precipitate appeared in due course. The precipitate was filtered and washed with CH_3CN (5 mL). Crystals suitable for single crystal X–ray diffraction analysis were grown by the slow evaporation of a 2:1 CH_2Cl_2/hexane solvent mixture.

Yield: 0.134 g, 89% (with respect to the green precipitate).

FTIR (KBr pellet, cm^{-1}): 3080, 3065, 2967, 2954, 2929, 2912, 2869, 1651, 1622, 1591, 1580, 1537, 1482, 1451, 1378, 1368, 1305, 1270, 1252, 1210, 1026, 976, 900, 804, 764, 737, 699.

ESI-MS (+) m/z for $[C_{40}H_{50}CuN_2O_2]^+$: Calcd, 653.33; found, 653.32.

UV–Vis/NIR (CH_2Cl_2) λ_{max}, nm (ε, $M^{-1}cm^{-1}$): 650(400), 440(9350), 295(17200).

Effective magnetic moment (μ_{eff}) at 25 °C: 1.95 μ_B (Evan's method).

Anal. Calcd for $C_{41}H_{52}Cl_4CuN_2O_2$: C, 60.78; H, 6.47; N, 3.46. Found: C, 61.02; H, 6.44; N, 3.37.

6.2.19: Formation of H_2 gas and regeneration of $Cu(L^{ISQ})_2$ from complex $\{Cu[L^{IBQ}]_2\}$, 4E

To a mixture of complex **4E**•CH_2Cl_2 (0.122 g, 0.15 mmol) and $NaBH_4$ (0.026 g, 0.75 mmol), dry acetonitrile (5 mL) was added under a N2 atmosphere. Bubbles of H_2 gas evolved immediately and the brown precipitate turned to a green precipitate. The generation of H_2 gas has been confirmed by using a TCD gas chromatographic analyzer (BRUKER 450 GC). Water (5 mL) was added to the reaction mixture and was stirred for 15 min at room temperature under air. The resultant green precipitate was filtered and washed with CH_3CN and recrystallized from a 5:1 CH_2Cl_2 : CH_3CN solution mixture.

The yield of $Cu(L^{ISQ})_2$ was 0.076 g, 78%.

6.2.20: Synthesis of $\{Co[L^{ISQ(o\text{-}NH_2\text{-}OPh)}]_2\}[ClO_4]$; 5A

To a solution of ligand $\mathbf{H_2L^{AP(o–NH_2–OPh)}}$ (0.101 g, 0.25 mmol) in CH_3CN (8 mL), $Co(ClO_4)$•$6H_2O$ (0.46 g, 0.12 mmol) and Et_3N (0.05 mL) were added sequentially under air. The reaction mixture was stirred for 3 h. The resultant green precipitate was collected by filtration and washed with cold CH_3CN (2 mL). Suitable crystals for X–ray diffraction analysis were obtained from a solution of CH_3CN by slow evaporation techniques.

Yield: 0.040 g, 33%.

FTIR (KBr pellet, cm^{-1}): 3447, 3356, 3319, 3252, 3074, 2964, 2906, 2868, 1619, 1576, 1498, 1480, 1461, 1364, 1308, 1255, 1210, 1097, 1031, 1000, 760, 750.

UV-Vis/NIR (CH_2Cl_2) λ_{max}, nm (ε, $M^{-1}cm^{-1}$): 924(14400), 824(9150), 614(12750), 352(11350).

ESI–MS (+) *m/z* for $[C_{52}H_{60}N_4O_4Co]^+$: Calcd, 863.39; found, 863.38.

6.2.21: Synthesis of $\{Ni[L^{ISQ(o\text{-}NH_2\text{-}OPh)}]_2\}$; 5B

A solution of ligand $\mathbf{H_2L^{AP(o–NH_2–OPh)}}$ (0.405 g, 1 mmol) with $Ni(ClO_4)_2$•$6H_2O$ (0.183 g, 0.5 mmol) and Et_3N (0.2 mL) was stirred for 3 h in CH_3CN (12 mL) under air. Thus resultant green precipitate was filtered and washed with CH_3CN. Crystals suitable for single crystal X–ray diffraction analysis were obtained from a CH_2Cl_2/CH_3CN (3:1) solvent mixture.

Yield: 0.270 g, 63%.

FTIR (KBr pellet, cm^{-1}): 3473, 3378, 3065, 2956, 2905, 2865, 1620, 1578, 1504, 1482, 1457, 1448, 1378, 1359, 1318, 1290, 1259, 1230, 1221, 1200, 1172, 1109, 1031, 1002, 921, 750, 739, 670, 538.

UV-Vis/NIR (CH_2Cl_2) λ_{max}, nm (ε, $M^{-1}cm^{-1}$): 908(29150), 728(4050), 593(2150), 293(25450).

ESI–MS (+) *m/z* for $[C_{52}H_{60}N_4O_4Ni]^+$: Calcd, 862.39; found, 862.38.

Anal. Calcd for $C_{52}H_{60}N_4O_4Ni$: C, 72.31; H, 7.00; N, 6.49. Found: C, 71.94; H, 7.09; N, 6.80.

6.2.22: Synthesis of {Ni[$L^{IBQ(o\text{-}NH_2\text{-}OPh)}$]$_2$}2[$PF_6$]; 5C

To a homogeneous solution of complex **5B** (0.270 g, 0.31 mmol) in CH_2Cl_2 (15 mL), fine–grained ferrocenium hexafluorophosphate (0.218 g, 0.66 mmol) was added and the reaction mixture was allowed to stir at room temperature for 3 h. The solvent was evaporated the crude was washed with hot hexane (3×10 mL). Crystal suitable for X–ray diffraction analysis was obtained from a 3:1 dichloromethane and hexane solvent mixture.

Yield: 0.300 g (Crude), 73%.

FTIR (KBr pellet, cm^{-1}): 3346, 3291, 2966, 2908, 2873, 1608, 1579, 1531, 1498, 1478, 1388, 1369, 1319, 1253, 1199, 1105, 1083, 1030, 844, 794, 764, 752, 739, 558.

UV-Vis/NIR (CH_2Cl_2) λ_{max}, nm (ε, $M^{-1}cm^{-1}$): 700(800), 515(6150), 382(8650), 264(20500).

6.2.23: Synthesis of {Cu[$L^{ISQ(o\text{-}NH_2\text{-}OPh)}$]$_2$}; 5D

To a stirred solution of $H_2L^{AP(o-NH_2-OPh)}$ (0.405 g, 1.0 mmol) in CH_3CN (20 mL), $CuCl_2$•$2H_2O$ (0.086 g, 0.5 mmol) or $Cu(ClO_4)_2$•$6H_2O$ (0.166 g, 0.5 mmol) was added. The resultant red solution turned to green on adding of 0.4 mL Et_3N. The green precipitate was filtered after 3 h of stirring and washed with acetonitrile. Crystalline solid suitable for single crystal X–ray analyzer was obtained from 3:1 mixture of dichloromethane and acetonitrile solvents.

Yield: 0.136 g, 30 %; 0.298 g, 66 % (crystalized from 2:1 diethyl ether and acetonitrile).

FTIR (KBr pellet, cm^{-1}): 3437, 3388, 3348, 3302, 3057, 2956, 2905, 2867, 2254, 1617, 1581, 1499, 1483, 1465, 1437, 1387, 1356, 1333, 1266, 1252, 1238, 1214, 1200, 1176, 1101, 1029, 915, 890, 851, 788, 744.

UV–Vis/NIR (CH_2Cl_2) λ_{max}, nm (ε, $M^{-1}cm^{-1}$): 1050(2350), 790(7500), 457(5350), 359 (15150), 293 (29150).

ESI–MS (+) *m/z* for $[C_{52}H_{60}CuN_4O_4]^+$: Calcd, 867.40; found, 867.40.

Anal. Calcd for $C_{52}H_{60}N_4O_4Cu$•CH_3CN: C, 71.30; H, 6.98; N, 7.70. Found: C, 71.61; H, 6.94; N, 7.26.

Appendices

1. Bond length parameter of optimized geometry
2. Crystallographic data

1. Bond length parameter of optimized geometry (Complex 1E)

Bond Type	Bond Length in Å (Experimental)	Bond Length in Å (Calculated)
Cu1–O1	1.967(2)	1.971
Cu1–N1	1.973(3)	2.059
Cu1–N2	2.108(2)	2.035
Cu1–Cl1	2.219(1)	2.296
Cu1–O2	2.418(2)	2.177
S1–C13	1.774(3)	1.787
S1–C12	1.776(3)	1.795
O1–C2	1.284(4)	1.272
N1–C1	1.354(3)	1.331
N1–C7	1.405(4)	1.405
O2–C24	1.229(3)	1.250
N2–C19	1.303(4)	1.323
N2–C18	1.432(4)	1.414
C1–C6	1.415(4)	1.429
C1–C2	1.443(4)	1.474
C21–C20	1.336(4)	1.366
C21–C22	1.470(4)	1.459
C21–C33	1.529(4)	1.534
C19–C20	1.435(4)	1.437
C19–C24	1.515(4)	1.499
C23–C22	1.344(4)	1.366
C23–C24	1.470(4)	1.459
C23–C37	1.532(4)	1.537
C13–C18	1.386(5)	1.414
C13–C14	1.395(4)	1.400
C7–C8	1.395(4)	1.407
C7–C12	1.405(4)	1.412
C2–C3	1.440(4)	1.445
C6–C5	1.358(4)	1.373
C25–C3	1.531(5)	1.537
C12–C11	1.387(4)	1.396
C3–C4	1.364(5)	1.375
C5–C4	1.426(5)	1.444
C5–C29	1.537(4)	1.537
C14–C15	1.380(5)	1.394
C18–C17	1.391(4)	1.409
C15–C16	1.365(5)	1.396
C16–C17	1.381(4)	1.390
C8–C9	1.376(5)	1.393
C9–C10	1.380(5)	1.397
C11–C10	1.375(5)	1.397

2. Crystallographic data

	2C	**2E**
CCDC No.	NA	993713
Empirical formula	$C_{80}H_{96}Cu_2N_4O_4Se_2 \bullet CHCl_3$	$C_{40}H_{48}ClCuN_2O_2S \bullet C_2H_3N$
Formula weight	1581.98	760.91
Crystal habit, colour	columnar / green	block / brown
Crystal size, mm^3	0.32 × 0.16 × 0.14	0.38 × 0.30 × 0.24
Temperature, *T*	296(2) K	296(2) K
Wavelength, λ (Å)	0.71073	0.71073
Crystal system	triclinic	monoclinic
Space group	*'P–1'*	*'P2$_1$/n'*
Unit cell dimensions	*a* = 14.8478(4) Å *b* = 16.2751(8) Å *c* = 17.1353(6) Å α = 85.629(3)°, β = 81.059(3)°, γ = 83.535(3)°	*a* = 10.9576(7) Å *b* = 10.9599(6) Å *c* = 34.1796(18) Å α = 90.00°, β = 95.760(6)°, γ = 90.00°
Volume, *V* ($Å^3$)	4057.1(3)	4084.1(4)
Z	2	4
Calculated density, $Mg \cdot m^{-3}$	1.295	1.238
Absorption coefficient, μ (mm^{-1})	1.568	0.688
F(000)	1640	1608
θ range for data collection	2.94° to 25.00°	2.97° to 25.00°
Limiting indices	$-17 \le h \le 17, -17 \le k \le 19, -19 \le l \le 20$	$-13 \le h \le 11, -9 \le k \le 13, -39 \le l \le 40$
Reflection collected/unique	30869/14281 [*R*(int) = 0.0390]	16972/7152 [*R*(int) = 0.0610]
Completeness to θ	99.8 % (θ = 25.00°)	99.8% (θ = 25.00°)
Max. and min. transmission	0.803/0.747	0.848/0.781
Refinement method	'SHELXL–97 (Sheldrick, 1997)'	'SHELXL–97 (Sheldrick, 1997)'
Data/restraints/parameters	14281/0/889	7152/0/464
Goodness–of–fit on F^2	1.028	1.045
Final *R* indices [$I > 2\sigma(I)$]	*R*1 = 0.0691, *wR*2 = 0.1707	*R*1 = 0.0514, *wR*2 = 0.1069
R indices (all data)	*R*1 = 0.1115, *wR*2 = 0.1959	*R*1 = 0.0816, *wR*2 = 0.1239
Largest diff. peak and hole	1.462 and –1.059 $e \cdot Å^{-3}$	0.507 and −0.570 e $Å^{-3}$

	3B	**3C**	**3D**
CCDC No.	NA	NA	NA
Empirical formula	$C_{80}H_{96}Cl_2Co_2N_4O_4S_2$	$C_{80}H_{96}Cl_2Co_2N_4O_4Te_2$	$C_{120}H_{146}Co_2N_6O_6S_3$
Formula weight	1430.49	1621.57	1982.47
Crystal habit, colour	block / blue	needle / blue	needle / blue
Crystal size, mm^3	0.20 × 0.18 × 0.14	0.22 × 0.14 × 0.12	0.24 × 0.16 × 0.12
Temperature, *T*	293(2) K	293(2) K	293(2) K
Wavelength, λ (Å)	0.71073	0.71073	0.71073
Crystal system	orthorhombic	orthorhombic	triclinic

Space group	*'Pbcn'*	*'Pbcn'*	*'P–1'*
Unit cell dimensions	a = 21.0719(8) Å b = 22.3733(13) Å c = 19.7259(10) Å α = 90.00°, β = 90.00°, γ = 90.00°	a = 21.0200(9) Å b = 22.3813(17) Å c = 20.2653(10) Å α = 90.00°, γ = 90.00°, β = 90.00°	a = 15.5859(7) Å b = 17.5588(10) Å c = 24.4355(15) Å α = 83.281(5)°, β = 77.809(4)°, γ = 77.747(4)°
Volume, V (Å^3)	9299.7(8)	9533.9(10)	6369.3(6)
Z	4	4	2
Calculated density, Mg·m^{-3}	1.022	1.130	1.034
Absorption coefficient, μ (mm^{-1})	0.500	1.044	0.358
F(000)	3024	3312	2116
θ range for data collection	3.04° to 25.00°	3.05° to 25.00°	2.93° to 25.00°
Limiting indices	$-25 \le h \le 23$, $-26 \le k \le 20$, $-23 \le l \le 15$	$-24 \le h \le 13$, $-26 \le k \le 26$, $-20 \le l \le 24$	$-18 \le h \le 18$, $-20 \le k \le 20$, $-29 \le l \le 28$
Reflection collected/unique	26441/8186 [R(int) = 0.0619]	23349/8345 [R(int) = 0.0863]	22383/8943 [R(int) = 0.0838]
Completeness to θ	99.7 % (θ = 25.00°)	99.4 % (θ = 25.00°)	99.8% (θ = 25.00°)
Max. and min. transmission	0.932/0.905	0.882/0.839	0.934/0.958
Refinement method	'SHELXL–97 (Sheldrick, 1997)'	'SHELXL–97 (Sheldrick, 1997)'	'SHELXL–97 (Sheldrick, 1997)'
Data/restraints/parameters	8186/0/436	8345/0/436	8943/0/1272
Goodness–of–fit on F^2	1.007	1.001	1.019
Final R indices [$I > 2\sigma(I)$]	$R1$ = 0.0761, $wR2$ = 0.1564	$R1$ = 0.0697, $wR2$ = 0.1241	$R1$ = 0.1063, $wR2$ = 0.2648
R indices (all data)	$R1$ = 0.1146, $wR2$ = 0.1717	$R1$ = 0.1387, $wR2$ =0.1462	$R1$ = 0.2301, $wR2$ = 0.3696
Largest diff. peak and hole	0.815 and –0.363 e·Å^{-3}	0.778 and –1.340 e·Å^{-3}	0.840 and –0.344 e·Å^{-3}

	4A	**4B**
CCDC No.	NA	NA
Empirical formula	$C_{52}H_{56}FeClN_4O_8$	$C_{52}H_{56}NiN_4O_8$
Formula weight	956.31	923.72
Crystal habit, colour	block / green	orthogonal / green
Crystal size, mm^3	0.32 × 0.22 × 0.20	0.24 × 0.16 × 0.14
Temperature, T	296(2) K	293(2) K
Wavelength, λ (Å)	0.71073	0.71073
Crystal system	monoclinic	monoclinic
Space group	*'P $2_1/c$'*	*'C2/c'*
Unit cell dimensions	a = 15.1678(9) Å b = 19.2024(11) Å c = 18.5648(12) Å	a = 27.2828(7) Å b = 9.8422(3) Å c = 18.6426(5) Å

	α = 90.00°, β = 110.006(4)°, γ = 90.00°	α = 90.00°, β = 105.003(3)°, γ = 90.00°
Volume, V (Å^3)	5080.9(5)	4835.3(2)
Z	4	4
Calculated density, Mg·m^{-3}	1.250	1.269
Absorption coefficient, μ (mm^{-1})	0.405	0.458
F(000)	2012	1952
θ range for data collection	1.58° to 25.00°	3.02° to 25.00°
Limiting indices	$-18 \le h \le 18$, $-21 \le k \le 22$, $-19 \le l \le 22$	$-32 \le h \le 32$, $-10 \le k \le 11$, $-12 \le l \le 22$
Reflection collected/unique	66316/8829 [R(int) = 0.0486]	9000/4251 [R(int) = 0.0259]
Completeness to θ	98.7 % (θ = 25.00°)	99.8% (θ = 25.00°)
Max. and min. transmission	0.922/0.899	0.938/0.916
Refinement method	'SHELXL–97 (Sheldrick, 1997)'	'SHELXL–97 (Sheldrick, 1997)'
Data/restraints/parameters	8829/0/607	4251/0/301
Goodness–of–fit on F^2	1.000	1.017
Final R indices [$I > 2\sigma(I)$]	R1 = 0.0510, wR2 = 0.1210	R1 = 0.0536, wR2 = 0.1411
R indices (all data)	R1 = 0.0742, wR2 = 0.1366	R1 = 0.0709, wR2 = 0.1548
Largest diff. peak and hole	0.716 and –0.549 e·Å^{-3}	1.034 and –0.288 e·Å^{-3}

	4C	**4D**	**4E**
CCDC No.	1446981	1446980	1446979
Empirical formula	$C_{52}H_{56}CuN_4O_8$	$C_{52}H_{56}Cl_2CuN_4O_8$	$C_{40}H_{50}Cl_2CuN_2O_2$• CH_2Cl_2
Formula weight	928.55	999.45	810.19
Crystal habit, colour	plate / green	columnar / red	block / red
Crystal size, mm3	0.24 × 0.14 × 0.12	0.18 × 0.12 × 0.10	0.36 × 0.28 × 0.24
Temperature, T	296(2) K	293(2) K	293(2) K
Wavelength, λ (Å)	0.71073	0.71073	0.71073
Crystal system	monoclinic	monoclinic	monoclinic
Space group	*'C2/c'*	*'C2/c'*	*'P2$_1$/c'*
Unit cell dimensions	a = 27.611(2) Å b = 9.7390(8) Å c = 18.7464(14) Å α = 90.00°, β = 105.248(8)°, γ = 90.00°	a = 33.6810(16) Å b = 16.0902(7) Å c = 11.2272(5) Å α = 90.00°, β = 98.919(4)°, γ = 90.00°	a = 9.5682(5) Å b = 20.2538(11) Å c = 11.7161(8) Å α = 90.00°, β = 99.951(5)°, γ = 90.00°
Volume, V (Å3)	4863.5(7)	6010.8(5)	2236.3(2)
Z	4	4	2
Calculated density, Mg·m–3	1.268	1.104	1.203
Absorption coefficient, μ (mm–1)	0.506	0.500	0.760
F(000)	1956	2092	850
θ range for data collection	1.53° to 25.10°	3.07° to 25.00°	2.95° to 25.00°
Limiting indices	$-32 \le h \le 32$, $-11 \le k \le$	$-40 \le h \le 37$, $-18 \le k$	$-11 \le h \le 8$, $-24 \le k \le$

	10, $-22 \le l \le 22$	≤ 19, $-6 \le l \le 13$	14, $-13 \le l \le 12$
Reflection collected/unique	17036/4163 [*R(int)* = 0.0729]	10830/ 5270 [*R(int)* = 0.0600]	9210 / 3929 [*R(int)* = 0.0261]
Completeness to θ	95.7 % (θ = 25.10°)	99.5% (θ = 25.00°)	99.8% (θ = 25.00°)
Max. and min. transmission	0.941/0.919	0.951/0.931	0.833/0.775
Refinement method	'SHELXL–97 (Sheldrick, 1997)'	'SHELXL–97 (Sheldrick, 1997)'	'SHELXL–97 (Sheldrick, 1997)'
Data/restraints/parameters	4163/0/301	5270/0/310	3929/0/247
Goodness–of–fit on F2	0.985	1.043	1.082
Final R indices [I > 2□(I)]	*R1* = 0.0600, *wR2* = 0.1482	*R1* = 0.0739, *wR2* = 0.1578	*R1* = 0.0520, *wR2* = 0.1485
R indices (all data)	*R1* = 0.1150, *wR2* = 0.1682	*R1* = 0.1398, *wR2* = 0.1956	*R1* = 0.0663, *wR2* = 0.1608
Largest diff. peak and hole	0.798 and –0.357 e·Å^{-3}	0.360 and –0.410 e·Å^{-3}	0.723 and –0.541 e·Å^{-3}

	5A	**5B**
CCDC No.	NA	NA
Empirical formula	$C_{52}H_{60}ClCoN_4O_9$	$C_{52}H_{60}NiN_4O_4$
Formula weight	979.42	863.75
Crystal habit, colour	block / black	tabular / green
Crystal size, mm^3	0.25 × 0.18 × 0.15	0.24 × 0.18 × 0.16
Temperature, *T*	293(2) K	293(2) K
Wavelength, λ (Å)	0.71073	0.71073
Crystal system	monoclinic	triclinic
Space group	*'C2/c'*	*'P–1'*
Unit cell dimensions	*a* = 12.5303(9) Å *b* = 24.6984(14) Å *c* = 17.5011(14) Å α = 90.00°, β = 110.040(9)°, γ = 90.00°	*a* = 7.9536(3) Å *b* = 12.2064(6) Å *c* = 12.2785(6) Å α = 96.557(4)°, β = 94.969(4)°, γ = 100.384(4)°
Volume, *V* (Å^3)	5088.2(6)	1157.8(1)
Z	4	1
Calculated density, Mg·m^{-3}	1.278	1.239
Absorption coefficient, μ (mm^{-1})	0.448	0.468
F(000)	2064	460
θ range for data collection	2.98° to 25.00°	2.95° to 25.00°
Limiting indices	$-14 \le h \le 8$, $-29 \le k \le 26$, $-19 \le l \le 20$	$-6 \le h \le 9$, $-14 \le k \le 14$, $-14 \le l \le 12$
Reflection collected/unique	6001/3922 [*R*(int) = 0.0292]	7534/4078 [*R*(int) = 0.0256]
Completeness to θ	87.3 % (θ = 25.00°)	99.9 % (θ = 25.00°)
Max. and min. transmission	0.874/0.824	0.928/0.904
Refinement method	'SHELXL–97 (Sheldrick, 1997)'	'SHELXL–97 (Sheldrick, 1997)'
Data/restraints/parameters	3922/0/311	4078/0/284

Goodness–of–fit on F^2	1.058	1.005
Final R indices [$I > 2\sigma(I)$]	$R1$ = 0.0801, $wR2$ = 0.2091	$R1$ = 0.0500, $wR2$ = 0.1195
R indices (all data)	$R1$ = 0.1104, $wR2$ = 0.2349	$R1$ = 0.0556, $wR2$ = 0.1239
Largest diff. peak and hole	0.727 and –0.441 e·Å^{-3}	0.355 and –0.274 e·Å^{-3}

	5C	**5D**
CCDC No.	NA	NA
Empirical formula	$C_{52}H_{60}N_4NiO_4$, 2(PF_6)	$C_{52}H_{60}CuN_4O_4$•C_2H_3N
Formula weight	1323.54	909.63
Crystal habit, colour	block / red	needle / green
Crystal size, mm^3	0.28 × 0.26 × 0.20	0.17 × 0.13 × 0.10
Temperature, T	293(2) K	293(2) K
Wavelength, λ (Å)	0.71073	0.71073
Crystal system	triclinic	triclinic
Space group	*'P–1'*	*' P–1'*
Unit cell dimensions	a = 11.2282(8) Å b = 11.8145(6) Å c = 13.6665(8) Å α = 66.696(5)°, β = 79.408(5)°, γ = 66.455(6)°	a = 12.0149(10) Å b = 14.0775(7) Å c = 17.1241(12) Å α = 92.836(5)°, β = 106.272(7)°, γ = 114.554(7)°
Volume, V (Å^3)	1525.70(16)	2482.8(3)
Z	1	2
Calculated density, Mg·m^{-3}	1.441	1.217
Absorption coefficient, μ (mm^{-1})	0.629	0.489
F(000)	682	966
θ range for data collection	3.01° to 25.00°	2.88° to 25.00°
Limiting indices	$-13 \le h \le 12$, $-13 \le k \le 14$, $-16 \le l \le 16$	$-14 \le h \le 14$, $-16 \le k \le 16$, $-20 \le l \le 20$
Reflection collected/unique	9236/5354 [R(int) = 0.0196]	16041/8702 [R(int) = 0.0606]
Completeness to θ	99.8 % (θ = 25.00°)	99.5 % (θ = 25.00°)
Max. and min. transmission	0.882/0.839	0.952/0.927
Refinement method	'SHELXL–97 (Sheldrick, 1997)'	'SHELXL–97 (Sheldrick, 1997)'
Data/restraints/parameters	5354/0/373	8702/0/592
Goodness–of–fit on F^2	1.040	1.041
Final R indices [$I > 2\sigma(I)$]	$R1$ = 0.0733, $wR2$ = 0.1988	$R1$ = 0.0748, $wR2$ = 0.1659
R indices (all data)	$R1$ = 0.0897, $wR2$ = 0.2152	$R1$ = 0.1227, $wR2$ = 0.2008
Largest diff. peak and hole	1.080 and –0.752 e·Å^{-3}	0.766 and –0.532 e·Å^{-3}

Volume 44 | Number 20 | 28 May 2015 | Pages 9307–9694

Dalton Transactions

An international journal of inorganic chemistry

www.rsc.org/dalton

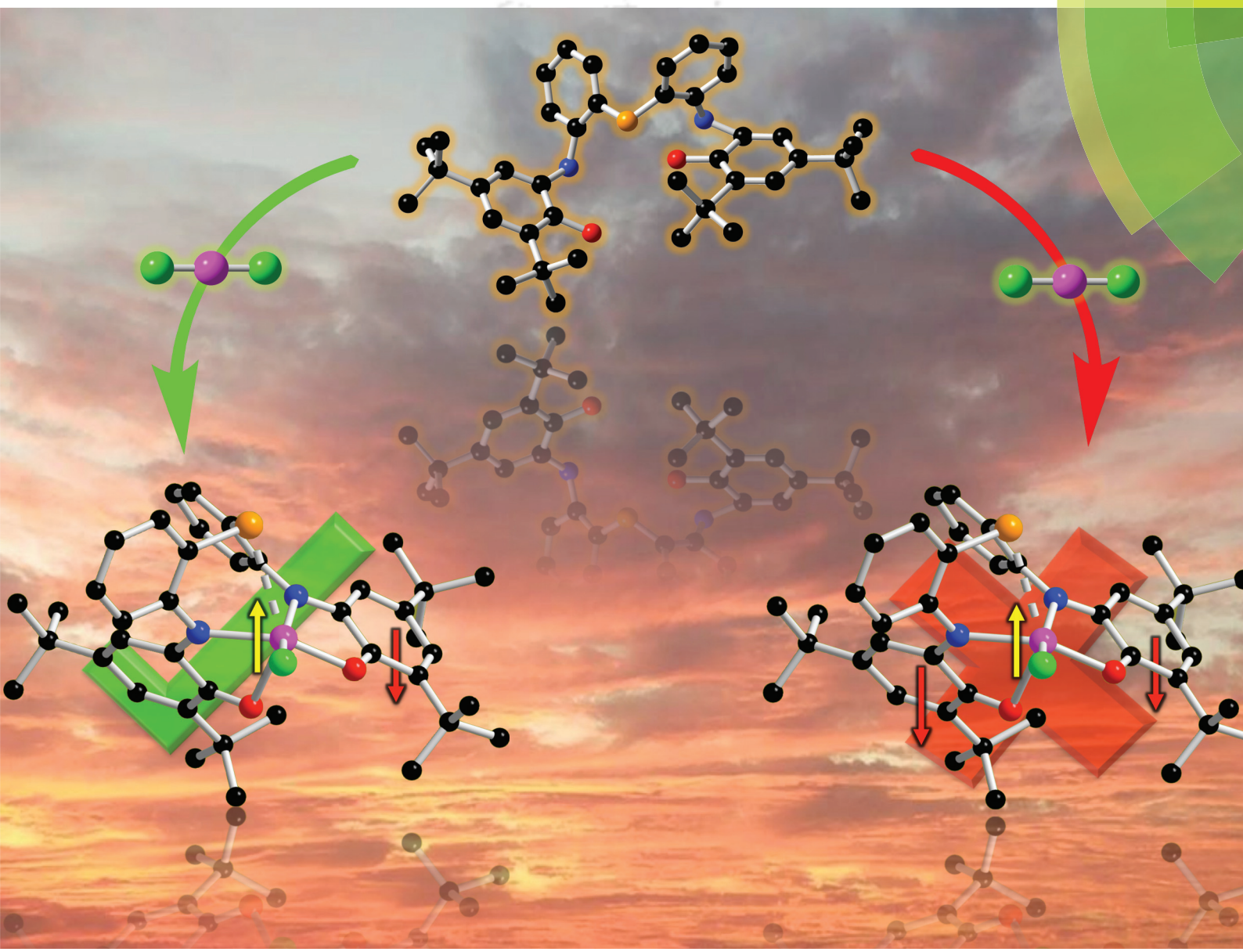

ISSN 1477-9226

PAPER

Bishwajit Ganguly, Chandan Mukherjee *et al.*
Unprecedented iminobenzosemiquinone and iminobenzoquinone coordinated mononuclear Cu(II) complex formation under air

Dalton Transactions

PAPER

View Article Online
View Journal | View Issue

Cite this: *Dalton Trans.*, 2015, **44**, 9375

Unprecedented iminobenzosemiquinone and iminobenzoquinone coordinated mononuclear Cu(II) complex formation under air†

Manas Kumar Mondal,[a] Abul Kalam Biswas,[b] Bishwajit Ganguly*[b] and Chandan Mukherjee*[a]

Received 22nd October 2014,
Accepted 23rd December 2014

DOI: 10.1039/c4dt03263b

www.rsc.org/dalton

Two non-innocent 2-anilino-4,6-di-*tert*-butylphenol units were connected through an *-ortho* bridging S atom and provided the ligand $H_4L^{S(AP/AP)}$. The ligand reacted with $CuCl_2{\cdot}2H_2O$ in the presence of Et_3N under air and generated a mononuclear Cu(II) complex (**1**, $[CuL^{S(IBQ/ISQ)}Cl]^0$). A single crystal X-ray diffraction analysis confirmed that in the complex one of the two 2-anilido-4,6-di-*tert*-butylphenol arms was present in its one-electron oxidized iminobenzosemiquinone form, while the other was in its two-electron oxidized iminobenzoquinone form. The monoradical-containing Cu(II) complex was diamagnetic in nature owing to a strong antiferromagnetic coupling between the single electron containing $d_{x^2-y^2}$ magnetic orbital of Cu(II) and the radical-centered unpaired electron.

Introduction

Galactose oxidase (GOase) is a fungal copper-containing mononuclear metalloenzyme that catalyses aerial oxidation of primary alcohols to the corresponding aldehydes with a concomitant reduction of oxygen to hydrogen peroxide.[1] The active site of GOase is composed of a Cu(II) ion that is surrounded by two histidine imidazole units and two tyrosinate units.[1b–c] In the catalytically active form the Cu(II) ion is coordinated to the Tyr272 radical in a distorted square planar geometry. Both the paramagnetic centers participate in the catalysis and undergo one-electron reduction each and, consequently, the substrate primary alcohol gets oxidized to an aldehyde.[1] The high catalytic efficiency and the structural simplicity have motivated chemists to synthesize functional and/or structural models of GOase; (i) to have efficient enzyme-like alcohol-oxidation catalysts, and (ii) to gain insight into the electronic structure. In this regard, a number of non-innocent ligands, which are defined as the organic moieties capable of changing their oxidation state upon coordination to metal ions, and their corresponding diradical-containing square planar or distorted square planar Cu(II) complexes have been synthesized and studied by X-ray crystallography and various other spectroscopic techniques, *e.g.* NMR, EPR, UV-Vis/NIR, *etc.*[2a–b] In the complexes reported to date, the coordinating ligands were present in their one-electron oxidized iminobenzosemiquinone $[(ISQ)^{1-}]$ form and the paramagnetic ground state was predominated by the presence of a single unpaired-electron on the Cu(II) centre by experiencing stronger antiferromagnetic coupling between the two paramagnetic radical centers compared to the Cu(II) centre and one radical center. In contrast to the trend, recently it has been found that a secondary interaction between the central Cu(II) centre and a tethered axial ligand can alter the coupling fashion and its magnitudes by lowering the O–Cu–O bond angle to <150° from the linearity and provides paramagnetic $S = 1/2$ ground state with a radical-centered unpaired electron.[2c–d]

2-Anilino-4,6-di-*tert*-butylphenol ($H_2L^{(AP)}$; Scheme 1) is a non-innocent ligand.[3] It reacts with copper ions under air and provides a diradical-containing square planar $[Cu^{II}L_2^{(ISQ)}]^0$ complex.[3] In the molecular structure of the complex it is found that the $[L^{(ISQ)}]^{1-}$ belonging the aniline phenyl ring and the 3,5-di-*tert*-butyl-1,2-iminobenzosemiquinone ring are almost perpendicular to each other. If two such kinds of $[L^{(ISQ)}]^{1-}$ or $[L^{(ISQ)}]^{1-}$ generating $L^{(AP)2-}$ moieties were connected through a common *-ortho* substituent (the *-ortho* substituent represents the substituent that is attached at the *-ortho* carbon atom to the aniline moiety), which would provide an almost perpendicular geometry between two aniline phenyl rings, then a

[a]*Department of Chemistry, Indian Institute of Technology, Guwahati, 781039 Assam, India. E-mail: cmukherjee@iitg.ernet.in; Fax: (+) 91-361-258-2349; Tel: (+) 91-361-258-2327*

[b]*Computation and Simulation Unit (Analytical Discipline and Centralized Instrument Facility), CSIR–Central Salt and Marine Chemicals Research Institute, Bhavnagar-364002, India. E-mail: ganguly@csmcri.org; Fax: +91-278-2567562*

†Electronic supplementary information (ESI) available: Experimental procedures and characterization data; mass, UV-Vis/NIR, CV. X-ray structural parameters and bond distances, and angles for **1**. Optimized geometry and the Cartesian coordinates of complex **1**. CCDC 993713. For ESI and crystallographic data in CIF or other electronic format see DOI: 10.1039/c4dt03263b

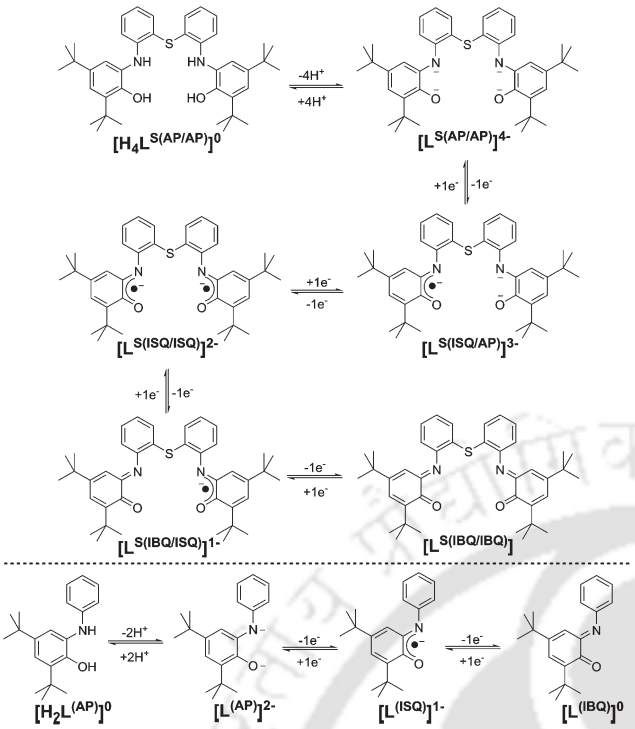

Scheme 1

diradical-coordinating Cu(II) complex could be formed where the radical-containing two paramagnetic centers would be almost perpendicular to each other. Hence, the electronic structure, including structure-dependent coupling between the paramagnetic centers, could be studied in a completely unexplored system. In this regard, we have synthesized the ligand $\mathbf{H_4L^{S(AP/AP)}}$ by placing an S atom at the *-ortho* positions of two aniline moieties.

Although the ligand has recently been reported by Limberg and coworkers,[4] we have independently synthesized the ligand and its corresponding Cu(II) complex (Scheme 2). Herein, we report the synthesis and characterization of complex (**1**) that is coordinated to the ($[L^{S(IBQ/ISQ)}]^{1-}$) form of the ligand.

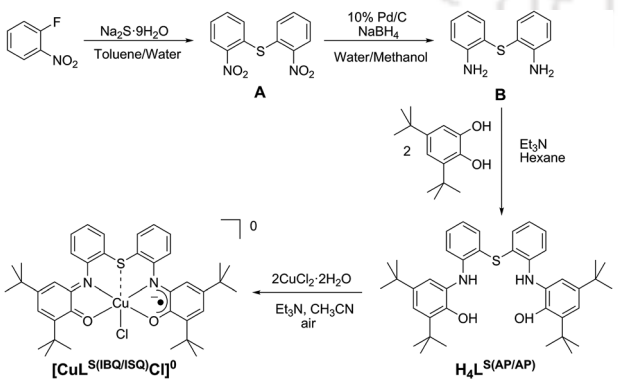

Scheme 2

Results and discussion

An aerial reaction of 1 : 2 $\mathbf{H_4L^{S(AP/AP)}}$ and $CuCl_2{\cdot}2H_2O$ in CH_3CN in the presence of Et_3N provided complex **1**·1CH_3CN in 52% yield.

The crystal structure of complex **1**·1CH_3CN has been determined by single-crystal X-ray crystallography at 296(2) K.[5] A crystalline solid suitable for X-ray diffraction measurements was obtained by slow evaporation of a 5 : 2 CH_2Cl_2–CH_3CN solvent mixture of **1**. The complex crystallized in the monoclinic space group $P2_1/n$. The molecular structure is presented in Fig. 1. Selected bond distances and bond angles are given in Table 1.

In the neutral complex **1**, the central Cu1 atom was six-coordinate with a highly distorted octahedral geometry. The ligand backbone was composed of mainly four C_6 rings. Among them, two C_6 rings each contained two *tert*-butyl groups, while the other two did not. Interestingly, alternating long–short–long C–C bond distances followed by three long bond distances were observed in the *tert*-butyl group-containing two C_6 rings. This type of distortion is known as quinoid-type distortion and has previously been observed for one-electron as well as two-electron oxidized phenyl ring systems.[2,6] All the C–C bond distances of the other two C_6 rings were almost the same and were within the 1.39 ± 0.01 Å range as expected for fully reduced phenyl rings. The C1–N1 = 1.354(3) and C2–O1 = 1.284(4) Å bond distances were in between their characteristic single bond and double bond values and indicated a partial double bond character for both the bonds.[2] These partial double bond characterizing C–N and C–O bonds along with the quinoid-type distortion emphasized an one-electron oxidized iminobenzosemiquinone (ISQ^{1-}) form for the C_6 ring composed of C1-to-C6 atoms.[6] The C19–N2 = 1.303(4) and C24–O2 = 1.229(3) Å bond distances were in accord with their characteristic double bond values, and hence, the quinoid-type distortion acquiring C_6 ring, which is constituted by C19-to-C24 atoms, along with C19–N2 and C24–O2 represented its two-electron oxidized iminobenzoquinone (IBQ^0) form.[7] Note that the angle between the iminobenzosemiquinone C_6 (C1-to-C6)

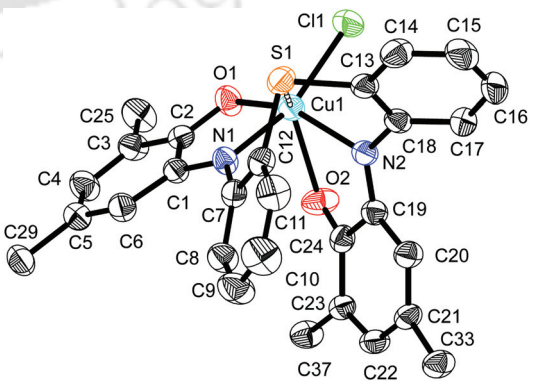

Fig. 1 The molecular structure of **1** has been shown; thermal ellipsoids are drawn at the 50% probability level. Methyl groups attached at C25, C29, C33, C37, hydrogen atoms, and CH_3CN are omitted for clarity.

Table 1 Selected bond distances (Å) and angles (°) for complex **1**·1CH_3CN

Cu1–O1	1.967(2)	C7–C8	1.395(4)
Cu1–N1	1.973(3)	C7–C12	1.405(4)
Cu1–N2	2.108(2)	C8–C9	1.376(5)
Cu1–S1	2.9954(11)	C9–C10	1.380(5)
Cu1–O2	2.418(2)	C11–C10	1.375(5)
S1–C13	1.774(3)	C12–C11	1.387(4)
S1–C12	1.776(3)	C13–C14	1.395(4)
O1–C2	1.284(4)	C13–C18	1.386(5)
O2–C24	1.229(3)	C14–C15	1.380(5)
N1–C1	1.354(3)	C15–C16	1.365(5)
N1–C7	1.405(4)	C16–C17	1.381(4)
N2–C19	1.303(4)	C18–C17	1.391(4)
N2–C18	1.432(4)	C19–C20	1.435(4)
C1–C6	1.415(4)	C19–C24	1.515(4)
C1–C2	1.443(4)	C21–C20	1.336(4)
C2–C3	1.440(4)	C21–C22	1.470(4)
C3–C4	1.364(5)	C23–C22	1.344(4)
C5–C4	1.426(5)	C23–C24	1.470(4)
C5–C29	1.537(4)	C41–N3	1.117(8)
C6–C5	1.358(4)		
O1–Cu1–N1	82.13(9)	C19–N2–Cu1	118.79(18)
O1–Cu1–N2	153.57(10)	C18–N2–Cu1	120.31(19)
N1–Cu1–N2	93.61(10)	N1–C1–C6	125.9(3)
O1–Cu1–Cl1	98.15(7)	N1–C1–C2	113.7(3)
N1–Cu1–Cl1	160.44(8)	N2–C19–C20	126.4(3)
N2–Cu1–Cl1	94.40(7)	N2–C19–C24	115.0(3)
O1–Cu1–O2	82.23(8)	C18–C13–S1	120.7(2)
N1–Cu1–O2	84.89(10)	C14–C13–S1	119.3(3)
N2–Cu1–O2	71.40(8)	C8–C7–N1	123.5(3)
Cl1–Cu1–O2	114.59(7)	C12–C7–N1	118.1(3)
C13–S1–C12	99.79(15)	O1–C2–C3	123.6(3)
C2–O1–Cu1	113.16(19)	O1–C2–C1	117.8(3)
C1–N1–C7	123.6(3)	C11–C12–S1	120.0(2)
C1–N1–Cu1	112.6(2)	C7–C12–S1	120.0(2)
C7–N1–Cu1	122.83(18)	C13–C18–N2	119.7(3)
C24–O2–Cu1	107.6(2)	C17–C18–N2	120.6(3)
C19–N2–C18	120.4(2)	N3–C41–C42	178.7(9)

plane and the iminobenzoquinone C_6 (C19-to-C24) plane was ~58°.

Two different oxidation states of the *tert*-butyl group-containing two C_6 rings were further reflected by Cu–N and Cu–O bond distances. The Cu1–N1 = 1.973(3) and Cu1–O1 = 1.967(2) Å bond distances were expectably found to be much shorter compared to Cu1–N2 = 2.108(2) and Cu1–O2 = 2.418(2) Å bond distances, and were in accord with the previously reported Cu(II)–O_{ISQ} and Cu(II)–N_{ISQ} bonds [O_{ISQ} and N_{ISQ} represent the O atom and the N atom of an iminobenzosemiquinone moiety attached to the Cu(II) atom], and Cu(II)–O_{IBQ} and Cu(II)–N_{IBQ} bonds [O_{IBQ} and N_{IBQ} represent the O atom and the N atom of an iminobenzoquinone moiety attached to the central Cu(II) atom], respectively.[2,6,7] Hence, from the X-ray crystallographic analysis it was evident that the two non-innocent 2-anilido-4,6-di-*tert*-butylphenolate moieties, which were bridged by the S1 atom with a bridging angle of ~100°, were present in complex **1** in two different oxidation states. The overall formal charge of the ligand in the complex was –I and the neutrality of the complex was maintained by the coordination of a mononegative chloride ion [Cu(II)–Cl1 = 2.2193(9)].

Complex **1** acquired two paramagnetic centers: (i) a Cu(II) ($3d^9$, $S_{Cu(II)}$ = 1/2), and (ii) a radical (S_R = 1/2). An S_t = 1 or an S_t = 0 ground state would be formed by experiencing a ferromagnetic or an antiferromagnetic coupling between the paramagnetic centers, respectively. Variable-temperature (2–300 K) magnetic susceptibility measurements showed a constant μ_{eff} = 0.96μ_B value in the temperature range (Fig. 4 and S4†). This indicated an antiferromagnetic coupling between the two S = 1/2 spins and the diamagnetic nature of complex **1**.

The electrochemical behavior of complex **1** was studied by cyclic voltammetry. Cyclic voltammograms (CVs) have been recorded in CH_2Cl_2 solutions containing 0.10 M [(^{n}Bu)$_4$N]ClO_4 as a supporting electrolyte at a glassy carbon working electrode, a platinum wire counter electrode, and an $Ag/AgNO_3$ reference electrode. Ferrocene was used as an internal standard, and potentials are referenced *versus* the ferrocenium/ferrocene couple (Fc^+/Fc).

Complex **1** was composed of one fully oxidized iminobenzoquinone, one one-electron oxidized iminobenzosemiquinone, and one chloride unit. The complex underwent a one-electron oxidation at +0.02 V (Fig. 2) and, consequently, the formation of a fully oxidized Cu(II)-diquinone species took place. This species underwent four successive one-electron reductions at −0.10, −0.27, −0.88, and −1.21 V, respectively (Fig. 2), and presumably generated a Cu(II)-diamidophenolate species.[2,6a,7] While the first two oxidation potentials of the reduced species were separated by 0.15 V and 0.13 V than those of the corresponding reduction potentials, the third oxidation potential had a 0.44 V separation than that of the corresponding reduction potential. This could be due to structural changes, *i.e.* loss of chloride ions followed by reduction or *vice versa*.

The UV-Vis/NIR spectrum of complex **1** was measured at 25 °C in the 300–2000 nm range and is presented in Fig. 3. The spectrum was dominated by intense charge transfer bands (inset of Fig. 3) in the UV and visible regions, while the bands that appeared in the near-infrared (NIR) region were moderately intense.

Time dependent density functional theory (TDDFT) calculations have been performed in the dichloromethane solvent (ε = 8.93) with the optimized geometry[8] using 50 singlet states at the B3LYP/6-31G(d,p) level of theory in order to rationalize the experimentally observed UV-Vis/NIR absorption bands (Fig. 5 and S5†) of **1**. The selection of CH_2Cl_2 for TDDFT calculations was due to the record of experimental absorption spectra in the medium. The absorption wavelength at 381 nm

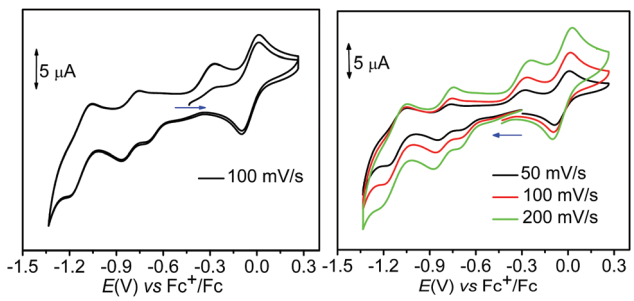

Fig. 2 Cyclic voltammograms of complex **1** measured in a CH_2Cl_2 solution. Left: two consecutive cycles. Right: rate dependence.

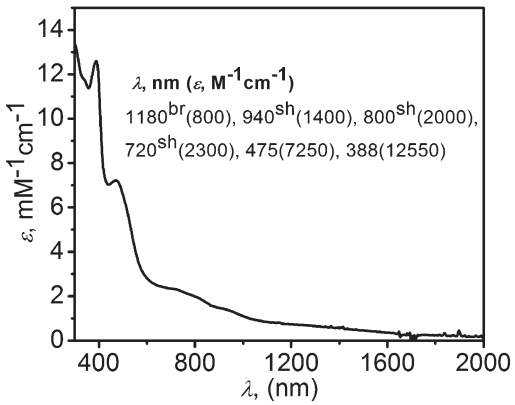

Fig. 3 UV-Vis/NIR spectrum of complex **1** measured in a CH_2Cl_2 solution at 25 °C; br and sh stand for broad and shoulder, respectively.

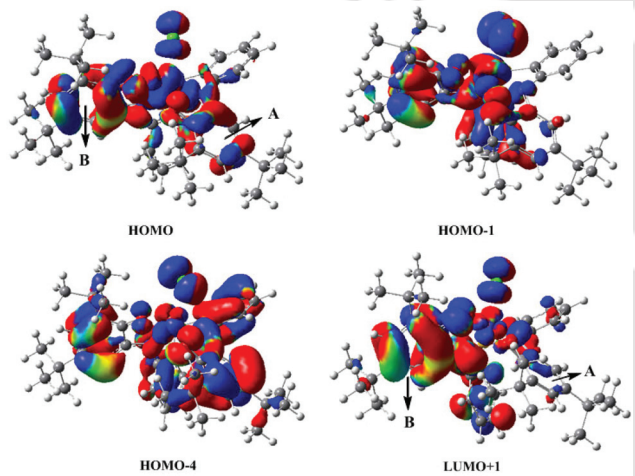

Fig. 4 B3LYP/6-31G(d,p) calculated frontier molecular orbitals for a complex in dichloromethane (white = H, gray = C, blue = N, red = O, lime = Cl, and coral = Cu).

(experimental absorption = 386 nm) corresponded to the intra-ligand charge transfer.[9] The experimental absorption band at 475 nm was because of ligand-to-metal charge transfer (LMCT) as obtained with TDDFT calculations at 490 nm. The frontier molecular orbitals responsible for the electronic transition at λ = 490 nm were HOMO−4 to LUMO+1 (Fig. 4). The absorption band at 941 nm was due to metal-to-ligand charge transfer, and the frontier molecular orbitals showed the electronic transition from HOMO−1 to LUMO+1 (Fig. 4) for the band. The TDDFT results also showed an absorption band at 1172 nm. The frontier molecular orbital analysis suggested that the band appeared due to an intramolecular ligand-to-ligand charge transfer process where a transition occurs from the HOMO of one *tert*-butyl group-containing phenyl ring **A** to the other *tert*-butyl group-containing phenyl ring **B** (LUMO+1) (Fig. 4).

Complex **1** formation was achieved through the initial generation of a green color solid (**2**), which was X-band EPR silent and hence, refuted its mononuclear diradical-containing Cu(II)

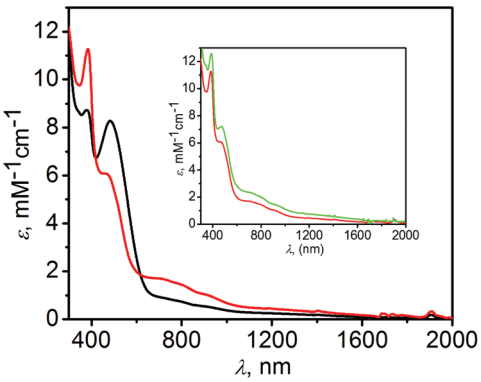

Fig. 5 UV-Vis/NIR spectrum of: black: **2** + 1 equivalent of $CuCl_2{\cdot}2H_2O$ (in CH_3CN), red: the formed red solution + Et_3N. Inset: the formed red solution + Et_3N, green: complex **1** (measured in CH_2Cl_2 solution at 25 °C).

form. Due to solubility problems and the unsatisfactory single crystal quality we were unable to characterize the green compound (**2**) structurally. However, a very close resemblance of the UV-Vis/NIR spectrum of the green solid (**2**) to that of the X-band EPR inactive dinuclear tetraradical-containing Cu(II) complex formed with the analogous $\mathbf{H_4L^{Se(AP/AP)}}$ ligand ($L^{Se(ISQ/ISQ)}$: Cu = 2 : 2; each ligand is coordinated to both Cu(II) centers)[10] supported indirectly the dinuclear nature of the green solid. A time-dependent UV-Vis/NIR study showed that the green compound, upon reacting with molecular oxygen in a CH_2Cl_2 solution, transformed to complex **1** (Fig. S6 and S7†). Unfortunately, the intermediate for the above transition could not be detected due to the very sluggish nature of the transformation.

The formation of complex **1** required two equivalents of $CuCl_2{\cdot}2H_2O$ compared to one equivalent of the $\mathbf{H_4L^{S(AP/AP)}}$ ligand. In order to understand the role of excess $CuCl_2{\cdot}2H_2O$ in complex **1** formation, 0.50 equivalent of **2** was added in a CH_3CN solution of $CuCl_2{\cdot}2H_2O$. The color of the solution instantaneously became dark-red and the green solid disappeared (Fig. 5, black line). The UV-Vis/NIR spectrum of the dark-red solution showed the formation of a strong band at 480 nm (ε = 8400 M^{-1} cm^{-1}) and indicated the generation of a diquinone species. In fact, the spectrum corroborated the previously reported Cu(II)-diquinone species.[7] Upon addition of 10 μL of Et_3N to the red solution, the color of the solution changed immediately to brown (Fig. 5, red line) and a precipitation started slowly. The UV-Vis/NIR spectrum of the solution implied the formation of complex **1** by a one-electron reduction of the initially formed Cu(II)-diquinone species (Fig. 5, inset). Hence, it can be argued that the concentration of $CuCl_2{\cdot}2H_2O$ along with Et_3N played a vital role in the formation of complex **1** from the green compound.

Conclusions

Both bidentate 2-anilino-4,6-di-*tert*-butylphenol [$H_2L^{(AP)}$] and -*ortho*-SMe substituted 2-{(2-methylthio)aniline}-4,6-di-*tert*-

butylphenol [$H_2L^{SMe(AP)}$] ligands provide the corresponding diradical-containing mononuclear {[$Cu^{II}L_2^{(ISQ)}$]^0, and [$Cu^{II}L_2^{SMe\ (ISQ)}{}_2$]^0} complexes, having an S_t = 1/2 ground state each. Although the presence of a tethered *-ortho*-SMe group promotes a geometrical deviation from square planar to distorted square planar *via* a weak secondary Cu–S coordination and causes an alteration in the ground state electronic configuration from (↑↑↓) to (↑↓↑), no anomaly in the ligand oxidation state of the coordinated ligands in both the complexes is observed.[2c–d] In contrast to those, herein it was found that an imposition of orthogonality between the two coordinatable bidentate H_2L^{AP} units by means of the *-ortho* bridging S atom provided a mononuclear Cu(II) complex (**1**) where one of the two coordinating $H_2L^{(AP)}$ units was present in its two-electron oxidized iminobenzoquinone form and the other was in its one-electron oxidized iminobenzosemiquinone form. The complex formation proceeded through the initial generation of a tetraradical-containing dinuclear Cu(II) green compound (**2**) and its further oxidation. The oxidation of the green compound proceeded by the $CuCl_2{\cdot}2H_2O$ and Et_3N duo as well as air and the process was possibly favored because of low oxidation potentials of the initially formed compound (Fig. S5 and S6†). Further studies using analogous ligands having the general formula $\mathbf{H_4L^{X(AP/AP)}}$ (X = O, Se, Te) are currently ongoing.

Experimental section

Materials

All the chemicals and solvents were obtained from commercial sources and were used as supplied, unless noted otherwise. 3,5-Di-*tert*-butylcatechol, 2-fluoronitrobenzene, 10% Pd/C, and $NaBH_4$ were purchased from Sigma-Aldrich. Solvents were obtained from Merck (India).

Physical methods

X-ray crystallographic data were recorded using a SuperNova (single source at offset, Eos) diffractometer equipped with a sealed tube with Mo-Kα radiation (λ = 0.71073 Å) at 296(2) K. Structures were solved with the Superflip, a structure solution program, using charge flipping and were refined by direct methods using SHELXS-97 and with full-matrix least squares on F^2 using SHELXL-97.[11] All the non-hydrogen atoms were refined anisotropically. IR spectra were recorded on a Perkin Elmer instrument at normal temperature preparing KBr pellets by grinding the sample with KBr (IR grade). UV-Vis/NIR spectra were recorded on a Perkin Elmer, Lambda 750, UV/VIS/NIR spectrometer preparing a known concentration of the samples in HPLC grade CH_2Cl_2 at room temperature using cuvettes of 1 cm width. EPR spectra were recorded on an X-Band Microwave Unit, JES-FA200 ESR spectrometer. Magnetic measurements were performed using a SQUID magnetometer at a 1 T external magnetic field at JNCASR, Bangalore, India. ESI-MS measurements were performed using a Q-TOF LC/MS mass spectrometer (6520, Agilent Technologies). NMR measurements were made using a Bruker (400 MHz) NMR machine.

Computational methods

The electronic transitions of the Cu complex have been calculated using time dependent density functional theory (TDDFT) calculations. First, the optimization and frequency calculation of the Cu-complex were performed at the B3LYP/6-31G(d,p) level of theory employing the polarizable continuum model (PCM)[12–16] using universal force field (UFF) atomic radii in acetonitrile solvent (ε = 35.69).[17] The absence of any imaginary frequencies in the calculated vibrational frequencies ensures that the optimized geometry corresponds to a true energy minimum. Furthermore, the TDDFT calculations have been performed in dichloromethane solvent (ε = 8.93) with the optimized geometry using 50 singlet states at the B3LYP/6-31G(d,p) level of theory. The calculated absorption spectra at this level of theory showed good agreement with the experimental absorption spectra for the Cu-complex.[18] All quantum chemical calculations were performed using Gaussian 09, Revision D.01 program (Table 2).[19]

Table 2 Crystallographic data and structure refinement parameters for **1**·1CH_3CN

Empirical formula	$C_{40}H_{48}ClCuN_2O_2S$, C_2H_3N
Formula weight	760.91
CCDC number	993713
Crystal habit, colour	Block/brown
Crystal size, mm^3	0.38 × 0.30 × 0.24
Temperature (T)	296(2) K
Wavelength, λ (Å)	0.71073
Crystal system	Monoclinic
Space group	$P2_1/n$
Unit cell dimensions	a = 10.9576(7) Å b = 10.9599(6) Å c = 34.1796(18) Å α = 90.00° β = 95.760(6)° γ = 90.00°
Volume, V (Å^3)	4084.1(4)
Z	4
Calculated density (Mg m^{-3})	1.238
Absorption coefficient, μ (mm^{-1})	0.688
F(000)	1608
θ range for data collection	2.97° to 25.00°
Limiting indices	$-13 \le h \le 11$, $-9 \le k \le 13$, $-39 \le l \le 40$
Reflection collected/unique	16 972/7152 [R(int) = 0.0610]
Completeness to θ	99.8% (θ = 25.00°)
Max. and min. transmission	0.848/0.781
Refinement method	SHELXL-97 (Sheldrick, 1997)
Data/restraints/parameters	7152/0/464
Goodness-of-fit on F^2	1.045
Final R indices [$I > 2\sigma(I)$]	R_1 = 0.0514, wR_2 = 0.1069
R indices (all data)	R_1 = 0.0816, wR_2 = 0.1239
Largest diff. peak and hole	0.507 and −0.570 e Å^{-3}

Synthesis of bis(*o*-nitrobenzene)sulfide, A. Bis(*o*-nitrobenzene)sulfide was synthesized as described by J.-Y. Liu *et al.*[20] Despite using *o*-chloronitrobenzene, as reported, here we have used *o*-fluoronitrobenzene.

TH-1576_126122004

Synthesis of bis(*o*-aminophenyl)sulfide, B. To a suspension of finely grained bis(*o*-nitrobenzene) sulfide (0.658 g, 2.38 mmol) in a water and methanol mixture (7 : 3; 15 mL), 10% Pd-charcoal (22 mg) was added, followed by the addition of sodium borohydride (1.085 g, 28.56 mmol) under an Ar atmosphere at 0 °C. The suspension was stirred at room temperature (30 °C) for 15 minutes and then stirred at 50 °C overnight under an Ar atmosphere. The reaction mixture was then cooled to room temperature and filtered through a celite pad. The filtrate was extracted with CH_2Cl_2 (3 × 30 mL), and the combined organic layer was washed with water followed by brine and, finally, dried over anhydrous Na_2SO_4. The solvent was evaporated to afford a white solid. Yield: 0.490 g, 95%. FTIR (KBr pellet, cm^{-1}): 3457, 3417, 3357, 3340, 1611, 1584, 1570, 1477, 1446, 1315, 1289, 1255, 1157, 1138, 1030, 1018, 759, 754, 686, 675, 668, 540, 498, 464. ^{1}H NMR (399.85 MHz, $CDCl_3$): δ 7.21 (d, J = 7.6 Hz, 2H), 7.12–7.09 (m, 2H), 6.73–6.67 (m, 4H), 4.20 (s, 4H) ppm. ESI-MS (+) m/z for $[C_{12}H_{12}N_2S + H]^+$: Calcd, 217.0794; found, 217.0808.

Synthesis of $[C_{40}H_{52}N_2O_2S]$, $H_4L^{S(AP/AP)}$. To a suspension of bis(*o*-aminophenyl) sulfide (0.489 g, 2.26 mmol) in hexane (20 mL), 3,5-di-*tert*-butylcatechol (1.005 g, 4.52 mmol) was added, followed by the addition of Et_3N (0.05 mL). The reaction mixture was then refluxed for 30 minutes and then stirred at room temperature (30 °C) for 5 h. A white precipitate was obtained in due course. The solid was filtered, washed with hexane (20 mL), and dried under air. Yield: 1.010 g, 71%. FTIR (KBr pellet, cm^{-1}): 3434, 3358, 3335, 3061, 2961, 2906, 2868, 1602, 1587, 1574, 1492, 1472, 1446, 1421, 1391, 1380, 1362, 1310, 1264, 1227, 1203, 1158, 1116, 1054, 1035, 977, 882, 824, 808, 768, 750, 718, 679, 648, 636, 617, 560, 487. ^{1}H NMR (600.17 MHz, $CDCl_3$): δ 7.40–7.38 (m, 2H), 7.21 (d, J = 2.4 Hz, 2H), 7.16–7.14 (m, 2H), 6.84–6.82 (m, 2H), 6.79 (d, J = 1.8 Hz, 2H), 6.48 (d, J = 7.8 Hz, 2H), 6.09 (s, 2H), 5.90 (s, 2H), 1.41 (s, 18H), 1.20 (s, 18H) ppm. ^{13}C NMR (100.55 MHz, $CDCl_3$): δ 149.7, 147.2, 142.6, 135.7, 133.4, 130.0, 127.1, 122.7, 122.0, 120.3, 118.5, 114.8, 35.2, 34.5, 31.8, 29.7 ppm. ESI-MS (+) m/z for $[C_{40}H_{52}N_2O_2S + H]^+$: Calcd, 625.3822; found, 625.3820.

Synthesis of $[CuL^{S(IBQ/ISQ)}Cl]^0 \cdot 1CH_3CN$ (1·1CH$_3$CN). To a suspension of $H_4L^{S(AP/AP)}$ (0.287 g, 0.46 mmol) in CH_3CN (5 mL), $CuCl_2 \cdot 2H_2O$ (0.157 g, 0.92 mmol) and Et_3N (0.2 mL) were added sequentially. The resulting reaction mixture was stirred for 24 h at room temperature (30 °C) under air when the initially formed blue-green precipitate was gradually transformed to a brown solid. The thus formed brown precipitate was filtered and washed with CH_3CN (10 mL). Recrystallization of the solid from a CH_2Cl_2–CH_3CN (5 : 2) solvent mixture provided a cube-shaped crystalline solid suitable for single-crystal X-ray diffraction study. The solid was separated and washed with CH_3CN (5 mL). Yield: 0.181 g, 52%. FTIR (KBr pellet, cm^{-1}): 3443, 3252, 3050, 2956, 2908, 2869, 2252, 1640, 1618, 1589, 1504, 1465, 1430, 1379, 1335, 1310, 1271, 1250, 1204, 1025, 899, 765, 748. ESI-MS (+) m/z for $[C_{40}H_{48}CuN_2O_2S]^+$: Calcd, 683.2832; found, 683.2832. Anal. Calcd for $C_{40}H_{48}ClCuN_2O_2S \cdot 1CH_3CN$: C, 66.37; H, 6.76; N, 5.53. Found: C, 66.29; H, 6.72; N, 5.39%.

Acknowledgements

This project was funded by CSIR [01(2817/14/EMR-II]. MKM and AKB thank IIT Guwahati and UGC (India), respectively, for their doctoral fellowship. CM is indebted to Prof. A. Sundaresan, JNCASR, Bangalore, India, for the SQUID measurements. Mr Samir Ghorai is acknowledged for X-ray single crystal measurements. We thank CIF and Department of Chemistry, IIT Guwahati, for instrumental facilities.

Notes and references

1 (*a*) J. Stubbe and W. A. van der Donk, *Chem. Rev.*, 1998, **98**, 705; (*b*) R. H. Holm, P. Kennepohl and E. I. Solomon, *Chem. Rev.*, 1996, **96**, 2239; (*c*) J. W. Whittaker, *Chem. Rev.*, 2003, **103**, 2347; (*d*) R. Banerjee, *Chem. Rev.*, 2003, 103, 2081; (*e*) N. Ito, S. E. V. Phillips, C. Stevens, Z. B. Ogel, M. J. Mcpherson, J. N. Keen, K. D. S. Yadav and P. F. Knowles, *Nature*, 1991, **350**, 87; (*f*) N. Ito, S. E. V. Phillips, K. D. S. Yadav and P. F. Knowles, *J. Mol. Biol.*, 1994, **238**, 794.

2 (*a*) P. Chaudhuri and K. Wieghardt, *Prog. Inorg. Chem.*, 2001, **50**, 151; (*b*) P. Chaudhuri, K. Wieghardt, T. Weyhermüller, T. K. Paine, S. Mukherjee and C. Mukherjee, *Biol. Chem.*, 2005, **386**, 1023; (*c*) S. Ye, B. Sarkar, F. Lissner, T. Schleid, J. van Slageren, J. Fiedler and W. Kaim, *Angew. Chem., Int. Ed.*, 2005, **44**, 2103; (*d*) R. Rakshit, S. Ghorai, S. Biswas and C. Mukherjee, *Inorg. Chem.*, 2014, **53**, 3333.

3 P. Chaudhuri, C. N. Verani, E. Bill, E. Bothe, T. Weyhermüller and K. Wieghardt, *J. Am. Chem. Soc.*, 2001, **123**, 2213.

4 R. Metzinger, S. Demeshko and C. Limberg, *Chem. – Eur. J.*, 2014, **20**, 4721.

5 CCDC 993713 (**1**·1CH$_3$CN) contains the supplementary crystallographic data for this paper. Disorderness in the solvent molecule CH_3CN was found in the molecular structure.

6 (*a*) C. Mukherjee, U. Pieper, E. Bothe, V. Bachler, E. Bill, T. Weyhermüller and P. Chaudhuri, *Inorg. Chem.*, 2008, **47**, 8943; (*b*) G. A. Abakumov, V. K. Cherkasov, V. I. Nevodchikov, V. A. Kuropatov, G. T. Yee and C. G. Pierpont, *Inorg. Chem.*, 2001, **40**, 2434; (*c*) K. J. Blackmore, J. W. Ziller and A. F. Heyduk, *Inorg. Chem.*, 2005, **44**, 5559; (*d*) C. Mukherjee, T. Weyhermüller, K. Wieghardt and P. Chaudhuri, *Dalton Trans.*, 2006, 2169; (*e*) S. Ghorai and C. Mukherjee, *Dalton Trans.*, 2014, **43**, 2169.

7 (*a*) C. Mukherjee, U. Pieper, E. Bothe, V. Bachler, E. Bill, T. Weyhermüller and P. Chaudhuri, *Inorg. Chem.*, 2008, **47**, 2740.

8 The optimization of complex **1** was performed at the B3LYP/6-31G(d,p) level of theory employing the polarizable continuum model (PCM) (for references: (*a*) M. Cossi and V. Barone, *J. Chem. Phys.*, 1998, **109**, 6246; (*b*) J. Tomasi and

M. Persico, *Chem. Rev.*, 1994, **94**, 2027; (*c*) M. Cossi, V. Barone, R. Cammi and J. Tomasi, *Chem. Phys. Lett.*, 1996, **255**, 327; (*d*) V. Barone, M. Cossi and J. Tomasi, *J. Comput. Chem.*, 1998, **19**, 404.) using universal force field (UFF) atomic radii in the acetonitrile solvent (ε = 35.69) (for reference: A. V. Marenich, C. J. Cramer and D. G. Truhlar, *J. Phys. Chem. B*, 2009, **113**, 6378).

9 (*a*) W. Li, F. Yang and Z. Wang, *Int. J. Quantum Chem.*, 2011, **111**, 2099; (*b*) S. Torres, G. Ferraudi, M. J. Aguirrea, M. Isaacsc, B. Matsuhiro, N. P. Chandĭa and L. Mendoza, *Helv. Chim. Acta*, 2011, **94**, 293.

10 C. Mukherjee, unpublished results.

11 G. M. Sheldrick, *Acta Crystallogr., Sect. A: Fundam. Crystallogr.*, 2008, **64**, 112.

12 M. Cossi and V. Barone, *J. Chem. Phys.*, 1998, **109**, 6246.

13 J. Tomasi and M. Persico, *Chem. Rev.*, 1994, **94**, 2027.

14 M. Cossi, V. Barone, R. Cammi and J. Tomasi, *Chem. Phys. Lett.*, 1996, **255**, 327.

15 V. Barone, M. Cossi and J. Tomasi, *J. Chem. Phys.*, 1997, **107**, 3210.

16 V. Barone, M. Cossi and J. Tomasi, *J. Comput. Chem.*, 1998, **19**, 404.

17 A. V. Marenich, C. J. Cramer and D. G. Truhlar, *J. Phys. Chem. B*, 2009, **113**, 6378.

18 A. M. Whyte, K. Awaga, B. Roach, F. J. White, D. K. Henderson, P. Richardson, P. A. Tasker and N. Robertson, *Inorg. Chem.*, 2011, **50**, 12867.

19 M. J. Frisch, G. W. Trucks, H. B. Schlegel, G. E. Scuseria, M. A. Robb, J. R. Cheeseman, J. A. Montgomery Jr., T. Vreven, K. N. Kudin, J. C. Burant, J. M. Millam, S. S. Iyengar, J. Tomasi, V. Barone, B. Mennucci, M. Cossi, G. Scalmani, N. Rega, G. A. Petersson, H. Nakatsuji, M. Hada, M. Ehara, K. Toyota, R. Fukuda, J. Hasegawa, M. Ishida, T. Nakajima, Y. Honda, O. Kitao, H. Nakai, M. Klene, X. Li, J. E. Knox, H. P. Hratchian, J. B. Cross, V. Bakken, C. Adamo, J. Jaramillo, R. Gomperts, R. E. Stratmann, O. Yazyev, A. J. Austin, R. Cammi, C. Pomelli, J. W. Ochterski, P. Y. Ayala, K. Morokuma, G. A. Voth, P. Salvador, J. J. Dannenberg, V. G. Zakrzewski, S. Dapprich, A. D. Daniels, M. C. Strain, O. Farkas, D. K. Malick, A. D. Rabuck, K. Raghavachari, J. B. Foresman, J. V. Ortiz, Q. Cui, A. G. Baboul, S. Clifford, J. Cioslowski, B. B. Stefanov, G. Liu, A. Liashenko, P. Piskorz, I. Komaromi, R. L. Martin, D. J. Fox, T. Keith, M. A. Al-Laham, C. Y. Peng, A. Nanayakkara, M. Challacombe, P. M. W. Gill, B. Johnson, W. Chen, M. W. Wong, C. Gonzalez and J. A. Pople, *Gaussian 09, Revision D.01*, Gaussian, Inc., Wallingford, CT, 2013.

20 J.-Y. Liu, Y.-S. Li, J.-Y. Liu and Z.-S. Li, *J. Mol. Catal. A: Chem.*, 2006, **244**, 99.

Dalton Transactions

PAPER

View Article Online
View Journal | View Issue

Cite this: *Dalton Trans.*, 2016, **45**, 13532

An unprecedented one-step synthesis of octahedral Cu(II)-bis(iminoquinone) complexes and their reactivity with $NaBH_4$†

Manas Kumar Mondal and Chandan Mukherjee*

A new non-innocent ligand, $H_2L^{AP(o\text{-}NO_2\text{-}OPh)}$, was synthesized. The ligand $H_2L^{AP(o\text{-}NO_2\text{-}OPh)}$ reacted with 0.5 equivalents of $CuCl_2{\cdot}2H_2O$ and provided the corresponding mononuclear four-coordinate [Cu(II)-bis(iminosemiquinone)] complex (**1**). Interestingly, the ligand upon reacting with 2 equivalents of $CuCl_2{\cdot}2H_2O$ in the presence of Et_3N and air provided the corresponding *trans*-dichloride-bound six-coordinate mononuclear Cu(II)-complex (**2**) in one step. To extend the validity of the newly developed one-step synthesis of the *trans*-dichloride-bound Cu(II)-bis(iminoquinone) complex using a non-innocent ligand and 2 equivalents of $CuCl_2{\cdot}2H_2O$, the previously reported non-innocent ligand H_2L^{AP} was further examined. Thus the formed *trans*-dichloride-bound Cu(II)-bis(iminoquinone) complex was designated as complex **3**. The complexes were characterized by IR, mass, UV-Vis/NIR, X-band EPR, and X-ray single crystal diffraction techniques. Molecular structure analysis confirmed that in **1** the oxidation state of the coordinating ligands was $[L^{ISQ(o\text{-}NO_2\text{-}OPh)}]^{1-}$, *i.e.*, one-electron oxidized iminosemiquinone. In **2** and **3**$\cdot CH_2Cl_2$, both the coordinated-ligands were present in their two-electron oxidized iminoquinone form. The iminoquinone-complex formation was found to proceed with the generation of CuCl salt. X-band EPR spectrum measurement confirmed that both the iminoquinone-complexes were paramagnetic and the unpaired electron was located at the $3d_{x^2-y^2}$ orbital of Cu(II) ions. When the Cu(II)-bis(iminoquinone) complex **3** was subjected to react with $NaBH_4$ in dry CH_3CN, H_2 gas was formed along with the generation of the corresponding Cu(II)-bis(iminosemiquinone) complex. GC analyses were performed for the identification of H_2 gas.

Received 18th June 2016,
Accepted 21st July 2016

DOI: 10.1039/c6dt02443b

www.rsc.org/dalton

Introduction

The participation of Cu-quinone species in various biological phenomena[1a–g] and $-CF_3$ group transferring reactions[1h] has motivated chemists for the synthesis of Cu-quinone complexes. One of the strategies for the synthesis of Cu-quinone complexes is the employment of a phenol unit-containing non-innocent ligand as a coordinating unit. Non-innocent ligands refer to the organic moieties, which upon complex formation change their redox state. These ligands in the presence of Cu-salt, air and a base provide Cu(II)-radical complexes, which upon further oxidation using external oxidants can be converted into the corresponding Cu(II)-quinone species.[1i,2]

Despite employing various external oxidants and Cu(II)-radical complexes to generate the corresponding Cu(II)-quinone species, we have found that *trans*-dichloride bound mononuclear Cu(II)-bis(iminoquinone) complexes can be synthesized in one step by reacting only 2 equivalents of $CuCl_2{\cdot}2H_2O$ with 1 equivalent of non-innocent N-substituted-2-aminophenol-type ligands in the presence of triethylamine (Et_3N) and air. Herein, we shall report the synthesis, characterization and probable formation route to the Cu(II)-bis(iminoquinone) complexes. The complex **3** has been further examined as the possible promoter to the generation of H_2 gas from the economically benign $NaBH_4$ in dry CH_3CN.

Results and discussion

A new non-innocent ligand $H_2L^{AP(o\text{-}NO_2\text{-}OPh)}$ was employed for this study (Scheme 1). The ligand was synthesized by reacting 1 : 1 compound **A** and 3,5-di-*tert*-butyl catechol in hexane in the presence of Et_3N and air. Ligand $H_2L^{AP(o\text{-}NO_2\text{-}OPh)}$ reacted with 0.5 equivalents of $CuCl_2{\cdot}2H_2O$ in CH_3CN in the presence

Department of Chemistry, Indian Institute of Technology Guwahati, Guwahati, 781039 Assam, India. E-mail: cmukherjee@iitg.ernet.in

†Electronic supplementary information (ESI) available: Characterization of ligands and complexes, infrared, mass spectra, NMR, UV–Vis/NIR, EPR spectra, GC-plots, and video-clip for H_2 gas production. CCDC 1446979–1446981. For ESI and crystallographic data in CIF or other electronic format see DOI: 10.1039/c6dt02443b

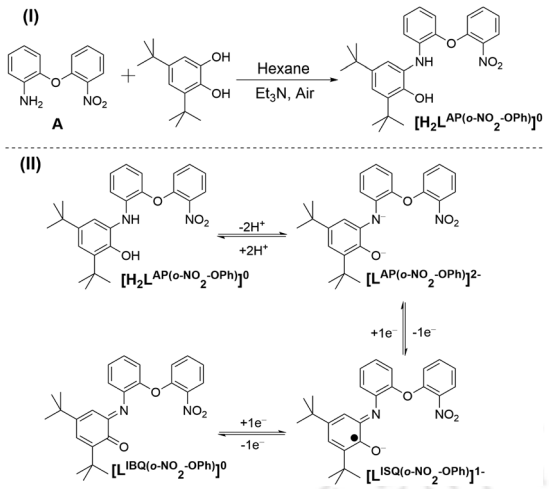

Scheme 1

of Et_3N under an aerial atmosphere for 2 hours and provided the corresponding square planar diradical-containing mononuclear complex (**1**) in 68% yield (Scheme 2). However, when the reaction was performed under the same reaction conditions despite using 2 equivalents of $CuCl_2{\cdot}2H_2O$, an octahedral mononuclear Cu(II)-bis(iminoquinone) complex (**2**) was formed in 39% yield. To extend the validity of the newly developed method for the one-step synthesis of the Cu(II)-bis(iminoquinone) complex to another non-innocent ligand, a well-defined non-innocent ligand, *N*-phenyl-4,6-di-*tert*-butyl-2-aminophenol (H_2L^{AP}),[4e] was employed. Indeed, the corresponding octahedral diquinone-coordinated Cu(II) complex (complex **3**) was formed in 65% yield under the same reaction conditions.

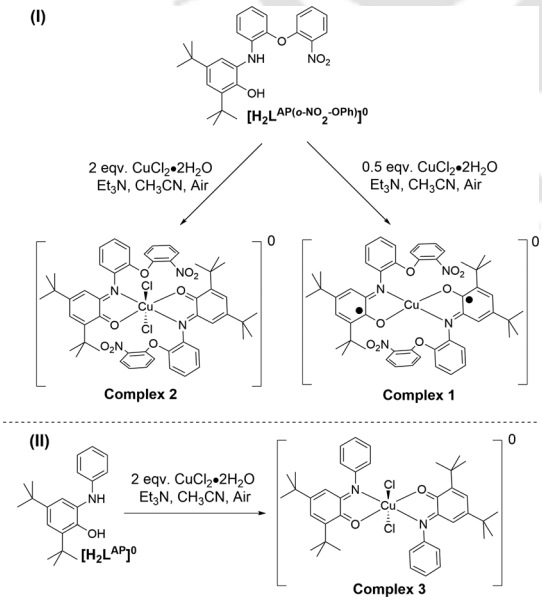

Scheme 2 Schematic representations of complexes **1**, **2** and **3** formation.

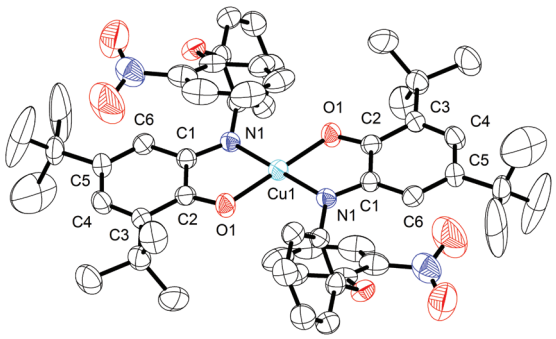

Fig. 1 ORTEP plot of complex **1**; thermal ellipsoids were drawn at the 40% probability level. H-atoms were omitted for clarity.

The molecular structure of complex **1** was determined by single crystal X-ray diffraction analysis at 296(2) K. The complex crystallized in the monoclinic space group *C*2/*c*. The ORTEP diagram of the molecular structure of the complex is shown in Fig. 1 and selected bond distances and bond angles are given in Table 1.

The complex molecule was neutral in charge and in the molecule the central Cu atom was four-coordinate where two

Table 1 Selected bond distances (Å) and bond angles (°) for the complexes

	1	**2**	**3**·CH_2Cl_2
Cu1–O1	1.929(3)	2.344(3)	2.414(2)
Cu1–N1	1.934(3)	2.025(4)	2.020(3)
Cu1–Cl1		2.273(1)	2.294(1)
O1–C2	1.301(4)	1.215(5)	1.215(4)
O2–C12	1.399(4)	1.386(6)	
O2–C13	1.372(4)	1.379(6)	
N1–C1	1.340(4)	1.298(5)	1.286(4)
N1–C7	1.422(4)	1.426(6)	1.432(4)
N2–O3	1.197(5)	1.234(8)	
N2–O4	1.186(5)	1.181(8)	
N2–C18	1.487(6)	1.444(9)	
C1–C2	1.454(5)	1.525(6)	1.522(4)
C2–C3	1.431(5)	1.471(6)	1.469(5)
C4–C3	1.371(5)	1.343(7)	1.342(4)
C4–C5	1.430(6)	1.464(7)	1.463(4)
C5–C6	1.361(5)	1.332(7)	1.341(5)
C1–C6	1.416(5)	1.436(6)	1.441(4)
O1–Cu1–O1*	180.0(2)	180.0(1)	180.0(1)
O1–Cu1–N1	83.4(1)	74.5(1)	73.5(1)
O1–Cu1–N1*	96.6(1)	105.5(1)	106.5(1)
N1–Cu1–Cl1		89.9(1)	88.2(1)
N1–Cu1–Cl1*		90.1 (1)	91.8(1)
Cl1–Cu1–Cl1*		180.0(1)	180.0(1)
Cl1–Cu1–O1*		92.13(9)	91.8(1)
Cl1–Cu1–O1		87.87(9)	88.2(1)
N1–Cu1–N1*	180.0(1)	180.0(1)	180.0(1)
C2–O1–Cu1	113.1(2)	108.7(3)	108.8(2)
C13–O2–C12	117.7(3)	118.0(4)	
C1–N1–C7	120.7(3)	122.7(4)	120.3(3)
C1–N1–Cu1	113.3(2)	120.4(3)	121.7(2)
C7–N1–Cu1	125.2(2)	116.9(3)	117.8(2)
O3–N2–C18	116.1(5)	117.4(8)	
O4–N2–C18	119.4(5)	119.9(8)	
O4–N2–O3	124.6(6)	122.6(8)	

The asterisk (*) symbol stands for symmetry operation, inversion center.

NO donor sets from two individual ligands occupied the coordination sites in a *trans*-fashion. The molecule acquired an inversion centre on the Cu1 atom. Hence, the nature of both the coordinated-ligands was the same. The geometry around the Cu atom was square planar as evident by the τ^3 = 0.00 value. The Cu1–O1 = 1.929(3) Å and Cu1–N1 = 1.934(3) Å bond distances suggested +II oxidation state of the Cu atom.[4]

The C–C bond distances of the *tert*-butyl group-containing C_6 rings were different from those of the other C_6 rings. The C–C bonds of the without *tert*-butyl group-containing C_6 rings ranged in between 1.362–1.399 Å and indicated the phenyl form of the C_6 rings. Contrarily, three alternating short–long–short C–C bonds [C3–C4 = 1.371(5), C4–C5 = 1.430(6), C5–C6 = 1.361(5) Å] followed by other three long C–C bonds [C1–C6 = 1.416(5), C1–C2 = 1.454(5), C2–C3 = 1.431(5) Å] were present in the *tert*-butyl group-containing C_6 rings. This type of distortion is known as quinoid-distortion and implied the non-aromatic character of the C_6 rings, *i.e.* oxidation of phenyl rings. The C1–N1 = 1.340(4) and C2–O2 = 1.301(4) Å bonds ranged in between those of single bond (C–N = 1.45, C–O = 1.36 Å) and double bond (C=N = 1.30, C=O = 1.22 Å) values, which implied an one-electron oxidized delocalized iminosemiquinone form ($[L^{ISQ(o\text{-}NO_2\text{-}OPh)}]^{1-}$, Scheme 1) of the coordinating ligands.[4] In short, the neutral mononuclear complex was a Cu(II)-bis(iminosemiquinone).

Single crystal X-ray diffraction measurements for complex **2** and complex **3**·CH_2Cl_2 were performed at 296(2) K. ORTEP drawings of the molecular structure of the complexes are shown in Fig. 2. Selected bond distances and bond angles are given in Table 1. Complex **2** and complex **3**·CH_2Cl_2 crystallized in the monoclinic space group $C2/c$ and $P2_1/c$, respectively.

Both the complexes were neutral and the central Cu atom was six-coordinate. The Cl, N, and O atoms were coordinated to the central Cu atom in a *trans*-fashion. The Cu1–N1 = 2.025(4)[**2**], 2.020(3)[**3**]; Cu1–O1 = 2.344(3)[**2**], 2.414(2)[**3**]; Cu1–Cl1 = 2.273(1)[**2**], 2.294(1)[**3**] (parenthesis indicates the complex) bond distances indicated distorted octahedral geometry around the Cu centre. While, Cu1–N1 bond distances were close to the bond distances found in complex **1**, Cu1–O1 bonds were significantly long compared to those found in complex **1**. This further implied that the oxidation state of the coordinated ligands in complex **2** as well as in complex **3** was different from that in complex **1**, *i.e.*, the coordinated ligands were not in their one-electron oxidized iminosemiquinone forms. Indeed, double bond characterizing C1–N1 = 1.298(5)[**2**], 1.286(4)[**3**] and C2–O2 = 1.215(5)[**2**], 1.215(4)[**3**] Å bond distances along with quinoid-distortion of the *tert*-butyl group-containing phenyl rings (Tables 1 and S13†) confirmed the two-electron oxidized iminoquinone ($[L^{IBQ(o\text{-}NO_2\text{-}OPh)}]^0$, Scheme 1)[2] form of the coordinated ligands. Thus, both complex **2** and complex **3** comprised of two chloride anions, two ligands in iminoquinone form and a Cu(II) ion.

The X-band EPR spectra of complex **1**, complex **2**, and complex **3**·CH_2Cl_2 were recorded at 77 K. The solubility of complex **1** was very low in most of the organic solvents *e.g.* CH_2Cl_2, $CHCl_3$, MeOH, EtOH, CH_3CN, and $PhCH_3$ and therefore, the spectrum was obtained in the solid state. For the other two complexes, the spectra were recorded in a 2 : 1 CH_2Cl_2/toluene solvent mixture. Experimental and simulated spectra are shown in Fig. 3.

The obtained-spectrum of complex **1** was broad and unresolved. This type of unresolved spectrum is common in solid-state EPR. Nevertheless, the experimentally obtained axial spectrum was well simulated using the following para-

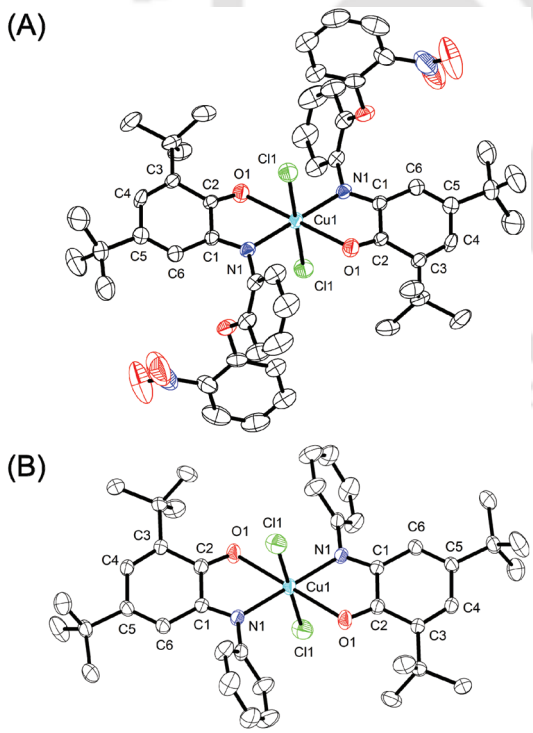

Fig. 2 ORTEP plots for complex **2** and complex **3**; thermal ellipsoids were drawn at the 40% probability level. H-atoms and CH_2Cl_2 solvent molecules (for complex **3**) were omitted for clarity.

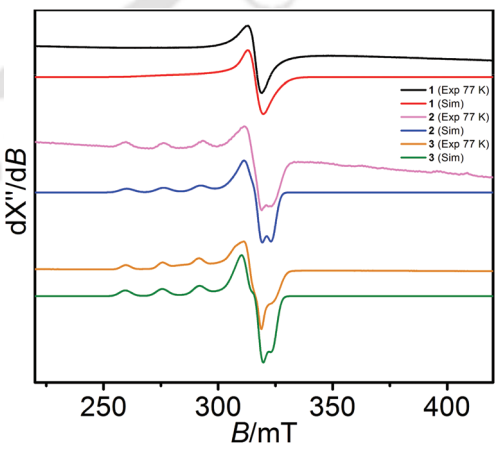

Fig. 3 X-band EPR spectrum of the complexes measured at 77 K. Conditions: X-band microwave frequency (GHz): 9.145 [**1**], 9.143 [**2**], 9.142 [**3**]; modulation frequency (kHz): 100 [**1**, **2**, **3**]; microwave power (mW): 0.998 [**1**], 0.995 [**2**, **3**]; amplitude (G): 1.0 [**1**, **3**], 3.0 [**2**].

meters: $g_1 = g_2 = 2.065$; $g_3 = 2.230$; $g_{iso} = 2.120$; $^{63/65}Cu(A_1, A_2, A_3) = (0, 0, 133) \times 10^{-4}$ cm^{-1}. $g_{iso} > 2.00$ and $g_3 > g_1 = g_2 > 2.00$ values indicated the existence of the unpaired-electron at the $3d_{x^2-y^2}$ orbital of the Cu(II) ion. $g_1 = g_2 \neq g_3$ implied that complex **1** acquired a tetragonal environment around the Cu(II) centre. Indeed, in the complex two distal C atoms from two different phenyl rings (Fig. S8 and S6†) occupied the axial positions. The Cu(II)–C_{Ph} (C_{Ph} stands for C atoms belonging to phenyl rings) units were having a distance of 3.13 Å. Therefore, complex **1** could also be described as axially elongated octahedral.[5]

In both complex **2** and complex **3**, the Cu(II) ion was the only paramagnetic centre (*vide supra*). Experimentally obtained EPR spectra were also a signature of Cu(II)-centred unpaired-electrons. The spectra were simulated using the following parameters: g_1 = 2.058[**2**], 2.057[**3**]; g_2 = 2.080[**2**], 2.085[**3**]; g_3 = 2.300[**2**], 2.303[**3**]; g_{iso} = 2.146[**2**], 2.148[**3**]; $^{63/65}Cu(A_1, A_2, A_3) = (0, 0, 160) \times 10^{-4}$ cm^{-1}[**2**], $(3, 3, 162) \times 10^{-4}$ cm^{-1}[**3**]. The simulated-data reinforced that the unpaired-electron was located at the Cu(II) centre ($g_{iso} > 2.00$) and the EPR signals appeared for axial Cu(II) systems with slight rhombic distortions. $g_3 > g_1, g_2$, and $A_3 \gg A_1, A_2$ further indicated the presence of unpaired electrons at the $d_{x^2-y^2}$ orbital of the Cu(II) ion.[5c,d]

It has been established by X-ray single crystal molecular structure analysis that complex **1** comprised of three paramagnetic centres (*vide supra*): two radical anions and one Cu(II) ion ($3d^9$), *i.e.*, one unpaired-electron on each paramagnetic centre. Variable-temperature magnetic susceptibility measurement at 1 T showed μ_{eff} = 1.80 μ_B at 5 K. The value remained almost constant till 150 K. Above the temperature, the μ_{eff} value increased gradually and reached μ_{eff} = 2.17 μ_B at 300 K. μ_{eff} = 1.80 μ_B at 5 K indicated that complex **1** had an S = 1/2 ground state with $g > 2.00$ (μ_{eff} = 1.73 μ_B; g = 2.00) and the increase of magnetic moment with temperature emphasized the presence of multi-paramagnetic centers. Thus the magnetic study further supported the Cu(II)-bis(iminosemiquinone) nature of complex **1**. This type of four-coordinate Cu(II)-bis(iminosemiquinone) system and similar magnetic behaviour have already been extensively studied[4h–j,m] and it has been established that an S = 1/2 ground state and the Cu(II)-centred EPR spectrum appeared due to stronger antiferromagnetic coupling between the two radical centres compared to a radical centre and the Cu(II) centre. Herein, the coupling between the two radicals was propagated through the Cu(II)-centered t_{2g} orbitals. Akin to the previous reports,[4h–j] herein, we have also observed that the antiferromagnetic coupling between two radicals (−270 cm^{-1}) dominated over the coupling between a radical and the Cu(II) centre (−10 cm^{-1}) [Fig. 4].

The electrochemical behavior of complexes **1**, **2** and **3**·CH_2Cl_2 has been recorded in CH_2Cl_2 solution containing 0.1 (M) $[(^nBu)_4N]ClO_4$ as the supporting electrolyte at a glassy carbon working electrode, a platinum wire counter electrode and an Ag/AgCl reference electrode. Ferrocenium hexafluorophosphate was used as an internal standard and all the potentials have been referenced *vs.* Fc^+/Fc couple. The cyclic voltammograms of complexes **1**, **2** and **3**·CH_2Cl_2 are shown in Fig. 5 and the corresponding redox potentials are summarized in Table 2.

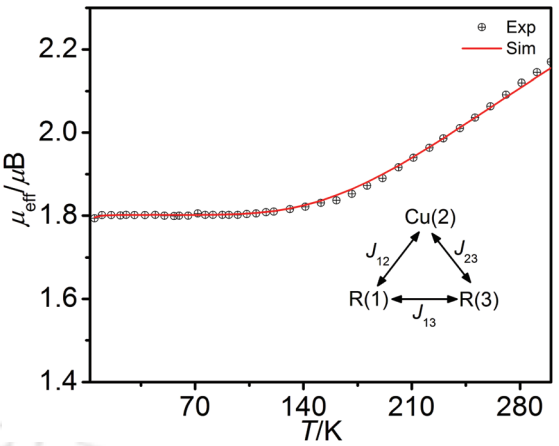

Fig. 4 μ_{eff} *vs.* T plot for **1**; B = 1.0 T. The experimental result was simulated by using the parameters: S_{Cu} = 1/2, S_R = 1/2, $g_{Cu(II)}$ = 2.08, g_R = 2.00, $J_{12} = J_{23}$ = −10.0 cm^{-1}, J_{13} = −270.0 cm^{-1}.

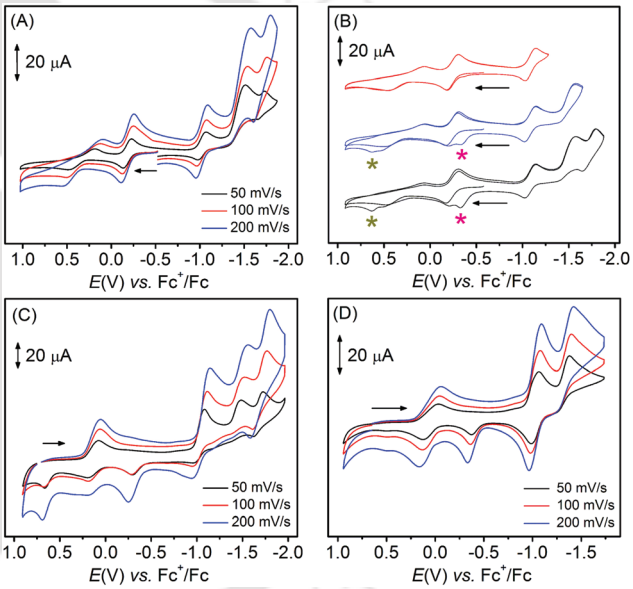

Fig. 5 Cyclic voltammograms of (A) complex **1**, (C) complex **2** and (D) complex **3**·CH_2Cl_2 measured in dichloromethane at 25 °C. (B) *Cyclic voltammograms of complex* **1** *at three different potentials and two consecutive cycles.*

Complex **1** was composed of a Cu(II) ion and two iminosemiquinone moieties. The complex underwent two successive ligand-centered oxidations at −0.129 and 0.492 V and a fully oxidized Cu(II)-bis(iminoquinone) species was developed.[4c,e,f,h] Thus obtained iminoquinone-coordinated Cu(II) species underwent five successive reductions at 0.119, −0.253, −1.074, −1.538 and −1.765 V during the cathodic scan. Two coordinated-iminoquinone moieties can accept a maximum of four electrons. Thus, the fifth reduction process corresponded to the reduction of Cu(II) to Cu(I). Therefore, it was apparent that a Cu(I)-bis(amidophenolate) species was formed after five successive reductions. During the oxidation of Cu(I)-bis(amido-

Table 2 Summary of redox potentials (V) of the complexes

Complex	E_{Ox} (V) *vs.* Fc^+/Fc	E_{Red} (V) *vs.* Fc^+/Fc	ΔE (V) *vs.* Fc^+/Fc	$E_{1/2}$ (V) *vs.* Fc^+/Fc
1	−1.605	−1.765	0.160	−1.685
		−1.538		
	−0.964	−1.074	0.110	−1.019
	−0.129	−0.253	0.124	−0.191
	0.492	0.119	0.373	0.306
2	−1.610	−1.769	0.159	−1.689
		−1.522		
	−0.956	−1.115	0.159	−1.036
	−0.289			
	0.181	0.054	0.127	0.118
	0.678			
3·CH_2Cl_2	−1.244	−1.401	0.157	−1.322
	−0.980	−1.081	0.101	−1.030
	−0.365			
	0.123	−0.045	0.168	0.039
	0.501			

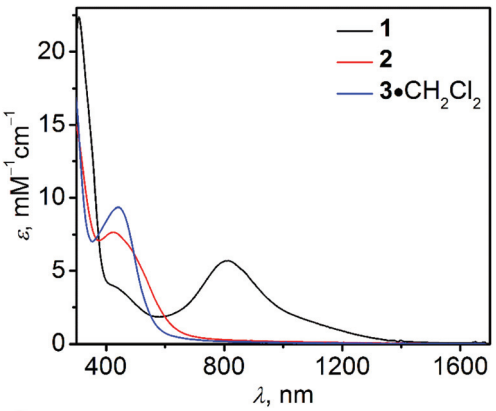

Fig. 6 UV-Vis/NIR spectra of complexes **1**, **2** and **3**·CH_2Cl_2 in CH_2Cl_2 at room temperature.

Table 3 Summary of the electronic absorption data for the complexes

Complex	λ_{max}, nm (ε, M^{-1} cm^{-1})
1	1049^{br} (1850), 812 (5700), 431^{sh} (3900), 308 (22 400)
2	650^{br} (850), 425 (7650), 305 (14 350)
3·CH_2Cl_2	650^{br} (400), 440 (9350), 295 (17 200)

br and sh stand for broad peak and shoulder peak, respectively.

phenolate) species, two additional oxidation waves appeared at −0.285 and 0.669 V as observed by two successive cyclic voltammograms' measurement (Fig. 5B, *). The reduction potential beyond −1.288 V was responsible for the appearance of those two additional oxidation waves (Fig. 5B). Thus the irreversible reduction wave at −1.538 V was attributed to the process of the $[Cu^{II}\{L^{AP(o\text{-}NO_2\text{-}OPh)}\}\{L^{ISQ(o\text{-}NO_2\text{-}OPh)}\}]^-/[Cu^{I}\{L^{AP(o\text{-}NO_2\text{-}OPh)}\}\{L^{ISQ(o\text{-}NO_2\text{-}OPh)}\}]^{2-}$ couple (Schemes 1 and S12†). Hence, the reduction at −1.685 V was due to the Cu(I)-coordinated ligand-centered reduction of iminosemiquinone species to the corresponding amidophenolate species.

In complexes **2** and **3**·CH_2Cl_2, both the coordinated-ligands were present in their two-electron oxidized iminoquinone form. In the complex, all the reduction waves were not completely discernible during the cathodic scan. Noteworthily, the reduction potential values, −1.115, −1.522, and −1.769 V, were almost the same as the reduction potential values of complex **1**. Thus, the loss of axial chloride ions presumably took place after the reduction of complex **2** at 0.181 V. Akin to complex **2**, all the redox waves of complex **3**·CH_2Cl_2 were also not well resolved. The observed reduction potentials at −1.030 and −1.322 V were close to the corresponding Cu(II)-bis(iminosemiquinone) complex.[4e] This implied the loss of axial chloride ions during the electron transfer in the potential range 0.645 to −0.880 V.

The electronic absorption (UV-Vis/NIR) spectra of complexes **1**, **2** and **3**·CH_2Cl_2 were recorded in dichloromethane at room temperature (25 °C). The spectra are shown in Fig. 6. The absorption band position along with the extinction coefficient values are summarized in Table 3. In the case of complex **1**, an intense band corresponding to ligand-to-ligand charge transfer appeared at 812 nm (ε = 5700 M^{-1} cm^{-1}). This band is typical of four coordinate Cu(II)-bis(iminosemiquinone) complexes.[4e,f,h] The band at 431 nm (ε = 3900 M^{-1} cm^{-1}) appeared due to metal-to-ligand charge transfer (MLCT). Thus, the electronic absorption feature of complex **1** further supported its Cu(II)-bis(iminosemiquinone) form. The absence of the charge transfer band in the NIR region in the UV-Vis/NIR spectra of both complexes **2** and **3** indicated the absence of coordinated iminosemiquinone moieties in the coordination sphere of the complexes. Both the complexes provided a absorption manifold at approximately 650 nm, which corresponded to the Cu(II)[$3d^9$]-centered d–d electronic transition (Table 3). The bands at 425 nm (**2**) and 440 nm (**3**) (parenthesis indicated the complex) appeared due to the π–π* transition of the Cu(II)-coordinated iminoquinone moieties.[2,4e]

In order to understand the solvent-effect in the one-step Cu(II)-bis(iminoquinone) complex formation, we have performed the reaction in EtOH by keeping the other reaction conditions the same. In the process, complex **2** was also formed in 46% yield. Hence, it can be argued that the Cu(II)-bis(iminoquinone) complex formation-reaction was independent of the nature of the used solvent, *i.e.* the reaction was not a solvent driven-process.

In a reaction, 2 equivalents of $CuBr_2$ or $Cu(ClO_4)_2{\cdot}6H_2O$ or $Cu(OAc)_2{\cdot}2H_2O$ upon reacting with 1 equivalent of either ligand $H_2L^{AP(o\text{-}NO_2\text{-}OPh)}$ or H_2L^{AP} in the presence of Et_3N and air in 2 hours reaction time did not provide the corresponding octahedral Cu(II)-bis(iminoquinone) species, rather diradical-containing square planar Cu(II) complexes were isolated as a green solid. This indicated that the Cu(II)-bis(iminoquinone) complex formation depended on the nature of the employed salt. The anion, associated with the Cu(II) ion, was then postulated to participate in the electron transfer,[6] *i.e.* in the oxidation of iminosemiquinone to iminoquinone.

In order to gain insight into the mechanistic path for the formation of complex **2** and complex **3**, we have reacted the corresponding 1 equivalent of each ligand with 2 equivalents of $CuCl_2{\cdot}H_2O$ in CH_3CN for 2 hours. Indeed, complex **2** and complex **3** were formed and during the formation of the complexes a colorless solid that was insoluble in CH_3CN, CH_2Cl_2, and $CHCl_3$ was isolated. The color of the solid in due course changed to light green under air. The colorless solid was X-band EPR silent, while the light green solid showed a Cu(II)-centred EPR spectrum (Fig. S18 and S11†). This implied that the initially isolated solid was CuCl, which under an aerial atmosphere changed to its Cu(II) form. Hence, it was evident that during the reaction Cu(II) was reduced to Cu(I). The electron-transfer was possibly an inner sphere process,[6] where at the initial stage two chloride ions from two individual $CuCl_2$ molecules formed two bridges with the central Cu(II) ion of a diradical-containing Cu(II) complex in a *trans*-fashion (Scheme 3). After that, one-electron transfer to each bound $CuCl_2$ unit from the two iminosemiquinone moieties through the Cu(II) centre took place and finally octahedral *trans*-dichloride-bound mononuclear Cu(II)-bis(iminoquinone) complexes and CuCl formed. A detailed mechanistic proposal is depicted in Scheme 3.

An iminoquinone moiety can accept two-electrons, hence, Cu(II)-bis(iminoquinone) complexes can be used as electron-acceptors or as multi-electron oxidising agents. Therefore, the complexes can be examined as catalysts or promoters for the generation of H_2 gas from BH_4^- species. Thus, such reactivity was preliminarily investigated employing more economical Cu(II)-bis(iminoquinone) complex $\mathbf{3}{\cdot}CH_2Cl_2$.[7] In dry CH_3CN, 1 : 5 complex $\mathbf{3}{\cdot}CH_2Cl_2$ and $NaBH_4$ were added (see the Experimental section). Instantaneously, H_2 gas started forming and was coming out from the reaction medium in bubble form (Fig. 7, also see the video clip attached in the ESI†). The gas was characterized by the gas chromatography (GC) technique (Fig. S19 and S12†). Noteworthily, under the same reaction conditions almost no H_2 gas was formed in the absence of the complex. In due course brown Cu(II)-bis(iminoquinone) complex $\mathbf{3}{\cdot}CH_2Cl_2$ transformed to a green precipitate, which was characterized by mass, IR and UV-Vis/NIR spectroscopic techniques and found as the corresponding Cu(II)-bis(iminosemiquinone) species $[Cu(L^{ISQ})_2]$[4e] (Scheme 4). The isolated yield of the crystalline Cu(II)-bis(iminosemiquinone) species after the reaction was 78% and the complex can be converted again to complex **3** in a different reaction set-up by using 3.0 equivalents of $CuCl_2{\cdot}2H_2O$ in CH_3CN (see the Experimental section #).

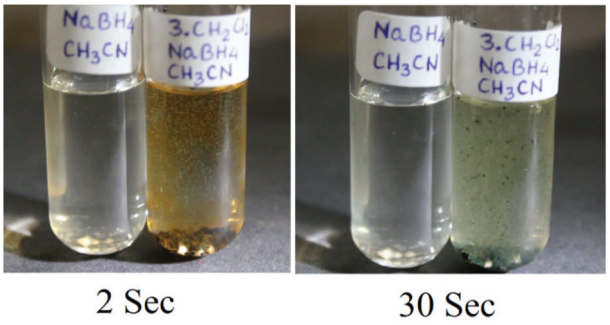

Fig. 7 Complex $\mathbf{3}{\cdot}CH_2Cl_2$ assisted generation of H_2 gas from $NaBH_4$ in dry CH_3CN.

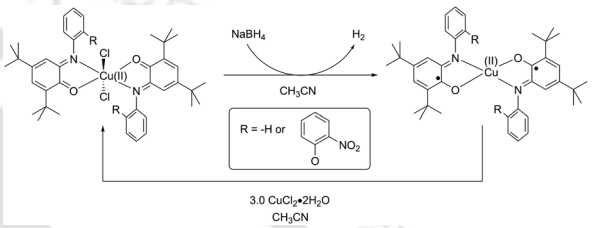

Scheme 4

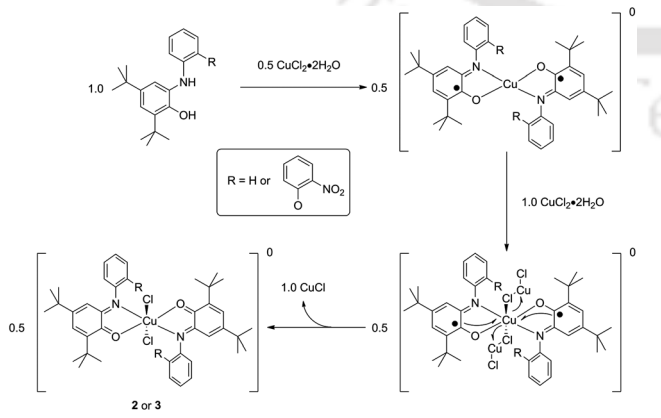

Scheme 3 Mechanistic proposal for the formation of complexes **2** and **3** by using 2 equivalents of $CuCl_2{\cdot}2H_2O$.

Conclusions

To summarize, herein, we presented an efficient and unprecedented method for the one-step and one-pot synthesis of the Cu(II)-bis(iminoquinone) complex using non-innocent ligands and 2 equivalents of $CuCl_2{\cdot}2H_2O$ in the presence of Et_3N and air. It has also been found that solo $CuCl_2{\cdot}2H_2O$ can also be employed as an oxidant for the synthesis of the Cu(II)-bis(iminoquinone) complex from its corresponding Cu(II)-bis(iminosemiquinone) complex (see the Experimental section #). Although it is too early to generalize, it seems that the method can be employed to the synthesis of Cu(II)-bis-(iminoquinone) complexes employing any non-innocent 2-aminophenol-type ligand.

Additionally, in preliminary investigation, herein, the Cu(II)-bis(iminoquinone) complex $\mathbf{3}{\cdot}CH_2Cl_2$ has been demonstrated as an efficient promoter for the production of H_2 gas from economically benign $NaBH_4$ in non-aqueous CH_3CN medium.

In this process about 78% of the corresponding Cu(II)-bis-(iminosemiquinone) complex is isolated. The isolated complex, in a different reaction set-up, can again be transmuted to the Cu(II)-bis(iminoquinone) complex by the solo use of $CuCl_2{\cdot}2H_2O$. Hence, a reversible cycle, *via* the regeneration process, can be established for the production of H_2 gas from $NaBH_4$. In our laboratory, further investigations will be carried out to examine the potential of Cu(II)-bis(iminoquinone) complexes as electrochemical-catalysts for the continuous generation of H_2 gas.

Experimental section

Materials

All the chemicals and solvents were obtained from commercial sources and were used as supplied, unless noted otherwise. 3,5-Di-*tert*-butylcatechol, 2-fluoronitrobenzene, 10% Pd/C, $NaBH_4$, and NaH were purchased from Sigma-Aldrich. Solvents were obtained from Merck (India). THF was dried before used. Mass spectra were obtained in HPLC grade acetonitrile solution.

Physical methods

X-ray crystallographic data for **1**, **2** and **3** were collected (Table 4) using a 'Super Nova, single source at offset, Eos diffractometer'. The structure was solved with the Superflip, structure solution program using Charge Flipping and refined by direct methods using 'SHELXS-97' and with full-matrix least squares on F^2 using 'SHELXL-97'.[8] In both cases, all the non-hydrogen atoms were refined anisotropically. IR spectra were recorded on a Perkin Elmer Instrument at normal temperature with KBr pellets by grinding the sample with KBr (IR Grade). UV-Vis spectra were recorded on a Perkin Elmer, Lambda 750, UV/VIS/NIR spectrometer by preparing a known concentration of the samples in HPLC grade CH_2Cl_2 at room temperature using a cuvette of 1 cm width. ^1H and ^{13}C NMR spectra were collected on an Agilent 400 MHz NMR machine. Mass spectral (MS) data were obtained from a quadrupole time-of-flight (QTOF)-MS spectrometer ('Waters, Model: Q-Tof Premier' or "Agilent 6520") and peaks are given in *m*/*z* (% of base peak). Variable temperature magnetic susceptibility measurements were performed using a superconducting quantum interference device (SQUID) magnetometer at 1 T external magnetic field. Simulations of the experimentally obtained magnetic measurements were performed using julX programme developed by Dr E. Bill.[9]

Synthesis of $H_2L^{AP(o\text{-}NO_2\text{-}OPh)}$

To a stirred solution of 2-(2-nitrophenoxy)aniline (2.798 g, 12.15 mmol) in hexane (20 mL), 3,5-di-*tert*-butylcatechol (2.701 g, 12.15 mmol) and Et_3N (0.02 ml) were added sequen-

Table 4 Crystallographic data and structure refinement parameters for complexes **1**, **2**, and **3**·CH_2Cl_2

	1	**2**	**3**·CH_2Cl_2
Empirical formula	$C_{52}H_{56}CuN_4O_8$	$C_{52}H_{56}Cl_2CuN_4O_8$	$C_{40}H_{50}Cl_2CuN_2O_2{\cdot}CH_2Cl_2$
Formula weight	928.55	999.45	810.19
Crystal habit, colour	Plate/green	Columnar/red	Block/red
Crystal size, mm^3	0.24 × 0.14 × 0.12	0.18 × 0.12 × 0.10	0.36 × 0.28 × 0.24
Temperature, *T*	296(2) K	293(2) K	293(2) K
Wavelength, λ (Å)	0.71073	0.71073	0.71073
Crystal system	Monoclinic	Monoclinic	Monoclinic
Space group	*C*2/*c*	*C*2/*c*	$P2_1/c$
Unit cell dimensions	*a* = 27.611(2) Å	*a* = 33.6810(16) Å	*a* = 9.5682(5) Å
	b = 9.7390(8) Å	*b* = 16.0902(7) Å	*b* = 20.2538(11) Å
	c = 18.7464(14) Å; α = 90.00°,	*c* = 11.2272(5) Å; α = 90.00°,	*c* = 11.7161(8) Å; α = 90.00°,
	β = 105.248(8)°, γ = 90.00°	β = 98.919(4)°, γ = 90.00°	β = 99.951(5)°, γ = 90.00°
Volume, *V* ($Å^3$)	4863.5(7)	6010.8(5)	2236.3(2)
Z	4	4	2
Calculated density (mg m^{-3})	1.268	1.104	1.203
Absorption coefficient, μ (mm^{-1})	0.506	0.500	0.760
F(000)	1956	2092	850
θ range for data collection	1.53° to 25.10°	3.07° to 25.00°	2.95° to 25.00°
Limiting indices	$-32 \le h \le 32$, $-11 \le k \le 10$,	$-40 \le h \le 37$, $-18 \le k \le 19$,	$-11 \le h \le 8$, $-24 \le k \le 14$,
	$-22 \le l \le 22$	$-6 \le l \le 13$	$-13 \le l \le 12$
Reflection collected/unique	17 036/4163	10 830/5270	9210/3929
	[*R*(int) = 0.0729]	[*R*(int) = 0.0600]	[*R*(int) = 0.0261]
Completeness to θ	95.7% (θ = 25.10°)	99.5% (θ = 25.00°)	99.8% (θ = 25.00°)
Max. and min. transmission	0.941/0.919	0.951/0.931	0.833/0.775
Refinement method	SHELXL-97 (Sheldrick, 2008)[8]	SHELXL-97 (Sheldrick, 2008)[8]	SHELXL-97 (Sheldrick, 2008)[8]
Data/restraints/parameters	4163/0/301	5270/0/310	3929/0/247
Goodness of fit on F^2	0.985	1.043	1.082
Final *R* indices [$I > 2\sigma(I)$]	R_1 = 0.0600	R_1 = 0.0739	R_1 = 0.0520
	wR_2 = 0.1482	wR_2 = 0.1578	wR_2 = 0.1485
R indices (all data)	R_1 = 0.1150	R_1 = 0.1398	R_1 = 0.0663
	wR_2 = 0.1682	wR_2 = 0.1956	wR_2 = 0.1608
Largest diff. peak and hole	0.798 and −0.357 e $Å^{-3}$	0.360 and −0.410 e $Å^{-3}$	0.723 and −0.541 e $Å^{-3}$

tially at room temperature (25 °C) under air. A reddish homogeneous solution was obtained on refluxing the reaction mixture for 14 h. Then it was allowed to attain room temperature and the stirring was continued for another 26 h. Pale yellow crude was obtained on evaporation of the solvent and the product was crystallized from hot methanol. Yield: 3.87 g, 73%. FTIR (KBr pellet, cm^{-1}): 3460, 3382, 3359, 2960, 2905, 2866, 1611, 1602, 1586, 1528, 1503, 1481, 1426, 1392, 1351, 1316, 1267, 1249, 1223, 1178, 1101, 1034, 978, 880, 796, 781, 749, 693, 568, 543. ^{1}H NMR (399.853 MHz, $CDCl_3$): δ 7.97 (dd, J = 8.4 Hz, J = 1.6 Hz, 1H), 7.57–7.51 (m, 1H), 7.23–7.19 (m, 2H), 7.10 (d, J = 8.0 Hz, 1H), 7.06–6.99 (m, 3H), 6.85–6.81 (m, 1H), 6.59–6.57 (m, 1H), 6.18 (s, 1H), 5.74 (s, 1H), 1.42 (s, 9H), 1.26 (s, 9H) ppm. ^{13}C NMR (100.542 MHz, $CDCl_3$): δ 151.0, 149.5, 142.6, 140.8, 139.2, 135.6, 134.5, 126.8, 126.5, 126.2, 123.2, 122.5, 122.0, 120.2, 119.7, 118.5, 115.7, 35.2, 34.6, 31.8, 29.7 ppm. ESI-MS (+) m/z for $[C_{26}H_{30}N_2O_4 + H]^+$: Calcd, 435.22; found, 435.23.

Synthesis of {Cu[$L^{ISQ(o\text{-}NO_2\text{-}OPh)}$]$_2$}; 1

$CuCl_2{\cdot}2H_2O$ (0.022 g, 0.125 mmol) was added to a stirred solution of ligand $H_2L^{AP(o\text{-}NO_2\text{-}OPh)}$ (0.109 g, 0.25 mmol) in CH_3CN (10 mL) at room temperature under air. To the solution Et_3N (0.05 mL) was added and the stirring was continued for 5 h. During the period, a green solid was precipitated out. The precipitate was filtered and washed with CH_3CN (10 mL). Recrystallization of the solid from a CH_2Cl_2/CH_3CN (10 : 1) solvent mixture provided green crystals suitable for single crystal X-ray diffraction analysis. Yield: 0.079 g, 68%. FTIR (KBr pellet, cm^{-1}): 3072, 2956, 2906, 2870, 1607, 1588, 1529, 1478, 1462, 1448, 1433, 1419, 1353, 1335, 1269, 1256, 1244, 1230, 1101, 861, 850, 764, 737. ESI-MS (+) m/z for $[C_{52}H_{56}N_4O_8Cu]^+$: Calcd, 927.35; found, 927.47. UV-Vis/NIR (CH_2Cl_2) λ_{max}, nm (ε, M^{-1} cm^{-1}): 1049(1850), 812(5700), 431(3900), 308(22 400). Anal. Calcd for $C_{52}H_{56}CuN_4O_8$: C, 67.26; H, 6.08; N, 6.03. Found: C, 66.94; H, 6.10; N, 6.18.

Synthesis of {Cu[$L^{IBQ(o\text{-}NO_2\text{-}OPh)}{}_2Cl_2$]}; 2

To a solution of ligand $H_2L^{AP(o\text{-}NO_2\text{-}OPh)}$ (0.217 g, 0.5 mmol) in CH_3CN (10 mL), $CuCl_2{\cdot}2H_2O$ (0.171 g, 1.0 mmol) was added at room temperature under air. Addition of Et_3N (0.1 mL) to the stirred solution caused a green precipitation. It changed to brown within 30 min of stirring. The stirring was continued for further 1.5 h. To the mixture, dichloromethane (20 mL) was added and the solution was then filtered through a Whatman filter paper. Evaporation of the solvent under reduced pressure yielded a brown solid, which was washed with CH_3CN (5 mL). The residue was then dissolved in a 2 : 1 CH_2Cl_2/hexane solvent mixture. Slow evaporation of the solvent mixture provided suitable crystals for single crystal X-ray diffraction analysis. Yield: 0.098 g, 39%. Yield: 0.116 g, 46% (when EtOH was used as a solvent in place of CH_3CN). FTIR (KBr pellet, cm^{-1}): 3070, 3037, 2964, 2938, 2910, 2870, 1656, 1622, 1606, 1580, 1526, 1478, 1447, 1381, 1354, 1307, 1247, 1217, 1196, 1108, 902, 888, 864, 854, 791, 776, 759, 747, 467. ESI-MS (+) m/z for $[C_{52}H_{56}N_4O_8Cu]^+$: Calcd, 927.35; found, 927.35. UV-Vis/NIR (CH_2Cl_2) λ_{max}, nm (ε, M^{-1} cm^{-1}): 650(850), 485(6500), 425(7650), 305(14 350). Effective magnetic moment (μ_{eff}) at 25 °C = 2.05 μ_B (Evan's method).[10] Anal. Calcd for $C_{52}H_{56}Cl_2CuN_4O_8{\cdot}0.33C_6H_{14}$: C, 63.15; H, 5.96; N, 5.46. Found: C, 64.01; H, 6.11; N, 5.87.

Synthesis of {[Cu(L^{IBQ})$_2Cl_2$]}·CH_2Cl_2; 3·CH_2Cl_2

To a stirred solution of ligand H_2L^{AP} (0.074 g, 0.25 mmol) in CH_3CN (10 mL), $CuCl_2{\cdot}2H_2O$ (0.86 g, 0.5 mmol) and Et_3N (0.05 mL) were added at room temperature under air. A green precipitate appeared in due course. The precipitate changed to brown within 30 min and the stirring was further continued for 1.5 h. The thus formed precipitate was filtered and washed with CH_3CN (5 mL). Crystals suitable for single crystal X-ray diffraction analysis were grown by slow evaporation of a 2 : 1 CH_2Cl_2/hexane solvent mixture. Yield: 0.066 g, 65%.

To a stirred solution of ligand H_2L^{AP} (0.150 g, 0.5 mmol) in CH_3CN (10 mL), $CuCl_2{\cdot}2H_2O$ (0.043 g, 0.25 mmol) was added at room temperature under air. Addition of Et_3N (0.10 mL) to the solution caused a green precipitation and the stirring was continued for 1 h. The precipitate was filtered and washed with CH_3CN (10 mL). Yield: 0.124 g, 0.19 mmol, 76%.[4e] The green precipitate was taken in CH_3CN (10 mL) and $CuCl_2{\cdot}2H_2O$ (0.099 g, 0.58 mmol) was added at room temperature under air. The reaction mixture was stirred for 1.5 h. A brown precipitate appeared in due course. The precipitate was filtered and washed with CH_3CN (5 mL). Crystals suitable for single crystal X-ray diffraction analysis were grown by the slow evaporation of a 2 : 1 CH_2Cl_2/hexane solvent mixture. Yield: 0.134 g, 89% (with respect to the green precipitate). FTIR (KBr pellet, cm^{-1}): 3080, 3065, 2967, 2954, 2929, 2912, 2869, 1651, 1622, 1591, 1580, 1537, 1482, 1451, 1378, 1368, 1305, 1270, 1252, 1210, 1026, 976, 900, 804, 764, 737, 699. ESI-MS (+) m/z for $[C_{40}H_{50}CuN_2O_2]^+$: Calcd, 653.33; found, 653.32. UV-Vis/NIR (CH_2Cl_2) λ_{max}, nm (ε, M^{-1} cm^{-1}): 650(400), 440(9350), 295(17 200). Effective magnetic moment (μ_{eff}) at 25 °C = 1.95 μ_B (Evan's method).[10] Anal. Calcd for $C_{41}H_{52}Cl_4CuN_2O_2$: C, 60.78; H, 6.47; N, 3.46. Found: C, 61.02; H, 6.44; N, 3.37.

Formation of H_2 gas and regeneration of Cu(L^{ISQ})$_2$ from complex 3·CH_2Cl_2

To a mixture of complex 3·CH_2Cl_2 (0.122 g, 0.15 mmol) and $NaBH_4$ (0.026 g, 0.75 mmol), dry acetonitrile (5 mL) was added under a N_2 atmosphere. Bubbles of H_2 gas evolved immediately and the brown precipitate turned to a green precipitate. The generation of H_2 gas has been confirmed by using a TCD gas chromatographic analyzer (BRUKER 450 GC). Water (5 mL) was added to the reaction mixture and was stirred for 15 min at room temperature under air. The resultant green precipitate was filtered and washed with CH_3CN and recrystallized from a 5 : 1 CH_2Cl_2 : CH_3CN solution mixture. The yield of Cu(L^{ISQ})$_2$ was 0.076 g, 78%.

Acknowledgements

This project is funded by SERB [EMR/2015/002491], India. MKM thanks IIT Guwahati for his doctoral-fellowship. The Department of Chemistry and CIF, IIT Guwahati are thankfully acknowledged for the instrumental facilities.

Notes and references

1 (*a*) Y. Izumi, H. Sawada, N. Sakka, N. Yamamoto, T. Kume, H. Katsuki, S. Shimohama and A. Akaike, *J. Neurosci. Res.*, 2005, **79**, 849; (*b*) G. F. Z. da Silva and L.-J. Ming, *Angew. Chem.*, 2007, **119**, 3401, (*Angew. Chem., Int. Ed.*, 2007, **46**, 3337); (*c*) R. Liu, B. Goodell, J. Jellison and A. Amirbahman, *Environ. Sci. Technol.*, 2005, **39**, 175; (*d*) T. Klabunde, C. Eicken, J. C. Sacchettini and B. Krebs, *Nat. Struct. Biol.*, 1998, **5**, 1084; (*e*) E. I. Solomon, U. M. Sundaram and T. E. Machonkin, *Chem. Rev.*, 1996, **96**, 2563; (*f*) H. Decker, T. Schweikardt and F. Tuczek, *Angew. Chem.*, 2006, **118**, 4658, (*Angew. Chem., Int. Ed.*, 2006, **45**, 4546); (*g*) C. M. Wilmot, *Biochem. Soc. Trans.*, 2003, **31**, 493; (*h*) C. Anthony, *Arch. Biochem. Biophys.*, 2004, **428**, 2; (*i*) J. Jacquet, E. Salanouve, M. Orio, H. Vezin, S. Blanchard, E. Derat, M. Desage-El Murr and L. Fensterbank, *Chem. Commun.*, 2014, **50**, 10394.

2 C. Mukherjee, T. Weyhermüller, E. Bothe and P. Chaudhuri, *Inorg. Chem.*, 2008, **47**, 2740.

3 A. Addison, T. Rao, J. Reedijk, J. van Rijn and G. Verschoor, *J. Chem. Soc., Dalton Trans.*, 1984, 1349.

4 (*a*) F. Thomas, *Eur. J. Inorg. Chem.*, 2007, 2379; (*b*) P. Chaudhuri and K. Wieghardt, *Prog. Inorg. Chem.*, 2002, **50**, 151; (*c*) R. Rakshit, S. Ghorai, S. Biswas and C. Mukherjee, *Inorg. Chem.*, 2014, **53**, 3333; (*d*) P. Chaudhuri, K. Wieghardt, T. Weyhermüller, T. K. Paine, S. Mukherjee and C. Mukherjee, *Biol. Chem.*, 2005, **386**, 1023; (*e*) P. Chaudhuri, C. N. Verani, E. Bill, E. Bothe, T. Weyhermüller and K. Wieghardt, *J. Am. Chem. Soc.*, 2001, **123**, 2213; (*f*) S. Ye, B. Sarkar, F. Lissner, T. Schleid, J. van Slageren, J. Fiedler and W. Kaim, *Angew. Chem., Int. Ed.*, 2005, **44**, 2103; (*g*) S. Ghorai and C. Mukherjee, *Chem. – Asian J.*, 2014, **9**, 3518; (*h*) C. Mukherjee, U. Pieper, E. Bothe, V. Bachler, E. Bill, T. Weyhermüller and P. Chaudhuri, *Inorg. Chem.*, 2008, **47**, 8943; (*i*) C. Mukherjee, T. Weyhermüller, E. Bothe and P. Chaudhuri, *Inorg. Chem.*, 2008, **47**, 11620; (*j*) C. Mukherjee, T. Weyhermüller, E. Bothe, E. Rentschler and P. Chaudhuri, *Inorg. Chem.*, 2007, **46**, 9895; (*k*) A. I. Poddel'sky, V. K. Cherkasov and G. A. Abakumov, *Coord. Chem. Rev.*, 2009, **253**, 291; (*l*) S. Ghorai, A. Sarmah, R. K. Roy, A. Tiwari and C. Mukherjee, *Inorg. Chem.*, 2016, **55**, 1370; (*m*) A. Paretzki, R. Hübner, S. Ye, M. Bubrin, S. Kämper and W. Kaim, *J. Mater. Chem. C*, 2015, **3**, 4801; (*n*) D. L. J. Broere, R. Plessius and J. I. van der Vlugt, *Chem. Soc. Rev.*, 2015, **44**, 6886.

5 (*a*) I. M. Procter, B. J. Hathaway and P. J. Nichollos, *J. Chem. Soc. A*, 1968, 1678; (*b*) R. S. Drago, *Physical Methods in Chemistry*, Philadelphia, 1977; (*c*) B. J. Hathaway and D. E. Billing, *Coord. Chem. Rev.*, 1970, **5**, 1; (*d*) E. Garribba and G. Micera, *J. Chem. Educ.*, 2006, **83**, 1229; (*e*) R. Rakshit and C. Mukherjee, *Eur. J. Inorg. Chem.*, 2016, 2731.

6 H.-C. Chang, F.-C. Lo, W.-C. Liu, T.-H. Lin, W.-F. Liaw, T.-S. Kuo and W.-Z. Lee, *Inorg. Chem.*, 2015, **54**, 5527.

7 Reaction of complex **2** with 5 equivalents of $NaBH_4$ in dry CH_3CN generated H_2 gas and provided complex **1** in 43% yield.

8 G. M. Sheldrick, *Acta Cryst.*, 2008, **A64**, 112.

9 E. Bill, *JulX* version 1.4.1, magnetic susceptibility simulation software, Max-Planck Institute, Germany.

10 C. Piguet, *J. Chem. Educ.*, 1997, **74**, 815.

ChemComm

COMMUNICATION

View Article Online
View Journal | View Issue

Cite this: *Chem. Commun.*, 2016, 52, 11995

Received 4th August 2016,
Accepted 22nd August 2016

DOI: 10.1039/c6cc06433g

www.rsc.org/chemcomm

Solid-state valence tautomeric octahedral $\{Co^{II}[(BQ\text{-}N\text{-}Cat)]_2\}^0$ complex formation *via* ligand-centered phenolic C–O bond breaking and Co–O bond making†

Manas Kumar Mondal,[a] Archana Tiwari[b] and Chandan Mukherjee*[a]

Ligand $H_4L^{O(AP/AP)}$ underwent ligand-centered C–O bond cleavage during a complexation reaction with Co(II)-salt. The thus formed octahedral $\{Co^{II}[(BQ\text{-}N\text{-}Cat)]_2\}^0$ complex showed valence tautomerization in the solid state. While the process was triggered by the presence of lattice solvent, the nature of the solvent molecule has less effect on the process.

Transition metal complexes, which are coordinated to redox-active ligands, have achieved great importance in the fields of biomimetic catalysis, C–H bond activation, C–C cross coupling, C–N bond activation, bistable as well as valence tautomeric complex formation, *etc.*[1–3] The redox-active ligands, which are coordinated to a metal ion, may exist in various oxidation states. Furthermore, a redox-active ligand coordinated to a metal ion in multiple numbers can exist in different oxidation states. Soper *et al.* have reported that the electrophilic and nucleophilic behaviours of square planar Co(III) complexes depend on the redox state of the coordinated redox-active ligands.[2] Redox-active ligand-coordinated cobalt complexes have recently been reported as catalysts for C–C coupling reactions.[1g,2] Apart from the catalytic reactivity, valence tautomerization between Co(III)-semiquinone and Co(II)-quinone electronic isomers is under progressive investigation because of the demand for the development of logic gates and bistable and spin-switch materials.[3] Thus, the study of cobalt complexes that are coordinated to redox-active ligands has drawn special attention.

2-Anilino-4,6-di-*tert*-butylphenol (H_2AP) is an established bidentate non-innocent ligand.[4] The square planar Co(III) complex that formed by the coordination of two equivalents of $[AP]^{2-}$ ligand, $[Co^{III}([AP]^{2-})_2]^-$, is known to behave as a strong nucleophile and undergoes $2e^-$ oxidative addition with alkyl halides. In this process, each $[AP]^{2-}$ ligand undergoes one-electron oxidation and consequently, alkyl-coordinated square pyramidal complexes having the general formula $[Co^{III}E([SQ]^{\bullet 1-})_2]$ (where E = CH_2Cl, alkyl) form. To initiate an oxidative C–C cross coupling reaction *via* the oxidative addition of both alkyl and halide units to the Co center in a Co complex requires *cis*-orientation between the alkyl and halide units. Therefore, *cis*-orientation is necessary between the two coordinated non-innocent ligands to create a vacant site for *cis*-coordination of alkyl halide. In the square planar $[Co^{III}([AP]^{2-})_2]^-$ complex the two coordinating-ligands orient in a *trans*-fashion. Thus, oxidative addition of both alkyl and halide units was not possible in the system.

As the foremost step to impose a non-coplanar arrangement between two radical-generation units, two H_2AP ligands were combined by a bridging O atom that connects the two ligands *via* the *ortho*-carbon atom of the two aniline moieties. The thus formed new ligand will be designated here as $H_4L^{O(AP/AP)}$ (Scheme 1; Fig. S8, ESI†). Because of the O-bridge the angle around the O atom would be ~105°, hence, two aniline rings of the two H_2AP units in ligand $H_4L^{O(AP/AP)}$ could not situate parallel to each other in coordination complexes. Hence, coplanar and *trans*-alignments of the radical-generating 3,5-di-*tert*-butyl

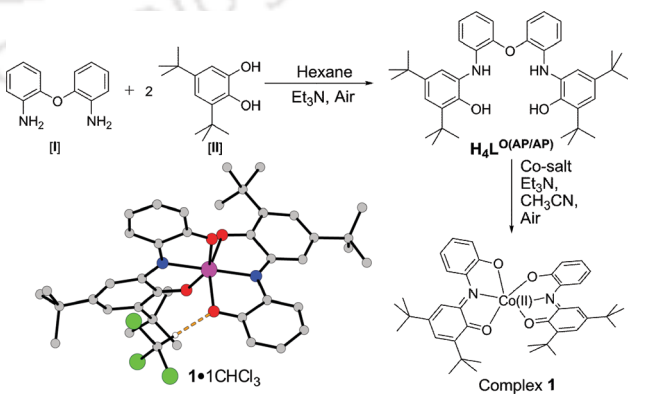

Scheme 1 Schematic representation of ligand $H_4L^{O(AP/AP)}$ and complex **1** formation. X-ray molecular structure of complex **1**·1$CHCl_3$.

[a] *Department of Chemistry, Indian Institute of Technology Guwahati, Guwahati, 781039, Assam, India. E-mail: cmukherjee@iitg.ernet.in*

[b] *Department of Physics, School of Physical Sciences, Sikkim University, Gangtok–737102, Sikkim, India*

† Electronic supplementary information (ESI) available: Synthesis, characterization and molecular structures of the ligand and the complexes, the proposed mechanism, and crystallographic data. See DOI: 10.1039/c6cc06433g

TH-1576_126122004

amidophenolate units could be restricted and the required vacant site for *cis*-coordination might be availed.

Ligand $H_4L^{O(AP/AP)}$ was synthesized in 64% yield by reacting 1 : 2 2,2′-oxodianiline (**I**) with 3,5-di-*tert*-butyl catechol (**II**) in hexane in air in the presence of triethyl amine (Et_3N) [Scheme 1]. The ligand reacted with an equivalent amount of $Co(ClO_4)_2{\cdot}6H_2O$ or $CoCl_2{\cdot}6H_2O$ in CH_3CN in air for 7 hours in the presence of Et_3N and provided a blue-green solid (complex **1**). The solid upon recrystallization from a 5 : 2 $CHCl_3$: CH_3CN solvent mixture appeared as rectangular-shaped crystals (**1**·1$CHCl_3$). However, the crystals were not stable during X-ray diffraction measurement (Table S2, ESI†) even at 100 K. Hence, the molecular structure analysis of the formed complex **1**·1$CHCl_3$ [Scheme 1; Fig. S8; Tables S1 and S2, ESI†] was not worthy enough for the definite assignment of the oxidation state of the central metal ion as well as the coordinated ligands. Nevertheless, from the crystallographic analysis it was evident that the complex was neutral, mononuclear-octahedral (*mer*), and the ligand backbone was different from that of the initially employed ligand for the complexation reaction, *i.e.*, a new tridentate ligand was formed during the reaction *via* ligand-centered phenolic C–O bond cleavage.

Two analogous tridentate ligands, as present in complex **1**·1$CHCl_3$, are already available in the literature[5] and it has been demonstrated that the ligands may exist in their three different stable oxidation states in their corresponding transition metal complexes (Scheme 2). Therefore, the composition of the neutral complex **1** can be either (a) a Co(II) ($S_{Co(II)} = 3/2$, high-spin) ion with two coordinated diamagnetic $(BQ\text{-}N\text{-}Cat)^{1-}$ ligands, *i.e.*, $\{Co^{II}[(BQ\text{-}N\text{-}Cat)]_2\}^0$ or (b) a Co(III) ($S_{Co(III)} = 0$, low-spin) ion with coordinated paramagnetic $(SQ\text{-}N\text{-}Cat)^{2-}$ [$S_L = 1/2$] and $(BQ\text{-}N\text{-}Cat)^{1-}$ ($S_{L'} = 0$) ligands, *i.e.*, $\{Co^{III}[(SQ\text{-}N\text{-}Cat)(BQ\text{-}N\text{-}Cat)]\}^0$ (Scheme 3).

In order to distinguish between the two possible compositions, X-band EPR measurement on **1**·0.3$CHCl_3$[6] was performed at 77 K in a CH_2Cl_2/toluene solvent mixture (Fig. 1A). A ligand-centered $S = 1/2$ signal with a reasonable ^{59}Co ($I = 7/2$) super-hyperfine interaction was established by the simulation of the experimental spectrum. The parameters obtained by the simulation were $g_1 = 2.007$, $g_2 = 2.007$, and $g_3 = 1.998$; $g_{iso} = 2.004$; $^{59}Co(A_1, A_2, A_3) = (7, 7, 27) \times 10^{-4}$ cm^{-1}. Interestingly, it was observed that the signal vanished at 295 K. The temperature-dependent signal also held true for solid-state X-band EPR measurements of the complex (Fig. 1B). The intensity of the signal decreases drastically at 295 K. In fact, the nature of the observed EPR signal was different than that of ligand-centered $S = 1/2$ and indeed, very weak in intensity, *i.e.*, almost X-band EPR silent. Therefore, it can be argued that in solution as well as in the solid state the complex underwent valence tautomerization; at low temperature

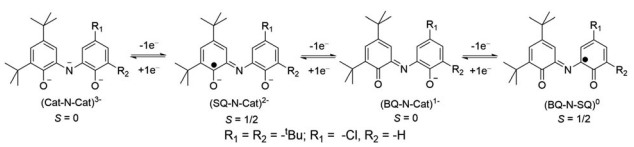

Scheme 2 Various possible oxidation states of $(Cat\text{-}N\text{-}Cat)^{3-}$ species.

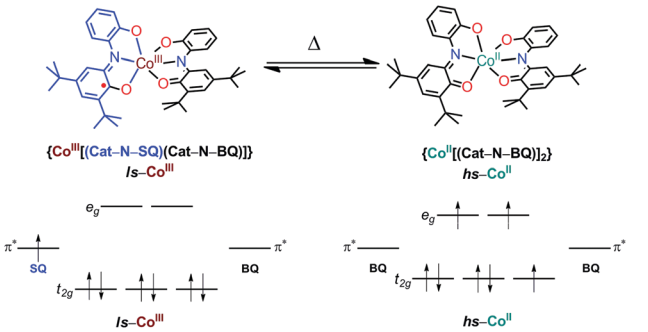

Scheme 3 Valence tautomeric species.

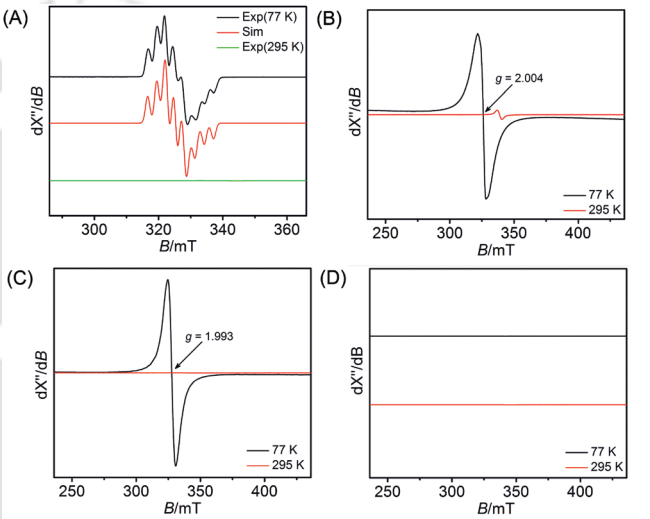

Fig. 1 X-band EPR spectra measured at 77 and 295 K; (A) complex **1**·0.3$CHCl_3$ in a CH_2Cl_2/toluene (2 : 1) solvent mixture; microwave frequency (GHz): 9.444; modulation frequency (kHz): 100; amplitude = 1.0; (B) complex **1**·0.3$CHCl_3$ in the solid state; microwave frequency (GHz): 9.142; modulation frequency (kHz): 100; amplitude (*G*) = 0.3; (C) complex **1**·0.8CH_3CN in solid state; microwave frequency (GHz): 9.138; modulation frequency (kHz): 100; amplitude (*G*) = 1.0; and (D) complex **1** in solid state; X-band microwave frequency (GHz): 9.143; modulation frequency (kHz): 100; amplitude (*G*) = 1.0.

(77 K) the composition of the complex was Co(III), $(SQ\text{-}N\text{-}Cat)^{2-}$ and $(BQ\text{-}N\text{-}Cat)^{1-}$, while at 295 K both the coordinated ligands were in the $(BQ\text{-}N\text{-}Cat)^{1-}$ form and the central metal was Co(II). Vanishing of the X-band EPR signal at 295 K was due to zero-field splitting (>0.3 cm^{-1}) that resulted upon high spin–orbit coupling at Co(II). Herein, it is noteworthy that valence tautomerization between octahedral $\{Co^{III}[(SQ\text{-}N\text{-}Cat)(BQ\text{-}N\text{-}Cat)]\}^0$ and $\{Co^{II}[(BQ\text{-}N\text{-}Cat)]_2\}^0$ is well known in solution; however, the phenomenon is absent in the solid state within the 2–295 K temperature range.[7]

Inspired by X-band EPR results, variable-temperature magnetic susceptibility measurement was carried out on a solid sample of complex **1**·0.3$CHCl_3$[6] at 1 T external magnetic field to reinforce the solid-state valence tautomeric nature of the complex. The $\chi_M T$ *vs.* T plot is depicted in Fig. 2. At 10 K, $\chi_M T = 0.44$ emu K mol^{-1} was observed. This value was closely commensurate with the

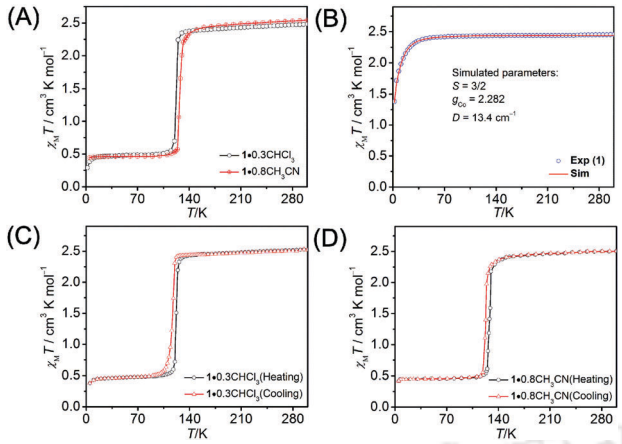

Fig. 2 $\chi_M T$ *vs.* T plots: (A) **1**·0.3CHCl$_3$ and **1**·0.8CH$_3$CN, (B) **1**, (C) hysteresis measurement of **1**·0.3CHCl$_3$ and (D) hysteresis measurement of **1**·0.8CHCl$_3$.

system having one-unpaired electron (an $S = 1/2$ spin). The value remained almost unchanged up to 118 K. Interestingly, in the 118 to 125 K temperature range a sharp transition in the magnetic moment to $\chi_M T = 2.34$ emu K mol^{-1} was observed. The magnetic moment attained at 125 K remained almost constant up to 300 K. This feature supported a valence tautomeric phenomenon in the system, where low-spin diamagnetic Co(III) was reduced to high-spin Co(II) by the ligand-centric SQ unit that then transformed to its one-electron oxidized BQ form (Scheme 3). Therefore, it can be argued that till 118 K the complex was existing in the $\{Co^{III}[(SQ\text{-}N\text{-}Cat)(BQ\text{-}N\text{-}Cat)]\}^0$ form, while above 125 K the complex continued to exist in the $\{Co^{II}[(BQ\text{-}N\text{-}Cat)]_2\}^0$ form. The critical temperature (T_c), which is defined as the temperature at which the free energy difference (ΔG) between the two inter-convertible species is nil, was 122 K.[8]

In order to understand the origin of the tautomerization, and such a rare and abrupt transition, initially we have tried to understand the solvent effect. Hence, complex **1** was recrystallized from (a) a 3 : 1 Et_2O : CH_3CN solvent mixture and (b) toluene. Crystals, which were obtained from the two crystallization processes, were measured by X-ray single crystal diffraction methods. Indeed, 1 equivalent of CH_3CN was found to exist in the crystal lattice of the crystal (**1**·1CH_3CN) that was obtained from the 3 : 1 Et_2O : CH_3CN solvent mixture (Fig. S8D, ESI†). The nonexistence of solvent molecule was confirmed in the crystal (complex **1**) that was obtained from toluene (Fig. S8C, ESI†). Noteworthily, the quality of crystals was not good enough for the assignment of acute and appropriate oxidation states of ligands as well as the metal center (Tables S1 and S2, ESI†).

Nevertheless, variable-temperature magnetic susceptibility measurements for **1**·0.8CH_3CN[6] and **1**[6] were carried out on solid samples at 1 T external magnetic field. The $\chi_M T$ *vs.* T plots are depicted in Fig. 2. The temperature-dependent change in $\chi_M T$ for **1**·0.8CH_3CN was very similar to that of **1**·0.3$CHCl_3$. However, T_c of **1**·0.8CH_3CN was slightly higher (~4.4 K) compared to that of **1**·0.3$CHCl_3$. Unlike solvated crystals, in the case of complex **1**, the $\chi_M T$ = 2.46 emu K mol^{-1} value remained almost constant in the temperature range 50–300 K. Upon further lowering the temperature, the $\chi_M T$ value decreased and reached 1.71 emu K mol^{-1} at 5 K. Herein, the decrease in the $\chi_M T$ value was due to zero-field splitting ($D = 13.4$ cm^{-1}, Fig. 2B) that arose because of strong spin–orbit coupling at the Co(II) center. Thus, it was apparently evident that in the absence of lattice solvent the complex remained in the $\{Co^{II}[(BQ\text{-}N\text{-}Cat)]_2\}^0$ form and no valence tautomerization took place.

The single-crystal volume of **1** increased with the incorporation of lattice solvent (Table S2, ESI†). Therefore, it was evident that the presence of lattice solvent molecules within the crystal lattice promoted flexibility or softness[3a,n] in the systems (Fig. S9 and S10, ESI†) and favored the required structural changes in the valence tautomeric transition. Crystal-structure packing analyses revealed that in complex **1** two adjacent molecules were firmly held by strong intermolecular H-bonds, while in complex **1**·1$CHCl_3$ and complex **1**·1CH_3CN the intermolecular H-bonds were weak in nature (Fig. 3). The strong H-bonds, which can be considered as a stabilizing factor, presumably prevented complex **1** from undergoing any required structural change for valence tautomerization. The abrupt transition within a very small (7 K) temperature range (Fig. 2) in **1**·0.3$CHCl_3$ and **1**·0.8CH_3CN reinforced a strong cooperative effect[3a,n] that was propagated through the lattice solvent network (Fig. S9 and S10, ESI†). Although, the crystallographic phases and the nature of the lattice solvent molecule were different for the different complexes (Fig. 4), no consequence on the nature of transition, transition temperature, and hysteresis

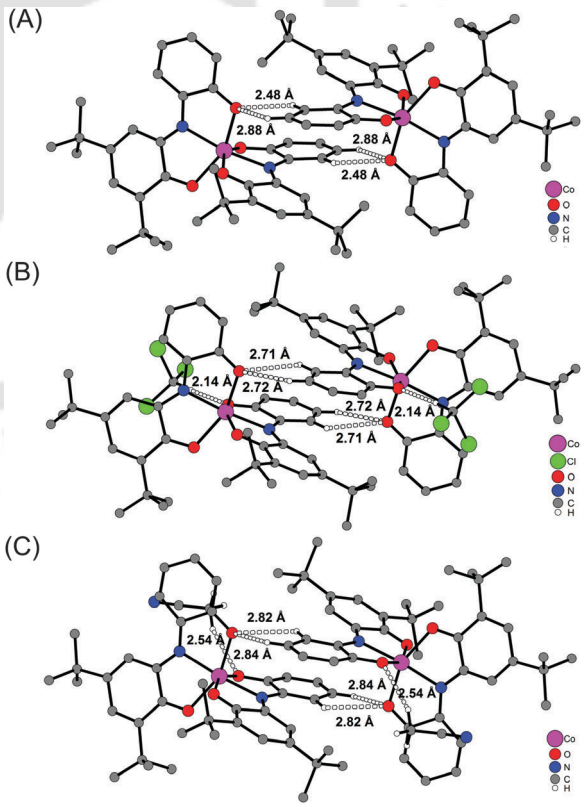

Fig. 3 H-bonds between the two adjacent molecules: (A) complex **1**, (B) complex **1**·1$CHCl_3$, and (C) complex **1**·1CH_3CN.

TH-1576_126122004

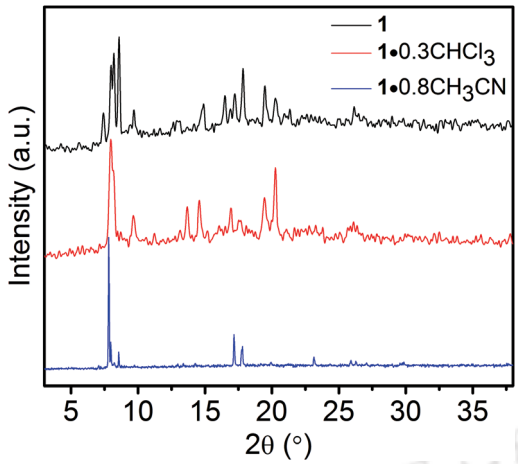

Fig. 4 X-ray powder diffractograms of crystalline samples of the complexes.

effect (Fig. 2C and D) was discerned. These experimental facts reinforced that no correlative inference can be formulated amongst T_c, solvent nature, and crystallographic phases.

To conclude, herein we have presented a new tetradentate non-innocent ligand $[H_4L^{O(AP/AP)}]$ which in the presence of Co(II)–salt, Et_3N and air forms a $\{Co^{II}[(BQ\text{-}N\text{-}Cat)]_2\}^0$ complex. During the complex formation, a weak interaction between the Co center and the bridging O atom is postulated (Scheme S3; Fig. S7, ESI†). This interaction drives the formation of Co–O bond *via* homolytic phenolic C–O bond cleavage. The complex undergoes valence tautomerization in solution (Fig. S11, ESI†) as well as in the lattice solvent-containing solid phase. From the solid state X-band EPR measurements, it was confirmed that at room temperature (295 K), the complex exists as $\{Co^{II}[(BQ\text{-}N\text{-}Cat)]_2\}^0$, while at a low temperature (77 K) it exists as $\{Co^{III}[(SQ\text{-}N\text{-}Cat)(BQ\text{-}N\text{-}Cat)]\}^0$.

Variable-temperature magnetic susceptibility measurements on **1**, **1**·0.3$CHCl_3$ and **1**·0.8CH_3CN again substantiate that the tautomerization is triggered by the presence of the lattice solvent molecule. Interestingly, the process and the T_c value are almost independent of the nature of lattice-solvent and the corresponding crystallographic phase. Although it appears that the valence tautomerization in the present system is governed by the change in the temperature-dependent lattice packing-structure, a good quality crystal-structure would lead to confirmation. Therefore, in the near future further studies will be conducted to have better quality crystals by using various other solvents for crystallization. Additionally, syntheses of other similar type of ligands, where various different substituents would be attached at the main ligand-backbone, and their corresponding Co-complexes will also be conducted to examine the packing effect on valence tautomerization.

This project was supported by SERB, India, EMR/2015/002491. MKM thanks the Indian Institute of Technology Guwahati (IITG) for his doctoral fellowship. Prof. Dr. Thorsten Glaser, Bielefeld University; CIF and the Department of Chemistry, IITG, are thankfully acknowledged for the instrumental facilities.

Notes and references

1 (*a*) D. L. J. Broere, R. Plessius and J. I. van der Vlugt, *Chem. Soc. Rev.*, 2015, **44**, 6886; (*b*) A. L. Smith, L. A. Clapp, K. I. Hardcastle and J. D. Soper, *Polyhedron*, 2010, **29**, 164; (*c*) S. Ghorai and C. Mukherjee, *Chem. Commun.*, 2012, **48**, 10180; (*d*) S. H. A. M. Leenders, R. Gramage-Doria, B. de Bruin and J. N. H. Reek, *Chem. Soc. Rev.*, 2015, **44**, 433; (*e*) S. Ghorai and C. Mukherjee, *Dalton Trans.*, 2014, **43**, 394; (*f*) V. Lyaskovskyy and B. de Bruin, *ACS Catal.*, 2012, **2**, 270; (*g*) M. van der Meer, Y. Rechkemmer, I. Peremykin, S. Hohloch, J. van Slageren and B. Sarkar, *Chem. Commun.*, 2014, **50**, 11104; (*h*) S. Ghorai and C. Mukherjee, *Chem. – Asian J.*, 2014, 3518; (*i*) S. Ghorai and C. Mukherjee, *RSC Adv.*, 2014, **4**, 24698; (*j*) L. G. Ranis, K. Werellapatha, N. J. Pietrini, B. A. Bunker and S. N. Brown, *Inorg. Chem.*, 2014, **53**, 10203.

2 A. L. Smith, K. I. Hardcastle and J. D. Soper, *J. Am. Chem. Soc.*, 2010, **132**, 14358 and references therein.

3 (*a*) E. Evangelio, C. Rodriguez-Blanco, Y. Coppel, D. N. Hendrickson, J. P. Sutter, J. Campo and D. Ruiz-Molina, *Solid State Sci.*, 2009, **11**, 793; (*b*) H. Spiering, T. Kohlhaas, H. Romstedt, A. Hauser, C. Bruns-Yilmaz, J. Kusz and P. Gütlich, *Coord. Chem. Rev.*, 1991, **111**, 275; (*c*) P. Gütlich, A. B. Gaspar and Y. Garcia, *Beilstein J. Org. Chem.*, 2013, **9**, 342; (*d*) N. Azzaroli, A. Lapini, M. D. Donato, A. Dei and R. Righini, *J. Phys. Chem. B*, 2013, **117**, 15492; (*e*) D. M. Adams and D. N. Hendrickson, *J. Am. Chem. Soc.*, 1996, **118**, 11515; (*f*) F. Novio, E. Evangelio, N. Vazquez-Mera, P. González-Monje, E. Bellido, S. Mendes, N. Kehagias and D. Ruiz-Molina, *Sci. Rep.*, 2013, **3**, 1708; (*g*) E. Evangelio and D. Ruiz-Molina, *Eur. J. Inorg. Chem.*, 2005, 2957; (*h*) P. Gütlich and A. Dei, *Angew. Chem., Int. Ed. Engl.*, 1997, **36**, 2734; (*i*) T. Tezgerevska, K. G. Alley and C. Boskovic, *Coord. Chem. Rev.*, 2014, **268**, 23; (*j*) A. Cui, k. Takahashi, A. Fujishima and O. Sato, *J. Photochem. Photobiol., A*, 2004, **161**, 243; (*k*) R. M. Buchanan and C. G. Pierpont, *J. Am. Chem. Soc.*, 1980, **102**, 4951; (*l*) C. G. Pierpont, *Coord. Chem. Rev.*, 2001, **217**, 99; (*m*) E. Evangelio and D. Ruiz-Molina, *C. R. Chim.*, 2008, **11**, 1137; (*n*) D. Kiriya, H. C. Chang and S. Kitagawa, *J. Am. Chem. Soc.*, 2008, **130**, 5515; (*o*) D. Kiriya, H. C. Chang, K. Nakamura, D. Tanaka, K. Yoneda and S. Kitagawa, *Chem. Mater.*, 2009, **21**, 1980; (*p*) R. D. Schmidt, D. A. Shultz and J. D. Martin, *Inorg. Chem.*, 2010, **49**, 3162; (*q*) F. Novio, J. Campo and D. Ruiz-Molina, *Inorg. Chem.*, 2014, **53**, 8742; (*r*) R. D. Schmidt, D. A. Shultz, J. D. Martin and P. D. Boyle, *J. Am. Chem. Soc.*, 2010, **132**, 6261.

4 P. Chaudhuri, C. N. Verani, E. Bill, E. Bothe, T. Weyhermüller and K. Wieghardt, *J. Am. Chem. Soc.*, 2001, **123**, 2213.

5 (*a*) C. L. Simpson, S. R. Boone and C. G. Pierpont, *Inorg. Chem.*, 1989, **28**, 4379; (*b*) A. Sasmal, E. Garribba, C. J. Gómez-García, C. Desplanches and S. Mitra, *Dalton Trans.*, 2014, **43**, 15958.

6 As obtained by microanalysis (C, H, N values).

7 (*a*) S. K. Larsen and C. G. Pierpont, *J. Am. Chem. Soc.*, 1988, **110**, 1827; (*b*) A. Caneschi, A. Cornia and A. Dei, *Inorg. Chem.*, 1998, **37**, 3419; (*c*) O. Cador, F. Chabre, A. Dei, C. Sangregorio, J. V. Slageren and M. G. F. Vaz, *Inorg. Chem.*, 2003, **42**, 6432.

8 Complex **1**·0.3$CHCl_3$: ΔH = 101 kJ mol^{-1}; ΔS = 825 J K^{-1} mol^{-1}; complex **1**·0.8CH_3CN: ΔH = 79 kJ mol^{-1}; ΔS = 618 J K^{-1} mol^{-1}; calculations were performed based on the mole-fraction formula as described in ref. 7*c*.

